



# Proteomic characterization of the biomolecular corona and its impact on cellular uptake

Dissertation

Zur Erlangung des Grades

´Doktor rerum naturalium (Dr. rer. nat.)´

Fachbereich Chemie, Pharmazie und Geowissenschaften

Johannes Gutenberg-Universität, Mainz (D77)

vorgelegt von

**Johanna Simon (geb. Reitz)**

Mainz, Mai 2018

[redacted]

Dekan: [redacted]

Prodekan: [redacted]

Gutachter 1: [redacted]

Gutachter 2: [redacted]

Date of oral examination: [redacted]

# Content

# Abstract

Once nanoparticles are exposed to a biological milieu, blood components rapidly interact with the nanoparticles´ surface, hereby giving the nanoparticle a biological fingerprint (´biomolecular corona´). This process determinately affects the pharmacological profile and therapeutic efficiency of any nanoparticle. Despite the great effort in the development of nanoparticles with a protein-repellent surface (for example surface functionalization with PEG), it is still under debate whether it is possible to completely prevent protein adsorption. Therefore, a thorough characterization of the adsorbed protein layer is needed to improve the biological properties of nanoparticles applied as drug delivery vehicles.

This work aimed to shed light onto the multiple interactions occurring at the nano-bio-interface. In a correlative analysis using transmission electron microscopy (TEM) and liquid chromatography coupled to mass spectrometry (LC-MS) it was possible to monitor the evolution of the protein corona. It was shown that the protein corona had a non-uniform structure and was not - as supposed - dense layer. For meaningful protein corona analysis, it is of great importance to perform *in vitro* studies under physiologically relevant conditions coming as close as possible to the *in vivo* situation. Here, as an example, a widely performed cell culture technique known as heat inactivation was investigated. Commonly, the protein source supplemented within the cell culture medium is heated up to 56 °C prior to use in order to avoid interference with *in vitro* assays. However, it was demonstrated that this procedure strongly affects the nanoparticle-protein interactions and further alters their cellular uptake behavior.

Clincial trials are the final step before nanoparticles are approved for therapeutic treatment. Beforehand, mouse studies are performed in order to evaluate the nanoparticles´ behavior *in vivo*. Based on this, it was investigated how the interspecies protein composition (mouse vs. human) influences the interaction with nanoparticles. Here, it was found that there is a severe discrepancy in the protein corona depending on the protein source. This needs to be considered in order to transfer knowledge gained from *in vivo* mouse experiments to clinical studies in human.

In nanomedicine the surface of the nanoparticles is commonly functionalized with hydrophilic polymers (e.g. poly(ethylene glycol) PEG) in order to prolong the circulation of nanoparticles in blood. This is known as the stealth effect, which is an established method since the early developments of nanoparticles applied as drug delivery vehicles. However, even up to now there is a limited knowledge about the principal mechanism behind this effect. To unravel this, the influence of polymer hydrophilicity on the protein adsorption pattern was investigated. This

was further correlated with the cellular interactions towards macrophages. It was shown that a defined surface hydrophilicity triggers a selective protein adsorption and that actually distinct proteins mediate the stealth effect. This knowledge now opens up the great potential to exploit protein corona formation. As an example, it was demonstrated that an engineered protein corona can prevent unspecific cellular uptake towards macrophages.

The overall goal of nanomedicine is the targeted transport of nanoparticles to the body region of interest (e.g. cancer cells). Therefore, the surface of the nanoparticles needs to be functionalized with targeting ligands to guide the nanoparticles´ way. Several studies indicated that the targeting properties of nanoparticles can be highly affected due to protein corona formation. Literature reports described that adsorbed proteins can completely cover up the targeting moiety, hereby preventing cellular recognition of the ligand on the nanoparticles´ surface and the cellular receptor. Therefore, in this work two different methods were developed, which allow an efficient surface functionalization and thereby enable targeted cell interactions even in the presence of the protein corona.

It was found that nanoparticles can be functionalized with antibodies through adsorption depending on the pH of the buffer system. Antibody functionalized nanoparticles were able to reach the targeted cell even after exposure to blood plasma and were able to withstand extended periods of incubation in a complex protein surroundings, hereby proving successful targeting properties.

Further, an alternative strategy is highlighted, which takes advantage of surfactants for the non-covalent functionalization of nanoparticles. Surfactants are surface-active substances and rapidly adsorb onto nanoparticles. To investigate whether this method allows targeted cell interactions, different surfactants were modified with a mannose ligand. It was shown that mannose modified surfactants can be used as a universal approach for the non-covalent functionalization of a broad range of nanoparticle to achieve targeted cell interactions even after incubation with blood plasma.

# Publication list

In this thesis, publication **1-9** will be presented in detail. Additionally, publications **10-19** are shortly summarized and extended information is provided in the respective publication.

**[1]** Kokkinopoulou, M*., **Simon, J*.,** Landfester, K., Mailänder, V., Lieberwirth, I. Visualization of the protein corona: towards a biomolecular understanding of nanoparticle-cell-interactions. *Nanoscale*, **2017**, *9* (25), 8858-8870. **(*shared first)**

**[2]** **Simon, J.,** Müller, J., Ghazaryan, A., Morsbach, S., Landfester, K., Mailänder, V. Protein denaturation by heat inactivation detrimentally affects biomolecular corona formation and cellular interactions. (to be submitted).

**[3]** Müller, L. K*., **Simon, J*.,** Rosenauer, C., Mailänder, V., Morsbach, S., Landfester, K. The transferability from animal models to humans: challenges regarding aggregation and protein corona formation of nanoparticles. *Biomacromolecules*, **2018**, 19 (2), 374-385. **(*shared first)**

**[4]** **Simon, J***., Kuhn, G*., Fichter, M., Landfester, K., Mailänder, V. Unraveling *in vivo* corona formation **(*shared first, to be submitted).**

**[5]** **Simon, J*.,** Wolf, T*. Klein, K. Landfester, K. Wurm, F.R., Mailänder, V. Hydrophilicity regulates the stealth properties of poly(phosphoester)-coated nanocarries. *Angewandte Chemie,* **2018**, 57, 5548-5553 **(*shared first)**

**[6]** **Simon, J***., Christmann, S*., Mailänder, V., Wurm, F. K., Landfester, K. Protein corona mediated stealth properties of biocompatible carbohydrate-based nanocarries. *Biomaterials* **(*shared first, under revision)**

**[7]** **Simon, J**., Müller, L. K., Kokkinopoulou, M., Lieberwirth, I., Morsbach, S., Landfester, K., Mailänder, V. Exploiting the biomolecular corona: Pre-coating of nanoparticles enables controlled cellular interactions. *Nanoscale* (under revision)

**[8]** Tonigold, M*., **Simon, J*.,** Estupinan, D., Kokkinopoulou, M., Reinholz, J., Kintzel, U., Kaltbeitzel, A., Renz, P., Domogalla, M. P., Steinbrink, K., Lieberwirth, I., Crespy, D., Landfester, K., Mailänder, V. Pre-adsorption of antibodies enables targeting of nanocarriers despite a biomolecular corona. *Nature Nanotechnology,* **(shared first, accepted by reviewers, editorial requests await approval)**

**[9]** **Simon, J.***, Bauer, K. N.,* Langhanki, J., Opatz, T., Landfester, K., Mailänder, V., Wurm F.R. Mannose functionalized poly(phosphoester)-based surfactants enable targeted cellular interactions. **(*shared first, to be submitted)**

**[10]** Müller, L. K., **Simon, J.,** Schöttler, S., Landfester, K., Mailänder, V., Mohr, K. Pre-coating with protein fractions inhibits nano-carrier aggregation in human blood plasma. *RSC Advances*, **2016**, *6* (99), 96495-96509.

**[11]** Piradashvili, K., **Simon, J.,** Paßlick, D., Höhner, J. R., Mailänder, V., Wurm, F. R., Landfester, K. Fully degradable protein nanocarriers by orthogonal photoclick tetrazole–ene chemistry for the encapsulation and release. *Nanoscale Horizons*, **2017**, *2* (5), 297-302.

**[12]** Schlegel, I., Renz, P., **Simon, J.,** Lieberwirth, I., Pektor, S., Bausbacher, N., Miederer, M., Mailänder, V., Muñoz-Espí, R., Crespy, D., Landfester, K. Highly Loaded Semipermeable Nanocapsules for Magnetic Resonance Imaging. *Macromolecular Bioscience*, **2018**, doi: 10.1002/mabi.201700387.

**[13]** Müller, J., Bauer, K. N., Prozeller, D., **Simon, J.,** Mailänder, V., Wurm, F. R., Winzen, S., Landfester, K. Coating nanoparticles with tunable surfactants facilitates control over the protein corona. *Biomaterials*, **2017**,*115*, 1-8.

**[14]** Wald, S., **Simon, J.,** Dietz, J. P., Wurm, F. R., Landfester, K. Polyglycerol Surfmers and Surfactants for Direct and Inverse Miniemulsion. *Macromolecular bioscience*, **2017**, doi: 10.1002/mabi.201700070.

**[15]** Wolf, T., Rheinberger, T., **Simon, J.**, Wurm, F. R. Reversible Self-Assembly of Degradable Polymersomes with Upper Critical Solution Temperature in Water. *Journal of the American Chemical Society*, **2017**, *139* (32), 11064-11072.

**[16]** Wolf, T., Hunold, J., **Simon, J.,** Rosenauer, C., Hinderberger, D., Wurm, F. R. Temperature responsive poly(phosphonate) copolymers: from single chains to macroscopic coacervates. *Polymer Chemistry*, **2018**, 9, 490-498.

**[17]** Müller, J., **Simon J.,** Rohne P., Koch-Brandt C., Mailänder V., Morsbach S., Landfester K. Denaturation via surfactants changes composition of protein corona *Biomacromolecules*, **2018**, doi: 10.1021/acs.biomac.8b00278

**[18]** Weber C., **Simon J.**, Mailänder V., Morsbach S., Landfester K. Preservation of the soft protein corona in distinct flow allows identification of weakly bound proteins. *Acta Biomaterialia*, **2018**, (under revision)

**[19]** Bros, M., Lutz, N., **Simon, J.,** Moll, L., Mailänder, V., Landfester, K., Grabbe, S. The protein corona as a confounding variable of nanoparticle-mediated targeted vaccine delivery. *Frontiers in Immunology* (under revision)

***Note:*** For each publication all LC-MS Excel files (raw data) are accessible via a link through the Elsevier online platform (Mendeley):

https://data.mendeley.com/datasets/48frcj8wry/draft?a=b4561032-1402-44ba-b23b-9ebd4f73b896

# Introduction

In modern medicine, nanotechnology is an emerging field, which aims to improve the therapeutic efficacy of drugs[1]. The development of multifunctional nanoparticle formulations is envisioned to revolutionize and improve current strategies for disease treatment[2]. The unique aspect of nanoparticles applied as drug delivery vehicles is the selective transport of therapeutics to the targeted site of interest[3]. With this, it is aimed to improve the bioavailability and reduce drug induced toxicity[4].

A first nanoparticle formulation based on liposomes (known as ´Doxil´) is already approved by the Food and Drug Administration (FDA) as a therapeutic for treating ovarian and other types of cancer[5-6]. However, the overall number of clinically applied nanoparticle systems is low and nanomedicine is still in the early developing stages[7]. Nanoparticles designed for biomedical applications have to encounter several challenges. A precise control of the physico-chemical properties (e.g. size, surface functionalization or charge) of the nanoparticles is required to ensure colloidal stability[8], efficient drug release[9] and a low toxicity[10].

On top of that, once applied under physiological conditions (e.g intravenously injected into blood) nanoparticles have to face the complex surrounding of various biomolecules[11]. Adsorption of blood proteins or lipids on the nanoparticle surface occurs rapidly within seconds (´biomolecular or ´protein corona´ formation) and this eventually gives the nanoparticle a new biological fingerprint. This fact was first widely overlooked. However, it has been now recognized that the cellular interactions and the physiological response of a nanoparticle are actually determined by its protein corona[12,13]. Therefore, to improve the nanoparticles´ properties and achieve a successful clinical translation, it is urgently needed to gain deeper knowledge about the principal mechanism governing protein corona formation.

This work aimed to understand the interactions occurring at the nano-bio-interface to achieve controlled cellular interactions of nanoparticles (Figure 1). Overall, this thesis is dived into three major parts. Briefly, **Chapter A** describes different parameters, which influence protein corona formations. Here, it was intended to characterize the biological identity of various nanoparticle formulation in order to understand the major driving forces mediating protein adsorption. **Chapter B** deals with the principal mechanism behind the ´stealth effect´ and its influence on protein corona formation. Last, in **Chapter C** different targeting strategies are presented, which enable controlled nanoparticle-cell interaction in the presence of the protein corona.

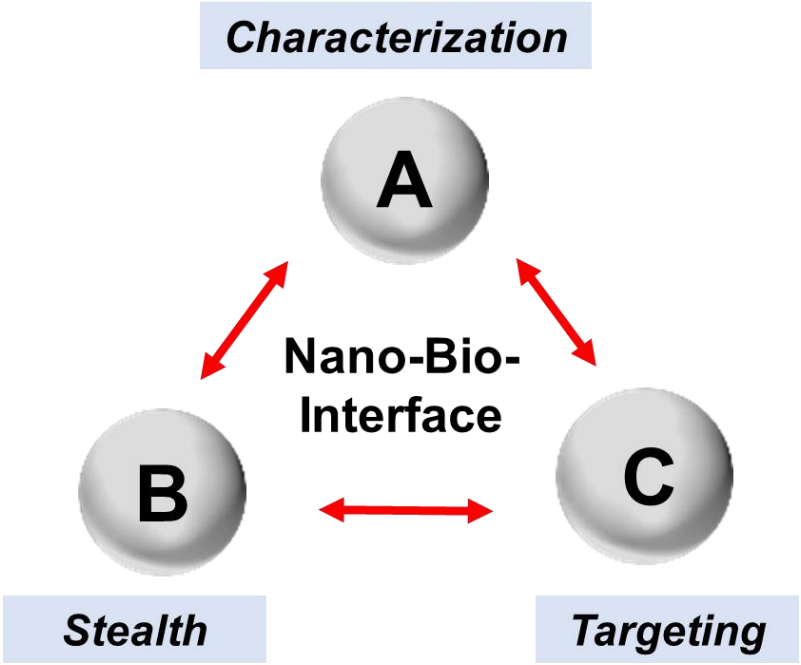


**Figure 1. Investigating the Nano-Bio-Interface.** The biological characterization of the protein corona is summarized in chapter A. The stealth properties of nanoparticles are studied in chapter B and the targeting efficiency in the presence of the protein corona is investigated in chapter C.

A thorough characterization of the protein corona composition is a key requirement to determine the biological signature of a nanoparticle. New analytical methods need to be developed in order to study the adsorbed protein layer around the nanoparticle. Additionally, for meaningful protein corona studies, advanced assays need to be established, which allow to investigate the protein corona under physiological relevant conditions and to mimic the *in vivo* situation. This issue is addressed in four different parts included in **Chapter A (´Charaterization of the biomolecular corona: Expanding analytical methods and exploring conditions´)**.

In the first study, transmission electron microscopy (TEM) was used to investigate the structure of the biomolecular corona. Further, with liquid chromatography coupled to mass spectrometry (LC-MS) it was possible to identify the corona composition. Lastly, in a correlative analysis via TEM and confocal laser scanning microscopy (cLSM), the cellular uptake process in the presence of the protein corona was explored. This study describes on one side new analytical methods (TEM) to analyze the structure of the protein corona and on the other side combines a set of established analytical tools, which allow to monitore the evolution of the protein corona.

The second study investigated the influence of heat inactivation of serum or plasma on cellular uptake of nanoparticles towards macrophages and its impact on corona formation. This study

is of importance as it underlines the difference between commonly applied *in vitro* experiments and the *in vivo* situation.

The third study compared the corona formation, cellular uptake and aggregation behavior of nanoparticles incubated with plasma obtained from different animal sources. This knowledge is important for the successfull translation of nanoparticles to clinical trials (human).

In the fourth study, corona formation under classical *in vitro* conditions was compared to the *in vivo* situation. This part shed light into the complex surrounding, which nanoparticles have to encounter after *in vivo* administration.

Attaching poly(ethylene glycol) on the nanoparticles´ surface is the standard method to obtain ´stealth properties´. With this it is aimed to reduced the protein interaction and hereby avoid unintended cellular uptake. Up to now, there is a limited understanding on the interactions of stealth nanoparticles and plasma proteins. Additionally, as PEG is a non-biodegradable polymer, alternative strategies are needed to obtain stealth properties. In **Chapter B (´Stealth coating for nanoparticles: Avoiding unintended cellular uptake´)** three different parts are included, which investigate the stealth effect.

In study five, the influence of nanoparticle surface hydrophilicity is correlated with protein corona formation and cellular uptake towards phagocytic cells. With this, the molecular mechanism behind the stealth effect was analyzed.

Study six investigated whether it is possible to achieve stealth properties if the surface of hydroxyethyl starch (HES) nanocapsules is functionalized with different sugar moieties. With this strategy it is aimed to obtain fully degradable stealth nanocarrier.

In part seven a bioinspired alternative stealth coating strategy is presented. Here, protein corona formation was exploited for targeted cell interactions.

The overall goal of nanoparticles used as drug delivery vehicles is the targeted interaction with specific cells. Therefore, the nanoparticles´ surface is functionalized with different targeting ligands. In **Chapter C (´Targeting strategies: Controlled cellular interactions in the presence of the protein corona´)**, two different methods, are presented, which enable targeted cell interaction taking into account protein corona formation.

In study eight, nanoparticles were functionalized with antibodies via adsorption using different pH values. The distinct influence of corona formation on the targeting properties of antibody-modified nanoparticles was investigated.

Study nine describes the synthesis of mannose-functionalized surfactants, which can be utilized as coating for various nanoparticles to target nanoparticles specifically towards dendritic cells.

# Chapter A

## Charaterization of the biomolecular corona: Expanding analytical methods and exploring conditions

In chapter A there are four different publications **(1-4)** summarized. In general, these studies aimed to provide a fundamental knowledge about biomolecular corona formation. In the following an introduction about the current state-of the art methodologies for protein corona analysis will be given. Afterwards each study is presented separately.

**[1]** [redacted] Visualization of the protein corona: towards a biomolecular understanding of nanoparticle-cell-interactions. *Nanoscale*, **2017**, 9 (25), 8858-8870. **(*shared first)**

**[2]** [redacted] Protein denaturation by heat inactivation detrimentally affects biomolecular corona formation and cellular interactions.

**[3]** [redacted] The transferability from animal models to humans: challenges regarding aggregation and protein corona formation of nanoparticles. *Biomacromolecules*, **2018**, 19 (2), 374-385. **(*shared first)**

**[4]** [redacted] Unraveling in vivo corona formation.

# Introduction

There is a steadily increasing interest in the development of novel nanomaterials for biomedical applications[14-15]. The rapid progress in the synthesis of smart, multi-functional nanoparticle formulations promises their successful performance *in vivo*[16]. However, even up to now the number of nanoparticle systems, which have reached clinical trials or are approved by the FDA is still low[17-18].

Already, in the 60s Vroman and colleagues[19] recognized that protein adsorption onto the surface of nanoparticles is a key factor, which significantly influences the biological behavior of nanoparticles. First studies using gel electrophoresis aimed to identify the adsorbed proteins and understand the kinetics of the adsorption process (´Vroman effect´)[20]. In recent years, the development of high-throughput analytical methods (e.g. liquid chromatography coupled to mass spectrometry) has enabled researchers to characterize the exact protein composition[21]. It is now widely accepted that nanoparticles are rapidly covered by proteins (´protein corona´) once they are introduced to a physiological environment (e.g. blood plasma)[22-24]. Over the last 10 years, there is an increasing number of reports, which summarize large protein data sets, enabling researchers now to understand the principal mechanisms, which mediates the interaction of nanoparticles and proteins[25]. Further, it was shown that other biomolecules (e.g. lipids, sugars, metabolites) additionally cover the nanoparticles´ surface and influence the biological interaction (´biomolecular corona´)[26-28].

In the following, the first part will review how the physico-chemical properties of the nanoparticle influence protein adsorption. Further, an overview of analytical methods, which are currently used to study protein corona formation, will be summarized. Next to this, different approaches, which are applied for protein corona studies, will be highlighted. To conclude, the final impact of protein corona formation on the cellular interactions will be discussed.

### A.1 Physico-chemical properties (material, charge, size)

Protein adsorption is generally driven by Van der Waals forces, electrostatic and electrosteric and hydrophobic interactions or hydrogen bonds (Figure A.1)[29-30]. Depending on the application, nanoparticles are synthesized from inorganic or organic materials[31]. Apolipoproteins were identified on a broad range of polystyrene nanoparticles[32], whereas complement proteins specifically bound to sugar coated nanoparticles[33-34]. Next, to this Deng *et al.* investigated the interaction of plasma proteins and different metal oxide nanoparticles ($TiO_2$, ZnO, $SIO_2$)[35]. All nanoparticles had the same surface charge, but the protein corona pattern differed greatly.

From the early times when nanoparticles were used as drug carrier vehicles, it is the main goal to achieve a long blood circulation in order to enable a targeted cell interaction[36]. Most commonly, the surface of the nanoparticles is modified with hydrophilic polymers such as poly(ethylene glycol). With this it is intended to reduce protein interactions and hereby avoid the rapid clearance of the nanoparticles by phagocytic cells[37-38]. Next to this, for a hydrophobic surface, the interactions of nanoparticles and proteins are favoured due to hydrophobic protein domains[39].

Surface charge is another factor, which determines protein adsorption[11]. A correlation between the isolectric point (pI) and the surface charge of the nanoparticles was found by Aggarwal *et al.*[31]. Proteins, which have a pI < 5.5 (e.g. albumin) preferably adsorbed to negatively charge polystyrene nanoparticles, whereas proteins with a pI > 5.5 (e.g. immunoglobuline, IgG) adsorbed to positively charged particles. Overall, it was suggested that Coulomb interactions are a main driving force for protein adsorption. The nanoparticle surface charge does not only determine the corona composition[40], but it can also influence the protein structure[41]. It was shown that bovine serum albumin (BSA) was denatured upon binding to positively charge nanoparticles, however remained its structure upon adsorption to negatively charged nanoparticle[42]. Depending on the structure of BSA, the nanoparticle was recognized via different cell receptors (scavenger vs. albumin receptor).

The nanoparticle size is known to determine the *in vivo* biodistribution[43]. Overall, smaller nanoparticles (< 100 nm) showed a more efficient cellular uptake towards cancer cells and were even able to cross the blood-brain barrier compared to larger nanoparticles[44-45]. On the protein level, Cedervall *et al.* determined that the protein composition was similar for nanoparticles with varying size (70 – 700 nm); hence, the overall protein amount differed. With an increasing surface area per particle, the protein amount increased[22].

Based on this, the particle composition itself mediates the competitive protein interactions and shapes corona formation[46].

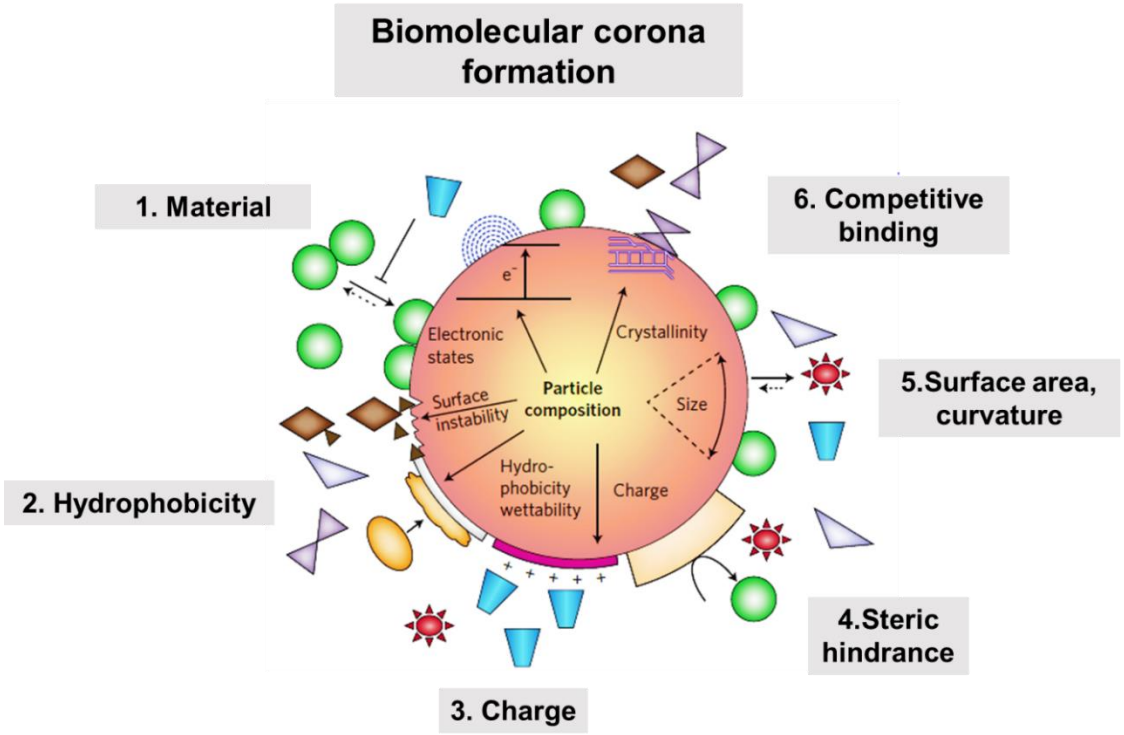


**Figure A. 1. Nanoparticle composition determines biomolecular corona formation.** Protein adsorption depends on the material characteristics and surface properties of the nanoparticle. Hydrophobic and electrostatic interactions mediate the competitive adsorption process. Figure is adaptated and modified from ´Understanding Biophysicochemical Interactions at the Nano-Bio Interface´. Copyright @ 2009 Springer Nature. Reprinted with permission from Nature Materials. *Ref.* Nature Materials 2009, 8, 543-557.

## A.2 Analytical methods

The protein corona is generally divided into two layers referred to as ´soft´ and ´hard´ protein corona[47]. The discriminating factor is the binding affinity of the proteins towards the nanoparticle[48]. Here, the hard corona consists of proteins, which are tightly bound and have low exchange rates, whereas the soft corona comprises proteins, which are loosely bound and readily desorb from the nanoparticles´ surface[29].

Most models suggest that hard corona proteins directly interact with the nanoparticle surface and on top of this, the soft corona forms an additional layer via protein-protein interactions with hard corona proteins[11]. As the soft corona is highly dynamic, analytical techniques are required which allow to study the direct interaction of the nanoparticles within the protein source and thereby do not disturb its loose structure[49].

Classical soft corona techniques give information about the size, structure and thermodynamics of the protein corona (Table A.1)[50]. With dynamic light scattering (DLS) it is

possible to determine the hydrodynamic radius of nanoparticles before and after protein coating via their diffusion coefficient using Stokes-Einstein relation[51]. Schmidt and coworkers have established a valuable method to investigate the aggregation behavior of nanoparticle introduced directly to concentrated human serum or plasma[52]. They were additionally able to correlate the aggregation behavior of nanoparticle determined under *in vitro* with the biodistribution of the nanoparticles *in vivo*[53]. Therefore, this method can be used as a pre-clinical screening to evaluate the *in vivo* behavior of nanoparticles. Fluorescence correlation spectroscopy (FCS) is a complementary approach to determine the size of the nanoparticles with protein corona[54].

Via transmission and scanning electron microscopy (TEM and SEM) it is possible to visualize the nanoparticle surrounded by the protein corona[55]. TEM studies mainly utilize a negative staining technique (with uranyl acetate) for enhanced contrast[56]. In addition, Kelly *et al.* have established an immunolabeling technique to characterize the spatial distribution of corona proteins[57]. Here, they took advantage of gold labelled antibodies to identify functional epitopes exposed by corona proteins.

**Table A. 1.** Direct analytical techniques are used to characterize the soft protein corona. These methods allow to study protein adsorption on the nanoparticles´ surface without the need of purification.

| **Direct techniques (*in situ*)** | | |
|---|---|---|
| **DLS** | Dynamic light scattering | size, aggregation |
| **FCS** | Fluorescence correlation spectroscopy | size, aggregation |
| **TEM** | Transmission electron microscopy | size, visualization |
| **SEM** | Scanning electron microscopy | size, visualization |
| **CD** | Circular dichroism spectroscopy | secondary structure |
| **nanoDSF** | Nano differential scanning fluorimetry | tertiary structure |
| **FT-IR** | Fourier-transform infrared spectroscopy | structure, affinity |
| **ITC** | Isothermal titration calorimetry | thermodynamics |

With circular dichroism spectroscopy (CD) and Fourier-transform infrared spectroscopy (FT-IR) the secondary structure of corona proteins is studied[42, 58]. These methods revealed that upon binding of proteins to the nanoparticles´ surface, the protein structure can be strongly disturbed leading to an unfolding and denaturation of corona proteins.

Protein stability and unfolding can additionally be analyzed by nano differential scanning fluorimetry (NanoTemper Technologies, Prometheus NT.48 instrument, Munich Germany). It is a label free methods, which monitores the intrinsic tryptophan and tyrosin fluorescence intensity (330 nm and 350 nm) of a protein upon heating. In general, the thermal unfolding transition midpoint $T_M$ (°C) is measured, which is defined as the point at which 50% of the protein is unfolded (extended information see Publication 13).

Another common *in situ* method is isothermal titration calorimetry (ITC)[59]. Proteins are titrated into a nanoparticle solution. Upon protein adsorption, the heat is measured and further the binding affinity, enthalpy and stoichiometry is determined[60].

In order to determine the hard corona proteins, nanoparticles are purified from excess unbound proteins (Table A.2). Therefore, these indirect methods wash off soft corona proteins and only analyze tightly bound proteins[61]. Nanoparticles surrounded by the hard protein corona are typically isolated via centrifugation, magnetic separation or size exclusion chromatography based on the nanoparticle material[62-63]. Several washing steps are required to ensure the sufficient removal of all unbound proteins. In a final step, the adsorbed hard corona proteins are released from the nanoparticle surfaces and further applied for protein analysis. SDS-PAGE and 2D-gel electrophoresis were used in pioneer works to investigate the overall corona pattern[29, 64]. This yielded a very limited amount of diverse proteins and was a tedious procedure. With the recent progress in the development of novel mass spectrometry techniques, it is now possible to identify the exact protein corona composition while also quantifying the relative amount of proteins in one setup. Overall, the hard corona pattern formed after *in vitro* plasma incubation is often dominated by 3-6 major corona proteins[65]. Further, LC-MS analysis allows to detect the low abundant corona proteins[66]. Common protein assays are utilized to determine the absolute amount of proteins bound to nanoparticles. Additionally, ζ-potential measurements are used to characterize the nanoparticle surface charge after protein coating[67].

Overall, the biological relevance of the soft corona *vs*. hard corona is still under debate[68-69]. There, have been reports, which suggest that the soft corona is of minor importance as it is sheared off under dynamic flow condition *in vivo.* To conclude, combing a set of different analytical methods is required in order to investigate the whole picture corona formation.

**Table A. 2. Indirect analytical techniques are used to characterize the hard protein corona**. Excess unbound proteins are removed before analysis and nanoparticles coated with tightly bound proteins are anaylzed.

| **Indirect techniques (*ex situ*)** | | |
|---|---|---|
| **SDS-PAGE** | 1D/2D Gel Electrophoresis | Separation |
| **ζ-Potential** | Electrophoresis | Charge |
| **LC-MS** | Liquid chromatography–mass spectrometry | Identification |
| **Assay** | Pierce, BCA Protein Assay | Amount |
| **QCM** | Quartz crystal microbalance | Mass change |

### A.3 Exposure condition (source, concentration, personalized, flow, *in vivo*)

Due to the rapid progress in the development of novel analytical tools to investigate corona formation, additional factors have been recognized, which critically determine protein corona formation. In the classical *ex vivo* or *in vitro* approach, nanoparticles are exposed to serum or plasma[70-71]. Therefore, blood is obtained, naturally coagulated and centrifuged to remove all cellular components (red and white blood cells) to generate serum. In contrast, for plasma preparation an anticoagulant (commonly citrate, EDTA or heparin) is added to prevent blood clotting. Due to the difference in the preparation of the protein source, the protein composition is also altered[72]. Serum does not contain proteins involved in the coagulation (e.g. fibrinogen), which are still present in plasma.

Generally, fetal bovine serum (FBS) is most commonly supplement in cell culture medium as protein source for cell maintenance[73]. Variations between the protein composition of human, mice or bovine serum have also been reported in various reports[74]. Therefore, it is anticipated that the protein source, which is used to study corona formation is a deterimental factor that needs considerations[75].

In a comprehensive report from Schöttler *et al*., the protein adsorption pattern of polystyrene nanoparticles exposed to FBS or human serum and plasma was compared[76]. Especially, the discrepancy between serum and plasma was prominent as nanoparticles exposed to plasma were surrounded by a high amount of fibrinogen. Additonally, they recognized the significant role of the chosen anticoagulant. Due to the incubation of nanoparticles in heparin plasma as in contrast to citrate plasma cellular uptake into macrophages was strongly enhanced, wheras

cellular internalization towards cancer cells was prevented. Therefore, it is of great importance to consider the chosen anticoagulant to compare the protein corona profil of different sudies[77].

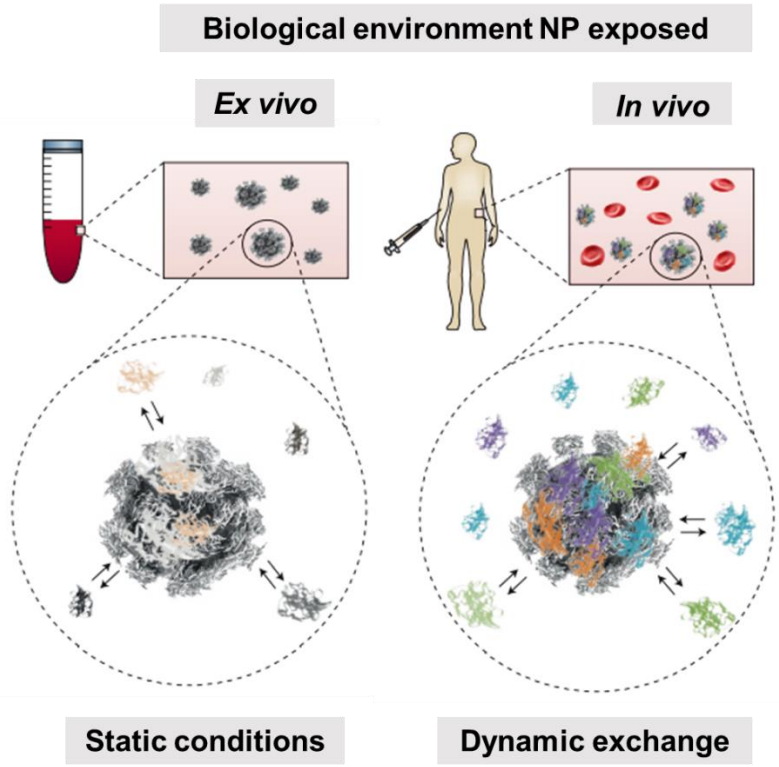


**Figure A. 2.** There is a distinct difference between the corona composition of nanoparticles under *ex vivo* conditions compared to the *in vivo* situation. Typical *ex vivo* approaches used plasma or serum to investigate protein adsorption. These experiments are usually under static conditions. In strong contrast, due to the blood flow the *in vivo* situation the protein corona is highly dynamic. Figure adaptated from ´Nanomedicine: Evolution of the nanoparticle corona´ and modified. Copyright @ 2017 Springer Nature. Reprinted with permission from Nature Nanotechnology. *Ref.* Nature Nanotechnology 2017, 6, 12(4), 288-290.

Next to the source itself, also the protein concentration shapes corona composition. Cell culture medium mainly contains 10% of FBS (~6 mg protein/mL). This is in contrast to the higher protein density in blood plasma (~60 mg protein/mL). Monopoli *et al.* saw a clear correlation for $SiO_2$ nanoparticles between an increasing plasma concentration and the thinkness of the protein corona (determined by DLS, SDS PAGE and protein assay)[68].

In 2015 there was the first report, which examined protein corona formation after nanoparticles were applied *in vivo*[78]. Liposomes were injected into mice, blood was recovered and liposomes surrounded by the *in vivo* protein corona were isolated via size exclusion chromatography. The

resulting pattern was strikingly different to the corona composition obtained after *in vitro* administration. Overall, there was a greater variety of proteins identifed after *in vivo* administration compared to the *in vitro* situation (Figure A.2)[79].

In a recent puplication (2017), Chen *et al.* emphasized the dynamics of the blood flow under *in vivo* conditions[33]. They investigated whether a preformed *in vitro* protein corona is replaced after *in vivo* administration. Here, they demonstrated that the *in vitro* protein coating is rapidily exchanged after *in vivo* exposure. This highlights the dynamic exchange of the *in vivo* protein corona.

These studies are first attempts in order to understand corona formation in a more complex surrounding. Moreover, they underline the importance to use and develop new methods to figure out the role of protein corona formation *in vivo*.

### A.4 Cellular impact

Depending on the corona composition, the cellular outcome can differ greatly[80-81]. This is most intriguingly shown in several studies, which compared the cellular internalization of nanoparticles in the absence or presence of the protein corona. For example, Treuel et*et al.* demonstrated that quantum dots show a high internalization rate in the absence of proteins (Figure A.3)[82]. However, after incubation with human serum albumin (HSA), cellular uptake was strongly suppressed. This goes along with other studies reporting a direct relationship between cellular uptake and protein concentration.

Lara *et al.* extended the knowledge about the interactions between the biomolecular corona and specific cellular receptors[83]. By using an immuno-mapping technique functional motifis of corona proteins were identified. They showed that the corona of $SiO_2$ nanoparticles consisted of lipoproteins and immunoglobulins. Both corona proteins exposed functional epitopes upon adsorption to the nanoparticles´ surface, which further allowed the recognition of the nanoparticles via low-density lipoprotein and Fc gamma receptors.

In a correlative study, cellular uptake of four different polystyrene nanoparticles was compared with the corona composition identified via label-free quantitative mass spectrometry. With this Ritz *et al*. were able to identify key proteins, which mediate the cellular uptake process[80]. As an example, apolipoprotein H (ApoH) was found to increase cellular interactions, whereas apolipoprotein A4 (ApoA4) or apolipoprotein C3 (ApoC3) significantly hampered the internalization process.

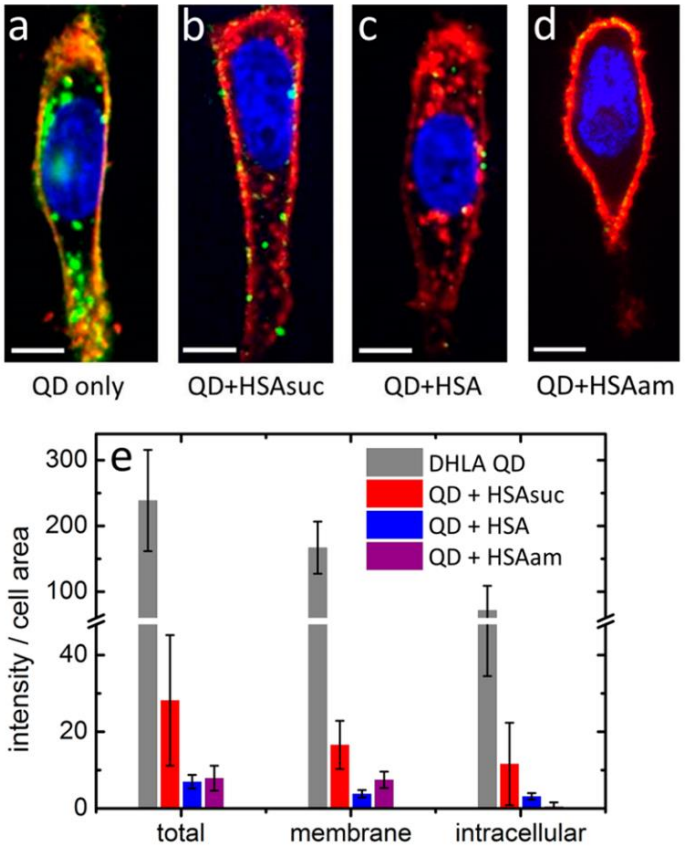


**Figure A. 3. Protein corona formation determines cellular interactions.** Cancer cells (Hela) were incubated with nanoparticles (quantum dots) in the absence of proteins (a) or in the presence of human serum albumin (b-d). Human serum albumin was modified with additional carboxy groups ($HSA_{suc}$) or ethylenediamine ($HSA_{am}$). Confocal images were taken and the cell membrane was stained in red, nucleus in blue and nanoparticles in green. Additional images were quantified (e). Figure adaptated from ´Impact of Protein Modification on the Protein Corona on Nanoparticles and NanoparticleCell Interactions´. Copyright @ 2014 American Chemical Society. Reprinted with permission from ACS Nano. *Ref.* ACS Nano 2014, 8, 8(1), 503-513

As highlighted above, the corona composition eventually determines the interaction of the nanoparticles and cells. Based on this, researchers have questioned whether the adsorbed protein layer is actually internalized with the nanoparticle and if this is the case, how this influences the intracellular processing. Therefore, Bertoli *et al.* fluorescently labeled the protein corona and monitored the internalization process via laser scanning microscopy[83]. They were able to prove that the corona is retained during cellular uptake and that actually the protein corona guides the intracellular trafficking of the nanoparticles.

Overall, these studies highlight the direct interplay between the corona composition and the cellular response[84]. Due to an increasing knowledge about the biomolecular corona formation and its physiological impact, it is no longer an unsurpassable barrier, which prohibits targeted

cell interactions. As protein corona formation is an inevitable process, it has been now realized that it can be used as an engineering tool to improve the nanoparticles´ properties for therapeutic applications.

# 1. Visualization of the protein corona: towards a biomolecular understanding of nanoparticle-cell-interactions

## Aim:

New analytical methods need to be developed in order to understand protein corona formation. This is the first study, which analyzed the morphology of the protein corona via transmission electron microscopy (TEM). On top of that, via proteomics (LC-MS) it was possible to monitor the evolution of the protein corona. Finally, the cellular impact of protein corona formation was investigated in correlative approach using flow cytometry, confocal laser scanning microscopy and TEM. Overall, the combination of various analytical tools provides a fundamental knowledge about the structure of the protein corona, its composition and cellular effect.

## Contribution:

I carried out the complete protein corona analysis (SDS-PAGE, LC-MS, Pierce Assay) and conducted the cellular uptake experiments (flow cytometry and cLSM). [redacted] performed the TEM images analysis. The project was supervised by [redacted]

## Copyright:

## Abstract

The use of nanocarriers in biology and medicine is complicated by the current need to understand how nanoparticles interact in complex biological surroundings. When nanocarriers come into contact with serum, proteins immediately adsorb onto their surface, enfolding the nanocarriers and forming a protein corona which then defines their biological identity. Although the composition of the protein corona has been widely determined by proteomics, its morphology still remains unclear. In this study we show for the first time how a protein corona is adsorbed onto polystyrene nanoparticles using transmission electron microscopy. We are able to demonstrate that the protein corona is not, as commonly supposed, a dense, layered shell coating the nanoparticle, but on the contrary an undefined, loose network of proteins. In addition, we are now able to visualize and discriminate between the *soft* and *hard* corona using centrifugation-based separation techniques together with proteomic characterization. The process of compositional change in the protein corona was analyzed after each of the multiple centrifugation steps in order to understand the evolution of the protein corona. The protein composition of the ~15 nm hard corona strongly depends on the surface chemistry of the respective nanomaterial, thus further affecting cellular uptake and intracellular trafficking. Large diameter protein corona resulting from pre-incubation with soft corona or Apo-A1 inhibits cellular uptake, confirming the stealth-effect mechanism. Taking this together, the knowledge on protein corona formation, composition and morphology is essential to design therapeutic effective nanoparticle systems.

## Introduction

On account of their small size, nanocarriers have distinct properties that make them excellent candidates for biomedical and biotechnological applications. Although their use is growing rapidly, crucial questions still arise about the interaction of nanocarriers with biological systems. When nanocarriers come into contact with biological fluids they adsorb proteins due to their high surface free energy.[1,2] The proteins that are adsorbed on the surface of nanocarriers form the so-called ‘protein corona’. The protein corona thus formed alters the size, aggregation state and properties of the nanoparticles and provides them with a biological identity, which differs from their synthetic identity.[3,4] The corona forms rapidly[5] and the composition changes only quantitatively.[6] It divides into the ‘hard’ and ‘soft’ corona, depending on the binding strength and exchange rate of the proteins. The hard corona is formed by the proteins with high binding affinities that are tightly bound and the soft corona by those proteins that are loosely bound and have high exchange rates. What the cell is finally able to recognize

is the particle-protein complex.[7] This means that the individual proteins present in each case are responsible for regulating the cellular uptake[8,9] and the intracellular fate.[10]

The proteomic composition[11], size and aggregation[12] effects of the protein corona are well-known, but its morphology has still to be examined. The protein corona is usually shown either as a uniform layer or as multiple layers covering the nanoparticle. For the first time we have been able to visualize the morphology of the protein corona and provide a 3D model of its structure by using transmission electron microscopy. In contrast to existing theories and sketches, we found that the protein corona forms a loose network which is attached to the nanoparticle.

In this paper we focus on three different polystyrene nanoparticles (plain, carboxyl-functionalized and amino-functionalized). These particles are easily synthesized in a wide range of sizes/surface functionalization and are ideal candidates for studying bio-nano interactions.[13] The protein corona morphology and composition of those nanoparticles were compared using TEM, DLS and LC-MS. Further we carefully monitored the process from initial corona formation directly after incubation in human serum and after each washing/ centrifugation steps. Using a 3D model reconstruction, we were able to quantify the amount of adsorbed protein covering the nanoparticles. Finally, endocytosis and intracellular trafficking of the nanoparticle coated *with* or *without* protein corona was investigated after incubation with macrophages. These studies offer a better understanding of the biological identity of the nanoparticles and will therefore contribute to a safer and more effective application in nanomedicine.

## Material and methods

**Transmission Electron Microscopy (TEM).** In order to observe the protein corona that was formed around the PS-NPs, the samples were first diluted with 1 mL water and then 2 µl were placed onto a lacey grid and let to dry. In the case of single protein binding studies, PS-NP (0.05 $m^2$) were incubated with individual proteins (100 µg) for 1 h, 37 °C and 2 µL of each sample was placed onto a lacey grid. The droplet method was applied with 4% uranyl acetate.[39]

Electron micrographs were taken on an Ultrascan 1000 (Gatan) charge-coupled device (CCD) camera. The TEM was operated at 200 kV. The Digital Micrograph software (Gatan) was used to collect the images.

In order to view the protein corona in 3D, tilt series over a tilt range of -65° to +65° were recorded at a magnification of 22000 ×. The SerialEM software (Mastronarde, 2005) was used to collect the tilt series.

**Cryo-TEM.** 10 µl of the sample was placed onto a 400 mesh copper grid covered with lacey film. The excess dispersion was removed by blotting with filter paper. The grid is plunged into liquid ethane (automated plunging system, Vitrobot FEI) and transferred in liquid nitrogen to the TEM. Prior to the preparation, the grids were treated with oxygen plasma to make the film hydrophilic.

**TEM (3D Reconstruction).** The alignments and the weighted back-projection-based reconstructions of raw tilt series were computed with eTomo (a program from the IMOD software package[40]).

The diameter of the particles and the protein corona that was formed around them was calculated with ImageJ.

**Dynamic Light Scattering.** Dynamic light scattering experiments were performed with an ALV-CGS 8F SLS/DLS 5022F goniometer equipped with eight simultaneously working ALV 7004 correlators, eight QEAPD Avalanche photodiode detectors and a a HeNe laser (632.8 nm, 25 mW output power) as light source at 37 °C. Nanoparticle dispersions (1 µL, 10 mg/mL) were measured in 1 mL of filtered Dulbecco`s magnesium- and calcium-free phosphate buffered saline (PBS) buffer solution (GIBCO, Invitrogen). Human serum was filtered through a Millex GS 220 nm filters (Millipore) into cylindrical quartz cuvettes (20mm diameter, Hellma, Müllheim) and nanoparticles were directly (1 µL) to the cuvette and incubated with human serum for 1 h at 37 °C before the measurement.

**Data evaluation dynamic light scattering.** Data was evaluated according to the method of Rausch *et al.*[23] Briefly, the sum of the autocorrelation functions (ACF) of the individual components (human serum or nanoparticle) was used as fixed parameters.

The ACF of human serum is approximated fitted by a sum of three exponential terms as given in equation S1:

$$g_{1,P}(t) = a_{1,P}\ \exp\left(-\frac{t}{\tau_{1,P}}\right) + \ a_{2,P}\ \exp\left(-\frac{t}{\tau_{2,P}}\right) + \ \ a_{3,P}\ \exp\left(-\frac{t}{\tau_{3,P}}\right) \qquad (1)$$

$a_i$ is the amplitude, $\tau_i = \frac{1}{q^2 D_i}$ the decay times, $q = \frac{4\pi n}{\lambda_0}\sin\left(\frac{\theta}{2}\right)$ the absolute scattering angle and $i$, $D_i$ Brownian diffusion coefficient. The ACF of the nanoparticles is fitted by a sum of two exponential terms (S2).

$$g_{1,NP}(t) = a_{1,NP}\ exp\left(-\frac{t}{\tau_{1,NP}}\right) + a_{2,NP}\ exp\left(-\frac{t}{\tau_{2,NP}}\right) \quad (2)$$

If nanoparticles are exposed to human serum the combination of the ACFs of serum and nanoparticles is analyzed. If no aggregation occurs, the resulting ACF of the mixture can be fitted by the sum of two individual ACFs $g_{1,m}(t)$, the so named *forced fit* (S3).

$$g_{1,m}(t) = f_P g_{1,P}(t) + f_{NP} g_{1,NP}(t) \quad (3)$$

If aggregation formation of nanoparticles in serum occurs, the ACF cannot be describe by sum of two components, so an additional term ACF $g_{1,agg}(t)$ for aggregates is needed (S4).

$$g_{1,agg}(t) = a_{1,agg}\ exp\left(-\frac{t}{\tau_{1,agg}}\right) \quad (4)$$

Therefore, the correlation function $g_{1,m}(t)$ consists of three terms including the aggregation terms with the intensity contribution $f_{agg}$.

$$g_{1,m}(t) = f_P g_{1,P}(t) + f_{NP} g_{1,NP}(t) + f_{agg} g_{1,agg}(t) \quad (5)$$

**ζ potential and particle charge detection.** The zeta (ζ) potential of the different polystyrene nanoparticle (20 µL) was measured with a Zeta Sizer Nano Series (Malvern Instrument, U.K) in 1 mM potassium chloride solution (2 mL). A combination of a particle charge detector PCD 02 (Mütek GmbH Germany) and a Titrino Automatic Titrator 702 SM (Metrohm AG Switzerland) was used to determine the amount of surface charged groups on nanoparticles. Titration experiments were performed with nanoparticles dispersion (10 mL) with a solid content of 1 mg/mL (0.1 wt%) at 20 °C. Amino groups were titrated against the negatively charged polyelectrolyte standard sodium poly(ethylene sulfonate) (Pes-Na) and for carboxyl groups positively charged poly(diallyl dimethyl ammonium chloride) (PDADAMC) was used. The amount of groups was calculated as previously described.[41]

**SDS-PAGE.** The protein sample (6 µg in 26 µL total volume) was mixed with 4 µL of NuPage Reducing Agent and 10 µL of NuPage LDS Sample Buffer NuPage, loaded on a 10% Bis-Tris-Protein Gels using NuPAGE MES SDS Running Buffer (all Novex, Thermo Fisher Scientific) and run for 1.5 h using SeeBlue Plus2 Pre-Stained (Invitrogen) as molecular marker. Gels were stained with SimplyBlue SafeStain (Novex, Thermo Fisher Scientific) at least for 4h and destained in distilled water overnight.

**Protein quantification.** The protein concentration of human serum or the desorbed hard corona proteins was quantified with the Pierce 660 nm protein Assay (Thermo Scientific; Germany) according to manufacturer's instructions and bovine serum albumin (Serva, Germany) was used a standard. Absorption was measured at 660 nm by a Tecan infinite M1000 plate reader.

**Human blood serum.** Human blood was obtained from the Department of Transfusion Medicine Mainz from healthy donors in accordance with the Declaration of Helsinki. Blood was clotted overnight according to the standard protocol to generate human serum. A serum pool from seven volunteers was used and storaged at -80 °C. To remove any protein aggregates after thawing, human serum was centrifuged for 30 min at 20 000 g before usage.

**Protein corona preparation.** A constant ratio between particle surface area and serum concentration was chosen to ensure reproducibility. A surface area of 0.05 $m^2$ nanoparticles (in a total volume of 300 µL) were incubated with 1 mL of human serum for 1 h, 37 °C. Previous studies have shown that the protein corona is formed stabile after 1 h.[42]

The hard protein corona surrounding nanoparticles was isolated via centrifugation and loosely or unbound proteins were removed. Nanoparticles were centrifuged for 1 h, 20 000 g (4 °C). The supernatant was collected for protein quantification. The remaining nanoparticle pellet was either re-suspended in water (final nanoparticle concentration of 10 mg/mL) and analyzed by TEM and DLS or washed with 1 mL of water. This procedure was repeated three times to ensure that all unbound proteins are removed. To elute bound proteins form the nanoparticles, the pellet was re-suspended in 2% SDS (62.5 mM Tris*HCl), heated up to 95 °C for 5 min and centrifuged for 1 h, 20 000 g (4 °C). The remaining supernatant was collected further analyzed by Pierce Assay, SDS-PAGE and LC-MS.

**In solution digestion.** Protein samples were applied to Pierce detergent removal columns (Thermo Fisher) to remove SDS prior to digestion. Proteins digestion was performed according to former instruction.[10,43] Briefly, proteins were precipitated overnight using ProteoExtract protein precipitation kit (CalBioChem) according to the manufactures instructions´. Proteins were isolated via centrifugation (14 000 g, 10 min), washed several times and re-suspend in RapiGest SF (Waters Cooperation) dissolved in ammonium bicarbonate (50 mM) buffer. Samples were incubated at 80 °C for 15 min. Protein disulfide bonds were reduced with dithithreitol (Sigma) at a final concentration of 5 mM. The reaction was performed at 45 min at 56 °C. Proteins were alkylated with idoacetoamide (final concentration 15 mM, Sigma) and incubated in the dark for 1 h. Digestion was carried out with a protein:trypsin ratio of 50:1 over 16h at 37 °C and the reaction was quenched by adding 2 µL hydrochloric acid (Sigma). To

remove degradation products of RapiGest SF, peptide samples were centrifuged for 14 000 g, 15 min (4 °C).

**Liquid chromatography coupled to mass spectrometry (LC-MS analysis).** Samples were diluted with 0.1% formic acid and spiked with 50 fmol/µL Hi3 Ecoli (Waters Cooperation) standard for absolute protein quantification[44]. Tryptic peptides were applied to a C18 analytical reversed phase column (1.7 µm, 75 µm × 150 mm) and a C18 nanoACQUITY trap column (5 µm, 180 µm × 20 mm) in a nanoACQUITY UPLC system. Two mobile phases (A) consisting of 0.1% (v/v) formic acid in water and 0.1% (v/v) formic acid with acetonitrile and gradient of 2% to 37% of mobile phase B over 70 min were used for separation. The nanoACQUITY UPLC system was coupled with a Synapt G2- Si mass spectrometer. Electrospray ionization (ESI) was conducted in positive ion mode using a NanoLockSpray source. The sample flow rate was set to 0.3 µL $min^{-1}$ and the reference component Glu-Fibrinopeptide was infused 150 fmol $µL^{-1}$ at a flow rate of 0.5 µL $min^{-1}$. The Synapt G2-Si was operated in resolution mode and data-independent acquisition ($MS^E$) experiments were carried out. A mass to charge range of 50–2000 Da, scan time of 1 s, ramped trap collision energy from 20 to 40 V was set and data was acquired over 90 min. MassLynx 4.1 was used for data acquisition and processing.

**Protein identification.** Continuum data was post lock mass corrected and further analyzed by Progenesis QI (2.0) using a reviewed human data base (Uniprot) for peptide and protein identification. Several processing parameters as noise reduction thresholds for low energy, high energy and peptide intensity were set to 120, 25, and 750 counts. The human data base was modified with the sequence information of Hi3 Ecoli standard for absolute quantification. The following criteria were chosen for protein and peptide identification: one missed cleavage, maximum protein mass 600 kDa, fixed carbamidomethyl modification for cysteine, variable oxidation for methionine and protein false discovery rate of 4%. To identify a protein at least two assigned peptides and five assigned fragments are required. Peptide identification is based on three assigned fragments and identified peptides with a score parameter below 4 were discharged. Based on the TOP3/Hi3 approach the amount of each protein in fmol was provided[45].

**Cell culture.** The murine macrophage cell line RAW264.7 were maintained in Dulbecco´s modified eagle medium (DMEM) supplemented with 10 % FCS, 100 U/mL penicillin, 100 mg/mL streptomycin and 2 mM glutamine (all from Invitrogen, Germany).

**Cell uptake experiments: Flow cytometry and confocal laser scanning microscopy.** For the cell uptake experiments, cells were seeded at a density of 150 000 cells/well in 24 well plates. 3 mm plasma-sterilized sapphire discs (M. Wohlwend GmbH, Sennwald, Switzerland)

covered with a 20 nm carbon layer before usage were added in the well plate. After 12 h, the cells were incubated in fresh serum-free medium for 2 h, before the nanoparticle dispersions were added at a concentration of 300 µg/mL to the cells.

Hard protein corona coated nanoparticles were prepared as described above (Protein corona preparation). Therefore, the nanoparticles were first incubated with human serum, centrifuged and washed to remove unbound proteins. Protein coated nanoparticles were re-suspended in serum free medium (final concentration: 300 µg/mL) and incubated with the cells for 1 h.

For flow cytometry experiments, adherent cells were washed with PBS and detached from the culture vessel with 2.5 % trypsin (Gibco, Germany) and measurements were performed on a CyFlow ML cytometer (Partec, Germany) with a 488 nm laser for excitation of BODIPY and a 527 nm band pass filter for emission detection. Data analysis was performed using FCS Express V4 software (DeNovo Software, USA) selecting the cells with a FSC/SSC plot, thereby excluding cell debris. The gated events were analyzed by the fluorescent signal (FL1) expressed as median fluorescence intensity (MFI).

In order to proof intracellular localization of nanoparticles, confocal laser scanning microscopy (cLSM) experiments were performed on a LSM SP5 STED Leica Laser Scanning Confocal Microscope (Leica, Germany), consisting of an inverse fluorescence microscope DMI 6000 CS equipped with a multi-laser combination using a HCX PL APO CS 63 x 1.4 oil objective. Bodipy-labbeled nanoparticles were excited with an argon laser (20 mW; λ=514 nm), detected at 530 - 550 nm (pseudocolored green) and the cell membran was stained with CellMaskOrange (2.5 µg/mL, Invitrogen) using a laser DPSS 561 nm (≈ 1.3 mW), detected at 570 - 600 nm (pseudocolored red).

**High pressure freezing and freeze substitution.** For a good preservation of the structure, the specimen was frozen under high pressure (2100 bars), using the high pressure freezing machine (Engineering Office M. Wohlwend GmbH, Switzerland). The specimen (sapphire discs with cells) was enclosed and protected in a small volume between two specimen carriers and locked inside the specimen pressure chamber. Liquid nitrogen was used as cooling medium. To enure high quality preservation, this technique was combined with freeze substitution and resin embedding. This included dehydration of the cryo-fixed samples at -90 °C by substituting the ice for an organic solvent (0.2 % osmium tetroxide, 0.1% uranyl acetate and 5 % water in aceton) inside the freeze substitution machine (EM, AFS 2, Leica Microsystems). After bringing the samples to room temperature, they were rinsed in pure aceton and infiltrated in EPON 812. On the next day, polymerization took place at 60 °C. Ultrathin sections were collected afterwards using a Leica ultramicrotime.

**Nanoparticle Synthesis.** Styrene (99%, Merck, Germany) and acrylid acid AA (99%, Aldrich, Germany) were freshly distilled under reduced pressure and stored at -18 °C. The following commercial products were used: 2-aminoethyl methacrylate hydrochloride (AEMH, 90%, Sigma-Aldrich, Germany), n-hexadecene (HD, Sigma-Aldrich), initiator 2,2'-azobis (2-methylbutyronitrile) (V59, Wako Chemicals, Germany) and Lutensol AT50 (BASF). The fluorescent dye Bodipy-1 was synthesized according to[46], which has the maximum of absorption at 523 nm and of emission at 536 nm. A stock solution of Lutensol was prepared (1.99 g Lutensol AT50 filled to 79.65 g with steril water). The nanoparticles were synthesized by free-radical miniemulsion polymerization according to.[14]

Plain PSNPs (referred as PS): 6.0529 g of styrene, 250.72 mg of hexadecane, 103.55 mg of the initiator V-59 and 5.99 mg Bodipy-1 were added to 24 g of water containing 0.6 g of Lutensol AT50.

Carboxy-functionalized PSNPs (referred as PS-COOH): 5.88286 g of styrene, 0.15258 g of AA, 251.28 mg of hexadecane, 99.71 mg of the initiator V-59 and 6.10 mg Bodipy-1 were added to 24 g of water containing 0.6 g of Lutensol AT50.

Amino-functionalized PSNPs (referred as PS-$NH_2$): 5.8887 g of styrene, 252.30 mg of hexadecane, 100.62 mg of the initiator V59 and 6.06 mg Bodipy-1 were mixed with 24 g water containing 0.12 g of AEMH and 0.6 g Lutensol AT-50.

After 1 h of stirring for pre-emulsification, the miniemulsion was prepared by ultrasonicating the mixture for 2 min by 450 W at 90% intensity (Branson sonifier W450 Digital, ½'' tip) at 0 °C. For polymerization, the temperature was increased to 72 °C and reaction proceeded overnight.

## Results and Discussion

The research presented here was carried out on a defined set of polystyrene nanoparticles (PS-NP), synthesized by free-radical mini-emulsion polymerization[14] and stabilized by the surfactant Lutensol AT-50 which has a polyethylene glycol (PEG) tail of 50 ethylene oxide units. All nanoparticles were purified under similar conditions. A detailed protocol is presented in the supplementary information 1. In contrast to other studies where particles with different properties were used such as material, size or charge[15,16,17] we focused on a set of PS-NPs with similar size and only varying surface modifications (PS, PS-COOH, PS-$NH_2$). For flow cytometry and confocal laser scanning microscopy analysis, nanoparticles were fluorescently

labeled using BODIPY (525/535 nm). Similar amounts of dye were covalently in-cooperated within the nanoparticles. Surface functionalities were introduced by co-polymerization of monomers containing carboxy- and amino-groups. The physico-chemical properties of nanoparticles such as charge, shape and size were characterized by ζ-potential measurements, transmission electron microscopy (TEM) and mulit-angle dynamic light scattering (DLS) in an aqueous solution and physiological buffer conditions (PBS).

Complementary analytical methods were applied to visualize the structure (TEM) of the protein corona and determine changes in size. The methods included multi-angle DLS as well as characterizing its composition by label-free, ultra-pressure liquid chromatography mass spectrometry (UPLC-MS).

The morphology of the protein corona was studied by TEM using a negative staining technique[18]. Proteins were embedded in a thin, free standing layer of dried trehalose containing heavy metal salts (e.g. uranyl acetate) providing high contrast samples, suitable for conventional electron tomography.[19-20] To assure that the corona morphology is not affected by the embedding into the trehalose film, additional cryo-TEM examinations have been performed. This showed no noticeable structural difference between cryo-TEM and trehalose embedding preparation. The protein corona of nanoparticles could be visualized for the first time using this technique and subsequently quantitatively analyzed using a 3-D reconstruction model.

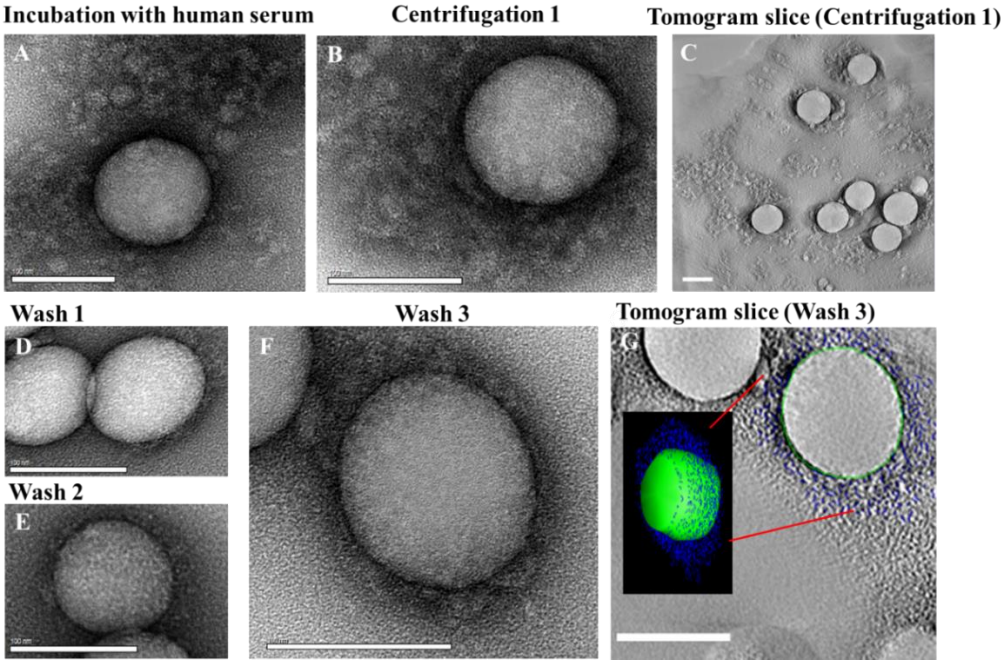


**Figure 1. 1.** TEM micrographs of the protein corona surrounding un-functionalized polystyrene nanoparticles. **A**: Hard and soft corona after incubation of un-functionalized PS-NPs in human serum and B: After centrifugation and removal of the supernatant, but before washing steps**. C:** Tomogram slice of an area such as **(B)**, scale bar: 100 nm. **D:** Hard corona after 1st wash, **E:** after 2nd wash, and **F:** after 3rd wash. **G:** Electron tomogram slice of the area presented in (F), superimposed by a 3D reconstruction. Scale bar: 100 nm. [redacted]

Directly after incubation of nanoparticles in human serum (Figure 1.1), un-functionalized polystyrene nanoparticles (PS) were surrounded by a protein cloud, which appeared to be larger than the diameter of the nanoparticle. Given the average diameter of 140 nm for un-functionalized polystyrene nanoparticles the average additional corona was estimated to be ~70 – 100 nm thick (Figure 1.1) and referred to as the *soft protein* corona. Interestingly, the soft protein corona is not shown by TEM to be as uniformly distributed and well-rounded, but rather as an undefined network surrounding the nanoparticle. Generally [2, 21] it is described as highly dynamic layer of proteins which have high exchange rates and low binding affinities towards the nanoparticle. By adding trehalose and uranyl acetate (UA) for TEM sample preparation, the highly dynamic structure is fixed. At this stage a “snapshot” of the nanoparticles surrounded by the soft corona was taken, revealing interestingly its non-uniform structure. In addition, cryo-TEM examinations corroborated the morphology of the protein corona observed by the trehalose-UA preparation. As a result structural artifacts caused by negative staining can be excluded. While there is extensive literature dealing with the subject of *hard protein* corona, only limited analytic methods used to study the soft protein corona are

available. Consequently, determining the biological relevance of the soft corona has been slowed down.[22] Hence, for *in vivo* application of nanocarriers it is essential to concentrate on studying the interactions of nanoparticles within a given protein source (serum, plasma) and to analyze their aggregation behavior in such complex surroundings as this can highly affect the biodistribution.[12]

By using multi-angle dynamic light scattering (DLS) it is possible to measure the average, hydrodynamic size of nanoparticles directly incubated in the protein source[23]. Multi-angle DLS was performed at 37 °C in human serum and we observed an average size increase of the hydrodynamic radius of about ~ 70 nm for functionalized PS-NPs. This size increase can be attributed to the protein corona formation and correlates well with the visualization of the protein corona in TEM images (Figure 1.1). The data evaluation procedure and the auto-correlation functions respectively shown for scattering angle of 30° can be found in the supplementary information 1.

As previously mentioned, in most studies dealing with the protein corona only proteins of the hard corona have been analyzed. These are tightly bound and have a high affinity towards nanoparticles.[24] The hard protein corona of nanoparticles is usually isolated using multiple centrifugation and washing steps to remove loosely or unbound proteins from nanoparticles surrounded by the hard corona.[25] Several other studies have compared the protein pattern obtained after centrifugation with different preparation techniques (e.g. magnetic separation, gel-filtration) and these studies have demonstrated that the general protein adsorption pattern is comparable.[26, 27]

Our goal was to analyze the evolution of the protein corona formed directly after incubation in human serum and after each purification/washing step by isolating protein coated nanoparticles via centrifugation. We monitored the morphological development of the protein corona for un-functionalized (Figure 1.1) and functionalized nanoparticles (Figure 1.3) by electron microscopy and analyzed the adsorption pattern quantitatively using LC-MS.

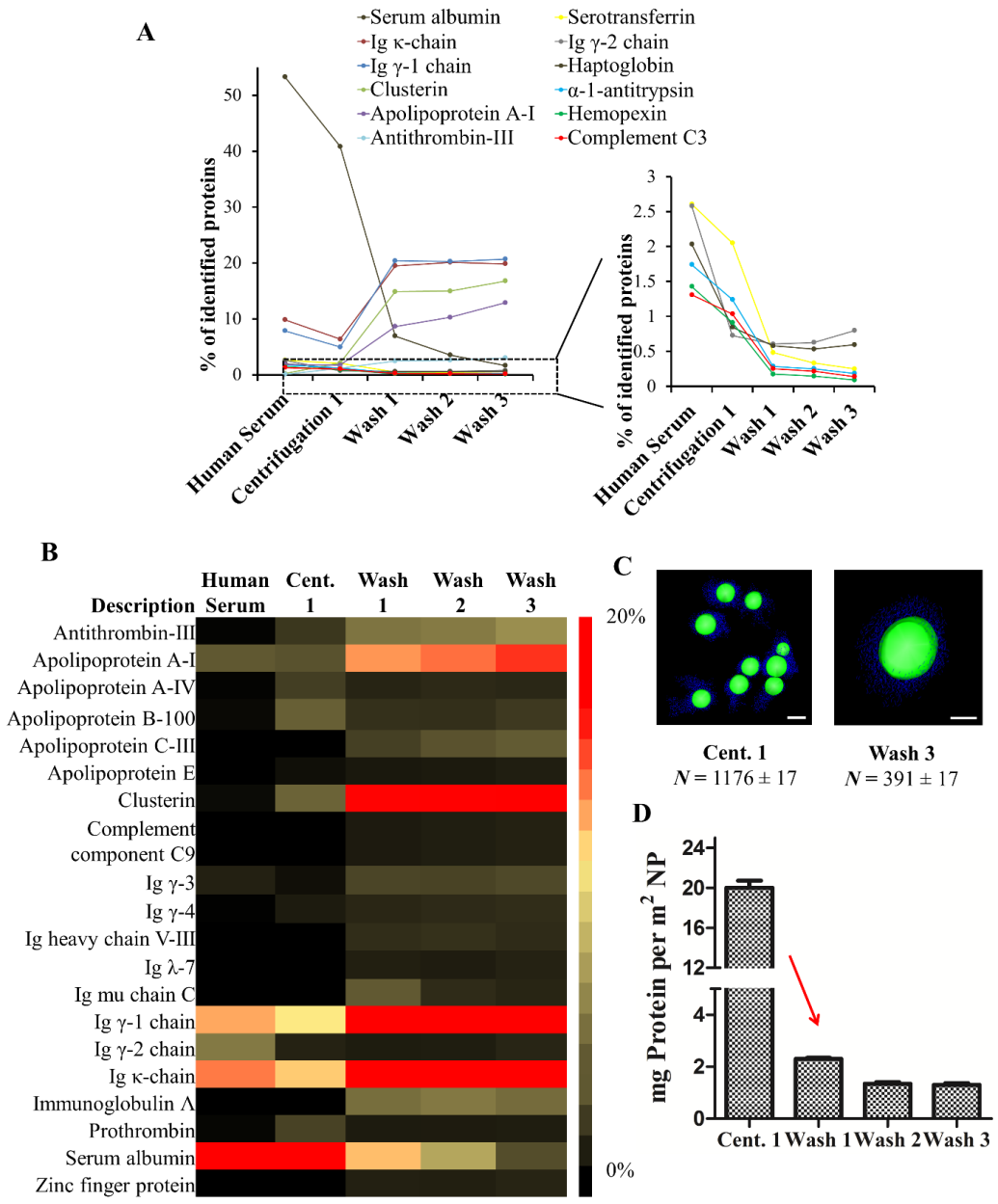


**Figure 1. 2.** Evolution of the hard protein pattern during sample preparation. **A.** The number of highly abundance serum proteins decreases and the abundance of the hard corona proteins increase after each washing step. **B.** The heat map illustrates the relative quantity of the most abundant proteins found in the hard corona. (Relative quantity of proteins identified amounting to > 1%, n = 4). **C**. 3D reconstruction of tomogram slices presented the nanoparticles surrounded by the protein corona. For TEM an average protein size of 10 nm in z-axis is assumed [redacted] **D.** Proteins were desorbed from un-functionalized PS nanoparticles with 2% SDS and the quantity of protein in mg per $m^2$ NP (± SD, n = 4) was measured by Pierce Assay.

After the first centrifugation, un-functionalized PS nanoparticles were surrounded by a substantial protein cloud (Figure 1.1) as observed directly after incubation. The 3D

reconstructions demonstrate the heterogeneity of the protein corona at this step. However, it is difficult to distinguish between tightly or loosely bound proteins associated to one nanoparticle and to unbound proteins. TEM images and DLS measurements reveal a high quantity of proteins adsorbing onto nanoparticles directly after incubation (Figure 1.2). This results in a marked increase in the size of the nanoparticles due to the formation of the soft corona. The soft corona was then washed off after several centrifugation steps and the nanoparticle-particle complex with tightly bound proteins (thus forming a hard corona) could then be isolated. This result is in agreement with the quantity of proteins quantified after each washing step which continuously decreases with wasching steps (Figure 1.2). The number of loosely and unbound proteins was significantly reduced after the first wash ($1^{st}$ centrifugation = 20.02 ± 1.00 mg *vs.* $1^{st}$ wash = 2.30 ± 0.10 mg per $m^2$ un-functionalized PS-NP). After the second and third washing steps, the quantity of adsorbed proteins did not decrease significantly. After the third and last wash the protein amount in the supernatant was below the detection limit indicating that the loosely/unbound proteins were effectively washed away. Using the 3D reconstruction presented (Figure 1.1) the number of proteins was counted every 10 nm in the z-axis (assuming that the average protein size is 10 nm). After the first centrifugation, un-functionalized nanoparticles were surrounded by ~ 1200 proteins. This number drastically decreased down to ~ 400 proteins after the final washing step.

There were no obvious structural differences observed in the nanoparticles-protein complexes when washed just once or three times (Figure 1.1). In addition, the ζ-potential of nanoparticles (-3.7 mV, measured in KCl) dramatically decreased to -21 mV after incubation in human serum, indicating protein adsorption and corona formation. Again, there were no major changes measured after the first, second and third washing steps. After the third and last wash, the corona thickness measured approximately 15 nm (Figure 1.1) by TEM. The proteins were tightly bound to the PS nanoparticles and covered most of each periphery. In order to determine statistical robustness, the radius of more than 20 particles from the TEM micrographs was measured (Figure 1.1). The hard corona radius measured by DLS was comparable (19 ± 2 nm).

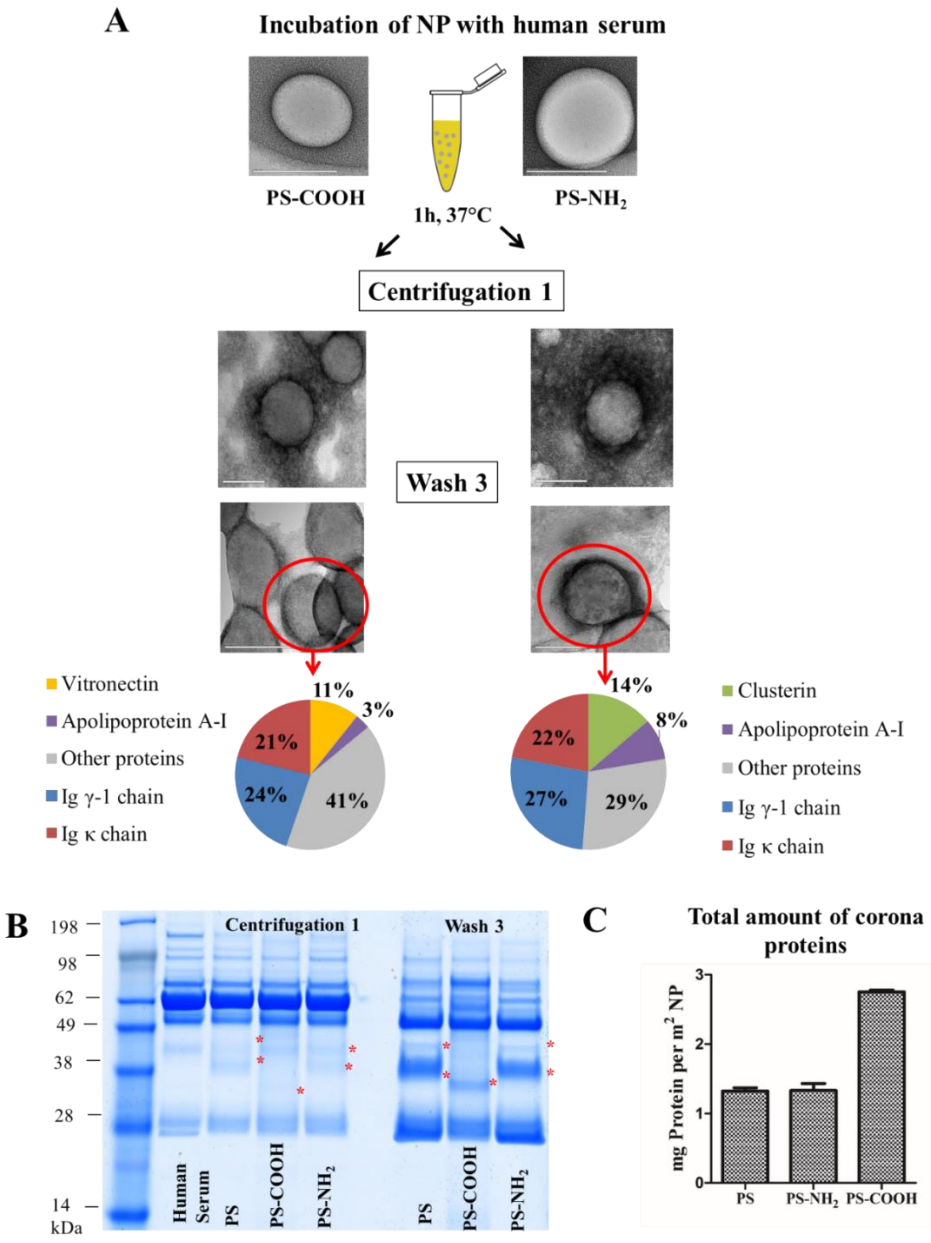


**Figure 1. 3.** Analyzing the protein corona pattern around functionalized nanoparticles (PS-COOH, PS-$NH_2$) by various analytic methods. **A.** NPs (total surface area of the sample: 0.05 $m^2$) were incubated in human serum (1 mL) for 1 h, 37 °C. The protein corona was visualized by TEM after the first centrifugation and third washing step. Hard corona proteins were identified, demonstrating that the protein pattern is highly dependent on surface functionalization [redacted] Proteins very analyzed by LC-MS (average of n = 4) and visualized by SDS-PAGE **B.** At a first glance the protein pattern of all nanoparticles incubated in human serum was very similar after the first centrifugation, but distinct protein bands can be seen even at this step (starred lanes “Centrifugation 1”). These proteins are further identified as hard corona proteins (“Wash 3”) **C.** The amount of bound proteins (in mg ± SD, n = 4) is quantified after desorption of proteins from nanoparticles using 2% SDS by Pierce assay.

In order to monitor the evolution of the hard protein corona, we analyzed the protein composition of un-functionalized PS-NPs after each purification step. The protein composition of the protein corona is significantly altered when compared to the composition of proteins in serum.[15-16] The relative amount of abundant serum proteins ( > 1%) was found to be drastically decreased in the case of human serum albumin, serotransferrin, haptoglobulin, hemopexin and complement C3 after the first centrifugation stage. All these proteins were detected in small quantities in the hard corona (Figure 1.2). In contrast, there was an enrichment of low abundance proteins (clusterin, apolipoprotein A1 and antithrombin-III) which are referred to as the hard corona proteins (Figure 1.2). Significantly, we were able to show that the relative abundance of the identified proteins remained stable after the first washing (Figure 1.2). Only slight changes in the protein pattern could be observed after the second and third washing steps. By doing this the equilibrium between proteins in solution and nanoparticle bound proteins changed rapidly and nanoparticles with tightly-bound hard corona proteins could be isolated. These results highlight the crucial purification step (after centrifugation 1 → wash 1) as here the equilibrium between unbound and nanoparticle bound proteins is critically shifted.

However, we know that the protein adsorption pattern is highly influenced by surface functionalization of nanoparticles.[24,28-29] We found that the absolute number of bound proteins per defined surface of nanoparticles is significantly higher (Figure 1.3) for negatively charged nanoparticles (PS-COOH) in comparison to un-functionalized (PS), or positively charged nanoparticles (PS-$NH_2$). In addition, vitronectin was highly enriched in the protein corona of PS-COOH (Figure 1.3) and PS-$NH_2$ particles specifically adsorbed clusterin. Clusterin was also found to be the major hard corona protein of poly(phosphoester)- and PEGylated modified PS-NPs.[29] The set of PS-NPs in this experiment was stabilized with Lutensol AT-50 which is a PEG-analog surfactant. In addition, there are specific proteins (immunoglobulin k, immunoglobulin γ or apolipoprotein AI) which were identified on all polystyrene nanoparticles under investigation. Previous studies[16,30,15, 31] support our findings as they recorded an enrichment of apolipoproteins in the hard corona of polystyrene nanoparticles.

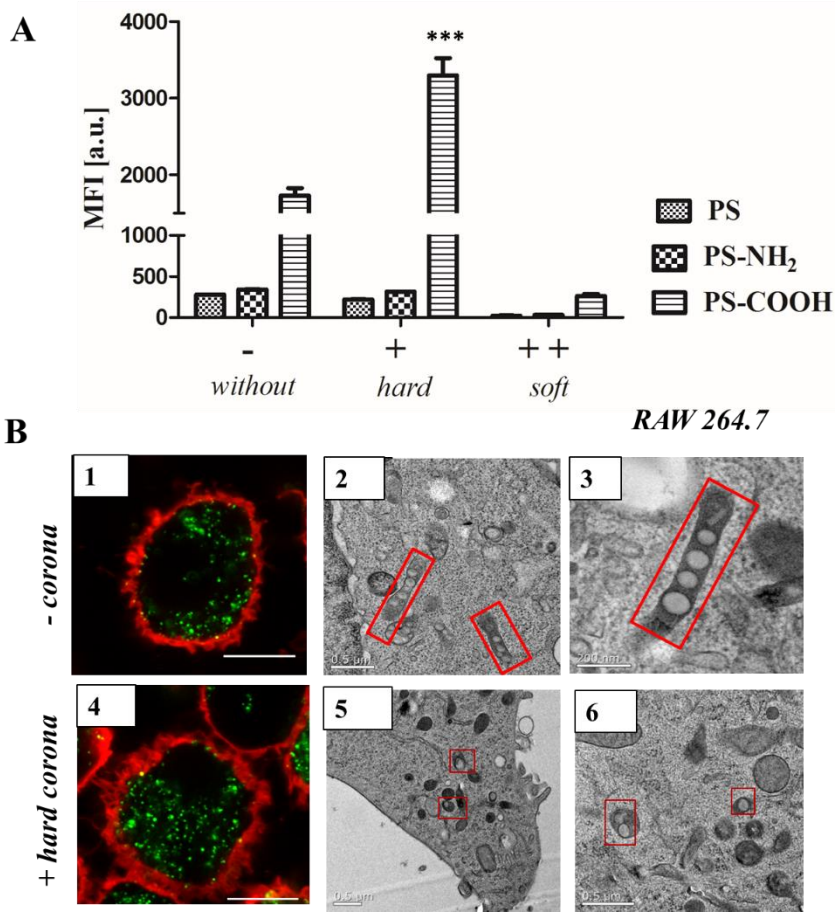


**Figure 1. 4. A.** Flow cytometry analysis: RAW264.7 cells were incubated with un-functionalized or functionalized polystyrene nanoparticles (300 µg/mL) for 1 h. The average of the median fluorescence intensity (MFI) of three independent experiments is shown (n=3). Prior to cellular uptake studies, nanoparticles were incubated with human serum for 1 h at 37 °C, centrifuged and washed to remove unbound proteins. Isolated hard corona coated nanoparticles (+) or uncoated nanoparticles (-) were added to serum free cell culture medium. Additionally, uncoated nanoparticles were added to cells cultured in 100% serum (++ soft corona) **B.** Confocal laser scanning microscopy images (1, 4) and TEM micrographs (2, 3, 5, 6) of high-pressure frozen macrophages treated with 300 µg/mL of un-functionalized nanoparticles without (-) or with hard protein corona (+). Scale bar: B1, B4 = 10 µm; B3 = 200 nm; B2, B5 and B6 = 0.5 µm. GraphPad Prism 5 Software was used for statistical analysis using a one-way ANOVA followed by Tukey's post-hoc multiple comparisons test. A *p*-value of < 0.001 was considered as highly significant***

After the first centrifugation, at a first glance, there were no major differences (SDS-PAGE, Figure 1.3) between the identified proteins with regard to the surface functionalization of the nanoparticle (PS, PS-COOH, PS-$NH_2$). Additionally, the protein pattern is comparable to the proteins identified in human serum. The major protein band (~ 62 kDa) is referred to as human serum albumin as it is the most abundant serum protein. At this stage it was not possible to

clearly separate nanoparticles with tightly surrounded proteins from the remaining proteins in solution because their protein concentration was much higher.

Interestingly, some distinct bands were detected in the SDS-PAGE (marked by a red star, Figure 1.3) even without performing any washing steps. These bands were identified as low abundance proteins in a detailed proteomic analysis by LC-MS (e.g. vitronectin, clusterin, apolipoprotein A1). The concentration of low abundance proteins is much higher on the NP than in the pristine human serum. These proteins were further enriched in subsequent washing steps and identified as the proteins of the hard corona (Figure 1.3). There were no significant structural differences (Figure 1.3) visualized in the soft and hard protein corona of functionalized nanoparticles. Additionally, the hard corona radius measured by TEM and DLS was comparable to un-functionalized nanoparticles (10 – 20 nm).

To visualize the binding of individual hard corona proteins, un-functionalized nanoparticles were incubated in the respective isolated proteins (clusterin, apolipoprotein A1 or IgG) for 1 h at 37 °C and the protein adsorption was analyzed by TEM (Figure 1.5). Micrographs show that in most cases the protein was present around the entire periphery of the nanoparticles. In addition, the corona diameter was quite large (~ 100 nm), as seen in the case of apolipoprotein A1 (Figure 1.5). However, the secondary structure of the proteins can be altered due to the adsorption on a surface[32,33] further determining the cellular uptake.[34 35]

Therefore, we further studied the interactions of protein corona coated nanoparticles (Figure 1.4 and 1.5) and a macrophages cell line, RAW264.7. Flow cytometry analysis, confocal laser scanning microscopy (CLSM) and TEM revealed the intracellular uptake of BODIPY-labeled PS-NPs and no adherence to the plasma membrane (Figure 1.4) Further, we investigated the difference between nanoparticles surrounded by the *hard* corona vs. *soft* corona. Hard corona coated nanoparticles incubated in serum were isolated via repetitive centrifugation and washing (3 times, as prepared for protein corona analysis) and added to serum free cell culture medium (+ hard corona). Additionally, nanoparticles were directly added to serum free culture medium (- corona) or cells cultured in 100% serum (++ soft corona).

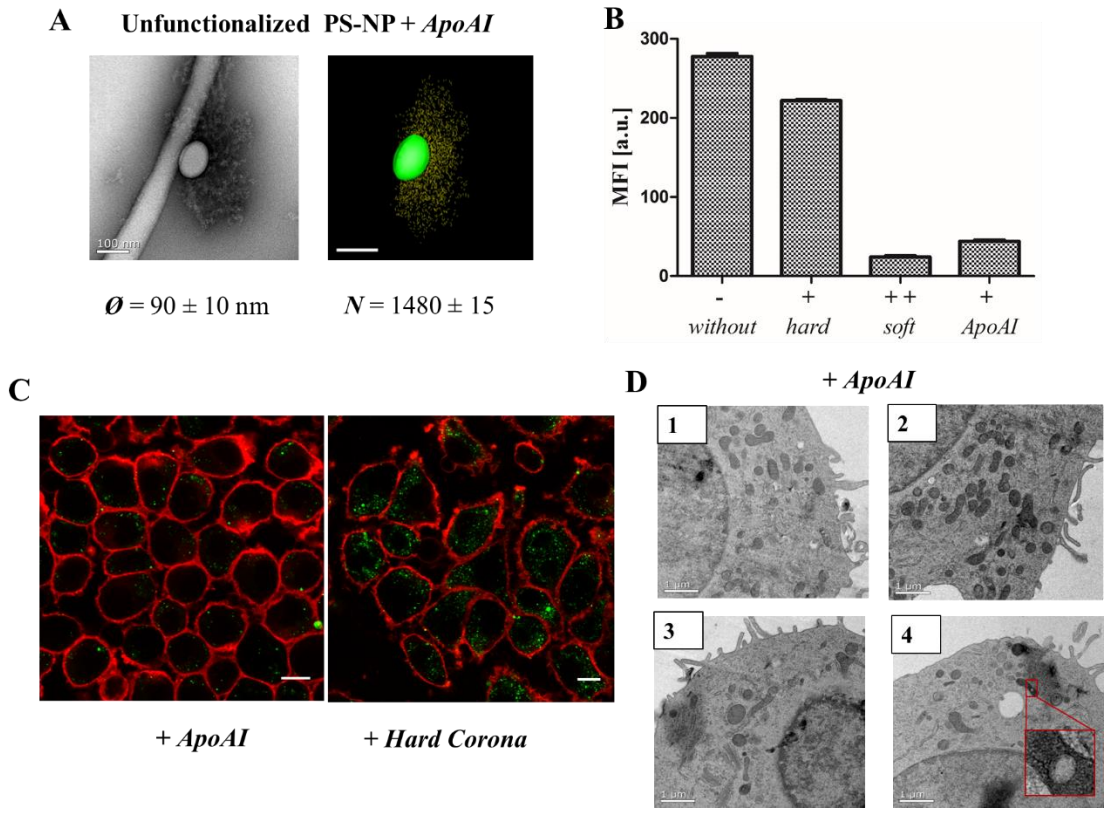


**Figure 1. 5. A.** TEM micrographs and 3D reconstruction images of un-functionalized PS-NP (0.05 $m^2$) incubated with ApoAI1 (100 µg) for 1 h, 37 °C. The additional corona diameter (~100 nm) and number of ApoAI proteins (>1400 proteins) surrounding un-functionalized PS-NP is comparable to the soft corona images (Figure 1.1 and 1.2). Scale bar: 100 nm. **B.** Flow cytometry analysis: RAW264.7 cells were incubated with 300 µg/mL of un-functionalized (-), protein corona coated (+/++) or ApoAI coated un-functionalized PS-NP for 1 h. **C.** Confocal laser scanning microscopy images of ApoAI or hard corona coated un-functionalized nanoparticles. The cell membrane is stained using CellmaskOrange (pseudo-coloured red) and BODIPY labeled nanoparticles are pseudo-coloured green. Scale bar: 10 µm **D.** TEM micrographs of high-pressure frozen macrophages treated with 300 µg/mL of un-functionalized nanoparticles pre-coated with ApoAI indicating a strongly reduced uptake of nanoparticles. Scale bar: 1 µm. [redacted]

Cellular uptake of soft corona coated nanoparticles (++) was strongly reduced in comparison to hard corona coated (+) or uncoated nanoparticles (-). Here, it was shown that the surface functionalization highly influenced uptake behavior (Figure 1.4). Un-functionalized and amino-functionalized nanoparticles were taken up to a significantly lower extent compared to carboxy-functionalized nanoparticles. Interestingly, this trend was observed *with* or *without* protein corona (Figure 1.4). Additionally, it was found that cellular uptake of PS-COOH nanoparticles was significantly enhanced for nanoparticles surrounded by hard corona proteins compared to uncoated PS-COOH ($p<0.001$ ***). This is remarkable as we demonstrate that

immunoglobulins are the major protein corona component (about 50%) for all investigated nanoparticles. As the morphology of the protein corona was visualized as an undefined loose network of proteins, this indicates that next to the presence of the protein corona the underlying surface functionalization affects cellular uptake.

Transmission electron microscopy (Figure 1.4) was used to compare the internalization mechanism and intracellular trafficking of un-functionalized nanoparticles without (-) or with hard protein corona (+). Numerous un-functionalized polystyrene nanoparticles were packed in long membrane structures (Figure 1.4) that resemble the uncoated carriers or early endosomes present in the CLIC/GEEC endocytosis pathway[36-37]. In the presence of protein corona, these structures were not observed. Instead, un-functionalized PS-NPs (either individually or in a group of 2-3) were packed in small vesicles, and were not found inside endosomes (Figure 1.4). These results indicate that in the presence of protein corona, the cells choose an alternative endocytosis pathway. Additional TEM micrographs are summarized in the supplementary information 1.

Several studies have shown that the secondary structure of the proteins can be altered by adsorption on a surface[32,33] and thus further determine cellular uptake.[34 35] As seen in the case of apolipoprotein AI (ApoAI), we found that the corona diameter after incubation with un-functionalized PS-NP was quite large (~ 100 nm, Figure 1.5). Therefore, we studied whether this affects the cellular uptake behavior. Un-functionalized nanoparticles were incubated with ApoAI and cellular uptake was analyzed by flow cytometry, cLSM, and TEM (Figure 1.5). It was found that due to pre-coating with ApoAI cellular uptake was strongly inhibited compared to uncoated (-) or hard corona coated nanoparticles (+), hence it was comparable to soft corona coated nanoparticle (++). Interstingly,the structural properties of the ApoAI and soft protein corona indicated strikingly similiar properties (Figure 1.5 vs. 1.2 average corona diameter and number of corona proteins).

## Conclusion

We were able to demonstrate the evolution of the protein corona during the centrifugation and washing procedures using the combined correlative approach of TEM and proteomics. By using these techniques, we could differentiate between the *soft* corona and the *hard* corona. Our findings on the morphology of the protein corona offer new insights into its real structure, which we determined to be a network-like, loosely interconnected agglomeration of proteins surrounding a nanoparticle.

In order to explore the effect of surface chemistry, we presented a qualitative and quantitative analysis of the protein corona of three differently surface functionalized PS-NPs and their influence on the composition of the protein corona. Furthermore, we proved that the uptake of un-functionalized PS-NPs pre-incubated with either soft corona or Apo-A1 was prevented. Understanding how NPs interact with proteins as well as the effect of the different corona morphologies and compositions on cellular mechanisms (like uptake and trafficking) are important factors in the design of NPs. This is particularly so for those NPs with regulated biological identities and physiological effects and also for experiments based on "personalized protein corona" intended for clinical applications as suggested by Hajipour *et al*. [38].

## Supplementary information

**Table 1. 1.** Physicochemical properties as hydrodynamic radius and ζ-potential of polystyrene nanoparticles determined by multi angle dynamic light scattering in aqueous solution and PBS. The fluorescence intensity of the BODIPY labeled nanoparticles (525/535 nm) was determined by Tecan Microplate Reader and normalized to the value for un-functionalized polystyrene nanoparticles.

| | $R_h$ ($H_2O$) | $R_h$ (PBS) | ζ-Potential | Fluorescence Intensity Factor |
|---|---|---|---|---|
| **PS** | 73 ± 7.3 nm | 75 ± 7.5 nm | - 3.70 mV | 1 |
| **PS- COOH** | 70 ± 7.0 nm | 72 ± 7.0 nm | - 7.21 mV | 1.16 |
| **PS- $NH_2$** | 74 ± 4.3 nm | 79 ± 7.9 nm | + 7.58 mV | 1.05 |

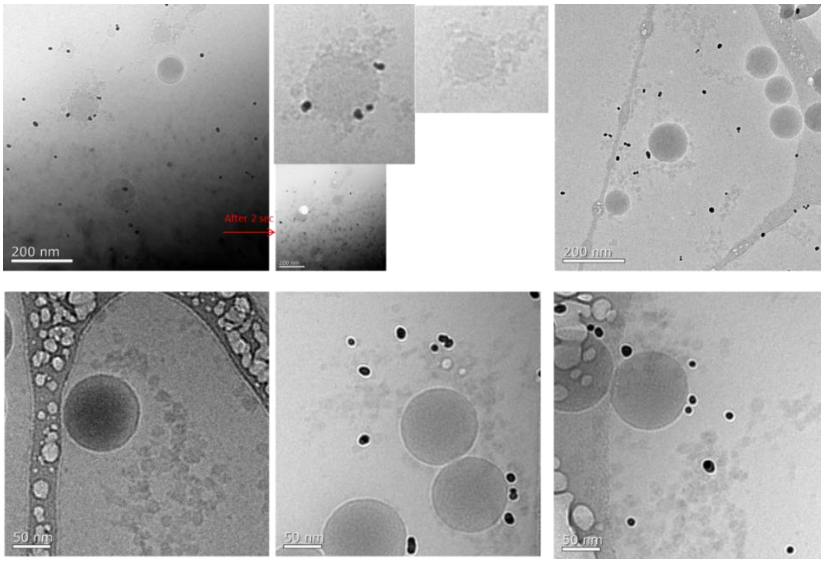


**Figure 1. 6.** Cryo-TEM micrographs of un-functionalized PS nanoparticles incubated with gold-labelled bovine serum albumin visualize the structure of the protein corona. Nanoparticles (0.05 $m^2$) were incubated with 100 µg of protein for 1 h at 37 °C before measurements were performed. [redacted]

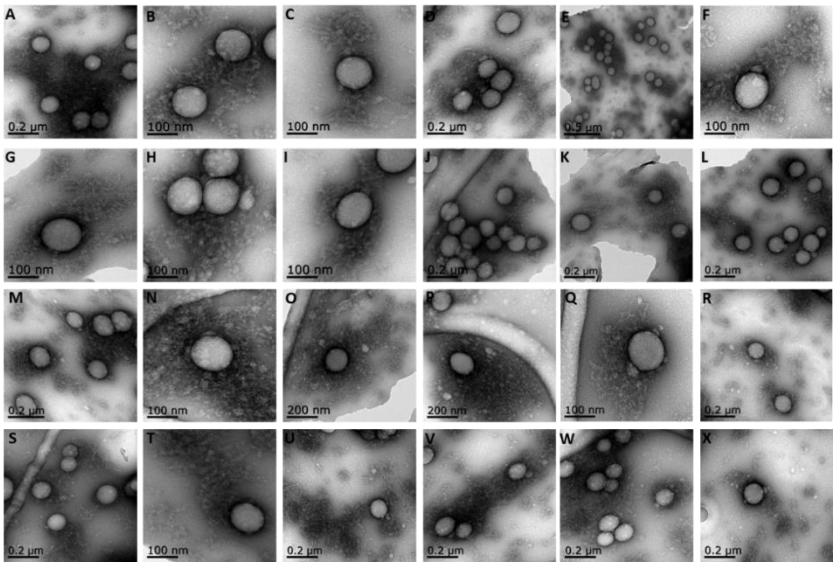


**Figure 1. 7.** TEM micrographs of un-functionalized PS nanoparticles incubated with human serum and centrifuged once (A). Nanoparticles are surrounded by a huge protein cloud. [redacted]

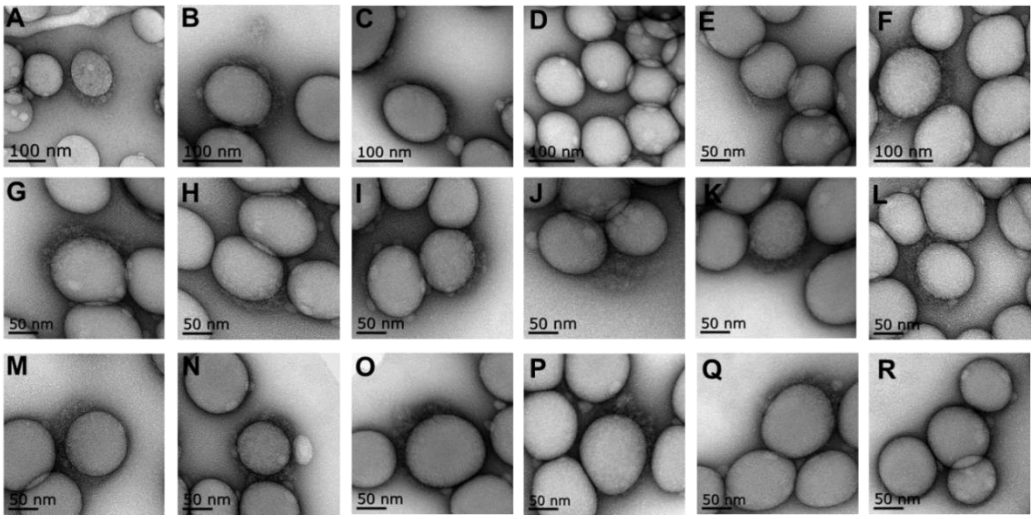


**Figure 1. 8.** TEM micrographs of un-functionalized PS nanoparticles incubated with human serum centrifuged and washed three times (D). The hard protein corona surrounding nanoparticles is visualized. [redacted]

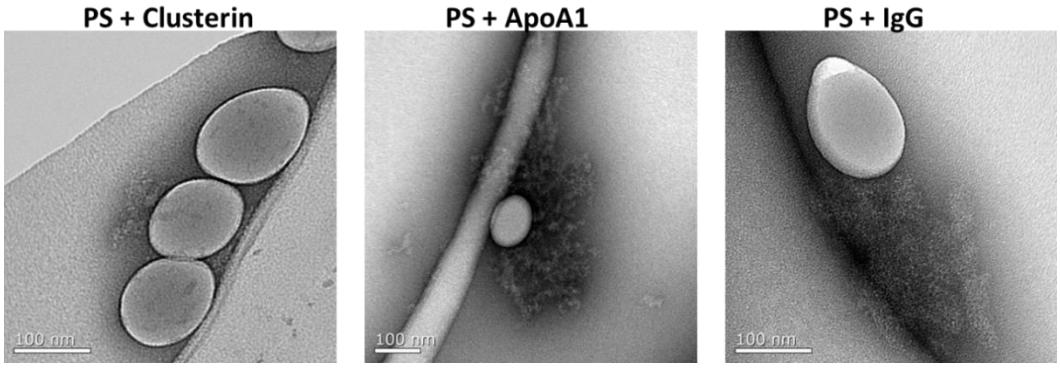


**Figure 1. 9.** TEM micrographs of un-functionalized PS incubated with identified hard corona proteins. Nanoparticles (0.05 $m^2$) were incubated with 100 µg of protein for 1 h at 37 °C before measurements were performed. [redacted]

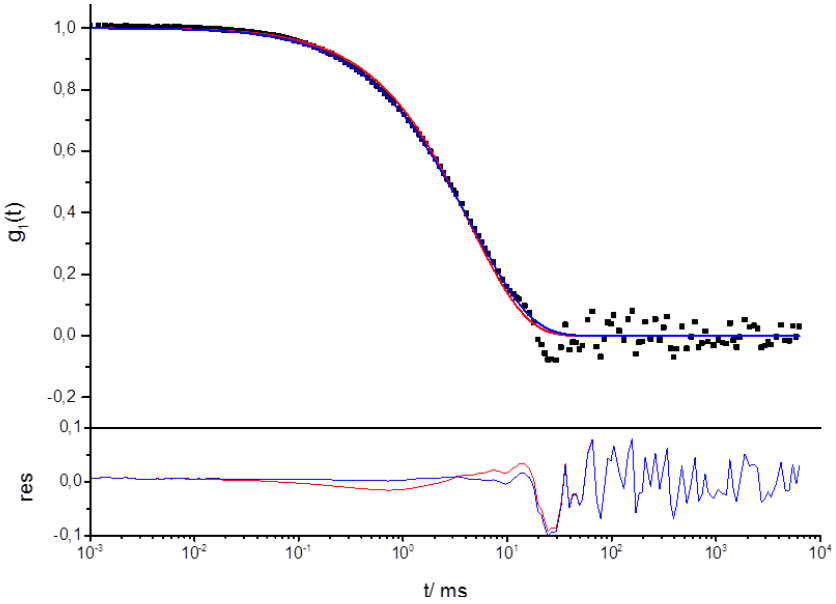


**Figure 1. 10.** Autocorrelation function of un-functionalized PS nanoparticles incubated with human serum exemplary shown for a scattering angle of 30°. [redacted]

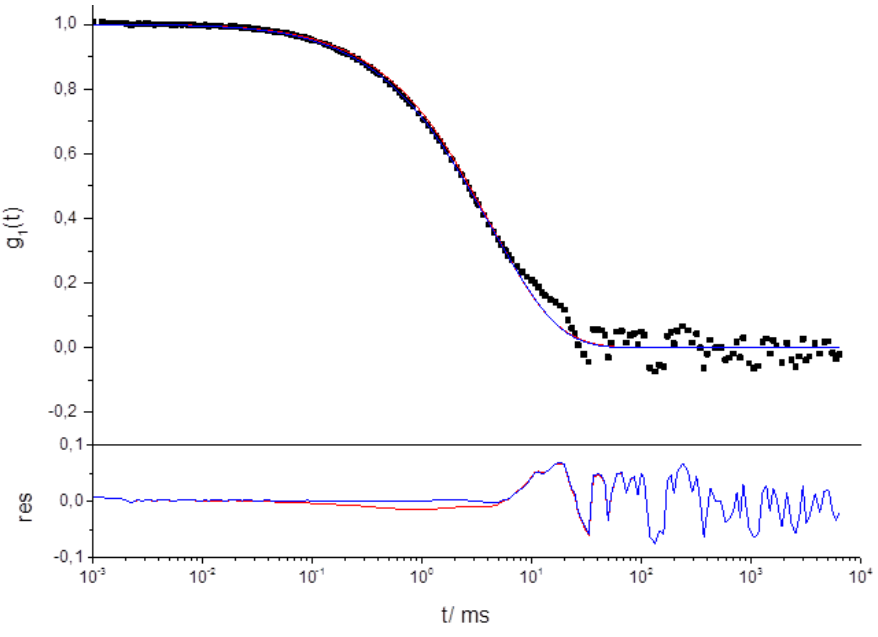


**Figure 1. 11.** Autocorrelation function of PS-$NH_2$ nanoparticles incubated with human serum exemplary shown for a scattering angle of 30°. [redacted]

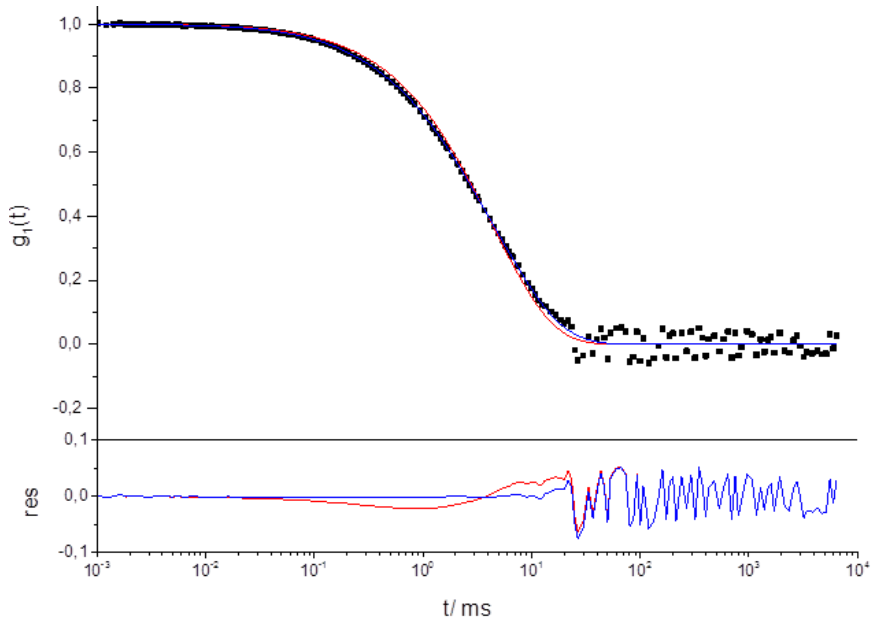


**Figure 1. 12.** Autocorrelation function of PS- COOH nanoparticles incubated with human serum exemplary shown for a scattering angle of 30°. [redacted]

**Table 1. 2.** *Soft* corona hydrodynamic radii of polystyrene nanoparticles incubated within human serum measured by multi angle dynamic light scattering. The size of the nanoparticles was measured directly within human serum. Nanoparticles are surrounded by a huge protein causing a size increase. Values are exemplary given for a scattering angle at 30° as the system has the greatest sensitivity towards detection of aggregation formation. [23] [redacted]

| | **Hydrodynamic radius (NP with *soft* corona) (Scattering angle 30°)** | **Intensity (I%)** |
|---|---|---|
| **PS** | 140 ± 14 nm | 22 |
| **PS- COOH** | 178 ± 18 nm | 21 |
| **PS- $NH_2$** | 188 ± 19 nm | 18 |

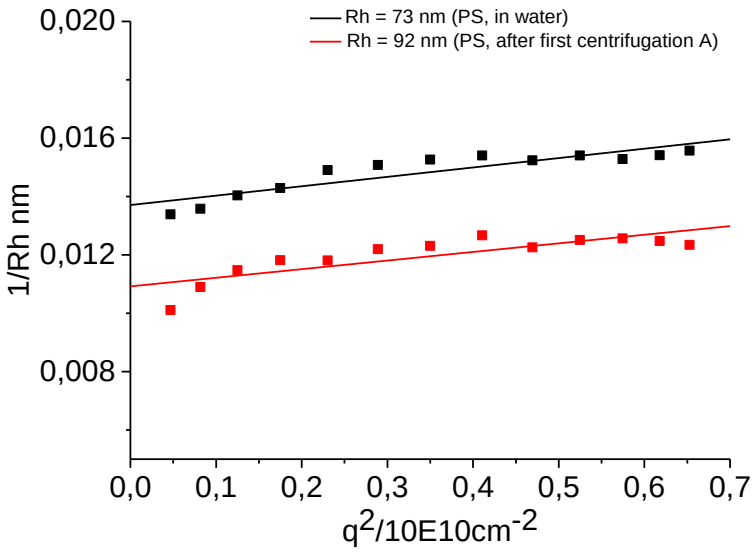


**Figure 1. 13.** Incubation of un-functionalized PS with human serum and further centrifugation to isolate NPs with hard protein corona (PS; A) in comparison to PS in water. There is a size increase of 19 ± 2 nm monitored by multi angle dynamic light scattering attributed to the hard protein corona around nanoparticles. The angular dependency of the inverse hydrodynamic radii of un-functionalized PS is demonstrated. [redacted]

**Table 1. 3.** *Hard* corona hydrodynamic radii of polystyrene nanoparticles incubated within human serum and centrifuged was measured by multi angle dynamic light scattering. [redacted]

| | **Hydrodynamic radius (NP with *hard* corona) $R_h$ ($H_2O$)** |
|---|---|
| **PS** | 92 ± 9.2 nm |
| **PS- COOH** | 80 ± 8.0 nm |
| **PS- $NH_2$** | 88 ± 8.8 nm |

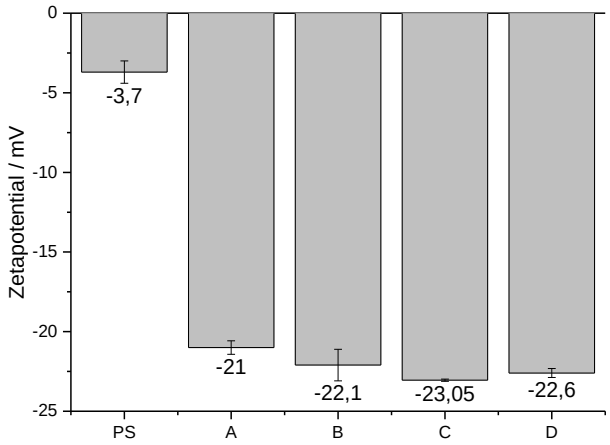


**Figure 1. 14.** Zeta-potential after incubation, centrifugation and washing of un-functionalized PS nanoparticles incubated with human serum. Due to protein adsorption the zeta-potential is strongly decreased. [redacted]

**Table 1. 4.** Amount of adsorbed protein in µg per 0.05 $m^2$ NP determined after each purification step (A = First centrifugation, B = 1. Wash, C = 2. Wash, D = Third wash)

| **Preparation PS** | **Amount of adsorbed protein per 0.05 m2 NP** |
|---|---|
| **A** | 781.9 ± 38.6 µg |
| **B** | 87.22 ± 2.42 µg |
| **C** | 50.51 ± 2.28 µg |
| **D** | 49.18 ± 3.00 µg |

| **Preparation PS- COOH** | **Amount of adsorbed protein per 0.05 m2 NP** |
|---|---|
| **A** | 1208.22 ± 101.38 µg |
| **D** | 137.35 ± 1.38 µg |

| **Preparation PS- $NH_2$** | **Amount of adsorbed protein per 0.05 m2 NP** |
|---|---|
| **A** | 1055.97 ± 18.78 µg |
| **D** | 66.70 ± 4.93 µg |

**Table 1. 5.** Protein concentration in the remaining supernatant after centrifugation and washing. After the third wash the protein concentration is below the detectable range of the Pierce assay.

| Supernatant | Concentration (mg/mL) |
|---|---|
| **A** | 47.97 ± 1.71 mg/mL |
| **B** | 1.43 ± 0.03 mg/mL |
| **C** | 0.07 ± 0.02 mg/mL |
| **D** | * (below 0.05 mg/mL) |

**Table 1. 6.** Amount of recovered nanoparticle after the first centrifugation and last washing steps for all nanoparticles measured via fluorescence intensity of nanoparticles at the initial concentration.

| Preparation | PS | PS- COOH | PS- NH2 |
|---|---|---|---|
| **A** | 71.7 ± 4.8 % | 83.6 ± 3.2 % | 86.8 ± 5.9 % |
| **D** | 68.3 ± 3.4 % | 72.7 ± 3.4 % | 66.8 ± 1.2 % |

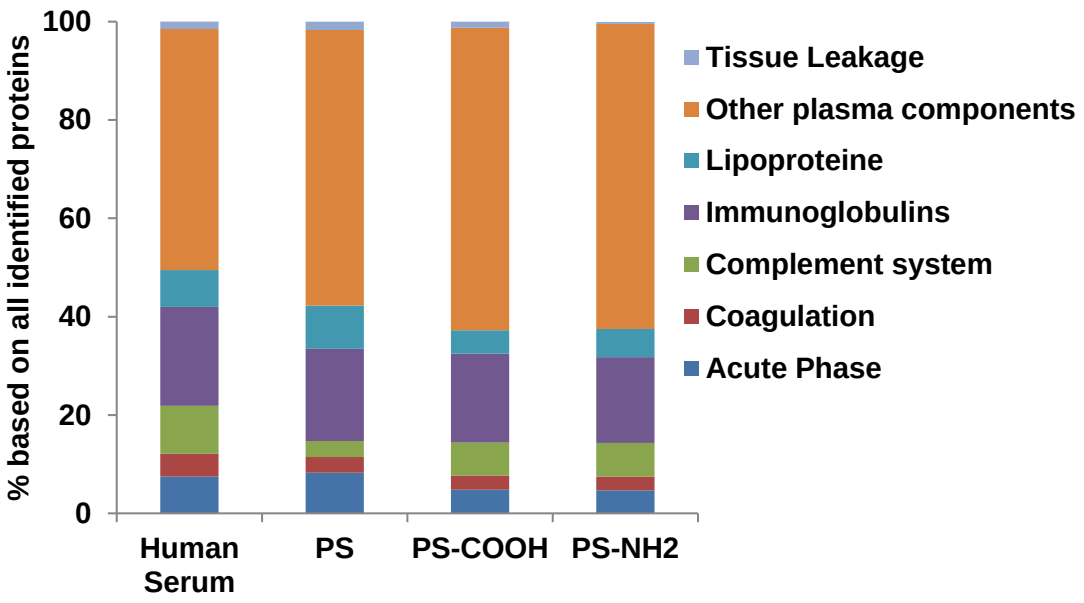


**Figure 1. 15.** LC-MS Protein classification of proteins associated with nanoparticles after the first centrifugation (A). There is no significant difference in the protein pattern for all nanoparticles.

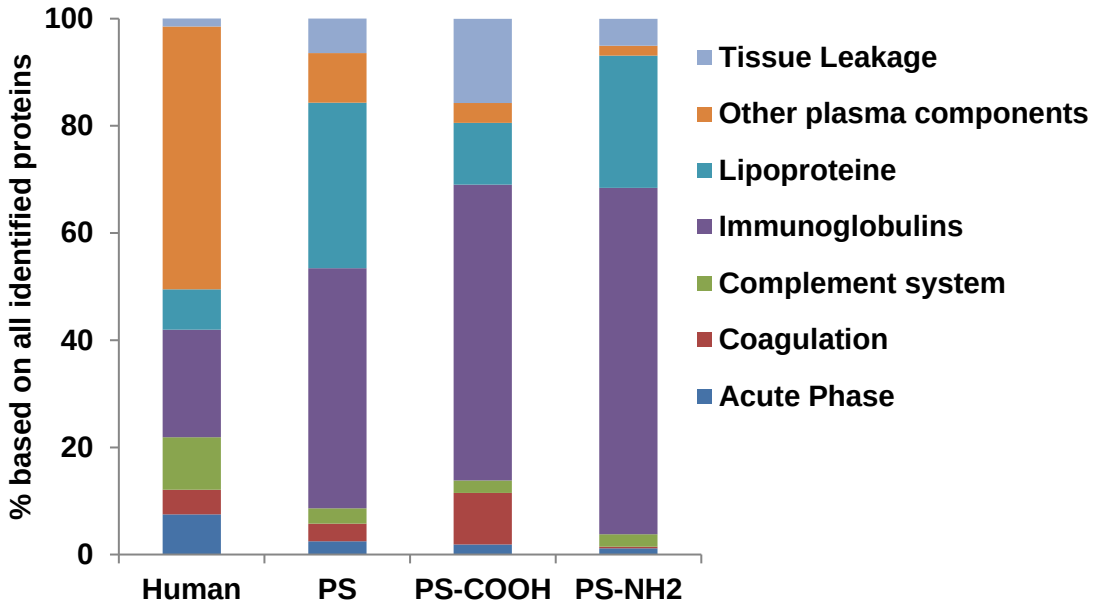


**Figure 1. 16.** LC-MS Protein classification of proteins associated with nanoparticles after the third wash (D). The distinct hard protein corona profile depends on surface functionalization of nanoparticles and highly differs from the protein composition in human serum.

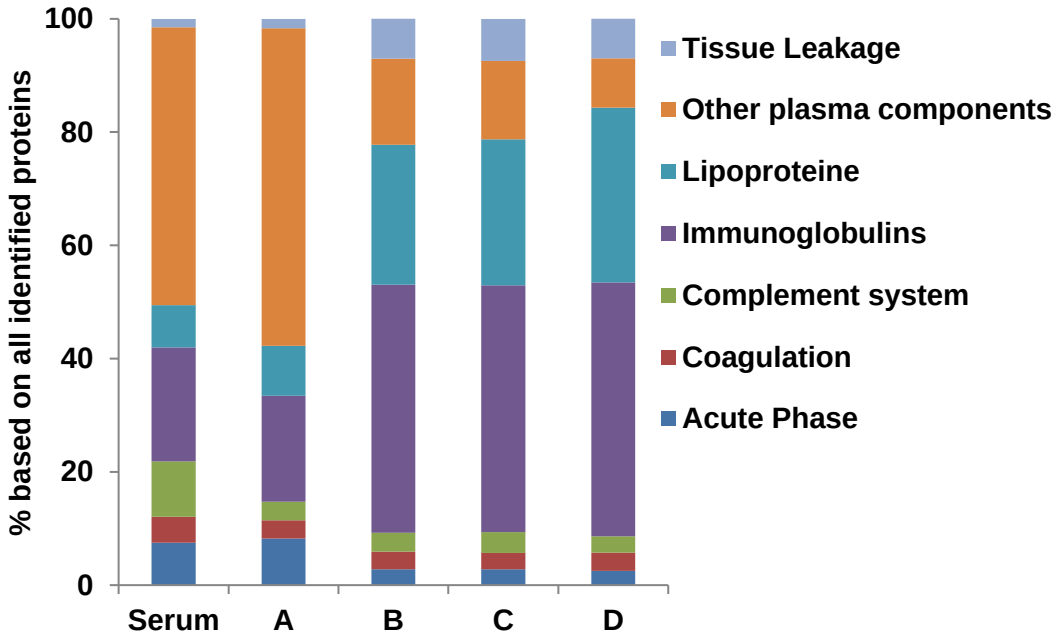


**Figure 1. 17.** LC-MS Protein classification of proteins associated with un-functionalized PS nanoparticles after each purification step. (A = First centrifugation, B = 1. Wash, C = 2. Wash, D = Third wash)

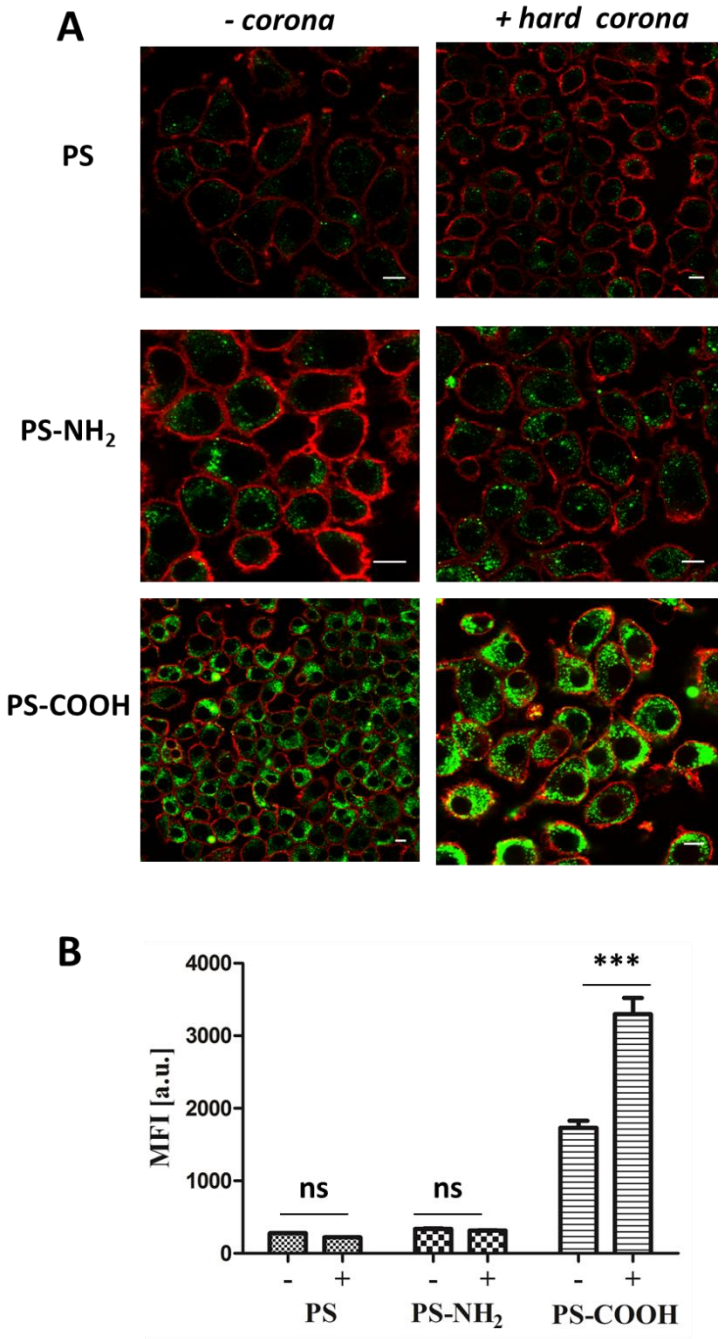


**Figure 1. 18. A.** Confocal laser scanning microscopy images: RAW264.7 cells were incubated with un-functionalized or functionalized polystyrene nanoparticles (300 µg/mL) for 1 h. Scale bar: 10 µm **B.** Flow cytometry experiments: RAW264.7 cells were incubated with un-functionalized or functionalized polystyrene nanoparticles coated with (+/-) or without hard protein corona (300 µg/mL) for 1 h. The average of the median fluorescence intensity of three independent experiments is shown (n=3). GraphPad Prism 5 Software was used for statistical analysis using a one-way ANOVA followed by Tukey's post-hoc multiple comparisons test. A *p*-value of < 0.001 was considered as highly significant***.

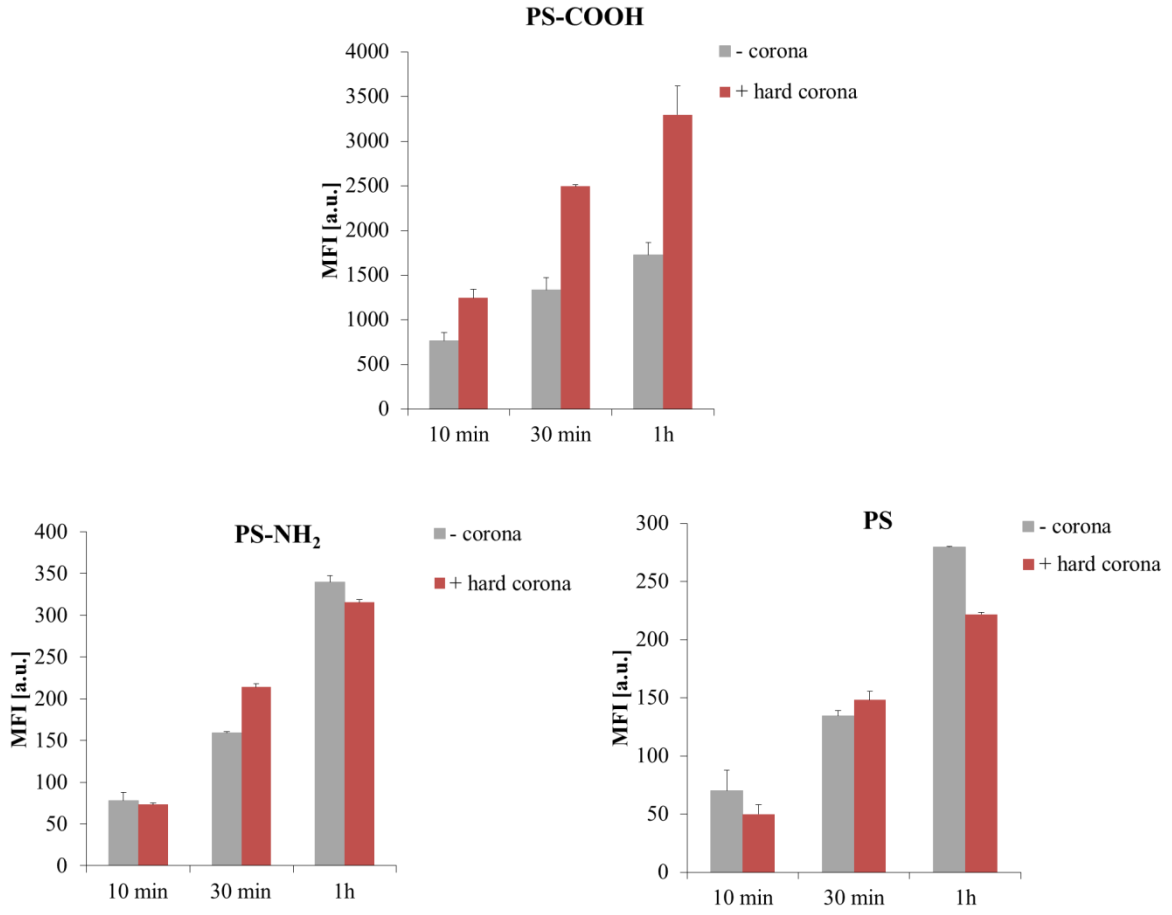


**Figure 1. 19.** Flow cytometry analysis: RAW264.7 cells were incubated with un-functionalized or functionalized polystyrene nanoparticles (300 µg/mL) for 10 min, 30 min or 1 h. Prior to cellular uptake studies, nanoparticles were incubated with human serum for 1 h at 37 °C, centrifuged and washed to remove unbound proteins. Isolated hard corona coated nanoparticles (+) or uncoated nanoparticles (-) were added to serum free cell culture medium. The average of the median fluorescence intensity (MFI) of three independent experiments is shown (n=3).

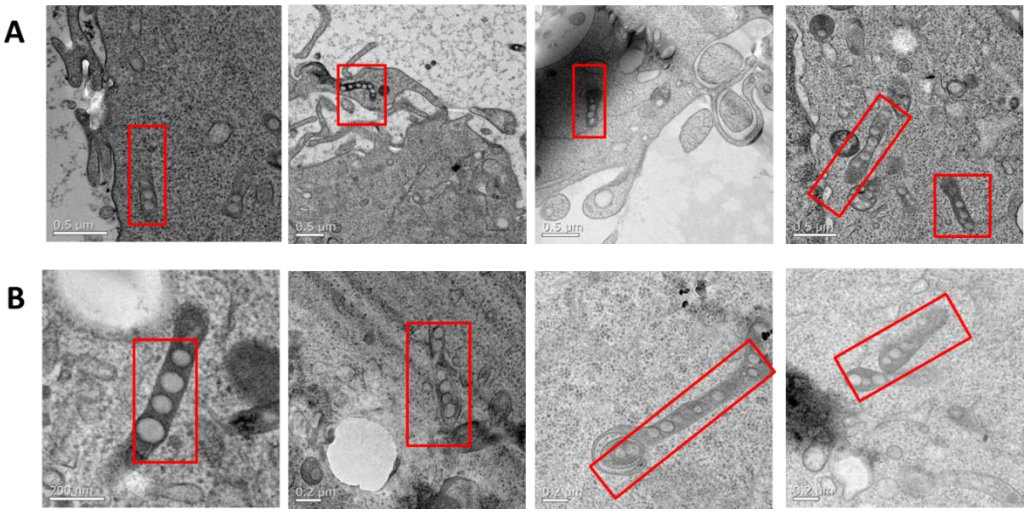


**Figure 1. 20.** TEM micrographs of high-pressure frozen macrophages treated with 300 µg/mL of un-functionalized nanoparticles without (-) hard protein corona for 1 h. Scale bar: A = 0.5 µm; B = 200 nm. Numerous un-functionalized polystyrene nanoparticles were packed in long membrane structures (CLIC/GEEC endocytosis pathway). [redacted]

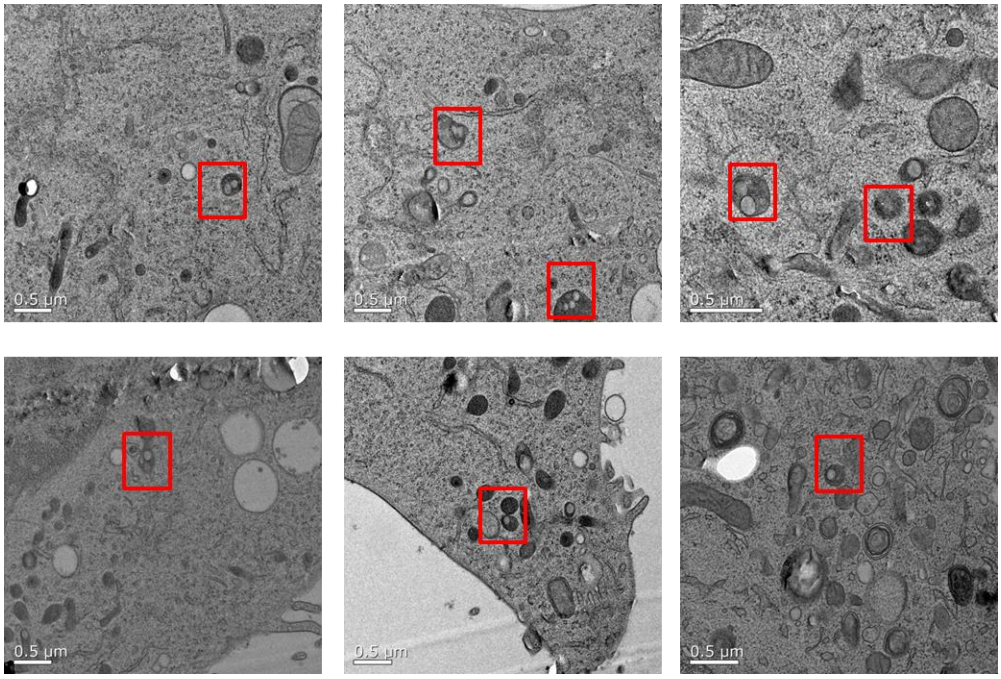


**Figure 1. 21.** TEM micrographs of high-pressure frozen macrophages treated with 300 µg/mL of un-functionalized nanoparticles with (+) hard protein corona for 1 h. (+). Scale bar: 0.5 µm Hard corona coated un-functionalized PS-NPs were packed in small vesicles (either individually or in a group of 2-3). [redacted]

# Literature


1. Mahmoudi, M.; Lynch, I.; Ejtehadi, M. R.; Monopoli, M. P.; Bombelli, F. B.; Laurent, S., Protein-nanoparticle interactions: opportunities and challenges. *Chem Rev* 2011, *111* (9), 5610-37.

2. Nel, A. E.; Madler, L.; Velegol, D.; Xia, T.; Hoek, E. M. V.; Somasundaran, P.; Klaessig, F.; Castranova, V.; Thompson, M., Understanding biophysicochemical interactions at the nano-bio interface. *Nat Mater* 2009, *8* (7), 543-557.

3. Kelly, P. M.; Åberg, C.; Polo, E.; O'Connell, A.; Cookman, J.; Fallon, J.; Krpetić, Ž.; Dawson, K. A., Mapping protein binding sites on the biomolecular corona of nanoparticles. *Nat. Nanotechnol.* 2015, *10* (5), 472-479.

4. Walkey, C. D.; Chan, W. C., Understanding and controlling the interaction of nanomaterials with proteins in a physiological environment. *Chem Soc Rev* 2012, *41* (7), 2780-99.

5. Cedervall, T.; Lynch, I.; Lindman, S.; Berggard, T.; Thulin, E.; Nilsson, H.; Dawson, K. A.; Linse, S., Understanding the nanoparticle-protein corona using methods to quantify exchange rates and affinities of proteins for nanoparticles. *Proc Natl Acad Sci U S A* 2007, *104* (7), 2050-5.

6. Tenzer, S.; Docter, D.; Kuharev, J.; Musyanovych, A.; Fetz, V.; Hecht, R.; Schlenk, F.; Fischer, D.; Kiouptsi, K.; Reinhardt, C.; Landfester, K.; Schild, H.; Maskos, M.; Knauer, S. K.; Stauber, R. H., Rapid formation of plasma protein corona critically affects nanoparticle pathophysiology. *Nat Nanotechnol* 2013, *8* (10), 772-81.

7. Walczyk, D.; Bombelli, F. B.; Monopoli, M. P.; Lynch, I.; Dawson, K. A., What the cell "sees" in bionanoscience. *Journal of the American Chemical Society* 2010, *132* (16), 5761-8.

8. Ritz, S.; Schöttler, S.; Kotman, N.; Baier, G.; Musyanovych, A.; Kuharev, J.; Landfester, K.; Schild, H.; Jahn, O.; Tenzer, S.; Mailaender, V., Protein corona of nanoparticles: distinct proteins regulate the cellular uptake. *Biomacromolecules* 2015, *16*, 1311-1321.

9. Lesniak, A.; Fenaroli, F.; Monopoli, M. P.; Aberg, C.; Dawson, K. A.; Salvati, A., Effects of the presence or absence of a protein corona on silica nanoparticle uptake and impact on cells. *ACS Nano* 2012, *6* (7), 5845-57.

10. Hofmann, D.; Tenzer, S.; Bannwarth, M. B.; Messerschmidt, C.; Glaser, S.-F.; Schild, H.; Landfester, K.; Mailänder, V., Mass Spectrometry and Imaging Analysis of Nanoparticle-Containing Vesicles Provide a Mechanistic Insight into Cellular Trafficking. *ACS Nano* 2014, *8* (10), 10077-10088.

11. Docter, D.; Distler, U.; Storck, W.; Kuharev, J.; Wünsch, D.; Hahlbrock, A.; Knauer, S. K.; Tenzer, S.; Stauber, R. H., Quantitative profiling of the protein coronas that form around nanoparticles. *Nat. Protoc.* 2014, *9* (9), 2030-44.

12. Mohr, K.; Sommer, M.; Baier, G.; Schöttler, S.; Okwieka, P.; Tenzer, S.; Landfester, K.; Mailänder, V.; Schmidt, M.; Meyer, R. G., Aggregation Behavior of Polystyrene-Nanoparticles in Human Blood Serum and its Impact on the in vivo Distribution in Mice. *J Nanomed Nanotechnol* 2014, *5* (2), 193.

13. Loos, C.; Syrovets, T.; Musyanovych, A.; Mailander, V.; Landfester, K.; Nienhaus, G. U.; Simmet, T., Functionalized polystyrene nanoparticles as a platform for studying bio-nano interactions. *Beilstein J Nanotechnol* 2014, *5*, 2403-12.

14. Landfester, K., Synthesis of colloidal particles in miniemulsions. *Annual Review of Materials Research* 2006, *36* (1), 231-279.

15. Tenzer, S.; Docter, D.; Rosfa, S.; Wlodarski, A.; Kuharev, J.; Rekik, A.; Knauer, S. K.; Bantz, C.; Nawroth, T.; Bier, C.; Sirirattanapan, J.; Mann, W.; Treuel, L.; Zellner, R.; Maskos, M.; Schild, H.; Stauber, R. H., Nanoparticle Size Is a Critical Physicochemical Determinant of the Human Blood Plasma Corona: A Comprehensive Quantitative Proteomic Analysis. *ACS Nano* 2011, *5* (9), 7155-7167.

16. Cedervall, T.; Lynch, I.; Foy, M.; Berggad, T.; Donnelly, S. C.; Cagney, G.; Linse, S.; Dawson, K. A., Detailed identification of plasma proteins adsorbed on copolymer nanoparticles. *Angew Chem Int Edit* 2007, *46* (30), 5754-5756.

17. Lundqvist, M.; Stigler, J.; Elia, G.; Lynch, I.; Cedervall, T.; Dawson, K. A., Nanoparticle size and surface properties determine the protein corona with possible implications for biological impacts. *Proc Natl Acad Sci U S A* 2008, *105* (38), 14265-70.

18. De Carlo, S.; Harris, J. R., Negative staining and cryo-negative staining of macromolecules and viruses for TEM. *Micron* 2011, *42* (2), 117-131.

19. Zhang, L.; Tong, H.; Garewal, M.; Ren, G., Optimized negative-staining electron microscopy for lipoprotein studies. *Biochim Biophys Acta* 2013, *1830* (1), 2150.

20. Renz, P.; Maria Kokkinopoulou, M.; Landfester, K.; Lieberwirth, I., Imaging of Polymeric Nanoparticles: Hard Challenge for Soft Objects. *Macromolecular Chemistry and Physics* 2016, *217* (71), 1879–1885.

21. Winzen, S., Complementary analysis of the hard and soft protein corona: sample preparation critically effects corona composition. *Nanoscale* 2015, *7*, 2992-3001.

22. Wegener, J., Measuring Biological Impacts of Nanomaterials. *Springer* 2016.

23. Rausch, K.; Reuter, A.; Fischer, K.; Schmidt, M., Evaluation of nanoparticle aggregation in human blood serum. *Biomacromolecules* 2010, *11* (11).

24. Walkey, C. D.; Olsen, J. B.; Guo, H.; Emili, A.; Chan, W. C., Nanoparticle size and surface chemistry determine serum protein adsorption and macrophage uptake. *Journal of the American Chemical Society* 2012, *134* (4), 2139-47.

25. Rahman, M.; Laurent, S.; Tawil, N.; Yahia, L.; Mahmoudi, M., *Protein-Nanoparticle-Interactions, The Bio-Nano Interface*. Springer-Verlag: 2013; Vol. 15.

26. Thode, K.; Luck, M.; Semmler, W.; Muller, R. H.; Kresse, M., Determination of plasma protein adsorption on magnetic iron oxides: sample preparation. *Pharm Res* 1997, *14* (7), 905-10.

27. Monopoli, M. P., Comparison of nanoparticles protein corona complexes isolated with different methods. *NanoLife* 2013, *3*.

28. Winzen, S.; Schoettler, S.; Baier, G.; Rosenauer, C.; Mailaender, V.; Landfester, K.; Mohr, K., Complementary analysis of the hard and soft protein corona: sample preparation critically effects corona composition. *Nanoscale* 2015, *7* (7), 2992-3001.

29. Schöttler, S.; Becker, G.; Winzen, S.; Steinbach, T.; Mohr , K.; Landfester, K.; Mailänder, V.; Wurm, F. R., Protein adsorption is required for stealth effect of poly(ethylene glycol)- and poly(phosphoester)-coated nanocarriers. *Nat. Nanotechnol.* 2016, *11*, 372-377.

30. Monopoli, M. P.; Aberg, C.; Salvati, A.; Dawson, K. A., Biomolecular coronas provide the biological identity of nanosized materials. *Nat Nano* 2012, *7* (12), 779-786.

31. Ritz, S.; Schöttler, S.; Kotman, N.; Baier, G.; Musyanovych, A.; Kuharev, J.; Landfester, K.; Schild, H.; Jahn, O.; Tenzer, S.; Mailänder, V., Protein Corona of Nanoparticles: Distinct Proteins Regulate the Cellular Uptake. *Biomacromolecules* 2015, *16* (4), 1311-1321.

32. Hlady, V. V.; Buijs, J., Protein adsorption on solid surfaces. *Curr Opin Biotechnol.* 1996, *7* (1), 72-77.

33. Gray, J. J., The interaction of proteins with solid surfaces. *Curr Opin Struct Biol.* 2004, *14* (1), 110-115.

34. Fleischer, C. C.; Payne, C. K., Nanoparticle surface charge mediates the cellular receptors used by protein-nanoparticle complexes. *J Phys Chem B* 2012, *116* (30), 8901-7.

35. Fleischer, C. C.; Payne, C. K., Secondary Structure of Corona Proteins Determines the Cell Surface Receptors Used by Nanoparticles. *J. Phys. Chem.* 2014, *118* (49), 14017-14026.

36. Hansen, C. G.; Nichols, B. J., Molecular mechanisms of clathrin-independent endocytosis. *Journal of Cell Science* 2009, 1713-1721.

37. Mayor, S.; Pagano, E., Pathways of clathrin-independent endocytosis. . *Nature Reviews* 2007, *8*, 603-612.

38. Hajipour, M. J.; Laurent, S.; Aghaie, A.; Rezaee, F.; Mahmoudi, M., Personalized protein coronas: a "key" factor at the nanobiointerface. *Biomaterials Science* 2014, *2* (9), 1210-1221.

39. De Carlo, S.; Harris, J. R., Negative staining and cryo-negative staining of macromolecules and viruses for TEM. *Micron.* 2011, *42*, 117-131.

40. Kremer, J. R.; Mastronarde, D. N.; McIntosh, J. R., Computer visualization of three-dimensional image data using IMOD. *J Struct Biol.* 1996, *116* (1), 71-76.

41. Musyanovych, A.; Rossmanith, R.; Tontsch, C.; Landfester, K., Effect of hydrophilic comonomer and surfactant type on the colloidal stability and size distribution of carboxyl- and amino-functionalized polystyrene particles prepared by miniemulsion polymerization. *Langmuir.* 2007, *23* (10), 5367-76.

42. Walczyk, D.; Baldelli Bombelli, F.; Monopoli, M. P.; Lynch, I.; Dawson, K. A., What the cell 'sees' in bionanoscience. *J. Am. Chem. Soc.* 2010, *132*, 5761-5768.

43. Tenzer, S., Nanoparticle size is a critical physicochemical determinant of the human blood plasma corona: a comprehensive quantitative proteomic analysis. *ACS Nano* 2011, *5*, 7155-7167.

44. Bradshaw, R. A.; Burlingame, A. L.; Carr, S.; Aebersold, R., Reporting protein identification data: the next generation of guidelines. *Mol Cell Proteomics* 2006, *5* (5), 787-8.

45. Silva, J. C.; Gorenstein, M. V.; Li, G. Z.; Vissers, J. P. C.; Geromanos, S. J., Absolute quantification of proteins by LCMSE: a virtue of parallel MS acquisition. *Mol. Cell. Proteomics* 2006, *5*, 144-156.

46. García-Moreno, I.; Costela, A.; Campo, L., 8-Phenyl-Substituted Dipyrromethene·BF2 Complexes as Highly Efficient and Photostable Laser Dyes. *J. Phys. Chem. A* 2004, *108* (16), 3315-3323.

# 2. Protein denaturation by heat inactivation detrimentally affects biomolecular corona formation and cellular interactions

## Aim:

Heat inactivation is a common cell culture procedure for *in vitro* experiments. Therefore, this study focuses especially on the effect of heat inactivation and its influence on protein corona formation. In general, it was demonstrated that the protein structure is highly affected due to heat inactivation. On top of that, this caused an altered protein corona profile and eventually affected cellular interactions. Therefore, this study demonstrates that the protein structure is one of the key parameters, which mediates protein corona formation.

## Contribution:

I conducted the complete protein corona analysis (SDS-PAGE, LC-MS, Pierce Assay) and cellular uptake experiments (flow cytometry). [redacted] performed the nanoDSF and ITC measurments. [redacted] Ghazaryan carried out the CD experiments. The project was supervised by [redacted]

## Abstract

Adsorption of blood proteins to the surface of nanoparticles has been shown to be a critically factor, which influences cellular interactions and eventually determines the successful application of nanoparticles as drug carriers *in vivo*. There is an increasing number of reports, which summarize large data sets of all identified corona proteins. However, up to now there is still a limited knowledge about the influence of the protein structure on the adsorption process. In this study, we focused on the effect of heat inactivation of serum and plasma, which is a common cell culture procedure to inactivate the complement system. Heat inactivation was performed at 56 °C for 30 min. We saw that the cellular uptake towards macrophages was significantly affected if nanoparticles were exposed to untreated and in contrast to heat treated serum. These results were further correlated with an altered corona composition depending on the treatment of the protein source. Overall, this proves that protein denaturation is one of the key parameters, which mediates protein corona formation.

## Introduction

The field of nanotechnology has made great progress in the development of novel nanoparticle formulations[1]. Innovative nanomaterials with varying surface modification[2], high encapsulation efficiencies[3] and controlled release properties[4] are promising candidates for targeted drug delivery[5]. However, even up to now, there is still a very limited number of reports, which could actually prove their successful performance *in vivo*[6]. This could be caused by the fact that there is still a huge gap between the synthetic design of nanocarries, their testing *in vitro* and their *in vivo* behavior[7-8].

Over the last decade, it has been recognized that the nanoparticle properties´ are significantly altered after contact with biological fluids (e.g. blood plasma)[9-11]. It has been shown that various biomolecules rapidly interact with the nanoparticle and immediately cover its surface (´termed as biomolecular corona´)[12]. Due to this, the physico-chemical properties of the nanoparticle such as size, charge or aggregation behavior are altered[13] and this further determines cellular uptake[14], toxicity[15] and body distribution[16]. Several studies showed that due to corona formation the intended targeting properties can be even completely lost, which underlines the significant influence of corona formation[17-18]. As a result, studies investigating the biomolecular corona have gained increased importance to understand and control this process[19].

Commonly, in cell culture, fetal bovine or human serum are used for cell maintenance and *in vitro* experiments[20]. Mirshafiee *et al*.[21] and Schöttler *et al.*[22] already reported that the protein source can significantly influence cellular uptake of nanoparticles and their protein adsorption pattern. A common procedure – mostly overlooked and also not always reported in the Material and Methods sections - in cell culture is heat inactivation of the respective protein source prior to use[23-24]. During this procedure, serum is typically heated up to 56 °C for 30 min. With this procedure, it is intended to inactive heat labile proteins, most notably complement proteins. These can interfere with other components in immunological assays and sometimes even promote the lysis of cells if cell binding antibodies are present[25]. Complement proteins were identified as parts of the biomolecule corona of different nanoparticle formulations and are known to mediate interactions with immune cells[26-27].

However, there is actually a limited knowledge to what extent heat inactivation affects other blood proteins. In addition, the majority of reports do not specify whether untreated or heat inactivated serum was used in the experimental setup.

Therefore, this study specifically focused on the effect of heat inactivation on the cellular uptake and corona formation of different nanoparticles. Here, we shed light onto the role of protein structure, which was found to critically influence the protein adsorption process. This basic knowledge is needed to understand corona formation and to transfer the knowledge gained from the *in vitro* studies for further *in vivo* experiments.

## Material and methods

**Polystyrene nanoparticles.** Polystyrene nanoparticles stabilized with the surfactant Lutensol-AT50 (BASF) were synthesized in accordance to previous reports using free-radical miniemulsion polymerization[43-44]. BOPIPY was incooperated into the nanoparticles for cell uptake studies[45].

**Hydroxyethyl starch (HES) nanocapsules.** HES nanocapsules were obtained by the inverse mini emulsion process[46]. The fluorescent dyesulforhodamine 101 (SR101) was incooperated into the nanocapsules.

**Cell culture.** RAW264.7 were maintained in Dulbecco´s modified eagle medium (DMEM) supplemented with 10 % FBS, 100 U/mL penicillin, 100 mg/mL streptomycin and 2 mM glutamine (Thermo Fisher).

**Cell uptake experiments by flow cytometry.** Cells (150 000 per well) were seeded out in 24-well plates overnight. The medium was changed to serum-free cell culture conditions for 2 h. Further nanoparticles (75 µg/mL) were added to cells for 2 h, 37 °C. Cells were washed with PBS, detached with 0.25 % Trypsin-EDTA (Gibco) and resuspended with PBS. Flow cytometry measurements were performed on a CyFlow ML cytometer (Partec) Data was analyzed by FCS Express V4 software (DeNovo Software).

**Pre-coating experiments.** Nanoparticles (0.05 $m^2$) were incubated with 100 µg Clusterin or ApoAI (untreated or heat treated as indicated) for 1 h, 37 °C, centrifuged and further used in cell uptake experiments.

**Human plasma and serum.** Serum and plasma was obtained from the Department of Transfusion Medicine Mainz from healthy donors in accordance with the Declaration of Helsinki.

**Heat inactivation.** Serum or plasma was heated up to 56 °C for 30 min and centrifuged afterwards for 30 min, 4 °C (20 000 g).

**Protein corona preparation.** Nanoparticles were incubated with the respective protein source and hard corona analysis was carried out as previously described[44].To detach the adsorbed corona proteins, the pellet was re-suspended in 2% SDS (62.5 mM Tris*HCl). The sample was heated up to 95 °C for 5 min, centrifuged (20 000 g, 4 °C, 1 h) and the supernatant was further used for protein analysis.

**LC-MS analysis.** Protein digestion was carried out as described in former reports[47,48]. Isolated peptide were diluted with 0.1% formic acid and spiked with 50 fmol/µL Hi3 Ecoli (Waters) for absolute protein quantification[49]. Samples were analyzed using a a nanoACQUITY UPLC system couple to a Synapt G2- Si mass spectrometer. Data was processed with MassLynx 4.1. Protein identification was carried out with Progenesis QI (2.0) using a reviewed human data base (Uniprot).For peptide and protein identification the parameter were set as described elsewhere[44, 50]

**Nano differential scanning fluorimetry (nanoDSF).** Proteins (Clusterin and ApoAI) were loaded into nanoDSF High Sensitivity capillaries (NanoTemper Technologies) and applied into a Prometheus NT.48 instrument. A linear thermal ramp program starting 20 °C to 95 °C (1 °C/min) was set and the tryptophan fluorescence was measured at 330 and 350 nm. Thermal unfolding curves of the single wavelength at 330 nm and the first derivative of the fluorescence ratio (F350/F330) are plotted against the temperature.

**Isothermal titration calorimetry (ITC).** Measurements were performed with a NanoITC Low Volume from TA Instruments (Eschborn) and experiments were conducted as previously described[33, 51]. Untreated or heat treated Custerin or ApoAI was titrated towards nanoparticles. Data was analyzed using the software NanoAnalyze**.**

## Results and discussion

Phagocytic cells such as macrophages (Figure 2.1) play an important role in the immune system as they engulf foreign material (e.g. nanoparticles)[28]. For this study, we chose non-covalently PEGylated polystyrene nanoparticles (named as PS-$PEG_{NC}$) as model system to investigate the cellular interactions with a macrophage cell line (RAW264.7) and the protein adsorption behavior with regard to the heat treatment of the protein source (material/methods see supplementary information 2).

Nanoparticles were incubated with untreated or heat inactivated serum/plasma (56 °C, 30 min) prior to cellular uptake studies. As a reference, cellular interactions of nanoparticles with macrophages in protein-free medium were investigated (´untreated´). In line with previous findings, in the presence of untreated serum or plasma cellular uptake was strongly decreased compared to untreated nanoparticles indicating stealth properties induced by corona proteins[29]. However, if nanoparticles were pre-coated with heat inactivated serum or plasma; we observed a significant increase in cellular uptake.

Several studies confirmed that PEGylation of nanoparticles did not completely prevent adsorption of blood proteins[30] and we demonstrated in previous studies that actually distinct proteins preferably adsorb onto stealth nanoparticles[29]. These so called ´stealth´ proteins (e.g. apolipoprotein J known as clusterin)[31] are necessary to reduce non-specific cellular uptake[32].

Therefore, we investigated the protein corona pattern of the here presented PS-$PEG_{NC}$ after incubation with untreated or heat inactivated human serum or plasma (Figure 2.1). As visualized by SDS PAGE there was a pronounced change in the corona pattern, if nanoparticles were incubated with heat inactivated serum compared to untreated serum (Figure 2.1). A detailed proteomic investigation was carried out and highlighted the distinct variations in the hard corona pattern. Clusterin was the major protein identified after incubation with untreated serum or plasma (> 50%). Next to this, apolipoprotein AI contributed to 15% (Figure 2.1). This is in line with previous reports, which reported the specific interaction of PEGylated nanocarries and clusterin[33] and a strong enrichment of lipoproteins in the protein corona[34].

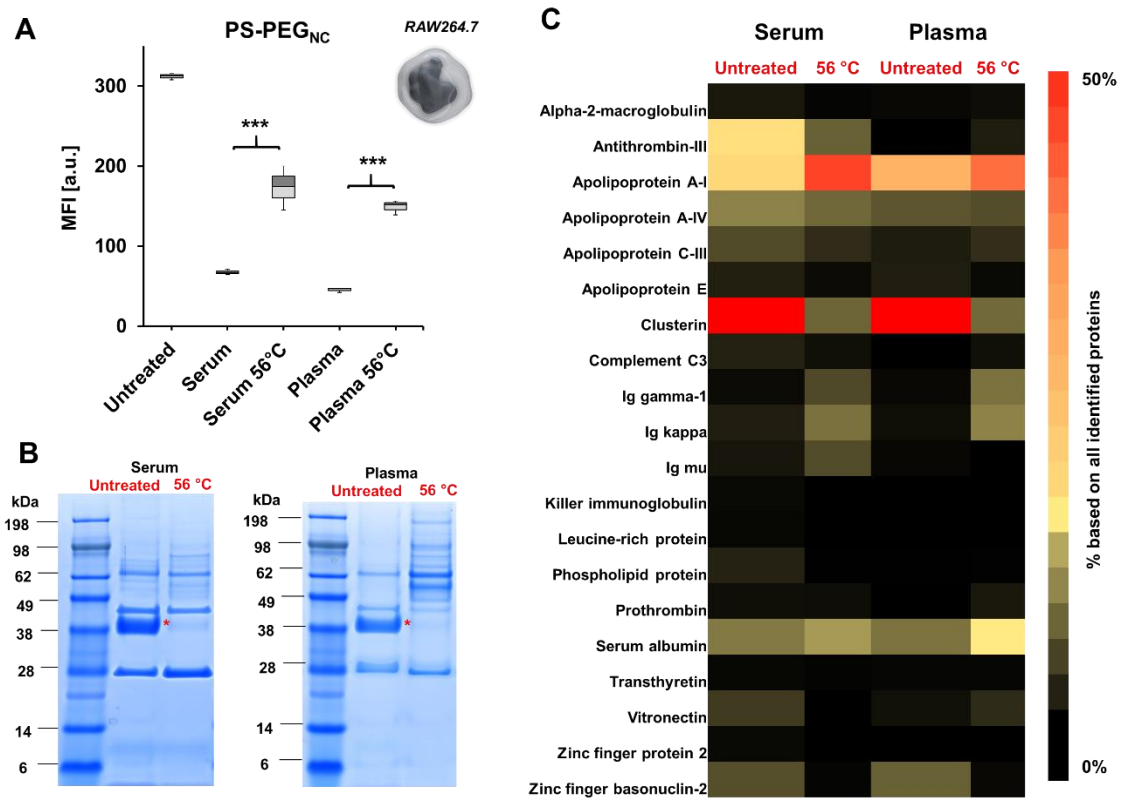


**Figure 2. 1.** Heat inactivation of human serum or plasma detrimentally affects cellular uptake and protein corona formation. **A)** The macrophage cell line RAW 264.7 was treated with nanoparticles (75 µg/mL) for 2 h, 37 °C. Non-covalently functionalized PEGylated polystyrene nanoparticles (PS-PEG$_{NC}$) were incubated with untreated or heat treated (56 °C, 30 min) human serum/plasma before cellular uptake experiments. The median fluorescence intensity (MFI) is shown from three independent replicates. The protein corona composition was visualized by SDS PAGE **(B)** and quantitatively analyzed by label free liquid chromatorgraphy mass spectrometry (LC-MS) **(C).** The most abundant proteins (TOP 25) are summarized in the heat map in order to highlight the major protein variations. The clusterin band (marked with a red star, B) appears under reducing conditions at a molecular weight of 38 kDa. $p < 0.05$*, $p< 0.01$** , $p<0.001$***

In strong contrast to this, we detected only minor amounts of clusterin in the corona after incubation with heat inactive serum or plasma (< 1%). Interestingly, the amounts of ApoAI remained high (Figure 2.1). In addition, we did not observe a significant difference in the absolute amount of proteins adsorbed to nanoparticles after incubation with untreated or heat inactive serum. This underlines that the distinct protein corona composition actually mediates the cellular interactions. Therefore, the increased cellular uptake after incubation with heat inactivated serum or plasma is a result of the altered protein corona composition, meaning that due to lower amounts of clusterin, cellular uptake is significantly increased.

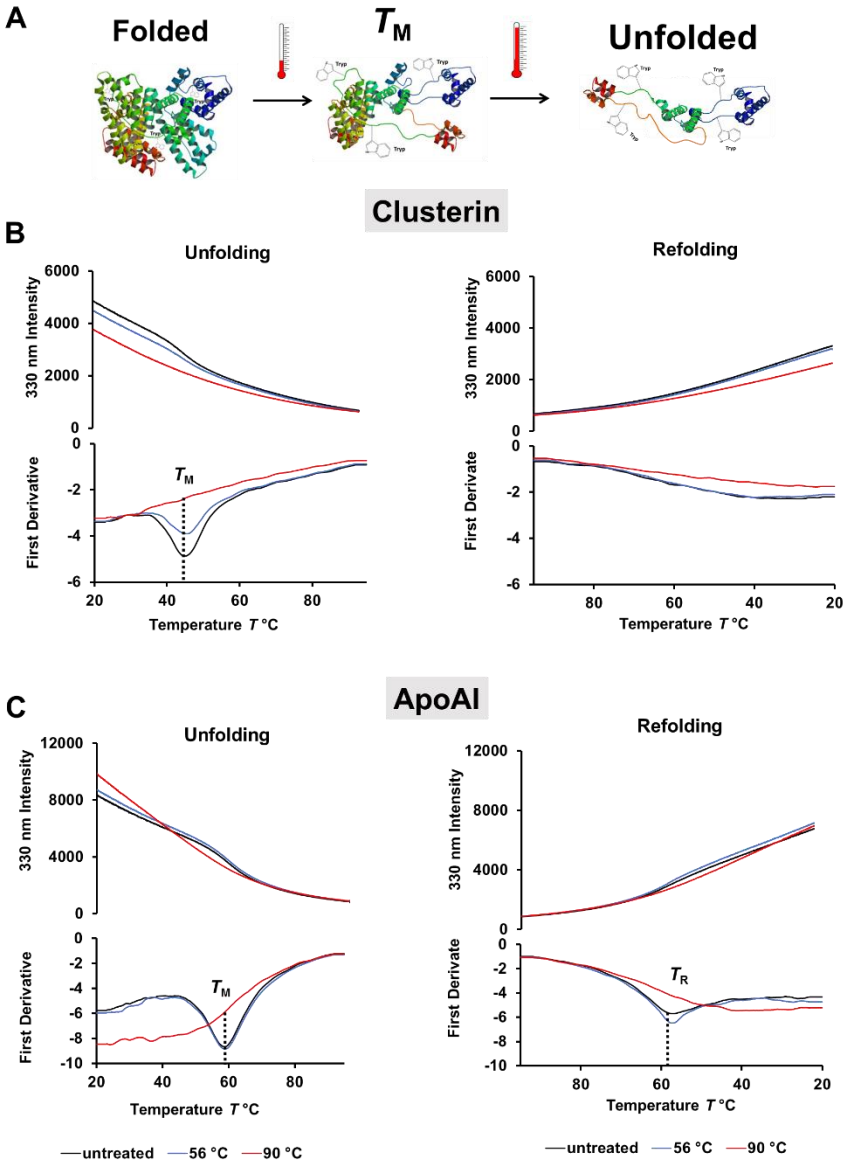


D

| | Clusterin | ApoAl |
|---|---|---|
| Melting point $T_M$ | 46.4 ± 1.3 °C | 58.2 ± 0.5 °C |
| Refolding $T_R$ | No | 57.1 °C |
| Heat inactivation 56 °C | ~ 40% unfolded | No effect |

**Figure 2. 2.** Clusterin is a heat-sensitive protein and readily unfolds. Differential scanning fluorimetry (nanoDSF) was used to monitor protein folding upon heating. **A)** Schematic illustration of the unfolding process and exposure of tryptophan residues. The melting temperature $T_M$ is defined as the point where the protein is 50% unfolded. **B)** Unfolding and refolding curves of clusterin. The fluorescence intensity at 330 nm and the corresponding first derivative are shown. The melting temperature $T_M$ is determined from the minimum of the first derivate. **C)** Monitoring the unfolding and refolding of ApoAI. **D)** Protein structure properties of clusterin and ApoAI as determined by nanoDSF. [redacted]

Along with the corona composition, the structure of proteins surrounding the nanoparticle is known to influence cellular uptake[35]. Interaction of proteins with nanoparticles can cause conformational changes in the protein structure, leading to an protein unfolding and subsequently causing surface exposure of unknown epitopes[36]. Additionally, temperature changes induce unfolding and denaturation of certain proteins[37].

With label-free differential scanning fluorimetry (nanoDSF), it is possible to study the unfolding process of proteins upon heating (Figure 2.2)[38]. The fluorescence intensity of tryptophan or tyrosine residues in a protein strongly depends on the structure of the proteins and therefore changes through temperature induced denaturation[39]. In those experiments the characteristic melting point $T_M$ of a protein is defined at a specific temperature, which is needed to unfold 50% of the protein. To explore the difference in protein corona composition when exposed to heat, the unfolding and refolding behavior of ApoAI and clusterin was investigated with nanoDSF (Figure 2.2). Here, it was found that clusterin had a significantly lower $T_M$ ~ 47 °C as compared to ApoAI $T_M$ ~ 59 °C (Figure 2.2). In addition, rarely observed for proteins, ApoAI was able to refold upon cooling in contrast to clusterin. At the heat inactivation temperature of 56 °C we found that about 40% of clusterin was already unfolded whereas the structure of ApoAI was not affected yet (Figure 2.2). Circular dichroism measurements confirmed that the secondary structure of clusterin was significantly altered upon heating.

To further investigate the structural involvement in protein-nanoparticle interactions, PS-$PEG_{NC}$ were incubated with the native single proteins – clusterin and ApoAI. Additionally, proteins were heated up to 56 °C or 90 °C prior to incubation in order to investigate if temperature induced denaturation affects the binding efficiency towards the nanoparticles and cellular interactions (Figure 2.3). The absolute amount of clusterin and ApoAI adsorbed to PS-$PEG_{NC}$ was quantified via a Pierce Assay. Here, we found that heat treatment of the single proteins did not affect the total amount of adsorbed proteins (Figure 2.3). In addition to this, we carried out isothermal calorimetry measurements. Untreated or heat treated (90 °C) and therefore completely denatured clusterin was titrated onto PS-$PEG_{NC}$. Interstingly, there were no significant differences in the binding affinity and all other binding parameters of heat treated clusterin compared to untreated clusterin towards PS-$PEG_{NC}$ (Figure 2.3).

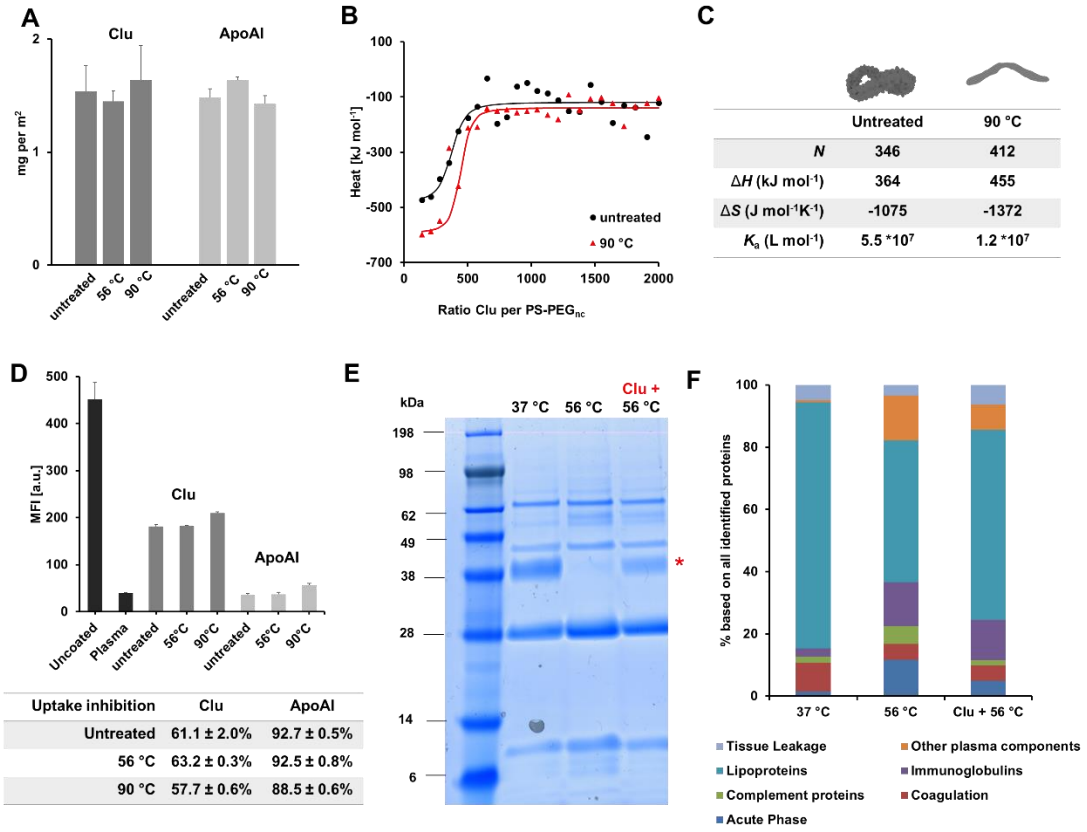


**Figure 2. 3.** Structural alteration of the singles protein did not affect the biological properties whereas in a complex protein mixture the protein structure mediates the adsorption. **A)** Clusterin and ApoAI were heat treated (56 °C or 90 °C for 30 min) and incubated with PS-PEG$_{nc}$ for 1 h. Unbound protein was removed via centrifugation/washing and the amount of protein adsorbed on the nanoparticle surface was determined via Pierce Assay. **B) + C)** Untreated or heat treated (90 °C) clusterin was titrated onto PS-PEG$_{nc}$ nanoparticles via isothermal titration calorimetry. The resulting integrated heats together with fits corresponding to an independent binding model are shown. In the table, parameters obtained by the fit procedure are given. [redacted] **D)** Cellular uptake of PS-PEG$_{NC}$ nanoparticles that were untreated and pre-treated with plasma, clusterin or ApoAI towards RAW 264.7 cells (75 µg/mL) was analyzed by flow cytometry. The median fluorescent intensity (MFI) of three independent measurements is shown. **E) + F)** Human serum was heated at 56 °C for 30 min. Native clusterin was further added to heat inactivated serum and the protein composition was analyzed via SDS PAGE **(E)** and LC-MS **(F).**

In order to investigate if the stealth properties of clusterin and ApoAI (meaning the ability to prevent interaction with phagocytic cells) are affected by structural alterations, cellular uptake of PS-PEG$_{NC}$ preincubated with native or heat treated ApoAI and clusterin towards macrophages was analyzed subsequently. It was found that pre-incubation with both proteins effectively reduced cellular uptake compared to uncoated nanoparticles (uptake inhibition ~

60%). On top of that, there was no difference whether proteins were heat treated or native (Figure 2.3). The nanoparticle behavior after incubation with the single proteins stands in strong contrast to incubation with the complex protein mixture (Figure 2.1). There, we showed that the interactions with untreated or heat treated serum and PEGylated nanocarriers strongly differed. We found that clusterin within the heat treated serum mixture was dramatically decreased in comparison to untreated serum.

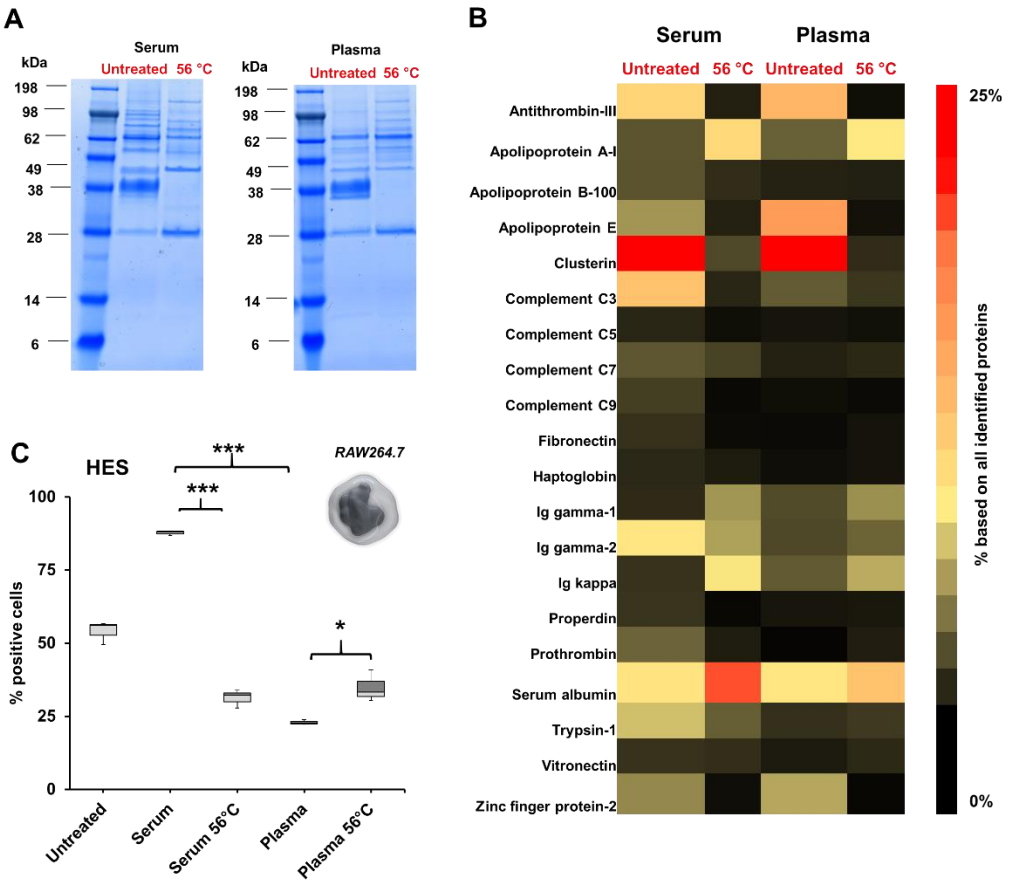


**Figure 2. 4.** Heat inactivation affects the adsorption behavior of complement proteins towards HES nanocapsules. **A)** The protein corona composition of HES nanocapsules was analyzed via SDS PAGE and LC-MS **(B).** There is an enrichment of complement proteins detected after incubation with human serum. Due to heat inactivation the adsorption of complement proteins is strongly diminished **C)** Cellular uptake of HES nanocapsules (75 µg/mL, 2 h) towards RAW264.7 cells after incubation with human serum or plasma. The amount of fluorescent positive cells (%) is shown for three independent replicates. $p < 0.05$*, $p < 0.01$**, $p < 0.001$***

To understand the structural involvement, which mediates the corona composition, serum was heat inactivated and native (untreated) clusterin was re-added to the protein mixture (Figure 2.3). The protein pattern was visualized by SDS PAGE and quantitatively analyzed by LC-MS

(Figure 2.3). We found that native clusterin, which was re-added to heat inactivated serum adsorbed to PS-$PEG_{NC}$ (clusterin band marked with a red star). This proves that in a complex protein mixture the protein structure critically determines the adsorption behavior, which eventually affects the cellular outcome.

To further reveal the influence of protein structure on corona formation, additional experiments were performed with a broad variety of different nanoparticle systems (supplementary information 2). Here, we chose covalently PEGylated PS-NPs (PS-$PEG_C$), carboxy- or amino-functionalized PS-NPs (PS-COOH and PS-$NH_2$) as well as biodegradable hydroxyethyl starch nanocapsules (HES; Figure 2.4). All nanoparticles were incubated with untreated or heat treated serum and plasma. As shown for PS-$PEG_{NC}$ there was a significant difference, if particles were incubated with untreated serum/plasma in comparison to the heat treated protein source (Figure 2.4).

Proteomic analysis highlighted the major differences in the corona composition for HES nanocapsules incubated with the respective protein source (Figure 2.4). As shown above the adsorption of clusterin was prevented when HES nanocapsules were incubated with heat inactive serum or plasma. While complement was not a prominent protein of the protein coronas in the experiments mentioned above, we found here that the corona of serum incubated nanocapsules was enriched with complement C3 (~ 6.8%). Interestingly, after heat treatment of serum, the amount of complement C3 was strongly decreased (~ 0.8%).

As widely reported complement proteins are heat-labile and undergo structural changes at 56 °C[25, 40]. This underlines that due to the structural alterations of the complement proteins the interactions with the nanoparticles are prevented (Figure 2.4). In addition, we found major differences in the corona pattern for serum compared to plasma (Figure 2.4). As already reported in literature, the protein source can influence corona formation[21-22]. For the here investigated HES nanocapsules the overall amount of complement proteins for human serum compared to human plasma differed strongly.

Complement proteins require calcium to maintain their native structure and function[41]. Citrate, which was used as anticoagulant for plasma generation in this study, specifically binds calcium[42]. This suggests that the structure of the complement proteins within human plasma is different compared to human serum, which eventually affects protein-nanoparticles interactions.

Additionally, cellular uptake studies of HES nanocapsules coated with serum or plasma (untreated vs. heat treated) linked the distinct role of the corona composition and cellular

interactions. Serum incubation strongly enhanced cellular uptake, which is mainly attributed to the involvement of complement proteins. Due to heat inactivation of serum or plasma incubation the overall amount of complement proteins was strongly decreased, which resulted in decreased cellular interactions. Heat inactivation of plasma slightly increased cellular uptake compared to untreated plasma ($p < 0.05$*). This is probably attributed to the lower amount of clusterin in the corona after heat inactivation, which is comparable to the results presented for PS-$PEG_{NC}$.

## Conclusion

Here, we showed that heat inactivation of serum or plasma critically affects cellular uptake and protein corona formation. We saw that the protein structure is the key factor, which mediates the adsorption process. Clusterin and complement proteins were identified as heat-labile proteins, which readily undergo temperature induced structural changes. Therefore, in a complex protein environment, the bound amount of the denatured proteins towards the nanoparticles was significantly decreased. Overall, the present study reveals the major role of the protein structure that needs to be considered in order to evaluate protein corona formation.

## Supplementary information

**Table 2. 1.** Physico-chemical properties of all investigated nanoparticle systems. [redacted]

| | **Diameter (nm)** | **Zeta Potential (mV)** |
|---|---|---|
| **PS-$PEG_{NC}$** | 120 ± 12 nm | - 6.7 mV |
| **HES** | 220 ± 22 nm | -19 mV |
| **PS-$PEG_{C}$** | 128 ± 12 nm | + 18.4 mV |
| **PS-COOH** | 116 ± 11 nm | - 7.2 mV |
| **PS-$NH_2$** | 126 ± 12 nm | + 7.6 mV |

**Table 2. 2.** Protein quantification of the absolute amount of protein bound to PS-PEG$_{NC}$ after incubation in the respective protein source via Pierce Assay. Values are given in mg per m$^2$ nanoparticles surface area.

| **PS-PEG$_{NC}$** | **Untreated** | **Heat inactivated** |
|---|---|---|
| Serum | 1.18 ± 0.04 mg/m$^2$ | 0.96 ± 0.03 mg/m$^2$ |
| Plasma | 1.04 ± 0.10 mg/m$^2$ | 1.51 ± 0.08 mg/m$^2$ |

**Table 2. 3.** Protein quantification of the absolute amount of protein bound to HES nanocapsules after incubation in the respective protein source via Pierce Assay. Values are given in mg per m$^2$ nanoparticles surface area.

| **HES** | **Untreated** | **Heat inactivated** |
|---|---|---|
| Serum | 0.53 ± 0.10 mg/m$^2$ | 0.49 ± 0.01 mg/m$^2$ |
| Plasma | 0.52 ± 0.12 mg/m$^2$ | 0.65 ± 0.04 mg/m$^2$ |

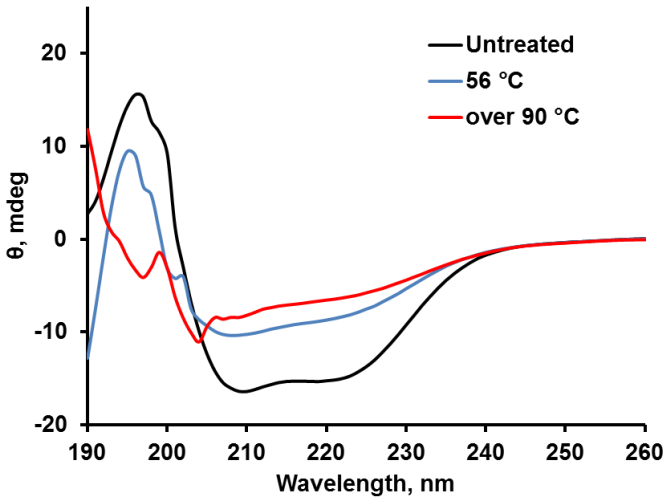


**Figure 2. 5.** CD spectra of untreated and heat treated clusterin. [redacted]Ghazaryan]

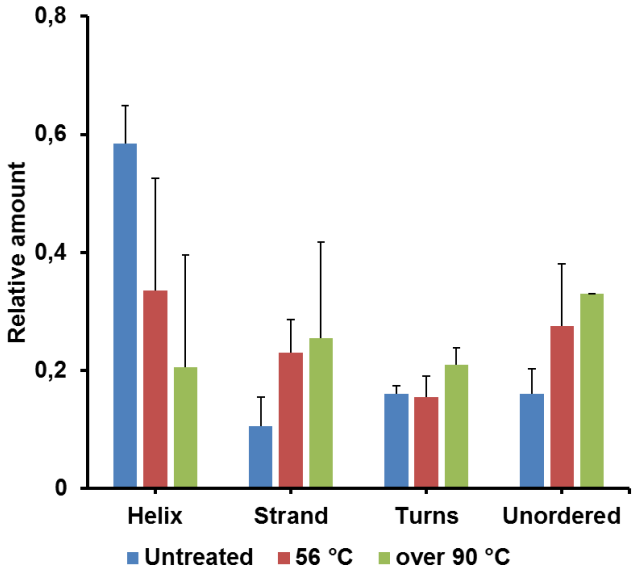


**Figure 2. 6.** Calculation of the structural alterations after heat treatment of clusterin using DichroWeb. [redacted] Ghazaryan)

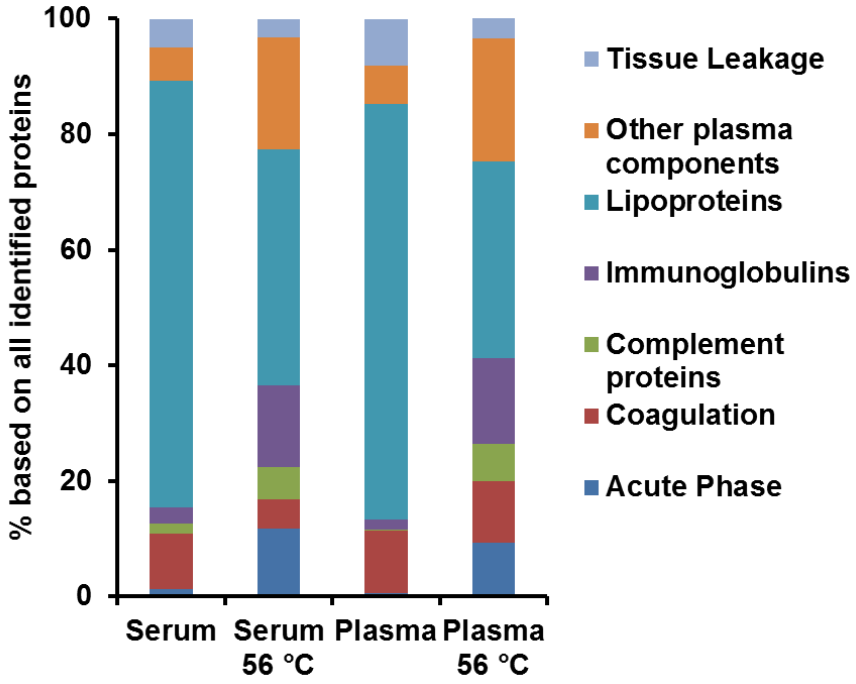


**Figure 2. 7.** Protein corona analysis of PS-PEG$_{NC}$. All identified proteins were classified into seven different classed based on their biological properties.

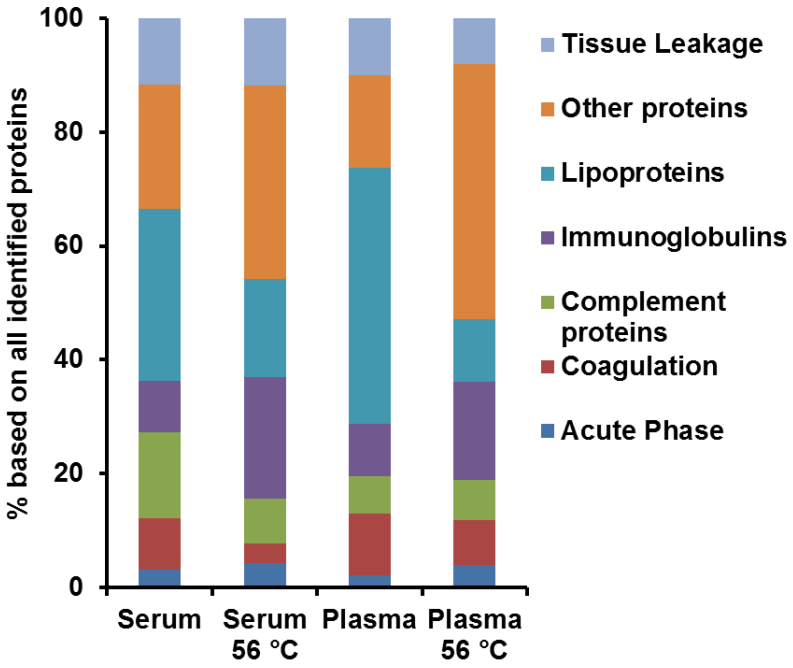


**Figure 2. 8.** Protein corona analysis of HES nanocapsules. All identified proteins were classified into seven different classed based on their biological properties.

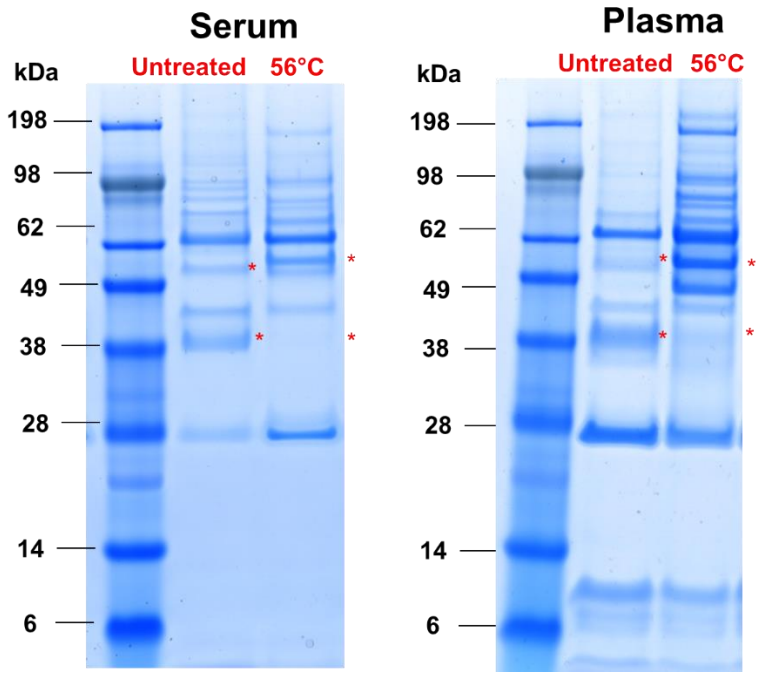


**Figure 2. 9.** Protein corona analysis of PS-PEG$_C$ visualized by SDS PAGE. Significant differences depending on the protein source are marked with a red star.

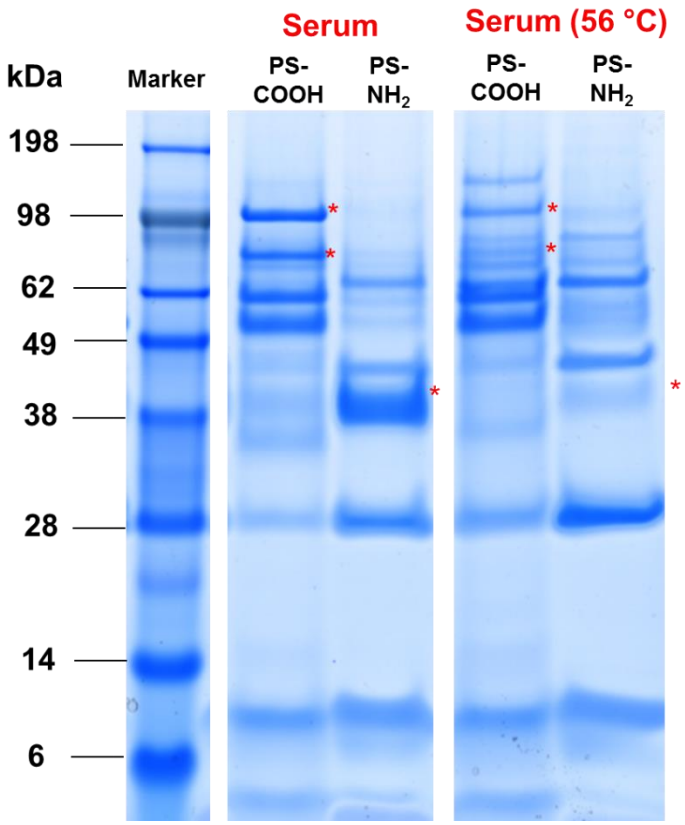


**Figure 2. 10.** Protein corona analysis of functionalized PS-NP (PS-COOH and PS-$NH_2$) visualized by SDS PAGE. Significant differences depending on the protein source are marked with a red star.

## Literature

1. Xu, X.; Ho, W.; Zhang, X.; Bertrand, N.; Farokhzad, O., Cancer nanomedicine: from targeted delivery to combination therapy. *Trends in molecular medicine* **2015,** *21* (4), 223-232.

2. Richards, D. A.; Maruani, A.; Chudasama, V., Antibody fragments as nanoparticle targeting ligands: a step in the right direction. *Chemical science* **2017,** *8* (1), 63-77.

3. Sun, S.-B.; Liu, P.; Shao, F.-M.; Miao, Q.-L., Formulation and evaluation of PLGA nanoparticles loaded capecitabine for prostate cancer. *International journal of clinical and experimental medicine* **2015,** *8* (10), 19670.

4. Rodzinski, A.; Guduru, R.; Liang, P.; Hadjikhani, A.; Stewart, T.; Stimphil, E.; Runowicz, C.; Cote, R.; Altman, N.; Datar, R., Targeted and controlled anticancer drug delivery and release with magnetoelectric nanoparticles. *Scientific reports* **2016,** *6*, 20867.

5. Yu, X.; Trase, I.; Ren, M.; Duval, K.; Guo, X.; Chen, Z., Design of nanoparticle-based carriers for targeted drug delivery. *Journal of nanomaterials* **2016,** *2016*.

6. Bobo, D.; Robinson, K. J.; Islam, J.; Thurecht, K. J.; Corrie, S. R., Nanoparticle-based medicines: a review of FDA-approved materials and clinical trials to date. *Pharmaceutical research* **2016,** *33* (10), 2373-2387.

7. Polo, E.; Collado, M.; Pelaz, B.; del Pino, P., Advances toward more efficient targeted delivery of nanoparticles in vivo: understanding interactions between nanoparticles and cells. *ACS nano* **2017,** *11* (3), 2397-2402.

8. Caracciolo, G.; Farokhzad, O. C.; Mahmoudi, M., Biological identity of nanoparticles in vivo: clinical implications of the protein corona. *Trends in biotechnology* **2017,** *35* (3), 257-264.

9. Ke, P. C.; Lin, S.; Parak, W. J.; Davis, T. P.; Caruso, F., A Decade of the Protein Corona. *ACS nano* **2017,** *11* (12), 11773-11776.

10. Cedervall, T.; Lynch, I.; Lindman, S.; Berggard, T.; Thulin, E.; Nilsson, H.; Dawson, K. A.; Linse, S., Understanding the nanoparticle-protein corona using methods to quantify exchange rates and affinities of proteins for nanoparticles. *Proc Natl Acad Sci U S A* **2007,** *104* (7), 2050-5.

11. Lynch, I.; Salvati, A.; Dawson, K. A., Protein-nanoparticle interactions: What does the cell see? *Nat Nanotechnol* **2009,** *4* (9), 546-7.

12. Monopoli, M. P.; Aberg, C.; Salvati, A.; Dawson, K. A., Biomolecular coronas provide the biological identity of nanosized materials. *Nature Nanotech.* **2012,** *7* (12), 779-86.

13. Tenzer, S.; Docter, D.; Rosfa, S.; Wlodarski, A.; Kuharev, J.; Rekik, A.; Knauer, S. K.; Bantz, C.; Nawroth, T.; Bier, C.; Sirirattanapan, J.; Mann, W.; Treuel, L.; Zellner, R.; Maskos, M.; Schild, H.; Stauber, R. H., Nanoparticle Size Is a Critical Physicochemical Determinant of the Human Blood Plasma Corona: A Comprehensive Quantitative Proteomic Analysis. *ACS Nano* **2011,** *5* (9), 7155-7167.

14. Li, Y.; Monteiro-Riviere, N. A., Mechanisms of cell uptake, inflammatory potential and protein corona effects with gold nanoparticles. *Nanomedicine* **2016,** *11* (24), 3185-3203.

15. Landgraf, L.; Christner, C.; Storck, W.; Schick, I.; Krumbein, I.; Dähring, H.; Haedicke, K.; Heinz-Herrmann, K.; Teichgräber, U.; Reichenbach, J. R., A plasma protein corona enhances the biocompatibility of Au@ Fe3O4 Janus particles. *Biomaterials* **2015,** *68*, 77-88.

16. Chinen, A. B.; Guan, C. M.; Ko, C. H.; Mirkin, C. A., The Impact of Protein Corona Formation on the Macrophage Cellular Uptake and Biodistribution of Spherical Nucleic Acids. *Small* **2017,** *13* (16).

17. Mirshafiee, V.; Mahmoudi, M.; Lou, K.; Cheng, J.; Kraft, M. L., Protein corona significantly reduces active targeting yield. *Chem. Commun.* **2013,** *49* (25), 2557-2559.

18. Salvati, A.; Pitek, A. S.; Monopoli, M. P.; Prapainop, K.; Bombelli, F. B.; Hristov, D. R.; Kelly, P. M.; Åberg, C.; Mahon, E.; Dawson, K. A., Transferrin-functionalized nanoparticles lose their targeting capabilities when a biomolecule corona adsorbs on the surface. *Nature Nanotech.* **2013,** *8* (2), 137-143.

19. Jain, P.; Pawar, R.; Pandey, R.; Madan, J.; Pawar, S.; Lakshmi, P.; Sudheesh, M., In-vitro in-vivo correlation (IVIVC) in nanomedicine: Is protein corona the missing link? *Biotechnology advances* **2017,** *35* (7), 889-904.

20. Arora, M., Cell Culture Media: A Review. *Materials and Methods* **2017**.

21. Mirshafiee, V.; Kim, R.; Mahmoudi, M.; Kraft, M. L., The importance of selecting a proper biological milieu for protein corona analysis in vitro: Human plasma versus human serum. *The international journal of biochemistry & cell biology* **2016,** *75*, 188-195.

22. Schöttler, S.; Klein, K.; Landfester, K.; Mailänder, V., Protein source and choice of anticoagulant decisively affect nanoparticle protein corona and cellular uptake. *Nanoscale* **2016,** *8* (10), 5526-5536.

23. Cancado, E.; Vilas-Boas, L. S.; Abrantes-Lemos, C. P.; Novo, N. F.; Porta, G.; Da Silva, L. C.; Laudanna, A. A., Heat serum inactivation as a mandatory procedure for antiactin antibody detection in cell culture. *Hepatology* **1996,** *23* (5), 1098-1104.

24. Soltis, R.; Hasz, D.; Morris, M.; Wilson, I., The effect of heat inactivation of serum on aggregation of immunoglobulins. *Immunology* **1979,** *36* (1), 37.

25. Soltis, R.; Hasz, D.; Morris, M.; Wilson, I., Studies on the nature of heat-labile anti-complementary activity in normal human serum. *Clinical and experimental immunology* **1979,** *37* (2), 310.

26. Shen, L.; Tenzer, S.; Storck, W.; Hobernik, D.; Raker, V. K.; Fischer, K.; Decker, S.; Dzionek, A.; Krauthauser, S.; Diken, M.; Nikolaev, A.; Maxeiner, J.; Schuster, P.; Kappel, C.; Verschoor, A.; Schild, H.; Grabbe, S.; Bros, M., Protein corona-mediated targeting of nano-carriers to B cells allows redirection of allergic immune responses. *J Allergy Clin Immunol* **2018**.

27. Chen, F.; Wang, G.; Griffin, J. I.; Brenneman, B.; Banda, N. K.; Holers, V. M.; Backos, D. S.; Wu, L.; Moghimi, S. M.; Simberg, D., Complement proteins bind to nanoparticle protein corona and undergo dynamic exchange in vivo. *Nature nanotechnology* **2017,** *12* (4), 387.

28. Gustafson, H. H.; Holt-Casper, D.; Grainger, D. W.; Ghandehari, H., Nanoparticle uptake: the phagocyte problem. *Nano today* **2015,** *10* (4), 487-510.

29. Schöttler, S.; Becker, G.; Winzen, S.; Steinbach, T.; Mohr, K.; Landfester, K.; Mailänder, V.; Wurm, F. R., Protein adsorption is required for stealth effect of poly (ethylene glycol)-and poly (phosphoester)-coated nanocarriers. *Nature nanotechnology* **2016,** *11* (4), 372.

30. Gref, R.; Lück, M.; Quellec, P.; Marchand, M.; Dellacherie, E.; Harnisch, S.; Blunk, T.; Müller, R., 'Stealth'corona-core nanoparticles surface modified by polyethylene glycol (PEG): influences of the corona (PEG chain length and surface density) and of the core composition on phagocytic uptake and plasma protein adsorption. *Colloids and Surfaces B: Biointerfaces* **2000,** *18* (3-4), 301-313.

31. Aoyama, M.; Hata, K.; Higashisaka, K.; Nagano, K.; Yoshioka, Y.; Tsutsumi, Y., Clusterin in the protein corona plays a key role in the stealth effect of nanoparticles against phagocytes. *Biochemical and biophysical research communications* **2016,** *480* (4), 690-695.

32. Kokkinopoulou, M.; Simon, J.; Landfester, K.; Mailänder, V.; Lieberwirth, I., Visualization of the protein corona: towards a biomolecular understanding of nanoparticle-cell-interactions. *Nanoscale* **2017,** *9* (25), 8858-8870.

33. Müller, J.; Bauer, K. N.; Prozeller, D.; Simon, J.; Mailänder, V.; Wurm, F. R.; Winzen, S.; Landfester, K., Coating nanoparticles with tunable surfactants facilitates control over the protein corona. *Biomaterials* **2017,** *115*, 1-8.

34. Bertrand, N.; Grenier, P.; Mahmoudi, M.; Lima, E. M.; Appel, E. A.; Dormont, F.; Lim, J.-M.; Karnik, R.; Langer, R.; Farokhzad, O. C., Mechanistic understanding of in vivo protein corona formation on polymeric nanoparticles and impact on pharmacokinetics. *Nature communications* **2017,** *8* (1), 777.

35. Fleischer, C. C.; Payne, C. K., Secondary structure of corona proteins determines the cell surface receptors used by nanoparticles. *The Journal of Physical Chemistry B* **2014,** *118* (49), 14017-14026.

36. Kim, Y.; Ko, S. M.; Nam, J. M., Protein–Nanoparticle Interaction-Induced Changes in Protein Structure and Aggregation. *Chemistry–An Asian Journal* **2016,** *11* (13), 1869-1877.

37. Tsai, A. M.; van Zanten, J. H.; Betenbaugh, M. J., I. Study of protein aggregation due to heat denaturation: a structural approach using circular dichroism spectroscopy, nuclear magnetic resonance, and static light scattering. *Biotechnology and bioengineering* **1998,** *59* (3), 273-280.

38. Strutz, W., Exploring Protein Stability by NanoDSF. *Biophysical Journal* **2016,** *110* (3), 393a.

39. Chaudhuri, R.; Cheng, Y.; Middaugh, C. R.; Volkin, D. B., High-throughput biophysical analysis of protein therapeutics to examine interrelationships between aggregate formation and conformational stability. *The AAPS journal* **2014,** *16* (1), 48-64.

40. Hamsten, C.; Skattum, L.; Truedsson, L.; von Döbeln, U.; Uhlén, M.; Schwenk, J. M.; Hammarström, L.; Nilsson, P.; Neiman, M., Heat differentiated complement factor profiling. *Journal of proteomics* **2015,** *126*, 155-162.

41. Snyderman, R.; Pike, M. C., Interaction of complex polysaccharides with the complement system: effect of calcium depletion on terminal component consumption. *Infection and immunity* **1975,** *11* (2), 273-279.

42. Mann, K.; Whelihan, M.; Butenas, S.; Orfeo, T., Citrate anticoagulation and the dynamics of thrombin generation. *Journal of Thrombosis and Haemostasis* **2007,** *5* (10), 2055-2061.

43. Landfester, K., Synthesis of colloidal particles in miniemulsions. *Annual Review of Materials Research* **2006,** *36* (1), 231-279.

44. Kokkinopoulou, M.; Simon, J.; Landfester, K.; Mailänder, V.; Lieberwirth, I., Visualization of the Protein Corona: towards a biomolecular understanding of nanoparticle-cell-interactions. *Nanoscale* **2017**.

45. García-Moreno, I.; Costela, A.; Campo, L., 8-Phenyl-Substituted Dipyrromethene·BF2 Complexes as Highly Efficient and Photostable Laser Dyes. *J. Phys. Chem. A* **2004,** *108* (16), 3315-3323.

46. Baier, G.; Baumann, D.; Siebert, J. r. M.; Musyanovych, A.; Mailänder, V.; Landfester, K., Suppressing unspecific cell uptake for targeted delivery using hydroxyethyl starch nanocapsules. *Biomacromolecules* **2012,** *13* (9), 2704-2715.

47. Hofmann, D.; Tenzer, S.; Bannwarth, M. B.; Messerschmidt, C.; Glaser, S.-F.; Schild, H.; Landfester, K.; Mailänder, V., Mass Spectrometry and Imaging Analysis of Nanoparticle-Containing Vesicles Provide a Mechanistic Insight into Cellular Trafficking. *ACS Nano* **2014,** *8* (10), 10077-10088.

48. Tenzer, S., Nanoparticle size is a critical physicochemical determinant of the human blood plasma corona: a comprehensive quantitative proteomic analysis. *ACS Nano* **2011,** *5*, 7155-7167.

49. Bradshaw, R. A.; Burlingame, A. L.; Carr, S.; Aebersold, R., Reporting protein identification data: the next generation of guidelines. *Mol Cell Proteomics* **2006,** *5* (5), 787-8.

50. Müller, L. K.; Simon, J.; Schöttler, S.; Landfester, K.; Mailänder, V.; Mohr, K., Pre-coating with protein fractions inhibits nano-carrier aggregation in human blood plasma. *RSC Advances* **2016,** *6* (99), 96495-96509.

51. Winzen, S.; Schoettler, S.; Baier, G.; Rosenauer, C.; Mailaender, V.; Landfester, K.; Mohr, K., Complementary analysis of the hard and soft protein corona: sample preparation critically effects corona composition. *Nanoscale* **2015,** *7* (7), 2992-3001.

# 3. The transferability from animal models to humans: challenges regarding aggregation and protein corona formation of nanoparticles

## Aim:

Clinical trials are the final step before nanoparticles can reach medical applications. Therefore, it is of great importance to investigate the influence of the interspecies protein composition (mouse vs. human). In this study, it was shown that there is a severe discrepancy between protein corona formation and aggregation behavior depending on the protein source. This knowledge is needed in order to evaluate whether results obtained from *in vivo* animal models are suitable to estimate the behavior of nanoparticles in clinical trials.

## Contribution:

I carried out the protein corona analysis (SDS-PAGE, LC-MS, Pierce Assay) and conducted the cellular uptake experiments (flow cytometry). [redacted] performed the DLS analysis. [redacted] supported the DLS analysis. The project was supervised by [redacted]

## Copyright:

## Abstract

Nanomaterials are interesting candidates for applications in medicine as drug delivery or diagnostic agents. For a safe application, they have to be evaluated *in vitro* and *in vivo* models to finally be translated to human clinical trials. However, often, those transfer processes fail and it is not completely understood whether *in vitro* models leading to these animal models can reliably be compared to the situation in humans. Especially, the interaction of nanomaterials with components from different blood plasma sources is difficult to compare and the outcomes of those interactions with respect to body distribution and cell uptake are unclear. Therefore, we investigated the interactions of differently functionalized polymeric and inorganic nanoparticles with human, mouse, rabbit and sheep plasma. The focus was put on the determination of aggregation events of the nanoparticles occurring in concentrated plasma and the correlation with the respectively formed protein coronas. Both the stability in plasma as well as the types of adsorbed proteins were found to strongly depend on the plasma source. Thus, we suggest evaluating the potential use of nanocarriers always in the plasma source of the chosen animal model for *in vitro* studies as well as in human plasma to pin down differences and eventually enable the transfer into clinical trials in humans.

## Introduction

The development of nanomaterials for biomedical applications has become of great interest in the last decades.[1] Especially when it comes to cancer treatment,[2] the encapsulation of drugs into nano-sized carriers is very attractive, since the so far used chemotherapeutics cause several cytotoxic side effects. The encapsulation of drugs offers the opportunity of targeting to the desired cells/tissue and by this increasing the mentioned specificity. The loading of drugs into nanomaterials protects the drug itself from degradation. A variety of nano-particular systems have been investigated for cancer therapy. They include polymeric nanoparticles,[3] liposomes,[4-5] metallic core nanoparticles,[6-7] dendrimers,[8] polymeric micelles[9-11] and viral nanoparticles.[12]

The evaluation processes a nanomaterial has to undergo prior to becoming an accepted pharmacy-medication is very time consuming and includes several critical steps. Animal models are often used in order to evaluate the potential nanomaterial prior to clinical trials with humans. These animal tests are even required before exposure to humans.[13] Nevertheless, the transfer from *in vivo* to humans bears several challenges and limitations.[14-15] Mak *et al.*

refer to that problem as “Lost in translation”.[16] Mouse models are the most commonly used one for testing drug candidates prior to clinical trials.[17] However, it has become clear that biological responses to certain treatments are not necessarily transferable from murine models to larger animals and finally to humans.

Concerning the application of nanocarriers as drug delivery systems the most critical assessment step prior to the evaluation of the pharmacological effect is the behavior in biological fluids. Most nanocarriers systems are being developed for intravenous injection, so that their first contact with biological material is the blood plasma. In that environment nanocarriers will rapidly get coated by physically adsorbed proteins and other biomolecules forming the ‘protein’ or ‘biomolecular corona’.[18-22] This new interface being seen by the body can result in different undesired responses like aggregation of nanocarriers, their rapid clearance from the blood stream by unspecific cell uptake or inflammation reactions of the body.[23-24] Therefore, there is an urgent need to understand protein corona formation[25] in order to develop nanomaterials for clinical application.[26] The physico-chemical properties[27] of the nanomaterial (e.g. size, shape, charge, surface functionalization and hydrophilicity) strongly affect protein corona formation.[28-30] Next to this, the protein source itself, which is used for *in vitro* studies (being either serum or plasma containing different anticoagulants) determines the protein composition.[31] Importantly, those corona differences were found to highly influence cellular uptake processes.[32-33] Apart from that Hajipour *et al.* could show that the corona pattern is altered for patients with different diseases due to a ´personalized plasma composition´. [34-35]

In previous studies[36] we found a direct connection between the aggregation behavior of nanoparticles in biological fluid and their *in vivo* biodistribution. Key proteins were identified which contribute to aggregation formation and hereby affecting cellular interactions.

Based on this we investigated the aggregation processes occurring for different nanomaterials in plasma from different animal sources and correlated those effects with the composition of the protein coronas formed. First, we investigated the differences in blood plasma composition between human, mouse, rabbit and sheep plasma. To mimic *in vivo* condition, we next tested the stability against aggregation of different nanoparticles using dynamic light scattering (DLS) in concentrated plasma. Lastly, the protein corona composition of the respective nanomaterials was determined by SDS-PAGE as well as liquid chromatography-mass spectrometry (LC-MS).

## Materials and Methods

**Materials.** Dulbecco´s phosphate buffered saline (DPBS) without calcium and magnesium was purchased from Gibco/life technologies, Germany. Magnetite nanoparticles coated with dextran (BNF-Dextran-redF) and hydroxyethyl starch (BNF-Starch-redF) were obtained by MicroMod, Germany with a solid content of 10 mg/mL and a magnetic core of 75-80% (w/w) as given by the manufacturer. BNF particles were prepared via a core shell method as described as described in literature[45-46]. Rabbit, sheep and mouse plasma were purchased from GeneTex, distributed by Biozol, Germany. In all cases, citrate was added as anti-coagulant. The protein concentration for all plasma pools was 60-70 mg/mL. Human citrate plasma, pooled from six donors, was obtained from the Blood Transfusion Center at the University Clinic of Mainz/Germany according to standard ethical guidelines and stored in aliquots at -80 °C before use. Mouse, rabbit and sheep plasma was pooled from 75-100 animals according to the manufacturer.

**Synthesis of polystyrene nanoparticles (PS-NPs).** A direct miniemulsion co-polymerization method according to previously published work was used to synthesize functionalized as well as non-functionalized polystyrene nanoparticles (NP).[47-48] Briefly, a total monomer amount of 6 g was used for each particle. In case of the non-functionalized NP this means 6 g styrene (Merck, Germany). For the functionalized particles, 5.88 g styrene and 0.12 g functionalized co-monomer were used. For the preparation of negatively charged polystyrene nanoparticles, acrylic acid (Sigma Aldrich, USA), 252 mg hexadecane (Sigma Aldrich) and 100 mg V59 (Wako chemicals, Japan) as initiator were added to a solution of 0.6 g Lutensol AT50 (BASF, Germany) in 24 mL water under vigorous stirring to prepare PS-COOH NPs. For the synthesis of positively charged polystyrene nanoparticles, 2-aminoethyl methacrylate hydrochloride (AEMH, Sigma Aldrich) was added to the water phase and combined with the disperse phase as described above to prepare PS-$NH_2$. After combining water and disperse phase, each preparation was stirred for one hour and the emulsions afterwards sonicated for two minutes at 90% intensity (Branson Sonifier, 1/2” tip, 450 W). After polymerization at 72 °C for 12 h, the NPs were purified by centrifugation and redispersion in water three times (17,572 g for 3-4 h). For cellular uptake studies nanoparticles were additionally copolymerized with BODIPY (523/535 nm) as previously described.[41]

**Particle charge detection (PCD).** The amount of amine or carboxyl groups on the particle surface was calculated from titration performed on a particle charge detector PCD 02 (Mütek GmbH, Germany) combined with a Titrino Automatic Titrator 702 SM (Metrohm AG, Switzerland). Carboxyl groups were titrated against positively charged poly(diallyl dimethyl

ammonium chloride) (PDADAMC) while amino groups were titrated against negatively charged polyelectrolyte standard sodium poly(ethylene sulfonate) (PES-Na). 10 mL of the dispersion under investigation with a solid content of 1 g/L in deionized water were titrated.

**Transmission electron microscopy (TEM).** Electron micrographs were taken on an Ultrascan 1000 (Gatan) charge-coupled device (CCD) camera operated at 200 kV. Images were collected using the Digital Micrograph software (Gatan). Nanoparticle dispersions in deionized water were used for sample preparation.

**Zeta potential measurements.** For determination of the zeta (ζ) potential of all nanoparticles a Malvern zetasizer nano series instrument was used. 20 µL of the respective dispersion was diluted in 2 mL 1mM KCl and filled into appropriate disposable folded capillary cells. For measurements of nanoparticles with a protein corona, the samples were prepared as described below, meaning that free plasma proteins were removed before the measurements.

**Protein corona preparation.** Each nanoparticle was incubated with blood plasma at a constant ratio of particle surface area to protein amount (0.05 $m^2$ particle surface area per 500 µL plasma) for one hour at 37 °C. Unbound proteins in the supernatant were separated from particles by centrifugation at 20 000 g for 30 min. The particle pellet was resuspended in PBS and washed by three centrifugation steps at 20 000 g for 30 min and subsequent redispersion in PBS.

**Dynamic light scattering (DLS).** All light scattering experiments were performed on a commercially available instrument from ALV GmbH, Germany consisting of an electronically controlled goniometer and an ALV-5000 multiple tau full-digital correlator. A HeNe laser with a wavelength of 632.8 nm and an output power of 25 mW (JDS Uniphase, USA, Type 1145P) was utilized as the light source. Concentrated plasma was filtered through Millex-GS 220 nm filters into cylindrical quartz cuvettes (18 mm inner diameter, Hellma, Germany). 1 µL of particle dispersion (1 wt% in PBS) were added without any filtering to avoid changes within the system under investigation.

**Pierce 660 nm Protein Quantification Assay.** The protein concentration of the different plasma sources or hard corona proteins was quantified using Pierce 660 nm protein Assay (Thermo Fisher, Germany) according to manufacturer's instruction and the absorption (660 nm) was measured by a Tecan infinite M1000 plate reader.

**SDS polyacrylamide gel electrophoresis (SDS-PAGE).** For SDS-PAGE 1.5 µg of each protein sample (in 6.5 µL MilliQ water) was mixed with 2.5 µL NuPAGE LDS sample buffer and

1 µL NuPAGE sample reducing agent and applied onto a NuPAGE 10% Bis Tris Protein gel (all Novex, Thermo Fisher Scientific, USA). The electrophoresis was carried out in NuPAGE MES SDS running buffer at 100 V for 2 h with a SeeBlue Plus2 Pre-Stained Standard (Invitrogen, USA) as a molecular marker. The gels were stained using the SilverQuest™ Silver Staining kit from ThermoFisher Scientific, USA and it was used as recommended by the manufacturer.

**Liquid chromatography-mass spectrometry (LC-MS).** Protein digestion was performed according to former instruction.[29, 49] Proteins were precipitated for at least 2 h using ProteoExtract protein precipitation kit, further recovered via centrifugation (14 000 g, 10 min), washed several times and re-suspended in RapiGest SF (Waters Cooperation). Protein reduction was carried out using dithiothreitol (final concentration 5mM, Sigma) for 45 min at 56 °C. Iodacetoamide (final concentration 15 mM, Sigma) was added for alkylation of proteins. A protein: trypsin ratio of 50:1 was chosen for digestion (16 h, 37 °C). The reaction was quenched with 2 µL hydrochloric acid (Sigma, Germany) and peptides were isolated via centrifugation 14 000 g (15 min, 4 °C).

Peptide samples were spiked with 50 fmol/µL Hi3 Ecoli (Waters Cooperation) standard for absolute protein quantification.[50] LC-MS analysis was carried out using a nanoACQUITY UPLC system coupled to a Synapt G2- Si mass spectrometer. The system is equipped with a C18 analytical reversed phase column (1.7 µm, 75 µm × 150 mm), a C18 nanoACQUITY trap column (5 µm, 180 µm × 20 mm) and a NanoLockSpray source. The mobile phase (A) consists of 0.1% (v/v) formic acid in water and mobile phase (B) is acetonitrile with 0.1% (v/v) formic acid. The reference component Glu-Fibrinopeptide was infused 150 fmol $\mu L^{-1}$ at a flow rate of 0.5 µL $min^{-1}$ and the sample flow rate was set to 0.3 µL $min^{-1}$. For data acquisition, the mass spectrometer was operated in resolution mode and data-independent acquisition ($MS^E$) experiments were carried. MassLynx 4.1 was used for data acquisition and processing.

Continuum data was post lock mass corrected and further analyzed by Progenesis QI (2.0) using a reviewed data bases (Uniprot) for peptide and protein identification. Several processing parameters as noise reduction thresholds for low energy, high energy and peptide intensity were set to 120, 25, and 750 counts. The data bases were modified with the sequence information of Hi3 Ecoli standard for absolute quantification. The following criteria were chosen for protein and peptide identification: one missed cleavage, maximum protein mass 600 kDa, fixed carbamidomethyl modification for cysteine, variable oxidation for methionine and protein false discovery rate of 4%. To identify a protein at least two assigned peptides and five assigned fragments are required. Peptide identification is based on three assigned fragments

and identified peptides with a score parameter below 4 were discharged. Based on the TOP3/Hi3 approach the amount of each protein in fmol was provided.[51]

**Cell culture***.* The murine macrophage cell line RAW264.7 was cultured in DMEM supplemented with 10% fetal bovine serum (FBS), 100 U/mL penicillin, 100 mg/mL streptomycin and 2 mM glutamine.

The human monocytic cell line THP-1 was maintained in RPMI supplemented with 10% fetal bovine serum (FBS), 100 U/mL penicillin, 100 mg/mL streptomycin and 2 mM glutamine. All materials were purchased from Thermo Fisher. Cells are grown in a humidified incubator at 37 °C and 5% $CO_2$. THP-1 cells were differentiated with phorbol 12-myristate 12-acetate (PMA, Sigma) at a concentration of 100 ng/mL for 3 days.

**Cellular interactions***.* RAW264.7 or differentiated THP-1 cells were seeded out in 24-well plates (100.000 cells per well) and kept overnight at 37 °C. Prior to cellular uptake experiments, cells were washed with PBS and kept in cell culture medium without proteins. Nanoparticles were incubated with human or mouse plasma as described above (protein corona preperation), centrifuged and applied to cell culture medium without additional proteins at a final concentration of 75 µg/mL. After 2 h, cells were detached using 2.5% Trysin (Gibco, Germany), washed and resupended in PBS. Flow cytometry analysis was conducted on an Attune NxT Flow Cytometer. Data was analyzed using the Attune NxT software. Cells were selected on a forward/sideware plot, excluding cell debris and the fluorescent signal (BODIPY) was analyzed. Mean values and standard deviations were determined from triplicates.

**Statistical analysis.** Student´s t-test was performed and calculated p values were considered to be significant for *$p < 0.05$, **$p < 0.01$, ***$p < 0.001$.

## Results and Discussion

Plasma from three typical *in vivo* models, namely rabbit, mouse and sheep was chosen and compared to human plasma (Figure 3.1). As a first step, dynamic light scattering (DLS) was used to characterize the different protein sources. In general, the autocorrelation function (ACF) of plasma can be described by a sum of three exponentials.[37] Each of them represents one size fraction of proteins in plasma. The first size fraction represents smaller proteins such as serum albumin or immunoglobulin G (IgG). The intermediate fraction comprises slightly bigger proteins like immunoglobulin M (IgM) or low density lipoproteins (LDL). The third size fraction is the biggest one and represents mostly lipoproteins, for example big chylomicrons. Depending on the plasma composition and the concentration of individual proteins, the

hydrodynamic radii of each size fraction can vary. Figure 3.1 shows the detected results for human, mouse, sheep and rabbit plasma.

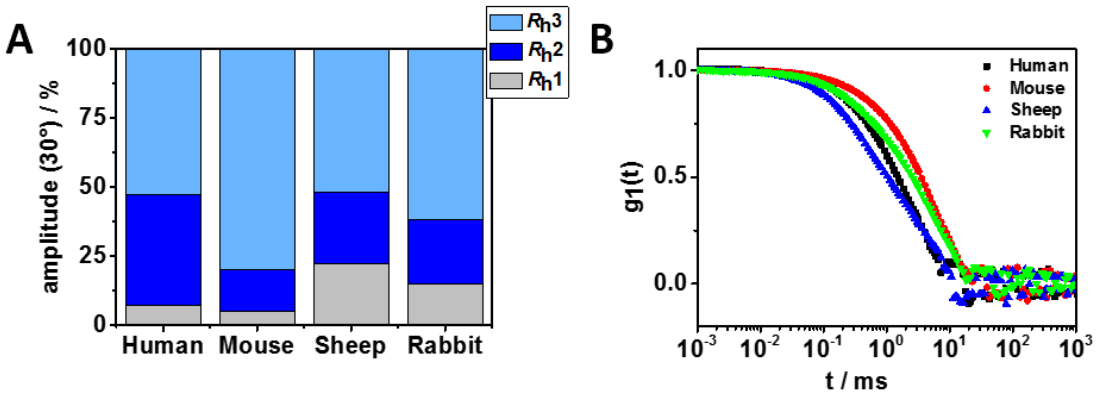


C

| | $R_h1$ / nm | $R_h2$ / nm | $R_h3$ / nm | average $R_h$ / nm | PDI |
|---|---|---|---|---|---|
| Human | 4 | 21 | 83 | 19 | 0.45 |
| Mouse | 3 | 18 | 101 | 35 | 0.49 |
| Sheep | 4 | 14 | 91 | 12 | 0.50 |
| Rabbit | 4 | 25 | 114 | 21 | 0.52 |

**Figure 3. 1. A)** Fluctuation of the intensity contributions of different size fractions for the different plasma sources and **B)** the corresponding autocorrelation functions at $\theta$ = 30°. **C)** Obtained hydrodynamic radii for the different size fractions from DLS together with the obtained polydispersity index (PDI) from a cumulant fit at a scattering angle of 90°. [redacted]

Each plasma source contains the already described three different size fractions. The sizes of each fraction (Figure 3.1) as well as their relative intensity amplitude in % vary over a wide range. Those variations can also directly be seen in the shapes of the ACFs that differ from each other. Mouse plasma for example contains a high amount of the species representing the largest size fraction. This results in the highest average hydrodynamic radius (average of all three fractions) $R_h$ = 35 nm, while e.g. sheep plasma only exhibits an average $R_h$ = 12 nm which is less than half of the size compared to the mouse plasma proteome. Thus, already from the average sizes and intensity contributions of each size fraction it is clear that the plasma from the different sources varies significantly in its composition. The different sizes of the largest size fractions ($R_h3$) additionally lead to differences in the overall polydispersity of the systems as described by the PDI.

To evaluate the composition in terms of proteins that can be identified in each plasma source, SDS-PAGE as well as liquid chromatography-mass spectrometry (LC-MS) analysis was carried out. For protein identification, only reviewed databases from Uniprot were chosen. Here, it should be noted the total number of all reviewed proteins varied significantly for the

investigated organism (human: ~20,000 proteins, mouse ~16,000 proteins, rabbit ~1,000 proteins, sheep ~500 proteins). Thus, especially the overall protein identification rate for rabbit and sheep proteins was affected. Since the number of identified peptides ions (~15,000) was similar for all investigated plasma sources, this indicates a higher amount of non-identified proteins in rabbit and sheep plasma. The identified proteins and their relative amounts in relation to all identified proteins are shown in Figure 3.2. The most abundant protein in all cases is serum albumin as expected. Most interestingly, the relative amount of immunoglobulins highly varied for mouse plasma (~1%) compared to human (~13%) and rabbit plasma (~7%). For mouse plasma, it has already been reported that the amount of immunoglobulins in plasma is significantly lower than in human plasma. This is of great importance as immunoglobulins are referred to as an important class of opsonins[38] which mediate interaction with phagocytic cells causing a rapid clearance of nanoparticles from the blood stream.

In general, the differences in blood plasma composition should mainly be related to inter-species differences since fluctuations between individual animals should be negligible due to the pooling of the plasma. The impact of these different plasma proteome compositions on particle stability was addressed in the next steps.

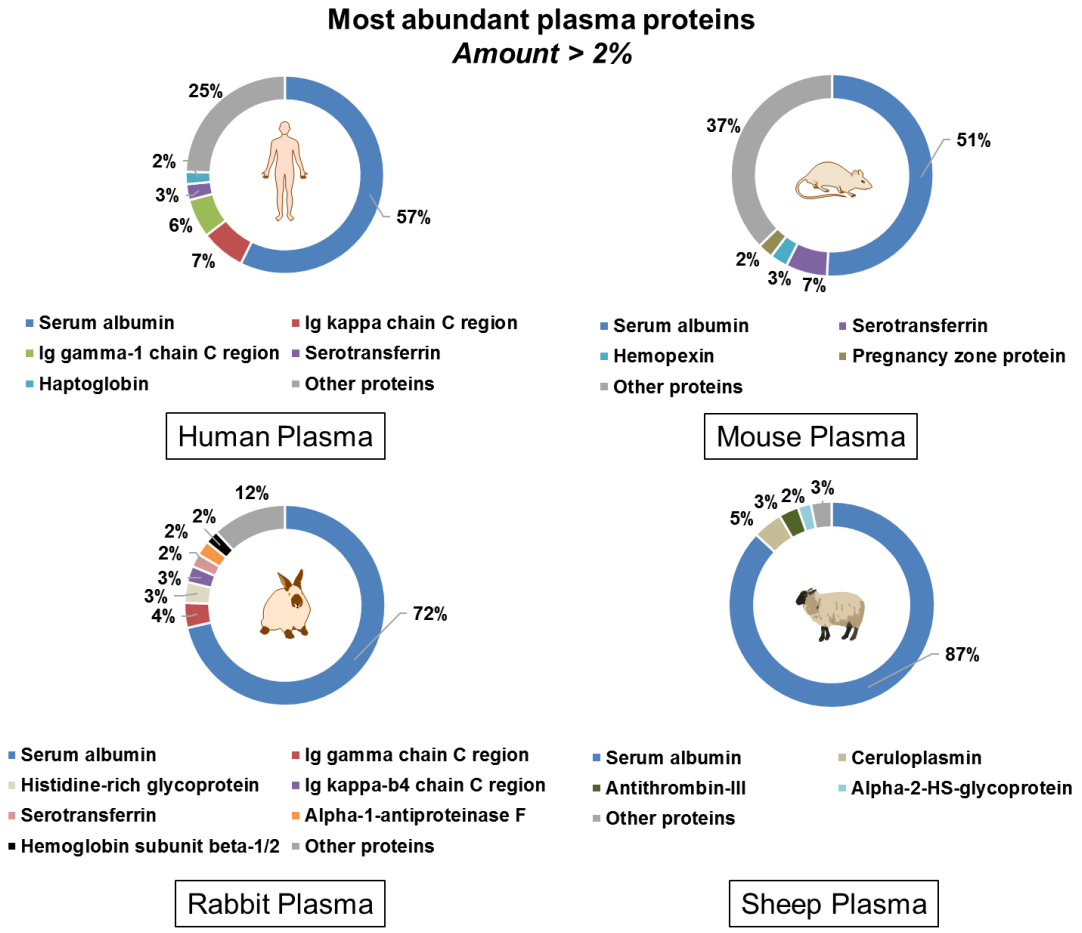


**Figure 3. 2.** Composition of the plasma from different animal sources as determined by LC-MS. Plasma proteins with an average amount > 2% based on all identified proteins are shown. [redacted]

Three differently functionalized polystyrene nanoparticles stabilized with the poly(ethylene glycol)-based surfactant Lutensol AT 50 as well as commercially available magnetite nanoparticles with two different coatings were used as model systems to monitor particle-protein interactions in the four different plasma sources. The chosen systems represent a broad range of available surface functionalities (amine and carboxyl groups) and materials often used for nanocarriers design such as dextran (DEX) and hydroxyethyl starch (HES). Particle charge detection, zeta potential measurements and dynamic light scattering were used in order to characterize the nanoparticles. The results for their size, number of functional groups and charge are summed up in Figure 3.3.

**A**

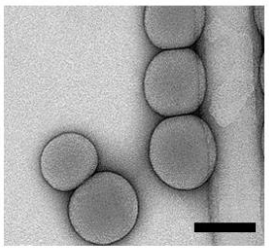

| Functionalization | PS | $PS\text{-}NH_2$ | PS-COOH |
|---|---|---|---|
| $R_h$ / nm (PDI) | 93 ± 9 (0.06) | 86 ± 9 (0.06) | 58 ± 7 (0.04) |
| Groups per NP | - | 4560 ± 360 | 45000 ± 800 |
| ζ potential / mV | -4 ± 1 | 4 ± 1 | -27 ± 1 |

**B**

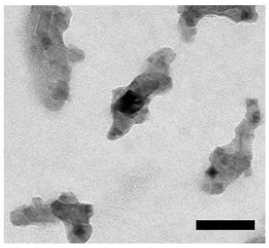

| Functionalization | DEX-coated | HES-coated |
|---|---|---|
| $R_h$ / nm (PDI) | 82 ± 8 (0.15) | 93 ± 9 (0.21) |
| ζ potential / mV | -5 ± 1 | 2 ± 1 |

**Figure 3. 3.** Transmission electron microscopy images and physicochemical parameters for analysed systems of **A)** polystyrene nanoparticles (PS-NPs) and **B)** magnetite nanoparticles coated with dextran (DEX) or hydroxyethyl starch (HES). Representative images of carboxy-functionalized polystyrene nanoparticles (PS-COOH) and hydroxyethyl starch (HES)-coated magnetic nanoparticles. Scale bar: 100 nm. PDIs of nanoparticles in DLS were determined by a cumulant fit of the DLS data at 90°. [redacted]

In order to mimic *in vivo* conditions, we directly introduced the particles into each plasma source without dilution and investigated their stability against aggregation by using DLS. Data were evaluated according to Rausch *et al*.[37]

Generally, the size increase of each particle depends a lot on the plasma source it is introduced into. For example, un-functionalized PS-NPs form aggregates in sheep plasma that are 166% bigger than the original species, while the same particle increases only 14% in size when introduced into mouse plasma (Figure 3.4). For magnetite NPs, we found that the surface coating (HES vs. DEX) did not significantly affect the aggregation behavior. However, as also shown for PS-NPs there are major differences between the four investigated plasma sources (Figure 3.4).

**A**

| particle sample ($R_h$) | $R_h$ aggregate / nm | $R_h$ aggregate / nm | $R_h$ aggregate / nm | $R_h$ aggregate / nm |
|---|---|---|---|---|
| PS (93 nm) | 155 ± 16 | 106 ± 11 | 247 ± 25 | 147 ± 15 |
| PS-COOH (58 nm) | 329 ± 33 | 133 ± 13 | 136 ± 14 | 86 ± 9 |
| PS-$NH_2$ (86 nm) | 220 ± 22 | 194 ± 19 | 185 ± 19 | 114 ± 11 |
| M-DEX (82 nm) | 394 ± 39 | 201 ± 20 | 515 ± 52 | 268 ± 27 |
| M-HES (93 nm) | 415 ± 42 | 289 ± 29 | 621 ± 62 | 214 ± 21 |

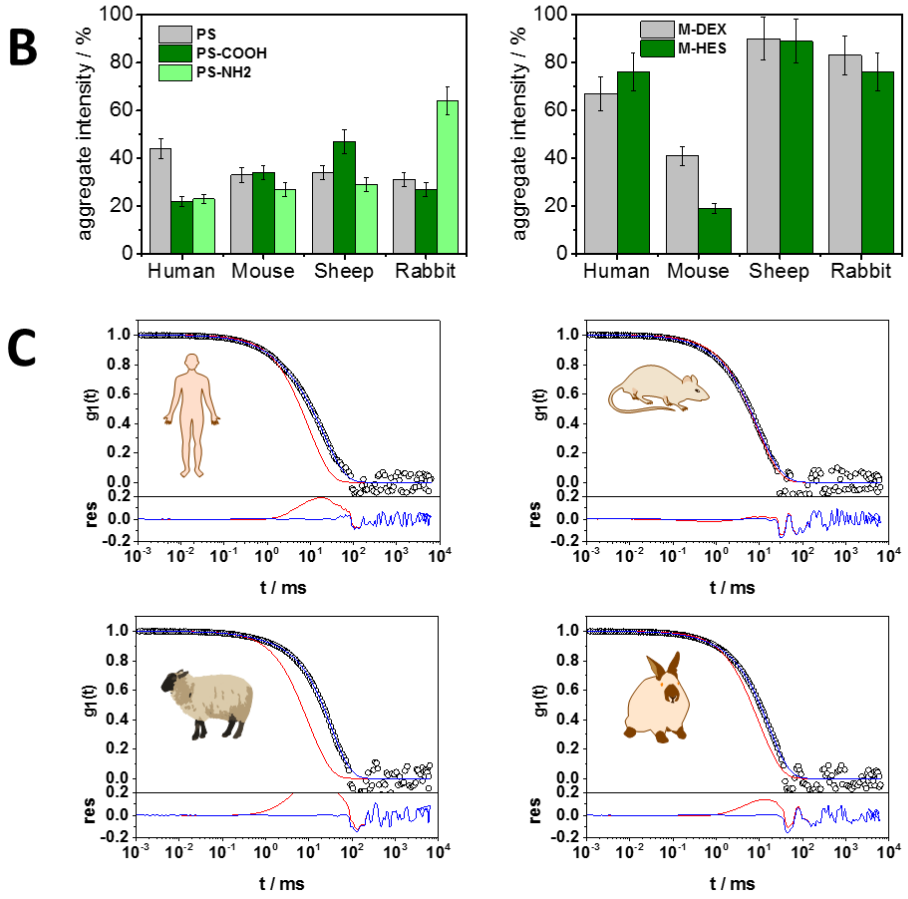


**Figure 3. 4.** Determination of aggregation tendency in concentrated plasma sources by dynamic light scattering (DLS). **A)** Summary of aggregate sizes determined in each plasma source. Colors indicate relative size increase as compared to pure NPs (small = blue, large = red) **B)** Intensity contribution of aggregate fractions for a scattering angle of 30°. **C)** (Top) Exemplary autocorrelation functions (ACFs) at a scattering angle of 30° of dextran coated magnetite nanoparticles (M-DEX) in each plasma source together with the corresponding fits with (blue line) and without (red line) an additional aggregate term. (Bottom) Residuals resulting from the difference between the data points and both fits. [redacted]

Taking this together, we observed the overall trend that the aggregation formation is less pronounced in mouse plasma compared to human or sheep plasma in terms of aggregate size as well as intensity contribution. As shown above (Figure 3.2), a lower amount of immunoglobulins was identified in mouse plasma compared to human plasma. We have previously investigated the influence of individual proteins and plasma fractions on the aggregation behavior of PS-NPs.[23] Especially IgG was found to highly influence the aggregation behavior of the nanoparticles. This indicates that probably due to the overall lower amount of IgG in mouse plasma less aggregation occurs in that plasma source. Especially this discrepancy between mouse and human plasma implies difficulties for the translation of results from mouse *in vivo* experiments to humans as the mouse model is often chosen for experiments that depend on particle/aggregate size like body distribution or cellular uptake.

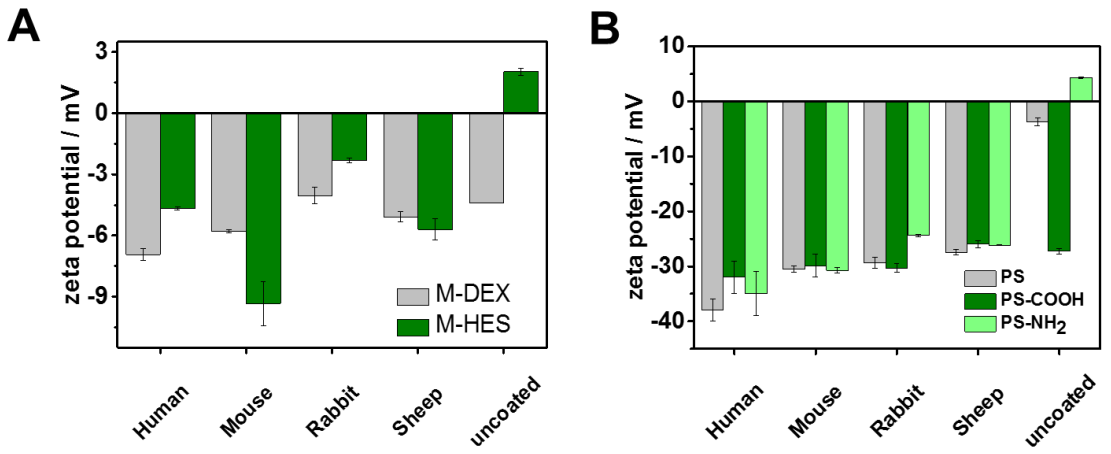


**Figure 3. 5.** Zeta potential of nanoparticles before and after coating with plasma proteins. **A)** Magnetite nanoparticles and **B)** polystyrene nanoparticles. The values are mean values from three individual measurements with error bars that represent the standard deviation.

In addition, the change of surface charge of each particle after incubation in every plasma source was monitored (Figure 3.5). Due to the fact, that most plasma proteins are negatively charged, the measured zeta potential becomes negative after protein corona formation. Small differences between the animal models can be observed. After incubation in human plasma, the values for zeta potential are most negative in the range between -32 and -38 mV, while the values after incubation in sheep plasma are around -26 mV. This could be relevant for cellular uptake and hence the body distribution. The differences observed for the magnetite NP surface charge before and after plasma incubation are smaller than the ones for PS-NPs. An explanation could be the reduced amount of adsorbed proteins calculated from the Pierce 660 nm assay (between 0.12 ± 0.03 and 0.27 ± 0.08 mg $m^{-2}$ NP). In comparison, this corresponds

to only ~10 - 40% of the amount found for PS-NPs depending on functionalization and plasma source.

Subsequently, SDS-PAGE was performed in order to visualize the protein patterns of the protein corona for all nanoparticles formed after incubation in the different plasma sources. Therefore, nanoparticles were incubated in plasma for 1 h at 37 °C using a constant ratio between a defined nanoparticle surface area and plasma volume (see material/methods supplementary information 3). Unbound proteins were removed via repetitive centrifugation and nanoparticles coated with strongly bound proteins were isolated. Proteins were desorbed from the nanoparticles and analysed by SDS-PAGE (Figure 3.6) or LC-MS (Figure 3.7 and 3.8). Undiluted plasma was chosen to mimic *in vivo* conditions as the concentration of the protein source[27, 39] additionally can influence corona formation (supplementary information 3).

For all investigated nanoparticles it is obvious that the protein corona significantly varies depending on the protein source. Comparing the different nanoparticle types, the un-functionalized and amino-functionalized PS-NPs share a similar protein pattern, greatly differing from the protein corona identified for carboxy-functionalized PS-NPs (Figure 3.6). This trend is consistent for all investigated plasma sources and highlights that a defined surface functionalization affects protein adsorption. In contrast to this, the protein pattern for inorganic magnetic nanoparticles M-DEX and M-HES (Figure 3.6) is similar after incubation in the respective protein source. But again, major differences between the different animal models can be observed.

To characterize the biological identity of the nanoparticles in more detail, the protein corona of each nanoparticle type in each plasma source was investigated by LC-MS. Exemplarily shown for un-functionalized PS-NPs (Figure 3.7), we found that independent from the plasma type, there are 4-6 major proteins which contribute to more than 50% of all identified corona proteins. Additionally, we observed that for all investigated plasma sources there is a strong enrichment of lipoproteins in the protein corona of un-functionalized PS-NPs. However, there are major differences between the exact protein compositions depending on the plasma source (Figure 3.7).

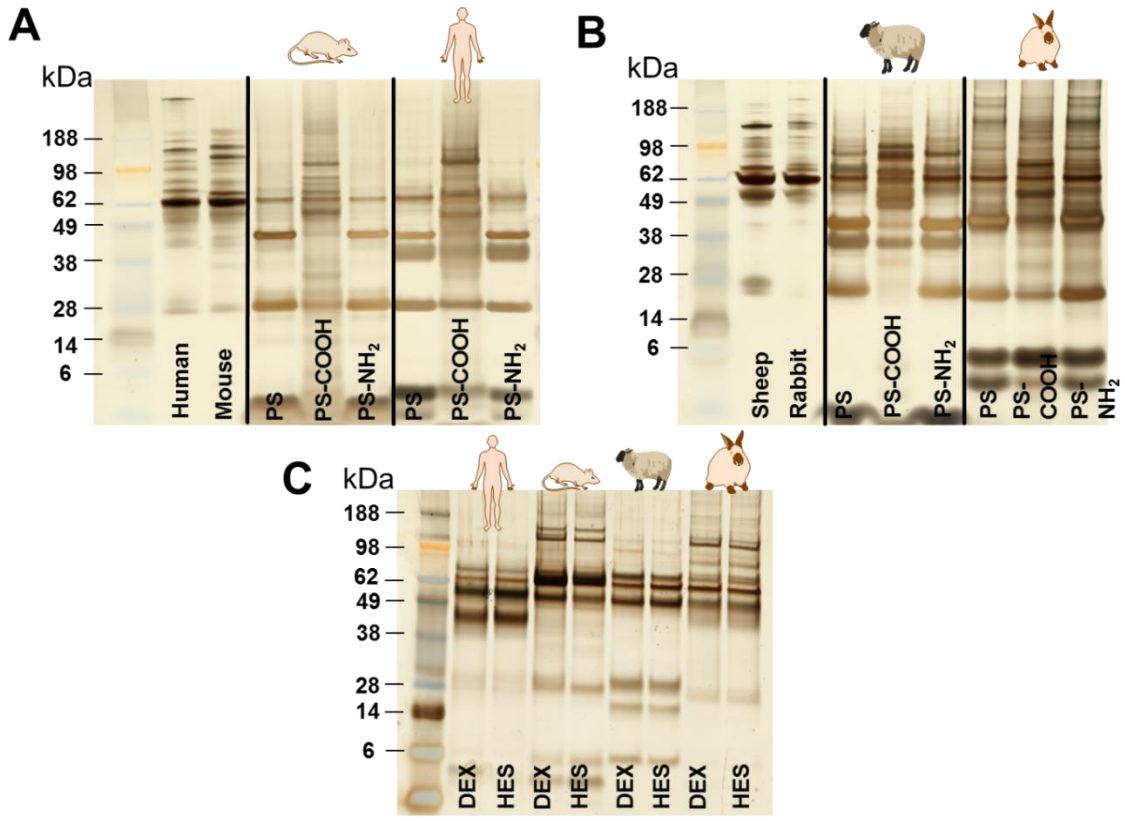


**Figure 3. 6.** SDS-PAGE of the protein coronas formed on polystyrene nanoparticles **(A),(B)** and magnetite nanoparticles **(C)** during incubation in plasma from the different sources. Pure plasma of each source is displayed as a reference in **(A)** and **(B).** [redacted]

A strong enrichment of clusterin was detected for the human corona. In contrast to this, the amount of clusterin in the mouse corona is significantly lower. Clusterin is known to specifically bind to PEGylated surfaces, contributing to the stealth effect and preventing cellular interactions with phagocytic cells.[40] Additionally, an enrichment of clusterin was also detected on the surface of carboxy- and amino-functionalized nanoparticles. All of the here investigated PS-NPs are stabilized with Lutensol which is a PEG analog surfactant. Summarizing the most abundant corona proteins (amount >1%) after incubation in human or mouse plasma highlights that there are major differences in the corona of carboxy-modified nanoparticles compared to un- or amino-functionalized nanoparticles. This is also in line with our previous investigations using human serum[36, 41] or various protein fractions.[23] Overall, the human corona of un-functionalized nanoparticles is enriched with different apolipoproteins (ApoAI, ApoAIV, ApoC-III or ApoE) whereas carboxy-functionalized nanoparticles preferably adsorbed vitronectin (32%) or fibrinogen (15%) indicating that this interaction is probably mediated by charge.

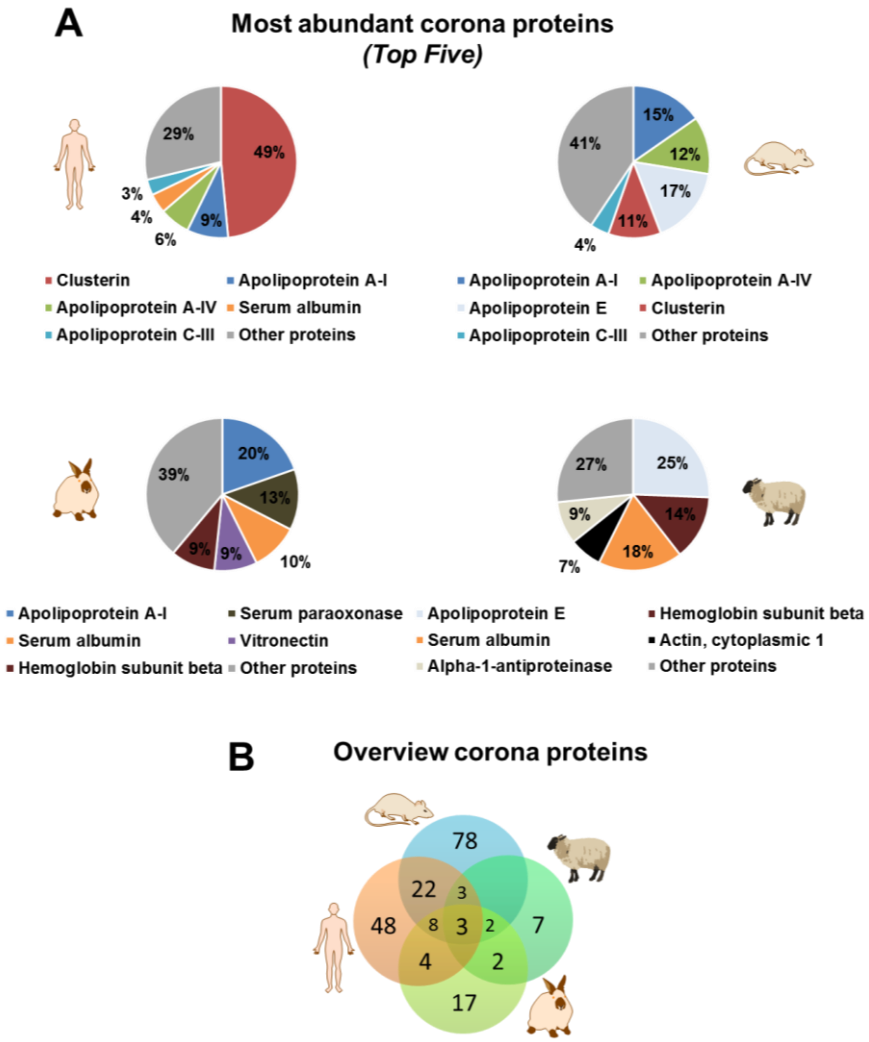


**Figure 3. 7**. **A)** Composition of the protein corona from different animal sources as determined by LC-MS exemplarily shown for un-functionalized PS-NPs. The five most abundant corona proteins based on all identified proteins are summarized. **B)** Venn diagram showing common proteins from the list of all identified proteins per animal source for PS and PS-$NH_2$. Not shown are the number of common proteins from human and sheep (0) and mouse and rabbit (6).

Analysing the protein corona for M-DEX particles the differences between the individual plasma sources become even very more pronounced (Figure 3.8). Here, even the most abundant corona proteins are different for all plasma types (kininogen-1 vs. carboxylesterase 1C or serum albumin). The differences between the different plasma sources are much more prominent than between particle functionalizations. In the same manner, the number of unique proteins in each corona also significantly increased (Figure 3.8). Again, for rabbit and sheep plasma probably not all proteins could be identified, but the overall trend of significantly different protein coronas was observed for all particles under investigation. Of most importance

for generally used *in vivo* models is the comparison between human and mouse plasma protein coronas.

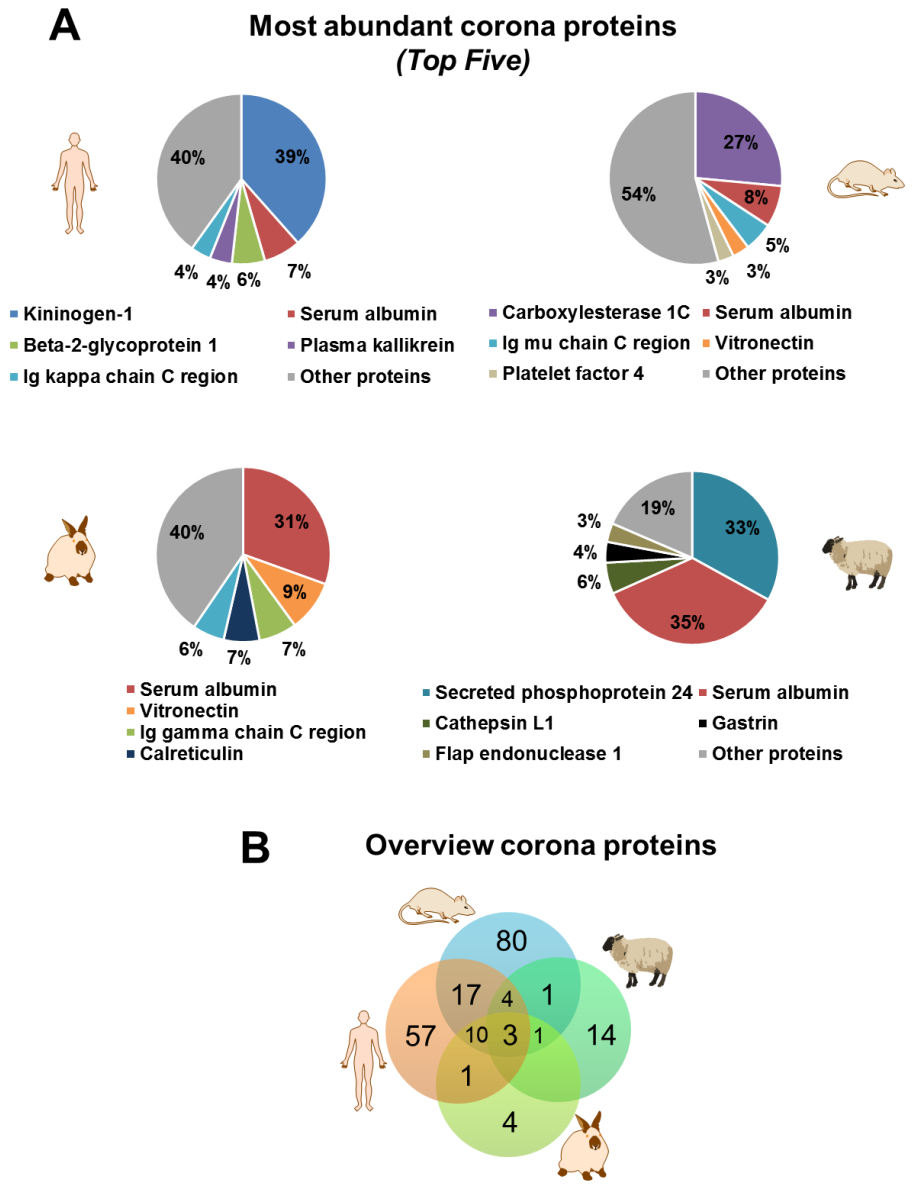


**Figure 3. 8. A)** Composition of the protein corona from different animal sources as determined by LC-MS exemplarily shown for dextran coated magnetite nanoparticles (M-DEX). The five most abundant corona proteins based on all identified proteins are summarized. **B)** Venn diagram showing common proteins from the list of all identified proteins per animal source for M-DEX and M-HES. Not shown are the number of common proteins from human and sheep (0) and mouse and rabbit (1).

The common proteins of both proteomes are actually much less than the unique proteins on both sides, making it quite obvious why translation from mouse *in vivo* models to human studies is often failing. Focusing on the most abundant corona proteins (amount >1%) for human and mouse plasma highlights the similarity between the corona for HES- and DEX-

coated nanoparticles. The polysaccharides hydroxyethyl starch and dextran are both used as volume expander.[42] Additionally, due to the structural similarities both materials showed protein repellent properties.[43] This is in line with the overall low protein amount detected on HES- and DEX-coated nanoparticles compared to PS-NPs.

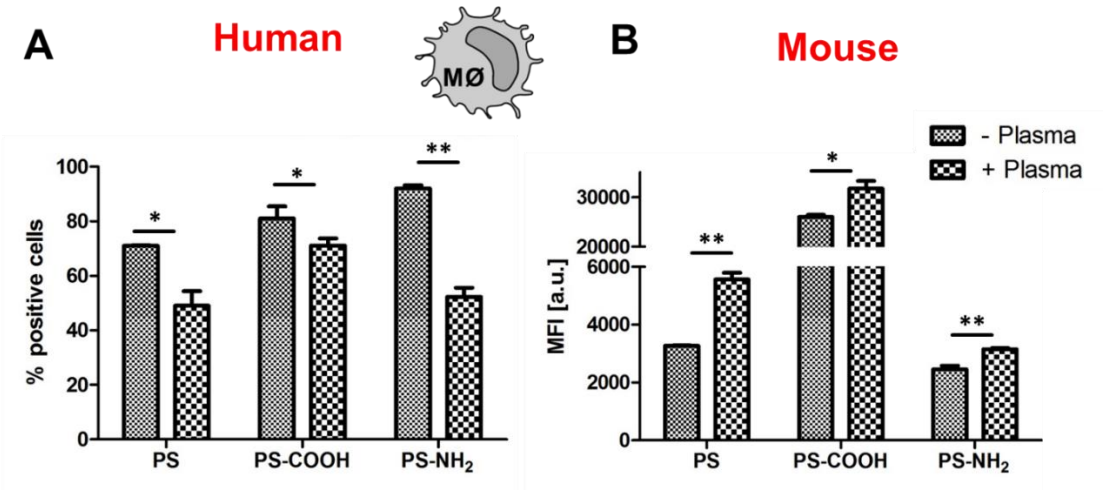


**Figure 3. 9.** Cellular interactions of polystyrene nanoparticles with macrophages. Nanoparticles were incubated with human **(A)** or mouse plasma **(B)** for 1 h at 37 °C, centrifuged and applied to cell culture medium without additional proteins (75 µg/mL) for 2 h. Values are given as mean ± SD (n=3). p <0.05*, p<0.01**, p<0.001***

Macrophages are immune cells which mediate the rapid clearance of nanoparticles from the blood stream. This process is driven by the adsorption of distinct proteins (‘opsonins‘) which favour cellular uptake. Immunoglobulins and complement proteins are known to support this interactions.[44] In contrast, there are several proteins identified which can have an opposite function (‘dysopsonins’) and hereby prevent cellular uptake.[40] As major differences in the corona composition for human and mouse plasma were identified, we evaluated the cellular uptake behavior of nanoparticles towards macrophages. Human THP-1 cells were differentiated to macrophages using PMA and the mouse-macrophage cell line RAW264.7 was chosen for a comparison.

Cellular uptake of uncoated and plasma coated polystyrene nanoparticles was compared. Overall, for the investigated polystyrene nanoparticles, coating with human plasma decreased cellular interactions (Figure 3.9). In strong contrast to this, the internalization of nanoparticles coated with mouse plasma in mouse macrophages is enhanced (Figure 3.9). As identified in our proteomic experiments, the relative amount of clusterin was significantly lower in the mouse corona compared to the human corona. This is in line with previous results which

describe the dysopsonic role of clusterin. Taking this together, it highlights the interplay between defined corona proteins and cellular interactions.

## Conclusion

The investigated blood plasma sources showed significant differences concerning their composition, especially in terms of immunoglobulin content and presence of other proteins. Those different blood proteomes resulted in pronounced discrepancies in the aggregation behavior of the different nanoparticles, implying different body distributions because of the size changes. Also, the composition of the protein coronas around the nanoparticles was found to differ immensely between the plasma sources, revealing even more unique proteins in many of the coronas than common ones could be found. Notably, the differences after incubation in the various plasma sources were in many cases more significant than between different surface functionalizations, which renders the chosen animal model even more important. Especially the discrepancy between mouse and human plasma implies difficulties for the transferability from animal *in vivo* models to clinical studies, as the mouse model is often used to investigate body distribution or cellular uptake of nanomaterials. Therefore, we suggest that 1) nanoparticles used *in vitro* or rather *in vivo* should be evaluated in the plasma of the used cell line type/animal model to ensure the transferability from *in vitro* to *in vivo* experiments. Additionally, 2) the same experiments – at least blood plasma stability and *in vitro* tests – should also be performed with human material/cell lines and be compared to the outcome in the respective animal models/studies. This could potentially yield predictions on whether e.g. the blood stability is the same and, therefore, if the results from animal models can be a valid estimation for the behavior in human organisms. Ideally, this way the most suitable animal model concerning the nanomaterial behavior in blood can be found.

## Supplementary information

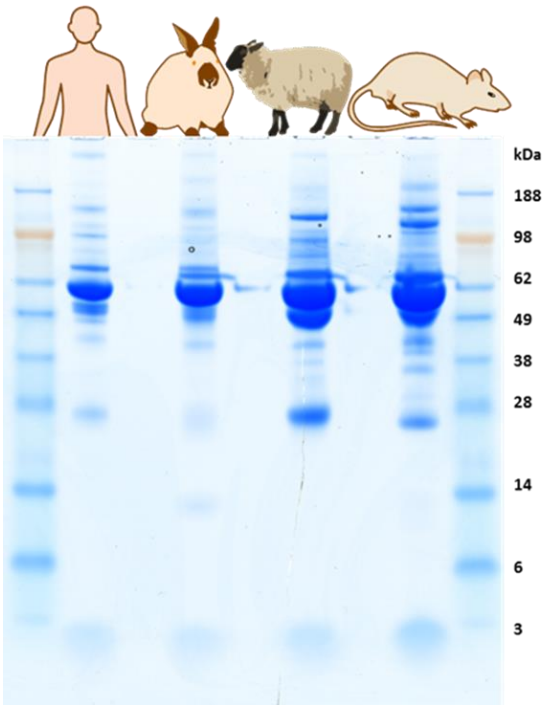


**Figure 3. 10.** SDS-PAGE of human, rabbit, sheep and mouse plasma visualized using Coomassie Blue staining. [redacted]

**Table 3. 1.** Protein concentration and pool size of all investigated plasma sources.

| | Pool size (N) | Protein concentration |
|---|---|---|
| **Human** | 6 | 66.9 ± 9.8 mg/mL |
| **Mouse** | 75-100 | 63.6 ± 6.3 mg/mL |
| **Sheep** | 75-100 | 62.9 ± 4.6 mg/mL |
| **Rabbit** | 75-100 | 69.0 ± 9.5 mg/mL |

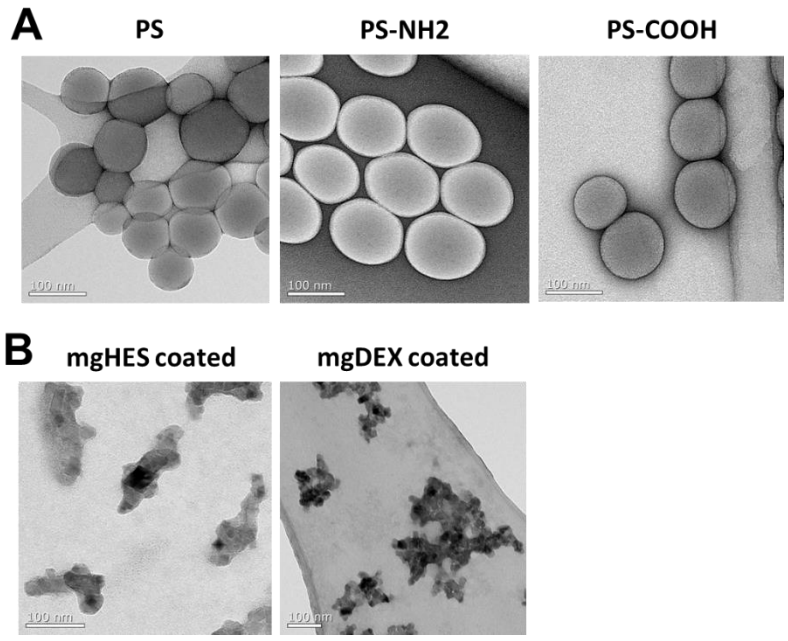


**Figure 3. 11.** TEM images of polystyrene nanoparticles with different surface functionalization **(A)** and magnetic nanoparticles coated with hydroxyethyl starch or dextran **(B).** Sale bar: 100 nm [redacted]

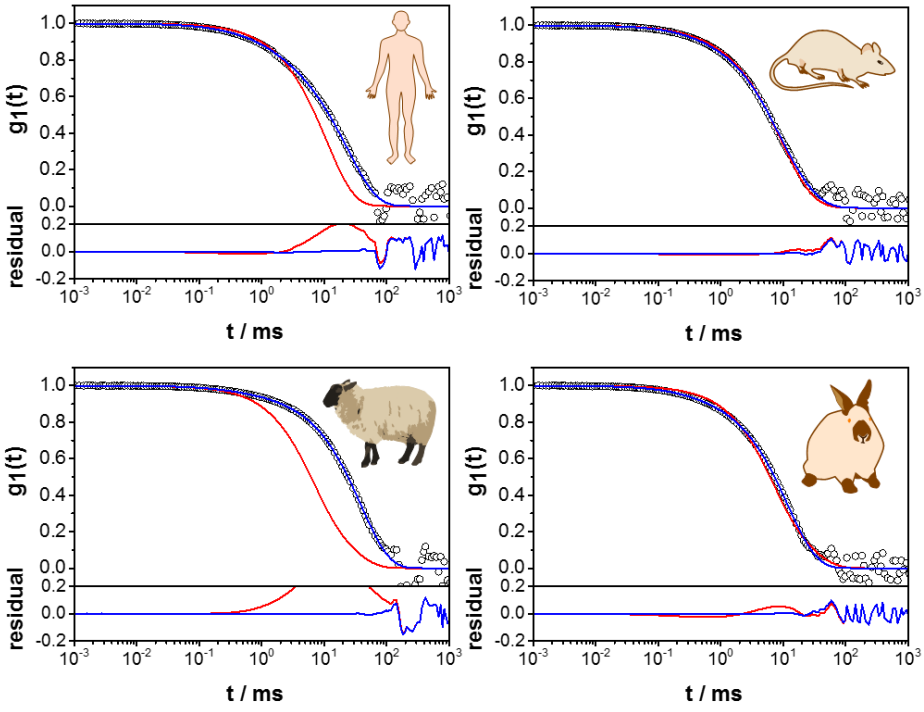


**Figure 3. 12.** ACF of BNF-HES in human, mouse, sheep and rabbit plasma at Θ = 30° including data points, force fit (red) and fit with aggregate formation (blue). ([redacted]

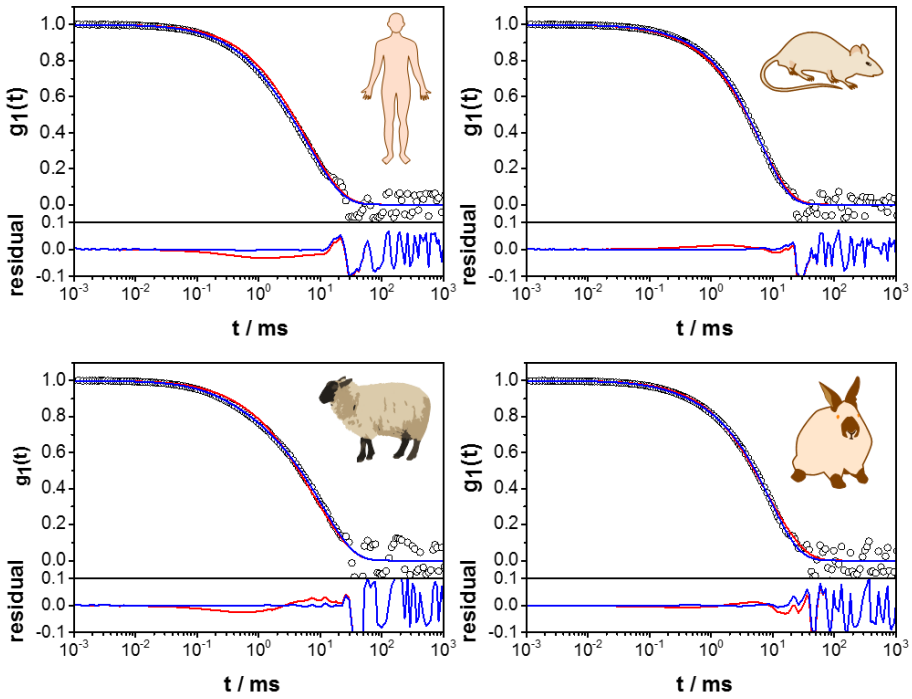


**Figure 3. 13.** ACF of PS in human, mouse, sheep and rabbit plasma at Θ = 30° including data points, force fit (red) and fit with aggregate formation (blue). [redacted]

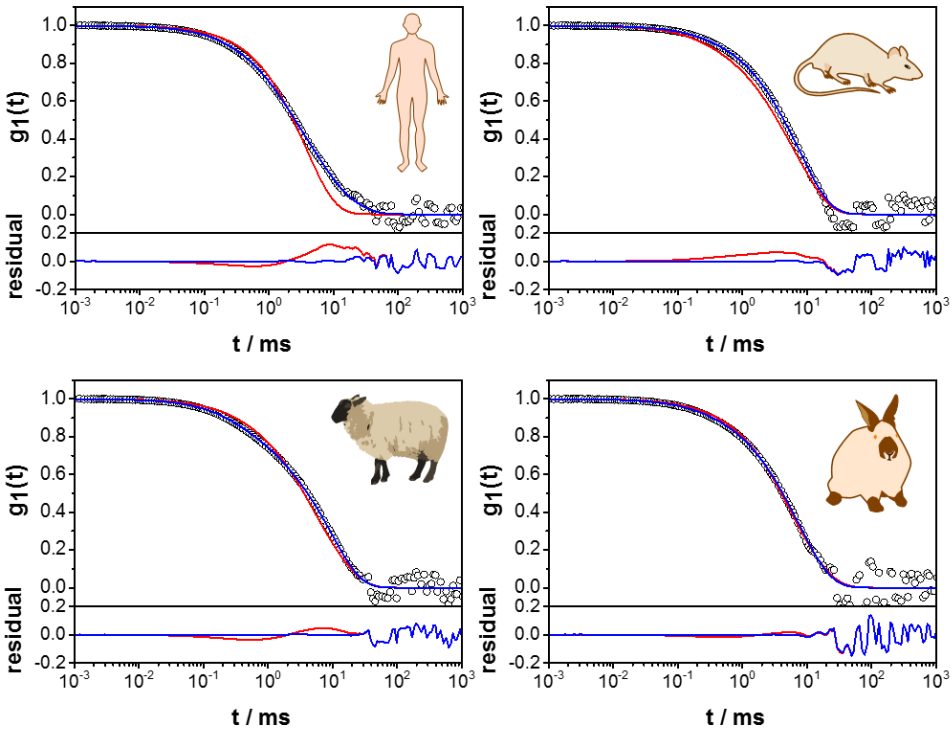


**Figure 3. 14.** ACF of PS-COOH in human, mouse, sheep and rabbit plasma at Θ = 30° including data points, force fit (red) and fit with aggregate formation (blue). [redacted]

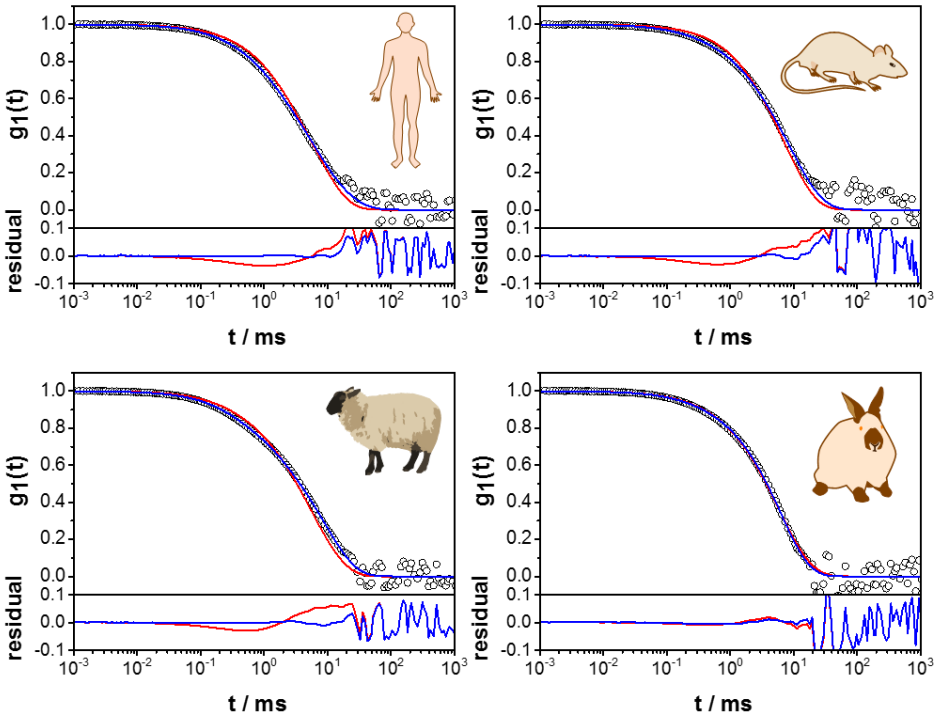


**Figure 3. 15.** ACF of PS-NH2 in human, mouse, sheep and rabbit plasma at Θ = 30° including data points, force fit (red) and fit with aggregate formation (blue). [redacted]

**Table 3. 2.** Protein amount adsorbed on HES and DEX magnetic nanoparticles after corona formation. Values are expressed as absolute protein amount in mg per $m^2$ nanoparticle surface area. [redacted]

| | **DEX** | **HES** |
|---|---|---|
| **Human** | 0.13 ± 0.08 mg | 0.17 ± 0.03 mg |
| **Mouse** | 0.16 ± 0.02 mg | 0.18 ± 0.04 mg |
| **Sheep** | 0.27 ± 0.08 mg | 0.13 ± 0.03 mg |
| **Rabbit** | 0.18 ± 0.02 mg | 0.12 ± 0.03 mg |

**Table 3. 3.** Protein amount adsorbed on polystyrene nanoparticles after corona formation. Values are expressed as absolute protein amount in mg per $m^2$ nanoparticle surface area. [redacted]

| | PS | PS-COOH | PS-$NH_2$ |
|---|---|---|---|
| **Human** | 0.65 ± 0.30 mg | 0.82 ± 0.21 mg | 0.80 ± 0.09 mg |
| **Mouse** | 1.01 ± 0.06 mg | 0.95 ± 0.12 mg | 1.00 ± 0.22 mg |
| **Sheep** | 0.65 ± 0.15 mg | 1.30 ± 0.28 mg | 0.69 ± 0.06 mg |
| **Rabbit** | 0.98 ± 0.02 mg | 1.10 ± 0.07 mg | 1.10 ± 0.14 mg |

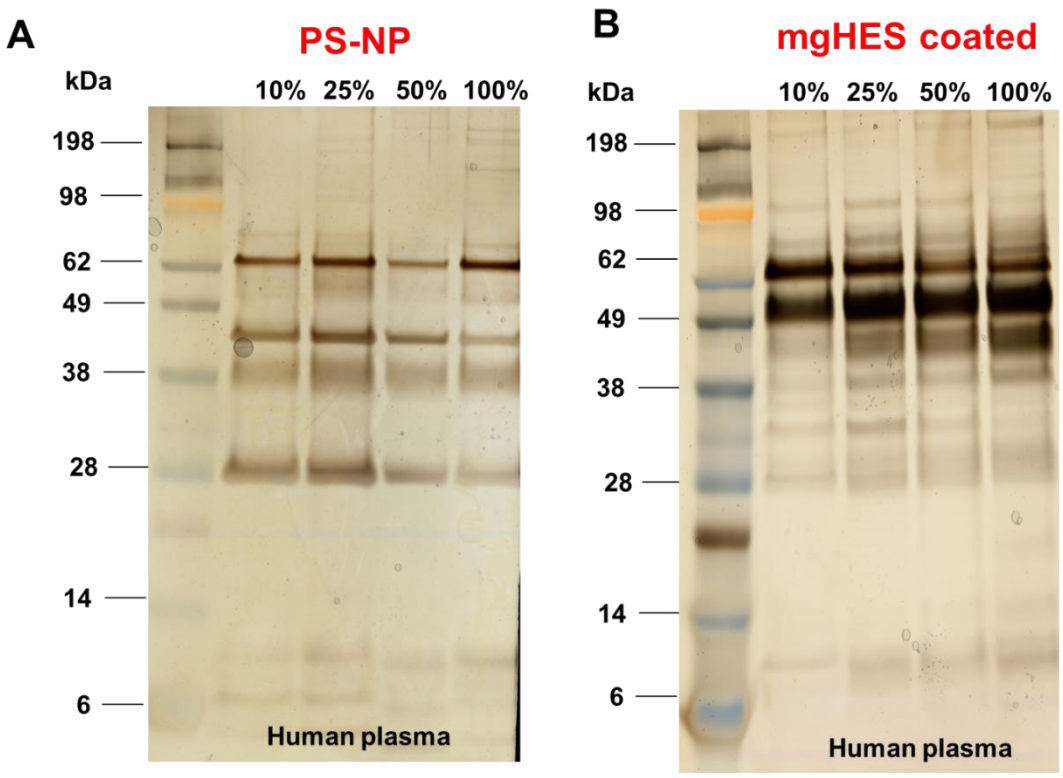


**Figure 3. 16.** Influence of protein concentration on corona formation. Unfunctionalized polystyrene **(A)** and HES **(B)** coated magnetic nanoparticles were incubated for 1 h, 37 °C with human plasma (10%, 25%, 50% or 100%). Proteins (2 µg) per lane were visualized by silver staining.

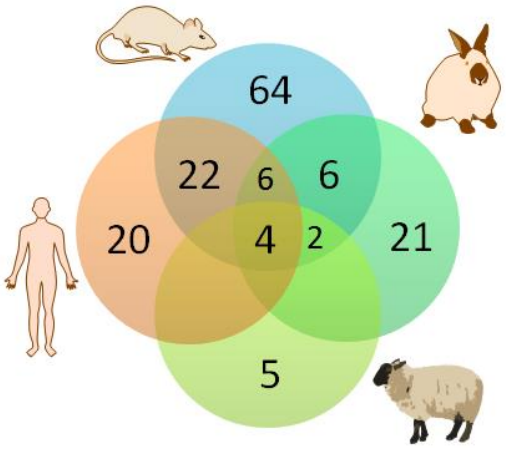


**Figure 3. 17.** Venn diagram showing common proteins from the list of all identified proteins per animal source for PS-COOH-NPs. Not shown are the number of common proteins from mouse and sheep (1) and human and rabbit (0).

**A**

**Human**

| % | PS | PS COOH | PS NH2 |
|---|---|---|---|
| Apolipoprotein A-I | 8.76 | 1.32 | 8.70 |
| Apolipoprotein A-IV | 6.45 | 0.21 | 9.69 |
| Apolipoprotein C-III | 3.34 | 0.57 | 1.11 |
| Apolipoprotein E | 1.97 | 1.22 | 2.12 |
| Beta-2-glycoprotein 1 | 0.07 | 11.55 | 0.05 |
| Clusterin | 48.50 | 11.47 | 49.61 |
| Fibrinogen alpha chain | 0.39 | 5.13 | 0.43 |
| Fibrinogen beta chain | 0.45 | 3.96 | 0.48 |
| Fibrinogen gamma chain | 0.49 | 6.00 | 0.63 |
| Histidine-rich glycoprotein | 0.00 | 7.56 | 0.00 |
| Ig kappa chain C region | 1.23 | 0.52 | 0.56 |
| Ig mu chain C region | 1.40 | 0.08 | 0.40 |
| Inter-alpha-trypsin inhibitor | 0.10 | 3.43 | 0.09 |
| Kininogen-1 | 0.07 | 3.81 | 0.06 |
| L-lactate dehydrogenase C chain | 2.39 | 0.00 | 2.13 |
| Phospholipid transfer protein | 1.16 | 0.00 | 1.27 |
| Serum albumin | 4.18 | 1.85 | 2.24 |
| Vitronectin | 2.46 | 31.87 | 4.88 |
| Zinc finger protein basonuclin-2 | 2.81 | 0.53 | 2.60 |

**B**

**Mouse**

| % | PS | PS COOH | PS NH2 |
|---|---|---|---|
| Alpha-2-HS-glycoprotein | 0.91 | 1.26 | 0.45 |
| Antithrombin-III | 0.35 | 2.76 | 0.32 |
| Apolipoprotein A-I | 15.32 | 4.17 | 15.28 |
| Apolipoprotein A-IV | 12.24 | 1.02 | 13.21 |
| Apolipoprotein C-III | 4.04 | 0.67 | 5.21 |
| Apolipoprotein C-IV | 1.77 | 1.02 | 2.04 |
| Apolipoprotein E | 16.61 | 3.56 | 13.43 |
| Beta-2-glycoprotein 1 | 0.41 | 17.79 | 0.35 |
| Clusterin | 11.17 | 3.21 | 13.62 |
| Coagulation factor V | 0.37 | 1.13 | 0.37 |
| Coagulation factor XII | 0.00 | 1.86 | 0.00 |
| Complement C1r-A | 0.36 | 2.00 | 0.22 |
| Complement factor H | 0.99 | 0.15 | 1.04 |
| Guanine nucleotide exchange factor | 1.55 | 0.00 | 2.55 |
| Haptoglobin | 0.78 | 0.17 | 1.00 |
| Heat shock protein | 1.78 | 0.07 | 1.55 |
| Ig mu chain C region | 2.18 | 1.06 | 1.67 |
| Inter alpha-trypsin inhibitor | 0.99 | 12.65 | 0.96 |
| Plasma protease C1 inhibitor | 0.32 | 1.22 | 0.27 |
| Serum albumin | 4.06 | 3.31 | 3.55 |
| Talin-1 | 1.41 | 0.05 | 1.24 |
| Transthyretin | 1.17 | 0.25 | 0.84 |
| Tyrosine-protein phosphatase | 0.87 | 0.00 | 1.02 |
| Vitronectin | 0.89 | 12.94 | 0.47 |
| Zinc finger protein | 0.00 | 1.21 | 0.00 |

**Figure 3. 18.** Heat map of most abundant corona proteins for polystyrene nanoparticles. Corona proteins which contribute to more than 1% (relative amount) are shown.

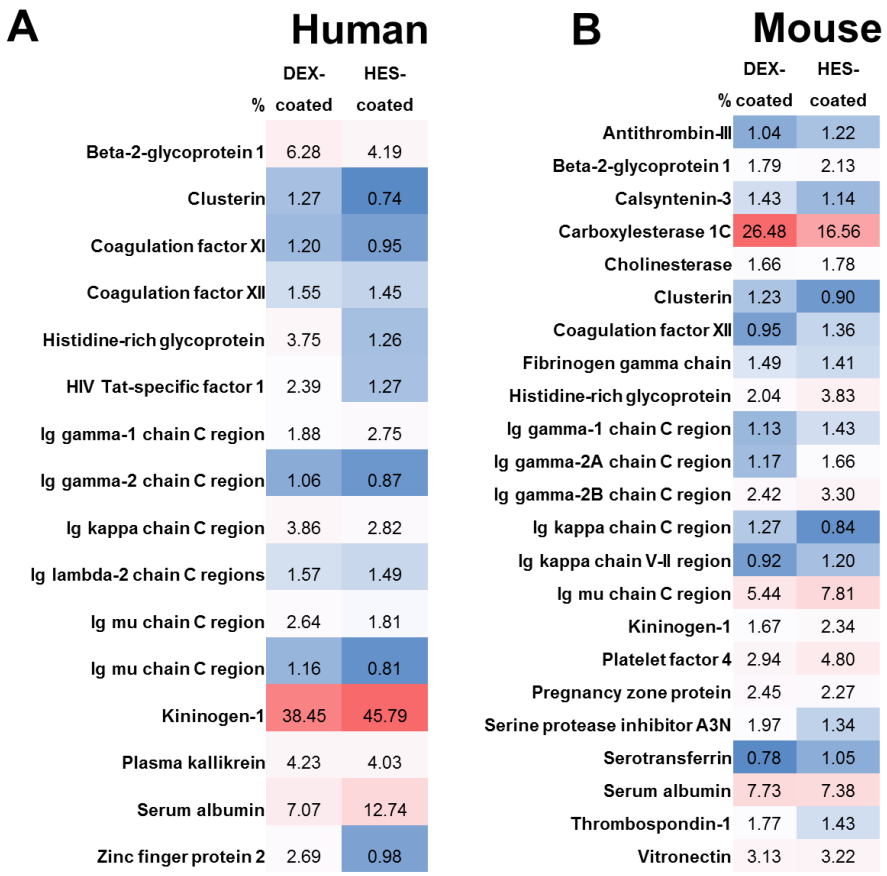


**Figure 3. 19.** Heat map of most abundant corona proteins for magnetic nanoparticles. Corona proteins which contribute to more than 1% (relative amount) are shown.

## Literature


1. Wagner, V.; Dullaart, A.; Bock, A.-K.; Zweck, A., The emerging nanomedicine landscape. *Nature biotechnology* **2006,** *24* (10), 1211-1217.

2. Akhter, S.; Ahmad, I.; Ahmad, M. Z.; Ramazani, F.; Singh, A.; Rahman, Z.; Ahmad, F. J.; Storm, G.; Kok, R. J., Nanomedicines as cancer therapeutics: current status. *Current cancer drug targets* **2013,** *13* (4), 362-378.

3. Betancourt, T.; Brown, B.; Brannon-Peppas, L., Doxorubicin-loaded PLGA nanoparticles by nanoprecipitation: preparation, characterization and in vitro evaluation. *Nanomedicine* **2007,** *2* (2), 219-232.

4. Schroeder, A.; Levins, C. G.; Cortez, C.; Langer, R.; Anderson, D. G., Lipid-based nanotherapeutics for siRNA delivery. *Journal of internal medicine* **2010,** *267* (1), 9-21.

5. Mohr, K.; Müller, S. S.; Müller, L. K.; Rusitzka, K.; Gietzen, S.; Frey, H.; Schmidt, M., Evaluation of Multifunctional Liposomes in Human Blood Serum by Light Scattering. *Langmuir* **2014,** *30* (49), 14954-14962.

6. Gavrilov, K.; Saltzman, W. M., Therapeutic siRNA: principles, challenges, and strategies. *The Yale journal of biology and medicine* **2012,** *85* (2), 187.

7. Jin, S.; Leach, J. C.; Ye, K., Nanoparticle-mediated gene delivery. *Micro and Nano Technologies in Bioanalysis: Methods and Protocols* **2009**, 547-557.

8. Patil, M. L.; Zhang, M.; Betigeri, S.; Taratula, O.; He, H.; Minko, T., Surface-modified and internally cationic polyamidoamine dendrimers for efficient siRNA delivery. *Bioconjugate chemistry* **2008,** *19* (7), 1396-1403.

9. Sutton, D.; Nasongkla, N.; Blanco, E.; Gao, J., Functionalized micellar systems for cancer targeted drug delivery. *Pharmaceutical research* **2007,** *24* (6), 1029-1046.

10. Francis, M. F.; Cristea, M.; Winnik, F. M., Polymeric micelles for oral drug delivery: why and how. *Pure and Applied Chemistry* **2004,** *76* (7-8), 1321-1335.

11. Moore, A.; Medarova, Z.; Potthast, A.; Dai, G., In Vivo Targeting of Underglycosylated MUC-1 Tumor Antigen Using a Multimodal Imaging Probe. *Cancer Research* **2004,** *64* (5), 1821-1827.

12. Flenniken, M. L.; Liepold, L. O.; Crowley, B. E.; Willits, D. A.; Young, M. J.; Douglas, T., Selective attachment and release of a chemotherapeutic agent from the interior of a protein cage architecture. *Chem. Commun.* **2005,** (4), 447-449.

13. Junod, S. W., FDA and clinical drug trials: a short history. *A Quick Guide to Clinical Trials: For People Who May Not Know It All* **2014**, 21-51.

14. McGonigle, P.; Ruggeri, B., Animal models of human disease: Challenges in enabling translation. *Biochemical Pharmacology* **2014,** *87* (1), 162-171.

15. Perel, P.; Roberts, I.; Sena, E.; Wheble, P.; Briscoe, C.; Sandercock, P.; Macleod, M.; Mignini, L. E.; Jayaram, P.; Khan, K. S., Comparison of treatment effects between animal experiments and clinical trials: systematic review. *BMJ* **2007,** *334* (7586), 197.

16. Mak, I.; Evaniew, N.; Ghert, M., Lost in translation: animal models and clinical trials in cancer treatment. *Am J Transl Res* **2014,** *6* (2), 114-8.

17. Seok, J.; Warren, H. S.; Cuenca, A. G.; Mindrinos, M. N.; Baker, H. V.; Xu, W.; Richards, D. R.; McDonald-Smith, G. P.; Gao, H.; Hennessy, L.; Finnerty, C. C.; López, C. M.; Honari, S.; Moore, E. E.; Minei, J. P.; Cuschieri, J.; Bankey, P. E.; Johnson, J. L.; Sperry, J.; Nathens, A. B.; Billiar, T. R.; West, M. A.; Jeschke, M. G.; Klein, M. B.; Gamelli, R. L.; Gibran, N. S.; Brownstein, B. H.; Miller-Graziano, C.; Calvano, S. E.; Mason, P. H.; Cobb, J. P.; Rahme, L. G.; Lowry, S. F.; Maier, R. V.; Moldawer, L. L.; Herndon, D. N.; Davis, R. W.; Xiao, W.; Tompkins, R. G.; Inflammation, t.; Host Response to Injury, L. S. C. R. P., Genomic responses in mouse models poorly mimic human inflammatory diseases. *Proceedings of the National Academy of Sciences* **2013,** *110* (9), 3507-3512.

18. Lynch, I.; Dawson, K. A., Protein-nanoparticle interactions. *Nano Today* **2008,** *3* (1–2), 40-47.

19. Walczyk, D.; Bombelli, F. B.; Monopoli, M. P.; Lynch, I.; Dawson, K. A., What the Cell "Sees" in Bionanoscience. *Journal of the American Chemical Society* **2010,** *132* (16), 5761-5768.

20. Monopoli, M. P.; Aberg, C.; Salvati, A.; Dawson, K. A., Biomolecular coronas provide the biological identity of nanosized materials. *Nat Nano* **2012,** *7* (12), 779-786.

21. Salvati, A.; Pitek, A. S.; Monopoli, M. P.; Prapainop, K.; Bombelli, F. B.; Hristov, D. R.; Kelly, P. M.; Aberg, C.; Mahon, E.; Dawson, K. A., Transferrin-functionalized nanoparticles lose their targeting capabilities when a biomolecule corona adsorbs on the surface. *Nat Nano* **2013,** *8* (2), 137-143.

22. Cedervall, T.; Lynch, I.; Lindman, S.; Berggård, T.; Thulin, E.; Nilsson, H.; Dawson, K. A.; Linse, S., Understanding the nanoparticle–protein corona using methods to quantify exchange rates and affinities of proteins for nanoparticles. *Proceedings of the National Academy of Sciences* **2007,** *104* (7), 2050-2055.

23. Müller, L. K.; Simon, J.; Schöttler, S.; Landfester, K.; Mailänder, V.; Mohr, K., Pre-coating with protein fractions inhibits nano-carrier aggregation in human blood plasma. *RSC Advances* **2016,** *6* (99), 96495-96509.

24. Deng, Z. J.; Liang, M.; Monteiro, M.; Toth, I.; Minchin, R. F., Nanoparticle-induced unfolding of fibrinogen promotes Mac-1 receptor activation and inflammation. *Nature Nanotech.* **2011,** *6* (1), 39-44.

25. Pozzi, D.; Caracciolo, G.; Capriotti, A. L.; Cavaliere, C.; La Barbera, G.; Anchordoquy, T. J.; Laganà, A., Surface chemistry and serum type both determine the nanoparticle–protein corona. *Journal of proteomics* **2015,** *119*, 209-217.

26. Solorio-Rodríguez, A.; Escamilla-Rivera, V.; Uribe-Ramírez, M.; Chagolla, A.; Winkler, R.; García-Cuellar, C.; De Vizcaya-Ruiz, A., A comparison of the human and mouse protein corona profiles of functionalized SiO 2 nanocarriers. *Nanoscale* **2017,** *9* (36), 13651-13660.

27. Monopoli, M. P.; Walczyk, D.; Campbell, A.; Elia, G.; Lynch, I.; Bombelli, F. B.; Dawson, K. A., Physical− chemical aspects of protein corona: relevance to in vitro and in vivo biological impacts of nanoparticles. *J. Am. Chem. Soc* **2011,** *133* (8), 2525-2534.

28. Lundqvist, M.; Stigler, J.; Elia, G.; Lynch, I.; Cedervall, T.; Dawson, K. A., Nanoparticle size and surface properties determine the protein corona with possible implications for biological impacts. *Proc Natl Acad Sci U S A* **2008,** *105* (38), 14265-70.

29. Tenzer, S.; Docter, D.; Rosfa, S.; Wlodarski, A.; Kuharev, J. r.; Rekik, A.; Knauer, S. K.; Bantz, C.; Nawroth, T.; Bier, C., Nanoparticle size is a critical physicochemical determinant of the human blood plasma corona: a comprehensive quantitative proteomic analysis. *ACS nano* **2011,** *5* (9), 7155-7167.

30. Moyano, D. F.; Saha, K.; Prakash, G.; Yan, B.; Kong, H.; Yazdani, M.; Rotello, V. M., Fabrication of corona-free nanoparticles with tunable hydrophobicity. *ACS nano* **2014,** *8* (7), 6748-6755.

31. Lundqvist, M.; Augustsson, C.; Lilja, M.; Lundkvist, K.; Dahlbäck, B.; Linse, S.; Cedervall, T., The nanoparticle protein corona formed in human blood or human blood fractions. *PloS one* **2017,** *12* (4), e0175871.

32. Mirshafiee, V.; Kim, R.; Mahmoudi, M.; Kraft, M. L., The importance of selecting a proper biological milieu for protein corona analysis in vitro: Human plasma versus human serum. *The international journal of biochemistry & cell biology* **2016,** *75*, 188-195.

33. Schöttler, S.; Klein, K.; Landfester, K.; Mailander, V., Protein source and choice of anticoagulant decisively affect nanoparticle protein corona and cellular uptake. *Nanoscale* **2016**.

34. Hajipour, M. J.; Laurent, S.; Aghaie, A.; Rezaee, F.; Mahmoudi, M., Personalized protein coronas: a "key" factor at the nanobiointerface. *Biomaterials Science* **2014,** *2* (9), 1210-1221.

35. Hajipour, M. J.; Raheb, J.; Akhavan, O.; Arjmand, S.; Mashinchian, O.; Rahman, M.; Abdolahad, M.; Serpooshan, V.; Laurent, S.; Mahmoudi, M., Personalized disease-specific protein corona influences the therapeutic impact of graphene oxide. *Nanoscale* **2015,** *7* (19), 8978-8994.

36. Mohr, K.; Sommer, M.; Baier, G.; Schöttler, S.; Okwieka, P.; Tenzer, S.; Landfester, K.; Mailänder, V.; Schmidt, M.; Meyer, R. G., Aggregation behavior of polystyrene-nanoparticles in human blood serum and its impact on the in vivo distribution in mice. *Journal of Nanomedicine & Nanotechnology* **2014,** *5* (2).

37. Rausch, K.; Reuter, A.; Fischer, K.; Schmidt, M., Evaluation of nanoparticle aggregation in human blood serum. *Biomacromolecules* **2010,** *11* (11), 2836-2839.

38. Aggarwal, P.; Hall, J. B.; McLeland, C. B.; Dobrovolskaia, M. A.; McNeil, S. E., Nanoparticle interaction with plasma proteins as it relates to particle biodistribution, biocompatibility and therapeutic efficacy. *Advanced Drug Delivery Reviews* **2009,** *61* (6), 428-437.

39. Mahmoudi, M.; Lynch, I.; Ejtehadi, M. R.; Monopoli, M. P.; Bombelli, F. B.; Laurent, S., Protein− nanoparticle interactions: opportunities and challenges. *Chemical reviews* **2011,** *111* (9), 5610-5637.

40. Schöttler, S.; Becker, G.; Winzen, S.; Steinbach, T.; Mohr, K.; Landfester, K.; Mailander, V.; Wurm, F. R., Protein adsorption is required for stealth effect of poly(ethylene glycol)- and poly(phosphoester)-coated nanocarriers. *Nature Nanotech.* **2016**.

41. Kokkinopoulou, M.; Simon, J.; Landfester, K.; Mailänder, V.; Lieberwirth, I., Visualization of the Protein Corona: towards a biomolecular understanding of nanoparticle-cell-interactions. *Nanoscale* **2017**.

42. Korttila, K.; Groehn, P.; Gordin, A.; Sundberg, S.; Salo, H.; Nissinen, E.; Mattila, M., Effect of hydroxyethyl starch and dextran on plasma volume and blood hemostasis and coagulation. *The Journal of Clinical Pharmacology* **1984,** *24* (7), 273-282.

43. Kang, B.; Opatz, T.; Landfester, K.; Wurm, F. R., Carbohydrate nanocarriers in biomedical applications: functionalization and construction. *Chemical Society Reviews* **2015,** *44* (22), 8301-8325.

44. Mirshafiee, V.; Kim, R.; Park, S.; Mahmoudi, M.; Kraft, M. L., Impact of protein pre-coating on the protein corona composition and nanoparticle cellular uptake. *Biomaterials* **2016,** *75*, 295-304.

45. Grüttner, C.; Müller, K.; Teller, J.; Westphal, F.; Foreman, A.; Ivkov, R., Synthesis and antibody conjugation of magnetic nanoparticles with improved specific power absorption rates for alternating magnetic field cancer therapy. *Journal of Magnetism and Magnetic Materials* **2007,** *311* (1), 181-186.

46. Natarajan, A.; Gruettner, C.; Ivkov, R.; DeNardo, G.; Mirick, G.; Yuan, A.; Foreman, A.; DeNardo, S., NanoFerrite particle based radioimmunonanoparticles: binding affinity and in vivo pharmacokinetics. *Bioconjugate chemistry* **2008,** *19* (6), 1211-1218.

47. Landfester, K.; Bechthold, N.; Tiarks, F.; Antonietti, M., Miniemulsion Polymerization with Cationic and Nonionic Surfactants: A Very Efficient Use of Surfactants for Heterophase Polymerization. *Macromolecules* **1999,** *32* (8), 2679-2683.

48. Holzapfel, V.; Musyanovych, A.; Landfester, K.; Lorenz, M. R.; Mailänder, V., Preparation of Fluorescent Carboxyl and Amino Functionalized Polystyrene Particles by Miniemulsion Polymerization as Markers for Cells. *Macromolecular Chemistry and Physics* **2005,** *206* (24), 2440-2449.

49. Hofmann, D.; Tenzer, S.; Bannwarth, M. B.; Messerschmidt, C.; Glaser, S.-F.; Schild, H.; Landfester, K.; Mailaender, V., Mass Spectrometry and Imaging Analysis of Nanoparticle-Containing Vesicles Provide a Mechanistic Insight into Cellular Trafficking. *ACS Nano* **2014,** *8* (10), 10077-10088.

50. Bradshaw, R. A.; Burlingame, A. L.; Carr, S.; Aebersold, R., Reporting Protein Identification Data: The next Generation of Guidelines. *Molecular & Cellular Proteomics* **2006,** *5* (5), 787-788.

51. Silva, J. C.; Gorenstein, M. V.; Li, G.-Z.; Vissers, J. P. C.; Geromanos, S. J., Absolute Quantification of Proteins by LCMSE : A Virtue of Parallel ms Acquisition. *Molecular & Cellular Proteomics* **2006,** *5* (1), 144-156.

# 4. Unraveling *in vivo* corona formation

## Aim:

Up to now, there is only a very few number of reports, which analyzed the protein corona under *in vivo* conditions. The dynamic nature of blood and the multiple interactions between blood proteins, cells and platelets are additional factors, which affect the nanoparticles´ behavior upon intravenous injection. In this study, we were able to isolate nanoparticles directly from the blood stream after *in vivo* administration and it was possible to further analyze the *in vivo* protein corona profile. Moreover, this pattern was compared to the common *in vitro* situation using serum or plasma. Major differences between the *in vitro* compared to the *in vivo* situation were noticed. Therefore, an alternative *ex vivo* approach was developed, which could mimic *in vivo* corona formation. Overall, this study presents a novel strategy, which allows analyzing protein corona formation under physiological condition coming close to the *in vivo* situation.

## Contribution:

I carried out the complete protein corona analysis (SDS-PAGE, LC-MS, Pierce Assay) and conducted the cellular uptake experiments (flow cytometry). [redacted] performed the mouse *in vivo* experiments. [redacted] supported the *in vivo* experiments. The project was supervised by [redacted]

## Abstract

Understanding the interaction of nanoparticles upon contact with a physiological environment is of urgent need to improve the properties of nanoparticles for therapeutic applications. Most commonly, the interaction of nanoparticles with plasma proteins are performed under *in vitro* conditions. However, it has been shown that this does not reflect the complex situation after *in vivo* administration. Therefore, here we focused on the investigation of magnetic nanoparticles with blood proteins under *in vivo* conditions. In time dependent experiments, we found that the *in vivo* corona profile did not change significantly over time. Hence, major differences were observed for nanoparticles incubated under *in vitro* conditions underlining the significance of *in vivo* protein corona studies. Via an *ex vivo* approach, we were able to show, that we could mimic *in vivo* corona formation. Based on this, we present a comprehensive analysis focusing on the interaction between nanoparticles and blood proteins under *in vivo* conditions. This knowledge is needed to characterize the true biological identity of nanoparticles.

## Introduction

It is now widely accepted that upon contact of nanoparticles with biological fluid (e.g. blood) proteins rapidly adsorb to the surface forming the ´biomolecular corona´[1-2]. On one side, this process highly affects the physico-chemical properties of the nanoparticles and on the other side; it eventually determines their biological behavior[3-5]. Depending on the nanoparticle system, a direct link between cellular interactions and specific proteins was proven. For example, poly(butyl cyanoacrylate) nanoparticles, which were coated with apolipoprotein E were able to cross the blood-brain barrier[6-7]. Next to this, due to corona formation the colloid stability and biocompatibility of inorganic Au@$Fe_3O_4$ Janus particles was enhanced[8]. In strong contrast to this, several reports recognized that protein adsorption can significantly influence the targeting properties of nanoparticles[9-10]. Here, it was shown that there was no cellular targeting of transferrin-functionalized nanoparticle after corona formation, meaning that the targeting ligands is completely covered up by plasma proteins[11]. Therefore, it is of urgent need to understand and control the interaction of nanoparticles upon contact with blood proteins in order to improve their therapeutic efficiency[12].

Most *in vitro* studies utilize serum or plasma to investigate protein adsorption on nanoparticles[13]. Even depending on the specific protein source (human vs. mice or serum vs. plasma)[14] there have been significant differences noticed in terms of cellular uptake and protein corona composition[15-16]. Overall, the *in vitro* experiments give the opportunity to characterize general interaction between nanoparticles and proteins. However, it is still under investigation

to what extent this can reflect the *in vivo* situation[17]. Recently, Chen *et al.* reported the highly dynamic nature of the *in vivo* protein corona[18]. They showed that complement protein (C3) bound to the nanoparticle surface; however, upon contact with the blood stream other proteins rapidly exchanged C3 from the nanoparticles´ surfaces. The complex nature of blood and flow velocity are therefore additionally factors, which should be taken into account in order to evaluate the nanoparticles´ behavior under *in vivo* conditions[19].

Based on this, we aimed to characterize the *in vivo* corona of magnetic nanoparticles after they were exposed to the blood stream of mice. Our workflow allowed the direct recovery of the nanoparticles from the blood stream without the need of plasma preparation prior to nanoparticle recovery as described in other reports[20-22]. Nanoparticles were extracted from the blood stream via magnetic separation after a period of circulation in the mice for up to 2 h. A thorough proteomic analysis was carried out to identify the distinct protein corona pattern. The identified corona composition was compared to an *ex vivo* approach using mice blood or to an *in vitro* system using serum or plasma with different anticoagulants. Additionally, cellular experiments were performed to correlate the corona composition with the cellular uptake of nanoparticles directly recovered from the blood or incubated under *ex vivo* or *in vitro* conditions.

## Material and methods

**Nanoparticles.** Magnetite nanoparticles coated with hydroxyethyl starch (named as mgHES) were obtained by MicroMod. Nanoparticle are labelled with a IR-Dye D750 for *in vivo* imaging. According to the manufacture nanoparticles have a magnetic core of 75-80% (w/w) and and a solid content 10 mg/mL. Nanoparticles were synthesized via the core shell method.[23-24]

**Mice.** C57BL/6J mice were kept under specific pathogen-free conditions and on a standard diet in the central animal facilities of the Johannes Gutenberg-University of Mainz. For *in vitro* studies, blood was obtained from C57BL/6 mice and applied to pre-coated Sarstedt tubes to generate serum or plasma (EDTA, Heparin or Citrate) according to the manufacture´s protocol.

***In vivo* experiment.** Mice were treated with commercial available Clodronate Liposomes to deplete macrophages[35]. The next day, mgHES nanoparticles (1 mg) were injected into the tail vein of mice. After defined time point (1 min, 10 min, 60 min, 120 min) blood was isolated via cardiac puncture into a LoBind tube (Eppendorf) containing heparin. Mice were sacrificed and the distribution of the nanoparticle into the different organs was analysed using an *in vivo* imaging system (IVIS®). The nanoparticle concentration remaining in the blood was determined by Tecan infinite M1000 plate reader. For *ex vivo* experiments blood was isolated from the mice and further applied to the nanoparticle dispersion. An average mouse blood

volume of 2 mL was assumed and therefore nanoparticle blood concentration of 0.5 mg/mL was chosen for *ex vivo* experiments.

**Protein corona.** Nanoparticles were recovered from the blood via magnetic separation. The nanoparticle pellet was washed with water (3 times) to remove loosely and unbound proteins. For *in vitro* study, nanoparticles (1 mg) were incubated with (1 mL) serum or plasma and the hard corona was magnetically isolated after 1 min or 2 h incubation at 37 °C. Proteins were desorbed from the nanoparticle surface using 2% SDS (62.5 mM Tris*HCl). The sample was heated up to 95 °C for 5 min. Via magnetic separation the nanoparticle pellet was separated and the supernatant was analysed.

**Pierce Assay.** To determine the protein concentration, the standard Pierce Assay was performed according to the manufactures instruction.

**SDS PAGE.** Proteins (1 µg) were mixed with NuPAGE LDS sample buffer, NuPAGE sample reducing agent and applied to NuPAGE 10% Bis Tris Protein gel (Thermo Fisher). The gel was run in NuPAGE MES SDS running buffer at 100 V for 1 h. SeeBlue Plus2 Pre-Stained Standard served as a molecular marker. Protein bands were visualized using the SilverQuest™ Silver Staining kit from ThermoFisher Scientific as recommended.

**LC-MS.** Proteomic analysis of the protein corona was carried out using Synapt G2-Si mass spectrometer coupled with a nanoACQUITY UPLC system under standard condition according to previously published protocols[36-38].

**Cell culture.** RAW264.7 were kept in Dulbecco´s modified eagle medium (DMEM) supplemented with 10 % FBS, 100 U/mL penicillin, 100 mg/mL streptomycin and 2 mM glutamine (Thermo Fisher).

**Cell uptake by flow cytometry.** 100 000 cells were seeded out into 24-well and incubated overnight at 37 °C. Protein corona coated nanoparticles (75 µg/mL) were added to cells for 2 h, 37 °C. For flow cytometry measurements, cells were washed with PBS, detached with 0.25% Trypsin-EDTA and centrifuged (500 g, 5 min). Samples were resuspended with PBS and analyzed by flow cytometry via Attune NxT Flow Cytometer.

## Results and discussion

Magnetic nanoparticles (Figure 4.1) which are covered with hydroxyethyl starch (mgHES)[23-24] were injected into C57BL/6 mice. After distinct time points (1 min – 2 h), blood was isolated via cardiac puncture. Nanoparticles were recovered from the blood via magnetic separation in order to identify the key proteins which adsorbed to the nanoparticles after *in vivo*

administration (material/methods see supplementary information 4). After animals were sacrificed, the *in vivo* biodistribution of the nanoparticles was visualized with an *in vivo* imaging system IVIS®. Representative images shown for a time point of 10 min, demonstrated that the nanoparticles did not accumulate in any specific organ. Nanoparticles were rather distributed over the whole organism.

Further, the remaining amount of nanoparticles in the blood was quantified after the different time point to investigate the circulation time. After 10 min ~ 80% of the nanoparticles were detected in blood. Even after 2 h, ~ 35% of the initial amount of nanoparticles remained in the blood (Figure 4.1). This relatively long circulation time is probably attributed to the hydroxyethyl starch (HES) coating. Various studies proved that nanoparticles modified with HES (HESylation)[25] showed a reduced cell interaction and prolong blood circulation times comparable to PEGylated nanoparticles[26-27]. For the here presented study, it allowed us to recover a sufficient amount of nanoparticles from the blood stream for further protein corona analysis.

The hard corona of nanoparticles isolated after *in vivo* administration was compared to the corona of nanoparticles, which were incubated under *in vitro* condition using serum or plasma. For plasma generation different anticoagulants were chosen (heparin, EDTA or citrate). In our previous studies we already found that the anticoagulant (in this case heparin) can influence protein adsorption and cellular uptake of nanoparticles[16]. Serum and plasma was obtained from the same mice strain used for the *in vivo* studies to minimize difference in the blood protein composition.

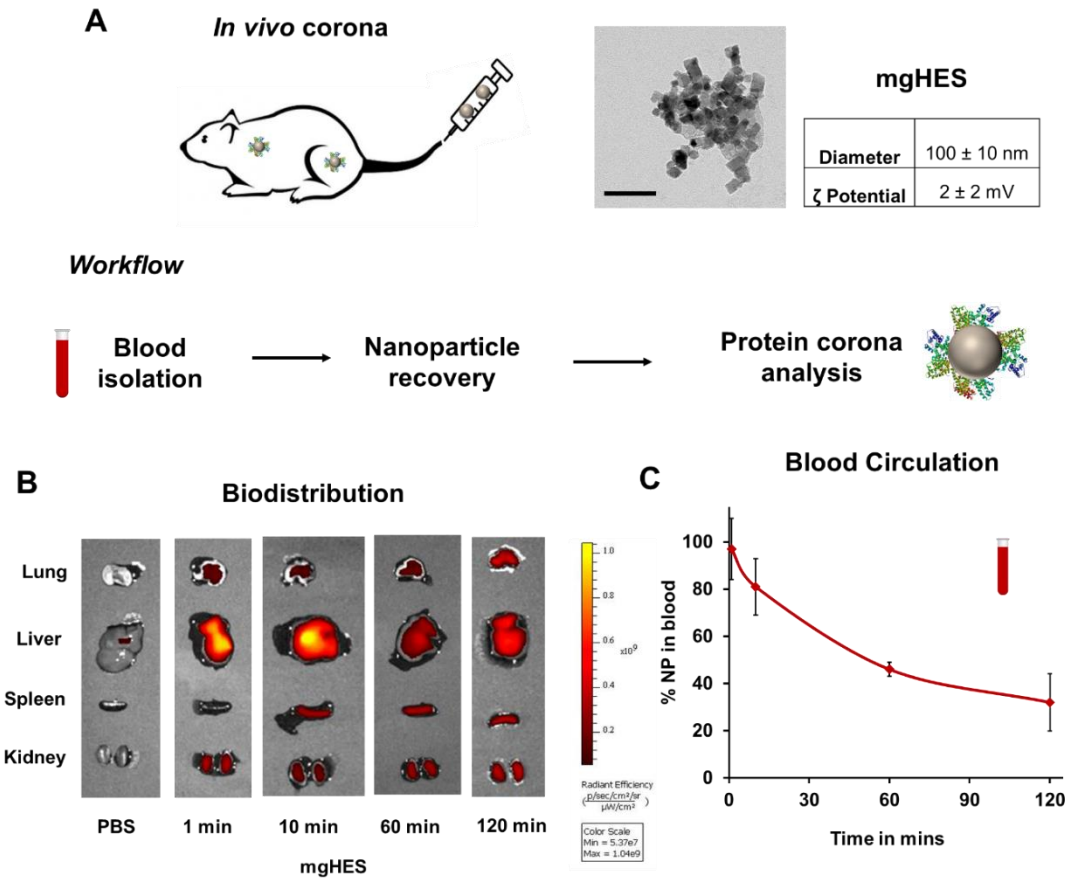


**Figure 4. 1.** Monitoring the biodistribution and blood circulation of magnetic HES nanoparticles *in vivo*. **A)** Magnetic HES nanoparticles (mgHES) were injected into mice and the blood was isolated after distinct time points (1 min – 2 h). Nanoparticles were recovered from the blood via magnetic separation and further the protein adsorption pattern surrounding the *in vivo* nanoparticles was anaylzed. **B)** The biodistribution of the nanoparticles into different organs was visualized by IVIS®. [redacted] **C)** The nanoparticle concentration in blood after distinct time points was measured via a Tecan Plate Reader and normalized based on the initial injected amount of nanoparticles.

As highlighted via SDS PAGE there are major difference in the hard corona pattern for nanoparticles after *in vivo* administration compared to the *in vitro* situation (Figure 4.2). The *in vitro* corona is mainly dominated by two or three major proteins whereas after *in vivo* administration nanoparticles are surrounded by a broad variety of proteins. Additionally, LC-MS analysis was carried out to determine the key corona proteins. The absolute number of identified proteins displayed the distinct difference between the *in vivo* situation compared to the *in vitro* situation. Overall, we found a significant higher number of proteins for the *in vivo* corona (467) compared to the *in vitro* corona (190). On top of that, the two corona types shared just 69 common proteins (Figure 4.2).

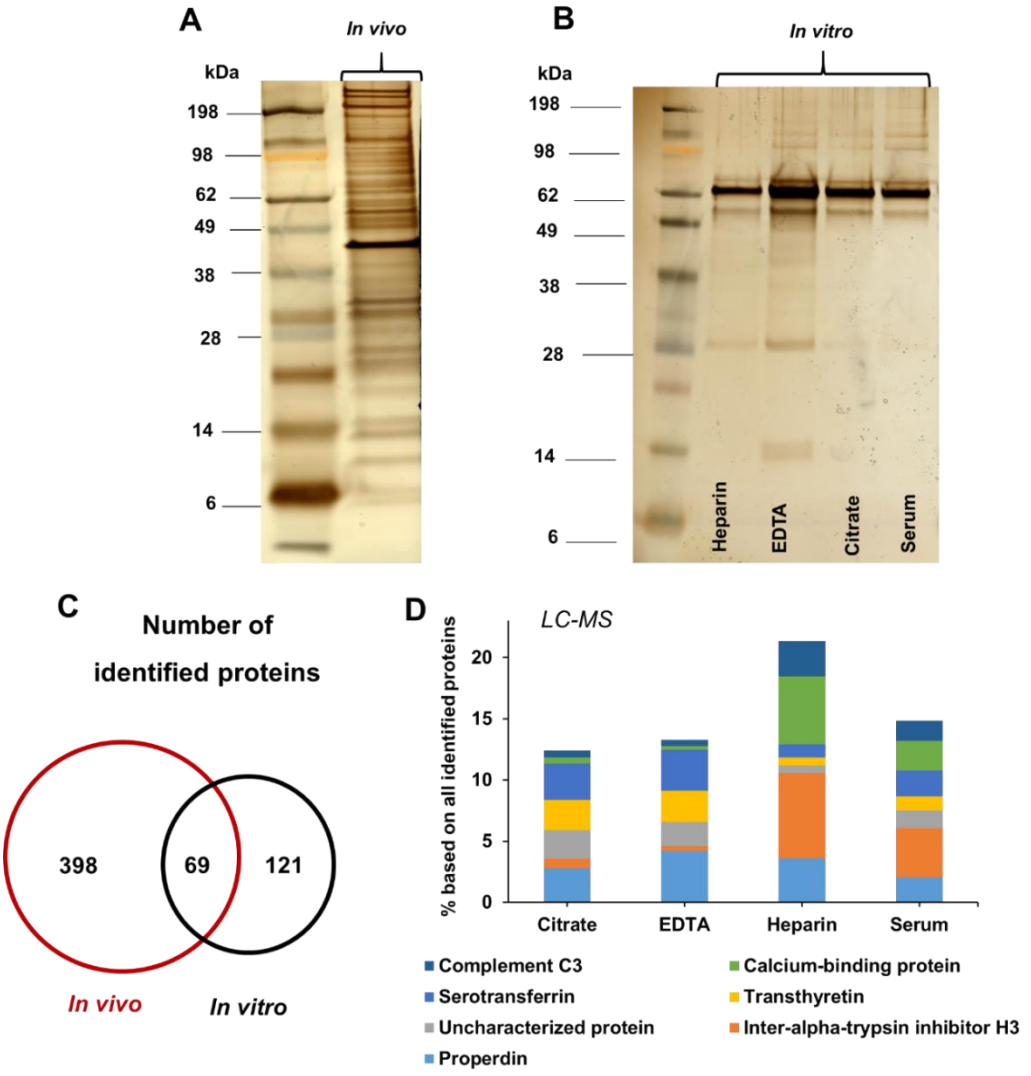


**Figure 4. 2.** The *in vivo* corona pattern is not comparable with the *in vitro* situation. **A)** Nanoparticles were recovered from the blood stream and purified for protein corona analysis via magnetic separation. **B)** In comparison to the *in vivo* situation, mgHES nanoparticles were incubated with serum or plasma (heparin, EDTA or citrat) for *in vitro* protein corona analysis. As visualized by SDS PAGE (A-B) the pattern for the *in vivo* and *in vitro* situation differed significantly. **C)** LC-MS analysis indicated that the total number of proteins identified for the *in vivo* corona was significantly higher compared to the *in vitro* situation. Both corona types shared a minor number of proteins. **D)** The most abundant proteins for the *in vitro* coronas were compared, which indicates that the anticoagulant and preparation method (serum or plasma) additionally influences corona formation.

As mentioned above, there have been studies, which reported significant difference for the *in vitro* protein corona pattern if nanoparticles where incubated with serum compared to plasma[28]. However, a detailed proteomic investigation considering all different anticoagulants is still missing. Here, we selected the most abundant corona proteins for the four different *in vitro* incubated nanoparticles (Figure 4.2). Overall, this showed that the corona composition of

citrate and EDTA is highly similar (additional SDS PAGE in supplementary information 4). In contrast, the protein pattern differed if nanoparticles were incubated with serum or heparin plasma. The protein composition after serum and heparin plasma incubation is additionally enriched with calcium-binding protein and complement C3. Both proteins bind and require calcium for their functionality[29-30]. Citrate and EDTA are both chelating calcium to prevent blood clotting during the process of plasma preparation[31]. This can explain the difference observed for the corona composition depending on the chosen anticoagulant.

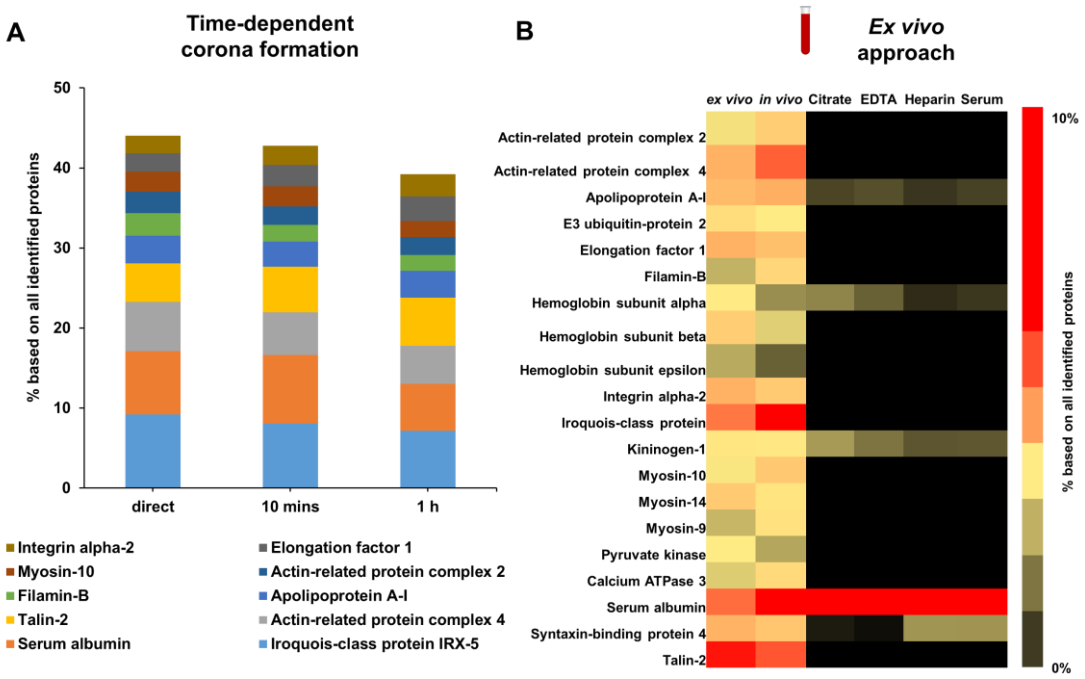


**Figure 4. 3.** *In vivo* protein corona formation occurs rapidly and does not change significantly over time. **A)** The protein corona composition *in vivo* was compared for three different time points (1 min, 10 min or 1 h). The 10 most abundant proteins contributed to ~45 % and indicated no significant difference in their relative abundance. **B)** To mimic *in vivo* corona formation, nanoparticles were incubated directly in blood (*ex vivo*). The heat map of the 25 most abundant corona proteins highlights the similarity between the *ex vivo* and *in vivo* corona.

To further characterize the *in vivo* corona composition, the protein pattern was monitored over time (direct recovery up to 60 min). We saw that the overall protein composition did not significantly change over time (Figure 4.3). As we observed the significant difference for the *in vitro* situation compared to the *in vivo* situation, we aimed for a strategy, which reflects the *in vivo* behavior. Here, we chose the *ex vivo* approach. Blood was isolated from mice and nanoparticles were directly applied to it. The *ex vivo* corona was purified in analogy to the *in*

*vivo* or *in vitro* corona. The heat map reflecting the 25 most abundant corona proteins highlights that the *ex vivo* corona is highly comparable to the *in vivo* corona (Figure 4.3). This is in strong contrast with the pattern for the *in vitro* corona. This indicated that the *ex vivo* approach reflects the *in vivo* situation most closely.

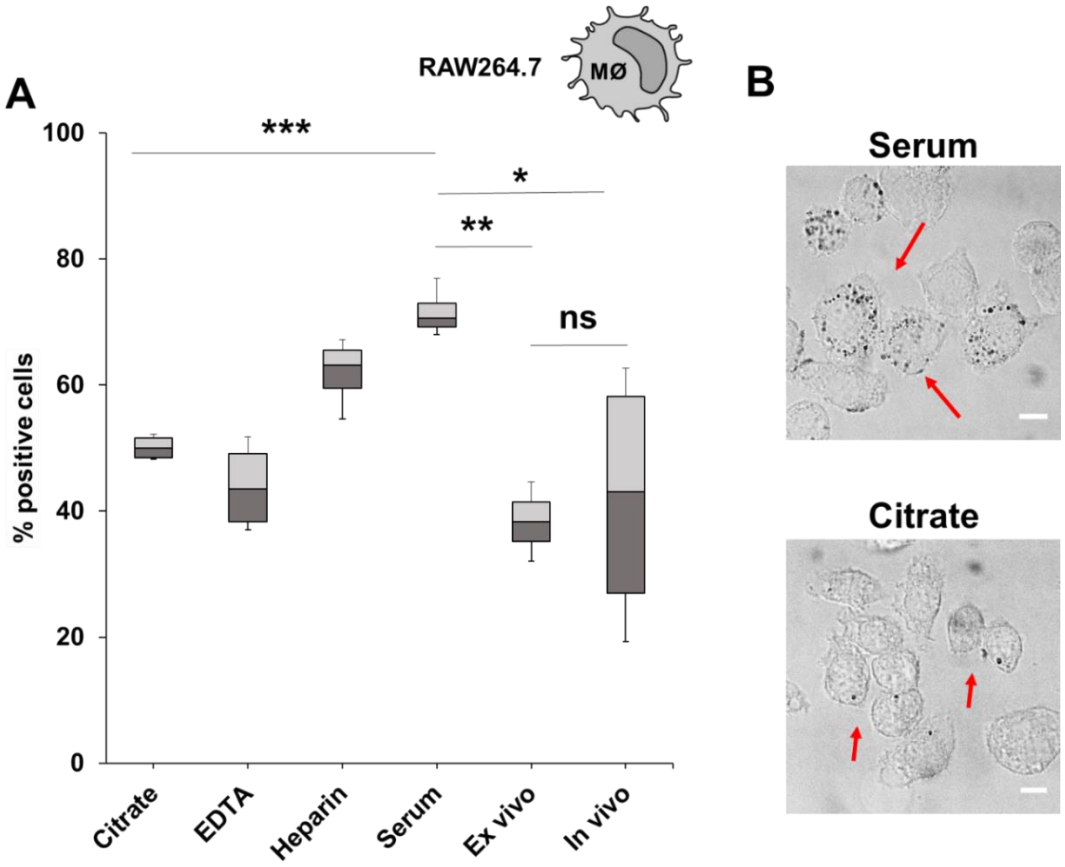


**Figure 4. 4**. Cellular uptake of protein corona coated nanoparticles depends on the anticoagulant and differs for nanoparticles recovered from the blood stream *(in vivo)* **A)** Nanoparticles were incubated with serum, plasma, blood or isolated after *in vivo* administration. Hard corona coated nanoparticles were subsequently added to macrophages (RAW264.7) for 2 h at a concentration of 75 µg/mL. Cellular uptake was analysed via flow cytometry. The amount of fluorescent positive cells is shown. **B)** Representative confocal images illustrate the intracellular distribution of the nanoparticles. RAW264.7 cells were treated with serum or citrate plasma coated nanoparticles for 2 h at a concentration of 75 µg/mL. Scale bar: 10 µm. $p < 0.05$* $p < 0.01$** $p < 0.001$**

As shown in a great number of reports, due to corona formation the cellular interactions are strongly altered[32-33]. Therefore, we wanted to study cellular uptake of nanoparticles coated with the *in vitro* corona compared to the *ex vivo* or *in vivo* corona. Cellular interaction towards a

mouse macrophage cell line (RAW264.7) was analyzed by flow cytometry and confocal imaging (Figure 4.4).

Already for the four *in vitro* incubated nanoparticles, we found significant differences in the cellular uptake behavior. In line with the corona composition, cellular internalization of citrate and EDTA coated nanoparticles is comparable. Those nanoparticles displayed a significant lower internalization rate compared to heparin or serum coated nanoparticles. As we identified an enrichment of complement proteins in the corona after serum or heparin incubation, this might explain the difference in the cellular uptake behavior. Complement proteins are widely identified in the corona of various nanoparticles and were shown to enhance interactions with immune cells[18, 34]. Lastly, we saw that cellular uptake of *ex vivo* and *in vivo* incubated nanoparticles is comparable (Figure 4.4). This underlines the similarity between the *ex vivo* approach and *in vivo* situation.

## Conclusion

In this study, we magnetically isolated nanoparticles directly from the blood stream after different time points. With this method, we were able to recover nanoparticles surrounded by the *in vivo* protein corona without extensive purification steps, which could alter the protein corona profile. We found that the *in vivo* protein corona differed significantly compared to *in vitro* incubated nanoparticles. Additionally, we noticed that the chosen anticoagulant should be carefully considered, as we observed major differences in the corona composition after incubation with serum or plasma supplemented with heparin, EDTA or citrate. For our here presented *ex vivo* approach, we found that the corona composition was comparable to the *in vivo* situation. Therefore, with this study we aimed to improve the understanding of the *in vivo* corona formation, which is urgently needed in order to reveal the nanoparticles´ behavior under physiological conditions.

## Supplementary information

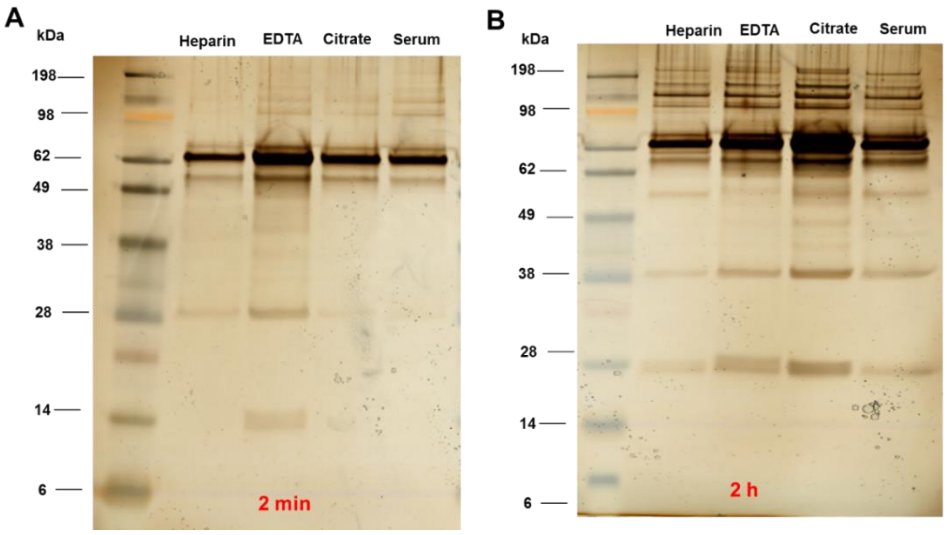


**Figure 4. 5.** mgHES nanoparticles were incubated with plasma or serum for 2 min **(A)** or 2 h **(B).** The hard corona was purified via magnetic separation. Proteins were desorbed from the nanoparticle surface and visualized by SDS PAGE.

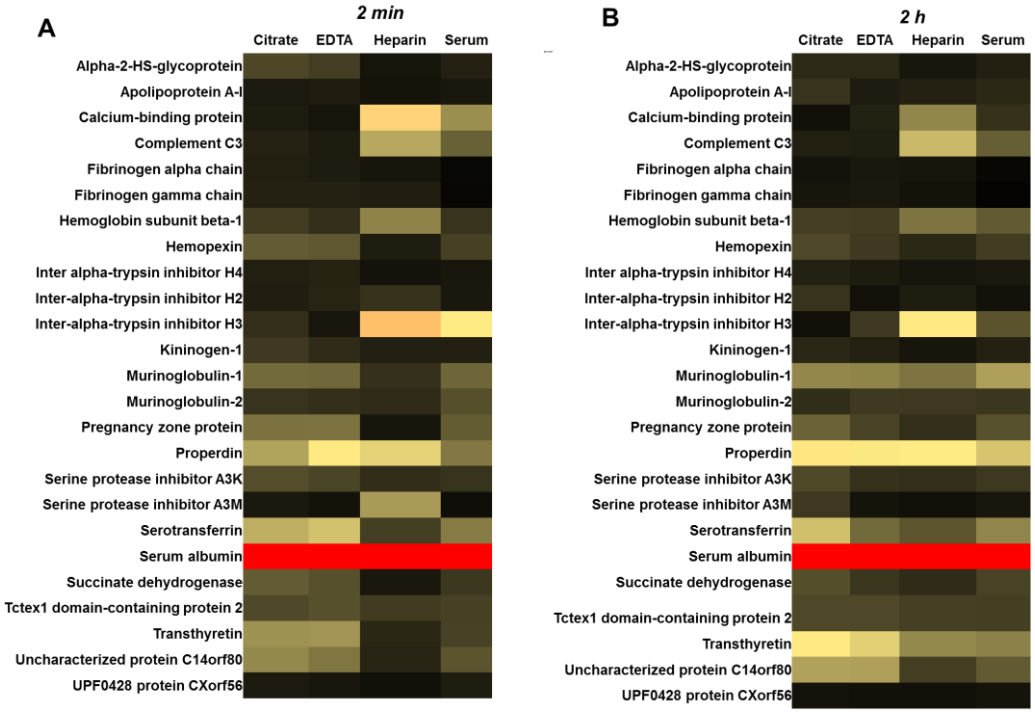


**Figure 4. 6.** Hard corona proteins after 2 min **(A)** or 2 h **(B)** *in vitro* incubation were analysed by LC-MS. The most abundant proteins (25) are summarized in the heat map.

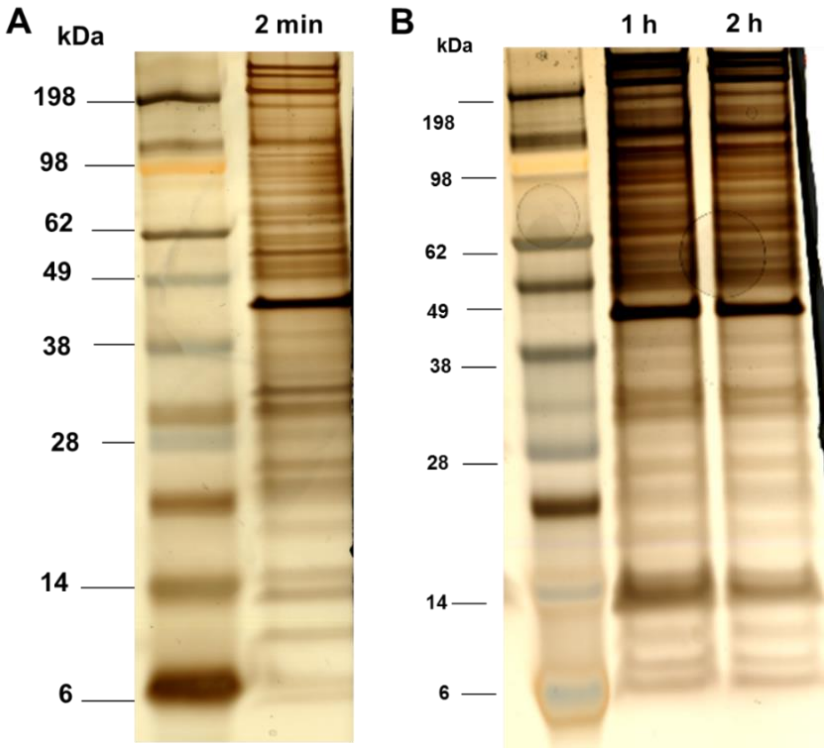


**Figure 4. 7.** mgHES nanoparticles were injected into mice, the blood was isolated after distinct time points (**A** = 2 min, **B** = 1 h or 2 h) and nanoparticles were recovered via magnetic separation. The hard corona pattern was visualized by SDS-PAGE.

## Literature

1. Monopoli, M. P.; Aberg, C.; Salvati, A.; Dawson, K. A., Biomolecular coronas provide the biological identity of nanosized materials. *Nature Nanotech.* **2012,** *7* (12), 779-86.

2. Ke, P. C.; Lin, S.; Parak, W. J.; Davis, T. P.; Caruso, F., A Decade of the Protein Corona. *ACS nano* **2017,** *11* (12), 11773-11776.

3. Yallapu, M. M.; Chauhan, N.; Othman, S. F.; Khalilzad-Sharghi, V.; Ebeling, M. C.; Khan, S.; Jaggi, M.; Chauhan, S. C., Implications of protein corona on physico-chemical and biological properties of magnetic nanoparticles. *Biomaterials* **2015,** *46*, 1-12.

4. Monopoli, M. P.; Pitek, A. S.; Lynch, I.; Dawson, K. A., Formation and characterization of the nanoparticle-protein corona. *Methods Mol Biol* **2013,** *1025*, 137-55.

5. Tenzer, S.; Docter, D.; Rosfa, S.; Wlodarski, A.; Kuharev, J.; Rekik, A.; Knauer, S. K.; Bantz, C.; Nawroth, T.; Bier, C.; Sirirattanapan, J.; Mann, W.; Treuel, L.; Zellner, R.; Maskos, M.; Schild, H.; Stauber, R. H., Nanoparticle Size Is a Critical Physicochemical Determinant of the Human Blood Plasma Corona: A Comprehensive Quantitative Proteomic Analysis. *ACS Nano* **2011,** *5* (9), 7155-7167.

6. Kreuter, J.; Shamenkov, D.; Petrov, V.; Ramge, P.; Cychutek, K.; Koch-Brandt, C.; Alyautdin, R., Apolipoprotein-mediated transport of nanoparticle-bound drugs across the blood-brain barrier. *Journal of drug targeting* **2002,** *10* (4), 317-325.

7. Wagner, S.; Zensi, A.; Wien, S. L.; Tschickardt, S. E.; Maier, W.; Vogel, T.; Worek, F.; Pietrzik, C. U.; Kreuter, J.; Von Briesen, H., Uptake mechanism of ApoE-modified nanoparticles on brain capillary endothelial cells as a blood-brain barrier model. *PloS one* **2012,** *7* (3), e32568.

8. Landgraf, L.; Christner, C.; Storck, W.; Schick, I.; Krumbein, I.; Dähring, H.; Haedicke, K.; Heinz-Herrmann, K.; Teichgräber, U.; Reichenbach, J. R., A plasma protein corona enhances the biocompatibility of Au@ Fe3O4 Janus particles. *Biomaterials* **2015,** *68*, 77-88.

9. Dai, Q.; Bertleff-Zieschang, N.; Braunger, J. A.; Björnmalm, M.; Cortez-Jugo, C.; Caruso, F., Particle Targeting in Complex Biological Media. *Advanced healthcare materials* **2017**.

10. Mirshafiee, V.; Mahmoudi, M.; Lou, K.; Cheng, J.; Kraft, M. L., Protein corona significantly reduces active targeting yield. *Chem. Commun.* **2013,** *49* (25), 2557-2559.

11. Salvati, A.; Pitek, A. S.; Monopoli, M. P.; Prapainop, K.; Bombelli, F. B.; Hristov, D. R.; Kelly, P. M.; Aberg, C.; Mahon, E.; Dawson, K. A., Transferrin-functionalized nanoparticles lose their targeting capabilities when a biomolecule corona adsorbs on the surface. *Nature Nanotech.* **2013,** *8* (2), 137-43.

12. Jain, P.; Pawar, R.; Pandey, R.; Madan, J.; Pawar, S.; Lakshmi, P.; Sudheesh, M., In-vitro in-vivo correlation (IVIVC) in nanomedicine: Is protein corona the missing link? *Biotechnology advances* **2017,** *35* (7), 889-904.

13. Lundqvist, M.; Augustsson, C.; Lilja, M.; Lundkvist, K.; Dahlbäck, B.; Linse, S.; Cedervall, T., The nanoparticle protein corona formed in human blood or human blood fractions. *PloS one* **2017,** *12* (4), e0175871.

14. Müller, L. K.; Simon, J.; Rosenauer, C.; Mailänder, V.; Morsbach, S.; Landfester, K., The transferability from animal models to humans: challenges regarding aggregation and protein corona formation of nanoparticles. *Biomacromolecules* **2018,** *19* (2), 374-385.

15. Caracciolo, G.; Pozzi, D.; Capriotti, A.; Cavaliere, C.; Piovesana, S.; La Barbera, G.; Amici, A.; Laganà, A., The liposome–protein corona in mice and humans and its implications for in vivo delivery. *J Mater Chem B* **2014,** *2* (42), 7419-7428.

16. Schöttler, S.; Klein, K.; Landfester, K.; Mailander, V., Protein source and choice of anticoagulant decisively affect nanoparticle protein corona and cellular uptake. *Nanoscale* **2016**.

17. Bertrand, N.; Grenier, P.; Mahmoudi, M.; Lima, E. M.; Appel, E. A.; Dormont, F.; Lim, J.-M.; Karnik, R.; Langer, R.; Farokhzad, O. C., Mechanistic understanding of in vivo protein corona formation on polymeric nanoparticles and impact on pharmacokinetics. *Nature communications* **2017,** *8* (1), 777.

18. Chen, F.; Wang, G.; Griffin, J. I.; Brenneman, B.; Banda, N. K.; Holers, V. M.; Backos, D. S.; Wu, L.; Moghimi, S. M.; Simberg, D., Complement proteins bind to nanoparticle protein corona and undergo dynamic exchange in vivo. *Nature nanotechnology* **2017,** *12* (4), 387.

19. Palchetti, S.; Pozzi, D.; Capriotti, A. L.; La Barbera, G.; Chiozzi, R. Z.; Digiacomo, L.; Peruzzi, G.; Caracciolo, G.; Laganà, A., Influence of dynamic flow environment on nanoparticle-protein corona: From protein patterns to uptake in cancer cells. *Colloids and Surfaces B: Biointerfaces* **2017,** *153*, 263-271.

20. Hadjidemetriou, M.; Al-Ahmady, Z.; Mazza, M.; Collins, R. F.; Dawson, K.; Kostarelos, K., In vivo biomolecule corona around blood-circulating, clinically used and antibody-targeted lipid bilayer nanoscale vesicles. *ACS nano* **2015,** *9* (8), 8142-8156.

21. Hadjidemetriou, M.; Al-Ahmady, Z.; Kostarelos, K., Time-evolution of in vivo protein corona onto blood-circulating PEGylated liposomal doxorubicin (DOXIL) nanoparticles. *Nanoscale* **2016,** *8* (13), 6948-6957.

22. Amici, A.; Caracciolo, G.; Digiacomo, L.; Gambini, V.; Marchini, C.; Tilio, M.; Capriotti, A.; Colapicchioni, V.; Matassa, R.; Familiari, G., In vivo protein corona patterns of lipid nanoparticles. *RSC Advances* **2017,** *7* (2), 1137-1145.

23. Grüttner, C.; Müller, K.; Teller, J.; Westphal, F.; Foreman, A.; Ivkov, R., Synthesis and antibody conjugation of magnetic nanoparticles with improved specific power absorption rates for alternating magnetic field cancer therapy. *Journal of Magnetism and Magnetic Materials* **2007,** *311* (1), 181-186.

24. Natarajan, A.; Gruettner, C.; Ivkov, R.; DeNardo, G.; Mirick, G.; Yuan, A.; Foreman, A.; DeNardo, S., NanoFerrite particle based radioimmunonanoparticles: binding affinity and in vivo pharmacokinetics. *Bioconjugate chemistry* **2008,** *19* (6), 1211-1218.

25. Liebner, R.; Mathaes, R.; Meyer, M.; Hey, T.; Winter, G.; Besheer, A., Protein HESylation for half-life extension: synthesis, characterization and pharmacokinetics of HESylated anakinra. *European Journal of Pharmaceutics and Biopharmaceutics* **2014,** *87* (2), 378-385.

26. Kang, B.; Opatz, T.; Landfester, K.; Wurm, F. R., Carbohydrate nanocarriers in biomedical applications: functionalization and construction. *Chemical Society Reviews* **2015,** *44* (22), 8301-8325.

27. Noga, M.; Edinger, D.; Kläger, R.; Wegner, S. V.; Spatz, J. P.; Wagner, E.; Winter, G.; Besheer, A., The effect of molar mass and degree of hydroxyethylation on the controlled shielding and deshielding of hydroxyethyl starch-coated polyplexes. *Biomaterials* **2013,** *34* (10), 2530-2538.

28. Mirshafiee, V.; Kim, R.; Mahmoudi, M.; Kraft, M. L., The importance of selecting a proper biological milieu for protein corona analysis in vitro: Human plasma versus human serum. *The international journal of biochemistry & cell biology* **2016,** *75*, 188-195.

29. Thielens, N.; Lohner, K.; Esser, A., Human complement protein C9 is a calcium binding protein. Structural and functional implications. *Journal of Biological Chemistry* **1988,** *263* (14), 6665-6670.

30. Ziccardi, R. J. In *The first component of human complement (C1): activation and control*, Springer seminars in immunopathology, Springer: 1983; pp 213-230.

31. Kirschfink, M.; Mollnes, T. E., Modern complement analysis. *Clinical and diagnostic laboratory immunology* **2003,** *10* (6), 982-989.

32. Cheng, X.; Tian, X.; Wu, A.; Li, J.; Tian, J.; Chong, Y.; Chai, Z.; Zhao, Y.; Chen, C.; Ge, C., Protein corona influences cellular uptake of gold nanoparticles by phagocytic and nonphagocytic cells in a size-dependent manner. *ACS applied materials & interfaces* **2015,** *7* (37), 20568-20575.

33. Kokkinopoulou, M.; Simon, J.; Landfester, K.; Mailänder, V.; Lieberwirth, I., Visualization of the Protein Corona: towards a biomolecular understanding of nanoparticle-cell-interactions. *Nanoscale* **2017**.

34. Shen, L.; Tenzer, S.; Storck, W.; Hobernik, D.; Raker, V. K.; Fischer, K.; Decker, S.; Dzionek, A.; Krauthauser, S.; Diken, M.; Nikolaev, A.; Maxeiner, J.; Schuster, P.; Kappel, C.; Verschoor, A.; Schild, H.; Grabbe, S.; Bros, M., Protein corona-mediated targeting of nano-carriers to B cells allows redirection of allergic immune responses. *J Allergy Clin Immunol* **2018**.

35. van Rooijen, N.; Hendrikx, E., Liposomes for specific depletion of macrophages from organs and tissues. *Liposomes: Methods and Protocols, Volume 1: Pharmaceutical Nanocarriers* **2010**, 189-203.

36. Kokkinopoulou, M.; Simon, J.; Landfester, K.; Mailänder, V.; Lieberwirth, I., Visualization of the protein corona: towards a biomolecular understanding of nanoparticle-cell-interactions. *Nanoscale* **2017,** *9* (25), 8858-8870.

37. Schöttler, S.; Becker, G.; Winzen, S.; Steinbach, T.; Mohr, K.; Landfester, K.; Mailänder, V.; Wurm, F. R., Protein adsorption is required for stealth effect of poly (ethylene glycol)-and poly (phosphoester)-coated nanocarriers. *Nature nanotechnology* **2016,** *11* (4), 372.

38. Docter, D.; Distler, U.; Storck, W.; Kuharev, J.; Wünsch, D.; Hahlbrock, A.; Knauer, S. K.; Tenzer, S.; Stauber, R. H., Quantitative profiling of the protein coronas that form around nanoparticles. *Nature protocols* **2014,** *9* (9), 2030.

# Chapter B

## Stealth coating for nanoparticles: Avoiding unintended cellular uptake

In chapter B there are three different publications **(5-7)** summarized. Overall, these studies aimed to investigate the stealth behavior of nanoparticles. In the following first an introduction about current strategies, which are applied to obtain stealth properties are presented and afterwards each publication is summarized.

**[5]** [redacted] Hydrophilicity regulates the stealth properties of poly(phosphoester)-coated nanocarries. *Angewandte Chemie,* **2018,** doi: 10.1002/anie.201800272. **(*shared first)**

**[6]** [redacted] Protein corona mediated stealth properties of biocompatible carbohydrate-based nanocarries. *Biomaterials,* **2018 (*shared first, under revision)**

**[7]** [redacted] Exploiting the biomolecular corona: Pre-coating of nanoparticles enables controlled cellular interactions. *Nanoscale,* **2018** (under revision)

## Introduction

One of the major drawbacks, which has been recognized since the early investigations of nanoparticles as drug delivery vehicles, is their rapid clearance from the bloodstream by the mononuclear phagocytic system (MPS)[85-86]. This implies that the nanoparticles are not able to reach the targeted cell. In contrast, long circulating substances can specifically accumulate in the tumor tissue, which is based on the enhanced permeability and retention (EPR) effect (details see chapter C)[87].

The MPS consists of phagocytic cells (e.g. monocytes and macrophages), which are located in the spleen, lymph node and liver (here named as ´Kupffer cells´)[88]. Further, the MPS is part of the innate immune system and is responsible for the recognition and internalization of foreign material (e.g. bacteria or fungi). Therefore, nanoparticles provide the ideal target for phagocytic cells, hereby limiting their therapeutic success[89].

The initial recognition of nanoparticles by phagocytic cells is driven by the adsorption of blood proteins towards the nanoparticle surface. This process is widely referred to as opsonization[36]. Commonly, immunoglobulins and complement proteins are classified as opsonins as they mediate cellular uptake of nanoparticles via Fc or complement receptors[36]. These receptors are highly expressed on the surface of phagocytic cells. In contrast, dysopsonins are proteins, which prevent cellular recognition. These proteins have been studied less.

In the following, various strategies will be described, which have been investigated to prolong the blood circulation time and improve the pharmacokinetic profile of nanoparticles. The most common and widely studied approach is the covalent attachment of poly (ethylene glycol) (PEG) to the surface of nanoparticles. Therefore, an additional part will highlight the influence of PEGylation on protein adsorption, cellular interactions and biodistribution of various nanoparticles. Moreover, novel alternative polymer classes will be presented, which can potentially used instead of PEG.

### B.1 Strategies

In the 1970s Davis and colleagues conjugated PEG to bovine serum albumin and bovine liver catalase[90]. They saw that the circulating lifetime of PEGylated proteins was significantly enhanced compared to unmodified ones. In this pioneering work, they proved that PEGylation is a feasible method to improve the pharmacokinetic profile of macromolecules. In the following years; the concept of PEGylation was extended to various molecules (including nanoparticles, peptides, antibodies or organic molecules) and it is today´s gold standard to achieve a prolonged blood circulation time[91-92]. Already in 1995, the FDA approved PEGylated

liposomes, which contain doxorubicine for cancer treatment. It was shown that PEGylated liposomes had an eightfold increased blood circulation time compared to bare liposomes[93].

However, in recent years there have been serious concerns raised against the use of PEG for biomedical applications. Various studies found that PEG can elicit antibody formation and that PEG is not, as reported in the initial studies, non-immunogenic[94]. Other studies confirmed that PEG can induce complement activation[95]. Next to this, PEG is a non-biodegradable material. Taking this together, it is of great interest to seek for alternative strategies, which enable prolonged blood circulation times of nanoparticles (Figure B.1).

In 2013, Rodriguez *et al.* developed an elegant strategy to improve the therapeutic efficiency of nanoparticles[96]. They used computationally designed peptides derived from the protein CD47 and attached this to the surface of nanobeads. *In vivo* studies confirmed enhanced blood circulation times in mice. CD47 is a signal-regulatory protein, which gives a ´don't eat me´ signal to the immune system. Therefore, nanoparticles, which are covered with CD47 peptides are not recognized by phagocytic cells.

Inspired by nature, researchers came up with several other biomimetic strategies. Initial studies used the membrane of red blood cells (RBC) to coat poly(lactic-co-glycolic acid) (PLGA) nanoparticles. They were able to proof a prolonged blood circulation of RBC coated nanoparticles up to 72 h[97].

Parodi *et al.* developed a similar concept[98]. The nanoparticles´ surface was covered with a leukocytic membrane and this prevented cellular uptake into phagocytic cells. Additionally, they saw that ´leukolike´ nanoparticles were able to interact with endothelial cells. *In vivo* studies confirmed the improved pharmacokinetic properties due to the leuko-coating and the successful accumulation of nanoparticles in the tumor tissue.

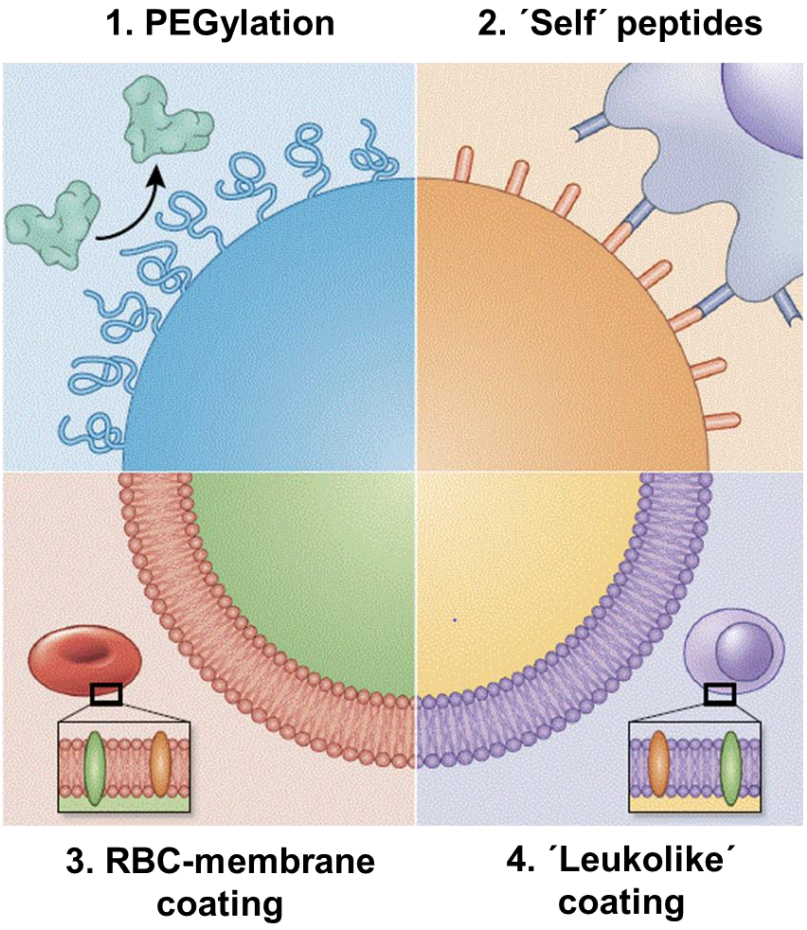


**Figure B. 1.** The surface of the nanoparticle is modified via different strategies to avoid the interaction of nanoparticles with phagocytic cells and hereby prolonging their blood circulation. 1) PEGylation is the classical approach to reduce protein interactions and prevent cellular uptake by macrophages. **2)** CD47 peptides are attached to the surface of nanoparticles to avoid interaction with the MPS. **3+4)** Biomimetic strategies use the cell membrane of red blood cells or leukocytes for particle coating. Figure adaptated and modified from ´Principles of nanoparticle design for overcoming biological barriers to drug delivery´. Copyright @ 2015 Springer Nature. Reprinted with permission from Nature Biotechnology. *Ref.* Nature Biotechnology 2015, 33(9), 941-951

### B.2 PEGylation

As poly(ethylene glycol) has ideal polymer properties for biomedical applications, it is one of the most widely used polymers in pharmaceutical industry[99]. PEG is non-toxic, has a high water solubility and can be synthesized in a broad molecular weight range (400 Da to 50 kDa) with a low polydispersity index (PDI < 1.1) via anionic ring opening polymerization of ethylene oxide[100]. Overall, PEG has flexible polymer chains and can obtain different conformations.

For nanoparticle modification, commonly PEG with a molecular weight between 1 kDa and 10 kDa is used. For smaller molecules e.g. siRNA or drugs, a higher molecular weight is chosen (20 kDa to 50 kDa) to prevent renal clearance[101].

Depending on the molecular weight and the density of PEG, it is either attached to the nanoparticle surface in a ´brush conformation´ or a ´mushroom-like structure´[102]. Most studies use NMR, dynamic light scattering or ζ-potential measurements to determine the degree of PEGylation quantitatively[103-104]. Furthermore, via theoretical calculation the PEGylation density is estimated assuming complete surface coverage of PEG for a given nanoparticle surface area. Perry *et al.* summarized several literature reports, which investigated the PEGylation density and correlated this with macrophage uptake and protein resistance[105]. Overall, it was concluded that a brush conformation is favorable to increase blood circulation times and biodistribution.

.

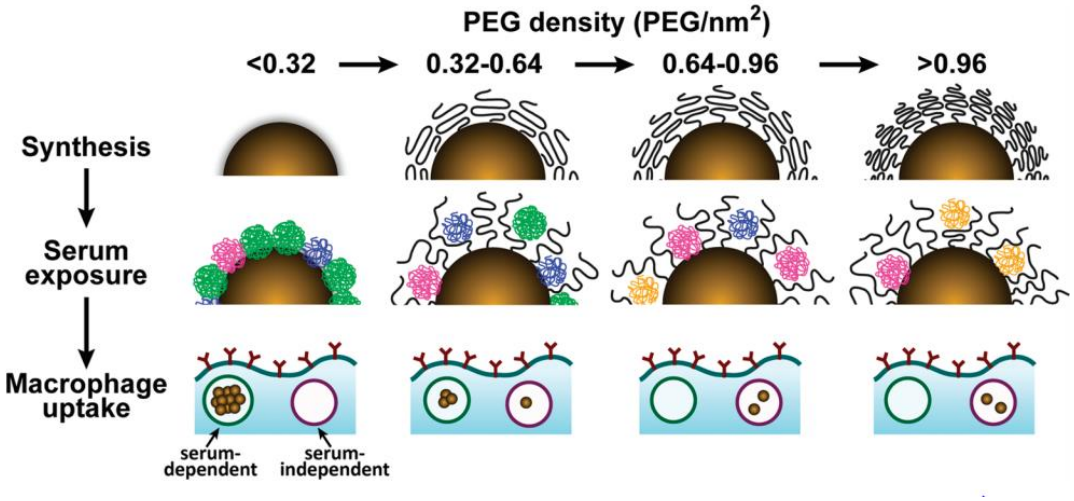


**Figure B. 2.** Correlation between the PEG density, its effect on protein adsorption and cellular interactions towards macrophages. Gold nanoparticles were modified with PEG using different densities. With increasing PEG density (0.32 PEG/nm$^2$ to 0.96/nm$^2$) the PEG volume decreased. Depending on the PEG density a distinct protein pattern was identified. Figure adaptated from ´Nanoparticle Size and Surface Chemistry Determine Serum Protein Adsorption and Macrophage Uptake´. Copyright @ 2012 American Chemical Society. Reprinted with Journal of the American Chemical Society. *Ref.* Journal of American Chemical Society 2012, 134(4), 2139-2147

Overall, it is accepted that due to PEGylation the protein interactions are strongly reduced. However, different reports proved that protein adsorption is not completely prevented[37, 106]. Walkey *et al*. studied the protein adsorption pattern of gold nanoparticles modified with different PEG densities (Figure B.2)[107]. With increasing PEG density, the overall protein adsorption

decreased, as expected. In addition, the protein corona composition was strongly altered. Unfunctionalized PEGylated nanoparticles were surrounded by a high number of proteins (e.g. complement proteins, referred to as cluster A proteins), which mediate cellular recognition by macrophages. Hence, for PEGylated nanoparticles, these proteins were identified in significantly lower amounts. Moreover, it was proven that highly PEGylated nanoparticles are surrounded by a different protein cluster (e.g. albumin, lipoproteins, referred to as cluster D proteins). Therefore, it was concluded that PEGylation does not completely prevent protein adsorption; hence it suppresses the adsorption of specific proteins.

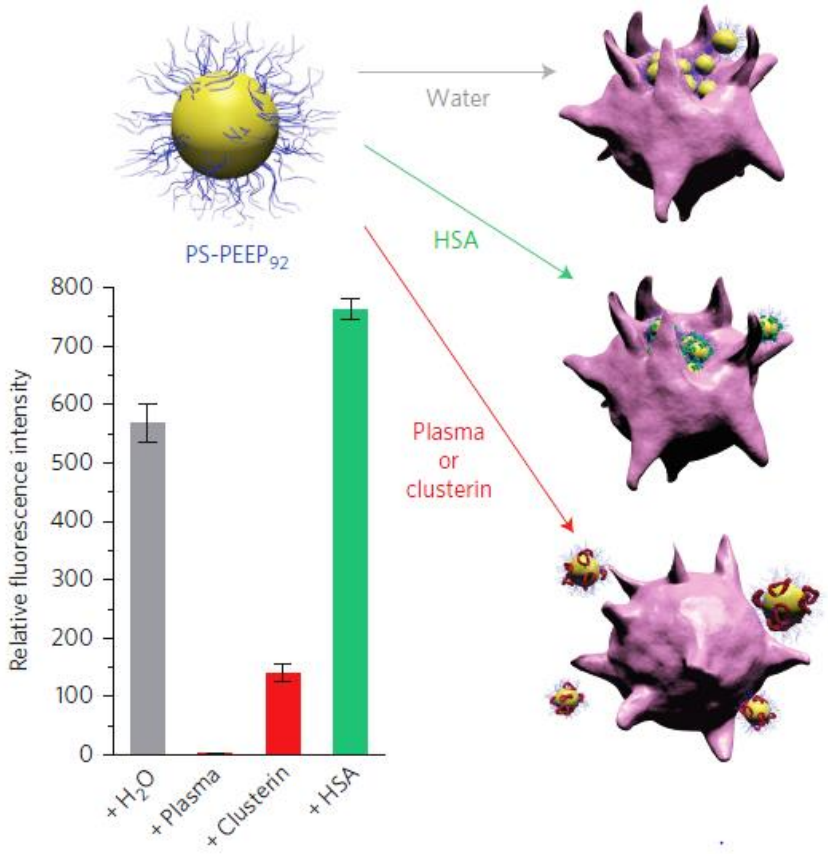


**Figure B. 3.** Clusterin effectively prevents cellular uptake into macrophages of poly(phosphoester) coated nanoparticles. Mass spectrometry analysis highlighted that the protein corona of stealth nanoparticles (PEG or poly(phosphoester)) is strongly enriched with clusterin. This led to the conclusion that distinct proteins mediate the stealth effect. Figure adaptated from ´Protein adsorption is required for stealth effect of poly(ethylene glycol)- and poly(phosphoester)-coated nanocarriers´. Copyright @ 2016 Springer Nature. Reprinted with Nature Nanotechnology. *Ref.* Nature Nanotechnology 2016, 11(4), 372-377

In 2016 Schöttler *et al.* carried out a detailed proteomic investigation to specify the corona of PEGylated nanoparticles (Figure B.3)[106]. The results were stunning as they highlighted that

protein adsorption is actually needed to prevent cellular uptake by macrophages. In the absence of proteins, PEGylated nanoparticles were highly internalized comparable to unmodified nanoparticles. In strong contrast, after plasma incubation cellular internalization of PEGylated nanoparticles was strongly diminished. LC-MS analysis demonstrated that PEGylated and poly(phosphoester) (as degradable polymer alternative to PEG) modified nanopartices are covered by a protein corona which is strongly enriched (~ 70%) with clusterin (also named apolipoprotein J). Additionally, they confirmed that due to pre-coating of nanoparticles with clusterin, cellular uptake towards macrophages was strongly reduced. This led to the conclusion that so-called ´stealth proteins´ (e.g. clusterin) preferably adsorb to PEG nanoparticles and actually mediate the stealth behavior[108].

Based on this observation, it highlights the great potential to exploit protein corona formation in order to achieve reduced cellular uptake by phagocytic cells. Engineering nanoparticles with targeted protein corona properties can enable researchers now to improve now the pharmacokinetic properties of nanoparticles.

### B.3 PEG Alternatives

As the interest about PEGylated products is increasing, a great number of studies also came up, which describe serious side effects induced by PEG[109]. It has been reported that intravenous injection of PEGlyated proteins induced hypersensitivity reactions, which provoked an anaphylactic shock[110]. Additionally, for an increasing number of patients anti-PEG antibodies were detected in the blood[111]. Therefore, it is of great interest to develop new strategies, which can be applied as alternative stealth coating for nanoparticles (Table B.1).

Poly(carboxybetaine)s are zwitterionic polymers that were successfully used to provide stealth properties to silica or gold nanoparticles and liposomes. Zwitterionic polymers form strong hydrogen bridges and therefore decrease protein interactions. Some first *in vivo* experiment compared the pharmacokinetic profile of zwitterionic-coated liposomes with PEGylated liposomes and could prove a similar behavior[112].

Poly(2-oxazoline)s are another potential alternative to PEG. Due to the structure of poly(2-oxazoline)s (POx) it is possible to obtain a broad range of derivatives. Additionally, they are very hydrophilic, biocompatible and non-toxic. There are already some first POx-modified therapeutics (named as Rotigotin for the treatment of Parkinson disease) in Phase-I clinical trials.

Poly(phosphoesters) were already investigated in the 1970s, however their potential as stealth material was just recently described[113]. Due to their hydrolytic or enzymatic degradation, they

are a promising material for biomedical applications. Further, they offer the possibility for multiple functionalizations and tunable polymer properties. Therefore, PPEs provide ideal characteristics to be used as stealth coating for nanoparticles.

**Table B. 1.** Overview of recently developed PEG alternatives, which are used as stealth coating material.

| Class | Type | Example |
|---|---|---|
| **Zwitterionic polymers** | Poly(carboxybetaine) PCB | Silica |
| **Poly(oxazoline)** | Poly(2-ethyl-2-oxazoline) PEtOx | Liposome |
| **Poly(phosphoester)** | Poly(ethyl ethylene phosphate) PEEP | Polystyrene |
| **Sugar derivates** | Hydroxyethyl starch HES | Capsules |
| **Protein** | Albumin | Nanogels |

Sugar derivates such as hydroxyethyl starch (HES), glucose or heparin are biocompatible, degradable, water-soluble and allow a high variety of synthetic modifications. Nanocapsules prepared from HES were shown to have a low unspecific cell uptake, reduced protein interaction and prolonged blood circulation (referred to as HESylation)[114]. Other studies modified metal nanoparticles, silica nanoparticles or liposomes with mannose or glucose (referred to as glyconanoparticles) which provided a stealth layer around the nanoparticle[115].

Proteins, which prevent interaction with phagocytic cells, are called dysopsonins. Takeuchi *et al.* saw that molecularly imprinted nanogels (MIP-NG) were covered with albumin after *in vivo* administration[116]. Due to the albumin rich protein corona the biodistribution profile could be tuned. Non-albumin imprinted nanogels mainly accumulated in the liver, whereas MIP-NG covered with albumin remained in the blood and were able to reach the tumor tissue. In a recent study (2017) Bertrand *et al.* studied the *in vivo* behavior of lipoprotein coated (ApoE and clusterin) PEGylated PLGA nanoparticles[104]. For nanoparticles with a low PEG densitiy, protein coating prolonged blood circulation suggesting the dysopsonic role of ApoE and clusterin.

To sum up, it was shown that the stealth behavior of nanoparticles is connected with protein corona formation. Even though PEGylation strongly reduces protein adsorption, it is not possible to completely prevent the interaction with proteins. Moreover, the adsorption of certain proteins (stealth proteins) is crucial to obtain a stealth behavior. The recent development in biomimetic strategies and the deeper understanding about protein corona formation offers now the possibility to synthesis advanced nanoparticle formulations.

# 5. Hydrophilicity regulates the stealth properties of poly(phosphoester)-coated nanocarriers

## Aim:

Commonly, the surface of nanoparticles is modified with hydrophilic polymers to prolong the blood circulation of nanoparticles (´stealth effect´). Although this effect is known since the early development of nanocarriers, the principal mechanism is barely understood. This study aimed to investigate the molecular mechanism behind the stealth effect. Therefore, the influence of polymer hydrophilicity on protein adsorption and cellular uptake towards phagocytic cells was explored. Overall, a clear correlation between polymer hydrophilicity, protein corona formation and cellular response was demonstrated. It was shown that the polymer hydrophilicity triggers a selective protein adsorption and that distinct proteins actually mediate cellular uptake.

## Contribution:

I carried out the complete protein corona analysis (SDS-PAGE, LC-MS, Pierce Assay) and conducted the cellular uptake experiments (flow cytometry, cLSM). [redacted] synthesized the polymers. [redacted] provided the nanoparticles. The project was supervised by [redacted]

## Copyright:

## Abstract

Increasing the plasma half-time is an important goal in the development and improvement of drugs and drug carriers. Attachment of polymer chains, especially hydrophilic poly(ethylene glycol) (PEG), the so-called PEGylation, is a well-established and effective method to increase the plasma half-time. Even though it was assigned to be a result of a decreased overall protein adsorption on the hydrophilic surface in combination with the adsorption of specific proteins the molecular reasons for the success of PEG and other hydrophilic polymers is still widely unknown. We investigate the influence of surface properties of poly(phosphoester)-coated nanocarriers, focusing especially on the surface hydrophilicity and on the protein adsorption behavior to control the stealth properties. We combine the precision of anionic ring-opening co-polymerization to poly(ethylene alkyl phosphonate)s with the grafting-onto process onto model polymer nanocarriers to control the surface hydrophilicity precisely. It was found that the overall protein amount is unchanged in spite of the hydrophilicity of the investigated nanocarriers. However, the protein type is dramatically altered which eventually mediates the interaction with immune cells.


## Introduction

Rapid clearance from the bloodstream and degradation are two major obstacles foreign materials, such as nanocarriers, must face when entering the body. This results in a reduced plasma half-time which, together with high toxicity of many drugs, limits the pharmaceutical efficacy of many drug carriers.[1,2,3]

An effective method to decrease the body clearance and the toxicity is the attachment of so-called “stealth” polymers (such as PEG),[4,5] which reduces the uptake of the “stealthed” carrier into immune cells (e.g. macrophages) and protect it from enzymatic degradation.[5] However, since PEG’s initial discovery as a “stealth” polymer in 1977 several drawbacks of PEGylation have been revealed. These include the lack of chemical modification, the formation of toxic degradation products under oxidative conditions, and the rising amount of patients showing anti-PEG antibodies.[6,7,8]

Consequently, PEG alternatives have been developed, with similar “stealth” behavior, but potentially fewer side-effects. The most promising ones are polysaccharides[9,10], poly(2-oxazolines)[11,12] and poly(phosphoester)s (PPEs).[13,14] It is noticeable, that all these “stealth” polymers differ significantly in their chemical structure and properties, but they all reduce protein binding significantly.

However, recent studies proved that reducing the protein adsorption alone is not sufficient to induce “stealth” properties, but rather the specific adsorption of certain blood proteins is necessary for a reduced cellular uptake.[13] Upon exposure of nanocarriers to blood plasma, proteins adsorb on the nanocarrier’s surface forming the so-called “protein corona”.[15] This protein layer highly alters the properties such as size, charge or aggregation behavior of nanocarriers and affects the body distribution, toxicity, and especially cellular interactions.[16,17] Therefore, controlling the protein corona is crucial in order to design therapeutic effective nanocarriers. Corona proteins enhancing the interactions with phagocytic cells are called opsonins. Typical examples are immunoglobulins and complement proteins. Also, few proteins with the opposite effect are known, prolonging the blood circulation and preventing cellular interactions.[18] From these dysopsonins, albumin is the most prominent, while also apolipoprotein J (clusterin) was identified as a dysopsonin and was detected in high amounts on PEGylated, PPE modified, and polysaccharide stealth nanocarriers.[9,13]

However, despite these new insights, an understanding of the stealth effect on the molecular level is still missing. Several studies cover the influence of surface charge[19,20] or hydrophilicity[21,22,23], particle size[21], and grafting density[24,25]. However, many of these studies lack detailed and quantitative investigation of the protein corona and only describe the cellular uptake behavior.

In this study, we investigated the interaction of PPE grafted model nanocarriers (NC) of different hydrophilicity by correlating their uptake into immune as well as cancer cells with their “stealth” behavior using detailed analysis of the protein adsorption pattern. Well-defined and degradable PPEs with adjustable hydrophilicity were prepared by the organocatalytic anionic ring-opening polymerization (oAROP) of cyclic phosphonates and grafted onto model nanocarriers. The cell-uptake of these nanocarriers into a macrophage cell-line was investigated and correlated with the adsorption pattern of human blood proteins. We observed an increased cellular uptake of the NC’s upon falling below a certain hydrophilicity threshold. Quantitative analysis of the protein amount adsorbed onto the NC’s proved no increase in protein adsorption even above this threshold, but a distinct change in the protein adsorption pattern.

## Material and methods

**Synthesis of poly(styrene) nanoparticles.** A macro emulsion was prepared with a continuous phase containing cetyl trimethyl ammonium chloride solution (25 %wt in water,

527 mg, 1.46 mmol) as surfactant and 2-aminoethyl methacrylate hydrochloride (547 mg, 3.32 mmol, 3 %wt to styrene) in 72.0 g sterile Milli-Pore water and a dispersed phase containing distilled styrene (17.1 g, 164 mmol), hexadecane (792 mg, 2.77 mmol) as ultrahydrophobe, BODIPY-methacrylate (17.3 mg, $3.7*10^{-2}$ mmol) as fluorescent dye and 2,2'-azobis(2-methyl butyronitrile) (V59) (301 mg, 1.56 mmol) as oil soluble azo initiator. Both phases were made homogenous by mechanical stirring and the continuous phase was added slowly to the stirring dispersed phase. The macro emulsion was stirred for 1 h at highest speed. To produce the mini emulsion, the macro emulsion was passed through a microfluidizer (Microfluidics USA, LM10) with a y-chamber 48 times at 103 MPa. The first 12 passes were discarded. The miniemulsion was directly transferred into a 100 mL flask and stirred in an oil bath at 72 °C. The polymerization was run for 12 h. The dispersion was purified by centrifugation (6 x 1.5 h, 12000 rpm), the supernatant always removed and the pellet re-dispersed in sterile Milli-pore water.

$D_h$ (DLS): 106.8 ± 9.1 nm (8.5 %); ξ-potential: + 47.4 ± 9.5 mV (20.0%); -$NH_2$ groups / particle (PCD): 29.000; $M_n$ (SEC, DMF, 0.1 mol LiBr, RI-detection, 333 K, PS standard): 107380 g $mol^{-1}$; Mw: 278004 g $mol^{-1}$, $Đ$ = 2.59.

**Representative procedure for the synthesis of P(1)$_x$ and P(1$_x$-co-2$_y$)-Mal.** The monomer(s) were weighed into a flame-dried Schlenk-tube, dissolved in dry benzene and dried by 3 times lyophilization. The monomers were dissolved in dry dichloromethane at a total concentration of 4 mol $L^{-1}$. A stock solution of initiator 2-(benzyloxy)ethanol in dry dichloromethane was prepared with a concentration 0.2 mol $L^{-1}$ and the calculated amount was added to the monomer solution via gas tight syringe (Hamilton®). A stock solution of DBU in dry dichloromethane was prepared with a concentration of 0.2 mol $L^{-1}$. The monomer solution and the catalyst solution were adjusted to 30 °C. The polymerization was initiated by the addition of the calculated volume of catalyst solution containing 3.0 equivalents of DBU in respect to the initiator. Polymerization was terminated after 16 h by the rapid addition 2.5 equivalents of 4-(maleinimido)phenyl isocyanate in 1 mL dry DMF. The yellow solution rapidly turned red, indicating the successful termination reaction. After 20 min, the amorphous polymers were purified by precipitation in cold diethyl ether, dialyzed against 2 L Milli-Q (Millipore®) water over night (1000 g $mol^{-1}$ cut off, regenerated cellulose membrane) and dried at reduced pressure. Yield: 95-97 % amorphous solid.

**Representative NMR data of P(1)$_x$-Mal.** $^1$H NMR (DMSO-$d_6$, 500 MHz, 298K, ppm): δ = 7.76 - 7.18 (m, aromatic C**H**), 6.91 (s, Maleimid C), 4.53 (s, aryl-C**H$_2$**-), 4.22 - 4.01 (m, backbone -C**H$_2$**-C**H$_2$**-), 3.63 (t, backbone terminal -C**H$_2$**-OH), 1.79 (dq, side-chain -P-C**H$_2$**-, $^2J_{HP}$ = 15.9 Hz, $^3J_{HP}$ = 7.7 Hz), 1.05 (dt, side-chain -C**H$_3$**, $^2J_{HP}$ = 20.2 Hz, $^3J_{HP}$ = 7.6 Hz).

$^{13}$C NMR (DMSO-d6, 125 MHz, 298K, ppm): δ = 138.78 (s, imide **C**), 133.78, 128.80, 127.97 (aromatic **C**), 64.56 (s, broad, backbone -**C**H$_2$-), 18.31 (d, $^1J_{CP}$ = 139.5 Hz, side-chain -P-**C**-), 6.71 (d, $^2J_{CP}$ = 6.75 Hz, side-chain -P-C-**C**).

$^{31}$P{H} NMR (DMSO-$d_6$, 201 MHz, 298K, ppm): δ = 34.53 (backbone), 34.26 (terminal).

**Representative NMR data of P(1$_x$-*co*-2$_y$)-Mal.** $^1$H NMR (DMSO-$d_6$, 500 MHz, 298K, ppm): δ = 7.76 - 7.18 (m, aromatic C**H**), 6.91 (s, Maleimid C**H**), 4.53 (s, aryl-C**H$_2$**-), 4.22 - 4.01 (m, backbone -C**H$_2$**-C**H$_2$**-), 3.63 (t, backbone terminal -C**H$_2$**-OH), 1.84 - 1.70 (m, side-chain -P-C**H$_2$**-), 1.63 - 1.56 (m, side-chain -P-C**H$_2$**-), 1.54 - 1.41 (m, side-chain -P-CH$_2$-C**H$_2$**-), 1.40 - 1.29 (m, side-chain -P-CH$_2$-CH$_2$-C**H$_2$**-), 1.05 (dt, side-chain -P-CH$_2$-C**H$_3$**, $^3J_{HP}$ = 20.1 Hz, $^3J_{HH}$ = 7.6 Hz), 0.86 (t, side-chain -P-CH$_2$-CH$_2$-CH$_2$-C**H$_3$**, $^3J_{HH}$ = 7.3 Hz).

$^{13}$C NMR (DMSO-d6, 125 MHz, 298K, ppm): δ = 138.78 (s, imide **C**), 133.78, 128.80, 127.97 (s, aromatic **C**), 64.56 (s, broad, backbone -**C**H$_2$-), 60.85 (s, aryl-**C**-), 24.66 (d, side-chain -P-**C**-, $^1J_{CP}$ = 145.0 Hz), 24.42 (d, side-chain –P-C-**C**-, $^2J_{CP}$ = 5 Hz), 23.41 (d, side-chain -P-C-C-**C**-, $^3J_{CP}$ = 16.3 Hz), 18.06 (d, side-chain -P-**C**-, $^1J_{CP}$ = 138.8 Hz), 13.90 (s, side-chain -P-C-C-C-**C**), 6.68 (d, side-chain -P-C-**C**, $^2J_{CH}$ = 6.3 Hz).

$^{31}$P{H} NMR (DMSO-$d_6$, 201 MHz, 298K, ppm): δ = 34.53 (backbone, Et-**P**), 34.26 (terminal, Et-**P**), 33.28 (backbone, $^n$Bu-**P**), 33.04 (terminal, $^n$Bu-**P**).

**Modification of poly(styrene) nanoparticles via Michael-addition.** For a typical Michael-addition 3 mL of particle dispersion (1 %$_{wt}$, 4.5*10$^{13}$ particles, 2.1*10$^{-6}$ mol NH$_2$ groups) were basified with 72 µL pyridine (pH 8.5) and stirred for 20 min at room temperature at 500 rpm. Then 2.5 eq. of polymer (in respect to the –NH$_2$ groups) dissolved in 1 mL sterile Milli-Pore water were added. The reaction was stirred for 24 h at room temperature and 500 rpm to ensure full conversion. The dispersion was purified by repeated centrifugation (3 x 1 h, 20000 rpm). Each time the supernatant was removed and the pellet re-dispersed in sterile Milli-Pore water (2 x 3 mL, 1 x 2 mL). After determination of the solid content the dispersion was adjusted to 1 %$_{wt}$ with sterile Milli-Pore water.

**Cell culture.** RAW264.7 cells were kept in DMEM and Hela cells were maintained in EMEM both supplemented with 10% FBS, 100 IU/mL penicillin and 100 µg/mL streptomycin.

**Flow cytometry.** Cells (10$^5$ cells) were seeded out in 24-well in cell culture medium and kept overnight at 37 °C. Prior to cell uptake studies, the cell culture medium was exchanged to cell culture medium without FBS. Nanocarriers were incubated with human plasma for 1 h to allow protein corona formation (details see protein corona preparation below). Protein coated nanocarriers were added to cell culture medium without FBS at a final concentration of 75

µg/mL and incubated with cells for 2 h at 37 °C (internalization) or 4 °C (binding). Cells were washed with PBS to remove free nanoparticles, detached with Trypsin-EDTA, centrifuged (500 g, 5 min) and resuspended in PBS.

Flow cytometry measurements were performed with a CyFlow ML cytometer (laser: 488 nm laser for Bodipy excitation; emission: 527 nm band pass filter). FCS Express V4 software was used for data analysis hereby selecting cells on a forward/sideward scatter plot, excluding cell debris. The fluorescent signal was expressed in a histogram and the median intensity was determined. The mean value and standard deviation from triplicates was calculated.

**Confocal laser scanning microscopy.** To verify the intracellular localization of nanocarriers cell images were taken with a Laser Scanning Confocal Microscope (Leica, LSM SP5 STED) consisting of a multi-laser combination and five detectors (range of 400 - 800 nm). Nanocarriers were detected at 530 - 545 nm (pseudo-colored in green) and the cell membrane was stained with CellMaskOrange (2.5 mg/mL) detected at 570 - 640 nm (pseudo-coloured in red). Images were evaluated with LAS AF 3000 software and Image J. For confocal analysis, cells were seeded out in 8-well ibidi dishes ($8*10^4$ cells) and the experiments were conducted in the same manner as flow cytometry experiments. Before images were taken, cells were fixed with 4% paraformaldehyde for 15 min at room temperature.

**Protein corona preparation.** As previously described a constant ratio between nanoparticle surface area and plasma was chosen[30-31] (0.05 $m^2$ PS-NC per 1 mL plasma). The dispersion was incubated at 37 °C, 300 rpm for 1 h and subsequently centrifuged (20 000 g, 1 h, 4 °C). The nanoparticle pellet was washed with PBS (3 times, 1 mL) to remove loosely and unbound proteins. For protein identification, the nanoparticle pellet was resuspended in 100 µL 2% SDS with 62.5 mM Tris hydrochloride solution and incubated for 5 min at 95 °C. The dispersion was centrifuged and the resulting supernatant contained desorbed corona proteins.

**Pierce Assay.** The protein concentration was determined by Pierce 660 nm protein Assay according to the manufactures´ instruction. Bovine serum albumin was used as standard. Absorbance was measured with a Tecan infinite plate reader.

**SDS-PAGE.** Proteins were analyzed by SDS-PAGE using NuPage 10% Bis-Tris Protein Gels. 7 µg of total protein was loaded for Coomassie staining and 1 µg of protein was applied if gels were stained with Pierce Silver Staining Kit. The protein sample volume was adjusted with water to a volume of 26 µL and mixed with 4 µL of NuPage Sample Reducing Agend and 10 µL of NuPage LDS Sample Buffer. Electrophoresis was carried out for 1.5 h at 100 V. Gels were either stained with Simply Blue Safe Stain overnight or Pierce Silver Staining Kit according to the manufactures´ instruction.

**In solution digestion.** Proteins were precipitated using ProteoExtract protein precipitation kit according to manufactors´ instruction and in solution digestion was performed as pervious reported [30-32]. For LC-MS measurements, samples were diluted with 0.1% formic acid and spiked with 50 fmol/µl Hi3 EColi Standard (Waters Corporation) for absolute peptide quantification.

**LC-MS meaurements and data analysis.** A Synapt G2-Si mass spectrometer coupled with a nanoACQUITY UPLC system was used for proteomic experiments. The system was operated as described in several reports. Data was processed and peptides were identified with Progenesis QI for Proteomics. Generated peptide masses were searched against a reviewed human protein sequence database downloaded from Uniprot. The database was modified with the sequence information of Hi3 Ecoli standard (Chaperone protein ClpB) for absolute quantification. For peptide identification, at least three assigned fragments are required. For protein identification, at least two assigned peptides and five assigned fragments are needed. Peptides with a score parameter less than 4 were rejected. Based on the TOP3/Hi3[33] approach, the amount of protein in fmol was generated.

## Results and discussion

To investigate the relationship between surface hydrophilicity and stealth behavior of nanocarriers, a well-defined system is essential. Amino-functionalized, fluorescent poly(styrene) nanoparticles prepared by radical miniemulsion polymerization were used as precise model nanocarriers to anchor the stealth polymers. Poly(ethylene alkyl phosphonate)s were synthesized via the living ring-opening copolymerization of 2-alkyl-2-oxo-1,3,2-dioxaphospholanes (material/methods see supplementary information 5)[13]. Well-defined, random copolymers with excellent control over the degree of polymerization and copolymer composition, as well as narrow molecular weight distributions were prepared.[24] To adjust the polymers' hydrophilicity, 2-ethyl-2-oxo-1,3,2-dioxaphospholane **(1)**, leading to hydrophilic polymers comparable to PEG, was copolymerized with 2-*n*-butyl-2-oxo-1,3,2-dioxaphospholane **(2)**, providing hydrophobic side-chains. The respective homopolymer properties, as well as detailed synthetic protocols for the oAROP, have been reported previously.[26,27,28] Commercial 4-(maleinimido)phenyl isocyanate was used for $\omega$-functionalization of the copolymers to introduce maleimide groups for *aza-Michael* addition with the surface amine groups. This combines the high control of polymer properties of oAROP with the isotropic surface coverage of the grafting-onto process.[24]

The SEC elugrams of all polymers were monomodal and showed narrow molecular weight distributions (*Đ* < 1.19). Attachment of the maleimide groups and copolymer formation was assured by $^{1}$H DOSY NMR spectroscopy. All $^{1}$H NMR resonances possess the same diffusion coefficient and are part of the same molecule.

Quantification of molecular weights, the degree of $\omega$-functionalization and the copolymer compositions were determined by $^{1}$H NMR spectroscopy via end-group analysis. Briefly, the resonances of the maleimide signals (6.96 - 6.46 ppm), as well as aromatic proton resonances (7.76 - 7.20 ppm), were compared with the initiators resonances (4.52 ppm) and the polymer backbone resonances (4.31 - 3.98 ppm). In all cases $\omega$-functionalities of > 97 % were achieved ($^{1}$H NMR). To obtain the copolymer composition, the relative $^{1}$H NMR resonances of the side-chain methylene groups at 1.05 ppm (ethyl -C**H**$_3$) and 0.87 ppm (*n*-butyl -C**H**$_3$) were compared. The results were further confirmed by comparing the $^{31}$P NMR resonances of **P(1)** at 34.5 ppm and **P(2)** at 33.4 ppm (Figure 5.1). The final copolymers contained 0, 8.6, and 32 mol% of hydrophobic *n*-butyl side-chains.

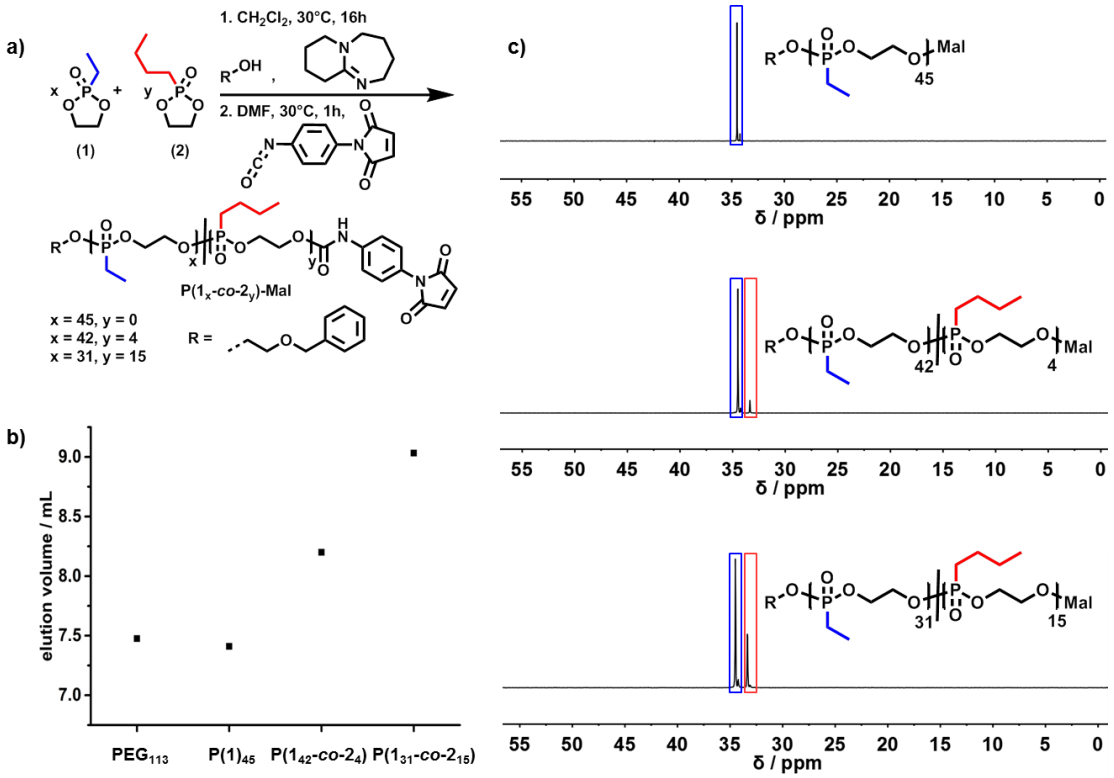


**Figure 5.** 1 **a)** Schematic presentation of the oAROP of (1) and (2) followed by $\omega$-functionalization to produce random copolymers P(1$_x$-*co*-2$_y$)-Mal. **b)** Elution volume of the investigated (co)polymers on rpHPLC to evaluate their hydrophilicity. **c)** $^{31}$P$^{24}$ NMR spectra (DMSO-d6, 298K) of the produced (co)polymers. [redacted]

The hydrophilicity of the copolymers was evaluated via reverse phase HPLC (rpHPLC). The elution volume from the hydrophobic column was used to gauge the macroscopic hydrophilicity of the polymer, as polymers of higher hydrophobicity elute later from the column due to stronger interactions. With an elution volume of 7.1 mL **P(1)$_{45}$-Mal** exhibits a similar hydrophilicity to the benchmark, ***m*-PEG$_{113}$-Mal** that elutes at 7.45 mL (chosen due to comparable $M_n$ values). Higher amounts of n-butyl side chains resulted in lower hydrophilicity and increasing elution volumens for **P(1$_{42}$-*co*-2$_4$)-Mal** and **P(1$_{31}$-*co*-2$_{15}$)-Mal** as shown in Figure 5.1). Additionally, this correlate well with the calculated partition coefficient (logP) values of the respective polymers.

To exclude the formation of pronounced hydrophobic patches in the form of gradients or block copolymer structures, $^{31}$P NMR spectroscopy assisted copolymerization kinetics were conducted according to previous studies.[24] The ratio of repetition unit **(1)** and **(2)** incorporated into the polymer backbone during the course of the polymerization was observed. This ratio (initial monomer feed ratio 1:1 for better visualization) stayed constant during the polymerization, proving the random incorporation of both monomers into the backbone.

To evaluate the effect of the copolymer hydrophilicity on the stealth properties of nanocarriers, model NCs based on poly(styrene nanoparticles ($D_h$ = 107 nm ± 9 nm) were prepared via free radical terpolymerization of styrene, 2-aminoethyl methacrylate and BODIPY-methacrylate in a cetyl trimethyl ammonium chloride (CTMA-Cl) stabilized miniemlusion process.[29] The maleimide-modified polymers were coupled to the amino groups on the NCs via the *aza-Michael* addition reaction in aqueous dispersion. Dissolving the NCs and analysis by SEC revealed that no free polymers remained in solution after purification by centrifugation. The average number of polymer chains per NC was determined from the ratio between the PS backbone resonances in $^1$H NMR spectroscopy (7.14 - 6.17 ppm) and the **PEG** or **PPn** resonances (3.60 - 3.55 ppm and 4.44 - 4.03 ppm, respectively).[13] On average, 5,300-6,300 chains were attached to each NC. In combination with the surface area obtained from the DLS diameter, a distance of 6-7 nm between two polymer chains was calculated (Figure 5.2). According to Perry *et al.,* the polymers should take a mushroom conformation under these conditions and hence provide a dense enough layer to induce stealth behavior.[25]

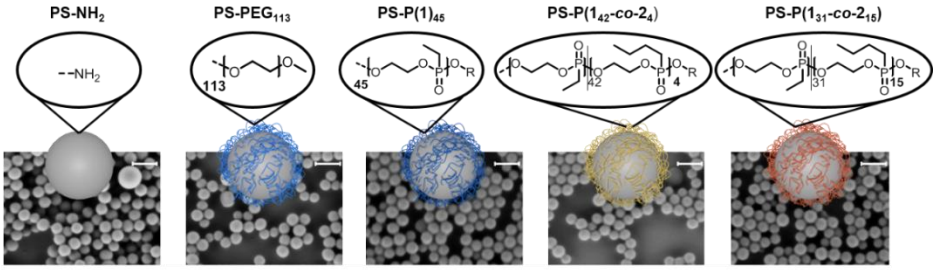


| modification | - | *m*-PEG$_{113}$ | P(1)$_{45}$ | P(1$_{42}$-co-2$_4$) | P(1$_{31}$-co-2$_{15}$) |
|---|---|---|---|---|---|
| chains / particle | - | 5300 | 5500 | 6300 | 5400 |
| $D_h$ ($H_2O$) / nm | 107 ± 9 | 124 ± 36 | 127 ± 28 | 105 ± 13 | 105 +61 |
| $D_h$ (NaCl 9 g $L^{-1}$) / nm | - | 115 ± 27 | 111 ± 17 | 106 ± 24 | 155 ± 16 |
| ζ-potential / mV | +47 ± 9 | + 7 ± 7 | - 24 ± 5 | - 16 ± 7 | - 22 ± 4 |
| ζ-potential in plasma / mV | -28 ± 9 | -33 ± 7 | -30 ± 19 | -30 ± 5 | -31 ± 7 |

**Figure 5. 2** Analytical data of model nanocarriers used herein. Scale bar: 200 nm. [redacted]

The size of the nanocarriers remained constant before and after coupling of the different polymers (Figure 5.2). The ζ-potential however, changed from + 47 mV to + 7 mV for ***m*-PEG** and ~ - 20 mV for all **PPn** modifications. Further, the functionalized NC stayed colloidal stable in NaCl solution (9 g $L^{-1}$) as opposed to the unmodified NC, indicating a shift from electrostatic, CTMA-Cl, to a steric stabilization by the polymer grafts and a successful conjugation. Finally, the ζ-potential of all NC after incubation in human plasma equilibrated to ~ -30 mV because of protein adsorption, similar to other reported nanocarriers in plasma.[13]

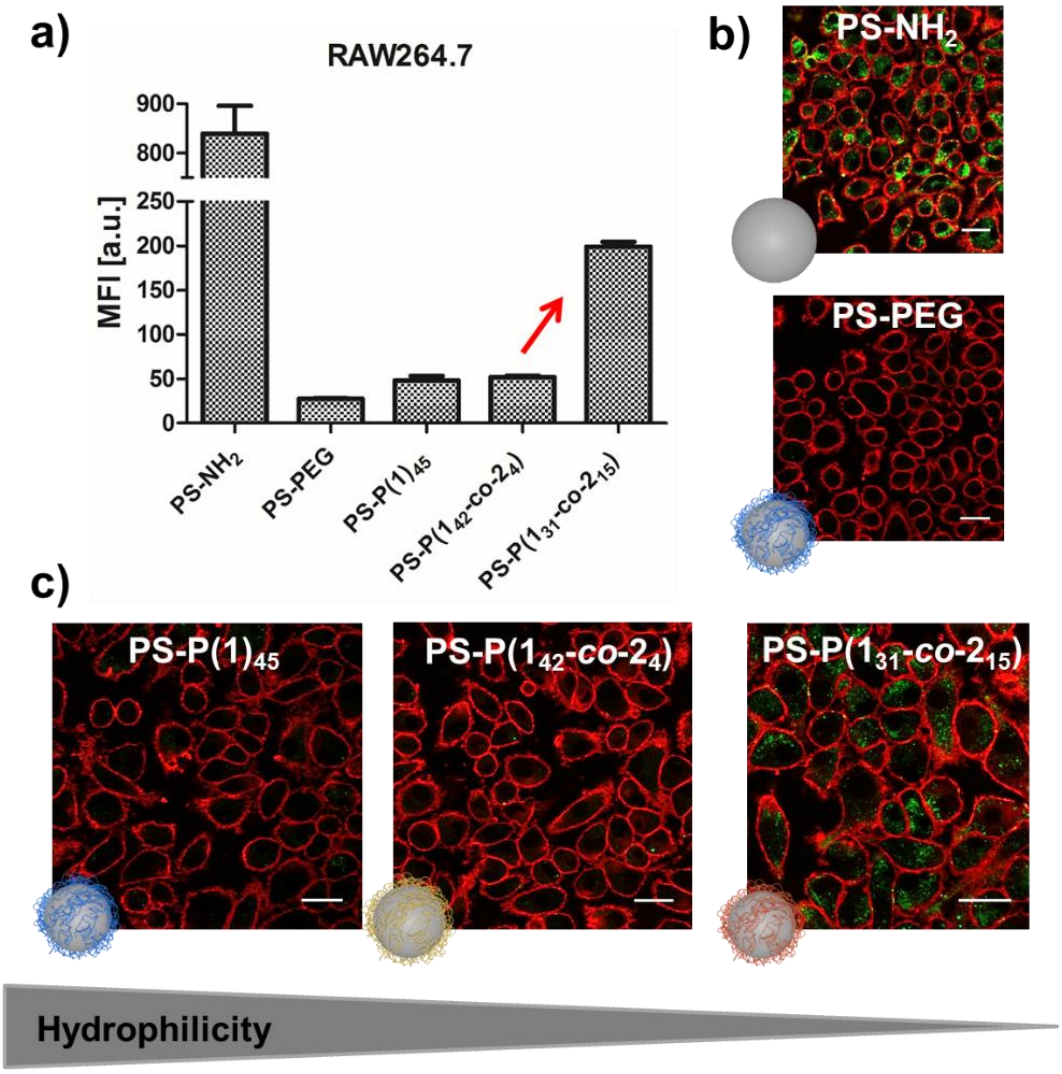


**Figure 5. 3.** Cellular interaction studies of pristine and polymer coated PS-NP after plasma incubation: **a)** Flow cytometry analysis **b-c)** Confocal laser scanning microscopy images. Values are expressed as mean ± SD of triplicates. The cell membrane is stained with CellMask Orange and pseudocolored in red and PS-NCs are pseudocolored in green. Scale bar:10 µm.

The main feature of stealth nanocarriers is the prolonged blood circulation time which is caused by reduced interactions with immune cells (e.g. phagocytic cells). Therefore, we study the cellular internalization of the here described nanocarriers towards the murine macrophage cell line, RAW 264.7 by flow cytometry and confocal laser scanning microscopy (cLSM).

To mimic *in vivo* conditions, the nanocarriers were incubated in human plasma prior to cell uptake experiments to allow the formation of the protein corona. Flow cytometry analysis indicates a high internalization rate of pristine NC (Figure 5.3). Additionally, strong co-

localization of the negatively charged cell membrane and positively charged nanocarriers is observed in cLSM images (Figure 5.3). For nanocarriers coated with PEG and the hydrophilic polymer **P(1)$_{45}$**, cellular uptake is strongly diminished. Interestingly, for nanocarriers coated with **P(1$_{42}$-*co*-2$_{4}$)** containing low amounts of hydrophobic *n*-butyl side chains, cellular uptake behavior remained unchanged (Figure 5.3). However, with increasing the hydrophobicity to **P(1$_{31}$-*co*-2$_{15}$)**, we observed an increase in cellular uptake. These first results indicate that a defined surface hydrophilicity enables controlled cellular interaction. Comparable results were obtained for HeLa cells (supplementary information 5). Additional, there is no unspecific binding or cell adhesion for polymer-coated nanocarriers compared to pristine NCs.

In general, a reduced protein adsorption has been reported for hydrophilic surfaces and with increasing hydrophobicity, the amount of protein adsorption also increases. All model nanocarriers were incubated with human plasma at 37 °C for 1 h and the hard corona proteins were isolated and quantified by the Pierce Assay (Figure 5.4). Compared to PS-$NH_2$ nanocarrier, a strongly reduced amount of proteins adsorbed to **PEG**ylated and **P(1)$_{45}$** modified NCs (Figure 5.4). However, increasing the hydrophobicity of the polymer shield on the nanocarriers did not influence the amount of protein adsorption (~ 0.5 mg per 0.05 $m^2$ surface area NC).

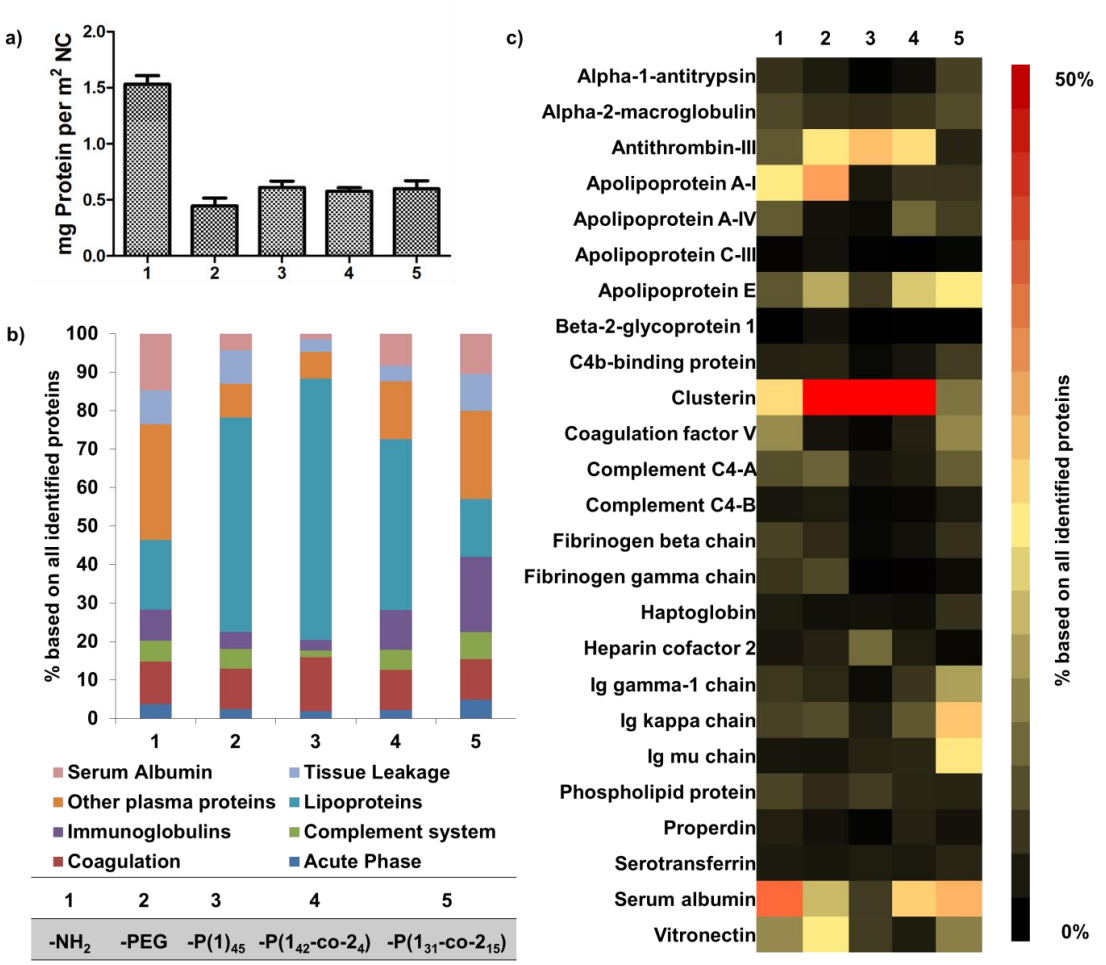


**Figure 5. 4.** Qualitative and quantitative protein corona analysis of pristine and polymer coated PS-NC **a)** Pierce Assay **b)** LCMS Protein Classification **c)** LCMS Protein Identification. Values are expressed as mean ± SD triplicates.

In the next step, we analyzed the protein corona via SDS-PAGE and liquid chromatography coupled to mass spectrometry (LC-MS) to assess the biological identity of the NC, i.e. after incubation in human plasma. In line with previous reports, the protein adsorption pattern of PS-$NH_2$ nanocarriers is dominated by albumin which is the most abundant plasma protein. On the NCs functionalized with the hydrophilic polymers **PEG** and **$P(1)_{45}$** a strong enrichment of apolipoproteins e.g. clusterin and ApoAI (Figure 5.4) were detected. When the more hydrophobic **$P(1_{42}$-*co*-$2_4)$** is coupled to the nanocarriers, no influence in the cellular uptake was found (Figure 5.3) and only minor differences in the protein corona pattern compared to **$P(1)_{45}$** were measured (Figure 5.4). However, there was a significantly different in the protein pattern adsorbed on nanocarriers with the most hydrophobic polymer **$P(1_{31}$-*co*-$2_{15})$** (Figure 5.4). Especially immunoglobulins, fibrinogen, and albumin were identified in substantial amounts, which are less pronounced on the other “stealth” nanocarriers (Figure 5.4).

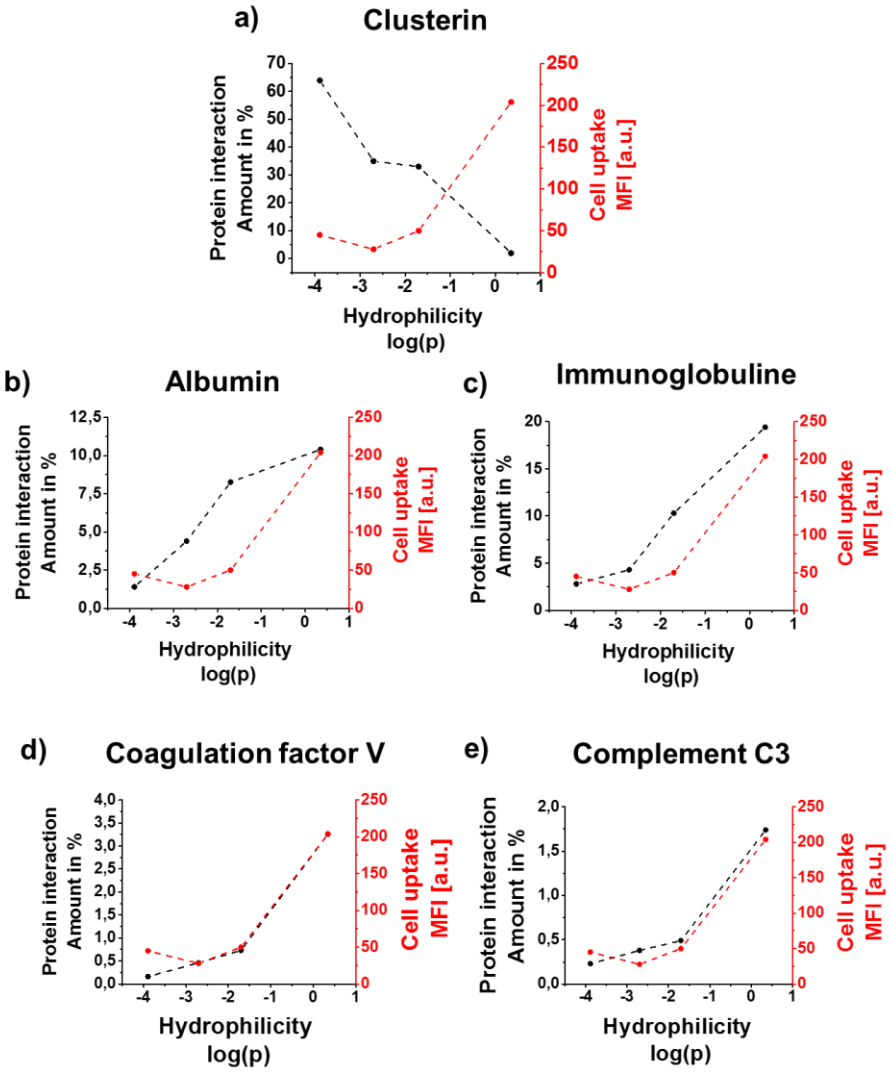


**Figure 5. 5.** Correlation between polymer hydrophilicity, cellular uptake and protein interaction.

NC covered with hydrophilic poly(phosphonates)s **P(1)$_{45}$** exhibit stealth behavior comparable to that of PEGylated NC under *in vitro* conditions. Additionally, we proved that NC coated either with hydrophilic *or* hydrophobic polymers exhibit an overall low protein binding (Figure 5.4). However, a clear correlation between polymer hydrophilicity (logP value), the protein adsorption pattern, and the resulting cellular interactions was found (Figure 5.5).

With increasing polymer hydrophobicicity (logP>0), cellular uptake was strongly enhanced whereas the overall amount of clusterin (dysopsonin) decreased (Figure 5.5) In contrast to this, the amount of IgG (opsonin), complement or coagulation proteins and albumin increased.

Additionally, we investigated the interaction of the different polymers with albumin and IgG. Here, we saw that the hydrophobic polymer induced an unfolding of the protein whereas the protein structure after exposure to the hydrophilic polymer was less affected. Due to the unfolding, hydrophobic regions of the protein are exposed to the surface, which further influence the adsorption process (supplementary information 5).

## Conclusion

In conclusion, this is an important step towards understanding and controlling the stealth effect of nanocarriers. This is the first study correlating a well-controlled surface hydrophilicity with quantitative high-resolution protein corona analysis and the interaction with immune cells. The degradable poly(phosphonate)s were prepared by the anionic ring-opening polymerization of cyclic phosphonates, producing ideal random copolymers with a controlled hydrophilicity. They were coupled to model nanocarriers and incubated with human blood plasma; the polymer structure does not change the amount of protein adsorbed but controls the protein pattern and this governs the cell interactions. This principal knowledge is needed to improve the properties of the nanocarriers for therapeutic applications.

## Supplementary information

**Table 5. 1.** Analytical data of maleinimide functionalized polymers. a) Monomer feed ratio. b) Monomer composition, $P_n$, and functionality f determined via $^1$H NMR (500 MHz) spectroscopy. c) Determined via SEC in DMF (RI detection, 333 K, vs. PEG). d) Elution volume on rpHPLC. e) logP value calculated from www.molinspiration.com [redacted]

| | (1) / (2) theo[a)] | (1) / (2) exp.[b)] | $P_n$[b)] | $M_n$[b)] | $Đ$[c)] | f %[b)] | V / mL[d)] | logP[e)] |
|---|---|---|---|---|---|---|---|---|
| **m-PEG$_{113}$-Mal** | - | - | 113 | 5000 | 1.03 | 97 | 4.45 | -2.27 |
| **P(1)$_{45}$-Mal** | - | - | 45 | 6100 | 1.19 | 99 | 7.10 | -3.89 |
| **P(1$_{42}$-*co*-2$_4$)-Mal** | 0,90 / 0,10 | 0,91 / 0,09 | 42 / 4 | 6300 | 1.17 | 99 | 8.19 | -1.73 |
| **P(1$_{31}$-*co*-2$_{15}$)-Mal** | 0,70 / 0,30 | 0,67 / 0,33 | 31 / 15 | 6700 | 1.18 | 97 | 9.03 | +0.35 |

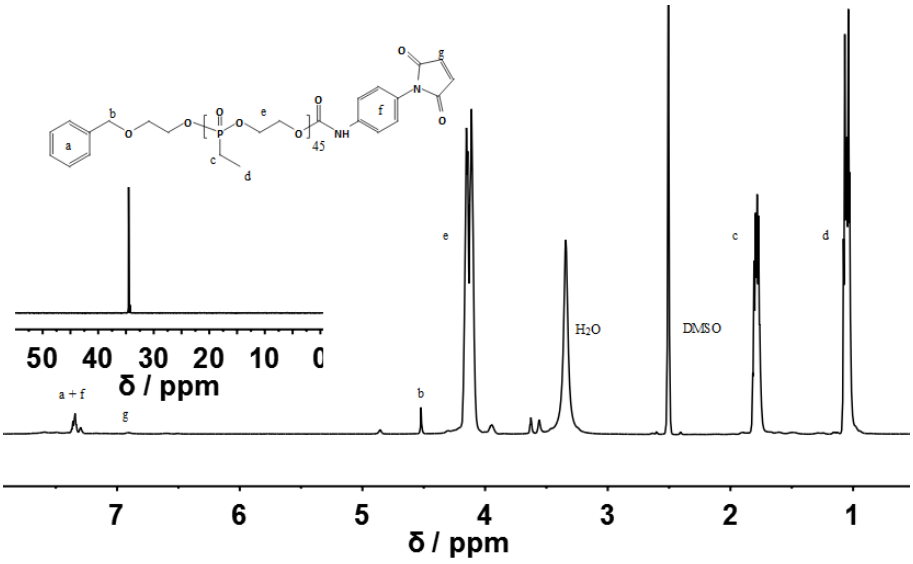


**Figure 5. 6.** $^1$H (500 MHz) and $^{31}$P (210 MHz, inset) NMR spectra of maleimide terminated poly(ethylene ethyl phosphonate) P(1)$_{45}$ in DMSO-$d_6$ at 298 K. [redacted]

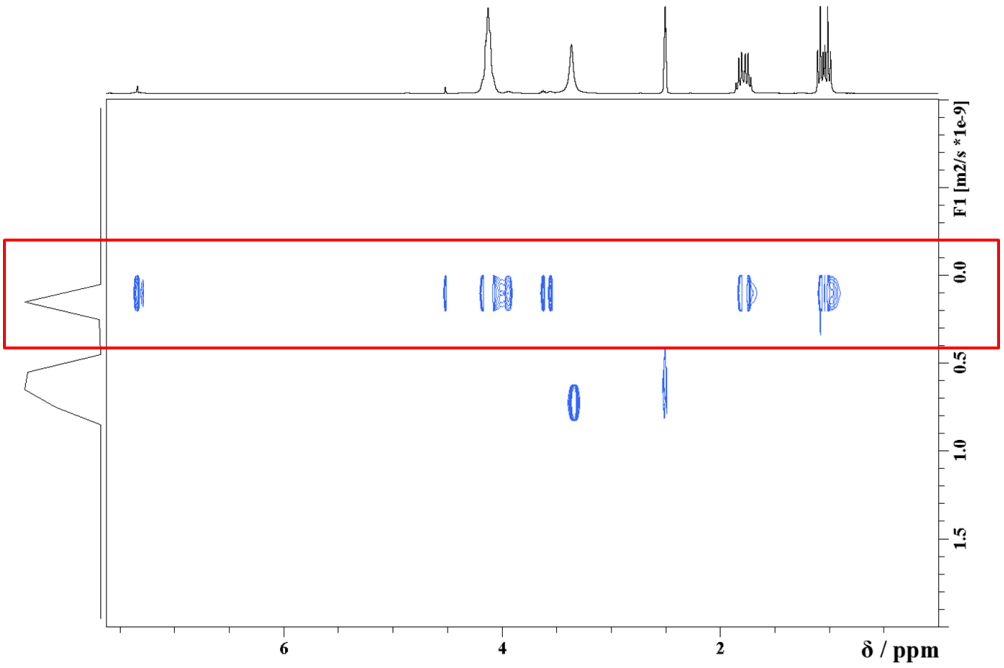


**Figure 5. 7.** $^{1}$H DOSY (500 MHz) NMR spectrum of maleimide terminated poly(ethylene ethyl phosphonate) P(1)$_{45}$ in DMSO-$d_6$ at 298 K. [redacted]

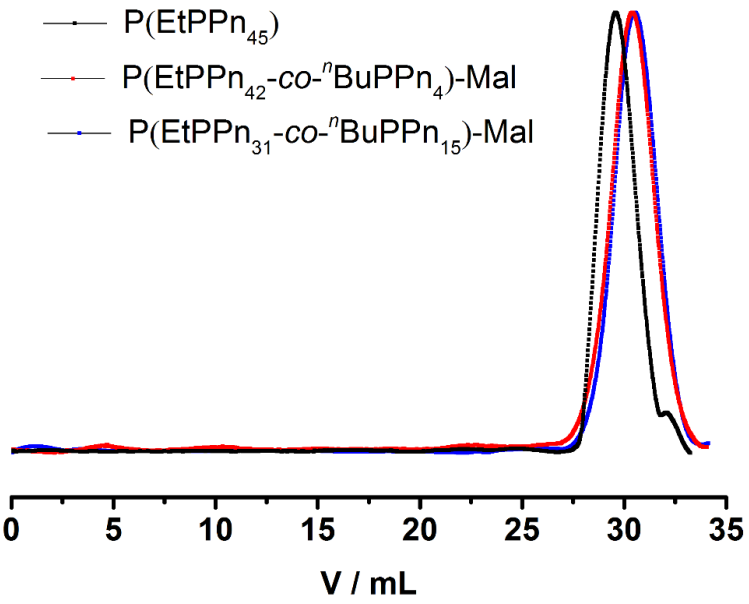


**Figure 5. 8.** SEC trace (RI detection) of poly(ethylene alkyl phosphonate) (co)polymers used in this study in DMF (0.1 g L$^{-1}$ LiBr) at 333 K. [redacted]

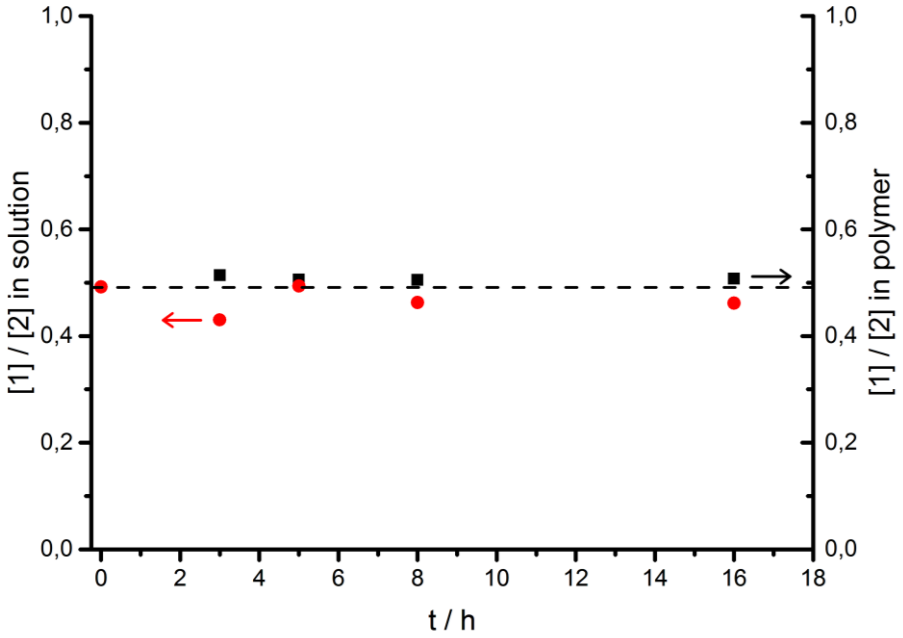


**Figure 5. 9.** $^{31}$P NMR (201 MHz) assisted copolymerization kinetics. [redacted]

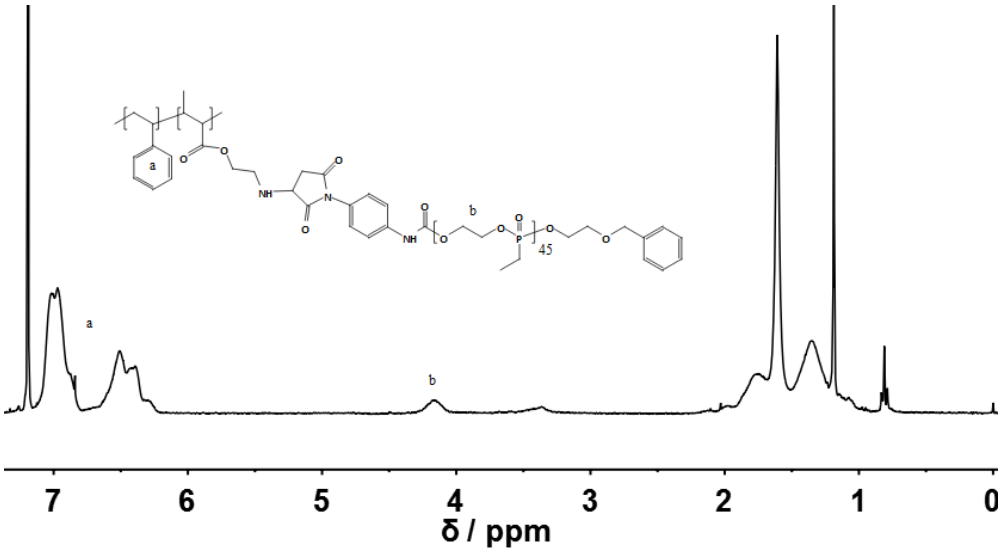


**Figure 5. 10**. $^{1}$H (500 MHz) NMR spectrum of polystyrene nanoparticles modified with hydrophilic poly(phosphonate) $P(1)_{45}$ ($PS\text{-}P(1)_{45}$) dissolved in $CDCl_3$ at 298 K. [redacted]

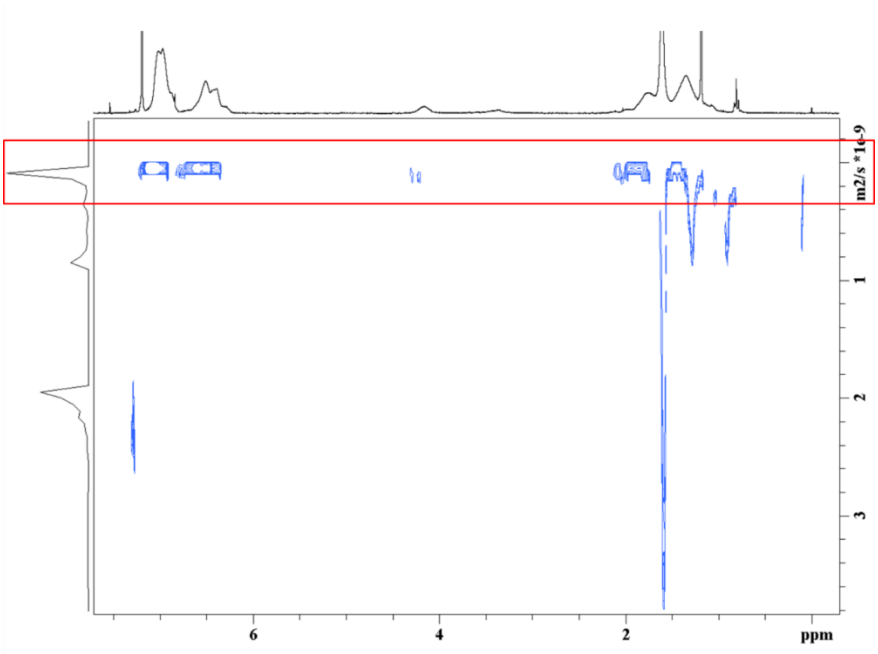


**Figure 5. 11.** $^{1}$H DOSY (500 MHz) NMR spectrum of polystyrene nanoparticles modified with hydrophilic poly(phosphonate) $P(1)_{45}$ ($PS\text{-}P(1)_{45}$) dissolved in $CDCl_3$ at 298 K. [redacted]

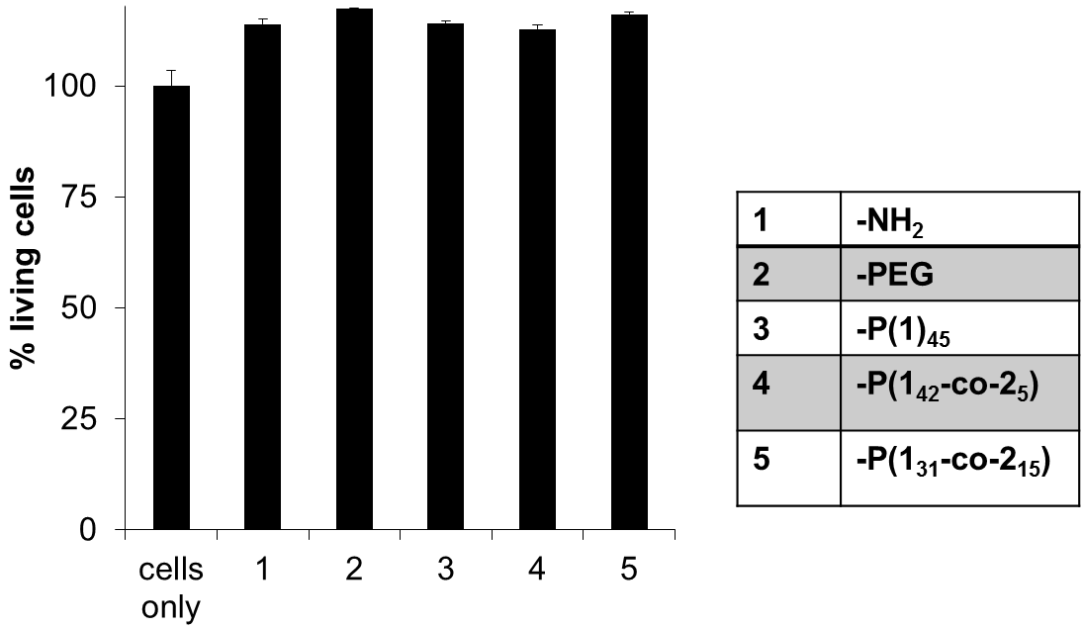


**Figure 5. 12.** Cytotoxicity assay of nanoparticles (75 µg/mL) incubated with RAW264.7 cells for 2 h. Cytotoxicity was determined by PI staining (2 µg/mL) whereas incubation without nanoparticles was defined as 100% viable. Values are expressed as mean ± SD of triplicates.

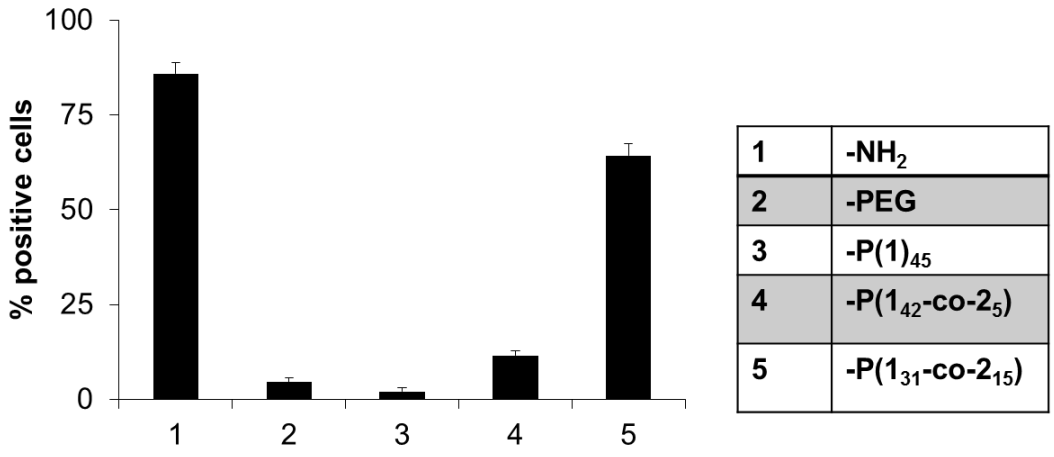


**Figure 5. 13.** Flow cytometry analysis of HeLa cells incubated with plasma coated PS-NC (75 µg/mL) for 3 h in serum-free medium. Values (% of fluorescent positive cells) are expressed as mean ± SD of duplicates.

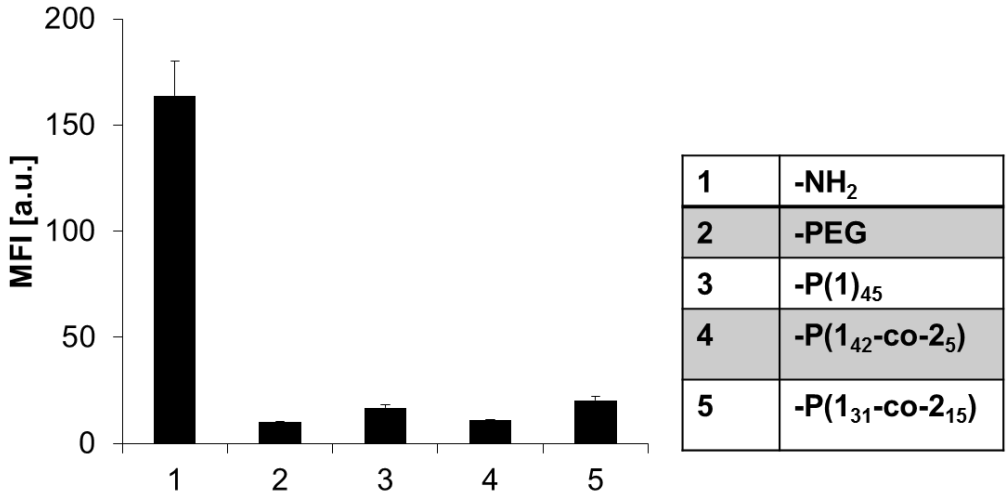


**Figure 5. 14.** Flow cytometry analysis of RAW264.7 cells incubated with plasma coated PS-NC (75 µg/mL) for 2 h in serum-free medium at 4 °C. Median Fluorescence intensity valules (MFI) are expressed as mean ± SD of triplicates. There is a strong unspecific binding to PS-$NH_2$ towards the cell membrane.

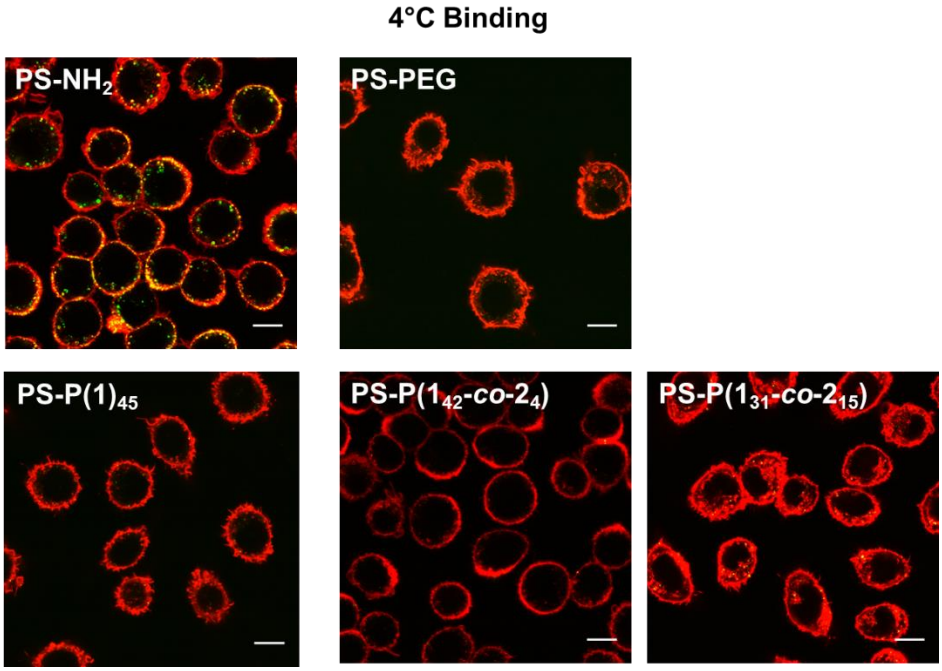


**Figure 5. 15.** cLSM images of RAW264.7 cells incubated with plasma coated PS-NC (75 µg/mL) for 2 h in serum-free medium. The cell membrane is stained with CellMask Orange and pseudocoloured in red and the PS-NCs are pseudocoloured in green. Scale bar: 10 µm.

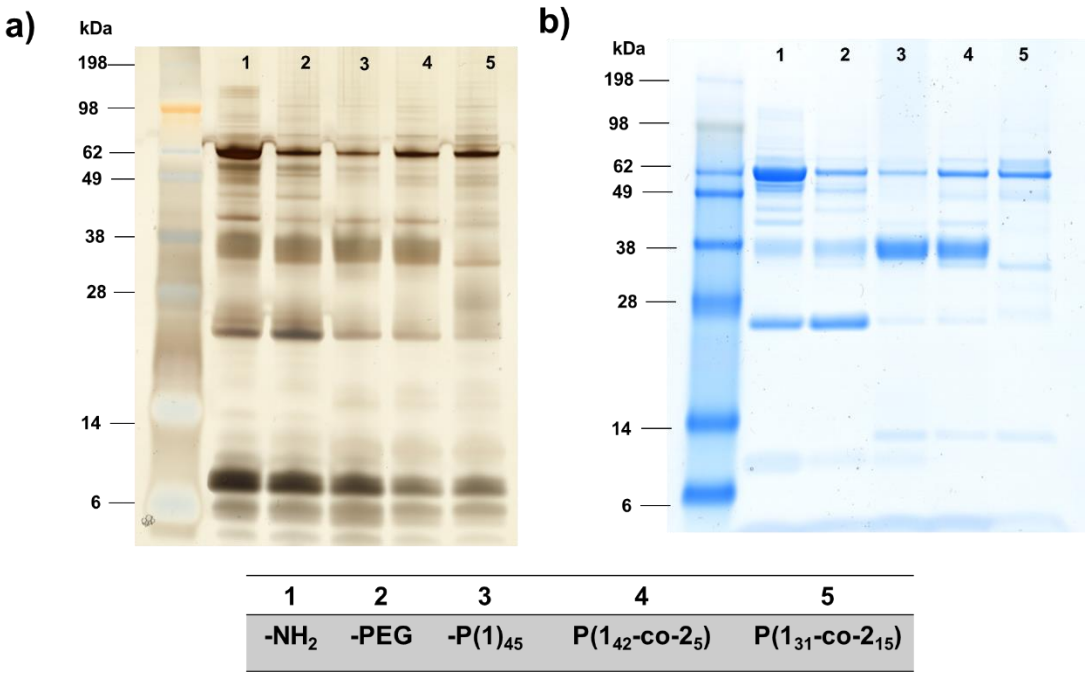


**Figure 5. 16.** SDS PAGE after protein corona analysis of PS-NC incubated with human plasma. Proteins were visualized by Silver Staining **(a)** or Coomassie blue **(b).**

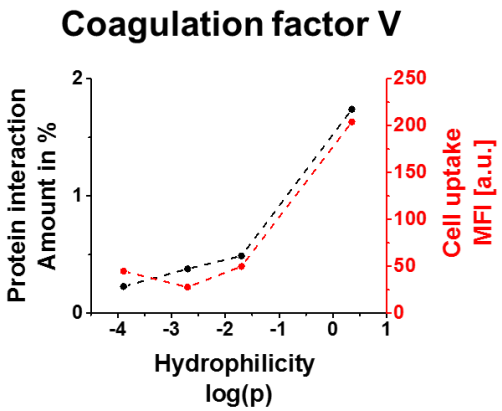


**Figure 5. 17.** Correlation between polymer hydrophilicity, cellular uptake and protein interaction.

**a)**

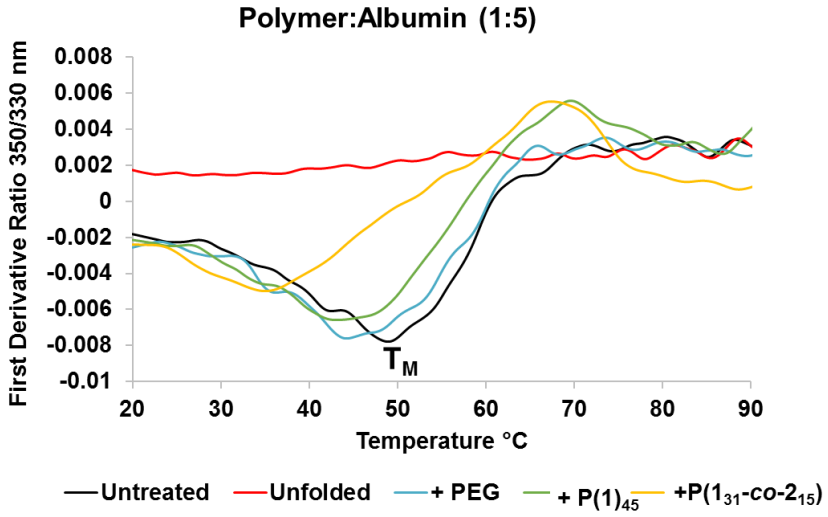


**b)**

| Albumin | Melting temperature $T_M$ |
|---|---|
| **Untreated** | 48.8°C |
| **+ PEG** | 44.6°C |
| **+ $P(1)_{45}$** | 43.6°C |
| **+$P(1_{31}$-*co*-$2_{15})$** | 35.0°C |

**Figure 5. 18. a)** Monitoring the unfolding human serum albumin exposed to different polymer solutions. Polymers (10 mg/mL) were added to albumin (1 mg/mL) in a ratio of 1:5 and analyzed by nanoDSF. This method determines protein stability based on intrinsic tryptophan and tyrosine fluoresence intensity at 350/330 nm. The first derivative of the ratio between 350/330 nm is shown. **b)** The melting point $T_M$ (50% of unfolded protein) is measured as the minimum of the curve. Proteins were treated with 2% SDS which servers a control for an unfolded protein.

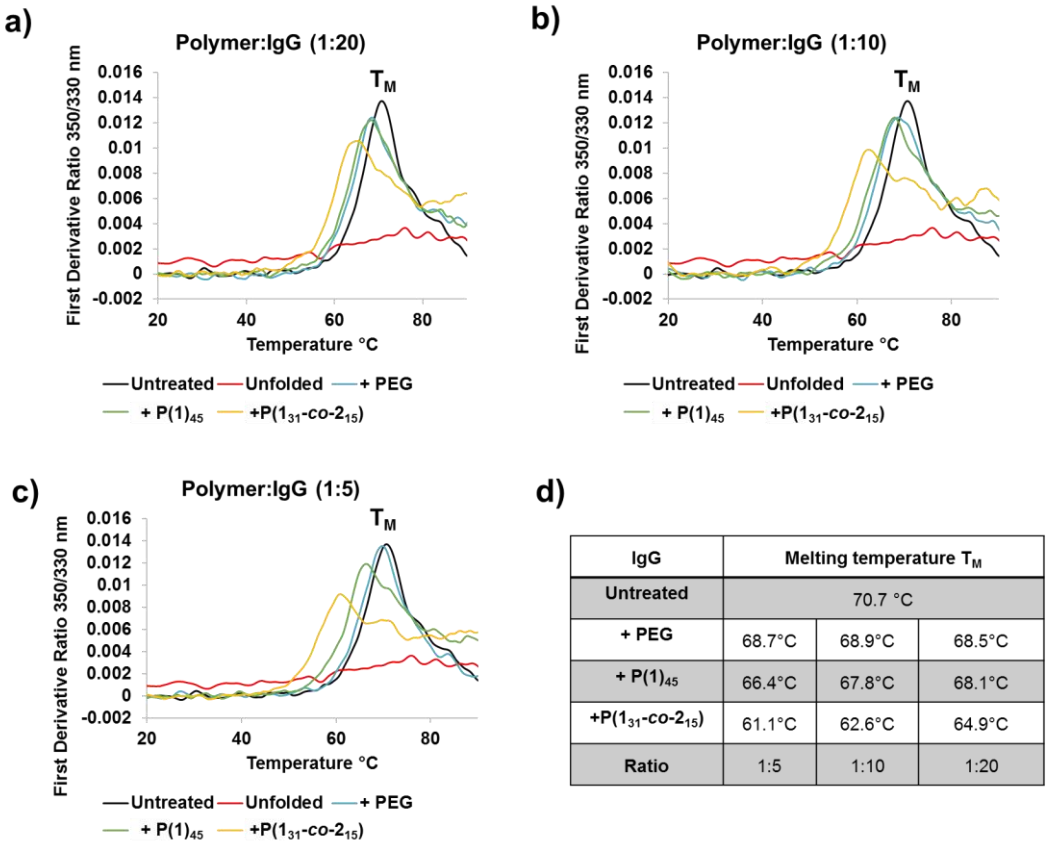


| IgG | Melting temperature $T_M$ | | |
|---|---|---|---|
| Untreated | 70.7 °C | | |
| + PEG | 68.7°C | 68.9°C | 68.5°C |
| + $P(1)_{45}$ | 66.4°C | 67.8°C | 68.1°C |
| +$P(1_{31}$-*co*-$2_{15})$ | 61.1°C | 62.6°C | 64.9°C |
| Ratio | 1:5 | 1:10 | 1:20 |

**Figure 5. 19.** Monitoring the unfolding immunoglobuline (IgG) exposed to different polymer solutions. Polymers (10 mg/mL) were added to IgG (1 mg/mL) in different ratios of **a)** 1:20 **b)** 1:10 **c)** 1:5 and analyzed by nanoDSF. The first derivative of the ratio between 350/330 nm is shown. **d)** The melting point TM (50% of unfolded protein) is measured as the maximum of the curve. Proteins were treated with 2% SDS which servers a control for an unfolded protein.

## Literature

1. Yoo, J. W.; Chambers, E.; Mitragotri, S., Factors that Control the Circulation Time of Nanoparticles in Blood: Challenges, Solutions and Future Prospects. *Curr Pharm Design* **2010,** *16* (21), 2298-2307.

2. Dawidczyk, C. M.; Kim, C.; Park, J. H.; Russell, L. M.; Lee, K. H.; Pomper, M. G.; Searson, P. C., State-of-the-art in design rules for drug delivery platforms: lessons learned from FDA-approved nanomedicines. *J Control Release* **2014,** *187*, 133-44.

3. Owens, D. E., 3rd; Peppas, N. A., Opsonization, biodistribution, and pharmacokinetics of polymeric nanoparticles. *Int J Pharm* **2006,** *307* (1), 93-102.

4. Suk, J. S.; Xu, Q.; Kim, N.; Hanes, J.; Ensign, L. M., PEGylation as a strategy for improving nanoparticle-based drug and gene delivery. *Adv Drug Deliv Rev* **2016,** *99* (Pt A), 28-51.

5. Knop, K.; Hoogenboom, R.; Fischer, D.; Schubert, U. S., Poly(ethylene glycol) in drug delivery: pros and cons as well as potential alternatives. *Angew. Chem. Int. Ed. Engl.* **2010,** *49* (36), 6288-308.

6. A. Abuchowski; J.R.McCoy; N.C.Palczuk; T. van Es; F.F.Davis, Effect ofcovalent attachment ofpolyethylene glycol on immunogenicity and circulating life of bovine liver catalase. *J. Biol. Chem.* **1977,** *252*, 3582–3586.

7. Kawai, F.; Kimura, T.; Fukaya, M.; Tani, Y.; Ogata, K.; Ueno, T.; Fukami, H., Bacterial oxidation of polyethylene glycol. *Applied and environmental microbiology* **1978,** *35* (4), 679-684.

8. Tagami, T.; Uehara, Y.; Moriyoshi, N.; Ishida, T.; Kiwada, H., Anti-PEG IgM production by siRNA encapsulated in a PEGylated lipid nanocarrier is dependent on the sequence of the siRNA. *Journal of controlled release* **2011,** *151* (2), 149-154.

9. Kang, B.; Okwieka, P.; Schottler, S.; Winzen, S.; Langhanki, J.; Mohr, K.; Opatz, T.; Mailander, V.; Landfester, K.; Wurm, F. R., Carbohydrate-Based Nanocarriers Exhibiting Specific Cell Targeting with Minimum Influence from the Protein Corona. *Angew Chem Int Ed Engl* **2015,** *54* (25), 7436-40.

10. Baier, G.; Baumann, D.; Siebert, J. M.; Musyanovych, A.; Mailander, V.; Landfester, K., Suppressing Unspecific Cell Uptake for Targeted Delivery Using Hydroxyethyl Starch Nanocapsules. *Biomacromolecules* **2012,** *13* (9), 2704-2715.

11. Bauer, M.; Lautenschlaeger, C.; Kempe, K.; Tauhardt, L.; Schubert, U. S.; Fischer, D., Poly(2-ethyl-2-oxazoline) as alternative for the stealth polymer poly(ethylene glycol): comparison of in vitro cytotoxicity and hemocompatibility. *Macromol Biosci* **2012,** *12* (7), 986-98.

12. Bludau, H.; Czapar, A. E.; Pitek, A. S.; Shukla, S.; Jordan, R.; Steinmetz, N. F., POxylation as an alternative stealth coating for biomedical applications. *Eur Polym J* **2017,** *88*, 679-688.

13. Schottler, S.; Becker, G.; Winzen, S.; Steinbach, T.; Mohr, K.; Landfester, K.; Mailander, V.; Wurm, F. R., Protein adsorption is required for stealth effect of poly(ethylene glycol)- and poly(phosphoester)-coated nanocarriers. *Nat Nanotechnol* **2016,** *11* (4), 372-7.

14. Bauer, K. N.; Tee, H. T.; Velencoso, M. M.; Wurm, F. R., Main-chain poly(phosphoester)s: History, syntheses, degradation, bio-and flame-retardant applications. *Progress in Polymer Science* **2017**.

15. Lynch, I.; Salvati, A.; Dawson, K. A., Protein-nanoparticle interactions: What does the cell see? *Nat Nanotechnol* **2009,** *4* (9), 546-7.

16. Lee, Y. K.; Choi, E. J.; Webster, T. J.; Kim, S. H.; Khang, D., Effect of the protein corona on nanoparticles for modulating cytotoxicity and immunotoxicity. *Int J Nanomedicine* **2015,** *10*, 97-113.

17. Ritz, S.; Schottler, S.; Kotman, N.; Baier, G.; Musyanovych, A.; Kuharev, J.; Landfester, K.; Schild, H.; Jahn, O.; Tenzer, S.; Mailander, V., Protein corona of nanoparticles: distinct proteins regulate the cellular uptake. *Biomacromolecules* **2015,** *16* (4), 1311-21.

18. Takeuchi, T.; Kitayama, Y.; Sasao, R.; Yamada, T.; Toh, K.; Matsumoto, Y.; Kataoka, K., Molecularly Imprinted Nanogels Acquire Stealth In Situ by Cloaking Themselves with Native Dysopsonic Proteins. *Angew Chem Int Ed Engl* **2017,** *56* (25), 7088-7092.

19. Bewersdorff, T.; Vonnemann, J.; Kanik, A.; Haag, R.; Haase, A., The influence of surface charge on serum protein interaction and cellular uptake: studies with dendritic polyglycerols and dendritic polyglycerol-coated gold nanoparticles. *Int J Nanomedicine* **2017,** *12*, 2001-2019.

20. Yoon, J.-Y.; Kim, J.-H.; Kim, W.-S., Interpretation of protein adsorption phenomena onto functional microspheres. *Colloids and Surfaces B: Biointerfaces* **1998,** *12* (1), 15-22.

21. Lindman, S.; Lynch, I.; Thulin, E.; Nilsson, H.; Dawson, K. A.; Linse, S., Systematic investigation of the thermodynamics of HSA adsorption to N-iso-propylacrylamide/N-tert-butylacrylamide copolymer nanoparticles. Effects of particle size and hydrophobicity. *Nano Lett* **2007,** *7* (4), 914-20.

22. Cedervall, T.; Lynch, I.; Foy, M.; Berggard, T.; Donnelly, S. C.; Cagney, G.; Linse, S.; Dawson, K. A., Detailed identification of plasma proteins adsorbed on copolymer nanoparticles. *Angew Chem Int Ed Engl* **2007,** *46* (30), 5754-6.

23. Gessner, A.; Waicz, R.; Lieske, A.; Paulke, B. R.; Mäder, K.; Müller, R. H., Nanoparticles with decreasing surface hydrophobicities: influence on plasma protein adsorption. *International Journal of Pharmaceutics* **2000,** *196* (2), 245-249.

24. Asai, M.; Zhao, D.; Kumar, S. K., Role of Grafting Mechanism on the Polymer Coverage and Self-Assembly of Hairy Nanoparticles. *ACS Nano* **2017**.

25. Perry, J. L.; Reuter, K. G.; Kai, M. P.; Herlihy, K. P.; Jones, S. W.; Luft, J. C.; Napier, M.; Bear, J. E.; DeSimone, J. M., PEGylated PRINT nanoparticles: the impact of PEG density on protein binding, macrophage association, biodistribution, and pharmacokinetics. *Nano Lett* **2012,** *12* (10), 5304-10.

26. Steinbach, T.; Ritz, S.; Wurm, F. R., Water-Soluble Poly(phosphonate)s via Living Ring-Opening Polymerization. *Acs Macro Lett* **2014,** *3* (3), 244-248.

27. Wolf, T.; Steinbach, T.; Wurm, F. R., A Library of Well-Defined and Water-Soluble Poly(alkyl phosphonate)s with Adjustable Hydrolysis. *Macromolecules* **2015,** *48* (12), 3853-3863.

28. Wolf, T.; Rheinberger, T.; Wurm, F. R., Thermoresponsive coacervate formation of random poly(phosphonate) terpolymers. *European Polymer Journal* **2017**.

29. Holzapfel, V.; Musyanovych, A.; Landfester, K.; Lorenz, M. R.; Mailander, V., Preparation of fluorescent carboxyl and amino functionalized polystyrene particles by miniemulsion polymerization as markers for cells. *Macromol Chem Physic* **2005,** *206* (24), 2440-2449.

30. Schöttler, S.; Becker, G.; Winzen, S.; Steinbach, T.; Mohr, K.; Landfester, K.; Mailander, V.; Wurm, F. R., Protein adsorption is required for stealth effect of poly(ethylene glycol)- and poly(phosphoester)-coated nanocarriers. *Nature Nanotech.* **2016**.

31. Kokkinopoulou, M.; Simon, J.; Landfester, K.; Mailänder, V.; Lieberwirth, I., Visualization of the Protein Corona: towards a biomolecular understanding of nanoparticle-cell-interactions. *Nanoscale* **2017**.

32. Hofmann, D.; Tenzer, S.; Bannwarth, M. B.; Messerschmidt, C.; Glaser, S.-F.; Schild, H.; Landfester, K.; Mailaender, V., Mass Spectrometry and Imaging Analysis of Nanoparticle-Containing Vesicles Provide a Mechanistic Insight into Cellular Trafficking. *ACS Nano* **2014,** *8* (10), 10077-10088.

33. Silva, J. C.; Gorenstein, M. V.; Li, G. Z.; Vissers, J. P.; Geromanos, S. J., Absolute quantification of proteins by LCMSE: a virtue of parallel MS acquisition. *Mol. Cell. Proteomics.* **2006,** *5* (1), 144-156.

# 6. Protein corona mediated stealth properties of biocompatible carbohydrate-based nanocarriers

## Aim:

Attaching poly(ethylene)glycol (PEG) to the surface of nanoparticles is the gold standard to increase the plasma half-life of nanocarriers. However, there a several drawbacks of PEG as it is a non-biodegradable polymer and potentially immunogenic. Therefore, this study investigated an alternative strategy using sugar derivates (HES, DEX or Glucose) as stealth coating for nanocarriers. It was shown that the cellular interactions towards phagocytic cells and the protein corona profile of sugar-modified nanocarriers are comparable to the PEGylated system. This highlights that biodegradable carbohydrates can be used as an alternative strategy to obtain stealth properties.

## Contribution:

I carried out the complete protein corona analysis (SDS-PAGE, LC-MS, Pierce Assay) and conducted the cellular uptake experiments (flow cytometry). [redacted] synthesized the nanocapsules. The project was supervised by [redacted]

## Abstract

Carbohydrates possess ideal properties for the synthesis of biocompatible nanocarriers. Hydroxyethyl starch was chosen as building material to produce biodegradable nanocarriers, which allow the encapsulation of drugs for targeted cell interactions. A mandatory feature for the successful application of nanocarriers in drug delivery is a prolong blood circulation time. Here, it is todays gold stand to attach polyethylene glycol (PEG) onto the surface. In comparison to this, we functionalized the surface with different sugar derivatives (HES, Dextran or Glucose) via copper-free click reaction in order to synthesize completely carbohydrate-based nanocarriers. Studying the interaction of sugar-modified nanocarriers and plasma proteins indicates a strong enrichment of ´stealth´ proteins (clusterin) which are also identified on PEGylated nanocarriers. Cellular uptake studies proved that there is no unspecific interaction between sugar modified nanocarriers and phagocytic cells hereby underlining the stealth properties.


## Introduction

Nanocarriers based on HES, ethoxylated starch, are promising candidates for nanometer-sized drug delivery vehicles for various water-soluble drugs in their interior. Encapsulation of the drugs is important to protect the drug against the environment as well as the healthy environment against the drugs and to release it selectively at the diseased place in the body.

However, if the nanocarriers are injected into the blood, proteins will adsorb on the nanocarriers' surface. Thus, the surface of the nanocarriers is shielded from the environment, which could change the properties of the nanocarrier in the body.[1-2] The nature and the amount of proteins adsorbing on the surface depends on the composition, the surface chemistry, charge, the environment and protein source.[2-3] Proteins adsorb on the nanocarrier surface due to hydrophobic interactions of the proteins and the nanocarrier surface, as well as hydrogen bonding, electrostatic and Van-der-Waals interactions.[2, 4] The protein coverage on the surface depends on the roughness of the surface and the size of the nanocarrier.[1, 4-5] Thus, different proteins can adsorb on the surface with strong or weak binding affinity. Depending on that, they are part of the so called *soft* or *hard* protein corona. Proteins with strong binding affinity to the surface are part of the hard protein corona. These proteins can only be removed from the surface with harsh conditions.[2] The soft protein corona includes proteins, which weakly adsorb at the nanocarrier surface and can be exchanged from the surface by proteins with strong adsorption properties.[2]

To reduce unspecific protein adsorption, the surface of the nanocarriers is functionalized with protein repellent materials. In addition to the often used PEG[6], poly(phosphoester)s[7] and polyglycerols (PG)[8] are known to reduce the protein adsorption on nanocarrier surfaces. Furthermore, polyoxazolines, poly(amino acids), polyamines, polybetaine and polysaccharides are discussed as alternative surface modifiers to reduce protein adsorption and to guarantee a long circulation time in the blood stream.[9] The advantages using polysaccharides as natural polymer instead of PEG[9] are their biodegradability, low toxicity and immunogenicity as well as their multiple functional groups for further functionalization for example with cell specific linkers or drugs.[10] First studies with hydroxyethyl starch nanocarriers underlined their protein repellent behavior and decreased unspecific uptake into HeLa cells.[11] Moreover, dextran as another polysaccharide decreased protein adsorption after grafted onto a polystyrene surface.[12] However, due to the multitude of saccharides, each chiral center might influence the interaction with proteins and needs to be carefully evaluated.

In general, chemical functionalization of a nanocarriers' surface shall be simple with high conversion. Thus, click reactions have been used, because they are easy to perform, with good yields, high rates, and if necessary simple purification.[13] A common click reaction is the copper-catalyzed 1,3-Huisgen reaction of an azide and an alkyne.[14] In addition, copper-free alternatives were investigated using strained alkynes like cyclooctynes.[15]

Herein, HES and dextran were functionalized with at least one azide group using an azido-isocyanate-urea as linker molecule. Additionally, monomeric glucose, which is part of both polysaccharides, was modified with an azide at β-position. These (poly)saccharides were then coupled to the surface of HES nanocarriers by the copper-free azide-alkyne cycloaddition to produce completely carbohydrate-based biocompatible and fully biodegradable nanocarriers. The protein composition on such nanocarriers surface was identified by SDS-PAGE and LC-MS as well as *in vitro* cell uptake studies towards phagocytic cells (macrophages and primary dendritic cells) and compared to PEGylated analogs. These results prove fully carbohydrate-based nanocarriers as a potential alternative to synthetic drug delivery vehicles, which might overcome accumulation in the body or immune responses due to their eventual degradation.

## Materials and methods

D-Glucose (Sigma-Aldrich, ≥99.5%), sodium azide ($NaN_3$, Sigma-Aldrich, *ReagentPlus*, ≥99.5%), 2-chloro-1,3-dimethylimidazolinium chloride (Sigma-Aldrich, DMC), Amberlite IR-120 (Sigma-Aldrich, hydrogen from), 2-chloroethylamine hydrochloride (Sigma-Aldrich, 99%), sodium hydroxide (NaOH, Fluka, ACS reagent, ≥ 97.0%), magnesium sulfate ($MgSO_4$, Fluka,

anhydrous, reagent grade, ≥99.5%), triphosgene (Sigma-Aldrich, reagent grade, 98%), poly(ethylene glycol) methyl ether azide (mPEG-azide, 5 kDa, Sigma-Aldrich), sodium dodecylsulfate (SDS, Fluka, ACS reagent grade, ≥99.0%), Cyanine 5-Oligonucleotide (Cy5 Oligo, Iba GmbH), toluene-2,4-diisocyanate (TDI, Sigma-Aldrich, 95%), Dibenzocyclooctyne-$PEG_4$-*N*-hydroxysuccinimidyl ester (DBCO-$PEG_4$-NHS ester, Jana Bioscience), citric acid (Sigma-Aldrich, ACS reagent, ≥99.5%), citric acid trisodium salt (Sigma-Aldrich, anhydrous, ≥98% (GC)), dextranase from *Penicillium sp.* (Sigma-Aldrich, lyophilized powder, 12.5 untis/mg solid) and hydrochloric acid (HCl 37%, VWR chemicals, AnalaR NORMAPUR Reag. Ph. Eur. for analysis) were used as received. Triethylamine (TEA, Fluka, HPLC, ≥99.5%) and 2,2′-(ethylenedioxy)bis(ethylamine) (Sigma-Aldrich, 98%) were stored over molecular sieve before use. Dextran (5.2 kDa, PSS Polymer Standard Service GmbH) and hydroxyethyl starch (HES, 8.2 kDa, Fresenius Kabi) were dried at 40 °C *in vacuo* overnight. HES (200kDa, 0.5 degree of substitution) was purchased from Fresenius Kabi and freeze-dried before used. Dichloromethane (DCM, Fisher Scientific), ethanol (VWR Chemicals, 96%), dimethylsulfoxide (DMSO, Sigma-Aldrich, anhydrous, ≥99.9%) and diethyl ether (Sigma-Aldrich, anhydrous, ≥99.7%) were used as received. The deuterated solvents chloroform-*d* ($CDCl_3$-*d*, Acros Organics, 99.8 atom% D), deuterium oxide ($D_2O$, Sigma-Aldrich, 99.9 atom% D) and dimethyl sulfoxide-$d_6$ (DMSO-$d_6$, Carl Roth, 99.8 atom% D) were used for NMR analysis as obtained.

The oil-soluble surfactant poly((ethylene-*co*-butylene)-*b*-(ethylene oxide)) was synthesized by anionic ring-opening polymerization of ethylene oxide using ω-hydroxypoly-(ethylene-*co*-butylene) as initiator in toluene with a poly(ethylene-*co*-butylene) block of 3700 g $mol^{-1}$ and a polyethylene oxide block of 3600 g $mol^{-1}$.[31]

**Methods.** $^1$H-NMR spectra were measured on a Bruker Avance 250 spectrometer (Bruker, Billerica, MA, USA) operating at a Lamor frequency of 250 MHz or a Bruker Avance 300 spectrometer (Bruker, Billerica, MA, USA) with a Lamor frequency of 300.23 MHz. As deuterated solvents $D_2O$, $CDCl_3$ and DMSO-$d_6$ were used. In 0.5 mL deuterated solvent around 15 mg of the product was dissolved and the spectra was calibrated according to the chemical shift of the used deuterated solvent (4.79 ppm for $D_2O$, 7.26 ppm for $CHCl_3$ or 2.5 ppm for DMSO-$d_6$).

$^{13}$C-NMR spectra were measured on a Bruker Avance 300 spectrometer (Bruker, Billerica, MA, USA) with a Lamor frequency of 300.23 MHz. 30 mg of the product was dissolved in 0.5 mL deuterated solvent ($D_2O$, $CHCl_3$ and DMSO-$d_6$) and the spectra were calibrated according to the chemical shift of the used deuterated solvent (77.16 ppm for $CHCl_3$ or 39.52 ppm for DMSO-$d_6$). Fourier transformed infrared spectroscopy (FT-IR) was performed using a

PerkinElmer Spectrum BX FT-IR spectrometer (PerkinElmer, Shelton, CT, USA) between wavelength of 4000 $cm^{-1}$ and 400 $cm^{-1}$ to determine successful azidation of the linker and the sugar derivatives. Therefore, the samples were mixed with potassium bromide (KBr), pressed and subsequently measured. At the Zeiss 1530 LEO Gemini microscope (Carl Zeiss, Oberkochen, Germany) the morphology and size of generated nanocapsules were analyzed. Therefore, 10 µL of the nanocapsule dispersion were diluted in 3 mL cyclohexane, dropped onto a silica wafer and dried under ambient conditions. Then, the wafer was placed under the microscope, working with an accelerating voltage of 0.2 kV and a distance of ~3 mm.
The zeta potential of 10 µL nanocapsule dispersion was measured at 25 °C in $10^{-3}$ mol/L in potassium chloride solution with a Zetasizer ZEN2600 from Malvern Instruments. An average of at least two measurements, each with at least ten runs is reported.
Nanocapsules were incubated with human plasma as described for hard protein corona analysis (see purification of hard corona below). After the final wash, nanocapsules coated with proteins were resuspended in water and 10 µL of the dispersion was measured with a Zetasizer. In addition, the hydrodynamic radii of the nanocapsules was determined by DLS using a Nicomp 380 Submicron particle Sizer (PSS-Nicomp, Particle Sizing System, Port Richey, Fl, USA) with a fixed angel of 90 °. To measure the size, 10 µL of the emulsion was diluted in 1 mL cyclohexane or water.

**Purification of hard protein corona.** Nanocapsules with a 0.05 $m^2$ surface area were incubated with 1 mL 100% human citrate plasma for 1 h at 37 °C to allow protein corona formation. Purification of hard protein corona was executed according prior instructions.[32,33] Briefly, nanocapsules were centrifuged three times for 30 min at 4 °C and 20,000 g followed by resuspension with 1 mL PBS at 4 °C. After the last washing step capsules were redispersed and incubated with 62.5 mM Tris-HCL supplemented with 2% SDS for 5 min at 95 °C and bound proteins were eluted from nanocapsules. To remove capsules in suspension the samples were centrifuged again for 30 min at 20 000 g and 4 °C. The Pierce 660 nm Protein Assay Reagent was used for protein quantification in combination with the Ionic Detergent Compatibility Reagent for Pierce 660 nm Protein Assay Reagent (both Thermo Scientific, Dreieich, Germany) corresponding the manufacturer instructions.

**Determination of the hard protein corona by SDS-PAGE.** 1 µg of the hard corona proteins was supplemented with sample buffer and reducing agent (Novex, Carlsbad, USA) for SDS polyacrylamide gel electrophoresis (SDS-PAGE) and afterwards incubated for 5 min at 95 °C. Then, SDS-PAGE was run for 1 h at 100 mV before protein bands were visualized by the

SilverQuest Silver Staining Kit (Thermo Scientific) corresponding the manufacturer instructions.

**Digestion of the protein corona for MS analysis.** SDS was eliminated via Pierce detergent removal columns (Thermo Fisher) prior to protein digestion. Tryptic digestion was performed as described by Tenzer et *al.*[5] with the following adjustments. Proteins were precipitated according to the manufactures instructions´ using ProteoExtract protein precipitation kit (CalBioChem). The resulting protein pellet was resuspended in RapiGest SF (Waters Cooperation) dissolved in 50 mM ammonium bicarbonate (Sigma-Aldrich) and afterwards incubated at 80 °C for 15 min. The addition of dithithreitol (Sigma-Aldrich) reduced the proteins to gain a final concentration of 5 mM and incubated for 45 min at 56 °C. Iodoacetamide (final concentration 15 mM, Sigma-Aldrich) was added and the solution was incubated for 1 h in the dark. Tryptic digestion with a protein:trypsin ratio of 50:1 was carried out over 16 h at 37 °C. The reaction was quenched by adding 2 µL hydrochloric acid (Sigma-Aldrich). Degradation products of RapiGest SF were removed via centrifugation (14 000 g, 15 min).

**LC-MS analysis.** For absolute protein quantification, the peptide samples were spiked with 10 fmol $\mu L^{-1}$ of $Hi^3$ Ecoli Standard (Waters Cooperation). Digested peptides were applied to a C18 nanoACQUITY Trap Column (5 µm, 180 µm x 20 mm,) and separated on a C18 analytic reversed phase column (1.7 µm, 75 µm x 150 mm) using a nanoACQUITY UPLC systems. The column is further coupled to a Synapt G2-Si mass spectrometer. A two phase mobile system consisting of phase (A) 0.1% (v/v) formic acid in water and phase (B) acetonitrile with 0.1% (v/v) formic acid was utilized at a sample flow rate of 300 µL $min^{-1}$ with a gradient of 2 – 37% mobile phase (A) to (B) over 70 min. As a reference component, Glu-Fibrinopeptide (150 fmol $\mu L^{-1}$, Sigma) was infused at a flow rate of 500 µL $min^{-1}$.
Electrospray ionization (ESI) was executed in positive ion mode with nanoLockSpray source and the mass spectrometer was operated in resolution mode performing data-independent acquisition ($MS^E$).

Data were recorded over 90 min with a mass to charge range (m/z) over 50 – 2000 Da, scan time of 1 s and ramped trap collision energy from 20 to 40 V. Each sample was run in triplicates. Data was arranged with MassLynx 4.1. For protein identification Progenesis QI for Proteomics Version 2.0 with continuum data using a reviewed human data base (Uniprot) was chosen. Several parameters as noise reduction thresholds for low energy, high energy and peptide intensity were set to 120, 250, and 750 counts. The peptide sequence of $Hi^3$ Ecoli standard (Chaperone protein CLpB, Waters Cooperation) was added to the database for absolute

quantification.[34] The following search criteria were used for protein and peptide identification: one missed cleavage, maximum protein mass 600 kDa, fixed carbamidomethyl modification for cysteine, variable oxidation for methionine and protein false discovery rate of 4%. At least two assigned peptides and five assigned fragments are required for protein identification and three assigned fragments for protein identification. A score parameter for identified peptides was set to 4 and quantitative protein identification was generated based on the $TOP^3/Hi^3$ approach, providing the amount of each identified protein in fmol.[35]

**Cell Culture RAW264.7**. Murine macrophage cell line RAW264.7 were cultured in Dulbecco's modified eagle medium (DMEM), supplemented with 10% fetal calf serum (FCS), 100 U $mL^{-1}$ penicillin, 100 mg $mL^{-1}$ streptomycin and 2 mM glutamine.

**Generation of monocyte derived dendritic cells (moDCs).** MoDCs were generated from healthy human donors from buffy coat according to the local ethics committee and Declaration of Helsinki. Peripheral blood mononuclear cells (PBMCs) were isolated by standard Ficol separation. MoDCs were obtained as previously described.[18]

**Cellular uptake studies.** Quantitative analysis of nanocapsules uptake into cells was analyzed by flow cytometry. 1 x $10^5$ cells per mL (RAW 264.7 or moDC) were allowed to attach in 24/48-well plates. Nanocapsules were incubated with human plasma as described above (hard corona analysis), centrifuged and added at a concentration of 75 µg $mL^{-1}$ (RAW264.7) or 50 µg $mL^{-1}$ (moDC) for 2 h.

RAW264.7 cells were detached with 2.5% trypsin (Gibco, Germany) and for moDCs 0.5mM EDTA/PBS was used. Flow cytometry measurements were performed on a CyFlow ML Cytometer. Data was analyzed using FCS Express V4 software by selecting the cells on a forward/sideward scatter plot. The fluorescent signal was expressed as median intensity. Mean values and standard deviations of three independent measurements (n = 3) are given.

**Synthesis.** All reactions involving air or moisture sensitive reagents or intermediates were conducted under an inert atmosphere of argon in glassware, which were dried in an oven before use. Reaction temperatures referred to the temperature of the particular cooling/heating bath.

**Synthesis of β-glucose azide.** Glucose was selectively functionalized with one azide group at the OH-β-position using the synthesis published by *Vinson et al*.[20]. Glucose (1.00 g, 5.6 mmol, 1 eq) and sodium azide (3.63 g, 55.8 mmol, 10 eq) were dissolved in water (20 mL) and added to a solution of 2-chloro-1,3-dimethylimidazolinium chloride (2.80 g, 16.6 mmol, 3 eq)

and TEA (7.80 mL, 55.9 mmol, 10 eq) under ice cooling. After stirring for 1 h at 0 °C, the mixture was concentrated at reduced pressure and mixed with ethanol (20 mL). The generated solid was separated by filtration and ethanol was removed from the filtrate at reduced pressure. The obtained solid was dried and redissolved in water (15 mL). After the water phase was washed five times with dichloromethane (10 mL), the water phase was stirred for 4 h with acidic Amberlite IR-120 at room temperature (RT). The Amberlite was activated before with 1 M sodium hydroxide solution. Then, the ion exchanger was removed by filtration and the filtrate was freeze-dried again to obtain the β-glucose azide as a white powder in 58% yield (0.58 g).

$^{1}$H-NMR ($D_2O$, 300 MHz): δ (ppm) = 4.73 (d, *J* = 8.8 Hz, 1H), 4.05 – 3.59 (m, 2H), 3.59 – 3.32 (m, 3H), 3.23 (h, *J* = 7.6 Hz, 1H). $^{13}$C-NMR ($D_2O$, 300 MHz): δ (ppm) = 90.1 ($C_1$), 77.9 ($C_5$), 75.7($C_3$), 72.82($C_2$), 69.17($C_4$), 60.53 ($C_6$). FT-IR v = 2120 $cm^{-1}$ (-$N_3$).

**Synthesis of 2-azido-1-ethylamine**. 2-Chloroethylamine hydrochloride (6 g, 0.052 mol, 1 eq) was dissolved with sodium azide (10.3 g, 0.158 mol, 3 eq) in MilliQ water (140 mL) and stirred for 20 h at 80 °C. After neutralization with sodium hydroxide (2.08 g, 0.052 mol, 1 eq), the product was extracted four times into diethyl ether (160 mL) and dried over magnesium sulfate. The solvent was partially removed under reduced pressure. At the end, 2-azido-1-ethylamine with a concentration of 81.6% (quantified by $^{1}$H-NMR spectroscopy), containing 2.28 g (yield 51%) in diethyl ether was obtained as yellow solution.
$^{1}$H-NMR ($CDCl_3$, 300 MHz) δ (ppm) = 3.37 (t, J = 5.6 Hz, 4H, $NH_2$-C*H*$_2$), 2.93-2.84 (m, 1H, $N_3$-C*H*$_2$), 1.44 (s, 1H, $NH_2$). $^{13}$C-NMR ($CDCl_3$, 300 MHz) δ (ppm) = 54.6(*C*$H_2$-$N_3$), 41.31 (*C*$H_2$-$NH_2$). FT-IR (ATR) v = 3380 (-$NH_2$), 3310 (-$NH_2$), 2101 (-$N_3$).

**Synthesis of 2,2'-(ethylenedioxy)bis(ethylisocyanate).** 2,2′-(ethylenedioxy)bis-(ethylamine) (2.5 mL, 0.017 mol, 1 eq) and TEA (11.28 mL, 0.081 mol, 4.8 eq) was dissolved in anhydrous DCM (6 mL) and dropwise added to a stirred solution of triphosgene (4.458 g, 0.015 mol, 0.9 eq) in anhydrous DCM (40 mL) under ice-cooling in an argon atmosphere. After complete addition, the mixture was stirred for 40 min at 4 °C, then for 1 h at RT and additionally heated for 5 ½ h under reflux. DCM was removed *in vacuo* and the product was extracted from the solid using anhydrous diethyl ether (two times 50 mL). The product was identified by $^{13}$C NMR and used without further purification for the next step.

$^{13}$C-NMR ($CDCl_3$, 300 MHz) δ (ppm) = 124.78 (O=*C*=N), 69.93 (*C*$H_2$-O), 69.91 (*C*$H_2$-O), 69.8(*C*$H_2$-O), 42.8 (*C*$H_2$-N).

**Synthesis of 1-(2-azidoethyl)-3-(2-(2-(2-isocyanatoethoxy)ethoxy)ethyl)urea and sugar functionalization.** 2-azido-1-ethylamine (1.17 g, 0.014 mol, 0.8 eq) was dissolved in anhydrous diethyl ether (2 mL) and added at a speed of 6 mL $h^{-1}$ by a syringe pump into the diisocyanate solution at -56 °C. Afterwards, anhydrous DMSO (5 mL) was added at ambient temperature and diethylether was removed *in vacuo*. The product was checked by FTIR and used without further purification for the next step. 500 µL of the 1-(2-azidoethyl)-3-(2-(2-(2-isocyanatoethoxy)ethoxy)ethyl)urea solution in DMSO was added dropwise into a sugar solution (250 mg of HES of 5.5 kDa or dextran of 5 kDa) in anhydrous DMSO (5 mL). The reaction was continued for 32 h, and the product was purified by dialysis against MilliQ water in a dialyzing tube with MWCO of 1 kDa for 4 days. After dialysis, the solution was freeze-dried to obtain the product (185 mg HES and 150 mg dextran). FT-IR of 1-(2-azidoethyl)-3-(2-(2-(2-isocyanatoethoxy)-ethoxy)ethyl)urea (ATR) v = 2339 (N=C=O), 2101 ($N_3$), 1676 (urethane), 1438 (N=C=O). **HES-azide.** FT-IR (ATR) v = 2111 ($N_3$). **Dextran-azide**. FT-IR (ATR) v = 2116 ($N_3$), 1740 (urethane).

**Synthesis of HES nanocapsules by inverse miniemulsion.** The nanocapsules were prepared as described in prior publications by polyaddition reactions at the cyclohexane-water droplet interfaces.[16-19] The dispersed phase consisted of HES (140 kDa, 130 mg), NaCl (10 mg), Cy5 Oligo solution (100 µL) and PBS buffer (240 µL). The dispersed phase was added to cyclohexane (7.5 g) containing P(E/B-*b*-EO) (80 mg). After stirring at 500 rpm for 30 min, the emulsion was subjected to ultrasonication under ice-cooling with a Branson W450-D sonifier equipped with a ½ inch tip for 3 min in a pulse-phase regime of 20 s and 10 s. 5 g cyclohexane and 55 mg P(E/B-b-EO) were added and the dispersion was stirred for 30 min at 500 rpm. After a second ultrasonication using same conditions as before, TDI (175 mg) and P(E/B-*b*-EO) (25 mg) dissolved in cyclohexane (2 g) were added dropwise to the miniemulsion and stirred for 24 h at 25 °C. The size and morphology of the obtained nanocapsules were analyzed by DLS and SEM measurements as described above.

**Nanocapsule transfer into water.** Before the nanocapsules were transferred into water, they were washed to remove unreacted monomer and excess of surfactant. Therefore, 2 mL nanocapsule dispersion were filled into a 2 mL Eppendorf tube and centrifuged by 4000 rpm for 45 min. The supernatant was removed and the nanocapsules were redispersed with 400 µL cyclohexane. The redispersed nanocapsules were slowly added into 5 mL of a 0.1 wt% prepared SDS solution while shaking in a sonication bath (Bandelin Sonorex, type RK 52H). The whole dispersion was stirred over night without cap at 1000 rpm at RT, to allow evaporation of cyclohexane. To remove the excess of SDS, the emulsion was dialyzed against

water for 1 day by changing the water three times. To obtain the solid content of the nanocapsule dispersion, three times 50 µL of the nanocapsule dispersion were freeze-dried overnight.

**Functionalization of the HES nanocapsule surface with DBCO-PEG$_4$-NHS.** After the solid content was adjusted to 1 wt%, the nanocapsules were functionalized with DBCO-PEG$_4$-NHS. Therefore, a DBCO-PEG$_4$-NHS (3.29 mg per mL nanocapsule dispersion, $5.06*10^{-6}$ mol) solution in anhydrous DMSO (167 µL) was added into 1 wt% nanocapsules dispersion. After stirring over night at room temperature and 1000 rpm, the dispersion was washed two times by centrifugation at 4500 rpm for 30 min. The amount of DBCO groups on the nanocapsules surface was determined by a fluorescent assay with 9-(azidomethyl)anthracene.[24]

**Coupling of β-glucose azide, HES-azide, dextrane-azide or mPEG-azide to the nanocapsule surface.** To 1 mL nanocapsule dispersion with 1 wt% solid content, a solution of the azide-derivative (3 eq per detected DBCO group, $2.24*10^{-6}$ mol) in DMSO (200 µL) was added and stirred for 4 days at 500 rpm at 4 °C. Afterwards, the dispersion was washed two times by centrifugation at 4500 rpm for 30 min. At the end, the solid content of the nanocapsule dispersion was analyzed by freeze-drying 50 µL of the dispersion and the amount of functionalization was determined using a fluorescent assay with 9-(azidomethyl)anthracene.[24]

## Results and Discussion

The all-carbohydrate nanocarriers were prepared by the polyaddition at the droplet-oil interface in inverse miniemulsions from HES with toluene-2,4-diisocyanate as the crosslinker according to previously published protocols (Figure 6.1).[16-19] The fluorescent dye Cyanine 5 (Cy5) was loaded to the dispersed phase and thus encapsulated into the nanocarriers to allow following of the cellular uptake (material/methods see supplementary information 6). The morphology and size of the nanocarriers were confirmed by SEM and DLS analysis (Figure 6.1 and Table 6.1).

All carbohydrates were functionalized with at least one azide group for the copper-free click reaction on the nanocarriers' surface. Glucose was functionalized at the anomeric position by a one-step reaction with sodium azide in combination with 2-chloro-1,3-dimethylimidazolinium chloride and triethylamine (Figure 6.1).[20-21] HES and dextran were modified in a three step

synthesis starting with 2,2'-(ethylenedioxy)bis(ethylamine), as shown in Figure 6.1. After the two amine groups were converted to isocyanate groups using triphosgene and triethylamine, one isocyanate group was transferred with 2-azidoethan-1-amine to obtain the water-soluble isocyanate-azide linker (1-(2-azidoethyl)-3-(2-(2-(2-isocyanatoethoxy)ethoxy)ethyl)urea). HES and Dextran were subsequently functionalized with the isocyanate-azide linker (supplementary information 6). The newly formed urethane bond was confirmed by FTIR analysis (Figure 6.1).

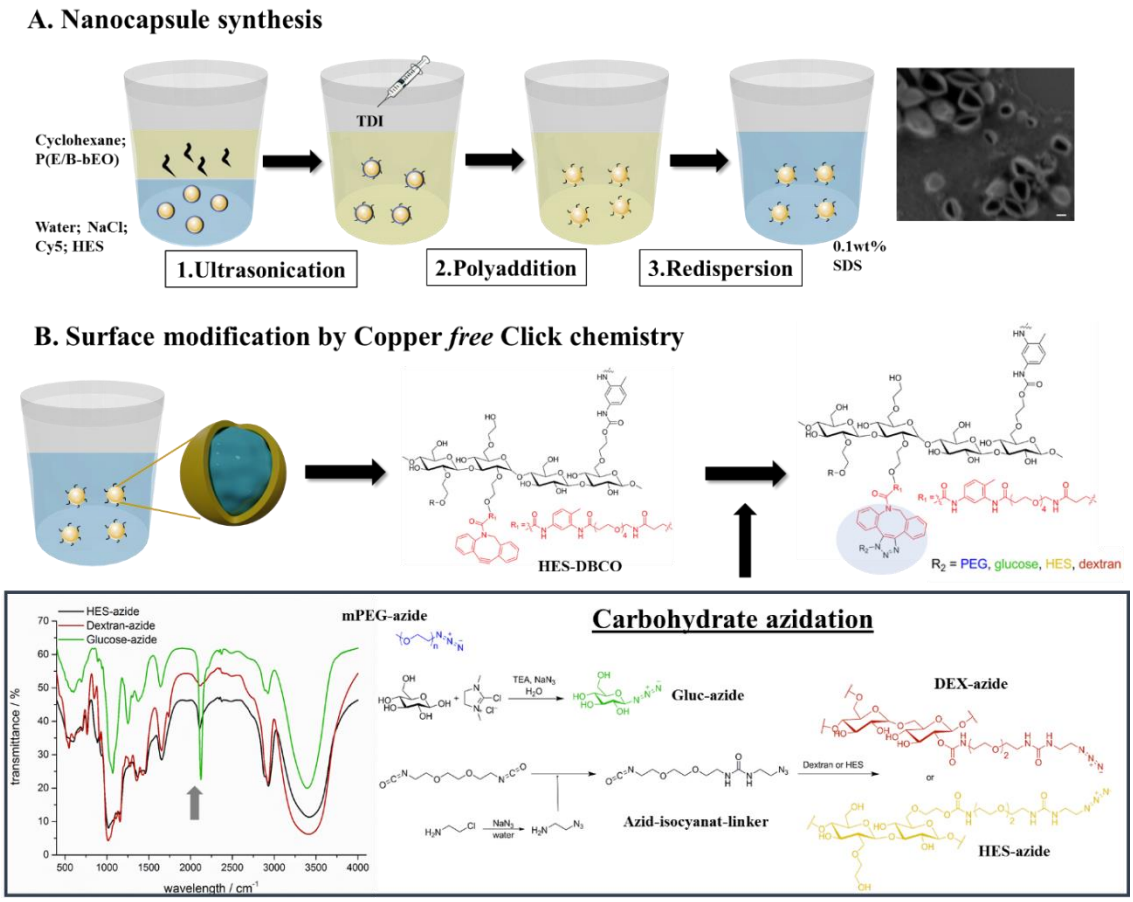


**Figure 6. 1. (A)** General scheme of hydroxyethyl starch (HES) nanocarriers synthesis by inverse miniemulsion polyaddition and their transfer into 0.1 wt% SDS solution. A mean diameter of around 300 nm was determined by scanning electron microscopy (scale bar 100 nm in cyclohexane) for all nanocarriers. **(B)** Nanocarriers were modified with strained dibenzylcycloocytne derivative (HES-DBCO) to introduce different carbohydrates (Glucose-azide (Gluc-azide), dextran-azide (DEX-azide) and HES-azide) as well as mPEG-azide on the surface by copper-free azide-alkyne click reaction. The carbohydrates were prior functionalized with azide groups and determined by infrared spectroscopy measurements. [redacted]

After transfer of the nanocarriers dispersion into water, the surface was functionalized with the strained cyclooctyne-derivative by activated ester chemistry (compare Figure 6.1) and the azide carbohydrates or mPEG-azide were linked to the surface by copper-free click reaction. An excess of the azide component was added (3 eq per triple bond).[22-23]

**Table 6. 1.** Results of modified HES nanocarriers with glucose (Gluc), dextran (DEX), HES, and mPEG.

| | d (PDI) / nm[a] | d (PDI) / nm[b] | DBCO / mol mL$^{-1}$[c] | DBCO / mol mL$^{-1}$[d] | ζ-potential / mV[e] | ζ-potential / mV[f] |
|---|---|---|---|---|---|---|
| **HES** | 240 (0.35) | 320 (0.10) | - | - | -08.07± 0.13 | -15.60 ± 0.50 |
| **HES-mPEG** | 240 (0.35) | 400 (0.13) | $2\cdot10^{-7}$ | $1.2\cdot10^{-7}$ | -12.10± 0.90 | -20.50 ± 0.80 |
| **HES-HES** | 240 (0.35) | 380 (0.06) | $2\cdot10^{-7}$ | $1.1\cdot10^{-7}$ | -13.00± 0.60 | -20.90 ± 0.50 |
| **HES-DEX** | 240 (0.35) | 420 (0.11) | $2\cdot10^{-7}$ | $8.8\cdot10^{-8}$ | -12.83± 0.13 | -20.35 ± 0.05 |
| **HES-Gluc** | 240 (0.35) | 400 (0.04) | $2\cdot10^{-7}$ | $6.7\cdot10^{-8}$ | -13.40± 0.60 | -15.20 ± 0.01 |

a) in cyclohexane, b) in water, c) before azide-alkyne reaction, d) after azide-alkyne reaction, e) in $1\cdot10^{-3}$ M KCl solution, f) in $1\cdot10^{-3}$ M KCl solution after incubation with human plasma.

The degree of carbohydrate functionalization was determined by a fluorescence assay. The fluorescence intensity of the reaction of 9-(azidomethyl)anthracene with the dibenzylcycloocytne groups (DBCO) on the surface of the nanocarriers was measured. Substraction of the measured intensities before and after attaching the carbohydrates gave the degree of functionalization (Table 6.1).[24] About 50 % (Table 6.1) based on the initial amount of DBCO groups were successfully functionalized with the respective azide component. All nanocarriers were characterized regarding size and ζ -potential indicating only minor differences between the different functionalized nanocarriers

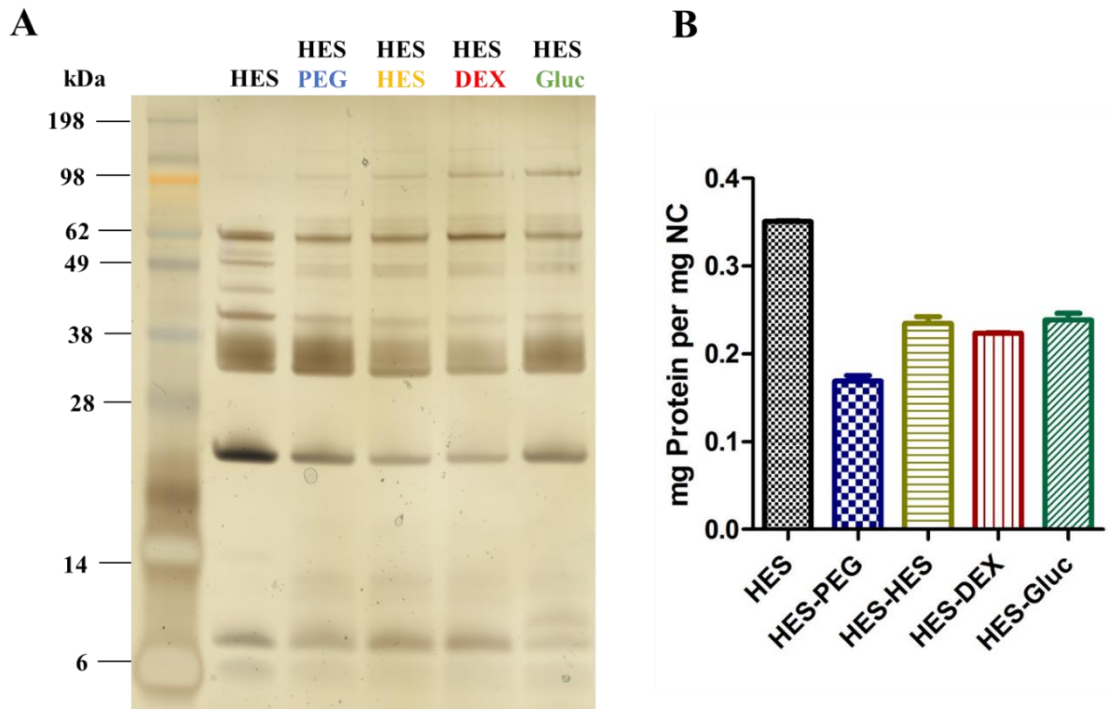


**Figure 6. 2**. Protein corona analysis. Nanocarriers (NC) were incubated for 1 h at 37 °C with 100% human plasma to allow protein corona formation. After purification of hard corona proteins (1 µg protein) was visualized by silver staining **(A)** and the total amount of hard corona proteins was quantified by Pierce Assay **(B).**

Previous studies proved the low unspecific cellular uptake of HES nanocarriers.[11] Additionally, the surface functionalization of nanocarriers with HES (i.e. “HESylation”) prolongs the blood circulation *in vivo* comparable with PEGylated carriers.[25] However, there is still a limited knowledge about the principal mechanism based on this effect. Therefore, we investigated such carbohydrate-modfied nanocarriers regarding their interactions with plasma proteins and phagocytic cells (macrophage and dendritic cells) in order to investigate their stealth properties.

Adsorption of plasma proteins to the surface of nanocarriers occurs rapidly[26] and alters the physico-chemical properties[27] and thus the interactions with cells.[28] To simulate the behavior in blood, the nanocarriers were incubated in human blood plasma for 1 h, 37 °C. Certain blood proteins adsorbed on the interface of the nanocarriers, resulting in a ζ -potential change of all nanocarriers after plasma incubation from -13 mV to -20 mV.

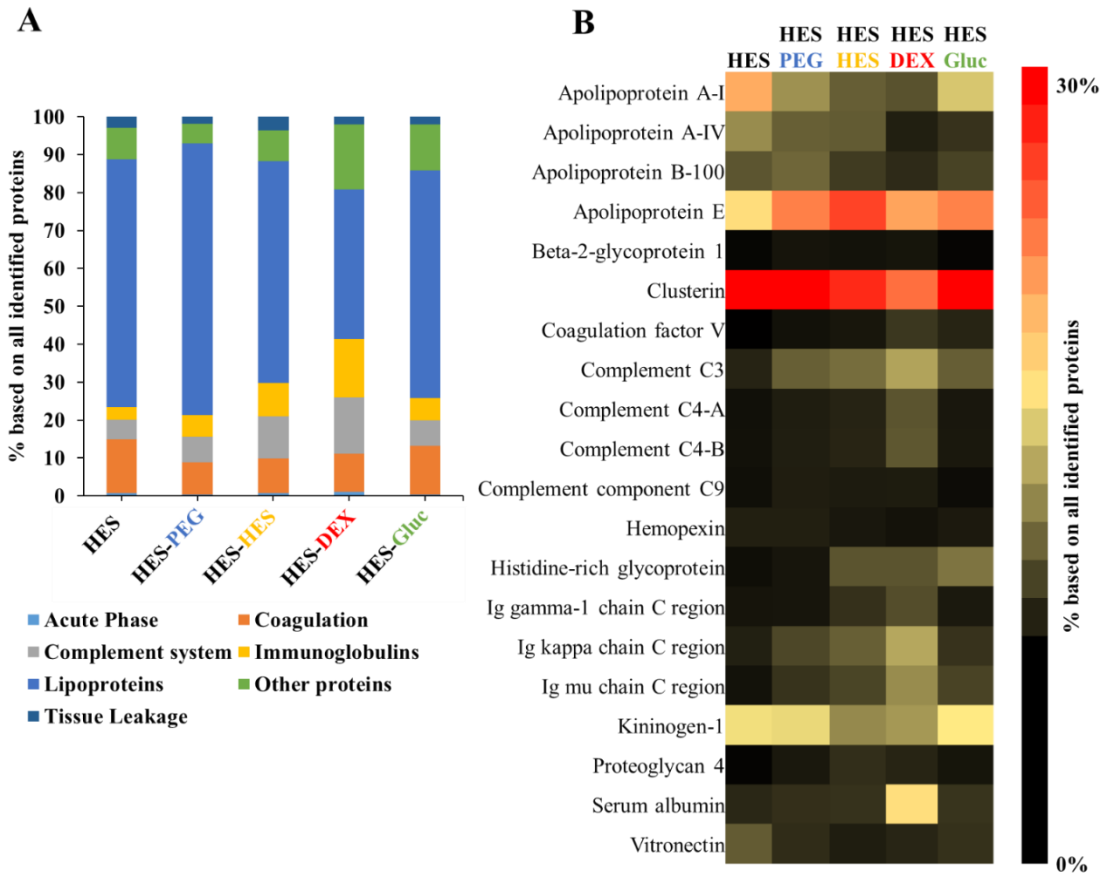


**Figure 6. 3.** Proteomic analysis of the protein corona of all HES nanocarriers. **(A)** Proteins were classified according to their biological function. **(B)** Heat map of the 20 most abundant corona proteins. The average amount (n=3) of each protein (fmol) was determined. Values are presented in % based on all identified proteins.

The protein-loaded nanocarriers were isolated by repetitive centrifugation and the remaining - so-called hard protein corona - was analyzed with respect to protein amount and type by SDS-PAGE and Pierce Assay (Figure 6.2). HES nanocarriers have been reported to exhibit an overall low protein adsorption, resulting in reasonable stealth properties.[6] However, the carbohydrate-functionalized HES nanocarriers (HES, DEX or Glucose) proved an even lower protein adsorption, which was comparable to PEGylated nanocarriers, rendering the carbohydrate functionalization an attractive pathway to increase the stealth properties of nanocarriers in general (Figure 6.2). Additionally, the protein pattern of the carbohydrate-modified nanocarriers visualized by SDS PAGE was similar to PEGylated nanocarriers, with only minor differences (Figure 6.2).

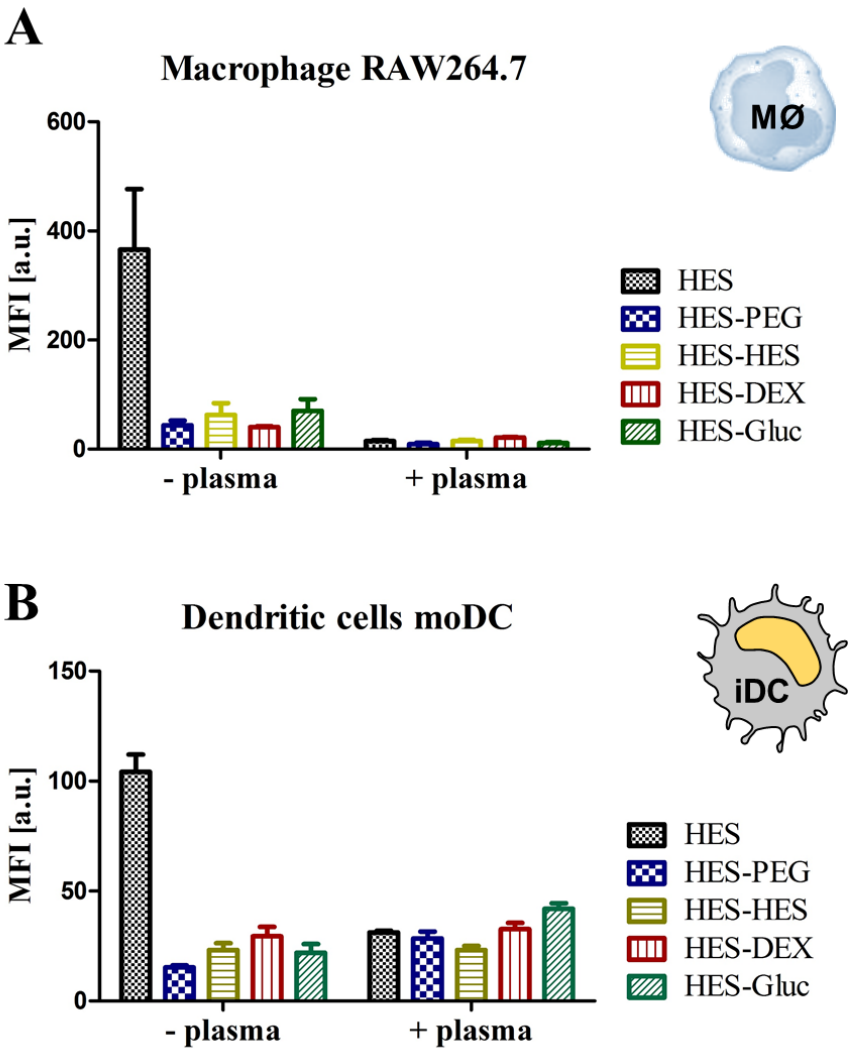


**Figure 6. 4.** Cellular interactions of HES nanocarriers with macrophage (RAW264.7) **A)** and monocyte derived dendritic cells (moDC, **B)** Nanocarriers were either incubated with human plasma (1 h, 37 °C) or directly added to cell culture medium without additional proteins. Values are expressed as median fluorescence intensity (MFI) and given as average of three independent measurements (n=3).

The quantitative analysis of the adsorbed blood proteins on the nanocarriers surface with liquid chromatography-coupled to mass spectrometry (LC-MS) proved the dominance of lipoproteins in the corona (40 – 70%, Figure 6.3). Especially clusterin (apolipoprotein J) was identified as the most abundant corona protein (> 30%). This is in line with previous reports, which highlighted the specific interaction of clusterin with stealth nanocarriers.[7, 29] Additionally, lower amounts of coagulation proteins (especially fibrinogen) and apolipoprotein A-I adsorbed to PEGylated and carbohydrate-modified nanocarriers compared to unfunctionalized nanocarriers (Figure 6.3). Taking this together, this demonstrates the specific interaction of plasma proteins and stealth nanocarriers.

Stealth nanocarriers have the major ability to evade interactions with immune cells.[30] Therefore, we investigated the cellular uptake towards macrophages and primary dendritic cells (moDCs). Nanocarriers were either directly introduced to cells or coated with plasma proteins before cell uptake studies (Figure 6.4). We found that the cellular interactions are comparable for both cell types. Most prominent, the unfunctionalized nanocarriers (HES) are taken up in the absence of additional proteins. PEGylated or sugar modified carriers display a low internalization rate. However, after plasma coating all nanocarriers exhibit a strongly reduced cellular uptake, caused by the selective protein adsorption from the blood plasma (e.g. clusterin).[7] Overall, this underlines the distinct role of corona proteins that mediate the stealth properties of nanocarriers. Further, these results indicate that the modification of nanocarriers with bio-based carbohydrate derivatives is a feasible alternative to PEGylation in order to produce fully biodegradable drug delivery systems.

## Conclusion

In conclusion, fully carbohydrate-based nanocarriers have been prepared by a combination of miniemulsion polymerization and surface modifications. HES nanocarriers were modified with different carbohydrates by copper-free click reaction, which proved to exhibit comparable stealth properties to the established PEG-modified nanocarriers. The use of bio-based and fully biodegradable alternatives for synthetic and non-degradable PEG offers a way to overcome accumulation of synthetic materials or immune responses against foreign polymers. Thus, these fully carbohydrate-based nanocarriers have the potential as alternative to synthetic drug delivery vehicles.

## Supplementary information

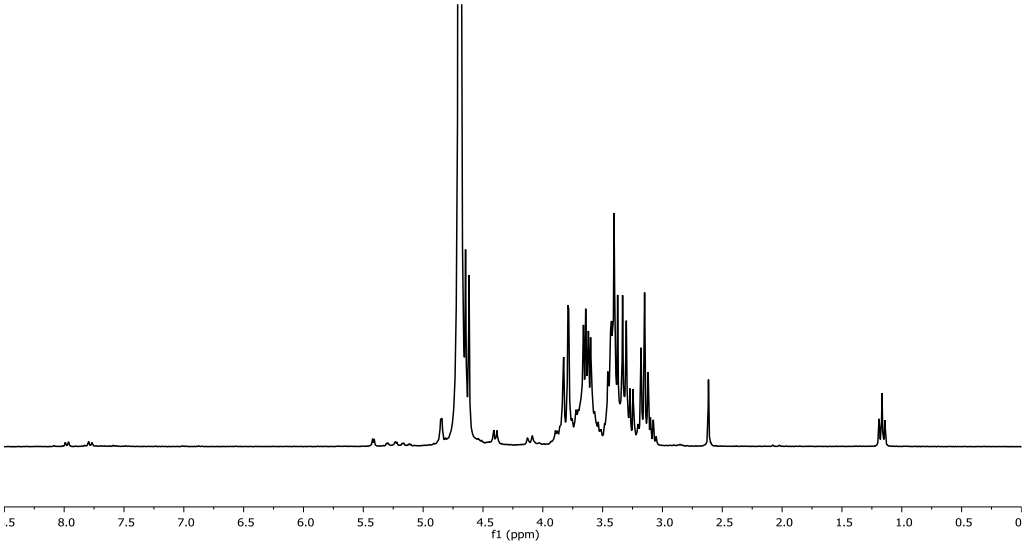


**Figure 6. 5.** $^{1}H$ NMR spectrum (300 MHz, $D_2O$) of β-glucose azide. (performed by Sarah Christmann)

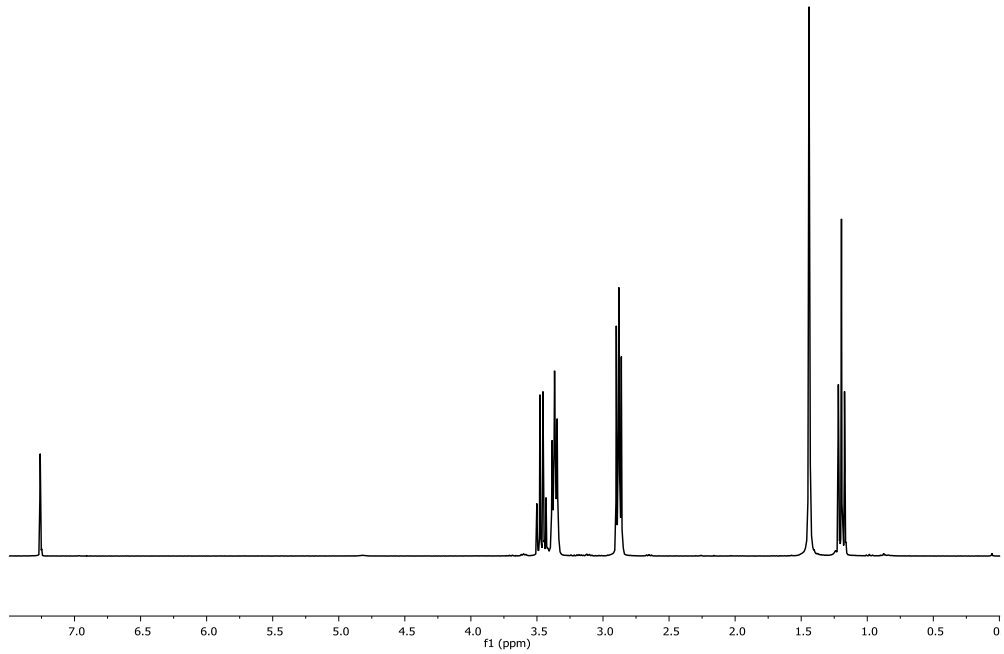


**Figure 6. 6.** $^{1}H$ NMR spectrum (300 MHz, $CDCl_3$) of 2-azido-1-ethylamine including diethyl ether. (performed by Sarah Christmann)

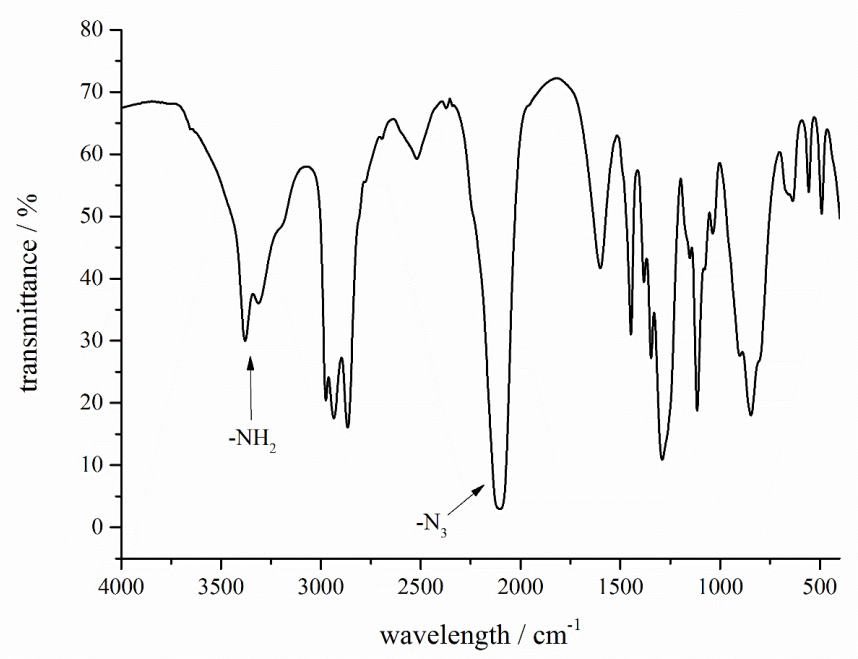


**Figure 6. 7.** FT-IR spectrum of 2-azido-1-ethylamine. (performed by Sarah Christmann)

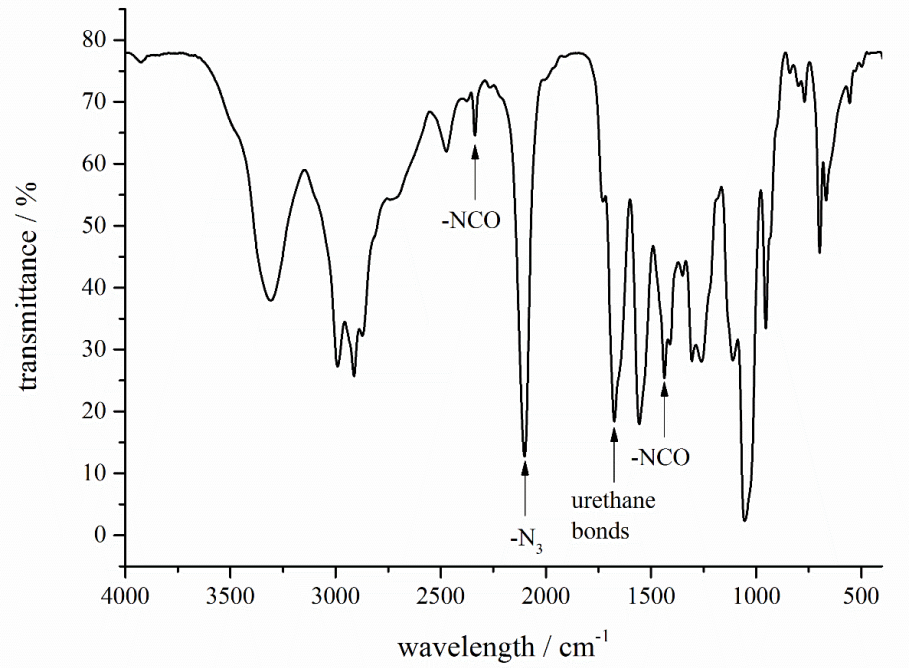


**Figure 6. 8.** FT-IR spectrum of 1-(2-azidoethyl)-3-(2-(2-(2-isocyanatoethoxy)ethoxy)-ethyl)urea.

# Literature


1. Mahmoudi, M.; Serpooshan, V., Large Protein Absorptions from Small Changes on the Surface of Nanoparticles. *The Journal of Physical Chemistry C* **2011,** *115* (37), 18275-18283.

2. Yang, S. T.; Liu, Y.; Wang, Y. W.; Cao, A., Biosafety and bioapplication of nanomaterials by designing protein-nanoparticle interactions. *Small* **2013,** *9* (9-10), 1635-53.

3. Lundqvist, M.; Stigler, J.; Elia, G.; Lynch, I.; Cedervall, T.; Dawson, K. A., Nanoparticle size and surface properties determine the protein corona with possible implications for biological impacts. *Proc Natl Acad Sci U S A* **2008,** *105* (38), 14265-70.

4. Schrade, A.; Mailander, V.; Ritz, S.; Landfester, K.; Ziener, U., Surface roughness and charge influence the uptake of nanoparticles: fluorescently labeled pickering-type versus surfactant-stabilized nanoparticles. *Macromol Biosci* **2012,** *12* (11), 1459-71.

5. Tenzer, S.; Docter, D.; Rosfa, S.; Wlodarski, A.; Kuharev, J.; Rekik, A.; Knauer, S. K.; Bantz, C.; Nawroth, T.; Bier, C.; Sirirattanapan, J.; Mann, W.; Treuel, L.; Zellner, R.; Maskos, M.; Schild, H.; Stauber, R. H., Nanoparticle Size Is a Critical Physicochemical Determinant of the Human Blood Plasma Corona: A Comprehensive Quantitative Proteomic Analysis. *ACS Nano* **2011,** *5* (9), 7155-7167.

6. Kang, B.; Okwieka, P.; Schöttler, S.; Seifert, O.; Kontermann, R. E.; Pfizenmaier, K.; Musyanovych, A.; Meyer, R.; Diken, M.; Sahin, U., Tailoring the stealth properties of biocompatible polysaccharide nanocontainers. *Biomaterials* **2015,** *49*, 125-134.

7. Schöttler, S.; Becker, G.; Winzen, S.; Steinbach, T.; Mohr, K.; Landfester, K.; Mailander, V.; Wurm, F. R., Protein adsorption is required for stealth effect of poly(ethylene glycol)- and poly(phosphoester)-coated nanocarriers. *Nature Nanotech.* **2016**.

8. Wald, S.; Simon, J.; Dietz, J. P.; Wurm, F. R.; Landfester, K., Polyglycerol Surfmers and Surfactants for Direct and Inverse Miniemulsion. *Macromol Biosci* **2017**.

9. Amoozgar, Z.; Yeo, Y., Recent advances in stealth coating of nanoparticle drug delivery systems. *Wiley Interdiscip Rev Nanomed Nanobiotechnol* **2012,** *4* (2), 219-33.

10. Pushpamalar, J.; Veeramachineni, A. K.; Owh, C.; Loh, X. J., Biodegradable Polysaccharides for Controlled Drug Delivery. *ChemPlusChem* **2016,** *81* (6), 504-514.

11. Baier, G.; Baumann, D.; Siebert, J. M.; Musyanovych, A.; Mailänder, V.; Landfester, K., Suppressing unspecific cell uptake for targeted delivery using hydroxyethyl starch nanocapsules. *Biomacromolecules* **2012,** *13* (9), 2704-2715.

12. Bosker, W. T. E.; Patzsch, K.; Stuart, M. A. C.; Norde, W., Sweet brushes and dirty proteins. *Soft Matter* **2007,** *3* (6), 754-762.

13. Kolb, H. C.; Finn, M. G.; Sharpless, K. B., Click Chemistry : Diverse Chemical Function from a Few Good Reactions. *Angew. Chem. Int. Ed.* **2001,** *40*, 2004-2021.

14. Huisgen, R., 1,3-Dipolar Cycloadditions *Proc. Chem. Soc* **1961**, 357-369.

15. Lutz, J. F., Copper-free azide-alkyne cycloadditions: new insights and perspectives. *Angew Chem Int Ed Engl* **2008,** *47* (12), 2182-4.

16. Baier, G.; Baumann, D.; Siebert, J. M.; Musyanovych, A.; Mailander, V.; Landfester, K., Suppressing Unspecific Cell Uptake for Targeted Delivery Using Hydroxyethyl Starch Nanocapsules. *Biomacromolecules* **2012,** *13* (9), 2704-2715.

17. Baier, G.; Musyanovych, A.; Dass, M.; Theisinger, S.; Landfester, K., Cross-Linked Starch Capsules Containing dsDNA Prepared in Inverse Miniemulsion as "Nanoreactors" for Polymerase Chain Reaction. *Biomacromolecules* **2010,** *11* (4), 960-968.

18. Freichels, H.; Wagner, M.; Okwieka, P.; Meyer, R. G.; Mailander, V.; Landfester, K.; Musyanovych, A., (Oligo)mannose functionalized hydroxyethyl starch nanocapsules: en route to drug delivery systems with targeting properties. *J Mater Chem B* **2013,** *1* (34), 4338-4348.

19. Landfester, K.; Musyanovych, A.; Mailander, V., From Polymeric Particles to Multifunctional Nanocapsules for Biomedical Applications Using the Miniemulsion Process. *J Polym Sci Pol Chem* **2010,** *48* (3), 493-515.

20. Vinson, N.; Gou, Y. Z.; Becer, C. R.; Haddleton, D. M.; Gibson, M. I., Optimised 'click' synthesis of glycopolymers with mono/di- and trisaccharides. *Polym Chem-Uk* **2011,** *2* (1), 107-113.

21. Tanaka, T.; Nagai, H.; Noguchi, M.; Kobayashi, A.; Shoda, S., One-step conversion of unprotected sugars to beta-glycosyl azides using 2-chloroimidazolinium salt in aqueous solution. *Chem Commun* **2009,** (23), 3378-3379.

22. Becer, C. R.; Hoogenboom, R.; Schubert, U. S., Click Chemistry beyond Metal-Catalyzed Cycloaddition. *Angew Chem Int Edit* **2009,** *48* (27), 4900-4908.

23. Ning, X.; Guo, J.; Wolfert, M. A.; Boons, G.-J., Visualizing metabolically labeled glycoconjugates of living cells by copper-free and fast huisgen cycloadditions. *Angew Chem Int Ed* **2008,** *47* (12), 2253-2255.

24. Baier, G.; Siebert, J. M.; Landfester, K.; Musyanovych, A., Surface Click Reactions on Polymeric Nanocapsules for Versatile Functionalization. *Macromolecules* **2012,** *45* (8), 3419-3427.

25. Kang, B.; Opatz, T.; Landfester, K.; Wurm, F. R., Carbohydrate nanocarriers in biomedical applications: functionalization and construction. *Chemical Society Reviews* **2015,** *44* (22), 8301-8325.

26. Tenzer, S.; Docter, D.; Kuharev, J.; Musyanovych, A.; Fetz, V.; Hecht, R.; Schlenk, F.; Fischer, D.; Kiouptsi, K.; Reinhardt, C., Rapid formation of plasma protein corona critically affects nanoparticle pathophysiology. *Nature nanotechnology* **2013,** *8* (10), 772-781.

27. Cedervall, T.; Lynch, I.; Lindman, S.; Berggard, T.; Thulin, E.; Nilsson, H.; Dawson, K. A.; Linse, S., Understanding the nanoparticle-protein corona using methods to quantify exchange rates and affinities of proteins for nanoparticles. *Proc Natl Acad Sci U S A* **2007,** *104* (7), 2050-5.

28. Kokkinopoulou, M.; Simon, J.; Landfester, K.; Mailänder, V.; Lieberwirth, I., Visualization of the Protein Corona: towards a biomolecular understanding of nanoparticle-cell-interactions. *Nanoscale* **2017**.

29. Müller, J.; Bauer, K. N.; Prozeller, D.; Simon, J.; Mailänder, V.; Wurm, F. R.; Winzen, S.; Landfester, K., Coating nanoparticles with tunable surfactants facilitates control over the protein corona. *Biomaterials* **2017,** *115*, 1-8.

30. Owens, D. E.; Peppas, N. A., Opsonization, biodistribution, and pharmacokinetics of polymeric nanoparticles. *International journal of pharmaceutics* **2006,** *307* (1), 93-102.

31. Schlaad, H.; Kukula, H.; Rudloff, J.; Below, I., Synthesis of alpha,omega-heterobifunctional poly(ethylene glycol)s by metal-free anionic ring-opening polymerization. *Macromolecules* **2001,** *34* (13), 4302-4304.

32. Schöttler, S.; Klein, K.; Landfester, K.; Mailänder, V., Protein source and choice of anticoagulant decisively affect nanoparticle protein corona and cellular uptake. *Nanoscale* **2016,** *8*, 5526-5536.

33. Ritz, S.; Schöttler, S.; Kotman, N.; Baier, G.; Musyanovych, A.; Kuharev, J. r.; Landfester, K.; Schild, H. r.; Jahn, O.; Tenzer, S.; Mailander, V., Protein Corona of Nanoparticles: Distinct Proteins Regulate the Cellular Uptake. *Biomacromolecules* **2015,** *16* (4), 1311-1321.

34. Bradshaw, R. A.; Burlingame, A. L.; Carr, S.; Aebersold, R., Reporting Protein Identification Data. *Mol Cell Proteomics* **2006,** *5*, 787-788.

35. Silva, J. C.; Gorenstein, M. V.; Li, G.-Z.; Vissers, J. P. C.; Geromanos, S. J., Absolute Quantification of Proteins by LCMS. *Mol Cell Proteomics* **2006,** *5*, 144-156.

# *7.* Exploiting the biomolecular corona: Pre-coating of nanoparticles enables controlled cellular interactions

## Aim:

Protein adsorption onto the nanoparticles´ surface is an inevitable process. Therefore, this study presents an alternative approach, which aimed to exploit protein corona formation to control cellular uptake. Immunoglobulins are proteins, which enhance unspecific cellular uptake of nanoparticles by phagocytic (Fc receptor expressing) cells. To avoid this unspecific cell interaction, immunoglobulins were removed from blood plasma. This protein mixture was further used to decorate the nanoparticles´ surface with an artificial protein corona coating. It was shown that the cellular interactions towards phagocytic cells were strongly reduced if nanoparticles were pre-coated. This highlights that protein corona formation can be exploited to obtain targeted cell interactions.

## Contribution:

I carried out the complete protein corona analysis (SDS-PAGE, LC-MS, Pierce Assay) and conducted the cellular uptake experiments (flow cytometry, cLSM). [redacted] performed the DLS analysis. [redacted] analyzed the protein corona by TEM. [redacted] conducted the ITC measurements. The project was supervised by [redacted]

## Abstract

Formation of the biomolecular corona ultimately determines the successful application of nanoparticles *in vivo*. Adsorption of biomolecules such as proteins is an inevitable process that takes place instantaneously upon contact with physiological fluid (e.g. blood). Therefore, strategies are needed to control this process in order to improve the properties of the nanoparticles and to allow targeted drug delivery. Here, we show that the design of the protein corona by a pre-formed protein corona with tailored properties enables controlled cellular interactions. Nanoparticles were pre-coated with immunoglobulin depleted plasma to create and design a protein corona that inhibits cellular uptake by immune cells. It was proven that a pre-formed protein corona remains stable even after nanoparticles were re-introduced to plasma. This opens up the great potential to exploit designed protein corona formation, which will significantly influence the development of novel nanomaterials.


## Introduction

Nanoparticle (NP) based drug delivery systems hold great promise as they offer the possibility for targeted cell interactions[1]. This eventually improves the drug bioavailability[2], minimizes toxic side effects[3] and reduces the drug dose[4]. Despite the recent progress in the development of novel nanoparticles, the majority of those systems show a low targeting efficiency *in vivo*[5].

Rapid recognition of nanoparticles by immune cells causes their fast clearance from the blood stream and therefore prevents interactions with targeted cells[6-7]. This process is mainly governed by the adsorption of blood proteins towards the nanoparticle surfaces. The adsorption happens immediately when nanoparticles enter the blood stream and has been termed ´biomolecular or protein corona formation´[8-10]. Specific proteins such as immunoglobulins[11] and complement proteins[12] are known to mediate interaction with phagocytic cells and hereby influence the clearance process (´opsonization´)[13-14].

To overcome this issue several approaches have been developed in order to mask the nanoparticles from phagocytic cells[15]. Coating the nanoparticle surface with hydrophilic polymers e.g. poly(ethylene glycol) (PEG) is the common strategy to prolong the blood circulation (´stealth effect´) and hereby enabling the nanoparticle to reach the desired target[16]. This effect has been widely described to be a result of reduced protein interactions with PEGylated surfaces[17]. However, several reports could prove that PEGylation can not completely abolish protein adsorption[18] and we were able to identify key proteins, which mediate the stealth effect[19-20]. On top of this, Hamad and colleagues[21] could show that PEG can even trigger the activation of the complement system.

Therefore, alternative strategies are needed to improve the properties of targeted nanoparticles *in vivo*[22]. Various studies have investigated the effect of corona formation on nanoparticle targeting[23]. It was found that nanoparticles can recruit specific proteins from plasma which eventually promote interactions with targeted cells[24]. Adsorption of apolipoproteins to polysorbate 80-coated nanoparticles was shown to enhance the transport of nanoparticles across the blood-brain barrier[25]. Additionally, Caracciolo *et al.* demonstrated that the adsorption of vitronectin can enhance cellular interactions with cancer cells[26]. Further, we already showed that due to a pre-formed protein corona nanoparticle aggregation in blood plasma is prevented[27]. This highlights the great potential to exploit corona formation.

In order to promote the field, we aimed to create a pre-formed protein corona, which enables controlled cellular interactions. Here, it was intended to engineer nanoparticles with stealth properties mediated only through corona proteins. Immunoglobulins (IgG) are one major class of proteins (´opsonins´), which are known to enhance cellular uptake by macrophages via interactions with the Fc receptor[28]. Therefore, we removed IgG from human plasma via affinity chromatography. This protein fraction (´IgG depleted plasma´) was chosen as a model protein coating in order to create a pre-formed protein corona, which prevents interactions with macrophages. To explore the stealth properties of the pre-formed protein, we analyzed the cellular interactions of uncoated and pre-coated nanoparticles with a macrophage cell line (RAW264.7). Next, the major aspect of our work focused on the question whether the pre-adsorbed corona proteins are exchanged or covered by other proteins over time when pre-coated nanoparticles are re-exposed to human plasma. This question needs to be addressed in order to reveal if nanoparticle pre-coating is an effective strategy to enable controlled cellular interactions *in vivo*. To answer this question, we carried out a detailed proteomic analysis (LC-MS). Additionally, dynamic light scattering (DLS) and isothermal titration (ITC) experiments were used to study the direct interaction of uncoated and pre-coated nanoparticles with plasma proteins.

Combining these we were able to demonstrate that a pre-formed protein corona remains stable, which further implies that pre-coating of nanoparticles is a feasible method to engineer the protein corona and to obtain tailored protein corona properties for targeted cell interactions.

## Material and methods

**Nanoparticle Synthesis.** Polystyrene nanoparticle stabilized with the non-ionic surfactant Lutensol AT50 (BASF, Ludwigshafen) were synthesized as previously reported[29, 36]. The fluorescent dye Bodipy[37] was in-cooperated for cellular uptake studies.

Briefly, nanoparticles were synthesized via free-radical copolymerization miniemulsion technique. For amino-functionalized nanoparticles 2-aminoethyl methacrylate hydrochloride (AEMH, 90%, Sigma-Aldrich) was used whereas for carboxy-functionalized nanoparticles acrylic acid AA (99%, Aldrich) was chosen.

**Dynamic Light Scattering (DLS).** Multi-angle dynamic light scattering experiments were performed with an ALV-CGS 8F SLS/DLS 5022F goniometer equipped with eight simultaneously working correlators, eight photodiode detectors and a HeNe laser (632.8 nm, 25 mW output power). Experiments were performed at 37 °C. Nanoparticle dispersions (1 µL, 10 mg/mL) were measured in 1 mL of filtered cell culture medium. Data was analyzed according to the method from Rausch *et al.*[33-34].

**ζ potential.** The zeta (ζ) potential of the different polystyrene nanoparticle (10 µL, 10 mg/mL) was measured in a 1 mM potassium chloride solution (1 mL) with a Zeta Sizer Nano Series (Malvern Instrument). Nanoparticle coated with proteins were prepared as described in the section protein corona preparation (below) before ζ potential measurements.

**Transmission Electron Microscopy (TEM).** To visualize the protein corona, nanoparticles were diluted with 1 mL water and further placed onto a lacey grid. Samples were stained with 4% uranyl acetate according to the method from Kokkinopoulou *et al.*[29, 38]. Images were taken with a Ultrascan 1000 (Gatan) charge-coupled device (CCD) camera.

**Human blood plasma.** Human plasma was obtained from the Department of Transfusion Medicine Mainz from healthy donors in accordance with the Declaration of Helsinki and stored at -80 °C. Before usage, human plasma was centrifuged at 20 000 g (30 min) to remove protein aggregates.

**Plasma fractionation.** Immunoglobulins (IgG) were removed from human plasma according to our previous established method[27]. A modified HPLC system was operated with a ToyoScreen AF-rProtein A HC-650F column (Tosoh Bioscoience) using 0.01 M Tris*HCl as running buffer. Human plasma was diluted 1:3 with running buffer, filtered and applied to the HPLC system. Bound IgG was recovered from the column using 0.2 M citric acid.

**Pre-coating with IgG depleted plasma.** Nanoparticles were incubated with IgG depleted plasma in a defined ratio between surface area and protein concentration. 0.05 $m^2$ nanoparticles were incubated with 5 mg of IgG depleted plasma for 1 h, 37 °C to allow corona formation. Further unbound proteins were removed via centrifugation.

**Protein corona preparation.** Nanoparticles (0.05 $m^2$) were incubated with human plasma (1 mL) for 1 h, 37 °C under constant agitation (300 rpm)[39]. To isolate the hard corona, nanoparticles were centrifuged (20 000 g, 1 h, 4 °C) and redispered in 1 mL of PBS. This

procedure was repeated 3 times as we have shown before that there are no unbound proteins in the supernatant[29]. The nanoparticle protein pellet was resuspended with 2% SDS + 62.5 mM Tris*HCL, incubated at 95 °C for 5 min and centrifuged again (20 000 g, 1 h, 4 °C). The supernatant contained desorbed corona proteins, which were further analyzed by SDS-PAGE, Pierce Assay and LC-MS.

**SDS-PAGE.** Hard corona proteins were separated using 10% Bis-Tris-Protein Gels and NuPAGE MES and SDS Running Buffer. Proteins (8 µg in 26 µL) were mixed with NuPage Reducing Agent (4 µL) and NuPage LDS Samples Buffer (10 µL). The gel was run for 1.5 h at 100 V with SeeBlue Plus2 Pre-Stained (Invitrogen) as molecular marker. Gels were stained with SimplyBlue SafeStain (Novex, Thermo Fisher Scientific) overnight and destained with water.

**Protein quantification.** The protein concentration was determined via Pierce 660 nm protein Assay (Thermo Scientific) according to manufacturer's instructions. Bovine serum albumin was used at standard and the absorption was measured at 660 nm with a Tecan infinite M1000 plate reader.

**LC-MS analysis.** Protein samples were prepared for proteomic analysis as described[19, 27, 40]. Briefly, proteins were precipitated using ProteoExtract protein precipitation kit (CalBioChem) according to the manufacturer's instructions. The resulting protein pellet was resuspended with RapiGest SF (Waters) in ammonium bicarbonate (50 mM). Samples were reduced (dithiothreitol, Sigma 5 mM, 45 min, 56 °C) and alkylated (idoacetoamide, Sigma15 mM, 1 h, dark). A protein:trypsin ratio of 50:1 was chosen for tryptic digestion (18 h, 37 °C). The reaction was quenched with 2 µL hydrochloric acid (Sigma).

Samples were spiked with 50 fmol/µL Hi3 Ecoli (Waters) for absolute protein quantification and diluted with 0.1% formic acid. Tryptic peptides were applied towards a nanoACQUITY UPLC system which was coupled with a Synapt G2- Si mass spectrometer. Electrospray ionization (ESI) was conducted in positive ion mode with a NanoLockSpray source. Measurements were performed in resolution mode and data-independent acquisition ($MS^E$) experiments were carried. Data was analyzed with MassLynx 4.1

For protein identification Progenesis GI (2.0) was used. Identified peptides were search against a reviewed human database downloaded from Uniprot. The analysis was carried out using the following criteria: one missed cleavage, max. protein mass 600 kDa, fixed modifications for cysteine and carbamidomethyl, variable oxidation for methionine and a false discovery rate of 4%. For peptide identification, three fragments need to be identified whereas protein identification requires five fragments and two peptides. The TOP3/Hi3[41] quantification approach was chosen to determine the amount of fmol for each protein.

**Cell culture.** RAW 264.7 cells were culture in Dulbecco´s modified eagle medium (DMEM) supplemented with 10 % FBS, 100 U/mL penicillin, 100 mg/mL streptomycin and 2 mM glutamine (all from Invitrogen).

**Flow cytometry and confocal laser scanning microscopy.** RAW 264.7 cells (150.000 cells/well) were seeded out in 24 well plates (1 mL) for flow cytometry analysis. For confocal images, cells were seeded out in µ-Dish 35 mm (ibidi) at a density of (100.000 cells/mL, 800 µL). After overnight incubation at 37 °C, cells were washed and cell culture medium without (-) or with human plasma (+) was added.

For nanoparticle uptake analysis, uncoated or pre-coated nanoparticles were applied to cells in medium without (-) or with plasma proteins (+) at a concentration of 75 µg/mL for 2 h. Afterwards, cells were washed with PBS and detached with 2.5 % trypsin from cell culture wells. Flow cytometry measurments were performed with a CyFlow ML cytometer (Partec, Germany). The fluorescent dye Bodipy was excited with a 488 nm laser. Data was analyzed with FCS Express V4 software (DeNovo Software, USA). Values are expressed as median fluorescence intensity (MFI) as mean of at least three independent experiments.

Confocal laser scanning microscopy (cLSM) images were taken o LSM SP5 STED Leica Laser Scanning Confocal Microscope (Leica, Germany). Nanoparticles were excited with an argon laser (488 nm) and are pseudocolored in green. The cell membrane was stained with CellMaskOrange (2.5 µg/mL, Invitrogen). The dye was excited with a laser DPSS 561 nm laser and the membrane was pseudocolored in red.

## Results and Discussion

As a model system, polystyrene nanoparticles (PS-NPs) stabilized with the PEG-based surfactant Lutensol AT50 were used in this study. Additionally, human plasma was depleted of immunoglobulins (IgG) as previously described[27]. IgG depleted plasma was isolated from human plasma via affinity chromatography using a Protein A column. The protein composition was determined by LC-MS and we were able to reduce the total amount of IgG from 28% down to 4%. Then, carboxy- and amino functionalized PS-NPs were incubated with IgG depleted plasma and characterized before and after incubation regarding size and ζ- potential (Table 7.1).

**Table 7. 1.** Physico-chemical properties of carboxy- and amino-functionalized polystyrene nanoparticles. NPs were pre-coated with IgG depleted plasma. The size refers to the newly formed NP-protein complex and was determined by multi-angle dynamic light scattering (DLS) and the ζ-Potential measured with a Malvern Zeta-sizer before and after protein coating. [redacted]

| | **PS-COOH** | | **PS-$NH_2$** | |
|---|---|---|---|---|
| **Protein Coating** | uncoated | coated | uncoated | coated |
| **Diameter** | 130 ± 13 nm | 164 ± 16 nm | 150 ± 15 nm | 162 ± 16 nm |
| **ζ – Potential** | -27 ± 8 mV | -17 ± 9 mV | +4 ± 1 mV | -29 ± 6 mV |

Dynamic light scattering experiments (DLS) indicate a minor size increase (~20 nm) after protein coating, which is attributed to protein corona formation[27, 29]. Additional transmission electron microscopy images (TEM) confirmed the protein layer surrounding the nanoparticles as found in previous reports[29] (Figure 7.1). To characterize the biological identity of nanoparticles after protein coating, the exact protein corona composition was identified by LC-MS (Figure 7.1).

Therefore, nanoparticles were incubated with IgG depleted plasma to allow corona formation, and afterwards centrifuged and washed (see material/methods supplementary 7)[9]. As shown before, the surface functionalization of the nanoparticles strongly influences the protein adsorption pattern[30-31]. Coated carboxy-functionalized nanoparticles (PS-COOH) were surrounded by a protein layer, which was strongly enriched by fibrinogen (~74%). In contrast, hemopexin (~38%) and clusterin (~20%) were the major hard corona proteins for coated amino-functionalized nanoparticles (PS-$NH_2$).

IgG depleted plasma was chosen as protein coating as it was intended to reduce the interaction of pre-coated nanoparticle with phagocytic cells in order to obtain stealth properties (Figure 7.2). Therefore, cellular uptake towards macrophages (RAW264.7) of uncoated and pre-coated nanoparticles was analyzed via flow cytometry and confocal laser scanning microscopy (Figure 7.2).

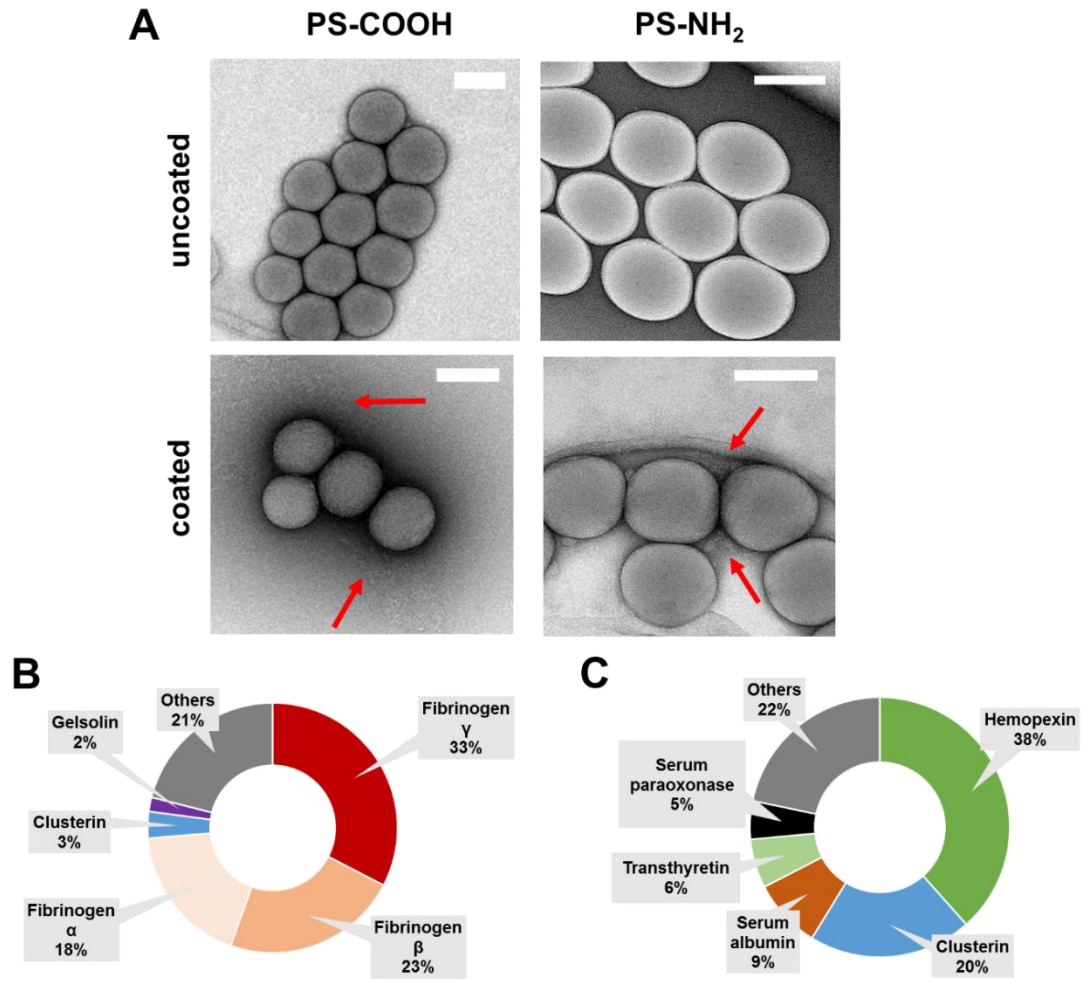


**Figure 7. 1.** Biological identity of PS-COOH and PS-$NH_2$ NPs. **A)** Representative TEM images of PS-NPs (PS-COOH and PS-$NH_2$) before (uncoated) and after (coated) pre-incubation with IgG depleted plasma. Red arrows highlight the lose protein corona network surrounding nanoparticles. Scale bar: 100 nm. LC-MS analysis of the protein composition after incubation with IgG depleted plasma. TOP 5 most abundant corona proteins are shown (**B** = PS-COOH and **C** = PS-$NH_2$). [redacted] Kokkinopoulou).

To present the principal mechanism, we first summarized a detailed analysis for PS-COOH nanoparticles (Figure 7.2 and 7.3). In the following section, we additionally focused on the investigations for PS-$NH_2$ nanoparticles (Figure 7.4).

Carboxy-functionalized nanoparticles were coated with IgG depleted plasma and applied to cell culture medium *without* additional proteins (marked as -plasma) or supplemented *with* plasma proteins (marked +plasma). This allowed to study the influence of the pre-coating on the cellular uptake of nanoparticles and to investigate if the preformed protein corona (coating

with IgG depleted plasma) is exchanged or remains stable after re-incubation with whole plasma (Figure 7.2).

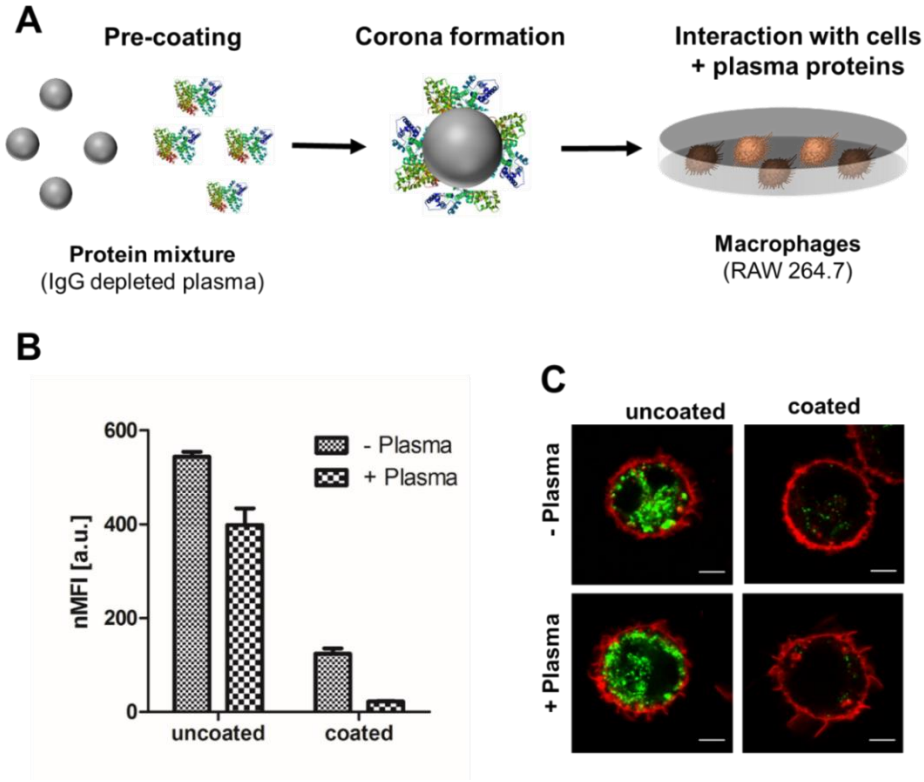


**Figure 7. 2**. **A)** Schematic overview: Exploiting protein corona formation. NPs are pre-coated with IgG depleted plasma to create an artificial protein corona, which prevents interactions with phagocytic cells. Macrophages (RAW264.7) were incubated with coated or pre-coated PS-COOH NPs (75 µg/mL) for 2 h at 37 °C. Cell uptake was analyzed by flow cytometry **(B)** and confocal laser scanning microscopy **(C).** Cells were kept in cell culture medium with (+) or without plasma proteins (-). Scale bar: 5 µm.

Flow cytometry analysis (Figure 7.2) and confocal laser scanning microscopy images clearly indicated the rapid uptake of *uncoated* PS-COOH nanoparticles in all cases (with or without plasma). Hence, cellular interactions of PS-COOH NPs *pre-coated* with IgG depleted plasma were strongly decreased (Figure 7.2). Most importantly, even if pre-coated NPs were re-introduced to plasma, cellular uptake was still reduced. This highlights that the obtained stealth properties due to the pre-formed protein corona were preserved meaning that pre-coating allowed us to control cellular uptake.

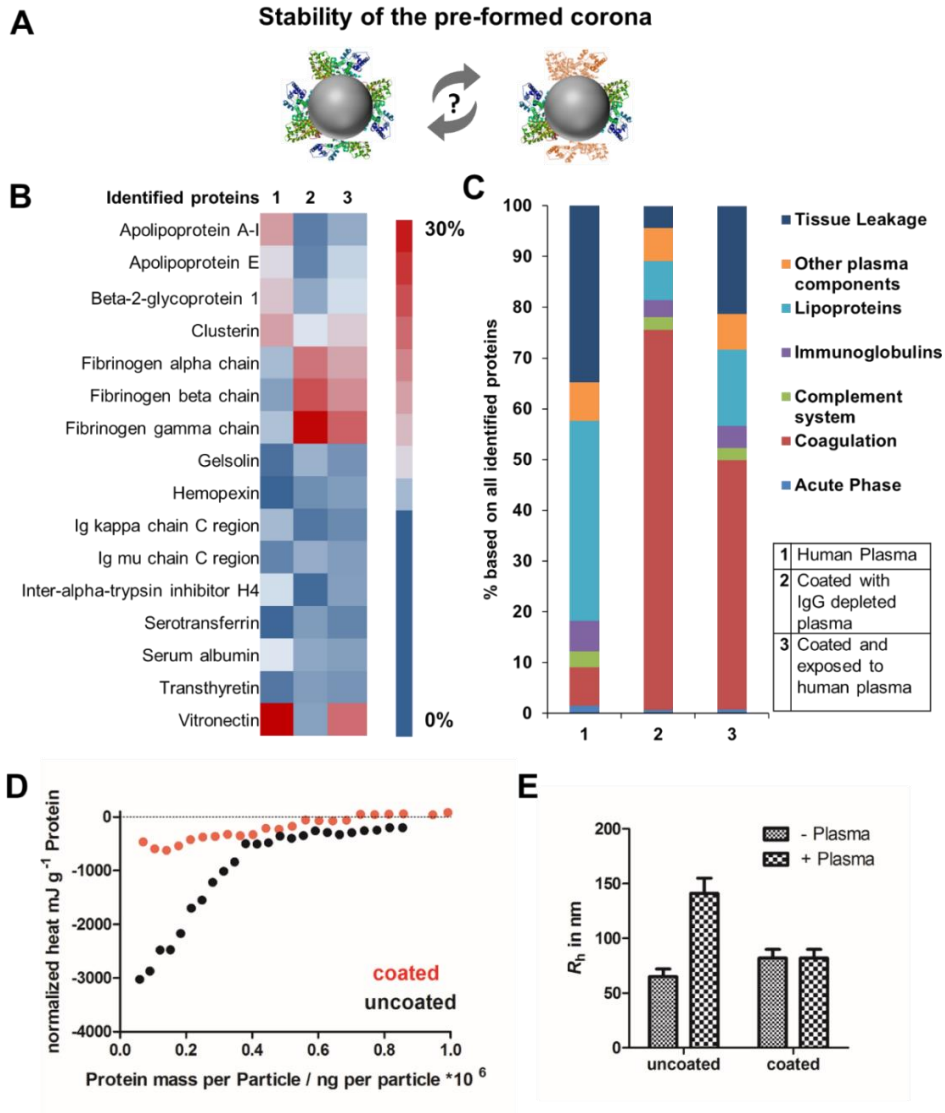


**Figure 7. 3. A)** Investigating the stability of a pre-formed protein corona. **B)** LC-MS analysis of the most abundant (amount > 1%) corona proteins after plasma incubation (1), pre-coating (2) or if pre-coated NPs were re-introduced to plasma (3). **C)** Protein classification of all identified proteins. **D)** ITC measurements. Titration of plasma to uncoated and pre-coated PS-COOH NPs. One representative measurement out of five replicates each is shown exemplarily. (performed by Svenja Morsbach) **E)** Multi-angle dynamic light scattering (DLS) analysis of uncoated and pre-coated PS-COOH NPs in human plasma. Hydrodynamic radii ($R_h$) is given in nm. [redacted]

Based on this, we now wanted to focus on the interaction between plasma proteins and uncoated or pre-coated nanoparticles once they were introduced to whole plasma. Here, it was questioned how pre-coating influences protein corona formation (Figure 7.3). The hard protein corona of uncoated as well as pre-coated nanoparticles formed after incubation in full plasma was isolated via repetitive centrifugation and analyzed by Pierce Assay, SDS PAGE and LC-

MS (Figure 7.3). We found that uncoated PS-COOH, which were incubated with full plasma, were surrounded by a protein corona, which was strongly enriched with vitronectin (~33%). In contrast to this, we did not identify vitronection as being highly abundant in the corona formed with IgG depleted plasma. Here, the hard corona of pre-coated nanoparticles was enriched with fibrinogen (Figure 7.3).

Next, we saw that there was no significant change in the protein adsorption pattern if pre-coated PS-COOH nanoparticles were re-introduced into whole plasma (Figure 7.3). This underlines the stability of the pre-formed protein corona (Figure 7.3). Hence, we noted minor differences in the corona composition. Re-adsorption of other plasma proteins (e.g. vitronectin) had occurred. Nevertheless, this did not affect cellular uptake decisively (Figure 7.2).

To further investigate the properties of the pre-formed corona, isothermal titration calorimetry experiments (ITC) were carried out (Figure 7.3 and raw data heat rates see supplementary 7). Plasma was titrated to uncoated and coated PS-COOH NPs. With ITC it is possible to study the binding or adsorption behavior of proteins towards nanoparticles *in situ*[9, 32]. We observed a strong binding of plasma proteins towards uncoated PS-COOH NPs (black circles). This interaction was diminished when NPs were pre-coated (red circles), which further highlights the stealth properties of the pre-formed protein corona. This is in accordance with the cellular uptake that was shown to be strongly reduced if nanoparticles were pre-coated (Figure 7.2).

As described in previous work, interactions of NPs with plasma proteins can cause aggregation of NPs hereby highly affecting their *in vivo* biodistribution[33]. With multi angle dynamic light scattering (DLS) it is possible to monitor the size of nanoparticles incubated with plasma[27, 34]. This method allows studying direct interactions of proteins and nanoparticles without applying any washing step. When uncoated PS-COOH nanoparticles were applied to plasma, an overall size increase of ~ 100 nm was measured indicating aggregation formation (Figure 7.3). In strong contrast to this, we did not observe any size increase for pre-coated PS-COOH nanoparticles after plasma incubation. This underlines that the pre-formed protein corona remains stable after re-exposure to plasma.

Overall, we were able to present here a set of different analytical methods that can be generally applied to investigate if a defined pre-coating can enable targeted cell interaction. For the here chosen model system using IgG depleted plasma we were able to prove that pre-coating offers the possibility to tailor the biological properties of the nanoparticles.

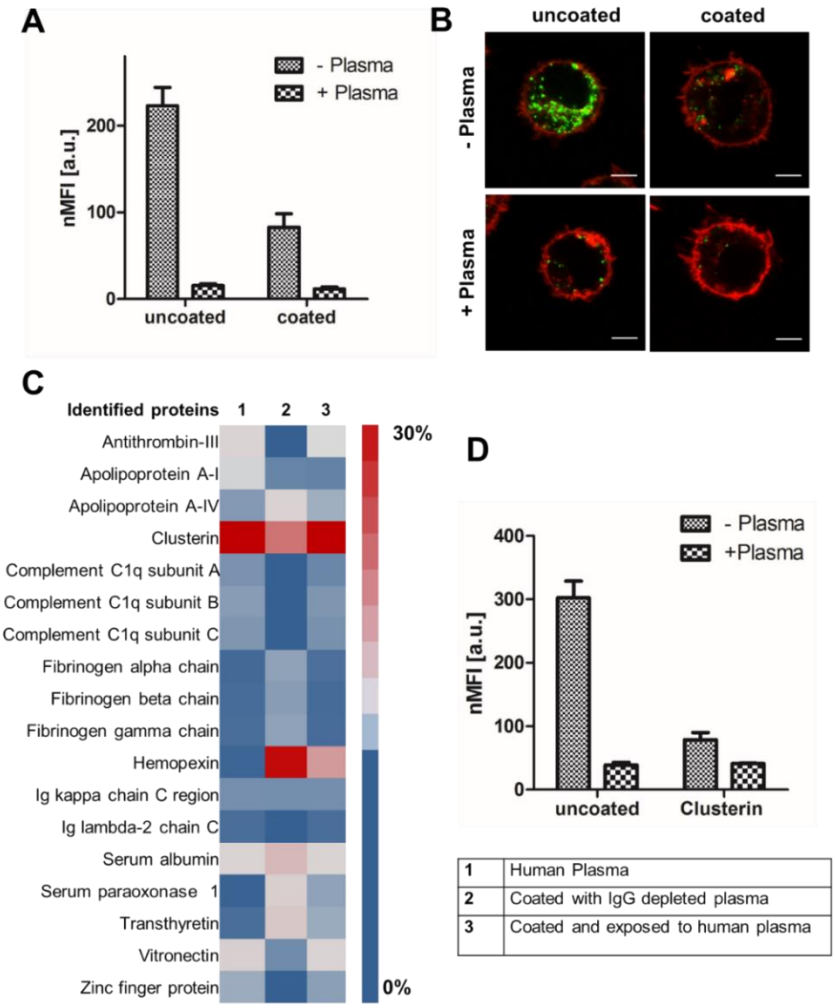


**Figure 7. 4. A) + B)** Cellular uptake of uncoated and pre-coated PS-$NH_2$ NPs towards macrophages (RAW 264.7) analyzed by flow cytometry and confocal laser scanning microscopy. Cells were kept in cell culture medium with (+) or without (-) plasma proteins. **C)** LC-MS analysis of the corona composition after plasma incubation (1), pre-coating (2) or if pre-coated NPs were re-introduced to plasma (3). **D)** Flow cytometry analysis of uncoated or clusterin coated PS-$NH_2$ NPs in the presence (+) or absence of human plasma (-).

As highlighted above (Figure 7.1) and intensively studied in literature the nanoparticle charge can significantly influence protein corona formation[30] and cellular uptake behavior[35]. Therefore, we additionally explored the influence of pre-coating with IgG depleted plasma for amino-functionalized nanoparticles (PS-$NH_2$) (Figure 7.4). First, cellular internalization of uncoated and pre-coated PS-$NH_2$ towards macrophages was studied followed by a detailed proteomic investigation of the hard protein corona.

For PS-$NH_2$ nanoparticles we found that only in the absence of proteins (-plasma) nanoparticles are highly internalized (Figure 7.4). If plasma proteins were present (+plasma),

cellular uptake was strongly reduced. Coated PS-$NH_2$ nanoparticles (with IgG depleted plasma) displayed a significantly lower internalization rate compared to uncoated PS-$NH_2$ in both cases (+with or -without plasma).

Analyzing the protein corona of uncoated PS-$NH_2$ indicates a strong enrichment of clusterin (~60%). Lower amounts of clusterin (~20%) were observed for nanoparticles incubated with IgG depleted plasma (Figure 7.4). Clusterin has been identified as major corona protein of PEGylated nanoparticles[16] and it was found that clusterin prevents interactions with macrophages[19]. The here presented PS nanoparticles are stabilized with the non-ionic surfactant Lutensol AT50, which has a PEG analog structure and therefore the interaction with clusterin is favored.

We were able to confirm that via pre-coating with clusterin cellular uptake of the here investigated PS-$NH_2$ is strongly decreased (Figure 7.4). However, it has to be noted that the uptake levels of PS-$NH_2$ after plasma incubation were even lower meaning that also other corona proteins, their orientation or even other biomolecules (e.g. sugar, lipids) may contribute to this effect. Overall, this demonstrates that PS-$NH_2$ nanoparticles are surrounded by a protein corona with *natural* stealth properties as due to plasma coating interactions with phagocytic cells are prevented.

## Conclusion

Here, we demonstrate that pre-coating of nanoparticles allows the defined design of the protein corona and offers the possibility to regulate cellular interaction. IgG depleted plasma was chosen as a coating system as it was intended to reduce the interaction of pre-coated nanoparticles with phagocytic cells. Overall, we were able to show that due to the pre-formed protein corona interactions with macrophages are inhibited. On top of that, it was confirmed that the obtained stealth properties are preserved even if pre-coated protein-corona engineered nanoparticles are re-introduced to plasma. This proves that directing corona formation is a feasible strategy to control cellular interactions.

## Supplementary information

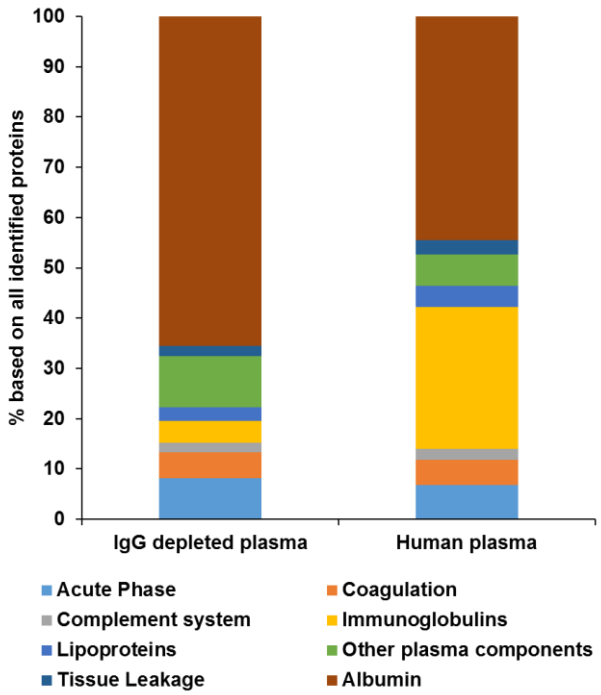


**Figure 7. 5.** LC-MS analysis of human plasma and IgG depleted plasma. Proteins were classified into 8 different classes according to their biological function. Values are given in % based on all identified proteins.

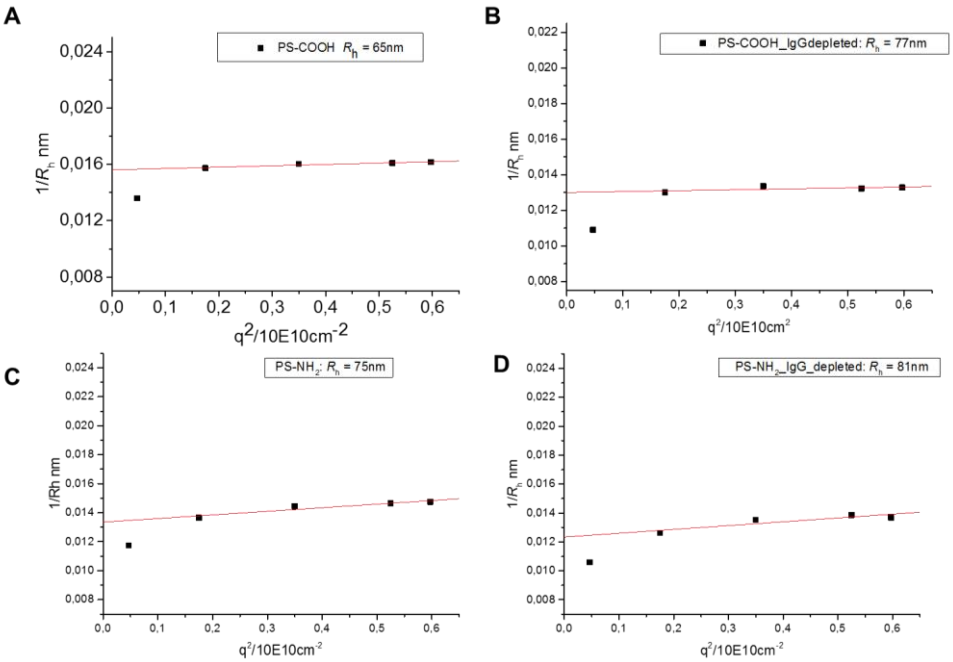


**Figure 7. 6.** Multi-angle dynamic light scattering (DLS) analysis. Angular dependency of the hydrodynamic radius $R_h$ for uncoated **(A, C)** and pre-coated **(B, D)** nanoparticles. PS-COOH are shown in (A, B) and PS-$NH_2$ in (C, D). [redacted]

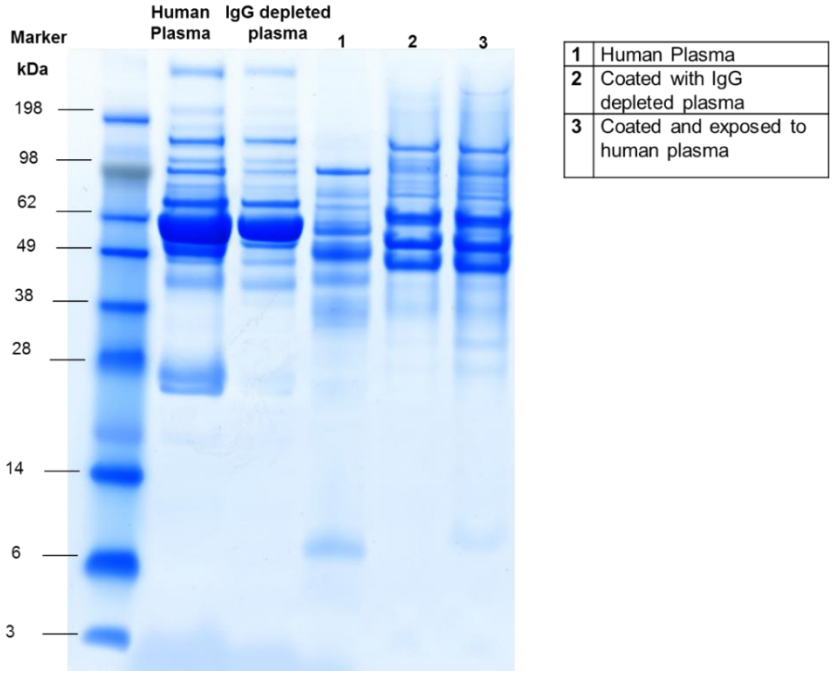


**Figure 7. 7.** SDS PAGE analysis of the hard corona pattern of PS-COOH nanoparticles. Human plasma and IgG depleted plasma serve as a reference. PS-COOH nanoparticles were incubated with human plasma (1), coated with IgG depleted plasma (2) or pre-coated and re-exposed to human plasma (3).

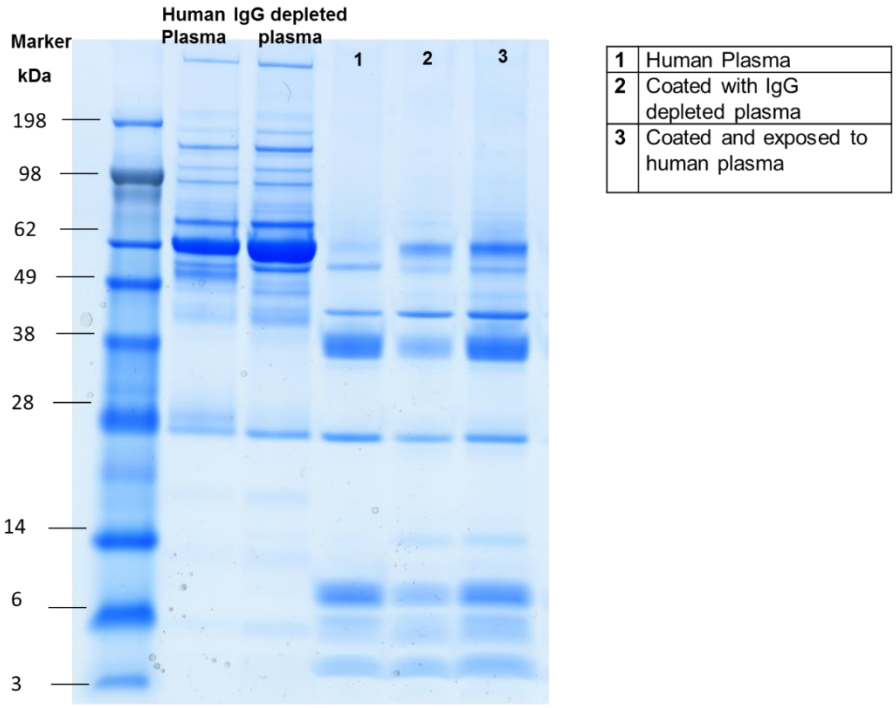


**Figure 7. 8.** SDS PAGE analysis of the hard corona pattern of PS-$NH_2$ nanoparticles. Nanoparticles were incubated with human plasma (1), coated with IgG depleted plasma (2) or pre-coated and re-exposed to human plasma (3). The hard corona was isolated as described in the material/methods part below.

**Table 7. 2**. Protein quantification via Pierce Assay of the hard protein corona. Values are given in mg per $m^2$ NP surface area ± s.d. of three independent experiments.

| **in mg/m²** | **Human Plasma** | **IgG depleted plasma** | **Coated and exposed to human plasma** |
|---|---|---|---|
| PS-COOH | 1.30 ± 0.13 | 3.10 ± 0.22 | 4.20 ± 0.47 |
| PS-NH2 | 0.96 ± 0.03 | 0.51 ± 0.08 | 1.06 ± 0.04 |

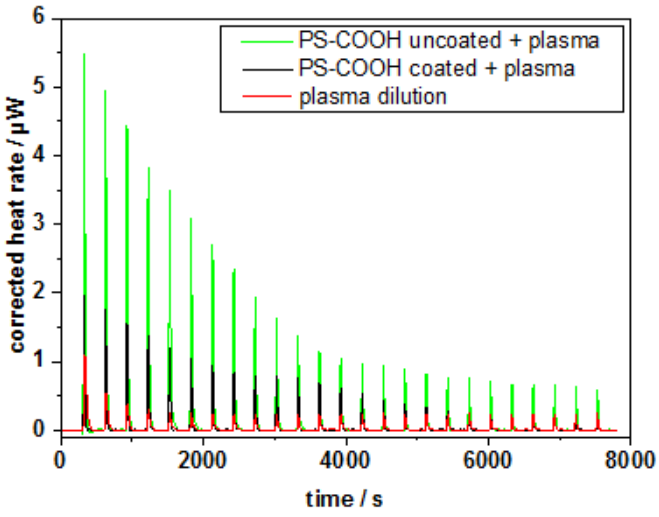


**Figure 7. 9.** Corrected heat rates of isothermal titration calorimetry experiments (ITC) experiments. The plasma dilution describes the titration of plasma into water and was subtracted from the adsorption measurements after integration. [redacted]

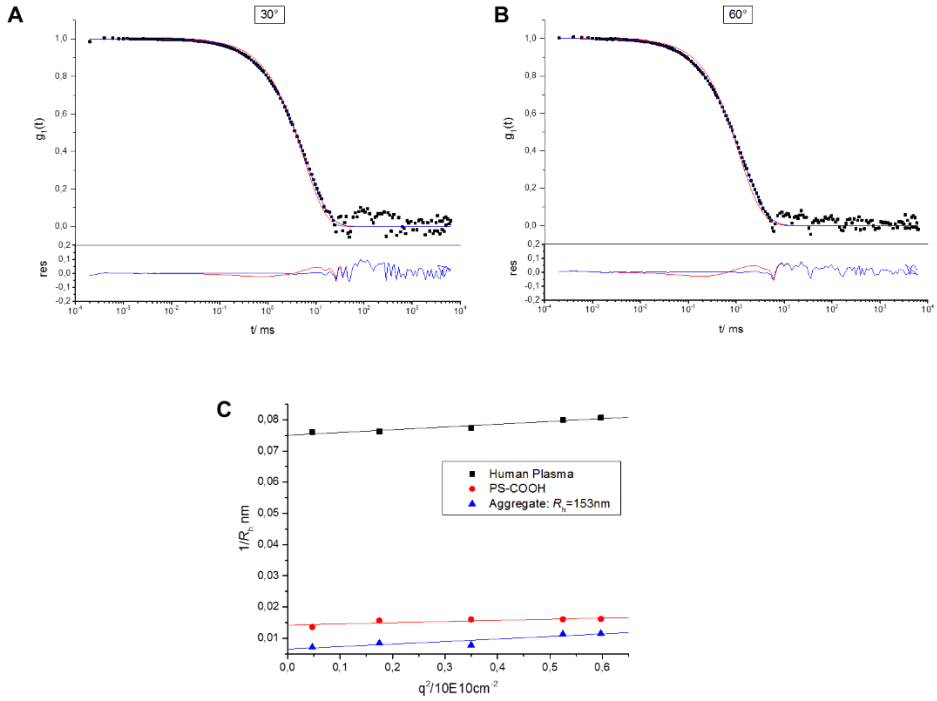


**Figure 7. 10.** Multi-angle dynamic light scattering analysis: PS-COOH nanoparticles incubated with human plasma at a scattering angle $\theta$ = 30° **(A)** or $\theta$ = 60° **(B). C)** Angular dependency of the hydrodynamic radius $R_h$ of PS-COOH nanoparticles (red), human plasma (black) and the aggregated formed in plasma (red). [redacted]

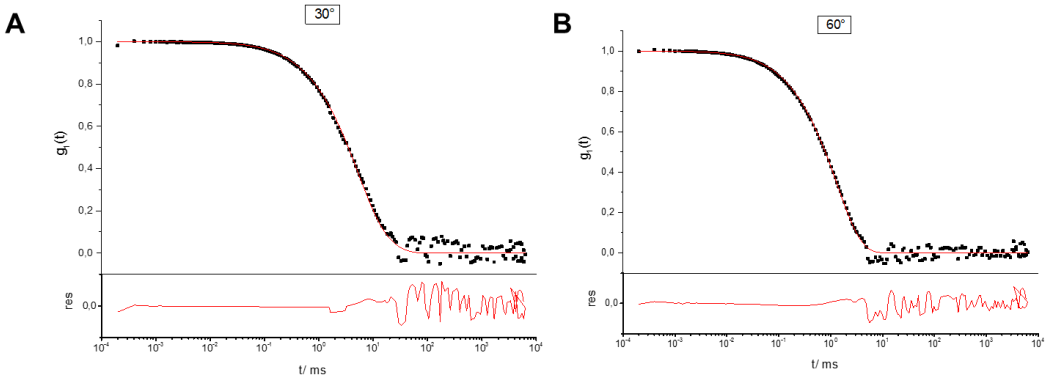


**Figure 7. 11.** Multi-angle dynamic light scattering analysis: *Upper graph:* Autocorrelation function $g_1(t)$ (black dots) of pre-coated PS-COOH nanoparticles incubated with human plasma at a scattering angle $\theta$ = 30° **(A)** or $\theta$ = 60° **(B).** The red line (–) represents the forced fit. There is no additional aggregation term needed indicating that the pre-coated nanoparticles remain stable in human plasma. [redacted]

## Literature

1. Blanco, E.; Shen, H.; Ferrari, M., Principles of nanoparticle design for overcoming biological barriers to drug delivery. *Nature biotechnology* **2015,** *33* (9), 941.

2. Peng, J.-R.; Qian, Z.-Y., Drug delivery systems for overcoming the bioavailability of curcumin: not only the nanoparticle matters. *Nanomedicine* **2014,** *9* (6), 747-750.

3. Liu, L.; Ye, Q.; Lu, M.; Lo, Y.-C.; Hsu, Y.-H.; Wei, M.-C.; Chen, Y.-H.; Lo, S.-C.; Wang, S.-J.; Bain, D. J., A new approach to reduce toxicities and to improve bioavailabilities of platinum-containing anti-cancer nanodrugs. *Scientific reports* **2015,** *5*, 10881.

4. Della Rocca, J.; Liu, D.; Lin, W., Are high drug loading nanoparticles the next step forward for chemotherapy? *Nanomedicine* **2012,** *7* (3), 303-305.

5. Park, K., Facing the truth about nanotechnology in drug delivery. *ACS nano* **2013,** *7* (9), 7442-7447.

6. Gustafson, H. H.; Holt-Casper, D.; Grainger, D. W.; Ghandehari, H., Nanoparticle uptake: the phagocyte problem. *Nano today* **2015,** *10* (4), 487-510.

7. Salvati, A.; Pitek, A. S.; Monopoli, M. P.; Prapainop, K.; Bombelli, F. B.; Hristov, D. R.; Kelly, P. M.; Aberg, C.; Mahon, E.; Dawson, K. A., Transferrin-functionalized nanoparticles lose their targeting capabilities when a biomolecule corona adsorbs on the surface. *Nature Nanotech.* **2013,** *8* (2), 137-43.

8. Ke, P. C.; Lin, S.; Parak, W. J.; Davis, T. P.; Caruso, F., A Decade of the Protein Corona. *ACS nano* **2017,** *11* (12), 11773-11776.

9. Winzen, S.; Schoettler, S.; Baier, G.; Rosenauer, C.; Mailaender, V.; Landfester, K.; Mohr, K., Complementary analysis of the hard and soft protein corona: sample preparation critically effects corona composition. *Nanoscale* **2015,** *7* (7), 2992-3001.

10. Monopoli, M. P.; Åberg, C.; Salvati, A.; Dawson, K. A., Biomolecular coronas provide the biological identity of nanosized materials. *Nature nanotechnology* **2012,** *7* (12), 779.

11. Daeron, M., Fc Receptors as Adaptive Immunoreceptors. *Curr Top Microbiol* **2014,** *382*, 131-164.

12. Shen, L.; Tenzer, S.; Storck, W.; Hobernik, D.; Raker, V. K.; Fischer, K.; Decker, S.; Dzionek, A.; Krauthauser, S.; Diken, M.; Nikolaev, A.; Maxeiner, J.; Schuster, P.; Kappel, C.; Verschoor, A.; Schild, H.; Grabbe, S.; Bros, M., Protein corona-mediated targeting of nano-carriers to B cells allows redirection of allergic immune responses. *J Allergy Clin Immunol* **2018**.

13. Owens III, D. E.; Peppas, N. A., Opsonization, biodistribution, and pharmacokinetics of polymeric nanoparticles. *International journal of pharmaceutics* **2006,** *307* (1), 93-102.

14. Mirshafiee, V.; Kim, R.; Park, S.; Mahmoudi, M.; Kraft, M. L., Impact of protein pre-coating on the protein corona composition and nanoparticle cellular uptake. *Biomaterials* **2016,** *75*, 295-304.

15. Amoozgar, Z.; Yeo, Y., Recent advances in stealth coating of nanoparticle drug delivery systems. *Wiley Interdisciplinary Reviews: Nanomedicine and Nanobiotechnology* **2012,** *4* (2), 219-233.

16. Kang, B.; Okwieka, P.; Schöttler, S.; Winzen, S.; Langhanki, J.; Mohr, K.; Opatz, T.; Mailänder, V.; Landfester, K.; Wurm, F. R., Carbohydrate-Based Nanocarriers Exhibiting Specific Cell Targeting with Minimum Influence from the Protein Corona. *Angew. Chem. Int. Ed.* **2015**.

17. Wörz, A.; Berchtold, B.; Moosmann, K.; Prucker, O.; Rühe, J., Protein-resistant polymer surfaces. *Journal of Materials Chemistry* **2012,** *22* (37), 19547-19561.

18. Kim, H. R.; Andrieux, K.; Delomenie, C.; Chacun, H.; Appel, M.; Desmaële, D.; Taran, F.; Georgin, D.; Couvreur, P.; Taverna, M., Analysis of plasma protein adsorption onto PEGylated nanoparticles by complementary methods: 2-DE, CE and Protein Lab-on-chip® system. *Electrophoresis* **2007,** *28* (13), 2252-2261.

19. Schöttler, S.; Becker, G.; Winzen, S.; Steinbach, T.; Mohr, K.; Landfester, K.; Mailander, V.; Wurm, F. R., Protein adsorption is required for stealth effect of poly(ethylene glycol)- and poly(phosphoester)-coated nanocarriers. *Nature Nanotech.* **2016**.

20. Schöttler, S.; Landfester, K.; Mailänder, V., Controlling the stealth effect of nanocarriers through understanding the protein corona. *Angewandte Chemie International Edition* **2016,** *55* (31), 8806-8815.

21. Hamad, I.; Hunter, A.; Szebeni, J.; Moghimi, S. M., Poly (ethylene glycol) s generate complement activation products in human serum through increased alternative pathway turnover and a MASP-2-dependent process. *Molecular immunology* **2008,** *46* (2), 225-232.

22. Bertrand, N.; Grenier, P.; Mahmoudi, M.; Lima, E. M.; Appel, E. A.; Dormont, F.; Lim, J.-M.; Karnik, R.; Langer, R.; Farokhzad, O. C., Mechanistic understanding of in vivo protein corona formation on polymeric nanoparticles and impact on pharmacokinetics. *Nature communications* **2017,** *8* (1), 777.

23. Dai, Q.; Bertleff-Zieschang, N.; Braunger, J. A.; Björnmalm, M.; Cortez-Jugo, C.; Caruso, F., Particle Targeting in Complex Biological Media. *Advanced healthcare materials* **2017**.

24. Takeuchi, T.; Kitayama, Y.; Sasao, R.; Yamada, T.; Toh, K.; Matsumoto, Y.; Kataoka, K., Molecularly Imprinted Nanogels Acquire Stealth In Situ by Cloaking Themselves with Native Dysopsonic Proteins. *Angewandte Chemie International Edition* **2017**.

25. Kreuter, J.; Shamenkov, D.; Petrov, V.; Ramge, P.; Cychutek, K.; Koch-Brandt, C.; Alyautdin, R., Apolipoprotein-mediated transport of nanoparticle-bound drugs across the blood-brain barrier. *Journal of drug targeting* **2002,** *10* (4), 317-325.

26. Caracciolo, G.; Cardarelli, F.; Pozzi, D.; Salomone, F.; Maccari, G.; Bardi, G.; Capriotti, A. L.; Cavaliere, C.; Papi, M.; Laganà, A., Selective targeting capability acquired with a protein corona adsorbed on the surface of 1, 2-dioleoyl-3-trimethylammonium propane/DNA nanoparticles. *ACS applied materials & interfaces* **2013,** *5* (24), 13171-13179.

27. Müller, L. K.; Simon, J.; Schöttler, S.; Landfester, K.; Mailänder, V.; Mohr, K., Pre-coating with protein fractions inhibits nano-carrier aggregation in human blood plasma. *RSC Advances* **2016,** *6* (99), 96495-96509.

28. Akula, S.; Mohammadamin, S.; Hellman, L., Fc receptors for immunoglobulins and their appearance during vertebrate evolution. *PloS one* **2014,** *9* (5), e96903.

29. Kokkinopoulou, M.; Simon, J.; Landfester, K.; Mailänder, V.; Lieberwirth, I., Visualization of the Protein Corona: towards a biomolecular understanding of nanoparticle-cell-interactions. *Nanoscale* **2017**.

30. Lundqvist, M.; Stigler, J.; Elia, G.; Lynch, I.; Cedervall, T.; Dawson, K. A., Nanoparticle size and surface properties determine the protein corona with possible implications for biological impacts. *Proc Natl Acad Sci U S A* **2008,** *105* (38), 14265-70.

31. Tenzer, S.; Docter, D.; Kuharev, J.; Musyanovych, A.; Fetz, V.; Hecht, R.; Schlenk, F.; Fischer, D.; Kiouptsi, K.; Reinhardt, C., Rapid formation of plasma protein corona critically affects nanoparticle pathophysiology. *Nature nanotechnology* **2013,** *8* (10), 772-781.

32. Müller, J.; Bauer, K. N.; Prozeller, D.; Simon, J.; Mailänder, V.; Wurm, F. R.; Winzen, S.; Landfester, K., Coating nanoparticles with tunable surfactants facilitates control over the protein corona. *Biomaterials* **2017,** *115*, 1-8.

33. Mohr, K.; Sommer, M.; Baier, G.; Schöttler, S.; Okwieka, P.; Tenzer, S.; Landfester, K.; Mailänder, V.; Schmidt, M.; Meyer, R. G., Aggregation behavior of polystyrene-nanoparticles in human blood serum and its impact on the in vivo distribution in mice. *Journal of Nanomedicine & Nanotechnology* **2014,** *5* (2).

34. Rausch, K.; Reuter, A.; Fischer, K.; Schmidt, M., Evaluation of nanoparticle aggregation in human blood serum. *Biomacromolecules* **2010,** *11* (11), 2836-2839.

35. Fleischer, C. C.; Payne, C. K., Secondary structure of corona proteins determines the cell surface receptors used by nanoparticles. *J. Phys. Chem. B.* **2014,** *118* (49), 14017-14026.

36. Musyanovych, A.; Rossmanith, R.; Tontsch, C.; Landfester, K., Effect of hydrophilic comonomer and surfactant type on the colloidal stability and size distribution of carboxyl- and amino-functionalized polystyrene particles prepared by miniemulsion polymerization. *Langmuir* **2007,** *23* (10), 5367-5376.

37. García-Moreno, I.; Costela, A.; Campo, L.; Sastre, R.; Amat-Guerri, F.; Liras, M.; López Arbeloa, F.; Bañuelos Prieto, J.; López Arbeloa, I., 8-Phenyl-Substituted Dipyrromethene BF2 Complexes as Highly Efficient and Photostable Laser Dyes. *J. Phys. Chem. A* **2004,** *108* (16), 3315-3323.

38. Renz, P.; Kokkinopoulou, M.; Landfester, K.; Lieberwirth, I., Imaging of Polymeric Nanoparticles: Hard Challenge for Soft Objects. *Macromol. Chem. Phys.* **2016,** *217* (17), 1879-1885.

39. Schöttler, S.; Klein, K.; Landfester, K.; Mailander, V., Protein source and choice of anticoagulant decisively affect nanoparticle protein corona and cellular uptake. *Nanoscale* **2016**.

40. Hofmann, D.; Tenzer, S.; Bannwarth, M. B.; Messerschmidt, C.; Glaser, S.-F.; Schild, H.; Landfester, K.; Mailaender, V., Mass Spectrometry and Imaging Analysis of Nanoparticle-Containing Vesicles Provide a Mechanistic Insight into Cellular Trafficking. *ACS Nano* **2014,** *8* (10), 10077-10088.

41. Silva, J. C.; Gorenstein, M. V.; Li, G. Z.; Vissers, J. P.; Geromanos, S. J., Absolute quantification of proteins by LCMSE: a virtue of parallel MS acquisition. *Mol. Cell. Proteomics.* **2006,** *5* (1), 144-156.

# Chapter C

## Targeting strategies: Controlled cellular interactions in the presence of the protein corona

In chapter C there are two different publications **(8-9)** summarized. In both studies it was aimed to develop targeting strategies in order to allow a specific cell recognition of nanoparticles even in the presence of the protein corona. In the following, first an introduction about current methods and challenges regaring targeting and protein corona formation will be summarized. Afterwards, the two publications are presented separately.

**[8]** [redacted] Pre-adsorption of antibodies enables targeting of nanocarriers despite a biomolecular corona. *Nature Nanotechnology,* **2018 (*shared first, accepted by reviewers, editorial requests await approval)**

**[9]** [redacted] Mannose functionalized poly(phosphoester)-based surfactants enable targeted cellular interactions. **(*shared first)**

## Introduction

The therapeutic efficiency of intravenously applied pharmaceutical products (e.g. chemotherapeutic agents) is often limited by the low amount, which is actually reaching the desired organ[117]. On top of that, the unspecific biodistribution of the drug causes severe side effects[118].

Therefore, nanoparticles designed as drug delivery vehicles promise targeted cell interactions in order to release the drug at the region of interest, hereby increasing the local drug dose and reducing toxic side effects[119]. To achieve this goal, several strategies are proposed to guide the nanoparticle to the desired place[120]. With this, it is aimed to control the drug biodistribution and further improve its therapeutic efficiency.

Even up to now, there is a limited number of reports, which proved the successful application of targeted drug loaded nanoparticles *in vivo.* This demonstrates that targeted drug delivery via nanoparticles remains a challenging task and nanoparticles applied under *in vivo* conditions have to break down several barriers[18].

In the following, different concepts will be discussed, which are commonly applied to achieve targeted cell interactions. Further, an overview of different targeting ligands, which are used for nanoparticle modifications, will be summarized. Lastly, the effect of protein corona formation on the targeting properties of nanoparticles will be discussed.

### C.1 Active/passive targeting

Targeted drug delivery via nanoparticles is commonly divided into two parts based on the mechanism of action (Figure C.1)[121-122]. In the 1980s, Maeda *et al*. saw that macromolecules specifically accumulate in the tumor tissue[123]. This process was referred to as the ´enhanced permeability and retention effect´ (EPR effect). A solid tumor has a unique vascular architecture meaning that there is an increased production of blood vessels due to tumor formation (referred to as hypervascularization). If tumor growth is abnormal, the blood vessels partially rupture, which further allows macromolecules to enter the tumor tissue. In addition, the tumor tissue is lacking an effective lymphatic drainage[124]. Therefore, macromolecules are retained in the tumor tissues, as the lymphatic system is not able to transport them out of the tissue. As no active transport mechanism is involved, it is a passive targeting strategy. Based on this effect, researchers aim to synthesize long circulating nanoparticle formulation in order to take advantage of the EPR effect[101]. However, the EPR effect is widely under debate. Due to the high diversity of tumor types and their heterogeneous growth, it is controversially discussed whether it has a clinical relevance[125].

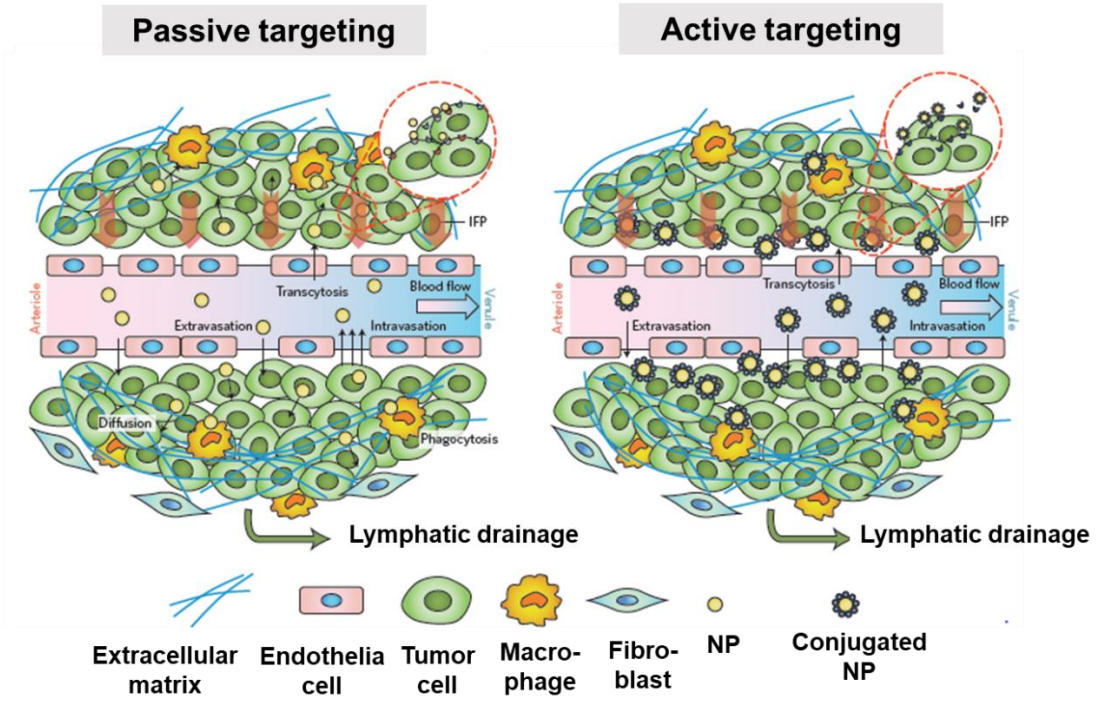


**Figure C. 1.** Schematic overview of different targeting strategies. Nanoparticles can reach the targeting cells via passive or active mechanism. Passive targeting is based on the EPR effect as long circulating nanoparticles specifically accumulate in the tumor tissue. Active targeting involves receptor mediated cellular uptake of nanoparticles via targeting ligands. Figure adaptated and modified from ´Designing nanomedicine for immuno-oncology´. Copyright @ 2017 Springer Nature. Reprinted with Nature Biomedical Engineering. *Ref.* Nature Biomedical Engineering 2017, 1.

In contrast to this, active targeting is based on the direct interaction of nanoparticles with specific cell receptors[126]. Nanoparticles are functionalized with targeting ligands, which enable receptor-mediated cellular uptake[127]. These strategies aim to direct the nanoparticle to the exact site of interest. Paul Ehrlich, a German Nobel laureate, postulated the term ´magic bullet´ in the 1900s[128]. He envisioned that a therapeutic agent should specifically remove microbes without affecting the whole body. Since then researchers are inspired to create a ´magic bullet´, which especially fights against incurable human diseases and does not affect the other tissues and cell types.

### C.2 Targeting ligands

In 2015 Cheng *et al.* reported a ´holistic approach´ for the design of targeted nanoparticles (Figure C.2)[129]. They described that for successful targeted drug delivery different aspects

needs to be considered. First, the application route (systemic, mucosal, dermal or CNS infusion) determines the selection of the nanoparticles´ properties. Depending on the biological milieu (skin, brain or blood), the targeting properties can be affected differently.

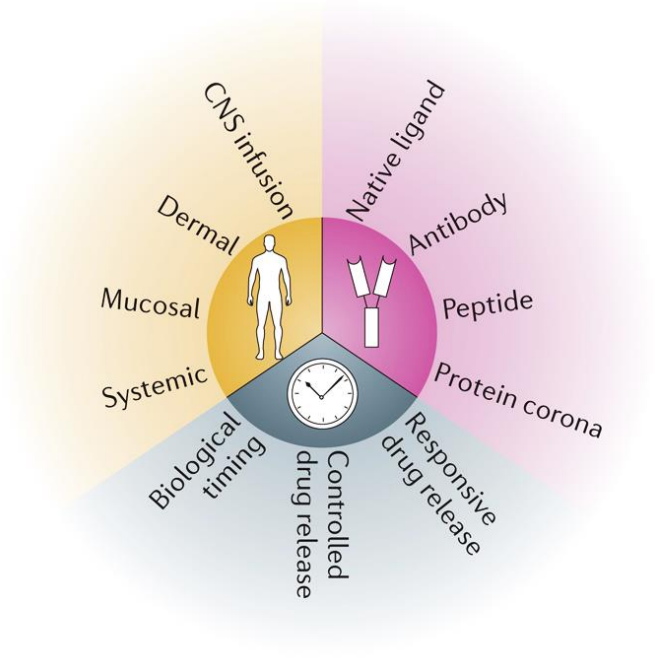


**Figure C. 2.** Achieving successful targeting via nanoparticles. Overview of key factors which need to be controlled in order to allow targeted cell interactions and an efficient drug delivery. Figure adaptated from ´A holistic approach to targeting disease with polymeric nanoparticles´. Copyright @ 2015 Springer Nature. Reprinted with permission from Nature Reviews Drug Discovery. *Ref.* Nature Reviews Drug Discovery 2015, 14(4), 239-247.

The choice of the targeting ligand depends on the desired cell interaction. Monoclonal antibodies are clinically used as therapeutics to treat specific cancer types (e.g. acute myelogenous leukemia)[130]. As a targeting ligand, most studies either use the whole antibodies or engineered antibody fragments. Antibodies consists of an antigen-binding region (Fab) and an additional Fc region. Phagocytic cells can recognize the Fc part of the antibodies via Fc receptors[131]. This interaction is unwanted for targeted cell interaction and hereby could reduce blood circulation. Therefore, antibody fragments without the Fc part (e.g. single chain or Fab fragments) are designed for the functionalization of targeted nanoparticles.

Next to this, other proteins (e.g. transferrin) are commonly applied to target nanoparticles towards the transferrin receptor, which is highly expressed on tumor cells[132]. Phage display libraries offer the possibility to identify specific peptides, which could be used as targeting ligands for specific cell receptors[133].

Additionally, several studies showed that carbohydrate (e.g. mannose) functionalization of nanoparticle enables recognition via DC-SIGN receptors expressed on dendritic cells[134-135]. Other small molecules such as folic acid were also conjugated to nanoparticles to specifically target cancer cells, which overexpress the folate receptor[136].

In general, it has to be noted that the covalent functionalization of nanoparticles is a challenging task. If proteins (e.g. antibodies) are coupled to the nanoparticle surface, synthetic strategies are needed, which do not disturb the protein structure and binding properties. Moreover, the functionalization of nanoparticles with targeting ligands can alter the physico-chemical properties of the nanoparticle (e.g. aggregation formation) and therefore need to be carefully controlled.

Lastly, an additional key requirement, which targeted nanoparticles needs to fulfil, is the ability to control drug release[9]. On one side, targeted drug delivery vehicles need to protect the drug during the administration journey until they reache the targeted cells. On the other side, once the nanoparticle has crossed the cellular barrier, the encapsulated drug should be efficiently released in order to achieve a targeted drug response.

### C.3 Corona influence

As blood proteins directly interact with the nanoparticles´ surface, the targeting properties can be significantly affected due to biomolecular corona formation. In 2013 Salvati *et al.* reported that it is not possible to achieve targeted cell interaction after protein corona formation (Figure C.3)[137]. It was shown that transferrin-functionalized nanoparticles are rapidly covered by plasma proteins, which further completely mask the targeting ligand. Therefore, the interaction between the targeting receptor and transferrin-functionalized nanoparticles were prevented. Since then various other groups showed that due to corona formation, the targeting properties were completely lost or strongly reduced[138-139].

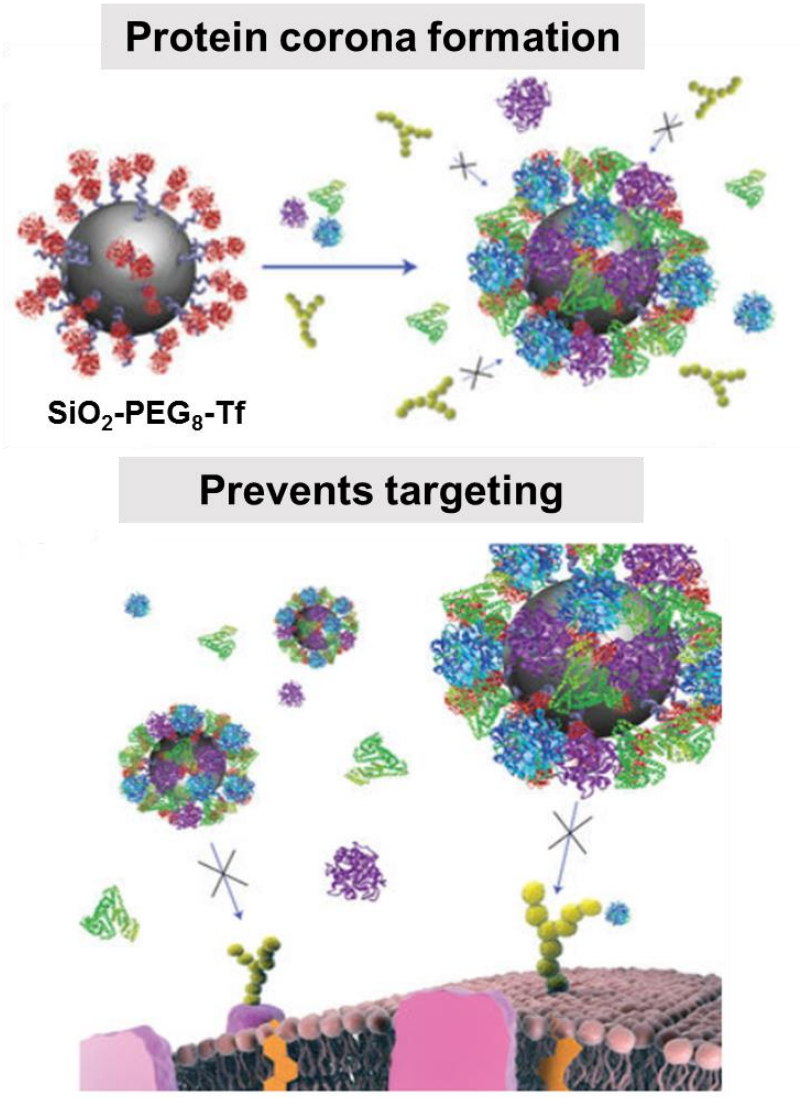


**Figure C. 3.** Protein corona formation prevents targeted cell interactions. Transferrin functionalized nanoparticles lose their targeting efficiency once blood proteins adsorb to the surface. Due to corona proteins, there is no interaction of the targeting ligand with the cell receptor. Figure adaptated and modified from ´Transferrin-functionalized nanoparticles lose their targeting capabilities when a biomolecule corona adsorbs on the surface´. Copyright @ 2013 Springer Nature. Reprinted with permission from Nature Nanotechnology. *Ref.* Nature Nanotechnology 2013, 8, 137-143.

Based on this, further studies aimed to improve the nanoparticles´ properties to achieve targeted cell interactions in the presence of the protein corona. Additionally, the process of biomolecular corona formation around targeted nanoparticles was intensively studied. Kang *et al.* developed PEGylated HES nanocapsules, which were additionally modified with mannose as a targeting ligand for dendritic cells[134]. They successfully proved targeted cell interaction after protein corona formation. It is suggested that the PEG layer below the targeting ligand as

well as the nanocapsule material itself (HES) effectively reduced protein adsorption and therefore corona proteins did not entirely cover up the targeting ligand.

Dai *et al*. investigated the targeting properties of affibody-functionalized nanoparticles (affibody = antibody-mimetic ligand) after incubation with albumin or human serum[140]. Depending on the corona type (albumin vs. human serum) the targeting properties were either enhanced or reduced. This study underlines that the distinct corona composition influences the targeting properties.

### C.4 Targeting via corona proteins

Inspired by the pioneer work from Kreuter *et al.* the concept of exploiting corona formation for targeted cell interaction has gained increasing interest. Already in 2002, he showed that polysorbate-80 coated poly(butyl cyanoacrylate) nanoparticles, which were pre-incubated with apolipoprotein E were able to cross the blood-brain barrier (Figure C.4)[141]. It was suggested that nanoparticles coated with ApoE mimic lipoproteins and are therefore taken up via receptor-mediated endocytosis[142].

Similar observations were reported from Caracciolo and colleagues[143]. It was demonstrated that lipid particles interact with plasma proteins and selectively adsorb vitronectin. The vitronectin-enriched protein corona mediated cellular uptake towards cancer cells, which express vitronectin αvβ3 integrin receptors.

In general, targeting via corona proteins requires an optimized nanoparticles system, which selective recruits specific proteins. Further, it needs to be controlled that the recruited plasma proteins remain functional on the nanoparticle surface for targeted cell interactions.

For example, Mirshafiee *et al.* demonstrated that even if nanoparticles were pre-coated with immunoglobulins cellular uptake into Fc receptor expressing cells was not enhanced[144]. This highlights that the orientation and accessibility of the recruited plasma proteins is essential for successful targeting via corona proteins.

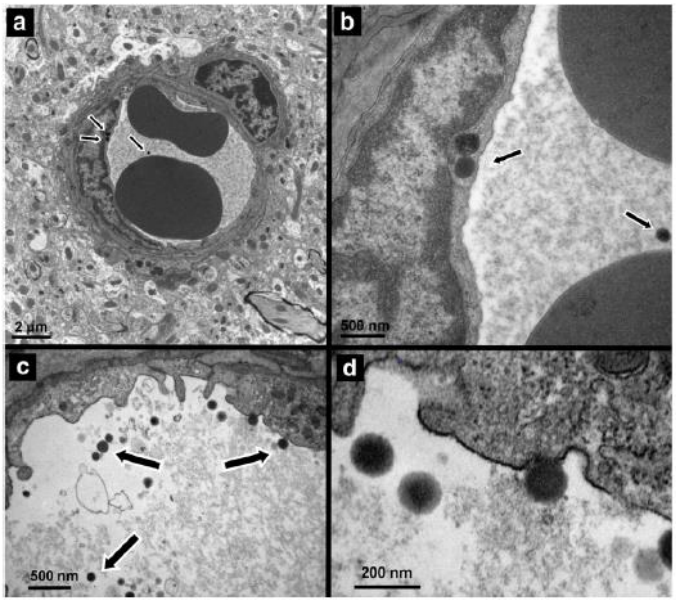


**Figure C. 4.** ApoE enables the transport of poly(butyl cyanoacrylate) nanoparticles across the blood-brain barrier. Protein corona formation mediates targeted cell interactions. Figure adaptated from ´Albumin nanoparticles targeted with Apo E enter the CNS by transcytosis and are delivered to neurones´. Copyright @ 2009 Elsevier. Reprinted with permission from Journal of Controlled Release. *Ref.* Journal of Controlled Release 2009, 137(1), 78-86.

# 8. Pre-adsorption of antibodies enables targeting of nanocarriers despite a biomolecular corona

## Aim:

The overall goal of nanoparticles applied as drug delivery vehicle, is the targeted transport of therapeutics to the desired body region. Therefore, the surface of nanocarriers is commonly functionalized with targeting ligands to guide the nanoparticles way. In this study, different strategies were investigated, which used antibodies for the surface functionalization of nanoparticles. It was demonstrated that the nanoparticles´ surface can be functionalized via simple adsorption of antibodies depending on the pH of the buffer systems. On top of that, it was proven that nanoparticles functionalized with adsorbed antibodies were able to reach the targeted cells even in the presence of the protein corona.

## Contribution:

I carried out the antibody functionalization of the nanoparticles and protein corona analysis. Cellular uptake experiments were conducted by me and [redacted]. [redacted] synthesized the nanoparticles. [redacted] conducted the transmission electron microscopy analysis. [redacted] contributed to the figure illustration and protein structure analysis. [redacted] and [redacted] performed the confocal electron microscopy experiments. [redacted] and [redacted] contributed with additional biological assays. The project was supervised by [redacted]

## Abstract

To promote drug delivery to exact sites and cell types, the surface of nanocarriers are functionalized with targeting antibodies or ligands, typically coupled by covalent chemistry. Once the nanocarrier is exposed to biological fluid like plasma however, its surface is inevitably covered with various biomolecules forming the protein corona, which masks the targeting ability of the nanoparticle. In this study, we show that we can use a pre-adsorption process to intentionally convey targeting antibodies to the surface of the nanocarrier. Pre-adsorbed antibodies remain functional and are not completely exchanged or covered up by the biomolecular corona, whereas coupled antibodies are more affected by this shielding. We conclude that pre-adsorption is potentially a versatile, efficient and rapid method of attaching targeting moieties to the surface of nanocarriers.

## Introduction

In this study, we demonstrate that the pre-adsorption of antibodies is an easier, more flexible and highly effective process in targeting nanocarriers towards the cell compared to the widely performed process of chemical coupling.

Nanotechnology in medicine and biology focuses on nanocarriers that deliver drugs to a specific site, organ, or cell type[1-2]. Targeting is achieved by the coupling of antibodies, ligands or other targeting moieties like sugars, to the surface of the nanocarrier[3]. Different coupling chemistries have been applied to bind proteins on the surface of nanocarriers in a covalent way[4-6]. The process of chemical coupling is, however, tedious and the antibodies sometimes lose their ability to bind to the antigen[7].

Salvati *et al.* have shown that the adsorption of proteins – termed protein corona[8] - can completely cover the chemically coupled targeting moiety[9]. Even surface modifications achieved by applying poly(ethylene glycol) cannot completely suppress protein adsorption. In fact, attracting specific proteins is the key factor in making nanocarriers unrecognizable to cells of the innate immune system, consequently hindering uptake[10].

Here, we use the pre-adsorption of antibodies or ligand as specific proteins to enable targeting. Adsorption of proteins, particularly antibodies, to a macroscopic, flat plastic surface is the standard procedure when coating plates for capturing an antigen out of solution. An example is the enzyme-linked sorbent assay (ELISA)[11]. To date, it was not clear if such an adsorbed antibody on a nanocarrier's surface could still be functional. Furthermore, during incubation in plasma or serum the targeting antibodies compete with the complex mixtures of serum or

plasma proteins forming the protein corona. These could cover up or replace the targeting antibody. Given this, the nanocarrier would no longer be targeting the correct cell type[12].

It has already been demonstrated that the targeting of chemically coupled nanocarriers can be achieved in media containing proteins[13-14] and even unspecific interactions can be suppressed[15]. However, many other studies observed that chemically coupled targeting moieties lose their binding after protein corona formation[9, 16-17]. Additionally, the protein corona can even guide intracellular uptake[18-20]. If pre-adsorption could enable stable and robust coverage, it would have a significant impact on the ease and versatility of using antibodies as targeting moieties.

In order to evaluate this approach, we chose an antibody that binds to an antigen of our target cell, the monocyte derived dendritic cell (moDC), a primary human cell type. It is a key player in responses of the immune system, as targeting specific receptors decisively alters the immunological outcome[21].

In previous studies, we identified a range of interesting surface expressed proteins of moDCs by proteomics[22]. Among all identified proteins, we chose CD63 as cellular target. CD63 is a member of the tetraspanin family and is found inside cells as well as on the cell surface[23].

Additionally, we demonstrate that the strategy of targeting by pre-adsorption can be expanded to several surface modified polymer nanoparticles and even to biodegradable nanocarriers made from hydroxyethyl starch (HES). Furthermore, antibodies against the CD3 antigen of T cells can be adsorbed and exert targeting properties. We could show that even a small bioactive protein like interleukin-2 (IL-2) adsorbs to HES nanocapsules and preserves its biological function. Taking this together, it appears that pre-adsorption is an interesting and easily established method for evaluating targeting antibodies and protein ligands.

## Material and methods

**Synthesis of oleate-capped iron oxide nanoparticles.** The preparation of hydrophobic oleate-stabilized iron oxide nanoparticles was performed according to a previous report[49]. Briefly, 60 mmol of $FeCl_2$-$4H_2O$ and 90 mmol of $FeCl_3$-$6H_2O$ were mixed in 100 mL of deionized water and mechanically stirred. 40 mL of concentrated ammonium hydroxide solution were added drop-wise over 5 min at room temperature. Afterwards, 5.0 g of oleic acid were added and the mixture was heated to 70 °C with constant stirring. After 1 h, the temperature was raised to 110 °C and the reaction continued for 2 h, keeping the volume constant by adding water sporadically. The resulting black precipitate was washed several times with water and dried overnight under vacuum at 40 °C.

**Synthesis of magnetic polystyrene nanoparticles functionalized with carboxylic acid groups.** Established practices reported in literature were followed with minor modifications[49] to obtain magneto-responsive polystyrene nanoparticles labelled with a fluorescent dye and functionalized with carboxylic acid groups.

**Immobilization of antibodies on magnetic polystyrene nanoparticles**

**Chemical Attachment.** The covalent attachment of antibodies to the surface of the magnetic nanoparticles was carried out by EDC coupling, a two-step process that involves the activation of a carboxyl group and subsequent conjugation with a primary amine.

*Activation*. The magnetic particles were diluted to a concentration of 5 mg/mL in MES buffer (50 mM, pH 6.1 adjusted with NaOH 0.1 M). 17.26 mg (0.15 mmol) of NHS and 5.75 mg (0.03 mmol) of EDC-HCl were added to 1 mL of this dispersion, and the mixture was shaken for 1 h at room temperature. The reaction mixture was later washed three times with MES buffer by magnetic purification to remove the unreacted material and diluted to a final volume of 1 mL.

*Conjugation*. 100 µL of the dispersion of NHS-activated particles were diluted with 4 mL of MES buffer. 100 µL of anti-CD63 (1.0 mg/mL) (Biolegend) or 40 µL of mouse IgG (2.5 mg/mL, Invitrogen) were dissolved in 4 mL of MES buffer and the nanoparticle dispersion was added drop-wise to the antibody solution. Finally, the combined reaction mixture was shaken for 4 h at room temperature and washed five times with water by magnetic purification. The final volume of the dispersion was adjusted to 2 mL.

**Physical Adsorption.** For the physical immobilization of the antibodies on the nanoparticles' surface, 100 µL of the particle dispersion before activation (5 mg/mL in MES, 50 mM, pH 6.1) were diluted with 4 mL of MES buffer. This diluted dispersion was then poured drop-wise onto a solution of an antibody, namely 100 µL of anti-CD63 (1.0 mg/mL) or 40 µL of mouse IgG (2.5 mg/mL) dissolved in 4 mL MES buffer. The mixture was incubated at room temperature for 4 h, washed twice by magnetic purification, and diluted to a final volume of 2 mL with water.

**Composition of the buffers used for nanoparticle modification at different pH**. pH 2.7: 125 mM Glycine-HCl; pH 5.5: 50 mM MES; pH 6.1: 50 mM MES; pH 7.5: 50 mM HEPES; pH 9.5: 50 mM $NaHCO_3$; pH 11.0: 50 mM $NaHCO_3$ and 100 mM NaOH. All buffers were adjusted with 1 N HCl or 1 N NaOH, respectively.

**Nanoparticle characterization.** Average hydrodynamic diameters of the particles were determined by dynamic light scattering (DLS) at 20 °C at a fixed angle of 90° with a PSS Nicomp particle sizer (380 Nicomp Particle Sizing Systems, USA). **ζ-**potential measurements were performed on a Malvern Instruments Zeta Nanosizer (Nicomp Particle Sizing Systems,

USA), diluting the samples in aqueous 1.0 mM KCl solution. For the experiments at different pH values, HCl 0.1 M or NaOH 0.1 M were used to adjust the pH. Transmission electron microscopy (TEM) was carried out on a Jeol 1400 (Jeol, Japan) operating at 120 kV. The particle dispersions were diluted with demineralized water, drop-casted on 300-mesh carbon-coated copper grids, and dried at room temperature for sample preparation. Thermogravimetric analysis (TGA) measurements were performed on a Mettler-Toledo 851 (Mettler-Toledo, USA) thermobalance with temperatures ranging from 35 °C to 1000 °C at a heating rate of 10 °C/min under nitrogen flow (30 mL/min). The solid content of the dispersions was determined gravimetrically after freeze-drying of the dispersions. Gel permeation chromatography (GPC) was used to determine the molecular weights distributions with a PSS SECcurity (Agilent Technologies 1260 Infinity (Agilent Technologies, USA). The freeze-dried samples were dissolved in THF and eluted at a flow rate of 1.0 mL/min at 30 °C. Polystyrene standards were used for calibration.

**Detection of antibodies on nanoparticle surfaces at different human serum (HS) concentrations by flow cytometry.** Nanoparticles (0.4 µg) were incubated with HS (10% or 100%) for 2 h at 37 °C to allow protein adsorption in a final volume of 19 µL. To detect mouse IgG1 or complete mouse IgG on the nanoparticle surface, the IgG1 antibody solution was incubated with 1 µL Zenon Alexa Fluor 647 mouse IgG1 labelling reagent (Invitrogen) for 5 min at room temperature. In contrast, complete mouse IgG was detected by staining with Alexa Fluor 633 anti-mouse (Life Technologies GmbH) for 30 min. In analogy, to detect the functional F(ab) region of the antibodies on the nanoparticles surface, secondary Alexa Fluor 647 labelled anti-mouse F(ab) fragment specific antibodies (Jackson ImmunoResearch) were used. Then, all solutions were filled up to 1 mL with PBS. Laser power was enhanced from 40 to 200 mW for better nanoparticle detection in flow cytometry. Nanoparticles were displayed in a dot plot at which the SSC and FL1 channel were scaled logarithmically. Recording of samples started 30 s after measurement to enable constant flow in the instrument. Quantification of Alexa Fluor 647 or 633 positive nanoparticles was performed by defining 0.5% of carboxylic acid functionalized nanoparticles as false positive.

**Detection of antibodies on nanoparticle surfaces via confocal laser scanning microscopy.** For cLSM measurements via Leica TCS SP5 II (Leica, Wetzlar, Germany) 0.4 µg nanoparticles were adjusted with PBS to a final volume of 19.5 µL and incubated with 0.5 µL Alexa Fluor 633 anti-mouse IgG for 30 min at room temperature. Nanoparticles were directly transferred without washing to microscopy chambers, which were coated with poly L-lysine (Sigma). Fluorescence signal of secondary antibodies co-localizing with particles was analysed for 80 events via ImageJ.

**Detection of antibody functionalization after HS incubation via transmission electron microscopy.** Characterization using TEM was carried out with a FEI Tecnai F20 (FEI, Hillsboro, OR, USA) equipped with an EDX at an acceleration voltage of 200 kV. The samples were prepared by diluting the particles in RPMI without 0% or 10% HS in comparison to 100% HS for 2 h at 37 °C. After the addition of secondary antibodies (12 nm Colloidal Gold-Antibody, Jackson ImmunoResearch) to each vial, one droplet was placed on 300-mesh Formvar coated copper grids. Subsequently, a drop of 1% trehalose containing 4 % uranyl acetate solution was added to the grid as previously reported[50]. Bright field images were acquired using a Gatan US1000 slow scan CCD camera (Gatan Inc.).

**Elemental analysis.** STEM was performed in combination with EDX to verify the elemental composition. This provides precise elemental maps by means of locally recording the spectrum of emitted X-rays. It should be noted that the resulting elemental maps only yield a relative concentration distribution.

**Cultured cell experiments.** Monocyte derived dendritic cells (moDCs) were generated from healthy human donor buffy coats which were obtained according to the vote of the local ethics committee and the Declaration of Helsinki. Isolation was preformed as previously described[14].

**Analysis of antibody binding to CD63 after nanoparticle modification.** Cell lysate of $10^6$ moDCs lysed with sample buffer (Invitrogen) was separated by SDS-PAGE. After polyacrylamide gel blotting with the iBlot dry blot system (Invitrogen), the membrane was blocked for 30 min with PBS, 3% BSA (Sigma-Aldrich) and subsequently washed twice for 5 min with purified water. Then the membranes were incubated with 7.5 µg/mL nanoparticles and as a positive control with 5 µg/mL anti-CD63 for 30 min. After the membrane was washed three times for 5 min with staining buffer composed of PBS, 1% BSA and 0.1% Tween 20 (Sigma-Aldrich), it was incubated for 30 min with secondary antibody solution (Invitrogen). Finally, the membrane was washed again three times for 5 min with a staining buffer and two times for 5 min with purified water before the luminescence signal of the secondary antibody was detected via the luminescent image analyzer LAS-3000 (Fujifilm Medical Systems USA, Stamfort).

**Detection of antibody conformation after adsorption and incubation at different pH values using nano differential scanning fluorimetry (nanoDSF).** CD63 antibody solutions (200 µg/mL) and nanoparticles coated with CD63 were prepared under different buffer conditions with varying pH values (described above). The solutions were loaded into nanoDSF High Sensitivity capillaries (NanoTemper Technologies) and placed into the Prometheus NT.48 instrument. For thermal unfolding experiments a linear thermal ramp program was chosen (1 °C/min, from 20 °C to 95 °C) and the tryptophan fluorescence was measured at 330

and 350 nm. Pristine, non-protein coated amino- and carboxy modified nanoparticles served as a reference. Thermal unfolding curves are plotted as the first derivative of the fluorescence ratio (F350/F330).

**Nanoparticle uptake in moDCs:** Around 100,000 moDCs in 200 µL DC-medium with 1600 IU/mL GMCSF and 500 IU/mL IL4 were seeded into the wells of a 24-well plate. Cells were incubated at different nanoparticle concentrations (0, 0.3, 1, 2, 3.75, 7.5 and 10 µg/mL) for 2 h under standard conditions. In contrast, when nanoparticle uptake was analysed at different HS concentrations, 100,000 moDCs were kept in RPMI-1640 without 0% or with 10% HS in comparison to 100% HS. Cells were incubated with nanoparticles for 2 h at the indicated concentration. Then moDCs were detached with PBS, 0.5 mM EDTA and subsequently washed once with 1 mL PBS. For flow cytometer measurements, moDCs were labelled with PI (2 µg/mL) to exclude dead cells from analysis. The percentage of fluorescently labelled moDCs was calculated by defining 1% of cells in the negative control as false positive. For cLSM analysis moDCs were resuspended with 200 µL DC-medium and seeded into 8-well chamber slides which were coated with poly L-lysine.

**Nanoparticle binding towards T-cells and CD3 blocking.** 100,000 Jurkat cells were incubated in RPMI containing 10% human serum and 25 µg/mL of nanoparticles were added for 6 h, 4 °C. Cells were centrifuged (300 g, 5 min) and washed with PBS in order to remove free nanoparticles before flow cytometer measurements. For blocking experiments: Cells were pre-treated with anti-CD3 antibodies (25 µg/mL) for 30 min, 4 °C. Afterwards cellular binding experiments were performed as described above.

**Purification of hard protein corona.** 1 mg of nanoparticles were incubated with 10% or 100% HS for 2 h at 37 °C. Purification of hard protein corona was performed as described before at 4 °C[18, 43]. Briefly, nanoparticles were pelleted by centrifugation at 20,000 g for 1 h and subsequently washed three times with 1 mL PBS. The pellet was resuspended in 2% SDS with 62.5 mM Tris hydrochlorid (Sigma) and incubated for 5 min at 95 °C. The samples were further centrifuged at 20,000 g for 1 h to remove nanoparticles and the supernatant containing desorbed hard corona proteins was stored at -20 °C.

**Statistical analysis.** All data are expressed as mean ± s.d. Each experiment was repeated at least three times, unless otherwise indicated. For comparing two experimental groups a two-sided student´s t-test was performed. Calculated p values were considered to be significant for *$p < 0.05$, **$p < 0.01$, ***$p < 0.001$. Differences are labelled n.s. for not significant.

**Protein structure analysis.** The 3D-structure and amino acid sequence of murine IgG1 (PDB ID: 1IGY) were obtained from the RCSB Protein Data Bank (PDB), the human CD63 (Uniprot ID: P08962) model structure and amino acid sequence were obtained from SWISS-MODEL.

Both structures were subsequently visualized, analysed and edited using Chimera 1.11.2. The structure of human serum albumin 1AO6 was obtained from RCSB Protein Data Bank (PDB) and is used in Figure 4 e,f to illustrate protein corona formation.

**Synthesis of amino functionalized polystyrene nanoparticles ($PS\text{-}NH_2$).** Amino-functionalized polystyrene nanoparticles were synthesized via free-radical miniemulsion copolymerization according to literature[53] **.** 2-aminoethyl methacrylate hydrochloride (AEMH) was used as co-monomer. The nanoparticles were stabilized with the non-ionic surfactant Lutensol AT50. Briefly, 6 g freshly distilled styrene, 250 mg of hexadecane, 100 mg of initiator V59 and 6 mg BODIPY were mixed with 120 mg AEHM and 600 mg Lutensol AT50. The mixture was ultrasonicated for 2 min (450 W, 90% intensity) at 0 °C and further polymerization (at 72 °C) was carried out overnight.

**Synthesis of hydroxyethyl starch (HES) nanocapsules.** As previously described[54] HES nanocapsules were obtained using polyaddition reaction at the droplet interface via miniemulsion. HES in solution (10 wt%, 1.4 g) was mixed with 20 mg NaCl, 100 µL Cy5Oligo solution and 150 µL CellTracker. 7.5 g cyclohexane containing 100 mg of P(E/B-*b*-EO) was added and the mixture was stirred for 1 h. Sonication was performed under ice-cooling with a Branson W450-D sonifier. Further, TDI (100 mg) and P(E/B-b-EO) (30 mg) were dissolved in 5 g cyclohexane, added dropwise and the emulsion was stirred for 24 h at RT. For purification, the nanocapsules were centrifuged and redispersion in cyclohexane (2 times). 0.1 wt% SDS was used to transfer the nanocapsules into aqueous medium. Excess SDS was removed via dialysis (24 h), centrifugation (1 time) and redispersion in water.

**Functionalization of $PS\text{-}NH_2$ nanoparticles and HES nanocapsules with antibodies by adsorption using different buffer conditions.** 200 µg of nanoparticles with amino groups or HES nanocapsules were incubated with 100 µg anti-CD63, mouse IgG1 or mouse IgG for 4 h at room temperature in 1 mL buffer possessing pH 2.7, 5.5, 6.1, 7.5, 9.5 and 11.0. In contrast, for carboxylic acid particles 120 µg were incubated with 50 µg antibodies. In addition, this solution was adjusted to 1 mL and incubated under the same conditions. The magnetic particles were separated from the supernatant by magnetic force and then washed with 1 mL ultrapure water. Non-magnetic particles were centrifuged for 30 min at 20,000 g and 4 °C to remove free antibodies and resuspended with 1 mL ultrapure water. Both washing steps were repeated three times. After the last step particles were resuspended in 200 µL ultrapure water. Concentrations of all particles were determined by fluorescence intensity in the Infinite® M1000 plate reader (Tecan Group Ltd.)

**Cell culture of T cells.** Jurkat cells (E6-1) were obtained from ATCC and kept in RPMI supplemented with 10% FBS, 100 IU/mL penicillin and 100 µg/mL streptomycin. Cells were

routinely checked (every three to six months) for Mycoplasma contamination using Microsart® AMP Mycoplasma Test Kit (Sartorius) according to the manufactures´ instruction.

**Cytotoxicity Assay.** 100,000 to 200,000 moDCs were incubated at different nanoparticle concentrations (0, 0.3, 1, 2, 3.75, 7.5 and 10 µg/mL) for 24 h under standard conditions. After detachment of moDCs with PBS/0.5 mM EDTA, cells were washed once with PBS. Cytotoxicity of nanoparticles towards moDCs was determined by staining with 2 µg/mL propidium iodide (PI, Sigma) just before measuring via Cyflow ML. In cell culture based experiments, laser power of the 488 nm laser was adjusted to 40 mW. To determine cytotoxicity of nanoparticles the negative control 0 µg/mL was defined as 100% viable.

**CTLL-2 Proliferationassay.** The IL-2-dependent CTTL-2 cell line has derived from a subclone of T cells that was isolated from a C57bl/6 mouse and relies on IL-2 for its proliferation and growth[55]. To investigate the biological activity of IL-2 (Cell Sciences) adsorbed to nanoparticles, CTLL-2 cells were incubated in 200 µl RPMI1640, supplemented with 10% FCS, 2mM L-glutamine and 50 µM and seeded at a density of $3x10^3$/well in 96 well plates. Nanocapsules were added at concentrations of 5 µg/mL, 1 µg/mL, 0.1 µg/mL, 0.01 µg/mL and 0.001 µg/mL. After 48h, proliferation of the cells was assessed by adding [$^3$H]-thymidine for 16-18h and subsequently measuring the amount of incorporated radioactive-labeled thymidine by a scintillation counter as counts per minute. For cell culture maintenance CTLL-2 cells were incubated in CTLL-2 medium, supplemented with 50 U/mL IL-2.

**Binding of nanoparticles to moDCs after HS incubation.** 7.5 µg/mL particles were incubated with 10% or 100% HS for 2 h at 37 °C and subsequently transferred to 100,000 moDCs for 2 h at 4 °C. Nanoparticle binding was determined at Cyflow ML and cLSM. Using flow cytometry, dead cells were excluded from analysis by PI staining (2 µg/mL), while moDCs were seeded for cLSM into 8-well chamber slides which were coated with poly L-lysine. Cells were allowed to attach for 30 min at 4 °C before they were fixed with 4% formaldehyde for 10 min. Cell membrane visualization was achieved by staining with Cellmask Orange™.

## Results and discussion

Polymeric nanoparticles with carboxyl surface groups (PS-COOH) were produced as a starting material by the miniemulsion technique[24] (Figure 8.1). The physicochemical properties as size and surface charge were analysed by transmission electron microscopy (TEM), dynamic light scattering (DLS) and ζ-potential measurements as a function of the pH value (material/methods see supplementary information 8).

Modifying the surface with a targeting antibody was achieved by chemical coupling via EDC-NHS chemistry or by adsorption under the same pH (Figure 8.1). We detected similar values for the ζ-potential, irrespective of whether the coupling reagent was added or only the antibody was present. The antibodies seemed to shield the negative charge in both states – adsorbed or coupled.

Anti-CD63 antibodies were detected on the nanoparticle surface by a secondary anti-IgG1 antibody against the F(c) region (Figure 8.1) of the targeting antibody. Similar amounts of anti-CD63 antibodies were detected for covalently coupled as well as adsorbed conditions (Figure 8.1). In addition, the fluorescence intensity of secondary antibodies co-localized to nanoparticles was analysed via confocal laser scanning microscopy (cLSM) and quantified via ImageJ. The red fluorescence intensity of antibody-functionalized nanoparticles was significantly higher compared to unfunctionalized nanoparticles (Figure 8.1).

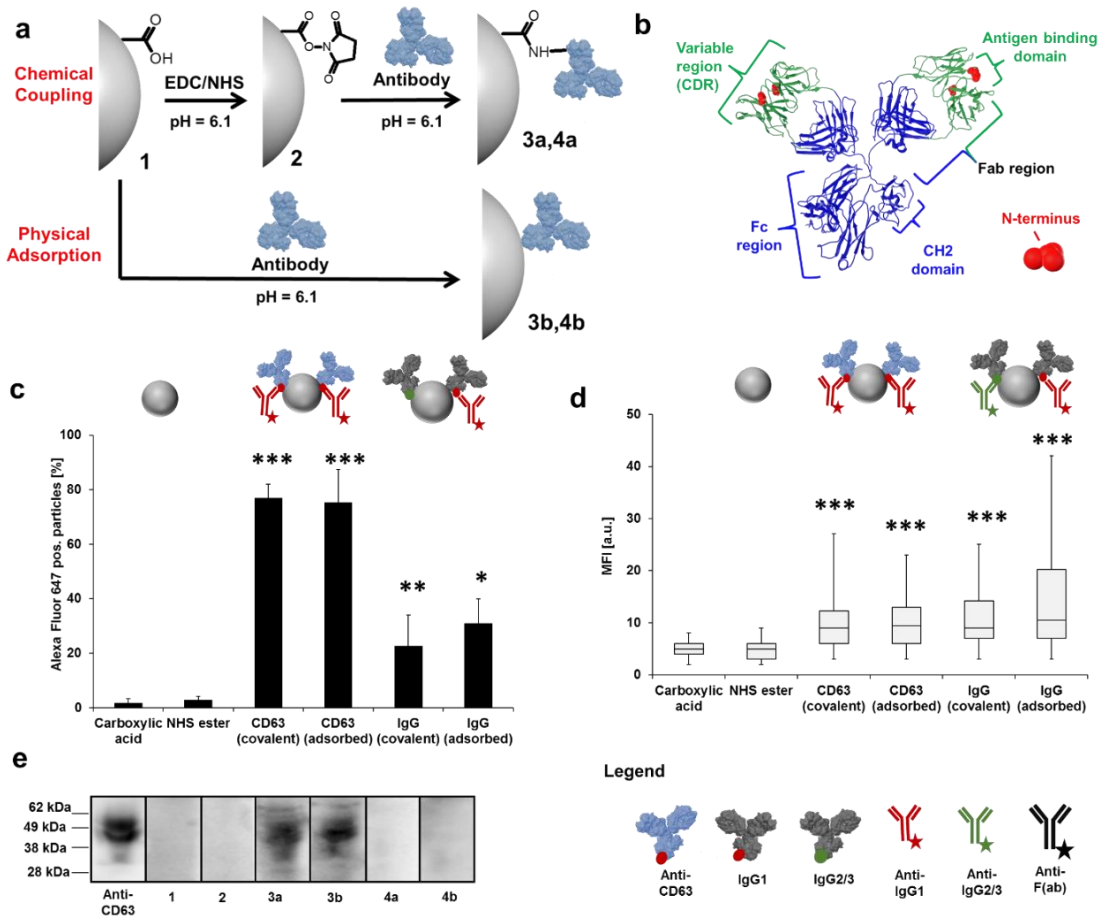


**Figure 8. 1. a,** Schematic representation of antibody immobilization on the surface of carboxylic nanoparticles (PS-COOH), depicting the pre-activation of the nanocarrier surface by EDC/NHS and antibody binding or incubation of the antibody under the same conditions but without EDC/NHS activation. **b,** 3D structure of IgG1 antibodies highlighting the constant part F(c) region, and the variable,

antigen binding site as part of the F(ab) region with the complementarity-determining region (CDR)[26]. **c,** Detection of antibodies with fluorescently labelled, monoclonal anti-IgG1 (red) antibodies by flow cytometry. Data is shown as the amount of Alexa Fluor 647 positive nanoparticles in % and is the mean ± s.d. of three independent experiments. **d,** Staining of nanoparticles with polyclonal anti-IgG antibodies (red/green). Polyclonal secondary antibodies are reacting to all subtypes of mouse IgG (red/green). Therefore, similar amounts of IgG and CD63 antibodies were detected on the nanoparticle surface. The median fluorescence intensity (MFI) was determined by cLSM and quantified via ImageJ. Data is represented as the mean ± s.d. of 80 counted events. **e,** Visualization of specific binding of anti-CD63 bound on nanoparticles to cell lysate by Western blot analysis**. f,** Figure legend. *p < 0.05, **p < 0.01, ***p < 0.001

Next, we tested if the antibodies present on the nanoparticles´ surface could still bind to their target, the CD63 antigen on the monocyte derived dendritic cell (moDC). In a modified Western blot we verified the nanoparticle binding to the target protein CD63 in a moDC cell lysate (Figure 8.1). This demonstrated that anti-CD63, either adsorbed or covalently coupled to the nanoparticle, still binds to the CD63 antigen. As CD63 is expressed in different degrees of glycosylation, the signal detected from free antibodies or nanoparticle bound antibodies (Figure 8.1) shows a distinct pattern of bands[25]. It is significant that positive control signals and anti-CD63 functionalized particles are similar, indicating an equal binding specificity after antibody immobilization. As a result, we were able to verify normal antibody functionality.

**Antibody adsorption improves uptake in target cells**

Based on this, we investigated the uptake behavior of the nanoparticles at different concentrations in moDCs after confirming that the nanoparticles had no negative effect on cell viability. Functionalization of nanoparticles with anti-CD63 significantly improves uptake into moDCs at all concentrations when compared to the control particles (Figure 8.2). cLSM and TEM images verified that nanoparticles ended up inside the cells in vesicles after 2 h of incubation (supplementary information 8).

Cellular uptake is usually investigated under cell culture conditions with a buffer ranging from pH 7.2 to 7.4. Tumour tissue has a lower pH value of about 6.5 and it has been shown that uptake can be influenced by this lower pH value[27]. In our examples, the difference between targeted and untargeted nanocarriers is still evident at this lower pH value (supplementary information 8).

Salvati *et al*.[9] have shown that adsorption of serum proteins can mask targeting proteins. The accessibility of a targeting ligand on the nanoparticle surface has been assessed in previous

studies by TEM[28] and flow cytometry[29-30]. These methods have been shown to be a valuable tool to detect functional motifs of the targeting ligand on the nanoparticle surface. When employing classical TEM (Figure 8.2) or scanning transmission electron microscopy (STEM), we used secondary antibodies against the F(c) region of the antibody coupled to 12 nm-gold particles. As the gold particles of the secondary antibody are hard to differentiate from those of the iron oxide cores embedded into the PS-COOH particles, we employed energy dispersive X-ray spectrometry (EDX) demonstrating that more electron dense spots on the TEM images were indeed gold. With TEM images (Figure 8.2) and flow cytometry analysis, we detected the anti-CD63 antibody on the nanoparticle surface even after incubation in 100% human serum (HS) and in 100% human plasma (HP). This indicates that the protein corona did not restrict access to the CD63 antibody. Results were confirmed by Western blot analysis of the desorbed protein corona detecting the pre-adsorbed CD63 antibody in this complex mixture.

However, on cellular level we found that the protein corona alters the interaction of nanoparticles and cells differentially (Figure 8.2). Here, we observed a direct correlation between increasing amounts of serum (10% to 100%) and reduced cellular targeting. When covalent functionalized nanoparticles were exposed to 100% serum, uptake was completely abolished. A similar trend was observed after plasma incubation. In strong contrast, adsorbed antibodies could reach the targeted cell even after exposure to 100% serum or plasma. This is intriguing. We hypothesized that the antibody orientation is the decisive factor.

While it is a standard procedure in antibody detection to use secondary antibodies against the F(c) region, we also investigated the accessibility of the F(ab) region of CD63 antibody by secondary F(ab) specific antibodies using flow cytometry (Figure 8.2). The F(ab) region contains the antigen-binding site, also termed complementarity-determining region (CDR, Figure 8.1) which is close to the N-terminus. Here, we saw that the accessibility of the F(ab) region was about half for the covalently bound anti-CD63 compared to that of the adsorbed counterpart (Figure 8.2).

Why should the F(ab) region be less exposed when chemically coupled? For chemical coupling, carboxyl groups on the nanoparticles´ surfaces are “activated” by EDC-NHS and subsequently react with the primary amine groups of the antibody[31]. There are primary amine groups of the lysine side chain as well as the N-terminus of each polypeptide chain (Figure 8.1). Mapping the lysine distribution of mouse IgG1[26] indicates that lysine residues are distributed over the F(c) and F(ab) region (lysine distribution F(ab): 58% vs. F(c): 42%).

In contrast, the N-terminal amino groups are all located within the F(ab) region (Figure 8.1) of the antibody closely to the CDR region. They are therefore closer to the antigen-binding site and possibly affect the accessibility of the F(ab) part if the covalent coupling to the

nanoparticles´ surface takes place in this region. This will also be true for the other amines in the F(ab) region when reacting with activated carboxy groups. As a result, one or both of the two the antigen binding sites of the antibody could be immobilized on the nanocarrier surface (Figure 8.2).

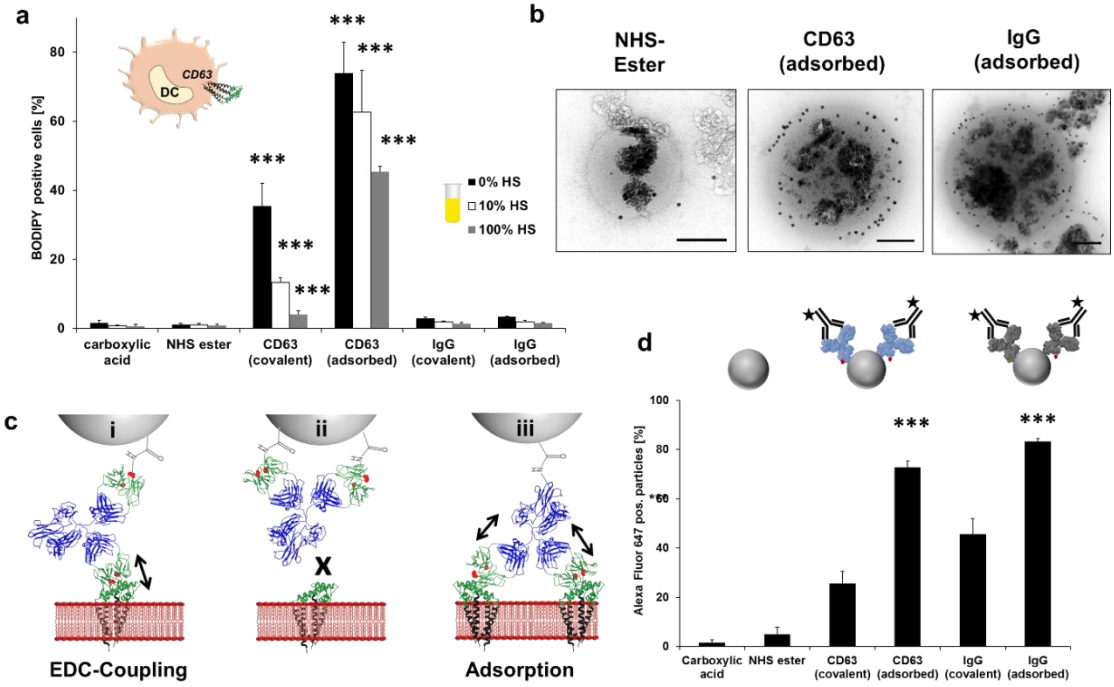


**Figure 8. 2.** Covalent anti-CD63 functionalized nanoparticles lose their targeting ability in the presence of the protein corona while adsorbed antibodies keep their targeting properties. **a,** Incubation of moDCs with nanoparticles (7.5 µg/mL) for 2 h, 4 °C in the presence of different human serum (HS) concentrations. The amount of nanoparticle (BODIPY) positive cells in % is shown. Data is represented as the mean ± s.d. of three independent experiments [redacted] **b,** Immunogold labelling: Representative TEM micrographs of nanoparticles incubated with HS and stained with secondary gold-coupled antibodies (12 nm colloidal gold-antibody). Scale bar: 200 nm [redacted] **c,** Detection of functional F(ab) regions on the nanoparticle surface using secondary F(ab)-specific antibodies (black). Data is shown as the amount of Alexa Fluor 647 positive nanoparticles in % and is the mean ± s.d. of three independent experiments. **d**, Schematic overview: Binding of anti-CD63 (representative structure of IgG1[26] shown) functionalized nanoparticles to cell membrane bound CD63 (Uniprot: P08962, Structure: SWISS-MODEL). *EDC-Coupling:* Antibodies are preferably bound via the N-terminus or lysine residues in the F(ab) region to the nanoparticle (i) or (ii). *Adsorption:* Antibodies preferably bind via the F(c) region to the nanoparticle (iii). *p < 0.05, **p < 0.01, ***p < 0.001.

The orientation of the adsorbed antibody seems to be favourable exposing a higher number of functional F(ab) parts (Figure 8.2) and hereby providing superior targeting properties

compared to covalently coupled antibodies. It is discussed that surface adsorption of proteins is higher closer to their isoelectric point[32]. We demonstrated by using nanoDSF measurements (Figure 8.3) that lower pH values induce the unfolding of the antibody. It has been described in the literature that the CH2-domain (Figure 8.1) located within the F(c)[33-34] region of antibodies is pH sensitive and readily unfolds exposing hydrophobic residues[35]. At a pH value of 6.1, which is slightly below the isoelectric point of IgG1[36], the adsorption process is probably supported by the interaction of the CH2-domain of the F(c) region and the nanoparticles. This process enables the effective orientation of F(ab) regions towards the CD63 antigen.

Putting it simply: the different modes of attaching an antibody to the surface of the nanocarrier – either by adsorption or chemical coupling – seems to determine its orientation and therefore accessibility to the antigen binding site of the two F(ab) regions (Figure 8.2).

**Antibody adsorption is pH-dependent**

As highlighted above, we clearly observed an improved targeting of nanoparticles with adsorbed antibodies, rather than covalently functionalized ones. Here, one decisive factor could be the pH value at which adsorption was performed. Radically different pH values can be found in the literature for antibody adsorption on surfaces[37-38].

Adsorption of proteins on nanoparticles can result in conformational changes which lead to an unfolding of the antibodies and therefore to a loss in their biological functionality[9, 39]. Conformational changes of anti-CD63 at different pH values were analysed by label-free differential scanning fluorimetry (nanoDSF, Figure 8.3). For a pH value ranging from 5.5 to 7.5 the point of the denaturation temperature ($T_M$) was around 70 °C (Figure 8.3), which is also reported for other antibodies[40]. Lower (pH 2.7) or higher (pH 9 – 11) values cause a strong decrease in the thermal transition temperatures indicating significant structural changes.

In order to determine an optimal pH value for antibody adsorption, the antibodies were incubated with PS-COOH nanoparticles at different buffer conditions (Figure 8.3). To evaluate the influence of the chemical modifications on the nanoparticles´ surface, an amino-functionalized polystyrene nanoparticle was used (PS-$NH_2$, ζ-potential = +4 ± 1 mV). While conformation was mainly preserved at a pH value of 6.1 for PS-COOH, a pH value of 2.7 proved to be preferable for PS-$NH_2$ regarding the conformational integrity of the antibody (Figure 8.3).

The impact of pH-dependent adsorption changes was subsequently analysed regarding uptake in moDCs. The best uptake was caused by adsorption at a pH value of 6.1 for PS-

COOH and at a pH value of 2.7 for PS-$NH_2$ particles. These results are in accordance with the conformation analysis (Figure 8.3) and amount of detected antibodies on the nanoparticle surface (Figure 8.3).

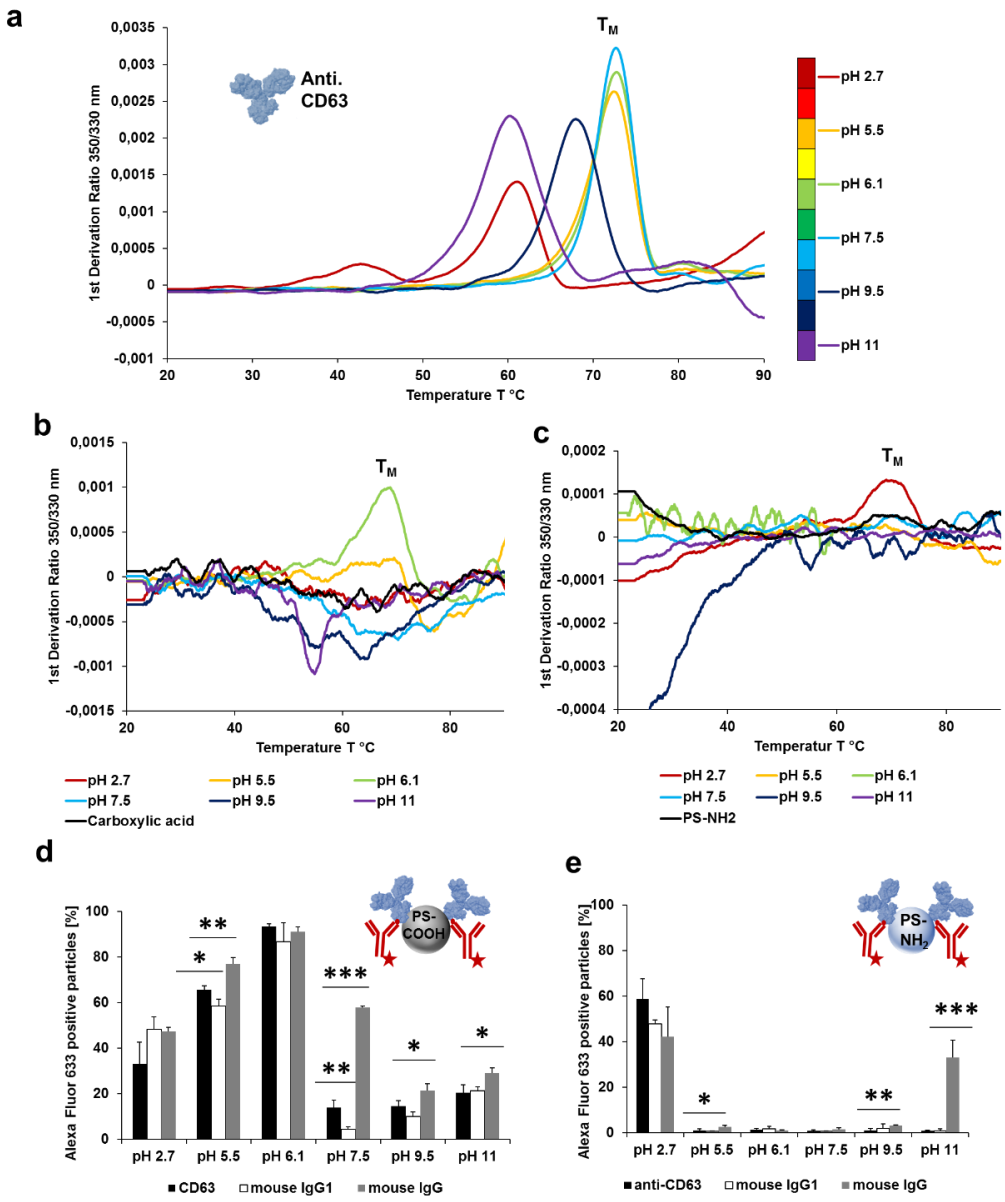


**Figure 8. 3. a,** Monitoring the unfolding of anti-CD63 at different pH values by nanoDSF. b-c, Structural analysis of adsorbed antibodies and determination of the melting temperature $T_M$ for PS-COOH **(b)** PS-$NH_2$ **(c).** Polystyrene nanoparticles were functionalized with antibodies at different pH values and then subjected to $T_M$ analysis. d-e, Secondary labelled polyclonal mouse IgG antibodies (red) were used to detect the adsorbed antibodies on the surface of carboxylic- **(d)** or amino-functionalized nanoparticles **(e).** Data is represented as the amount of Alexa Fluor 633 positive nanoparticles in % as mean ± s.d. of three independent experiments. *p < 0.05, **p < 0.01, ***p < 0.001. ([redacted]
[redacted]

Our findings would indeed be relevant if these results could be applied to other antibodies, ligands and nanocarrier systems. In fact, we found similar results for the anti-CD3 antibody adsorbed onto PS-$NH_2$ nanoparticles. Additionally, we applied our concept to a more hydrophilic and biodegradable nanocarrier system using hydroxyethyl starch (HES) nanocapsules. In this case, the pH value crucially affects the adsorption behavior of anti-C63 antibodies. We continued by studying the pH-dependent interaction of a small biomolecule – interleukin-2 (IL-2) and HES-nanocapsules. Interestingly, we saw that IL-2 tends to adsorb to HES-nanocapsules at pH 6.1 – 7.5, whereas adsorption of anti-CD63 is favoured at a pH value of 2.7. HES nanocarriers which adsorbed anti-CD63 antibodies showed superior uptake in the presence of serum and plasma compared to un-functionalized and control IgG nanocarries (supplementary information 8). Also, IL-2 functionalized nanocarriers exhibited cellular effects similar to our previous reported results[41].

Taking this together, we were able to demonstrate that by determining the optimal pH buffer for a defined nanoparticle-protein system we can influence and enhance the adsorption process.

**Impact of the protein corona on nanoparticle modification**

A major field of discussion concerning the targeting ability of nanoparticles focuses on the influence of protein corona formation after nanoparticles are introduced to serum or plasma. Questions to be addressed are: **i)** determination of proteins adsorbed, **ii)** masking of the targeting moiety causing a loss in the targeting effect, **iii)** mistargeting by proteins present in the protein corona **iv)** targeting by new epitopes exposed by adsorption of protein corona proteins or **v)** displacement of targeting antibodies by other serum proteins.

Adsorption of proteins to the nanoparticle surface alters the physico-chemical properties of any nanomaterial[42]. Incubation of nanoparticles in serum or plasma results in changes to the ζ-potential. The protein source itself, either serum or plasma, also impacts the composition of adsorbed proteins and even cellular uptake[43-44]. As a result, the characterization of the protein corona by label-free, quantitative mass spectrometry is essential in order to characterize the biological identity of nanoparticles **(i)**. For the two major nanoparticle systems under investigation (PS-COOH and PS-$NH_2$), we identified minor differences in the hard corona proteome of nanoparticles incubated in plasma as well as serum. By comparing the protein pattern for anti-CD63 modified nanoparticles and their isotype counterpart, we found hardly any differences. This suggests that the specific targeting properties of adsorbed anti-CD63 antibodies are not caused by corona proteins.

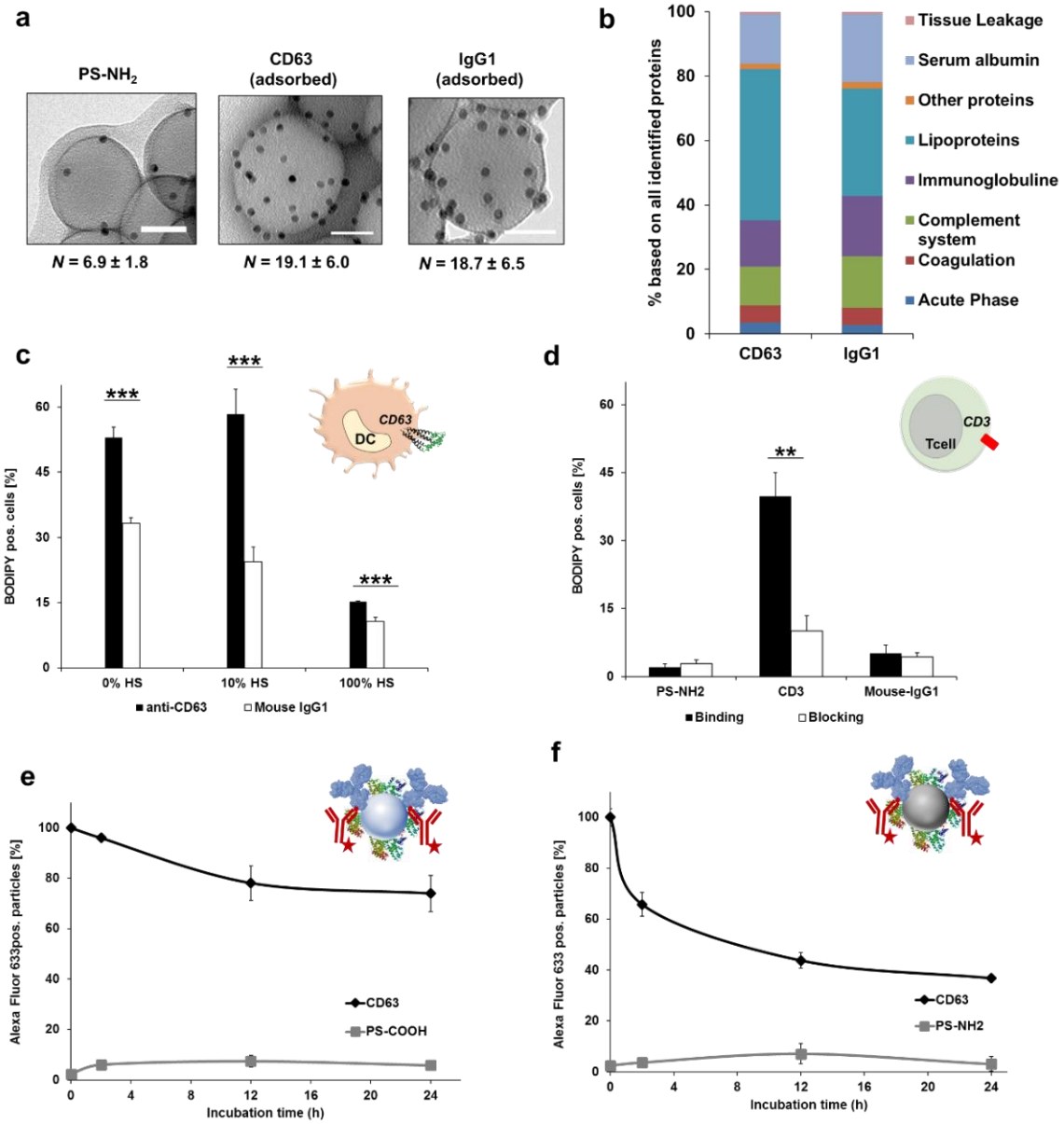


**Figure 8. 4. a,** Immunogold-labelling (12 nm colloidal gold-antibody) of antibody functionalized PS-$NH_2$ nanoparticles. Scale bar: 50 nm [redacted] **b,** LC-MS analysis. Proteins were classified based on their biological function. **c,** Incubation of moDCs with PS-$NH_2$ (9 µg/mL) for 2 h, 37 °C in the presence of different HS concentrations. [redacted] **d,** Incubation of Jurkat T cells with PS-$NH_2$ (25 µg/mL) for 6 h, 4 °C in the presence of HS. In addition, T cells were pre-treated with anti-CD3 for 30 min, 4 °C before nanoparticles were added. **e-f,** Anti-CD63 functionalized nanoparticles PS-COOH and PS-$NH_2$ were incubated with 100% HS for 2 h, 12 h and 24 h. The remaining amount of bound antibodies on the surface was determined by flow cytometry using secondary anti-mouse-IgG antibodies (red). Initial values (time point 0 h) were set as 100%. Data is shown as the amount of Alexa Fluor 633 positive nanoparticles as mean ± s.d of three independent experiments. *$p < 0.05$, **$p < 0.01$, ***$p < 0.001$.

To study the influence of corona formation for amino-functionalized nanoparticles, we visualized (Figure 8.4) and quantified the amount of antibodies on the surface of the nanoparticle before and after serum incubation by TEM and flow cytometry. As shown for PS-COOH, both methods indicate that the corona formation does not hinder accessibility of the anti-CD63 antibodies to the secondary labelled antibodies.

Based on this, we investigated the cellular interaction of anti-CD63 adsorbed on PS-$NH_2$ with dendritic cells and of anti-CD3 with T cells in the presence of proteins (Figure 8.4). Protein adsorption did not affect uptake in 10% HS (Figure 8.4) or even 100% human plasma. In 100% HS uptake was decreased but still significantly better when CD63 was adsorbed **(ii)**.

Adsorption of proteins as a protein corona onto the nanoparticle surface can cause structural alteration to the proteins[39, 45], further exposing epitopes which additionally could interact with targeted cells[3, 39]

To exclude the effect of mistargeting by corona proteins we performed blocking experiments (Figure 8.4). Here, we demonstrated that in the presence of proteins the targeting of the anti-CD3 functionalized nanoparticles is completely eliminated if the CD3 receptor was blocked (Figure 8.4). Additionally, a downregulation of the CD63 antigen on moDCs showed a corresponding decrease in uptake **(iii)**. To further exclude that the targeting properties are not governed by corona proteins (e.g. immunoglobulins[46] or complement proteins[47]), we performed additional receptor blocking experiments.These results proved that the targeting is undoubtedly based on the antigen binding part of the antibody, which is located on the two F(ab) regions **(iv)**. Finally, we checked to see if the adsorbed targeting anti-CD63 antibody was replaced over time (Figure 8.4) by other adsorbing corona proteins **(v)**. We were able to detect 80% of the initial antibody after 24 h for the PS-COOH nanoparticle and at least 40% for the PS-$NH_2$ nanoparticle (Figure 8.4). This is in line with the higher influence of 100% HS for CD63 adsorbed on PS-$NH_2$ (Figure 8.4) versus the PS-COOH (Figure 8.2). Additionally, cell uptake experiments confirmed that the specific targeting effect of adsorbed anti-CD63 nanoparticles is functional even after 12 h of serum incubation. Bringing the *in vitro* studies closer to *in vivo* situations[48], functionalized nanoparticles were introduced to whole blood with all cells and components. There was no replacement of targeting antibody from the nanoparticle surface.

## Conclusions

Here, we demonstrate that antibody modifications of nanocarriers by adsorption can be a valid and unexpectedly robust method of nanocarrier functionalization. Modification of particles by adsorption should be analysed under different buffer conditions to achieve optimal results, especially when being exposed to complex protein environments. We also foresee that

chemical coupling needs to and will evolve more sophisticated methods to attach biomolecules in a more controlled way on the surface of nanocarriers.

## Supplementary information

**Table 8. 1.** Characterization of unfunctionalized nanoparticles. The average size of the different nanoparticles was measured with a PSS Nicomp particle sizer. ζ-potential measurements were performed on a Malvern Instruments Zeta Nanosizer. Mean values ± s.d. from three meausrements are given. [redacted]

| | Name | Material | Functionalization | $D_h$ in nm | ζ-potential in mV |
|---|---|---|---|---|---|
| **A** | PS-COOH | Polystyrene, magnetic core | Carboxylic Acid | 230 ± 140 | - 72 ± 6 |
| **B** | PS-$NH_2$ | Polystyrene | Amino | 150 ± 15 | +4 ± 1 |
| **C** | HES | Hydroxyethyl starch | - | 460 ± 50 | -7 ± 1 |

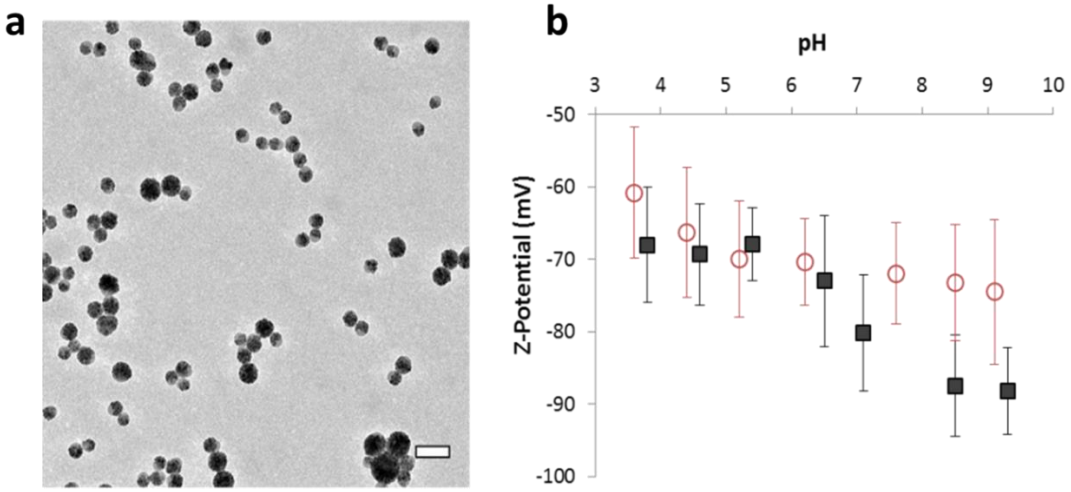


**Figure 8. 5. a,** Transmission electron micrograph of hybrid poly(styrene-*co*-acrylic acid)/magnetite nanocomposites (scale bar 200 nm). **b,** Deprotonation of the carboxylic acid moieties present on the particles surface was followed by ζ-potential measurements (black solid squares). For comparison, the ζ-potential profile at different pH values for unfunctionalized polystyrene / magnetite nanoparticles is shown in the plot (open red circles). Mean values ± s.d. from three meausrements are given. (performed by [redacted]

**Table 8. 2.** Characterization of PS-COOH nanoparticles (A) after incubation with 100% plasma and serum. ζ-potential measurements were performed on a Malvern Instruments Zeta Nanosizer. Mean values ± s.d. from three meausrements are given.

| Sample | Functionalization | Serum ζ-potential in mV | Plasma ζ-potential in mV |
|---|---|---|---|
| **A1** | Carboxylic acid | -17.0 ± 1.2 | -22.2 ± 0.5 |
| **A2** | NHS Ester | -18.0 ± 0.6 | -20.0 ± 0.9 |
| **A3a** | CD63 (covalent) | -18.0 ± 1.0 | -20.6 ± 1.2 |
| **A3b** | CD63 (adsorbed) | -14.0 ± 1.9 | -14.5 ± 1.4 |
| **A4a** | IgG (covalent) | -18.5 ± 0.2 | -18.7 ± 1.1 |
| **A4b** | IgG (adsorbed) | -14.9 ± 0.8 | -17.8 ± 0.5 |

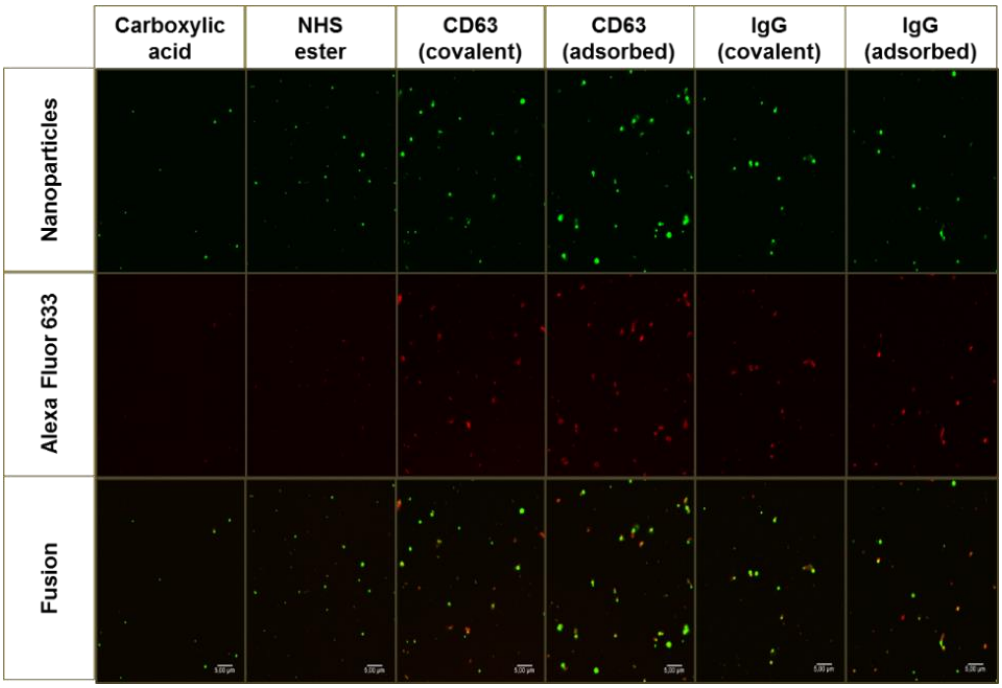


**Figure 8. 6.** Alexa Fluor 633 anti-mouse antibodies were incubated for 30 min with 0.4 µg PS-COOH nanoparticles. Visualization of antibody binding was executed via cLSM imaging. The median fluorescence intensity (MFI) was determined by cLSM images shown above and quantified via ImageJ. Data is represented as the mean ± s.d. of 80 events and shown in Fig. 1d. [redacted]

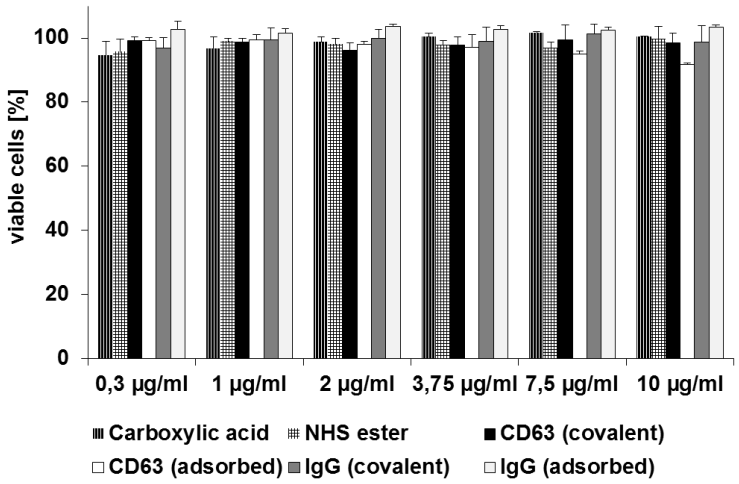


**Figure 8. 7.** Cytotoxicity assay of nanoparticles at different concentrations in moDCs. Nanoparticles (0.3, 1, 2, 20, 3.75, 7.5 or 10 µg/mL) were incubated for 24 h under standard conditions. Cytotoxicity was determined by PI staining (2 µg/mL) whereas incubation without nanoparticles was defined as 100% viable. [redacted]

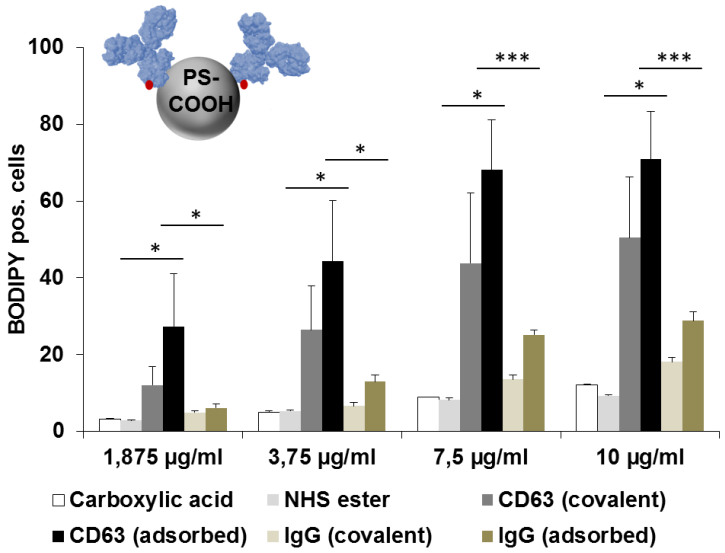


**Figure 8. 8.** Anti-CD63 functionalization significantly enhances uptake in moDCs. MoDCs were treated with nanoparticle concentrations (1.875, 3.75, 7.5 and 10 µg/mL) for 2 h, 37 °C in standard cell culture medium and cellular uptake was analyzed by flow cytometry. [redacted]

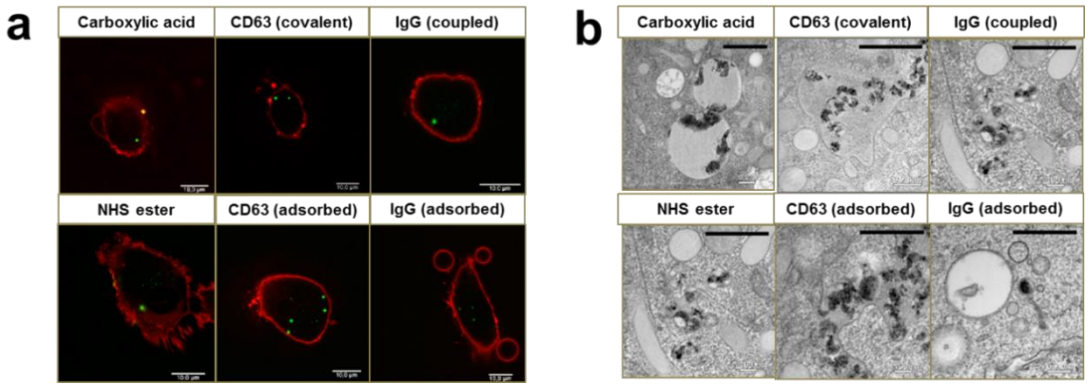


**Figure 8. 9.** 7.5 µg/mL nanoparticles (PS-COOH) were incubated for 2 h with moDCs under standard conditions. **a,** Confocal analysis. After detachment of cells and seeding in microscopy chambers, moDCs were stained with Cellmask Orange™ to label the cell membrane (red). Fluorescence signal of nanoparticles is displayed in green. Scale bar: 10 µm. (performed by Manuel Tonigold) **b,** TEM pictures of cells were analyzed after fixation by high pressure freezing. Scale bar: 0.5 µm. [redacted]

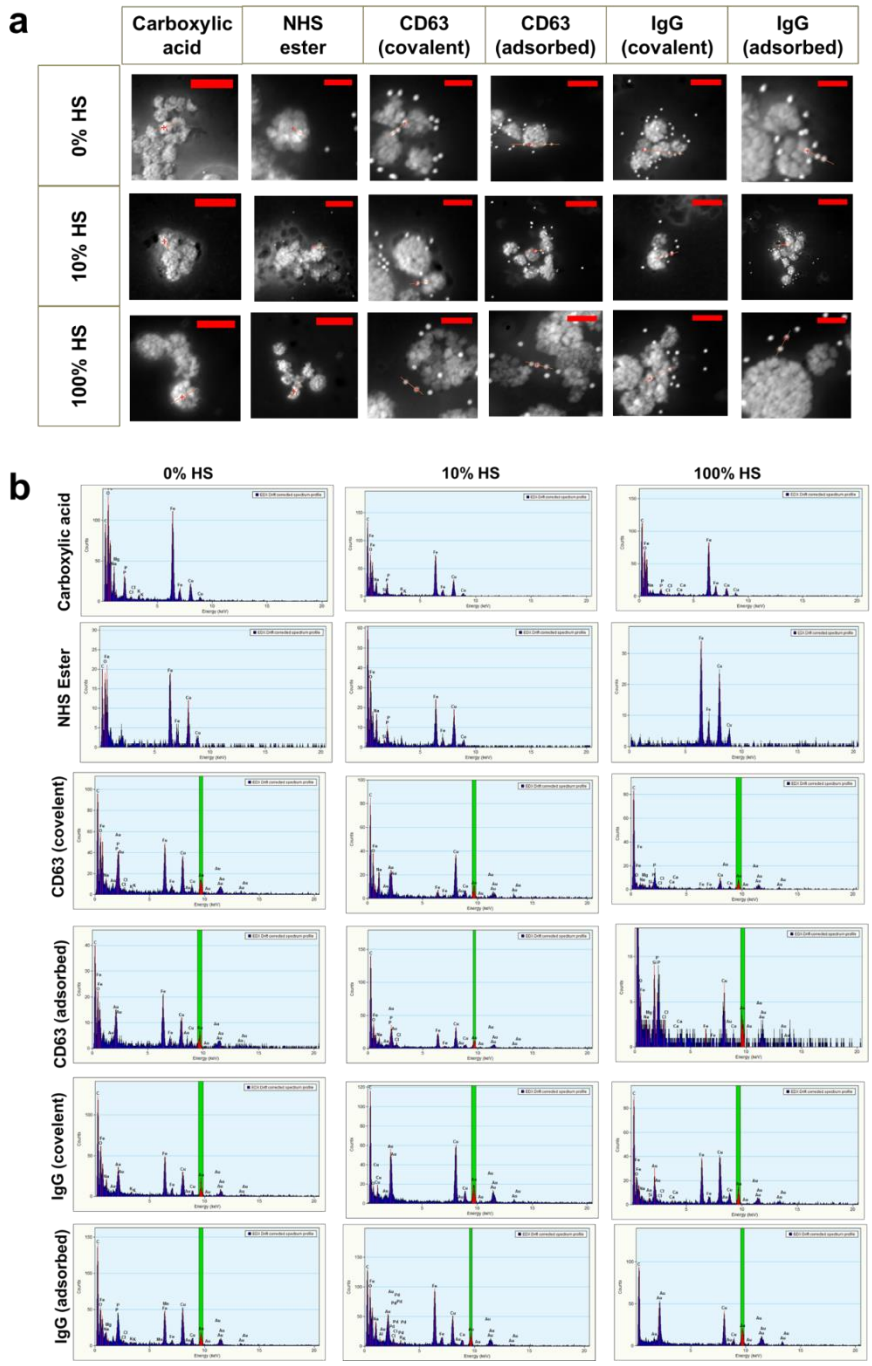


**Figure 8. 10**. IgG antibodies on the surface were labelled with secondary gold-coupled antibodies (12 nm colloidal gold-antibody) after incubation with different amounts of HS. Gold counts on the red line at STEM pictures **(a)** were determined by EDX **(b).** Scale bar: 50 nm. [redacted]

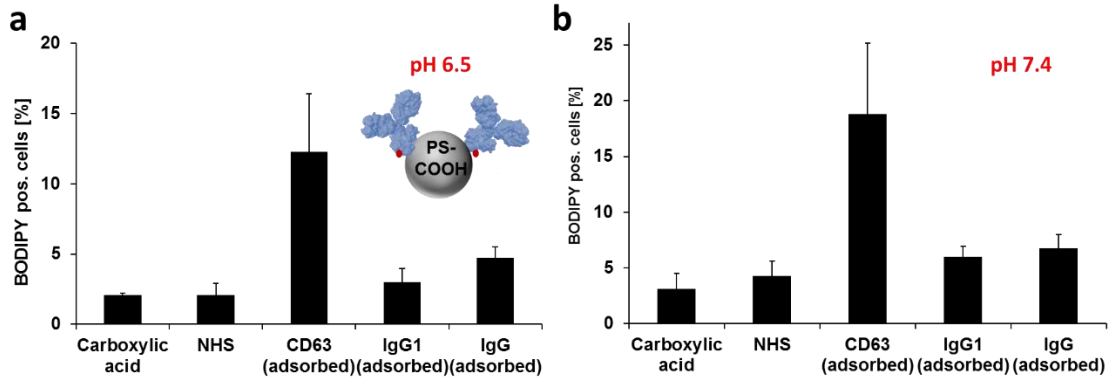


**Figure 8. 11.** Effective targeting even at lower pH as it is present in tumor tissue. The pH of the cell culture medium was adjusted to pH 6.5. MoDCs were either kept in culture medium (pH 7.4) or low pH medium (pH 6.5) and incubated with nanoparticles (5 µg/mL) for 2 h at 4 °C.

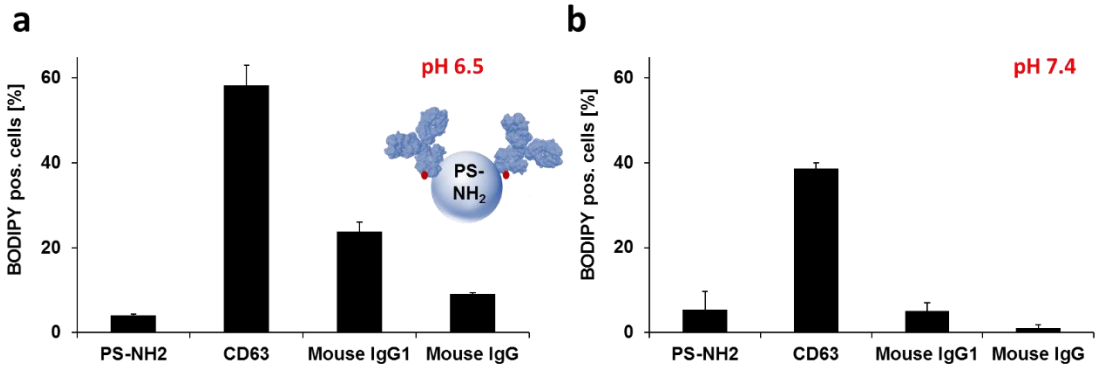


**Figure 8. 12.** Effective targeting even at lower pH as it is present in tumor tissue. The pH of the cell culture medium was adjusted to pH 6.5. MoDCs were either kept in regular cell culture medium (pH 7.4) or low pH medium (pH 6.5) and incubated with nanoparticles (25 µg/mL) for 2 h at 37 °C.

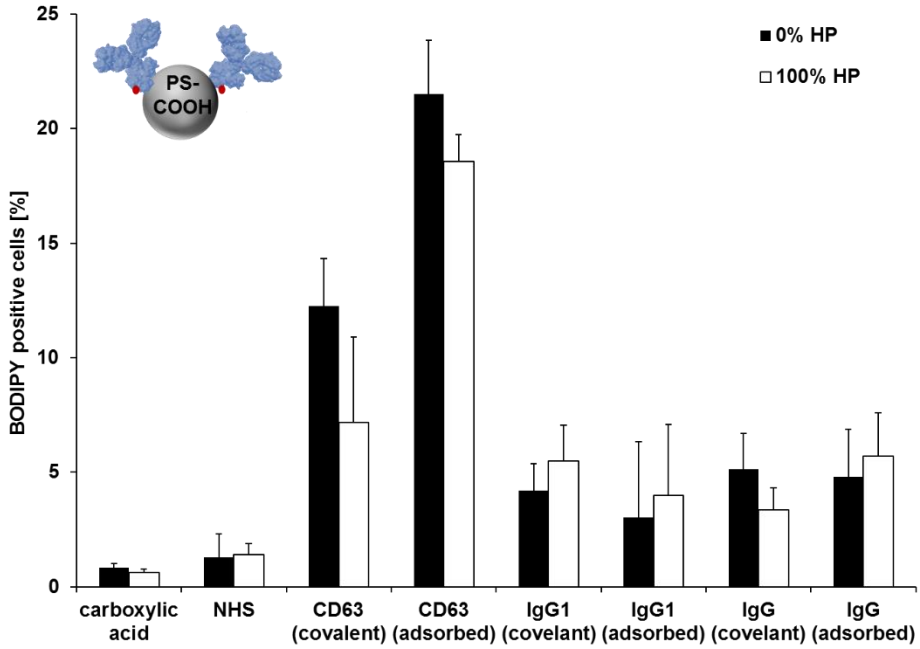


**Figure 8. 13.** Human plasma (HP) does not affect the targeting ability of CD63 adsorbed PS-COOH nanoparticles. Nanoparticles (5 µg/mL) were pre-treated with 100% human plasma (HP) and incubated with moDCs for 2 h at 4 °C.

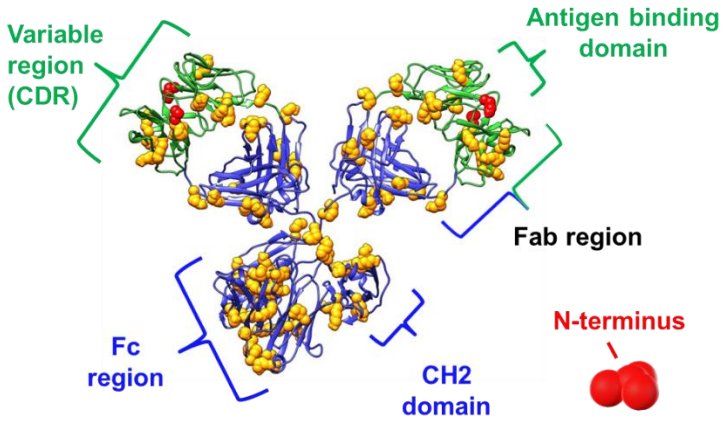


**Figure 8. 14.** 3D-Structure of IgG1 highlighting the distribution of lysine residues (yellow) and the N-terminus (red)[26]. Chimera 1.11.2 was used as software tool. The F(c) parts contains 36 lysine residues whereas the F(ab) part consists 50 lysine residues. The N-terminus (red) is located within the F(ab) region (green). [redacted]

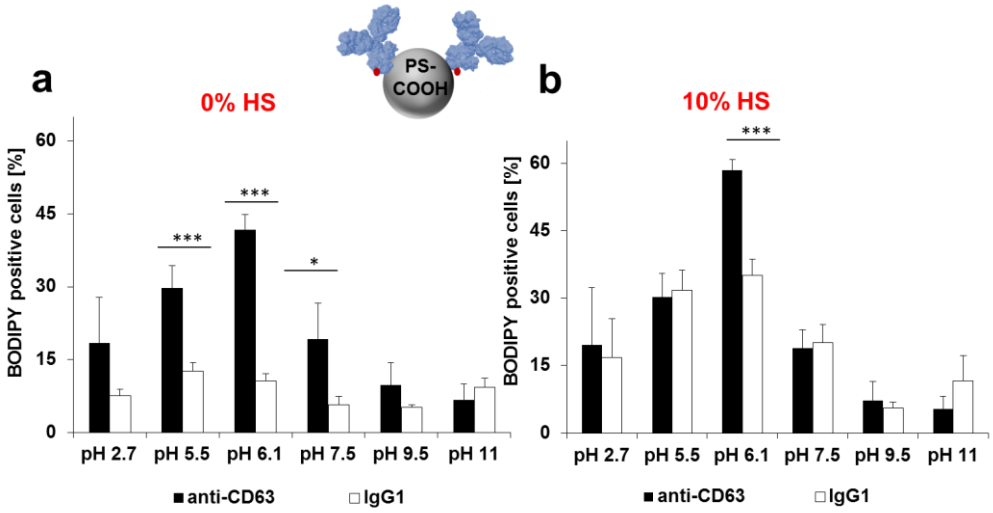


**Figure 8. 15**. Different buffer conditions during antibody modification enhance uptake in moDCs. 100,000 moDCs were treated with 7.5 µg/mL PS-COOH polystyrene particles for 2 h under standard conditions. Human serum (HS) dependence was determined by using different HS concentrations (**a,** 0% and **b,** 10%) during incubation. Binding of particles was analyzed by flow cytometry at which dead cells were excluded by PI staining. [redacted]

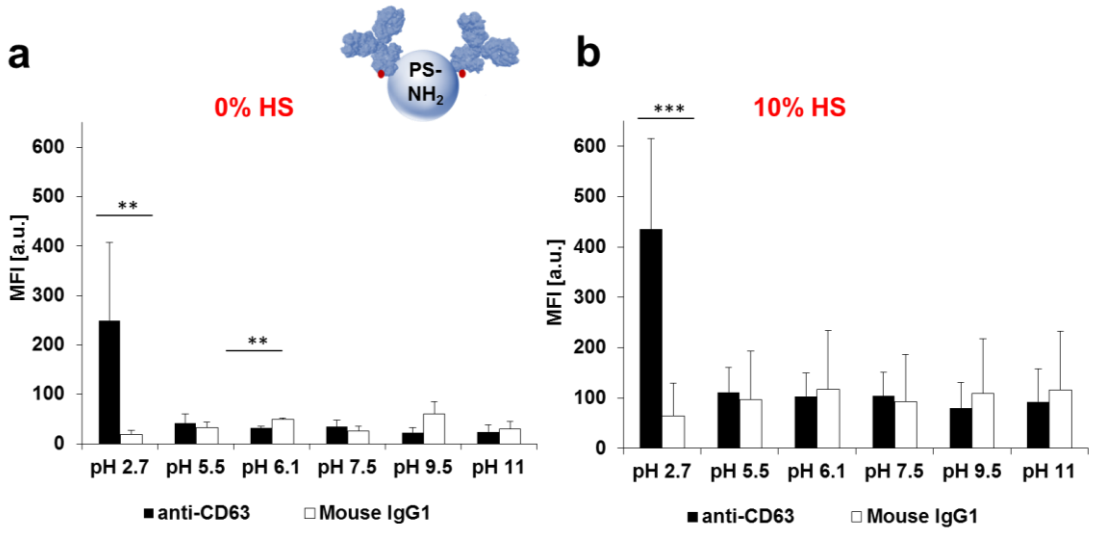


**Figure 8. 16.** Different buffer conditions during antibody modification enhance uptake in moDCs. 100,000 moDCs were treated with 9 µg/mL PS-$NH_2$ polystyrene particles for 2 h under standard conditions. HS dependence was determined by using different HS concentrations (a, 0% and b, 10%) during incubation. [redacted]

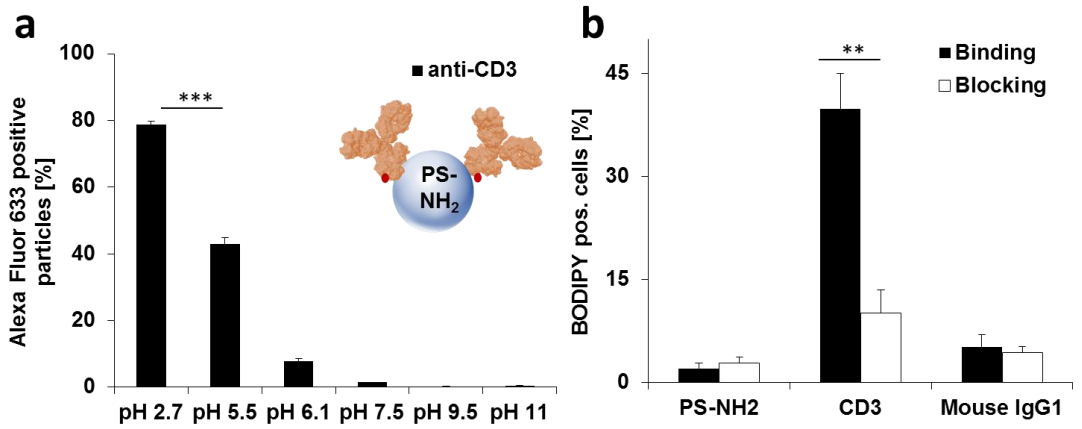


Figure 8. 17. **a,** Amino-functionalized nanoparticles (0.4 µg) were incubated with anti-CD3 antibodies at different pH values. The amount of bound mouse anti-CD3 was determined by flow cytometry using polyclonal fluorescent mouse IgG antibodies (%) and values are given as mean ± s.d. of three independent experiments**. b,** Targeting of CD3 on the surface of T cells. Jurkat cells were treated with nanoparticles (25 µg/mL) for 6 h, 4 °C in the presence of human serum. *For blocking studies:* Jurkat cells were pre-treated with anti-CD3 (25 µg/mL) for 30 min, 4 °C before nanoparticles were added.

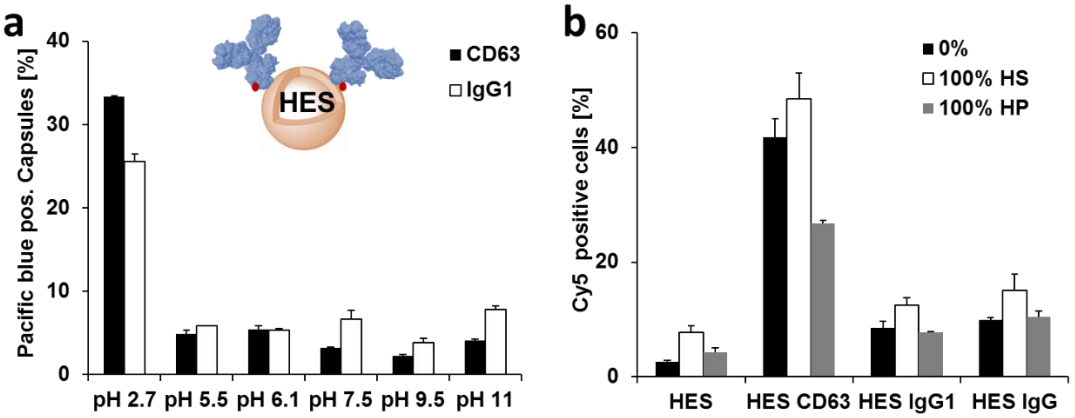


**Figure 8. 18.** Extending the investigated nanoparticle system. **a,** Biodegradable hydroxyethyl starch (HES) nanocapsules (0.4 µg) were functionalized with anti-CD63 antibodies at different pH values. The amount of bound mouse IgG was determined by flow cytometry (%) using polyclonal fluorescent mouse IgG antibodies. [redacted] **b,** Nanocapsules (5 µg/mL) were treated with 100% human serum (HS) or 100% human plasma (HP) and further incubated with moDCs for 2 h, 4 °C.

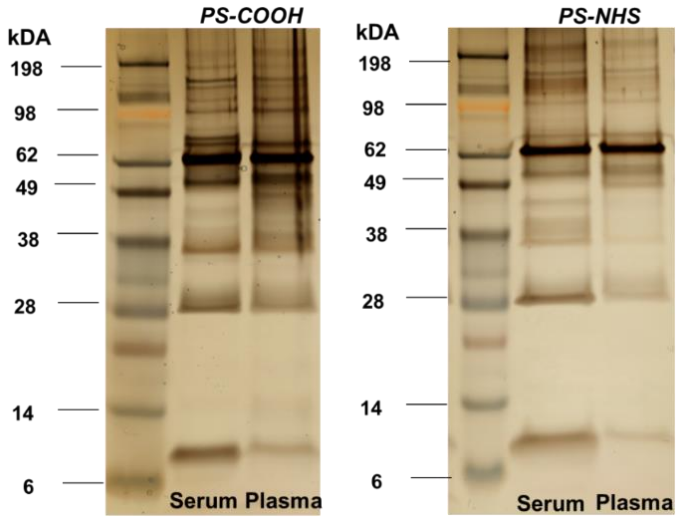


**Figure 8. 19.** SDS-PAGE: For protein corona analysis: Nanoparticles were incubated with 100% human serum or 100% human plasma for 2 h, isolated via centrifugation and washed three times to remove unbound proteins. Hard corona proteins were desorbed from the particles using 2% SDS, separated by SDS-PAGE and stained with a Silver Staining Kit.

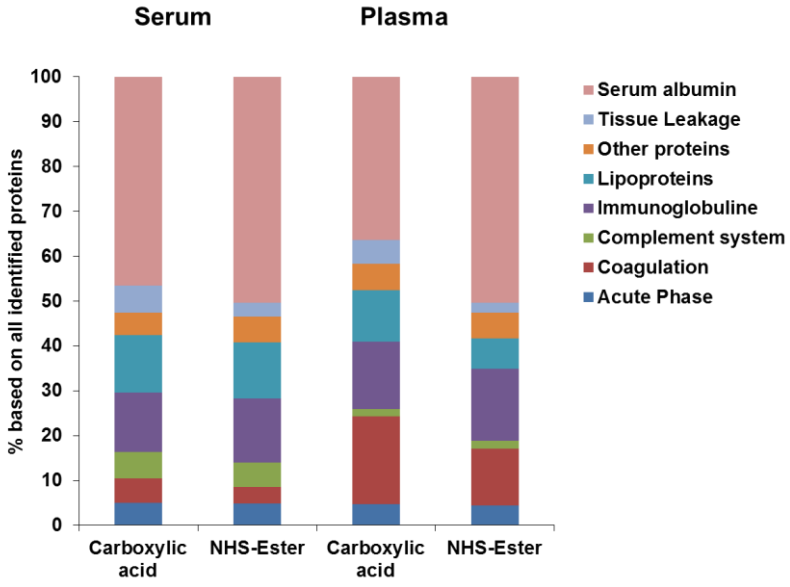


**Figure 8. 20.** LC-MS Analysis. Protein classification of hard corona proteins. Proteins were digested, analyzed by LC-MS as described in the supplementary methods and classified based on their biological function. Values are expressed in % based on the total amount of all identified proteins and the mean ± s.d of two technical replicates was calculated.

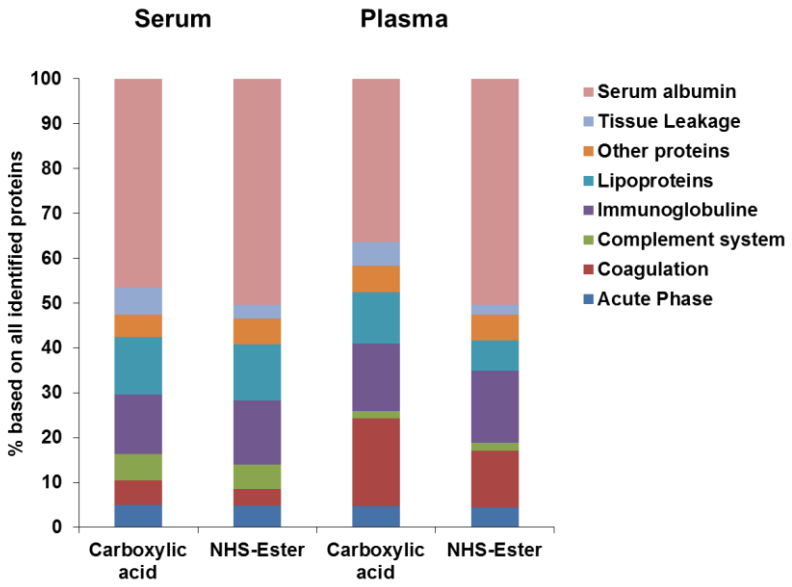


**Figure 8. 21.** LC-MS Analysis. Protein classification of hard corona proteins. Proteins were digested, analyzed by LC-MS as described in the methods section below and classified based on their biological function. Values are expressed in % based on the total amount of all identified proteins calculated from the average of two technical replicates.

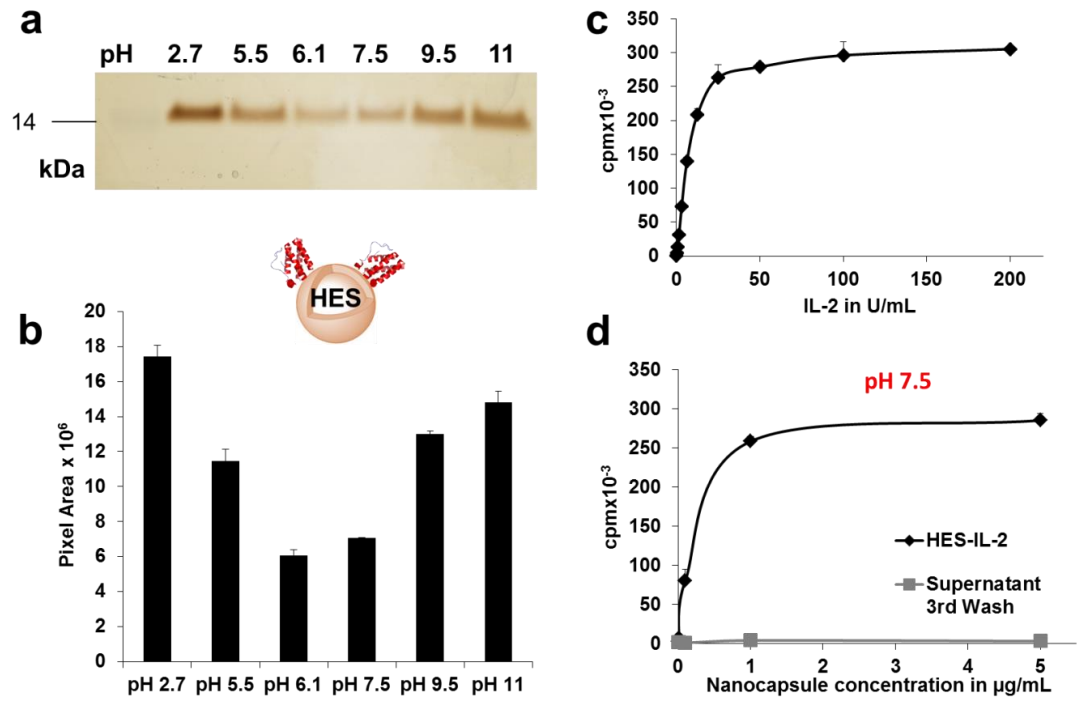


**Figure 8. 22.** Adsorption of IL-2 towards HES nanocapsules. **a-b,** Adsorption as a pH dependent process. The supernatant after the first centrifugation was visualized by SDS-PAGE, quantitatively analyzed via ImageJ and expressed in Pixel Area x $10^6$. Values are given as mean ± s.d. of three

measurements. c, IL-2 reference titration on IL-2 dependent murine CTLL-2 cells. Proliferation was measured by [$^3$H]-thymidine incorporation. Counts per minute (cpm) were plotted against the IL-2 concentration. d, Titration of HES-IL-2 (Adsorption pH 7.5) titration (0.001 – 5 µg/mL) and the supernatant after 3$^{rd}$ wash on CTLL-2 cells. We observed a strong dose-dependent proliferation for HES-IL-2 treated cells in comparison to cells treated with the supernatant of the final wash (3$^{rd}$ wash). This indicates a successful functionalization of HES nanocapsules with biological active IL-2. **c-d,** Values are expressed as mean ± s.d. of three independent experiments. [redacted]

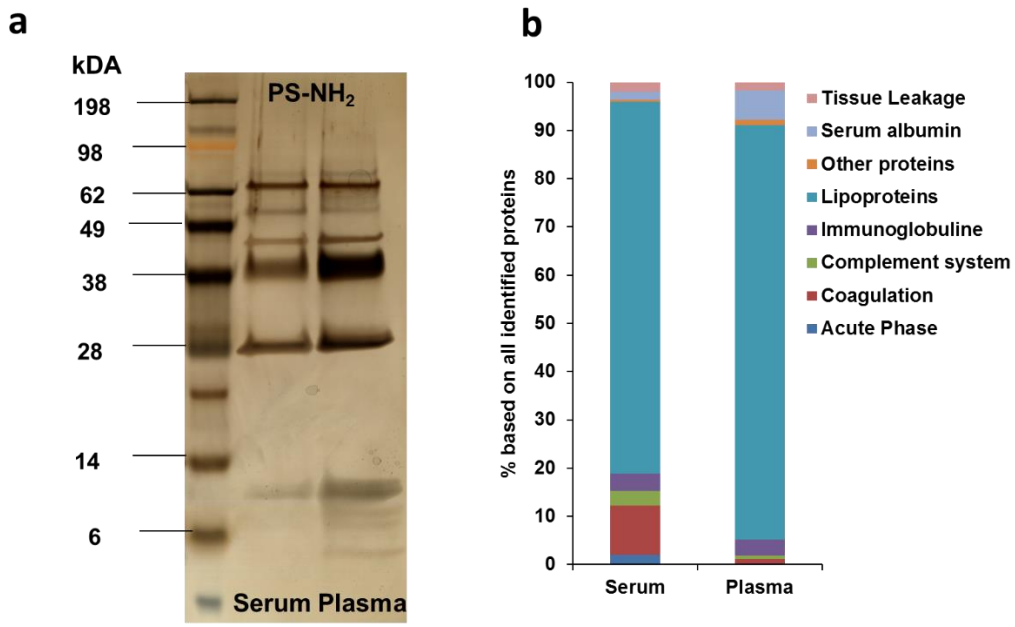


**Figure 8. 23.** Hard corona proteins were desorbed from the particles using 2% SDS, separated by SDS-PAGE **(a)** and stained with a Silver Staining Kit. Further LC-MS **(b)** analysis reveals the distinct protein pattern. Proteins were classified based on their biological function.

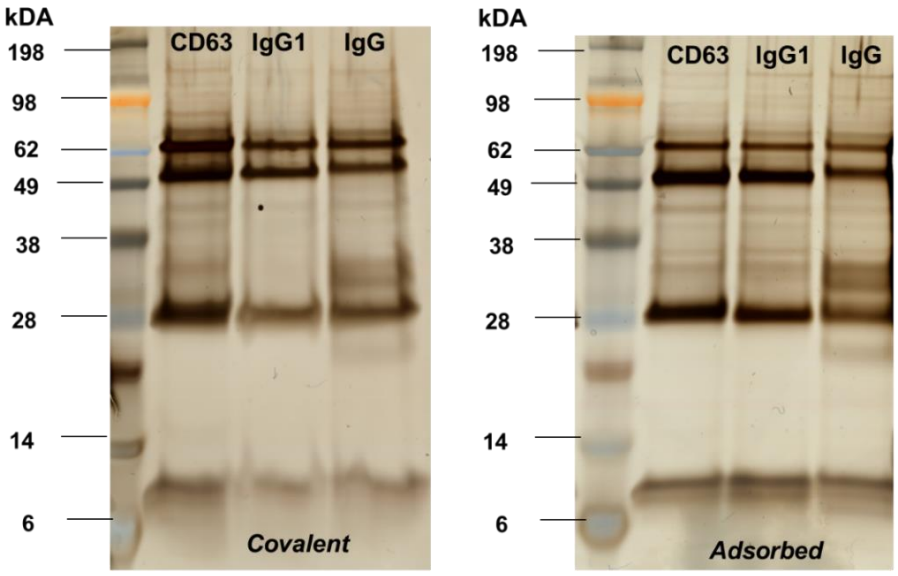


**Figure 8. 24.** Adsorbed and covalent functionalized PS-COOH nanoparticle share a similar protein corona. Hard corona proteins were desorbed from the particles using 2% SDS, separated by SDS-PAGE and stained with a Silver Staining Kit.

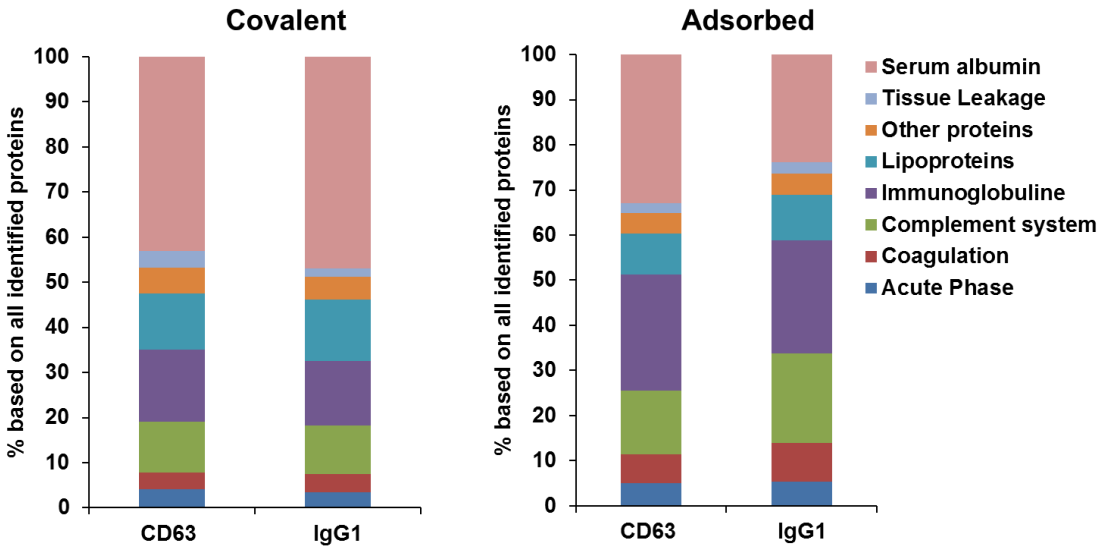


**Figure 8. 25.** LC-MS Analysis. Protein classification of hard corona proteins. Proteins were classified based on their biological function. Values are expressed in % based on the total amount of all identified proteins calculated from the average of two technical replicates.

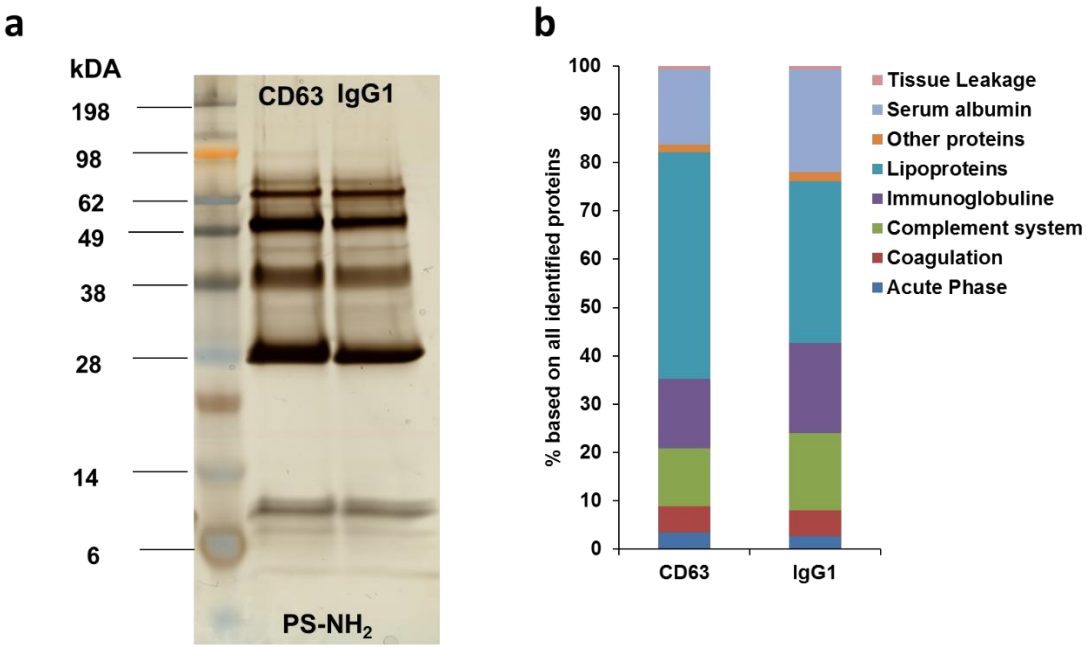


**Figure 8. 26. a,** SDS-PAGE: Nanoparticles were incubated with 100% serum for 2 h, isolated via centrifugation and washed three times to remove unbound proteins. **b,** LC-MS. Proteins were classified based on their biological function. Values are expressed in % based on the total amount of all identified proteins calculated from the average of two technical replicates.

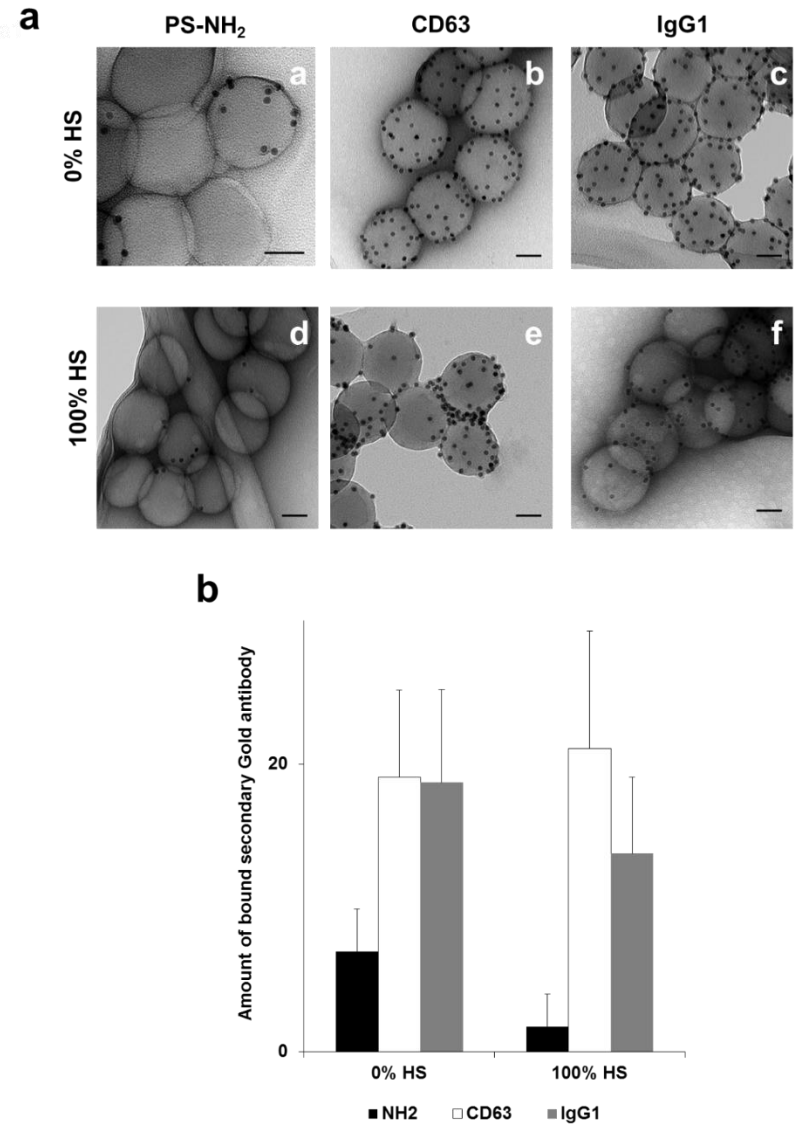


**Figure 8. 27. a,** Adsorbed antibodies are not hidden by the presence of the protein corona. a, TEM images of anti-CD63 functionalized PS-$NH_2$ were labelled with secondary gold-coupled antibodies (12 nm colloidal gold-antibody) before and after serum exposure. Scale bar: 50 nm **b,** Statistical analysis of the absolute amount of gold particles counted on the surface of nanoparticles. An average number of n=50 nanoparticles were analyzed for each condition. Values are expressed as mean ± s.d. [redacted]

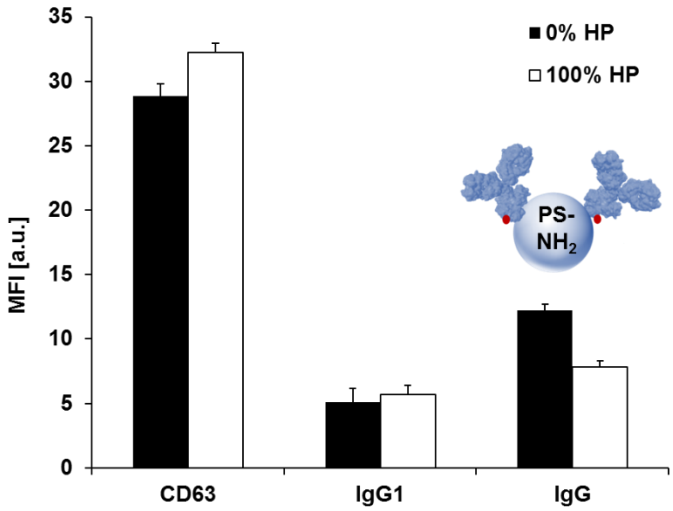


**Figure 8. 28.** Nanoparticles (25 µg/mL) were pre-treated with 100% human plasma (HP) and incubated with moDCs for 2 h at 4 °C. The median fluorescence intensity (MFI) was determined by flow cytometry.

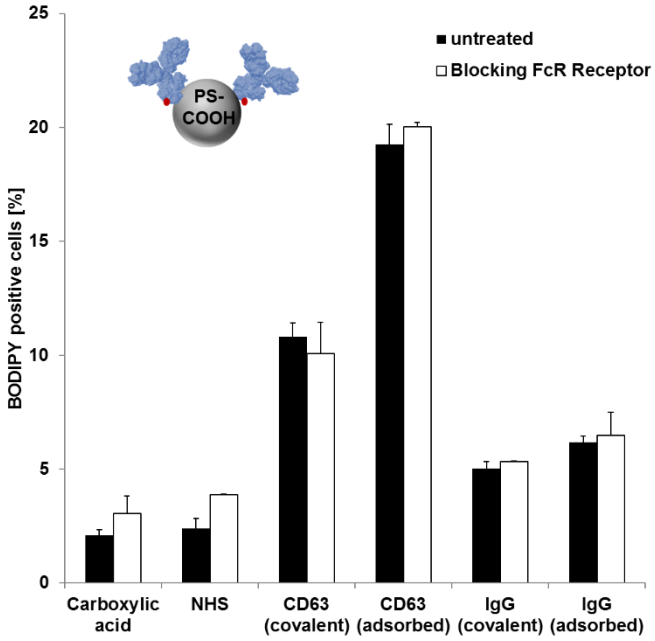


**Figure 8. 29.** MoDCs were pre-incubated with FcR blockings solution according to the manufactures´ instruction (Biolegend). Nanoparticles (5 µg/mL) were incubated with 100% HS for 2 h, 37 °C and subsequently added to moDCs for 2 h at 4 °C. The blocking solution was kept in the cell culture medium to ensure an efficient blocking during the incubation of nanoparticles and cells.

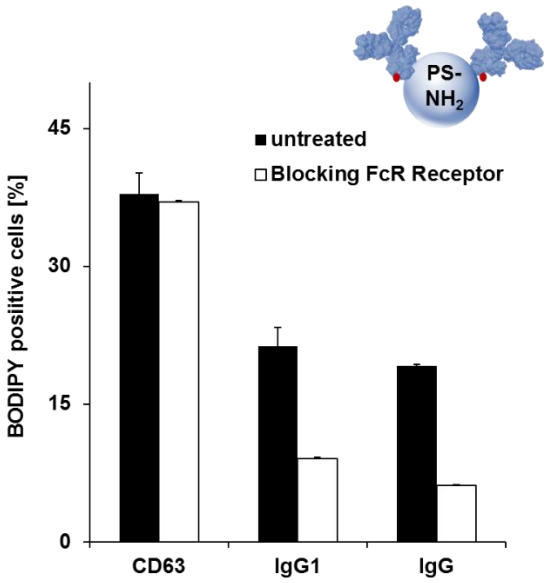


**Figure 8. 30.** Blocking FcR receptor does reduce cellular binding of CD63 modified PS-$NH_2$. Nanoparticles were incubated with 100% human serum for 2 h, 37 °C and subsequently added to moDCs for 2 h at 4 °C (10 µg/mL).

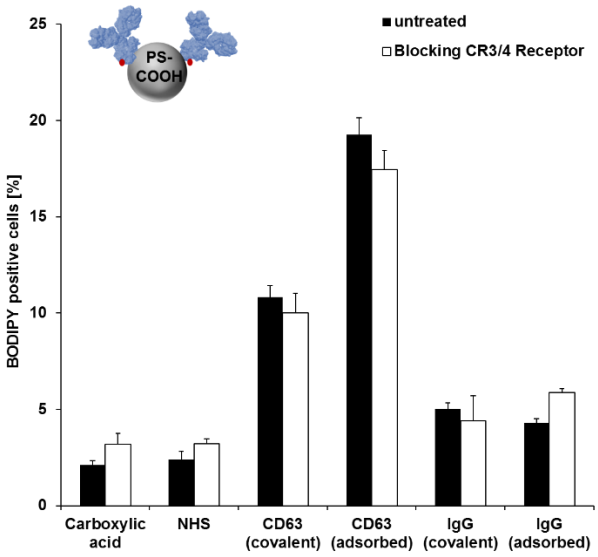


**Figure 8. 31.** Blocking complement receptor (CR3/4) does not prevent cellular binding of CD63 modified PS-COOH. As complement factors are found in the protein corona we pre-incubated MoDCs with CD11b/CD11c blocking antibodies (100 µg/mL, 30 min, 4 °C)[57]. Nanoparticles were incubated with 100% human serum for 2 h, 37 °C and subsequently added to moDCs for 2 h at 4 °C (5 µg/mL).

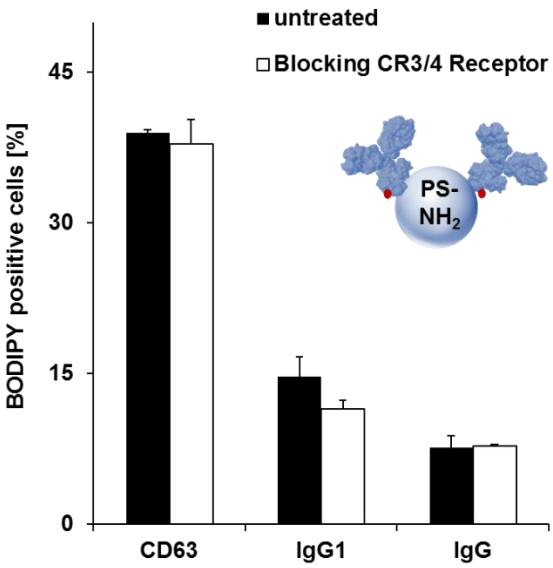


**Figure 8. 32**. MoDCs were pre-incubated with CD11b/CD11c (100 µg/mL, 30 min, 4 °C)[57]. Nanoparticles were incubated with 100% human serum for 2 h, 37 °C and subsequently added to moDCs for 2 h at 4 °C (10 µg/mL).

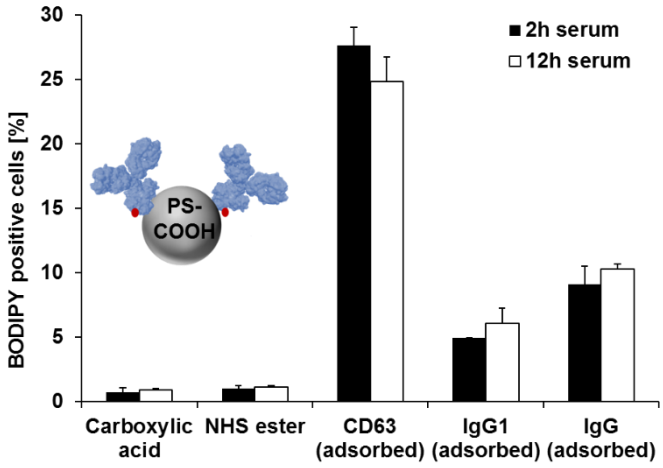


**Figure 8. 33.** PS-COOH (5 µg/mL) were incubated with 100% human serum for 2 h or 12 h and further added to moDCs for 2 h, at 4 °C.

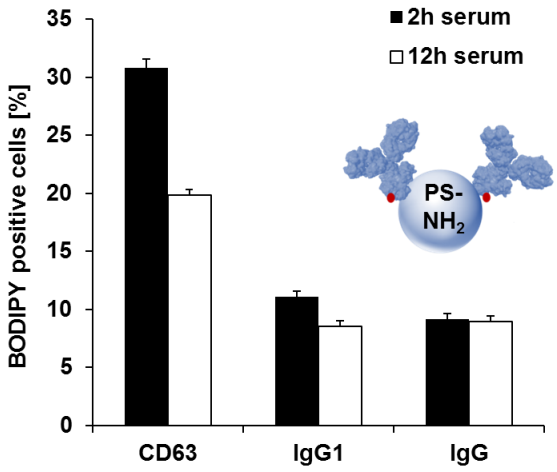


**Figure 8. 34.** Antibodies are not exchanged over time by other proteins and do not lose their targeting ability. PS-$NH_2$ (25 µg/mL) were incubated with 100% human serum for 2 h or 12 h and further added to moDCs for 2 h, at 37 °C.

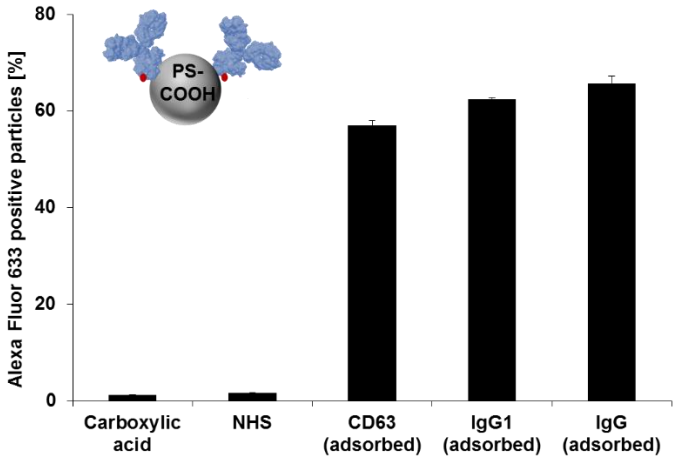


**Figure 8. 35**. PS-COOH (1 mg) were directly introduced to human blood (1 mL) and incubated for 2 h. Nanoparticles were magnetically isolated and washed three times with PBS. The remaining amount of bound antibodies was identified using secondary mouse IgG antibodies (%).

# Literature


1. Cheng, C. J.; Tietjen, G. T.; Saucier-Sawyer, J. K.; Saltzman, W. M., A holistic approach to targeting disease with polymeric nanoparticles. *Nat. Rev. Drug. Discov.* **2015,** *14* (4), 239-247.

2. Blanco, E.; Shen, H.; Ferrari, M., Principles of nanoparticle design for overcoming biological barriers to drug delivery. *Nature Biotech.* **2015,** *33*, 941-951.

3. Zyuzin, M. V.; Yan, Y.; Hartmann, R.; Gause, K. T.; Nazarenus, M.; Cui, J.; Caruso, F.; Parak, W. J., Role of the Protein Corona Derived from Human Plasma in Cellular Interactions between Nanoporous Human Serum Albumin Particles and Endothelial Cells. *Bioconj. Chem.* **2017,** *28* (8), 2062-2068.

4. Carter, T.; Mulholland, P.; Chester, K., Antibody-targeted nanoparticles for cancer treatment. *Immunotherapy* **2016,** *8* (8), 941-958.

5. Puertas, S.; Batalla, P.; Moros, M.; Polo, E.; del Pino, P.; Guisán, J. M., Taking advantage of unspecific interactions to produce highly active magnetic nanoparticle-antibody conjugates. *ACS Nano* **2011,** *5*, 4521-4528.

6. Dai, Q.; Bertleff-Zieschang, N.; Braunger, J. A.; Björnmalm, M.; Cortez-Jugo, C.; Caruso, F., Particle Targeting in Complex Biological Media. *Adv. Healthc. Mater.* **2017**.

7. Kocbek, P.; Obermajer, N.; Cegnar, M.; Kos, J.; Kristl, J., Targeting cancer cells using PLGA nanoparticles surface modified with monoclonal antibody. *J. Control. Release* **2007,** *120* (1), 18-26.

8. Monopoli, M. P.; Aberg, C.; Salvati, A.; Dawson, K. A., Biomolecular coronas provide the biological identity of nanosized materials. *Nature Nanotech.* **2012,** *7* (12), 779-86.

9. Salvati, A.; Pitek, A. S.; Monopoli, M. P.; Prapainop, K.; Bombelli, F. B.; Hristov, D. R.; Kelly, P. M.; Åberg, C.; Mahon, E.; Dawson, K. A., Transferrin-functionalized nanoparticles lose their targeting capabilities when a biomolecule corona adsorbs on the surface. *Nature Nanotech.* **2013,** *8* (2), 137-143.

10. Schöttler, S.; Becker, G.; Winzen, S.; Steinbach, T.; Mohr, K.; Landfester, K.; Mailander, V.; Wurm, F. R., Protein adsorption is required for stealth effect of poly(ethylene glycol)- and poly(phosphoester)-coated nanocarriers. *Nature Nanotech.* **2016**.

11. Zangar, R. C.; Daly, D. S.; White, A. M., ELISA microarray technology as a high-throughput system for cancer biomarker validation. *Expert Rev. Proteomics.* **2006,** *3* (1), 37-44.

12. Dai, Q.; Yan, Y.; Guo, J.; Björnmalm, M.; Cui, J.; Sun, H.; Caruso, F., Targeting Ability of Affibody-Functionalized Particles Is Enhanced by Albumin but Inhibited by Serum Coronas. *ACS Macro Lett.* **2015,** *4* (11), 1259-1263.

13. Dai, Q.; Yan, Y.; Ang, C. S.; Kempe, K.; Kamphuis, M. M.; Dodds, S. J.; Caruso, F., Monoclonal antibody-functionalized multilayered particles: targeting cancer cells in the presence of protein coronas. *ACS Nano* **2016,** *9* (3), 2876-2885.

14. Kang, B.; Okwieka, P.; Schöttler, S.; Winzen, S.; Langhanki, J.; Mohr, K.; Opatz, T.; Mailänder, V.; Landfester, K.; Wurm, F. R., Carbohydrate-Based Nanocarriers Exhibiting Specific Cell Targeting with Minimum Influence from the Protein Corona. *Angew. Chem. Int. Ed.* **2015**.

15. Ju, Y.; Dai, Q.; Cui, J.; Dai, Y.; Suma, T.; Richardson, J. J.; Caruso, F., Improving Targeting of Metal-Phenolic Capsules by the Presence of Protein Coronas. *ACS applied materials & interfaces* **2016,** *8* (35), 22914-22.

16. Mirshafiee, V.; Mahmoudi, M.; Lou, K.; Cheng, J.; Kraft, M. L., Protein corona significantly reduces active targeting yield. *Chem. Commun.* **2013,** *49* (25), 2557-2559.

17. Zarschler, K.; Prapainop, K.; Mahon, E.; Rocks, L.; Bramini, M.; Kelly, P.; Stephan, H.; Dawson, K., Diagnostic nanoparticle targeting of the EGF-receptor in complex biological conditions using single-domain antibodies. *Nanoscale* **2014,** *6* (11), 6046-6056.

18. Ritz, S.; Schöttler, S.; Kotman, N.; Baier, G.; Musyanovych, A.; Kuharev, J. r.; Landfester, K.; Schild, H. r.; Jahn, O.; Tenzer, S.; Mailander, V., Protein Corona of Nanoparticles: Distinct Proteins Regulate the Cellular Uptake. *Biomacromolecules* **2015,** *16* (4), 1311-1321.

19. Caracciolo, G.; Palchetti, S.; Colapicchioni, V.; Digiacomo, L.; Pozzi, D.; Capriotti, A. L.; La Barbera, G.; Laganà, A., Stealth effect of biomolecular corona on nanoparticle uptake by immune cells. *Langmuir* **2015,** *31* (39), 10764-10773.

20. Behzadi, S.; Serpooshan, V.; Tao, W.; Hamaly, M. A.; Alkawareek, M. Y.; Dreaden, E. C.; Brown, D.; Alkilany, A. M.; Farokhzad, O. C.; Mahmoudi, M., Cellular uptake of nanoparticles: journey inside the cell. *Chemical Society reviews* **2017,** *46* (14), 4218-4244.

21. Ring, S.; Maas, M.; Nettelbeck, D. M.; Enk, A. H.; Mahnke, K., Targeting of autoantigens to DEC205(+) dendritic cells in vivo suppresses experimental allergic encephalomyelitis in mice. *J. Immunol.* **2013,** *191* (6), 2938-47.

22. Hofmann, D.; Tenzer, S.; Bannwarth, M. B.; Messerschmidt, C.; Glaser, S.-F.; Schild, H.; Landfester, K.; Mailaender, V., Mass Spectrometry and Imaging Analysis of Nanoparticle-Containing Vesicles Provide a Mechanistic Insight into Cellular Trafficking. *ACS Nano* **2014,** *8* (10), 10077-10088.

23. Mantegazza, A. R.; Barrio, M. M.; Moutel, S.; Bover, L.; Weck, M.; Brossart, P.; Teillaud, J.-L.; Mordoh, J., CD63 tetraspanin slows down cell migration and translocates to the endosomal-lysosomal-MIICs route after extracellular stimuli in human immature dendritic cells. *Blood* **2004,** *104* (4), 1183-1190.

24. Ramirez, L. P.; Landfester, K., Magnetic Polystyrene Nanoparticles with a High Magnetite Content Obtained by Miniemulsion Processes. *Macromol. Chem. Phys.* **2003,** *204*, 22-31.

25. Helenius, A.; Mellman, I., Glycoproteins of the Lysosomal Membrane. *J. Cell Biol.* **1985,** *100*.

26. Harris, L. J.; Skaletsky, E.; McPherson, A., Crystallographic structure of an intact IgG1 monoclonal antibody. *J. Mol. Biol.* **1998,** *275* (5), 861-872.

27. Mizuhara, T.; Saha, K.; Moyano, D. F.; Kim, C. S.; Yan, B.; Kim, Y. K.; Rotello, V. M., Acylsulfonamide-Functionalized Zwitterionic Gold Nanoparticles for Enhanced Cellular Uptake at Tumor pH. *Angew. Chem. Int. Ed.* **2015,** *54* (22), 6567-6570.

28. Kelly, P. M.; Aberg, C.; Polo, E.; O'Connell, A.; Cookman, J.; Fallon, J.; Krpetic, Z.; Dawson, K. A., Mapping protein binding sites on the biomolecular corona of nanoparticles. *Nature Nanotech.* **2015,** *10* (5), 472-9.

29. Lo Giudice, M. C.; Herda, L. M.; Polo, E.; Dawson, K. A., In situ characterization of nanoparticle biomolecular interactions in complex biological media by flow cytometry. *Nature Commun.* **2016,** *7*, 13475.

30. Herda, L. M.; Hristov, D. R.; Lo Giudice, M. C.; Polo, E.; Dawson, K. A., Mapping of Molecular Structure of the Nanoscale Surface in Bionanoparticles. *J. Am. Chem. Soc.* **2017,** *139* (1), 111-114.

31. Estupiñán, D.; Bannwarth, M. B.; Mylon, S. E.; Landfester, K.; Muñoz-Espí, R.; Crespy, D., Multifunctional clickable and protein-repellent magnetic silica nanoparticles. *Nanoscale* **2016,** *8* (5), 3019-3030.

32. Wang, K.; Zhou, C.; Hong, Y.; Zhang, X., A review of protein adsorption on bioceramics. *Interface Focus.* **2012,** *2* (3), 259-277.

33. Ito, T.; Tsumoto, K., Effects of subclass change on the structural stability of chimeric, humanized, and human antibodies under thermal stress. *Protein Sci.* **2013,** *22* (11), 1542-1551.

34. Chaudhuri, R.; Cheng, Y.; Middaugh, C. R.; Volkin, D. B., High-throughput biophysical analysis of protein therapeutics to examine interrelationships between aggregate formation and conformational stability. *AAPS J.* **2013,** *16* (1), 48-64.

35. Latypov, R. F.; Hogan, S.; Lau, H.; Gadgil, H.; Liu, D., Elucidation of acid-induced unfolding and aggregation of human immunoglobulin IgG1 and IgG2 Fc. *J. Biol. Chem.* **2012,** *287* (2), 1381-1396.

36. Boswell, C. A.; Tesar, D. B.; Mukhyala, K.; Theil, F. P.; Fielder, P. J.; Khawli, L. A., Effects of charge on antibody tissue distribution and pharmacokinetics. *Bioconjug. Chem.* **2010,** *21* (12), 2153-2163.

37. Torcello-Gómez, A.; Santander-Ortega , M. J.; Peula-García, J. M.; Maldonado-Valderrama, J.; Gálvez-Ruiz, M. J.; Ortega-Vinuesa, J. L.; Antonio Martín-Rodríguez, A., Adsorption of antibody onto Pluronic F68-covered nanoparticles: link with surface properties. *Soft Matter* **2011,** *7* (18), 8450-8461.

38. Qian, W.; Yao, D.; Yu, F.; Xu, B.; Zhou, R.; Bao, X.; Zuhong, L., Immobilization of antibodies on ultraflat polystyrene surfaces. *Clin. Chem.* **2000,** *46* (9), 1456-1463.

39. Fleischer, C. C.; Payne, C. K., Secondary structure of corona proteins determines the cell surface receptors used by nanoparticles. *J. Phys. Chem. B.* **2014,** *118* (49), 14017-14026.

40. Temel, D. B.; Landsman, P.; Brader, M. L., Orthogonal Methods for Characterizing the Unfolding of Therapeutic Monoclonal Antibodies: Differential Scanning Calorimetry, Isothermal Chemical Denaturation, and Intrinsic Fluorescence with Concomitant Static Light Scattering. *Methods Enzymol.* **2016,** *567*, 359-389.

41. Frick, S. U.; Domogalla, M. P.; Baier, G.; Wurm, F. R.; Mailaender, V.; Landfester, K.; Steinbrink, K., Interleukin-2 Functionalized Nanocapsules for T Cell-Based Immunotherapy. *ACS Nano* **2016,** *10* (10), 9216-9226.

42. Maffre, P.; Brandholt, S.; Nienhaus, K.; Shang, L.; Parak, W. J.; Nienhaus, G. U., Effects of surface functionalization on the adsorption of human serum albumin onto nanoparticles - a fluorescence correlation spectroscopy study. *Beilstein J. Nanotechnol.* **2014,** *7* (5), 2036-2047.

43. Schöttler, S.; Klein, K.; Landfester, K.; Mailänder, V., Protein source and choice of anticoagulant decisively affect nanoparticle protein corona and cellular uptake. *Nanoscale* **2016,** *8* (10), 5526-5536.

44. Pozzi, D.; Caracciolo, G.; Capriotti, A. L.; Cavaliere, C.; La Barbera, G.; Anchordoquy, T. J.; Laganà, A., Surface chemistry and serum type both determine the nanoparticle-protein corona. *J Proteomics.* **2015,** *119*, 209-217.

45. Deng, Z. J.; Liang, M.; Monteiro, M.; Toth, I.; Minchin, R. F., Nanoparticle-Induced Unfolding of Fibrinogen Promotes Mac-1 Receptor Activation and Inflammation. *Nature Nanotech.* **2011,** *6* (1), 39-44.

46. Mirshafiee, V.; Kim, R.; Park, S.; Mahmoudi, M.; Kraft, M. L., Impact of protein pre-coating on the protein corona composition and nanoparticle cellular uptake. *Biomaterials* **2016,** *75*, 295-304.

47. Chen, F.; Wang, G.; Griffin, J. I.; Brenneman, B.; Banda, N. K.; Holers, V. M.; Backos, D. S.; Wu, L.; Moghimi, S. M.; Simberg, D., Complement proteins bind to nanoparticle protein corona and undergo dynamic exchange in vivo. *Nature Nanotech.* **2017,** *12* (4), 387-393.

48. Caracciolo, G.; Farokhzad, O. C.; Mahmoudi, M., Biological Identity of Nanoparticles In Vivo: Clinical Implications of the Protein Corona. *Trends Biotechnol* **2017,** *35* (3), 257-264.

49. Bannwarth, M. B.; Utech, S.; Ebert, S.; Weitz, D. A.; Crespy, D.; Landfester, K., Colloidal Polymers with Controlled Sequence and Branching Constructed from Magnetic Field Assembled Nanoparticles. *ACS Nano* **2015,** *9* (3), 2720-2728.

50. Renz, P.; Kokkinopoulou, M.; Landfester, K.; Lieberwirth, I., Imaging of Polymeric Nanoparticles: Hard Challenge for Soft Objects. *Macromol. Chem. Phys.* **2016,** *217* (17), 1879-1885.

51. Nikiforow, I.; Adams, J. r.; König, A. M.; Langhoff, A.; Pohl, K.; Turshatov, A.; Johannsmann, D., Self-stratification during film formation from latex blends driven by differences in collective diffusivity. *Langmuir* **2010,** *26* (16), 13162-13167.

52. García-Moreno, I.; Costela, A.; Campo, L.; Sastre, R.; Amat-Guerri, F.; Liras, M.; López Arbeloa, F.; Bañuelos Prieto, J.; López Arbeloa, I., 8-Phenyl-Substituted Dipyrromethene BF2 Complexes as Highly Efficient and Photostable Laser Dyes. *J. Phys. Chem. A* **2004,** *108* (16), 3315-3323.

53. Musyanovych, A.; Rossmanith, R.; Tontsch, C.; Landfester, K., Effect of hydrophilic comonomer and surfactant type on the colloidal stability and size distribution of carboxyl- and amino-functionalized polystyrene particles prepared by miniemulsion polymerization. *Langmuir* **2007,** *23* (10), 5367-5376.

54. Baier, G.; Baumann, D.; Siebert, J. M.; Musyanovych, A.; Mailänder, V.; Landfester, K., Suppressing unspecific cell uptake for targeted delivery using hydroxyethyl starch nanocapsules. *Biomacromolecules* **2012,** *13* (9), 2704-2715.

55. Gillis, S.; Smith, K. A., Long term culture of tumour-specific cytotoxic T cells. *Nature* **1977,** *268* (516), 154-156.

56. Silva, J. C.; Gorenstein, M. V.; Li, G. Z.; Vissers, J. P.; Geromanos, S. J., Absolute quantification of proteins by LCMSE: a virtue of parallel MS acquisition. *Mol. Cell. Proteomics.* **2006,** *5* (1), 144-156.

57. Sándor, N.; Kristóf, K.; Paréj, K.; Pap, D.; Erdei, A.; Bajtay, Z., CR3 is the dominant phagocytotic complement receptor on human dendritic cells. *Immunobiology* **2013,** *218* (4), 652-663.

# 9. Mannose functionalized poly(phosphoester)-based surfactants enable targeted cell interactions

## Aim:

Surfactants are surface-active polymers and readily adsorb onto nanoparticles. Therefore, in this study, different degradable poly(phosphoester)-based surfactants were synthesized, which contained a targeting unit (mannose) to allow a specific cellular recognition by dendritic cells. It was shown functionalization of nanoparticles with mannose containing surfactants allowed targeted cell interaction even after incubation with blood plasma. Therefore, the assembling of mannosylated poly(phosphoester)-based surfactants is a feasible strategy for the surface modification of nanoparticles to achieve targeted cell uptake.

## Contribution:

I carried out the complete protein corona analysis (SDS-PAGE, LC-MS, Pierce Assay) and conducted the cellular uptake experiments (flow cytometry, cLSM). [redacted] synthesized the surfactants and prepared the nanoparticles. [redacted] synthesized the mannose derivate. The project was supervised by [redacted]

## Abstract

Targeted nanoparticles promise a selective delivery of drugs to the body region of interest. This improves on one side the therapeutic efficiency and on the other side reduces drug-induced side effects. Therefore, advanced nanoparticle formulations are engineered with specific targeting ligands to guide the nanoparticles way to specific cells. Here, we present the synthesis of mannose functionalized poly(phosphoester)-based surfactants, which can be applied for surface coating of various nanoparticles. Primary monocyte derived dendritic cells (moDCs) specifically recognized mannose functionalized nanoparticles via the mannose receptor hereby proofing targeted cell interactions. It is widely accepted that adsorption of blood proteins towards the nanoparticle surface can significantly influence the targeting efficiency of nanoparticles. In a thorough proteomic characterization, we identified the distinct protein corona pattern after incubation with human plasma. Additionally, we showed that despite corona formation mannose functionalized nanoparticles are efficiently taken up by moDCs. This highlights that mannose functionalized poly(phosphoester)-based surfactants can be applied as universal coating to achieve targeted cell interaction.

## Introduction

In recent years, targeted drug delivery via nanoparticles has gained increasing attention as it allows the side selective delivery of therapeutics and hereby reduces toxic side effects. Nanoparticles have to fulfill several criteria for their successful application[1-2]. Unspecific interaction of nanoparticles with immune cells (e.g. macrophages) results in reduced blood circulation times, which prevents the interaction of nanoparticles with targeted cells[3-4]. To guide the nanoparticle to the targeted cell, the surface is commonly modified with targeting ligands. Here, various strategies including biomolecules[5], antibodies[6] or small molecules[7] were developed to modify the nanoparticles´ surface and obtain targeted cell interactions. In a general approach, the targeting ligand is covalently attached to the surface of the nanoparticle. However, these strategies are challenging and often result in a low functionalization degree[8] [9]. Therefore, alternative and more convenient methods are needed.

Surfactants are amphiphilic polymers and can be used for the non-covalent surface modification of nanoparticles[10-11]. Based on this, we developed poly(phosphoester)-based surfactants for the non-covalent surface modification of different nanoparticles. Poly(phosphoester)-based polymers are biodegradable and biocompatible and therefore an interesting polymer class for biomedical applications[12-13]. The poly(phosphoester)-based surfactants were synthesized by ring opening polymerization and further functionalized with

mannose. Mannose was chosen as targeting ligand to enable cellular recognition by dendritic cells (DC) via the mannose receptor.[14-15] The mannose receptor (CD206/CD209) is known to bind to glycoproteins of pathogens via mannose, fucose or N-acetlyglucosamine[16]. Dendritic cells are specialist antigen-presenting cells, which subsequently mediate T cell immunity[17-18]. Therefore, new vaccine strategies aim to specifically deliver antigens towards dendritic cells using targeted nanoparticles[19].

However, designing targeted nanoparticles for *in vivo* application bears additional challenges[20]. Once nanoparticles are introduced to blood, proteins rapidly cover its surface (´biomolecular corona formation´) and hereby critically alter the nanoparticles´ physico-chemical properties[21-22]. Several reports already recognized that the targeting ligand can even be completely buried by proteins and further cellular interactions are prevented[23-24]. Therefore, the influence of corona formation on the targeting ability of mannose functionalized nanoparticles was specifically studied. We carried out a detailed proteomic investigation to identify the distinct protein corona pattern.

## Material and methods

**Cell culture.** Monocytes and monocyte derived dendritic cells (moDC) were isolated from human buffy coats according to the vote of the local ethics committee and the Declaration of Helsinki as previously reported[33-34]. Briefly, peripheral blood mononuclear cells (PBMCs) were isolated by Ficoll separation and plated into 6-well plates in DC-medium (RPMI + 2% human serum, 100 IU/mL penicillin, 100 µg/mL streptomycin). Cells were incubated for 1 h at 37 °C and non-adherent cells were further discarded by washing the plates with PBS (3-4 times). Adherent cells were either directly frozen and further used for monocyte experiments or differentiated into monocyte derived dendritic cells (moDCs). For generate moDCs, cells were incubated with 800 IU/mL granulocyte-macrophage colony-stimulating factor (GMCSF) and 500 IU/mL interleukin IL4 (both PromoCell). Afterwards 48 h the medium was refreshed with 1600 IU/mL GMCSF and 500 IU/mL IL4 and incubation for 72 h was followed. MoDCs were detached from the wells with 0.5 mM PBS-EDTA solution.

**Surface marker.** 100 000 cells were resuspended in 100 µL PBS and the following antibodies were used to label the surface marker for the mannose receptor (APC anti-human CD206 MMR Antibody (Biolegend) and APC anti-human CD209 MMR Antibody (Biolegend)). Antibodies (5 µL) were added to cells for 30 min, 4 °C. Surface marker expression was analyzed by flow cytometry via Attune NxT Flow Cytometer.

**Cell uptake by flow cytometry.** 100 000 cells were seeded in DC medium with human serum into 48-well and incubated overnight at 37 °C. Nanoparticles (150 µg/mL) coated with or without plasma proteins (see below protein corona preparation) were added to DC medium without human serum and incubated with cells for 2 h, 37 °C. Cells were detached with 0.5 mM PBS-EDTA, centrifuged (480 g, 5 min) and resuspended in PBS. Samples were analyzed by flow cytometry via Attune NxT Flow Cytometer.

**For blocking studies:** Mannan (3 mg/mL) was dissolved in DC medium without human serum and added to cells for 30 min, 4 °C. For further blocking studies, mannan was kept in the cell culture medium during the incubation of cells and nanoparticles.

**Confocal laser scanning microscopy.** To proof the intracellular localization of the nanoparticles, cell uptake experiments were conducted in the same manner as described for flow cytometer experiments. Images were taken with a LSM SP5 STED Leica Laser Scanning Confocal Microscope (Leica). Nanoparticles (BODIPY) were excited with an argon laser (514 nm) and the cell membrane was stained with CellMaskOrange (2.5 µg/mL) which was exited with a DPSS 561 nm laser. Nanoparticles are pseudo-colored in green and the cell membrane is pseudo colored in red.

**Lectin assay.** To detect mannose on the surface of the nanoparticles (1 µg) were incubated with Wheat Germ Agglutinin (WGA, Thermo) conjugated to Texas Red (1 µg) for 30 min in the dark. Nanoparticles with bound WGA were detected by flow cytometry.

**Human plasma.** Human plasma was obtained from the Department of Transfusion Medicine Mainz from healthy donors. A plasma pool from ten volunteers was used and stored at - 80 °C.

**Protein corona preparation.** Nanoparticles (0.05 $m^2$) were incubated with 1 mL of human plasma for 1 h. Hard corona coated nanoparticles were isolated via centrifugation (20 000 g, 1 h, 4 °C) and washing with PBS (3 times, 1 mL). For cell uptake studies, nanoparticles were washed one time and added to cell culture medium.

To analyze the protein pattern surrounding the nanoparticles, the pellet was resuspended in 2% SDS (62.5 mM Tris*HCl) and heated up to 95 °C for 5 min. The dispersion was centrifuged (20 000 g, 1 h, 4 °C) again and the supernatant was analyzed by Pierce Assay, SDS-PAGE and LC-MS.

**SDS-PAGE.** Protein solutions (1 µg in 26 µL) were mixed with 4 µL of NuPage Reducing Agent and 10 µL of NuPage LDS Sample Buffer NuPage The sample was heated up to 70 °C for 10 min and loaded on a 10% Bis-Tris-Protein Gels using NuPAGE MES SDS Running Buffer

(Thermo Fisher Scientific). The gel was run for 1 h at 100 V and the band were visualized by Silver Staining using the commercial SilverQuest Silver Staining Kit.

**Protein quantification.** The protein concentration was determined by Pierce 600 nm protein Assay according to the manufactures instruction.

**In solution digestion.** To remove SDS, protein solutions were applied to Pierce detergent removal columns (Thermo Fisher). Digestion was performed to previously estabilished protocols.[35,36] A protein:trypsin ratio of 50:1 was chosen and the reaction was carried out over 14 h at 37 °C.

**Liquid chromatography coupled to mass spectrometry (LC-MS analysis).** Peptide samples were diluted with with 0.1% formic acid. Hi3 Ecoli was added at a concentration of 50 fmol/µL for absolute protein quantification[37]. A nanoACQUITY system containing a C18 analytical reversed phase column (1.7 µm, 75 µm × 150 mm) and a C18 nanoACQUITY trap column (5 µm, 180 µm × 20 mm) was used. Mobile phase A consists of 0.1% (v/v) formic acid in water and mobile phase B of 0.1% (v/v) formic acid with acetonitrile. For separation a gradient of 2% to 37% of mobile phase B over 70 min was used. The UPLC system was coupled to a Synapt G2- Si mass spectrometer performing electrospray ionization (ESI) in positive ion mode using a NanoLockSpray source. Glu-Fibrinopeptide was infused as reference component. The mass spectrometer was operated in resolution mode and d data-independent acquisition ($MS^E$) experiments were carried out. Data was processed with MassLynx 4.1

**Protein identification.** To identify proteins, a reviewed human data base (Uniprot) was downloaded and analysis was carried out with Progenesis QI (2.0). Parameters for protein identification were set as described before[38]. The human data base was modified with the sequence information of Hi3 Ecoli standard for absolute protein quantification. The amount of each protein in fmol was obtained via the TOP3/Hi3 approach[39].

**Synthesis of PS nanoparticles.** Nanoparticles were prepared via mini emulsion copolymerization technique. Therefore, the continuous phase contained sodium dodecyl sulfate (SDS) (60 mg, 0.21 mmol) as surfactant in water (24 g) and the dispersed phase contained distilled styrene (6 g, 57.6 mol) or methyl methacrylate (MMA) (6 g, 59.9 mmol), hexadecane (250 mg, 0.9 mmol) Bodipy methacrylate (6 mg, $1.3 \cdot 10^{-5}$ mol) and azoisobutyronitrile (AIBN) (100 mg, 0.6 mmol). Both phases were homogenized and the continuous phase was added slowly to the dispersed phase. The emulsion was stirred for 1 h, ultrasonicated with a Branson Sonifier (1/2“ tip, 6.5 nm diameter) for 3 min under ice cooling and further heated up to 72 °C. The emulsion was stirred overnight.

**Synthesis of surfactants.** The detailed synthesis and characterization of all surfactants is described in the dissertation of Kristin Bauer (MPI-P, AK Landfester, December 2017).

**Loading of nanoparticles with surfactants.** The nanoparticle dispersion (2 %) was washed with water (1 mL), centrifuged (20 000 g, 1 h) and resuspended in the respective surfactant solution (1%, 1 mL).

## Results and discussion

The polymer structure of the poly(phosphoester) surfactants is comparable to the structure of the PEG analog surfactant Lutensol AT-50. In previous studies, polystyrene nanoparticle were coated with unfunctionalized poly(phopshoester)-based surfactants Phos-S(1) and it was shown the protein and cell interactions of nanoparticles coated with poly(phosphoester)-based surfactants are comparable to Lutensol AT-50 coated nanoparticles[25]. It was proven that cellular internalization towards macrophages is significantly reduced for poly(phosphoester) and Lutensol AT-50 coated nanoparticle in comparison to uncoated nanoparticles indicating stealth properties[26]. Therefore, Phos-S(1) based surfactants served as a reference to compare the cellular interaction to mannose functionalized surfactants. The targeting surfactants Phos-S(2)-Man has a block polymer structure with an equal ratio of Phos-S(1) and Phos-S(3). The targeting surfactant Phos-S(3) has a homo polymer structure and each unit contains one mannose residue. All three surfactants have about 40 repeating units. Therefore, Phos-S(3) contains about 40 mannose units whereas Phos-S(2) has about 20 mannose units.

The poly(phosphoester)-based surfactants were synthesized in a two-step process. Phosphoester monomers were polymerized via ring opening polymerization as described[27]. For the targeting surfactants, a precursor monomer with a methacrylate groups were chosen. The mannose linker contained a free thiol-group and therefore, it was possible to link the mannose unit via a Thiol-Michael addition click reaction to the methacrylate unit of the poly(phosphoester) surfactant[28].

As surfactants have an amphiphilic structure, they readily adsorb to the nanoparticles´ surface. Therefore, it is possible to functionalize the nanoparticle surface in a non-covalent approach[29].

In the here presented study, polystyrene (PS) and poly(methyl metacrylate) nanoparticles (PMMA) were coated with the different poly(phosphoester)-based surfactants.

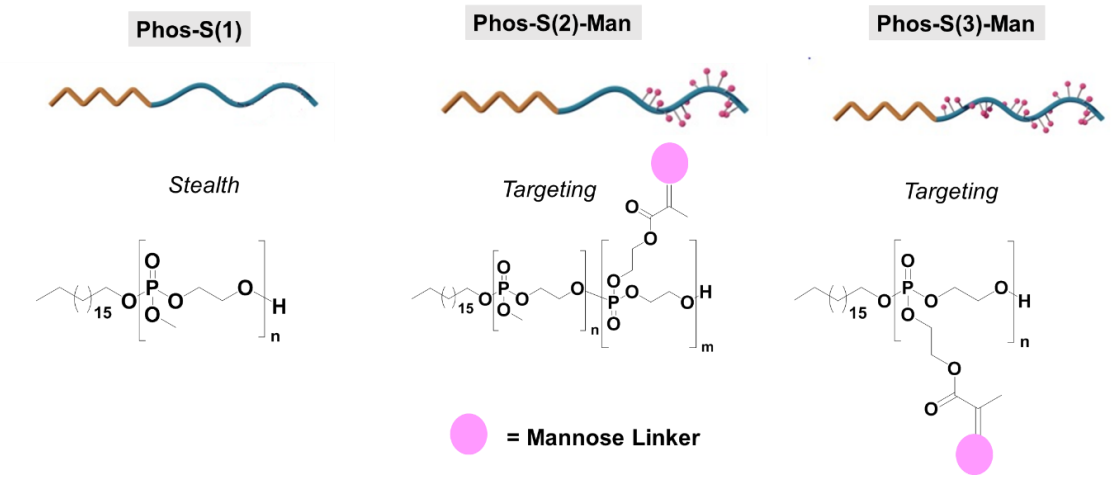


**Figure 9. 1.** Chemical structure of poly(phosphoester)-based surfactants. **Phos-S(1)** is an unfunctionalized poly(phosphoester)-based surfactant, which served as control. **Phos-S(2)-Man** has a block polymer structure and contains terminal mannose units. **Phos-(3)-Man** has homo polymer structure and each repeat units contains mannose. [redacted] The mannose linker was synthesized by [redacted] and contained a thiol-group. The reaction scheme is given in the supplementary information Figure S9.1.

In order to evaluate whether coating of nanoparticles with mannose functionalized surfactants allows targeted cell interactions, flow cytometry analysis towards primary monocyte derived dendritic cells (moDCs) was analyzed (Figure 9.1). As described above the structure of Phos-S(1) is comparable to the PEG analog surfactant Lutensol AT50 and it was already shown in previous studies that PS nanoparticles coated with unfunctionalized poly(phosphoester)-based surfactants exhibit reduced cellular interactions towards macrophages. Flow cytometry analysis (Figure 9.1) and confocal laser microscopy images (Figure 9.1) confirmed that nanoparticles coated with Phos S(1) exhibit a low binding affinity towards moDCs (material/methods see supplementary information 9).

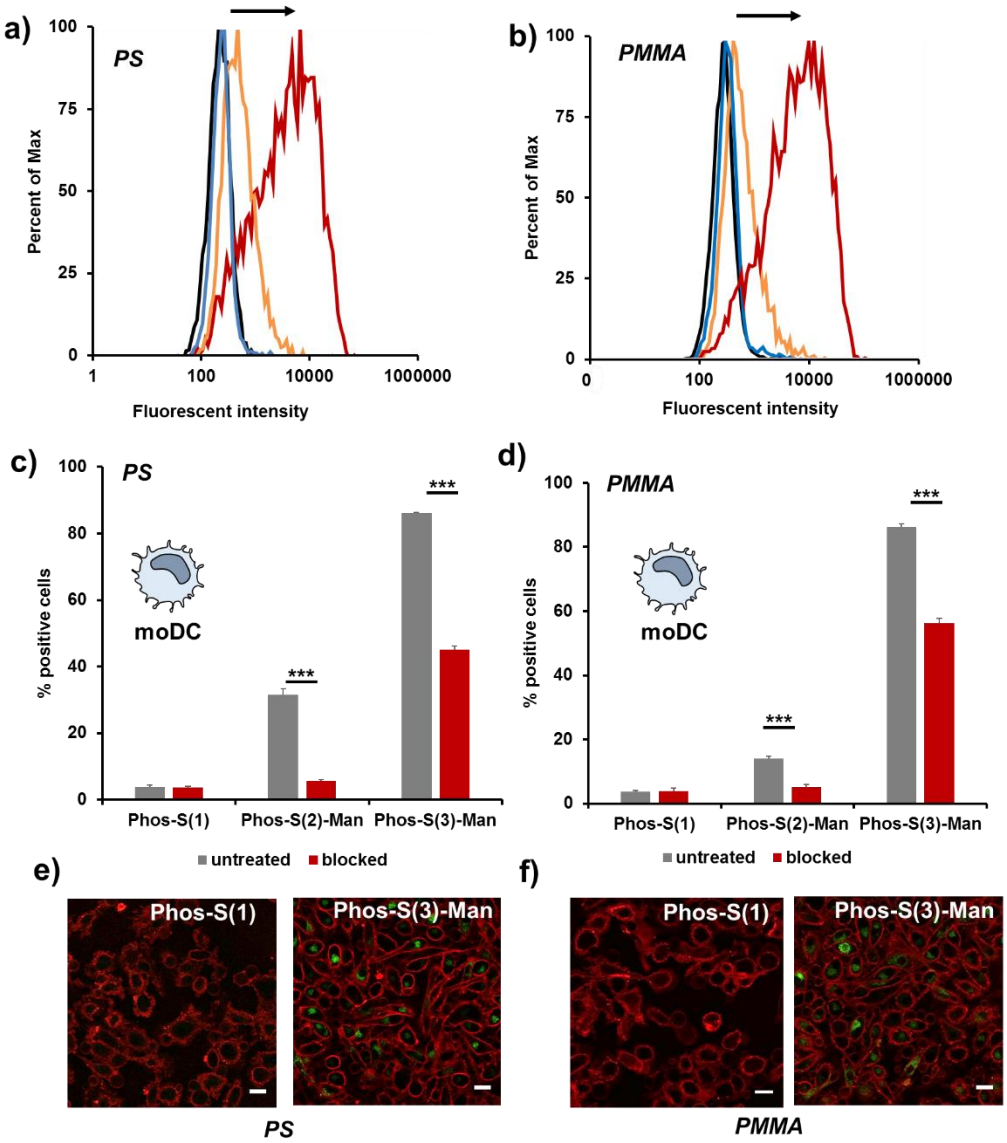


**Figure 9. 2**. **a, b)** Flow cytometry analysis of Phos-S(1) (blue), Phos-S(2)-Man (orange) or Phos-S(3)-Man (red) polymer coated nanoparticles (polystyrene or PMMA). **c, d)** Dendritic cells were treated with nanoparticles (150 µg/mL) for 2 h, 37 °C in cell culture medium without proteins (grey bar). Cellular uptake was quantified by flow cytometry and the amount of fluorescent positive cells (%) is shown. For blocking experiments, cells were pre-treated with mannan (3 mg/mL) for 30 min at 4 °C (red bar) **e, f)** Confocal laser scanning microscopy (cLSM). The cell membrane is visualized with CellMask Orange and pseudo-coloured in red whereas the nanoparticle is pseudo-coloured in green. Scale bar: 20 µm.

In strong contrast to this, if nanoparticle were coated with the targeting surfactants Phos-S(2)-Man or Phos-S(3)-Man we clearly demonstrate a significant increase in cellular uptake (Figure 9.1). This gave first hints, that coating of nanoparticles with mannosefunctionalized surfactants enables controlled cellular interactions. Additionally, we observed that Phos-S(3)-Man coated

nanoparticles displayed a significant stronger cellular internalization compared to Phos-S(2)-Man coated nanoparticles. Based on the chemical structure of the surfactants, the amount of mannose is higher for Phos-S(3)-Man compared to Phos-S(2)-Man. Further, we performed a binding assay using a fluorescent-labelled lectin to detect mannose on the surface of the nanoparticles. Via a flow cytometry based lectin assay, we also identified a higher amount of mannose on the surface of Phos-S(3)-Man coated nanoparticles compared to Phos-S(2)-Man (supplementary information 9).

In order to proof, that the cellular interaction of mannose coated nanoparticles is actually mediated via the mannose receptor (CD206/CD209) blocking experiments were performed (Figure 9.1). Cells were pre-treated with mannan, which binds to the mannose receptor (CD206/CD209) and cellular uptake analysis was followed. Here, we saw that nanoparticle internalization was strong reduced, if cells were pre-treated with mannan indicating cellular uptake of mannose functionalized NPs is receptor-mediated.

As reported, the interaction of plasma proteins can dramatically affect the targeting efficiency of nanoparticles.[20] Here, several studies showed that the targeting ligand can be covered completely after corona formation.[23] Therefore, we wanted to thoroughly characterize the influence of protein adsorption on the targeting properties and additionally investigate the distinct protein corona pattern of mannose functionalized nanoparticles.

Nanoparticles were pre-coated with human plasma to allow corona formation prior to cellular uptake towards moDCs (Figure 9.2). We found that cellular interactions of PS-NPs and PMMA-NPs differed after plasma incubation. Flow cytometry experiments indicated that PS-NPs which were coated with Phos-S(3)-Man exhibit a lower targeting efficiency after corona formation (Figure 9.2).

Interestingly, this effect was not observed for PMMA nanoparticles (Figure 9.2). On top of this, we even found an enhanced cellular uptake for PMMA NPs coated with Phos-S(2)-Man due to corona formation (Figure 9.2). This in intriguing. In order to further proof the receptor mediated cellular interactions of nanoparticles in the presence of the protein corona, cellular uptake towards monocytes was investigated. Monocytes are the precursor cells of dendritic cells. Those cells express low levels of the mannose receptor (CD206/CD209) in contrast to dendritic cells for which we confirmed a high expression level of CD206/CD209. Nanoparticles coated with the mannose surfactants Phos-S(2)/(3)-Man, which were incubated with plasma exhibited a low internalization rate towards monocytes (Figure 9.2). This further underlines the specific interaction of mannose functionalized nanoparticles with dendritic cells even in the presence of the protein corona.

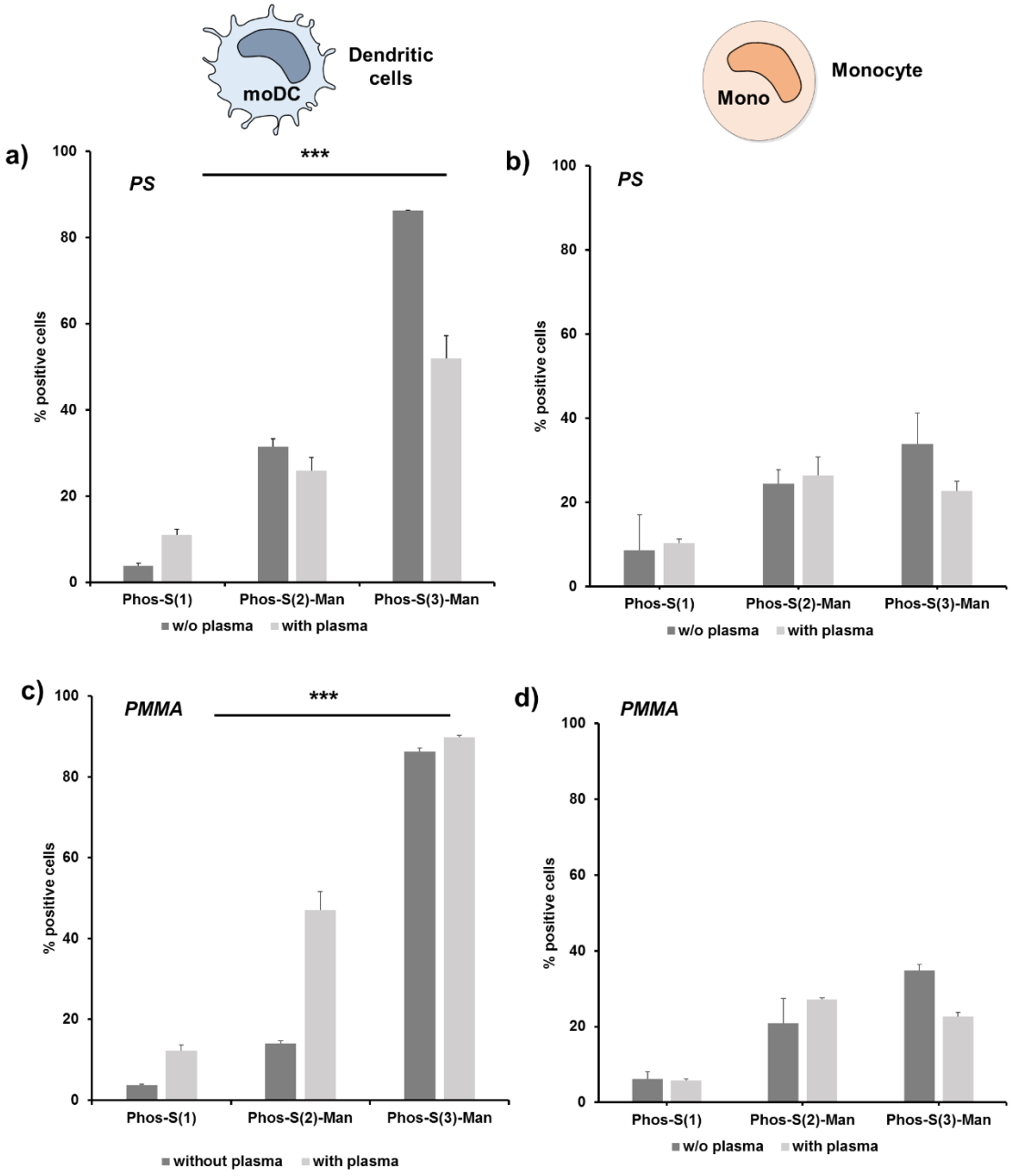


**Figure 9. 3.** Surfactant coated polystyrene nanoparticles were exposed to plasma and cellular uptake (150 µg/mL, 2 h) towards dendritic cells **(a,c)** or monocytes **(b,d)** was quantified via flow cytometry. The amount of fluorescent positive cells (%) is shown.

In order to understand the influence of protein adsorption, a detailed LC-MS analysis was carried out to detect the key corona proteins. All identified proteins were classified into 8 different classes depending on their biological function (Figure 9.3). Overall, the corona composition Phos-S(1) coated nanoparticles is comparable to Phos-S(2)-Man or Phos-S(3)-Man coated nanoparticles.

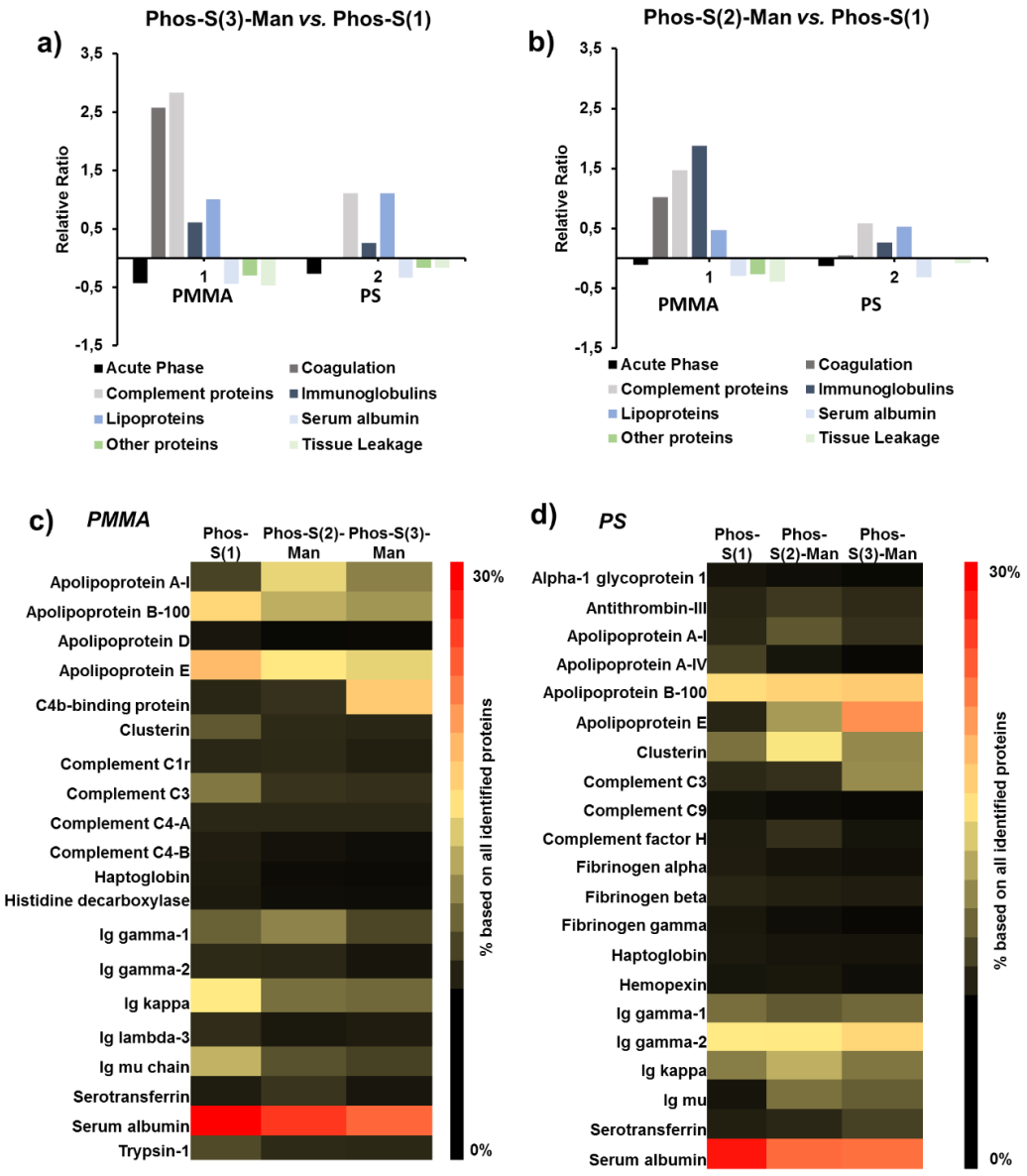


**Figure 9. 4.** Hard corona proteins were analysed via LC-MS and classified into eight different group. The relative amount for Phos-S(3)-Man **(a)** or Phos-S(2)-Man **(b)** coated nanoparticles in comparison to Phos-S(1) coated nanoparticles was calculated. **c,d)** The most abundant proteins (TOP 20) are visualized via heat map.

To point out specific differences in the protein adsorption pattern of nanoparticles coated with unfunctionalized surfactant Phos-S(1) compared to the functionalized ones Phos-S(2)/(3)-Man, the relative ratio for each protein group was calculated (Figure 9.3). This offered the possibility to highlight specific protein groups, which were enriched or reduced in the corona for Phos-S(2)/(3)-Man coated nanoparticles compared to Phos-S(1) functionalized NPs. Here, we found that the corona of PMMA nanoparticles coated with Phos-S(3)-Man is enriched with complement and coagulation proteins. Especially, complement proteins are known to enhance

interaction with immune cells.[30] Additionally, an enriched number of immunoglobulins was identified for PMMA NPs coated with Phos-S(2)-Man (Figure 9.3). These proteins are referred to the class of opsonins, which enhance cellular recognition via Fc receptor.[31]

In contrast to this, the corona of PS-NPs coated with Phos-S2/3-Man is less enriched with complement proteins and immunoglobulins (Figure 9.3). Moreover, the amount of lipoproteins is comparably high for PS-NPs. Lipoproteins (e.g. Clusterin) were identified in the corona of PEGylated nanoparticles and reduced cellular interactions towards macrophages.[32]

Taking this together, these results can explain the difference in the cellular uptake behavior of PS-NPs coated with the mannose surfactants compared to PMMA-NPs. PS-NPs coated with Phos-S(3)-Man showed a reduced cellular internalization after plasma coating, which is probably attributed to the dominant amounts of lipoproteins in the protein corona. In contrast, the corona of PMMA-NPs coated with Phos-S(2)/(3)-Man additionally contained complement proteins and immunoglobulins, which enhance cellular recognition. Overall, with this we present a direct link of the corona composition and the cellular outcome.

## Conclusion

In this study, we presented that coating of nanoparticles with mannose functionalized poly(phosphoester)-based surfactants enables targeting towards dendritic cells. A detailed proteomic investigation highlighted the distinct role of the protein corona on cellular uptake and targeting efficiency. Overall, we were able to proof that even in the presence of the protein corona mannose functionalized nanoparticles can reach the targeted cells.

## Supplementary information

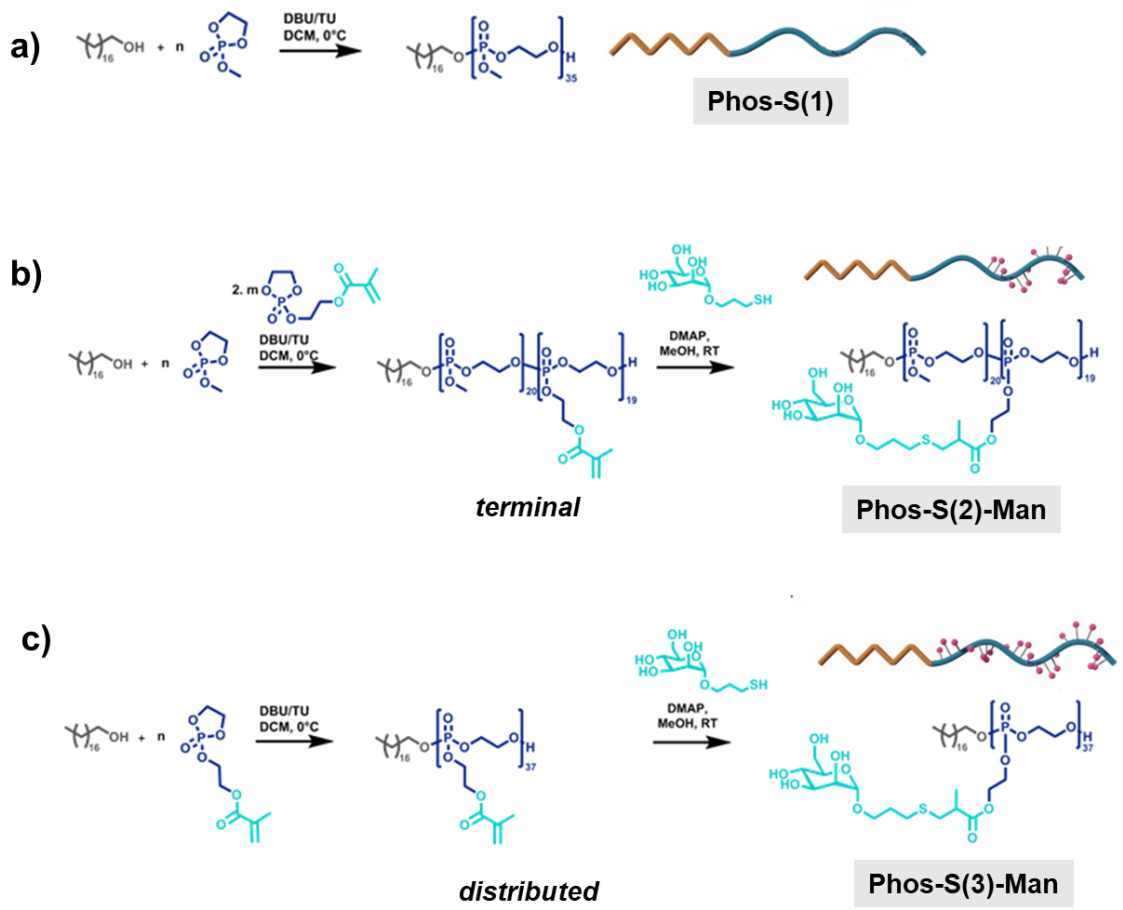


**Figure S9. 1.** Synthesis of polyphosphoester surfactants by ring-opening polymerization (ROP) of cyclic phosphoester monomers and subsequent mannosylation by thiol-Michael addition **a)** ROP of MEP leading to Phos-S(1) carrying no mannose moieties (´stealth surfactant´´) **b)** Synthesis of block copolymer Phos-S(2) and subsequent mannosylation leading to Phos-S(3)-Man (block copolymer, termina mannose unit). **c)** Synthesis of Phos-S(3) by ROP of OPEMA and subsequent mannosylation by thiol-Michael addition leading to Phos-S(2)-Man (homopolyer, distributed mannose unit).

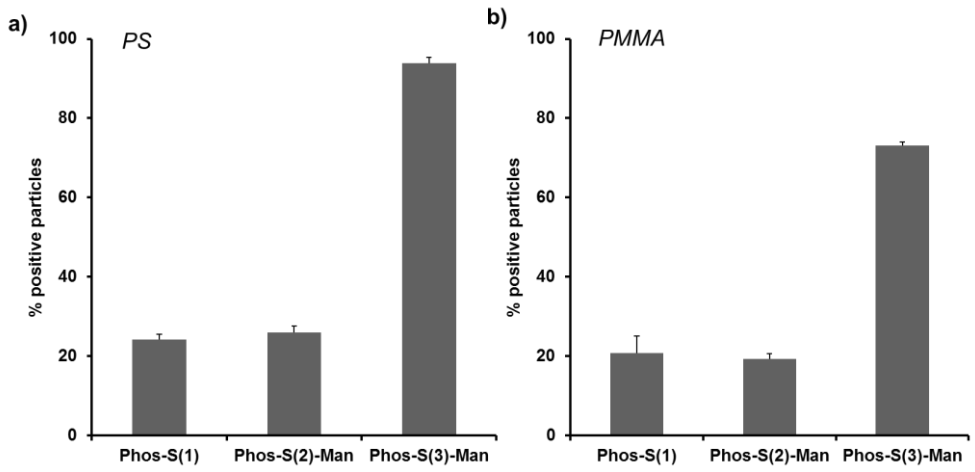


**Figure S9. 2.** Nanoparticles were incubated with Alexa633 conjugated to Wheat Germ Agglutinin (WGA lectin) for 30 min at room temperature. The amount of bound WGA to mannose on the nanoparticle surface was detected by flow cytometry. Values are given in % as Alexa 633 positive nanoparticles.

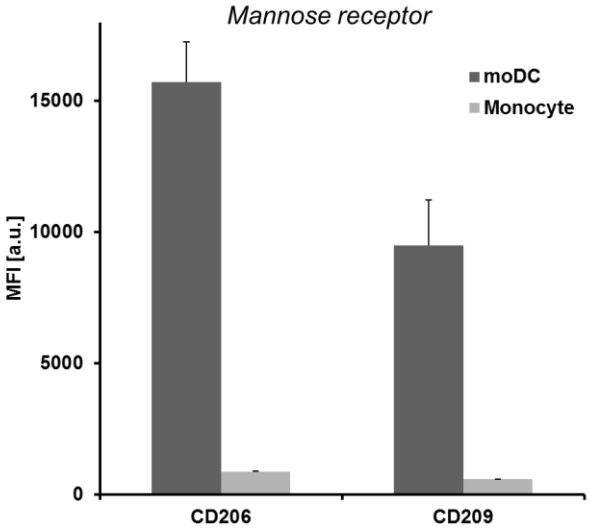


**Figure S9. 3.** Monocytes or monocyte derived dendritic cells were incubated with Alexa647 labelled secondary antibodies against the mannose receptor (CD206 and CD209) for 30 min at 4 °C. Flow cytometry measurements were performed and the median fluorescent intensity values (MFI) are given.

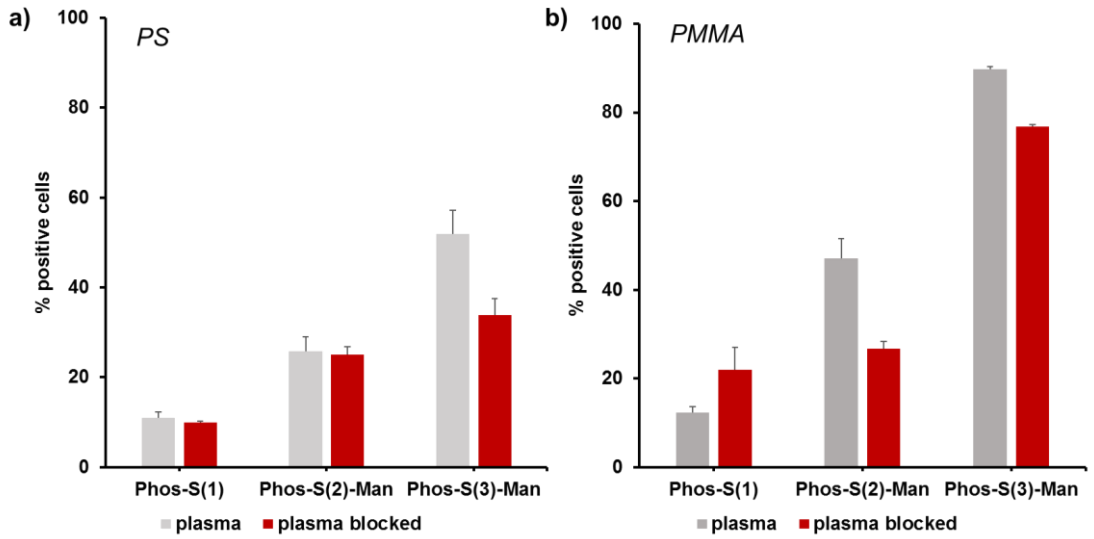


**Figure S9. 4.** Surfactant coated PS nanoparticles **(a)** or PMMA nanoparticles **(b)** were exposed to plasma and cellular uptake (150 µg/mL, 2 h) towards dendritic cells was quantified via flow cytometry. Cells were untreated prior to uptake analysis or pre-treated with mannan (3 mg/mL, 30 min) The amount of fluorescent positive cells is shown (%).

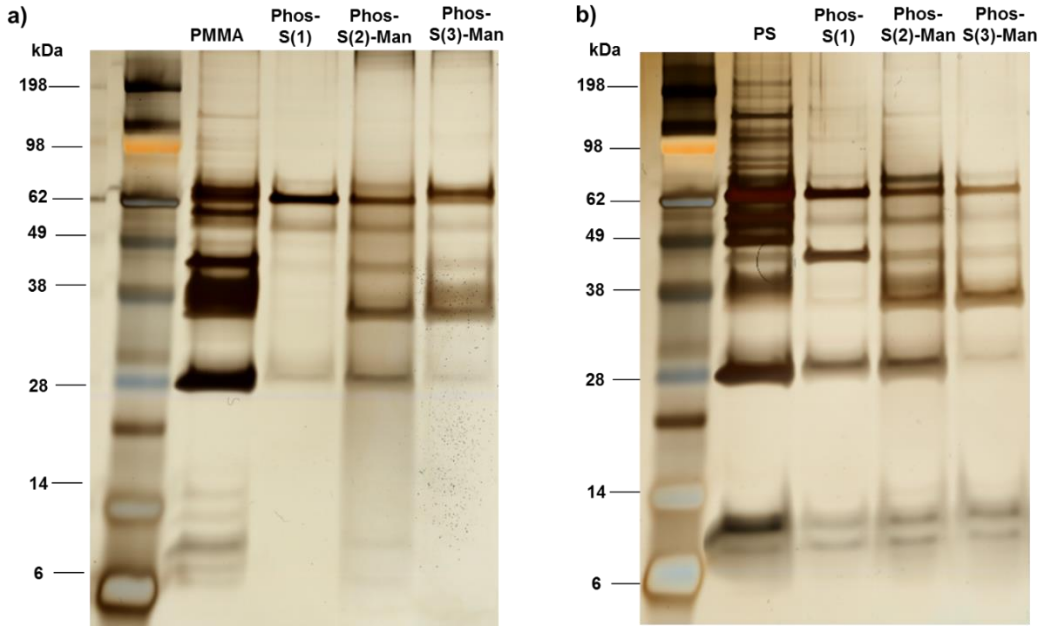


**Figure S9. 5.** Unfunctionalized and surfactant coated PMMA **(a)** and PS **(b)** were incubated with human plasma for 1 h at 37 °C. The hard corona proteins were isolated as described in the material and methods section. Silver staining was used to visualize the corona pattern.

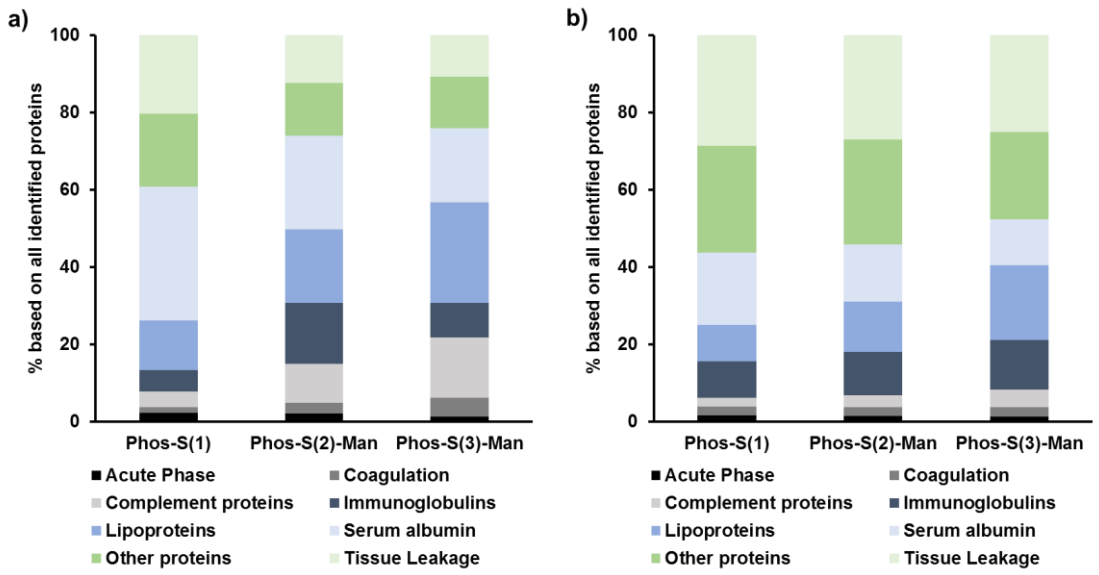


**Figure S9. 6.** The hard corona proteins of PMMA **(a)** and PS **(b)** nanoparticles were analysed by LC-MS. All proteins were classified into 8 different classes depending on their biological function.

# Literature

1. Singh, R.; Lillard Jr, J. W., Nanoparticle-based targeted drug delivery. *Experimental and molecular pathology* **2009,** *86* (3), 215-223.

2. D Friedman, A.; E Claypool, S.; Liu, R., The smart targeting of nanoparticles. *Current pharmaceutical design* **2013,** *19* (35), 6315-6329.

3. Blanco, E.; Shen, H.; Ferrari, M., Principles of nanoparticle design for overcoming biological barriers to drug delivery. *Nature biotechnology* **2015,** *33* (9), 941.

4. Song, G.; S Petschauer, J.; J Madden, A.; C Zamboni, W., Nanoparticles and the mononuclear phagocyte system: pharmacokinetics and applications for inflammatory diseases. *Current rheumatology reviews* **2014,** *10* (1), 22-34.

5. Johnsen, K. B.; Burkhart, A.; Melander, F.; Kempen, P. J.; Vejlebo, J. B.; Siupka, P.; Nielsen, M. S.; Andresen, T. L.; Moos, T., Targeting transferrin receptors at the blood-brain barrier improves the uptake of immunoliposomes and subsequent cargo transport into the brain parenchyma. *Scientific reports* **2017,** *7* (1), 10396.

6. Carter, T.; Mulholland, P.; Chester, K., Antibody-targeted nanoparticles for cancer treatment. *Immunotherapy* **2016,** *8* (8), 941-958.

7. Stella, B.; Arpicco, S.; Peracchia, M. T.; Desmaële, D.; Hoebeke, J.; Renoir, M.; D'Angelo, J.; Cattel, L.; Couvreur, P., Design of folic acid-conjugated nanoparticles for drug targeting. *Journal of pharmaceutical sciences* **2000,** *89* (11), 1452-1464.

8. Nobs, L.; Buchegger, F.; Gurny, R.; Allémann, E., Surface modification of poly(lactic acid) nanoparticles by covalent attachment of thiol groups by means of three methods. *International Journal of Pharmaceutics* **2003,** *250* (2), 327-337.

9. Juillerat-Jeanneret, L., The targeted delivery of cancer drugs across the blood–brain barrier: chemical modifications of drugs or drug-nanoparticles? *Drug Discovery Today* **2008,** *13* (23), 1099-1106.

10. Heinz, H.; Pramanik, C.; Heinz, O.; Ding, Y.; Mishra, R. K.; Marchon, D.; Flatt, R. J.; Estrela-Lopis, I.; Llop, J.; Moya, S., Nanoparticle decoration with surfactants: molecular interactions, assembly, and applications. *Surface Science Reports* **2017,** *72* (1), 1-58.

11. Pellegrino, T.; Manna, L.; Kudera, S.; Liedl, T.; Koktysh, D.; Rogach, A. L.; Keller, S.; Rädler, J.; Natile, G.; Parak, W. J., Hydrophobic nanocrystals coated with an amphiphilic polymer shell: a general route to water soluble nanocrystals. *Nano letters* **2004,** *4* (4), 703-707.

12. Wang, H.; Su, L.; Li, R.; Zhang, S.; Fan, J.; Zhang, F.; Nguyen, T. P.; Wooley, K. L., Polyphosphoramidates That Undergo Acid-Triggered Backbone Degradation. *ACS Macro Letters* **2017,** *6* (3), 219-223.

13. Du, J.-Z.; Du, X.-J.; Mao, C.-Q.; Wang, J., Tailor-Made Dual pH-Sensitive Polymer–Doxorubicin Nanoparticles for Efficient Anticancer Drug Delivery. *J Am Chem Soc* **2011,** *133* (44), 17560-17563.

14. Ezekowitz, R. A.; Sastry, K.; Bailly, P.; Warner, A., Molecular characterization of the human macrophage mannose receptor: demonstration of multiple carbohydrate recognition-like domains and phagocytosis of yeasts in Cos-1 cells. *The Journal of Experimental Medicine* **1990,** *172* (6), 1785-1794.

15. Banchereau, J.; Steinman, R. M., Dendritic cells and the control of immunity. *Nature* **1998,** *392* (6673), 245-252.

16. Taylor, M. E.; Conary, J. T.; Lennartz, M. R.; Stahl, P. D.; Drickamer, K., Primary structure of the mannose receptor contains multiple motifs resembling carbohydrate-recognition domains. *Journal of Biological Chemistry* **1990,** *265* (21), 12156-62.

17. Hsu, F. J.; Benike, C.; Fagnoni, F.; Liles, T. M.; Czerwinski, D.; Taidi, B.; Engleman, E. G.; Levy, R., Vaccination of patients with B–cell lymphoma using autologous antigen–pulsed dendritic cells. **1996,** *2*, 52.

18. Condon, C.; Watkins, S. C.; Celluzzi, C. M.; Thompson, K.; Falo Jr, L. D., DNA–based immunization by in vivo transfection of dendritic cells. **1996,** *2*, 1122.

19. Choi, B.; Moon, H.; Hong, S. J.; Shin, C.; Do, Y.; Ryu, S.; Kang, S., Effective delivery of antigen–encapsulin nanoparticle fusions to dendritic cells leads to antigen-specific cytotoxic T cell activation and tumor rejection. *ACS nano* **2016,** *10* (8), 7339-7350.

20. Dai, Q.; Bertleff-Zieschang, N.; Braunger, J. A.; Björnmalm, M.; Cortez-Jugo, C.; Caruso, F., Particle Targeting in Complex Biological Media. *Advanced healthcare materials* **2017**.

21. Lundqvist, M.; Stigler, J.; Elia, G.; Lynch, I.; Cedervall, T.; Dawson, K. A., Nanoparticle size and surface properties determine the protein corona with possible implications for biological impacts. *Proc Natl Acad Sci U S A* **2008,** *105* (38), 14265-70.

22. Tenzer, S.; Docter, D.; Kuharev, J.; Musyanovych, A.; Fetz, V.; Hecht, R.; Schlenk, F.; Fischer, D.; Kiouptsi, K.; Reinhardt, C., Rapid formation of plasma protein corona critically affects nanoparticle pathophysiology. *Nature nanotechnology* **2013,** *8* (10), 772-781.

23. Salvati, A.; Pitek, A. S.; Monopoli, M. P.; Prapainop, K.; Bombelli, F. B.; Hristov, D. R.; Kelly, P. M.; Aberg, C.; Mahon, E.; Dawson, K. A., Transferrin-functionalized nanoparticles lose their targeting capabilities when a biomolecule corona adsorbs on the surface. *Nature Nanotech.* **2013,** *8* (2), 137-43.

24. Mirshafiee, V.; Mahmoudi, M.; Lou, K.; Cheng, J.; Kraft, M. L., Protein corona significantly reduces active targeting yield. *Chem. Commun.* **2013,** *49* (25), 2557-2559.

25. Müller, J.; Bauer, K. N.; Prozeller, D.; Simon, J.; Mailänder, V.; Wurm, F. R.; Winzen, S.; Landfester, K., Coating nanoparticles with tunable surfactants facilitates control over the protein corona. *Biomaterials* **2017,** *115*, 1-8.

26. Schöttler, S.; Becker, G.; Winzen, S.; Steinbach, T.; Mohr, K.; Landfester, K.; Mailänder, V.; Wurm, F. R., Protein adsorption is required for stealth effect of poly (ethylene glycol)-and poly (phosphoester)-coated nanocarriers. *Nature nanotechnology* **2016,** *11* (4), 372.

27. Bauer, K. N.; Tee, H. T.; Velencoso, M. M.; Wurm, F. R., Main-chain poly (phosphoester) s: History, syntheses, degradation, bio-and flame-retardant applications. *Progress in Polymer Science* **2017,** *73*, 61-122.

28. Nair, D. P.; Podgórski, M.; Chatani, S.; Gong, T.; Xi, W.; Fenoli, C. R.; Bowman, C. N., The thiol-Michael addition click reaction: a powerful and widely used tool in materials chemistry. *Chemistry of Materials* **2013,** *26* (1), 724-744.

29. Doane, T.; Burda, C., Nanoparticle mediated non-covalent drug delivery. *Advanced drug delivery reviews* **2013,** *65* (5), 607-621.

30. Shen, L.; Tenzer, S.; Storck, W.; Hobernik, D.; Raker, V. K.; Fischer, K.; Decker, S.; Dzionek, A.; Krauthauser, S.; Diken, M.; Nikolaev, A.; Maxeiner, J.; Schuster, P.; Kappel, C.; Verschoor, A.; Schild, H.; Grabbe, S.; Bros, M., Protein corona-mediated targeting of nano-carriers to B cells allows redirection of allergic immune responses. *J Allergy Clin Immunol* **2018**.

31. Daeron, M., Fc Receptors as Adaptive Immunoreceptors. *Curr Top Microbiol* **2014,** *382*, 131-164.

32. Schöttler, S.; Becker, G.; Winzen, S.; Steinbach, T.; Mohr, K.; Landfester, K.; Mailander, V.; Wurm, F. R., Protein adsorption is required for stealth effect of poly(ethylene glycol)- and poly(phosphoester)-coated nanocarriers. *Nature Nanotech.* **2016**.

33. Kang, B.; Opatz, T.; Landfester, K.; Wurm, F. R., Carbohydrate nanocarriers in biomedical applications: functionalization and construction. *Chemical Society Reviews* **2015,** *44* (22), 8301-8325.

34. Kang, B.; Okwieka, P.; Schöttler, S.; Seifert, O.; Kontermann, R. E.; Pfizenmaier, K.; Musyanovych, A.; Meyer, R.; Diken, M.; Sahin, U., Tailoring the stealth properties of biocompatible polysaccharide nanocontainers. *Biomaterials* **2015,** *49*, 125-134.

35. Hofmann, D.; Tenzer, S.; Bannwarth, M. B.; Messerschmidt, C.; Glaser, S.-F.; Schild, H.; Landfester, K.; Mailänder, V., Mass Spectrometry and Imaging Analysis of Nanoparticle-Containing Vesicles Provide a Mechanistic Insight into Cellular Trafficking. *ACS Nano* **2014,** *8* (10), 10077-10088.

36. Tenzer, S., Nanoparticle size is a critical physicochemical determinant of the human blood plasma corona: a comprehensive quantitative proteomic analysis. *ACS Nano* **2011,** *5*, 7155-7167.

37. Bradshaw, R. A.; Burlingame, A. L.; Carr, S.; Aebersold, R., Reporting protein identification data: the next generation of guidelines. *Mol Cell Proteomics* **2006,** *5* (5), 787-8.

38. Kokkinopoulou, M.; Simon, J.; Landfester, K.; Mailänder, V.; Lieberwirth, I., Visualization of the Protein Corona: towards a biomolecular understanding of nanoparticle-cell-interactions. *Nanoscale* **2017**.

39. Silva, J. C.; Gorenstein, M. V.; Li, G. Z.; Vissers, J. P. C.; Geromanos, S. J., Absolute quantification of proteins by LCMSE: a virtue of parallel MS acquisition. *Mol. Cell. Proteomics* **2006,** *5*, 144-156.

# Chapter D

During my PhD, I have contributed to additional projects. Results are either submitted or already published as indicated (see publication list **10-19**). In the following each project is shortly summarized **(aim)** and the contribution of each author are mentioned.

**[10] Pre-coating with protein fractions inhibits nano-carrier aggregation in human blood plasma.**

**Aim.** The success of a nanomaterial designed for biomedical applications depends strongly on its “biological identity” meaning the physicochemical properties the material adopts after contact with a physiological medium e.g. blood. Critical issues are here the size stability of the nanomaterial against aggregation in blood induced by blood proteins and the composition of the protein corona. These factors further determine the particles' fate in vivo and in vitro. While this has been seen to occur inevitably we demonstrate here that a preformed and hereby predetermined protein corona steers the nanomaterials behavior concerning aggregation in human blood plasma and uptake behavior in macrophages. Fractionation of human blood plasma was applied to enrich human serum albumin (HSA), immunoglobulin G (IgG) as well as various low abundant protein mixtures. The exact composition of these protein fractions was analyzed via quantitative, label-free liquid-chromatography mass-spectrometry (LC-MS). The protein fractions were further applied to form a predetermined protein corona on differently functionalized polystyrene nanoparticles. The change of the nanoparticles' physicochemical properties after incubation with the defined protein fractions or whole human plasma was studied by dynamic light scattering (DLS) to determine size changes. DLS was also used to investigate the stability of the protein-coated nanoparticles when reintroduced in human plasma. In addition, we found that cellular uptake of nanomaterials was strongly influenced by the artificially created protein corona.

**Contribution.** I conducted the cellular uptake experiments. Dynamic light scattering experiments were performed by Laura Müller. LC-MS analysis was done by Susanne Schöttler. The project was supervised by Katharina Landfester, Volker Mailänder and Kristin Mohr.

**Copyright.** The following part **(10)** is based on the publication *RSC Advances,* **2016**, *6* (99), 96495-96509.

**[11] Fully degradable protein nanocarriers by orthogonal photoclick tetrazole–ene chemistry for the encapsulation and release.**

**Aim.** The encapsulation of sensitive drugs into nanocarriers retaining their bioactivity and achieving selective release is a challenging topic in current drug delivery design. Established protocols rely on metal-catalyzed or unspecific reactions to build the (mostly synthetic) vehicles which may inhibit the drug's function. Triggered by light, the mild tetrazole–ene cycloaddition enables us to prepare protein nanocarriers (PNCs) preserving at the same time the bioactivity of the sensitive antitumor and antiviral cargo Resiquimod (R848). This catalyst-free reaction was designed to take place at the interface of aqueous nanodroplets in miniemulsion to produce core–shell PNCs with over 90% encapsulation efficiency and no unwanted drug release over storage for several months. Albumins used herein are major constituents of blood and thus ideal biodegradable natural polymers for the production of such nanocarriers. These protein carriers were taken up by dendritic cells and the intracellular drug release by enzymatic degradation of the protein shell material was proven. Together with the thorough colloidal analysis of the PNCs, their stability in human blood plasma and the detailed protein corona composition, these results underline the high potential of such naturally derived drug delivery vehicles.

**Contribution.** I performed the LC-MS analysis and SDS-PAGE. Nanocapsules were synthesized by Keti Piradashvili and Julian Höhner. David Paßlick conducted the cellular uptake experiments. The project was supervised by Volker Mailänder, Frederik Wurm and Katharina Landfester.

**[12] Highly Loaded Semipermeable Nanocapsules for Magnetic Resonance Imaging.**

**Aim.** Magnetic resonance imaging has become an essential tool in medicine for the investigation of physiological processes. The key issues related to contrast agents, i.e., substances that are injected in the body for imaging, are the efficient enhancement of contrast, their low toxicity, and their defined biodistribution. Polyurea nanocapsules containing the gadolinium complex Gadobutrol as a contrast agent in high local concentration and high relaxivity up to 40 s-1 mmol-1 L are described. A high concentration of the contrast agent inside the nanocapsules can be ensured by increasing the crystallinity in the shell of the nanocapsules. Nanocapsules from aliphatic polyurea are found to display higher crystallinity and higher relaxivity at an initial Gadobutrol concentration of 0.1 mM than aromatic polyurea nanocapsules. The nanocapsules and the contrast agent are clearly identified in cells. After injection, the nanocarriers containing the contrast agent are mostly found in the liver and in the spleen, which allow for a significant contrast enhancement in magnetic resonance imaging.

**Contribution.** I analyzed the protein corona. Isabel Schlegel synthesized the nanocapsules. Patricia Renz performed the TEM measurements and cellular uptake experiments. Stefanie Pektor, Nicole Bausbacher and Matthias Miederer supported the *in vivo* studies. The project was supervised by Ingo Lieberwirth, Volker Mailänder, Rafael Muñoz-Espí, Daniel Crespy and Katharina Landfester.

**[13] Coating nanoparticles with tunable surfactants facilitates control over the protein corona.**

**Aim.** Nanoparticles with long blood circulation time are a prerequisite for targeted drug delivery. To make the nanoparticles invisible for phagocytizing cells, functional moieties on the particle surface are believed to be necessary to attract specific so-called 'stealth' proteins forming a protein 'corona'. Currently, covalent attachment of those moieties represents the only way to achieve that attraction. However, that approach requires a high synthetic effort and is difficult to control. Therefore, we present the coating of model nanoparticles with biodegradable polymeric surfactants as an alternative method. The thermodynamic parameters of the coating process can be tuned by adjusting the surfactants' block lengths and hydrophilicity. Consequently, the unspecific protein adsorption and aggregation tendency of the particles can be controlled, and stealth proteins inhibiting cell uptake are enriched on their surface. This non-covalent approach could be applied to any particle type and thus facilitates tuning the protein corona and its biological impact.

**Contribution.** I conducted the protein corona analysis and cell uptake. The ITC measurements were carried out by Julius Müller. Kristin Bauer synthesized the surfactants and Domenik Prozeller performed the zeta potential measurements. The project was supervised by Volker Mailänder, Frederik Wurm, Svenja Morsbach (Winzen) and Katharina Landfester.

**[14] Polyglycerol Surfmers and Surfactants for Direct and Inverse Miniemulsion**

**Aim.** Poly(ethylene glycol)-based surfactants are a prominent example for nonionic surfactants. Poly(glycerol) (PG) is discussed as a polyfunctional alternative, however, it is not yet used to stabilize miniemulsions. The anionic polymerization of glycidyl ethers is used to prepare surfactants for direct or inverse emulsions and ambident surfactants by adjusting the copolymer composition. Orthogonal-protected poly(glycerol) block copolymers, using ethoxyethyl glycidyl ether and allyl glycidyl ether (AGE) or tert-butyl glycidyl ether (tBuGE), are synthesized. After cleavage of the acetal groups, these all-polyglycerol surfactants (PG-b-PtBuGE) or multifunctional surfmers (PG-b-PAGE), are used in direct and inverse miniemulsion polymerizations. Polystyrene nanoparticles are obtained by free-radical miniemulsion polymerization, in which the allyl-functionalized copolymers act as surfmer. In inverse miniemulsion, hydroxyethyl starch nanocarriers are synthesized with PG-b-PAGE as surfmer, transferred into aqueous PG-b-PtBuGE solution, and functionalized by thiol-ene addition. The PG-b-PtBuGE with equal block length ratio is used as a surfactant for direct and inverse miniemulsions. With the PG being covalently bound to the nanocarriers, a desorption during protein adsorption does not occur. It is believed that these surfactants are promising alternatives to conventional surfactants with additional functionality.

**Contribution.** I carried out the protein corona analysis. Surfactants and nanoparticles were synthesized by Sarah Christmann (Wald) and Julia Dietz. The project was supervised by Frederik Wurm and Katharina Landfester.

**[15] Reversible Self-Assembly of Degradable Polymersomes with Upper Critical Solution Temperature in Water.**

**Aim.** Temperature-induced self-assembly of block copolymers allows the formation of smart nanodimensional structures. Mostly, nondegradable lower critical solution temperature (LCST) segments are applied to prepare such dynamic aggregates. However, degradable upper critical phase separation (UCST) block copolymers that would allow the swelling or disassembly at elevated temperatures with eventual backbone hydrolysis have not been reported to date. We present the first well-defined degradable poly(phosphonate)s with adjustable UCST. The organocatalytic anionic ring-opening copolymerization of 2-alkyl-2-oxo-1,3,2-dioxaphospholanes provided functional polymers with excellent control over molecular weight and copolymer composition. The prepolymers were turned into thermoresponsive polymers by thiol-ene modification to introduce pendant carboxylic acids. By this means, non cell-toxic, degradable polymers exhibiting UCST behavior in water between 43 and 71 °C were produced. Block copolymers with PEG as a nonresponsive water-soluble block can self-assemble into well-defined polymersomes with narrow size distribution. Depending on the responsive block, these structures either swell or disassemble completely upon an increased temperature.

**Contribution.** I performed the toxcicity assays. Thomas Wolf and Timo Rheinberger synthesized the polymersomes. The project was supervised by Frederik Wurm.

**[16] Temperature responsive poly (phosphonate) copolymers: from single chains to macroscopic coacervates.**

**Aim.** Temperature-induced self-assembly of block copolymers allows the formation of smart nanodimensional structures. Mostly, nondegradable lower critical solution temperature (LCST) segments are applied to prepare such dynamic aggregates. However, degradable upper critical phase separation (UCST) block copolymers that would allow the swelling or disassembly at elevated temperatures with eventual backbone hydrolysis have not been reported to date. We present the first well-defined degradable poly(phosphonate)s with adjustable UCST. The organocatalytic anionic ring-opening copolymerization of 2-alkyl-2-oxo-1,3,2-dioxaphospholanes provided functional polymers with excellent control over molecular weight and copolymer composition. The prepolymers were turned into thermoresponsive polymers by thiol-ene modification to introduce pendant carboxylic acids. By this means, non cell-toxic, degradable polymers exhibiting UCST behavior in water between 43 and 71 °C were produced. Block copolymers with PEG as a nonresponsive water-soluble block can self-assemble into well-defined polymersomes with narrow size distribution. Depending on the responsive block, these structures either swell or disassemble completely upon an increased temperature.

**Contribution.** I performed the toxcicity assays. Thomas Wolf and Johannes Hunold synthesized the polymers. The project was supervised by Frederik Wurm.

**[17] Denaturation via surfactants changes composition of protein corona**

**Aim.** The use of nanocarriers as drug delivery vehicles brings them into contact with blood plasma proteins. Polymeric nanocarriers require some sort of surfactant to ensure colloidal stability. Formation of the protein corona is therefore not only determined by the intrinsic properties of the nanocarrier itself, but also by the accompanying surfactant. Although it is well known that surfactants have an impact on protein structure, only few studies were conducted on the specific effect of surfactants on the composition of protein corona of nanocarriers. Therefore, we analyzed the composition of the protein corona on “stealth” nanoparticles with additional surfactant (cetyltrimethylammonium chloride, CTMA-Cl) after plasma incubation. Additional CTMA-Cl lead to an enrichment of apolipoprotein-A1 and vitronectin in the corona, while less clusterin could be found. Further, the structural stability of apolipoprotein-A1 and clusterin was monitored for a wide range of CTMA-Cl concentrations. Clusterin turned out to be more sensitive to CTMA-Cl, with denaturation occurring at lower concentrations.

**Contribution.** I prepared the surfactant coated nanoparticles carried out the protein corona analysis (SDS-PAGE, Pierce Assay and LC-MS). [redacted] performed the nanoDSF and isothermal titration calorimetry (ITC) experiments. [redacted] supplied the clusterin. The project was supervised by [redacted]

**[18] Preservation of the soft protein corona in distinct flow allows identification of weakly bound proteins**

**Aim.** Nanoparticles that are used for targeted drug delivery come in contact with biological liquid and proteins will adsorb to the nanocarrier's surface to form the so called 'protein corona'. The protein corona is what defines the biological identity of the nanoparticle in the body and determines the biological response towards the nanocarrier. To get a better idea of this protein corona and to make nanomedicine safe and reliable it is absolutely necessary to characterize the adsorbed proteins. Currently, centrifugation is the common method to isolate the protein corona for further investigations. However, with this method it is only possible to investigate the strongly bound proteins, also referred to as 'hard corona'. Therefore, we want to introduce a new separation technique to separate nanoparticles including the soft protein corona containing also loosely bound proteins for further characterizations. The used separation technique is the asymmetric flow filed-flow fractionation (AF4). We were able to separate the nanopartices with proteins forming the soft protein corona, and also could show, that the hard protein corona is what influences the cell uptake behavior.

**Contribution.** I carried out the LC-MS analysis and cell uptake experiments. Claudia Weber performed the asymmetric flow filed-flow fractionation. The project was supervised by [redacted]

**[19] The protein corona as a confounding variable of nanoparticle-mediated targeted vaccine delivery.**

**Aim.** Nanocarrier are almost inevitably coated with a protein corona after exposure to blood plasma or lymphatic fluid. This plasma protein corona can affect the trafficking of the NC within the body as well as their cellular targeting and uptake to a significant extent, potentially resulting in loss of the desired effects as well as altered functional properties of the NC. In contrast, the protein corona may also be exploited to extend their plasma half-life, thereby optimizing cell-specific targeting and immunotherapeutic effects, or even to re-direct NC to specific cell types or organs in vivo.

**Contribution.** In a collaborative work the review was written with Matthias Bros, Lutz Nuhn, Lorna Moll, Volker Mailänder, Katharina Landfester and Stephan Grabbe.

# Zusammenfassung

Durch den Kontakt von Nanopartikeln mit biologischen Medien, kommt es rasch zu einer Interaktion zwischen den Blutbestandteilen und der Nanopartikeloberfläche, wodurch der Nanopartikel eine biologische Identität erhält (´Biomolekül-Korona´). Dieser Prozess beeinflusst das pharmakokinetische Profil und die therapeutische Effizienz von allen Nanopartikeln. Obwohl es viele Bestrebungen zur Entwicklung von Nanopartikeln mit einer proteinabweisenden Oberfläche (beispielsweise mit PEG) gibt, ist es immer noch umstritten, ob es generell möglich ist die Proteinadsorption komplett zu verhindern. Aus diesem Grund ist eine genaue Charakterisierung der adsorbierten Proteinschicht unerlässlich. Denn durch diese Kenntnisse ist es möglich die biologischen Eigenschaften der Nanopartikel für einen effizienten Wirkstofftransport zu verbessern.

Im Rahmen dieser Arbeit werden verschiedene Interaktionen an der Nano-Bio-Grenzfläche untersucht. Durch eine kombinatorische Analyse mittels Transmissionselektronenmikroskopie (TEM) und hochauflösender Massen-spektrometrie (LC-MS) war es möglich die Entwicklung der Protein-Korona zu verfolgen. Diese ist nicht, wie erwartet, eine dicht gepackte Proteinschicht, sondern zeichnet sich durch eine inhomogene Struktur aus. Für eine aussagekräftige Analyse der Protein-Korona ist es unerlässlich die Studien unter physiologisch relevanten Bedingungen durchzuführen, die der komplexen Situation *in vivo* so nahe wie möglich kommen. Ein Negativbeispiel stellt die Hitzeinaktivierung dar. Dabei handelt es sich um ein gängiges methodisches Verfahren, das im Rahmen der Zellkultur Verwendung findet. Durch das Erhitzen der Proteinquelle des Zellkulturmediums sollen störende Einflüsse bei *in vitro* Versuchen vermieden oder verringert werden. Es stellte sich jedoch heraus, dass dadurch auch die Protein-Nanopartikel Interaktionen erheblich beeinflusst werden.

Klinische Studien sind der letzten Schritt bevor Nanopartikel eine medikamentöse Anwendung finden können. Zuvor werden typischerweise Mausstudien durchgeführt, um die Eigenschaften der Nanopartikel *in vivo* zu untersuchen. Aus diesem Grund wurde der Einfluss der artspezifischen Proteinzusammensetzung (Maus vs. Mensch) auf die Interaktion mit Nanopartikeln untersucht. Hier zeigten sich je nach Proteinquelle erhebliche Unterschiede in der Protein-Korona und Zellinteraktion.

In der Nanomedizin wird die Oberfläche von Nanopartikeln üblicherweise mit hydrophilen Polymeren (beispielsweise mit PEG) modifiziert, um die Zirkulation der Nanopartikel im Blut zu verlängern. Dies wird als Stealth-Effekt (´Tarnkappen-Effekt´) beschrieben und ist seit den frühen Anfängen der Nanomedizin eine etablierte Methode. Jedoch fehlte bisher ein grundlegendes Verständnis über den molekularen Mechanismus, auf dem dieser Effekt beruht. Um dies zu ergründen, wurde der Einfluss der Polymerhydrophilie auf die

Proteinadsorption untersucht und dieses mit der Zellaufnahme in Makrophagen korreliert. Es stellte sich heraus, dass je nach Oberflächenhydrophilie eine bestimmte Proteinadsorption induziert wird und spezifische Proteine den Stealth-Effekt vermitteln. Durch dieses Wissen ist es nun möglich, die Protein-Korona gezielt auszunutzen. Hier zeigte sich, dass durch eine maßgeschneiderte Protein-Korona eine unspezifische Aufnahme in Makrophagen verhindern werden kann.

Das allumfassende Ziel der Nanomedizin ist ein gerichteter Transport von Nanoträgern zur Zielzelle (´Targeting´). Hierfür wird die Oberfläche von Nanopartikeln mit spezifischen Liganden modifiziert. In vielen Studien wurde jedoch bereits beobachtet, dass durch die Protein-Korona die Targeting Eigenschaften der Nanopartikel erheblich beeinflusst werden können. Hier zeigte sich, dass Korona-Proteine den Liganden auf der Nanopartikeloberfläche komplett überdecken können, wodurch es zu keiner Interaktion zwischen den Rezeptoren auf der Zielzelle und dem Nanopartikel kommt. Aus diesem Grund wurden in dieser Arbeit verschiedene Methoden entwickelt, die eine effiziente Oberflächenfunktionalisierung von Nanopartikeln ermöglichen und somit auch in Anwesenheit der Korona eine gezielte Zellinteraktion erlauben.

Eine Möglichkeit zur Oberflächenmodifikation von Nanopartikeln bietet die Adsorption von Antikörpern bei einem bestimmten pH-Wert. Hier konnte ein gezielter Transport der Antikörper funktionalisierten Nanopartikel zur Zielzelle auch in Anwesenheit von Blutproteinen erfolgreich nachgewiesen werden.

Eine alternative Methode stellt der Einsatz von Tensiden zur nicht-kovalenten Oberflächenmodifikation von Nanopartikeln dar. Da Tenside oberflächenaktive Substanzen sind, können diese über eine nicht-kovalente Wechselwirkung an die Nanopartikeloberfläche binden. Um zu untersuchen, ob dieses Konzept für ein spezifisches Targeting von Nanopartikeln genutzt werden kann, wurden verschiedene Tenside mit einem Mannose Ligand modifiziert. Es zeigte sich, dass durch die Adsorption der Mannose funktionalisierten Tenside an die Oberfläche von verschiedenen Nanopartikeln, eine gezielte Zellinteraktion auch nach Inkubation mit Blutplasma ermöglicht wird.

# Summary and outlook

The gap between the rapid development of sophisticated nanoparticle formulations and their unsuccessful application *in vivo* highlights that there is a limited understanding about the behavior of nanoparticles under physiological conditions. Therefore, this work aimed to shed light into the interactions occurring at the nano-bio-interface. This knowledge is needed to design novel nanoparticle formulations, which allow controlled cell interactions.

Overall, this work describes three major topics, which need to be considered in order to assess the biological properties of nanoparticles. A comprehensive analysis of the biological fingerprint, which nanoparticles obtain after incubation with serum or plasma is essential to understand their further cellular interactions (**Chapter A**). Stealth properties are a major requirement of long circulating nanoparticles. Therefore, the molecular mechanism of the stealth effect needs to be evaluated (**Chapter B**). Finally, the key characteristic of nanoparticles designed as drug delivery vehicles are targeted and controlled cellular interactions (**Chapter C**). In the following, the main message of each chapter will be highlighted. Additionally, the major finding of all studies will be shortly summarized and based on this future experiment will be discussed.

**Chapter A: Protein structure and physiological environment (e.g. plasma, serum or blood) highly determine biomolecular corona formation.**

Study 1 showed that the protein corona has a non-uniform structure and is not – as supposed – a dense layer. This indicates that also targeting moieties on the surface of the nanoparticles can be attached and would allow controlled cellular interactions despite protein adsorption.

Study 2 underlined the urgent need to perform protein corona analysis under physiological relevant conditions. Heat inactivation of serum or plasma determinedly affected the protein adsorption pattern and therefore it does not reflect the *in vivo* situation.

Study 3 demonstrated that there are major differences between the corona formed in mouse plasma compared to human. This implies difficulties to translate *in vivo* (mouse) experiments to the clinical studies (human).

Study 4 showed that the *in vivo* corona has a broad complex protein pattern, which differed strongly from the composition obtained after *in vitro* incubation. This underlines the importance to establish methods, which mimic the i*n vivo* situation.

The knowledge about protein-nanoparticle interaction under *in vitro* conditions has increased extensively. Due to the development of new analytical methods, it should now be aimed to

understand *in vivo* corona formation. Further, it is of importance to evaluate cellular uptake in a complex cell surrounding (e.g. isolated spleen cells or whole blood) to understand the multiple interactions between nanoparticles and cells.

**Chapter B: A defined protein corona composition can mediate stealth properties.**

Study 5 correlated the nanoparticle surface hydrophilicity with protein adsorption and cellular uptake towards phagocytic cells. It was demonstrated that a defined surface hydrophilicity triggers selective protein adsorption, which mediates the stealth effect.

Study 6 found that the attachment of sugar molecules (HES, DEX or Glucose) provides stealth properties to nanoparticles. Therefore, it is possible to obtain fully degradable stealth nanoparticles via surface modification with sugar derivates.

Study 7 highlighted that corona formation can be exploited to decrease cellular interactions with macrophages.

Alternative methods to the conventional PEGylation strategy are needed. As it is now understood that proteins are involved in the stealth effect, selective protein adsorption can be exploited to prolong blood circulation *in vivo*.

**Chapter C: Advanced targeting strategies for the surface functionalization of nanoparticles enable controlled cell interactions despite corona formation.**

Study 8 demonstrated an easy approach to functionalize nanoparticles with antibodies. It was found that depending on a chosen pH the adsorption of antibodies to the nanoparticle surface is favored.

Study 9 showed that mannose functionalized poly(phosphoester) based surfactants can be used as non-covalent surface functionalization for a variety of nanoparticles to achieve targeted recognition of nanoparticles via the mannose receptor.

As it was proven that it is possible to achieve targeted cell interactions under *in vitro* conditions, it is now needed to evaluate the targeting efficiency *in vivo.* Additionally, it is aimed to find alternative strategies for the controlled covalent attachment of antibodies or other targeting ligands to the surface of nanoparticles. Moreover, a dual modification of the nanoparticle surface with stealth polymers or proteins and targeting ligands needs to be achieved and investigated under *in vivo* conditions.

# Literature

Combined references from the general introduction (page 5-8) and the individuell introduction parts in chaper A, B and C.


1. Moghimi, S. M.; Hunter, A. C.; Murray, J. C., Nanomedicine: current status and future prospects. *The FASEB journal* **2005,** *19* (3), 311-330.

2. Wei, C.; Wei, W.; Morris, M.; Kondo, E.; Gorbounov, M.; Tomalia, D. A., Nanomedicine and drug delivery. *Medical Clinics* **2007,** *91* (5), 863-870.

3. Mirza, A. Z.; Siddiqui, F. A., Nanomedicine and drug delivery: a mini review. *International Nano Letters* **2014,** *4* (1), 94.

4. Onoue, S.; Yamada, S.; Chan, H.-K., Nanodrugs: pharmacokinetics and safety. *International journal of nanomedicine* **2014,** *9*, 1025.

5. Gabizon, A.; Catane, R.; Uziely, B.; Kaufman, B.; Safra, T.; Cohen, R.; Martin, F.; Huang, A.; Barenholz, Y., Prolonged circulation time and enhanced accumulation in malignant exudates of doxorubicin encapsulated in polyethylene-glycol coated liposomes. *Cancer research* **1994,** *54* (4), 987-992.

6. Barenholz, Y. C., Doxil®—the first FDA-approved nano-drug: lessons learned. *Journal of controlled release* **2012,** *160* (2), 117-134.

7. Polyak, B.; Cordovez, B., How can we predict behavior of nanoparticles in vivo? Future Medicine: 2016.

8. Gambinossi, F.; Mylon, S. E.; Ferri, J. K., Aggregation kinetics and colloidal stability of functionalized nanoparticles. *Advances in colloid and interface science* **2015,** *222*, 332-349.

9. Rodzinski, A.; Guduru, R.; Liang, P.; Hadjikhani, A.; Stewart, T.; Stimphil, E.; Runowicz, C.; Cote, R.; Altman, N.; Datar, R., Targeted and controlled anticancer drug delivery and release with magnetoelectric nanoparticles. *Scientific reports* **2016,** *6*, 20867.

10. Yang, Y.; Qin, Z.; Zeng, W.; Yang, T.; Cao, Y.; Mei, C.; Kuang, Y., Toxicity assessment of nanoparticles in various systems and organs. *Nanotechnology Reviews* **2017,** *6* (3), 279-289.

11. Docter, D.; Westmeier, D.; Markiewicz, M.; Stolte, S.; Knauer, S.; Stauber, R., The nanoparticle biomolecule corona: lessons learned–challenge accepted? *Chemical Society Reviews* **2015,** *44* (17), 6094-6121.

12. Lynch, I.; Salvati, A.; Dawson, K. A., Protein-nanoparticle interactions: what does the cell see? *Nature nanotechnology* **2009,** *4* (9), 546.

13. Jain, P.; Pawar, R.; Pandey, R.; Madan, J.; Pawar, S.; Lakshmi, P.; Sudheesh, M., In-vitro in-vivo correlation (IVIVC) in nanomedicine: Is protein corona the missing link? *Biotechnology advances* **2017,** *35* (7), 889-904.

14. Xia, Y., Nanomaterials at work in biomedical research. *Nature materials* **2008,** *7* (10), 758.

15. Yang, H.; Xia, Y., Bionanotechnology: enabling biomedical research with nanomaterials. *Advanced Materials* **2007,** *19* (20), 3085-3087.

16. Polo, E.; Collado, M.; Pelaz, B.; del Pino, P., Advances toward more efficient targeted delivery of nanoparticles in vivo: understanding interactions between nanoparticles and cells. *ACS nano* **2017,** *11* (3), 2397-2402.

17. Bobo, D.; Robinson, K. J.; Islam, J.; Thurecht, K. J.; Corrie, S. R., Nanoparticle-based medicines: a review of FDA-approved materials and clinical trials to date. *Pharmaceutical research* **2016,** *33* (10), 2373-2387.

18. Desai, N., Challenges in development of nanoparticle-based therapeutics. *The AAPS journal* **2012,** *14* (2), 282-295.

19. Vroman, L., Effect of adsorbed proteins on the wettability of hydrophilic and hydrophobic solids. *Nature* **1962,** *196* (4853), 476.

20. Vroman, L.; Adams, A.; Fischer, G.; Munoz, P., Interaction of high molecular weight kininogen, factor XII, and fibrinogen in plasma at interfaces. *Blood* **1980,** *55* (1), 156-159.

21. Tenzer, S.; Docter, D.; Rosfa, S.; Wlodarski, A.; Kuharev, J. r.; Rekik, A.; Knauer, S. K.; Bantz, C.; Nawroth, T.; Bier, C., Nanoparticle size is a critical physicochemical determinant of the human blood plasma corona: a comprehensive quantitative proteomic analysis. *ACS nano* **2011,** *5* (9), 7155-7167.

22. Cedervall, T.; Lynch, I.; Lindman, S.; Berggård, T.; Thulin, E.; Nilsson, H.; Dawson, K. A.; Linse, S., Understanding the nanoparticle–protein corona using methods to quantify exchange rates and affinities of proteins for nanoparticles. *Proceedings of the National Academy of Sciences* **2007,** *104* (7), 2050-2055.

23. Tenzer, S.; Docter, D.; Kuharev, J.; Musyanovych, A.; Fetz, V.; Hecht, R.; Schlenk, F.; Fischer, D.; Kiouptsi, K.; Reinhardt, C., Rapid formation of plasma protein corona critically affects nanoparticle pathophysiology. *Nature nanotechnology* **2013,** *8* (10), 772-781.

24. Van Hong Nguyen, B.-J. L., Protein corona: A new approach for nanomedicine design. *International journal of nanomedicine* **2017,** *12*, 3137.

25. Ke, P. C.; Lin, S.; Parak, W. J.; Davis, T. P.; Caruso, F., A Decade of the Protein Corona. *ACS nano* **2017,** *11* (12), 11773-11776.

26. Raesch, S. S.; Tenzer, S.; Storck, W.; Rurainski, A.; Selzer, D.; Ruge, C. A.; Perez-Gil, J.; Schaefer, U. F.; Lehr, C.-M., Proteomic and lipidomic analysis of nanoparticle corona upon contact with lung surfactant reveals differences in protein, but not lipid composition. *ACS nano* **2015,** *9* (12), 11872-11885.

27. Müller, J.; Prozeller, D.; Ghazaryan, A.; Kokkinopoulou, M.; Mailänder, V.; Morsbach, S.; Landfester, K., Beyond the Protein Corona–Lipids Matter for Biological Response of Nanocarriers. *Acta biomaterialia* **2018**.

28. Wan, S.; Kelly, P. M.; Mahon, E.; Stöckmann, H.; Rudd, P. M.; Caruso, F.; Dawson, K. A.; Yan, Y.; Monopoli, M. P., The "sweet" side of the protein corona: effects of glycosylation on nanoparticle–cell interactions. *ACS nano* **2015,** *9* (2), 2157-2166.

29. Treuel, L.; Docter, D.; Maskos, M.; Stauber, R. H., Protein corona–from molecular adsorption to physiological complexity. *Beilstein journal of nanotechnology* **2015,** *6*, 857.

30. Wolfram, J.; Yang, Y.; Shen, J.; Moten, A.; Chen, C.; Shen, H.; Ferrari, M.; Zhao, Y., The nano-plasma interface: implications of the protein corona. *Colloids and Surfaces B: Biointerfaces* **2014,** *124*, 17-24.

31. Aggarwal, P.; Hall, J. B.; McLeland, C. B.; Dobrovolskaia, M. A.; McNeil, S. E., Nanoparticle interaction with plasma proteins as it relates to particle biodistribution, biocompatibility and therapeutic efficacy. *Advanced drug delivery reviews* **2009,** *61* (6), 428-437.

32. Giudice, M. C. L.; Herda, L. M.; Polo, E.; Dawson, K. A., In situ characterization of nanoparticle biomolecular interactions in complex biological media by flow cytometry. *Nature communications* **2016,** *7*, 13475.

33. Chen, F.; Wang, G.; Griffin, J. I.; Brenneman, B.; Banda, N. K.; Holers, V. M.; Backos, D. S.; Wu, L.; Moghimi, S. M.; Simberg, D., Complement proteins bind to nanoparticle protein corona and undergo dynamic exchange in vivo. *Nature nanotechnology* **2017,** *12* (4), 387.

34. Shen, L.; Tenzer, S.; Storck, W.; Hobernik, D.; Raker, V. K.; Fischer, K.; Decker, S.; Dzionek, A.; Krauthäuser, S.; Diken, M., Protein corona–mediated targeting of nanocarriers to B cells allows redirection of allergic immune responses. *Journal of Allergy and Clinical Immunology* **2018**.

35. Deng, Z. J.; Mortimer, G.; Schiller, T.; Musumeci, A.; Martin, D.; Minchin, R. F., Differential plasma protein binding to metal oxide nanoparticles. *Nanotechnology* **2009,** *20* (45), 455101.

36. Owens III, D. E.; Peppas, N. A., Opsonization, biodistribution, and pharmacokinetics of polymeric nanoparticles. *International journal of pharmaceutics* **2006,** *307* (1), 93-102.

37. Gref, R.; Lück, M.; Quellec, P.; Marchand, M.; Dellacherie, E.; Harnisch, S.; Blunk, T.; Müller, R., 'Stealth'corona-core nanoparticles surface modified by polyethylene glycol (PEG): influences of the corona (PEG chain length and surface density) and of the core composition on phagocytic uptake and plasma protein adsorption. *Colloids and Surfaces B: Biointerfaces* **2000,** *18* (3-4), 301-313.

38. Pelaz, B.; del Pino, P.; Maffre, P.; Hartmann, R.; Gallego, M.; Rivera-Fernandez, S.; de la Fuente, J. M.; Nienhaus, G. U.; Parak, W. J., Surface functionalization of nanoparticles with polyethylene glycol: effects on protein adsorption and cellular uptake. *Acs Nano* **2015,** *9* (7), 6996-7008.

39. Ashby, J.; Pan, S.; Zhong, W., Size and surface functionalization of iron oxide nanoparticles influence the composition and dynamic nature of their protein corona. *ACS applied materials & interfaces* **2014,** *6* (17), 15412-15419.

40. Lundqvist, M.; Stigler, J.; Elia, G.; Lynch, I.; Cedervall, T.; Dawson, K. A., Nanoparticle size and surface properties determine the protein corona with possible implications for biological impacts. *Proceedings of the National Academy of Sciences* **2008,** *105* (38), 14265-14270.

41. Fleischer, C. C.; Payne, C. K., Nanoparticle–cell interactions: molecular structure of the protein corona and cellular outcomes. *Accounts of chemical research* **2014,** *47* (8), 2651-2659.

42. Fleischer, C. C.; Payne, C. K., Secondary structure of corona proteins determines the cell surface receptors used by nanoparticles. *The Journal of Physical Chemistry B* **2014,** *118* (49), 14017-14026.

43. Hoshyar, N.; Gray, S.; Han, H.; Bao, G., The effect of nanoparticle size on in vivo pharmacokinetics and cellular interaction. *Nanomedicine* **2016,** *11* (6), 673-692.

44. Betzer, O.; Shilo, M.; Opochinsky, R.; Barnoy, E.; Motiei, M.; Okun, E.; Yadid, G.; Popovtzer, R., The effect of nanoparticle size on the ability to cross the blood–brain barrier: an in vivo study. *Nanomedicine* **2017,** *12* (13), 1533-1546.

45. Shang, L.; Nienhaus, K.; Nienhaus, G. U., Engineered nanoparticles interacting with cells: size matters. *J Nanobiotechnol* **2014,** *12* (5), b26.

46. Nel, A. E.; Mädler, L.; Velegol, D.; Xia, T.; Hoek, E. M.; Somasundaran, P.; Klaessig, F.; Castranova, V.; Thompson, M., Understanding biophysicochemical interactions at the nano–bio interface. *Nature materials* **2009,** *8* (7), 543.

47. Lynch, I.; Cedervall, T.; Lundqvist, M.; Cabaleiro-Lago, C.; Linse, S.; Dawson, K. A., The nanoparticle–protein complex as a biological entity; a complex fluids and surface science challenge for the 21st century. *Advances in colloid and interface science* **2007,** *134*, 167-174.

48. Winzen, S.; Schoettler, S.; Baier, G.; Rosenauer, C.; Mailaender, V.; Landfester, K.; Mohr, K., Complementary analysis of the hard and soft protein corona: sample preparation critically effects corona composition. *Nanoscale* **2015,** *7* (7), 2992-3001.

49. Pederzoli, F.; Tosi, G.; Vandelli, M. A.; Belletti, D.; Forni, F.; Ruozi, B., Protein corona and nanoparticles: how can we investigate on? *Wiley Interdisciplinary Reviews: Nanomedicine and Nanobiotechnology* **2017,** *9* (6).

50. Carrillo-Carrion, C.; Carril, M.; Parak, W. J., Techniques for the experimental investigation of the protein corona. *Current opinion in biotechnology* **2017,** *46*, 106-113.

51. Carril, M.; Padro, D.; del Pino, P.; Carrillo-Carrion, C.; Gallego, M.; Parak, W. J., In situ detection of the protein corona in complex environments. *Nature Communications* **2017,** *8* (1), 1542.

52. Rausch, K.; Reuter, A.; Fischer, K.; Schmidt, M., Evaluation of nanoparticle aggregation in human blood serum. *Biomacromolecules* **2010,** *11* (11), 2836-2839.

53. Mohr, K.; Sommer, M.; Baier, G.; Schöttler, S.; Okwieka, P.; Tenzer, S.; Landfester, K.; Mailänder, V.; Schmidt, M.; Meyer, R. G., Aggregation behavior of polystyrene-nanoparticles in human blood serum and its impact on the in vivo distribution in mice. *Journal of Nanomedicine & Nanotechnology* **2014,** *5* (2).

54. Nienhaus, G. U.; Maffre, P.; Nienhaus, K., Studying the protein corona on nanoparticles by FCS. In *Methods in enzymology*, Elsevier: 2013; Vol. 519, pp 115-137.

55. Sasidharan, A.; Riviere, J. E.; Monteiro-Riviere, N. A., Gold and silver nanoparticle interactions with human proteins: impact and implications in biocorona formation. *Journal of Materials Chemistry B* **2015,** *3* (10), 2075-2082.

56. Renz, P.; Kokkinopoulou, M.; Landfester, K.; Lieberwirth, I., Imaging of Polymeric Nanoparticles: Hard Challenge for Soft Objects. *Macromolecular Chemistry and Physics* **2016,** *217* (17), 1879-1885.

57. Kelly, P. M.; Åberg, C.; Polo, E.; O'connell, A.; Cookman, J.; Fallon, J.; Krpetić, Ž.; Dawson, K. A., Mapping protein binding sites on the biomolecular corona of nanoparticles. *Nature nanotechnology* **2015,** *10* (5), 472.

58. Satzer, P.; Svec, F.; Sekot, G.; Jungbauer, A., Protein adsorption onto nanoparticles induces conformational changes: Particle size dependency, kinetics, and mechanisms. *Engineering in life sciences* **2016,** *16* (3), 238-246.

59. Welsch, N.; Lu, Y.; Dzubiella, J.; Ballauff, M., Adsorption of proteins to functional polymeric nanoparticles. *Polymer* **2013,** *54* (12), 2835-2849.

60. Müller, J.; Bauer, K. N.; Prozeller, D.; Simon, J.; Mailänder, V.; Wurm, F. R.; Winzen, S.; Landfester, K., Coating nanoparticles with tunable surfactants facilitates control over the protein corona. *Biomaterials* **2017,** *115*, 1-8.

61. Capjak, I.; Goreta, S. Š.; Jurašin, D. D.; Vrček, I. V., How protein coronas determine the fate of engineered nanoparticles in biological environment. *Archives of Industrial Hygiene and Toxicology* **2017,** *68* (4), 245-253.

62. Milani, S.; Baldelli Bombelli, F.; Pitek, A. S.; Dawson, K. A.; Rädler, J., Reversible versus irreversible binding of transferrin to polystyrene nanoparticles: soft and hard corona. *ACS nano* **2012,** *6* (3), 2532-2541.

63. Bonvin, D.; Chiappe, D.; Moniatte, M.; Hofmann, H.; Ebersold, M. M., Methods of protein corona isolation for magnetic nanoparticles. *Analyst* **2017,** *142* (20), 3805-3815.

64. Jansch, M.; Stumpf, P.; Graf, C.; Rühl, E.; Müller, R., Adsorption kinetics of plasma proteins on ultrasmall superparamagnetic iron oxide (USPIO) nanoparticles. *International journal of pharmaceutics* **2012,** *428* (1-2), 125-133.

65. Walkey, C. D.; Chan, W. C., Understanding and controlling the interaction of nanomaterials with proteins in a physiological environment. *Chemical Society Reviews* **2012,** *41* (7), 2780-2799.

66. Distler, U.; Kuharev, J.; Navarro, P.; Tenzer, S., Label-free quantification in ion mobility–enhanced data-independent acquisition proteomics. *nature protocols* **2016,** *11* (4), 795.

67. Zanganeh, S.; Spitler, R.; Erfanzadeh, M.; Alkilany, A. M.; Mahmoudi, M., Protein corona: Opportunities and challenges. *The international journal of biochemistry & cell biology* **2016,** *75*, 143-147.

68. Monopoli, M. P.; Walczyk, D.; Campbell, A.; Elia, G.; Lynch, I.; Baldelli Bombelli, F.; Dawson, K. A., Physical− chemical aspects of protein corona: relevance to in vitro and in vivo biological impacts of nanoparticles. *Journal of the American Chemical Society* **2011,** *133* (8), 2525-2534.

69. Brun, E.; Sicard–Roselli, C., Could nanoparticle corona characterization help for biological consequence prediction? *Cancer nanotechnology* **2014,** *5* (1), 7.

70. Monopoli, M. P.; Åberg, C.; Salvati, A.; Dawson, K. A., Biomolecular coronas provide the biological identity of nanosized materials. *Nature nanotechnology* **2012,** *7* (12), 779.

71. Hadjidemetriou, M.; Kostarelos, K., Nanomedicine: evolution of the nanoparticle corona. *Nature nanotechnology* **2017,** *12* (4), 288.

72. Tang, H.-Y.; Beer, L. A.; Speicher, D. W., In-depth analysis of a plasma or serum proteome using a 4D protein profiling method. In *Serum/Plasma Proteomics*, Springer: 2011; pp 47-67.

73. Bettger, W. J.; McKEEHAN, W. L., Mechanisms of cellular nutrition. *Physiological reviews* **1986,** *66* (1), 1-35.

74. Faca, V. M.; Song, K. S.; Wang, H.; Zhang, Q.; Krasnoselsky, A. L.; Newcomb, L. F.; Plentz, R. R.; Gurumurthy, S.; Redston, M. S.; Pitteri, S. J., A mouse to human search for plasma proteome changes associated with pancreatic tumor development. *PLoS medicine* **2008,** *5* (6), e123.

75. Solorio-Rodríguez, A.; Escamilla-Rivera, V.; Uribe-Ramírez, M.; Chagolla, A.; Winkler, R.; García-Cuellar, C.; De Vizcaya-Ruiz, A., A comparison of the human and mouse protein corona profiles of functionalized SiO 2 nanocarriers. *Nanoscale* **2017,** *9* (36), 13651-13660.

76. Schöttler, S.; Klein, K.; Landfester, K.; Mailänder, V., Protein source and choice of anticoagulant decisively affect nanoparticle protein corona and cellular uptake. *Nanoscale* **2016,** *8* (10), 5526-5536.

77. Mirshafiee, V.; Kim, R.; Mahmoudi, M.; Kraft, M. L., The importance of selecting a proper biological milieu for protein corona analysis in vitro: Human plasma versus human serum. *The international journal of biochemistry & cell biology* **2016,** *75*, 188-195.

78. Hadjidemetriou, M.; Al-Ahmady, Z.; Mazza, M.; Collins, R. F.; Dawson, K.; Kostarelos, K., In vivo biomolecule corona around blood-circulating, clinically used and antibody-targeted lipid bilayer nanoscale vesicles. *ACS nano* **2015,** *9* (8), 8142-8156.

79. Vilanova, O.; Mittag, J. J.; Kelly, P. M.; Milani, S.; Dawson, K. A.; Rädler, J. O.; Franzese, G., Understanding the kinetics of protein–nanoparticle corona formation. *ACS nano* **2016,** *10* (12), 10842-10850.

80. Ritz, S.; Schöttler, S.; Kotman, N.; Baier, G.; Musyanovych, A.; Kuharev, J. r.; Landfester, K.; Schild, H. r.; Jahn, O.; Tenzer, S.; Mailander, V., Protein Corona of Nanoparticles: Distinct Proteins Regulate the Cellular Uptake. *Biomacromolecules* **2015,** *16* (4), 1311-1321.

81. Lesniak, A.; Fenaroli, F.; Monopoli, M. P.; Åberg, C.; Dawson, K. A.; Salvati, A., Effects of the presence or absence of a protein corona on silica nanoparticle uptake and impact on cells. *ACS nano* **2012,** *6* (7), 5845-5857.

82. Treuel, L.; Brandholt, S.; Maffre, P.; Wiegele, S.; Shang, L.; Nienhaus, G. U., Impact of protein modification on the protein corona on nanoparticles and nanoparticle–cell interactions. *ACS nano* **2014,** *8* (1), 503-513.

83. Lara, S.; Alnasser, F.; Polo, E.; Garry, D.; Lo Giudice, M. C.; Hristov, D. R.; Rocks, L.; Salvati, A.; Yan, Y.; Dawson, K. A., Identification of receptor binding to the biomolecular corona of nanoparticles. *ACS nano* **2017,** *11* (2), 1884-1893.

84. Lee, Y. K.; Choi, E.-J.; Webster, T. J.; Kim, S.-H.; Khang, D., Effect of the protein corona on nanoparticles for modulating cytotoxicity and immunotoxicity. *International journal of nanomedicine* **2015,** *10*, 97.

85. Gustafson, H. H.; Holt-Casper, D.; Grainger, D. W.; Ghandehari, H., Nanoparticle uptake: the phagocyte problem. *Nano today* **2015,** *10* (4), 487-510.

86. Jenkin, C. R.; Rowley, D., The role of opsonins in the clearance of living and inert particles by cells of the reticuloendothelial system. *Journal of Experimental Medicine* **1961,** *114* (3), 363-374.

87. Torchilin, V., Tumor delivery of macromolecular drugs based on the EPR effect. *Advanced drug delivery reviews* **2011,** *63* (3), 131-135.

88. Fraser, I.; Gordon, S., An overview of receptors of MPS cells. In *Macrophages and Related Cells*, Springer: 1993; pp 1-27.

89. Storm, G.; Belliot, S. O.; Daemen, T.; Lasic, D. D., Surface modification of nanoparticles to oppose uptake by the mononuclear phagocyte system. *Advanced drug delivery reviews* **1995,** *17* (1), 31-48.

90. Abuchowski, A.; Van Es, T.; Palczuk, N.; Davis, F., Alteration of immunological properties of bovine serum albumin by covalent attachment of polyethylene glycol. *Journal of Biological Chemistry* **1977,** *252* (11), 3578-3581.

91. Suk, J. S.; Xu, Q.; Kim, N.; Hanes, J.; Ensign, L. M., PEGylation as a strategy for improving nanoparticle-based drug and gene delivery. *Advanced drug delivery reviews* **2016,** *99*, 28-51.

92. Mishra, P.; Nayak, B.; Dey, R., PEGylation in anti-cancer therapy: An overview. *asian journal of pharmaceutical sciences* **2016,** *11* (3), 337-348.

93. Martin, F. J., Pegylated liposomal doxorubicin: scientific rationale and preclinical pharmacology. *ONCOLOGY-WILLISTON PARK THEN HUNTINGTON-* **1997,** *11*, 11-20.

94. Garay, R. P.; El-Gewely, R.; Armstrong, J. K.; Garratty, G.; Richette, P., Antibodies against polyethylene glycol in healthy subjects and in patients treated with PEG-conjugated agents. Taylor & Francis: 2012.

95. Hamad, I.; Hunter, A.; Szebeni, J.; Moghimi, S. M., Poly (ethylene glycol) s generate complement activation products in human serum through increased alternative pathway turnover and a MASP-2-dependent process. *Molecular immunology* **2008,** *46* (2), 225-232.

96. Rodriguez, P. L.; Harada, T.; Christian, D. A.; Pantano, D. A.; Tsai, R. K.; Discher, D. E., Minimal" self" peptides that inhibit phagocytic clearance and enhance delivery of nanoparticles. *Science* **2013,** *339* (6122), 971-975.

97. Hu, C.-M. J.; Zhang, L.; Aryal, S.; Cheung, C.; Fang, R. H.; Zhang, L., Erythrocyte membrane-camouflaged polymeric nanoparticles as a biomimetic delivery platform. *Proceedings of the National Academy of Sciences* **2011,** *108* (27), 10980-10985.

98. Parodi, A.; Quattrocchi, N.; Van De Ven, A. L.; Chiappini, C.; Evangelopoulos, M.; Martinez, J. O.; Brown, B. S.; Khaled, S. Z.; Yazdi, I. K.; Enzo, M. V., Synthetic nanoparticles functionalized with biomimetic leukocyte membranes possess cell-like functions. *Nature nanotechnology* **2013,** *8* (1), 61.

99. Harris, J. M.; Dust, J. M.; McGill, R. A.; Harris, P. A.; Edgell, M. J.; Sedaghat-Herati, R. M.; Karr, L. J.; Donnelly, D. L., New polyethylene glycols for biomedical applications. ACS Publications: 1991.

100. Herzberger, J.; Niederer, K.; Pohlit, H.; Seiwert, J.; Worm, M.; Wurm, F. R.; Frey, H., Polymerization of ethylene oxide, propylene oxide, and other alkylene oxides: Synthesis, novel polymer architectures, and bioconjugation. *Chemical reviews* **2015,** *116* (4), 2170-2243.

101. Jokerst, J. V.; Lobovkina, T.; Zare, R. N.; Gambhir, S. S., Nanoparticle PEGylation for imaging and therapy. *Nanomedicine* **2011,** *6* (4), 715-728.

102. Nicholas, A. R.; Scott, M. J.; Kennedy, N. I.; Jones, M. N., Effect of grafted polyethylene glycol (PEG) on the size, encapsulation efficiency and permeability of vesicles. *Biochimica et Biophysica Acta (BBA)-Biomembranes* **2000,** *1463* (1), 167-178.

103. Xu, Q.; Ensign, L. M.; Boylan, N. J.; Schön, A.; Gong, X.; Yang, J.-C.; Lamb, N. W.; Cai, S.; Yu, T.; Freire, E., Impact of surface polyethylene glycol (PEG) density on biodegradable nanoparticle transport in mucus ex vivo and distribution in vivo. *ACS nano* **2015,** *9* (9), 9217-9227.

104. Bertrand, N.; Grenier, P.; Mahmoudi, M.; Lima, E. M.; Appel, E. A.; Dormont, F.; Lim, J.-M.; Karnik, R.; Langer, R.; Farokhzad, O. C., Mechanistic understanding of in vivo protein corona formation on polymeric nanoparticles and impact on pharmacokinetics. *Nature communications* **2017,** *8* (1), 777.

105. Perry, J. L.; Reuter, K. G.; Kai, M. P.; Herlihy, K. P.; Jones, S. W.; Luft, J. C.; Napier, M.; Bear, J. E.; DeSimone, J. M., PEGylated PRINT nanoparticles: the impact of PEG density on protein binding, macrophage association, biodistribution, and pharmacokinetics. *Nano letters* **2012,** *12* (10), 5304-5310.

106. Schöttler, S.; Becker, G.; Winzen, S.; Steinbach, T.; Mohr, K.; Landfester, K.; Mailänder, V.; Wurm, F. R., Protein adsorption is required for stealth effect of poly (ethylene glycol)-and poly (phosphoester)-coated nanocarriers. *Nature nanotechnology* **2016,** *11* (4), 372.

107. Walkey, C. D.; Olsen, J. B.; Guo, H.; Emili, A.; Chan, W. C., Nanoparticle size and surface chemistry determine serum protein adsorption and macrophage uptake. *Journal of the American Chemical Society* **2012,** *134* (4), 2139-2147.

108. Aoyama, M.; Hata, K.; Higashisaka, K.; Nagano, K.; Yoshioka, Y.; Tsutsumi, Y., Clusterin in the protein corona plays a key role in the stealth effect of nanoparticles against phagocytes. *Biochemical and biophysical research communications* **2016,** *480* (4), 690-695.

109. Amoozgar, Z.; Yeo, Y., Recent advances in stealth coating of nanoparticle drug delivery systems. *Wiley Interdisciplinary Reviews: Nanomedicine and Nanobiotechnology* **2012,** *4* (2), 219-233.

110. Shah, S.; Prematta, T.; Adkinson, N. F.; Ishmael, F. T., Hypersensitivity to polyethylene glycols. *The Journal of Clinical Pharmacology* **2013,** *53* (3), 352-355.

111. Wang, X.; Ishida, T.; Kiwada, H., Anti-PEG IgM elicited by injection of liposomes is involved in the enhanced blood clearance of a subsequent dose of PEGylated liposomes. *Journal of Controlled Release* **2007,** *119* (2), 236-244.

112. Cao, Z.; Jiang, S., Super-hydrophilic zwitterionic poly (carboxybetaine) and amphiphilic non-ionic poly (ethylene glycol) for stealth nanoparticles. *Nano Today* **2012,** *7* (5), 404-413.

113. Bauer, K. N.; Tee, H. T.; Velencoso, M. M.; Wurm, F. R., Main-chain poly (phosphoester) s: History, syntheses, degradation, bio-and flame-retardant applications. *Progress in Polymer Science* **2017,** *73*, 61-122.

114. Kang, B.; Opatz, T.; Landfester, K.; Wurm, F. R., Carbohydrate nanocarriers in biomedical applications: functionalization and construction. *Chemical Society Reviews* **2015,** *44* (22), 8301-8325.

115. Ahmed, M.; Narain, R., Glyconanoparticles for gene delivery. In *Nanomaterials for biomedicine*, ACS Publications: 2012; pp 81-105.

116. Takeuchi, T.; Kitayama, Y.; Sasao, R.; Yamada, T.; Toh, K.; Matsumoto, Y.; Kataoka, K., Molecularly imprinted nanogels acquire stealth in situ by cloaking themselves with native dysopsonic proteins. *Angewandte Chemie International Edition* **2017,** *56* (25), 7088-7092.

117. Bazak, R.; Houri, M.; El Achy, S.; Kamel, S.; Refaat, T., Cancer active targeting by nanoparticles: a comprehensive review of literature. *Journal of cancer research and clinical oncology* **2015,** *141* (5), 769-784.

118. Kumar, R.; Roy, I.; Ohulchanskky, T. Y.; Vathy, L. A.; Bergey, E. J.; Sajjad, M.; Prasad, P. N., In vivo biodistribution and clearance studies using multimodal organically modified silica nanoparticles. *ACS nano* **2010,** *4* (2), 699-708.

119. Allen, T. M.; Cullis, P. R., Drug delivery systems: entering the mainstream. *Science* **2004,** *303* (5665), 1818-1822.

120. Yu, M. K.; Park, J.; Jon, S., Targeting strategies for multifunctional nanoparticles in cancer imaging and therapy. *Theranostics* **2012,** *2* (1), 3.

121. Sutradhar, K. B.; Amin, M. L., Nanotechnology in cancer drug delivery and selective targeting. *ISRN Nanotechnology* **2014,** *2014*.

122. Jiang, W.; von Roemeling, C. A.; Chen, Y.; Qie, Y.; Liu, X.; Chen, J.; Kim, B. Y., Designing nanomedicine for immuno-oncology. *Nature Biomedical Engineering* **2017,** *1* (2), 0029.

123. Maeda, H.; Wu, J.; Sawa, T.; Matsumura, Y.; Hori, K., Tumor vascular permeability and the EPR effect in macromolecular therapeutics: a review. *Journal of controlled release* **2000,** *65* (1-2), 271-284.

124. Maeda, H., Vascular permeability in cancer and infection as related to macromolecular drug delivery, with emphasis on the EPR effect for tumor-selective drug targeting. *Proceedings of the Japan Academy, Series B* **2012,** *88* (3), 53-71.

125. Swartz, H. M.; Khan, N.; Buckey, J.; Comi, R.; Gould, L.; Grinberg, O.; Hartford, A.; Hopf, H.; Hou, H.; Hug, E., Clinical applications of EPR: overview and perspectives. *NMR in Biomedicine* **2004,** *17* (5), 335-351.

126. Bi, Y.; Hao, F.; Yan, G.; Teng, L.; J Lee, R.; Xie, J., Actively targeted nanoparticles for drug delivery to tumor. *Current drug metabolism* **2016,** *17* (8), 763-782.

127. D Friedman, A.; E Claypool, S.; Liu, R., The smart targeting of nanoparticles. *Current pharmaceutical design* **2013,** *19* (35), 6315-6329.

128. Strebhardt, K.; Ullrich, A., Paul Ehrlich's magic bullet concept: 100 years of progress. *Nature Reviews Cancer* **2008,** *8* (6), 473.

129. Cheng, C. J.; Tietjen, G. T.; Saucier-Sawyer, J. K.; Saltzman, W. M., A holistic approach to targeting disease with polymeric nanoparticles. *Nature reviews Drug discovery* **2015,** *14* (4), 239.

130. Barrett, A. J., Antibody darts on target for acute myelogenous leukemia. *Annals of translational medicine* **2017,** *5* (4).

131. Andersen, M. N.; Al-Karradi, S. N.; Kragstrup, T. W.; Hokland, M., Elimination of erroneous results in flow cytometry caused by antibody binding to Fc receptors on human monocytes and macrophages. *Cytometry Part A* **2016,** *89* (11), 1001-1009.

132. Yhee, J. Y.; Lee, S. J.; Lee, S.; Song, S.; Min, H. S.; Kang, S.-W.; Son, S.; Jeong, S. Y.; Kwon, I. C.; Kim, S. H., Tumor-targeting transferrin nanoparticles for systemic polymerized siRNA delivery in tumor-bearing mice. *Bioconjugate chemistry* **2013,** *24* (11), 1850-1860.

133. Wu, C.-H.; Liu, I.-J.; Lu, R.-M.; Wu, H.-C., Advancement and applications of peptide phage display technology in biomedical science. *Journal of biomedical science* **2016,** *23* (1), 8.

134. Kang, B.; Okwieka, P.; Schöttler, S.; Winzen, S.; Langhanki, J.; Mohr, K.; Opatz, T.; Mailänder, V.; Landfester, K.; Wurm, F. R., Carbohydrate-based nanocarriers exhibiting specific cell targeting with minimum influence from the protein corona. *Angewandte Chemie International Edition* **2015,** *54* (25), 7436-7440.

135. Sehgal, K.; Dhodapkar, K. M.; Dhodapkar, M. V., Targeting human dendritic cells in situ to improve vaccines. *Immunology letters* **2014,** *162* (1), 59-67.

136. Stella, B.; Arpicco, S.; Peracchia, M. T.; Desmaële, D.; Hoebeke, J.; Renoir, M.; D'Angelo, J.; Cattel, L.; Couvreur, P., Design of folic acid-conjugated nanoparticles for drug targeting. *Journal of pharmaceutical sciences* **2000,** *89* (11), 1452-1464.

137. Salvati, A.; Pitek, A. S.; Monopoli, M. P.; Prapainop, K.; Bombelli, F. B.; Hristov, D. R.; Kelly, P. M.; Åberg, C.; Mahon, E.; Dawson, K. A., Transferrin-functionalized nanoparticles lose their targeting capabilities when a biomolecule corona adsorbs on the surface. *Nature nanotechnology* **2013,** *8* (2), 137.

138. Mirshafiee, V.; Mahmoudi, M.; Lou, K.; Cheng, J.; Kraft, M. L., Protein corona significantly reduces active targeting yield. *Chemical communications* **2013,** *49* (25), 2557-2559.

139. Dai, Q.; Bertleff-Zieschang, N.; Braunger, J. A.; Björnmalm, M.; Cortez-Jugo, C.; Caruso, F., Particle Targeting in Complex Biological Media. *Advanced healthcare materials* **2017**.

140. Dai, Q.; Yan, Y.; Guo, J.; Björnmalm, M.; Cui, J.; Sun, H.; Caruso, F., Targeting ability of affibody-functionalized particles is enhanced by albumin but inhibited by serum coronas. *ACS Macro Letters* **2015,** *4* (11), 1259-1263.

141. Kreuter, J.; Shamenkov, D.; Petrov, V.; Ramge, P.; Cychutek, K.; Koch-Brandt, C.; Alyautdin, R., Apolipoprotein-mediated transport of nanoparticle-bound drugs across the blood-brain barrier. *Journal of drug targeting* **2002,** *10* (4), 317-325.

142. Wagner, S.; Zensi, A.; Wien, S. L.; Tschickardt, S. E.; Maier, W.; Vogel, T.; Worek, F.; Pietrzik, C. U.; Kreuter, J.; Von Briesen, H., Uptake mechanism of ApoE-modified nanoparticles on brain capillary endothelial cells as a blood-brain barrier model. *PloS one* **2012,** *7* (3), e32568.

143. Caracciolo, G.; Cardarelli, F.; Pozzi, D.; Salomone, F.; Maccari, G.; Bardi, G.; Capriotti, A. L.; Cavaliere, C.; Papi, M.; Laganà, A., Selective targeting capability acquired with a protein corona adsorbed on the surface of 1, 2-dioleoyl-3-trimethylammonium propane/DNA nanoparticles. *ACS applied materials & interfaces* **2013,** *5* (24), 13171-13179.

144. Mirshafiee, V.; Kim, R.; Park, S.; Mahmoudi, M.; Kraft, M. L., Impact of protein pre-coating on the protein corona composition and nanoparticle cellular uptake. *Biomaterials* **2016,** *75*, 295-304.

# TOC Table of Contents

**[1] Visualization of the protein corona: towards a biomolecular understanding of nanoparticle-cell-interactions**

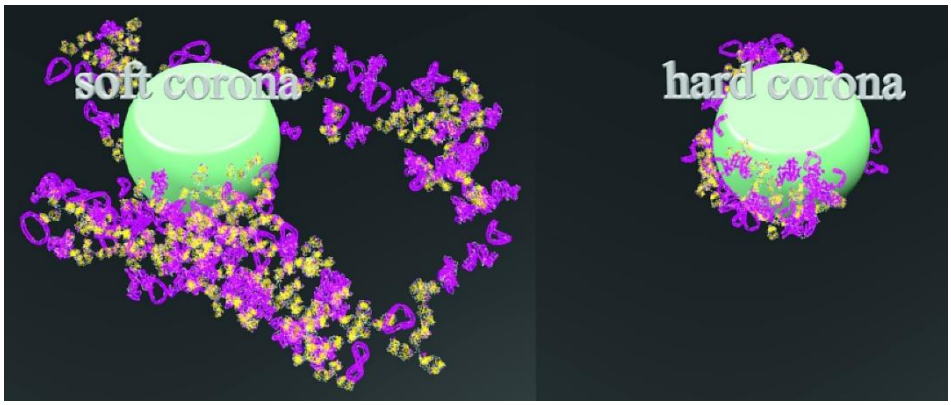


**[2] Protein denaturation by heat inactivation detrimentally affects biomolecular corona formation and cellular interactions**

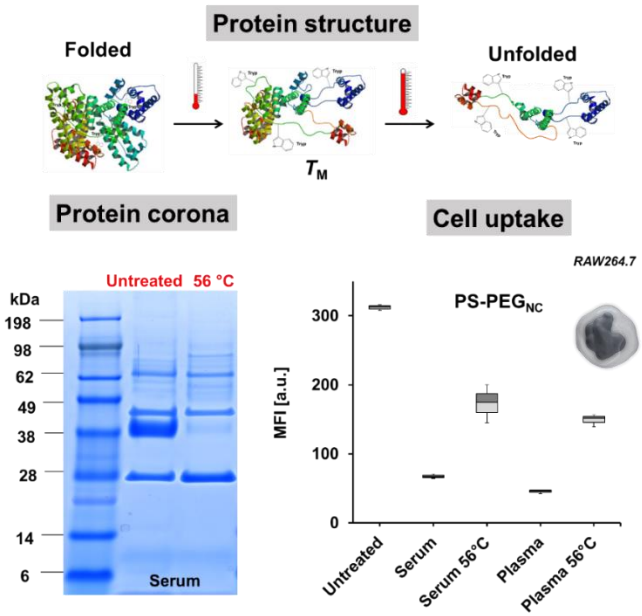

**[3] The transferability from animal models to humans: challenges regarding aggregation and protein corona formation of nanoparticles.**

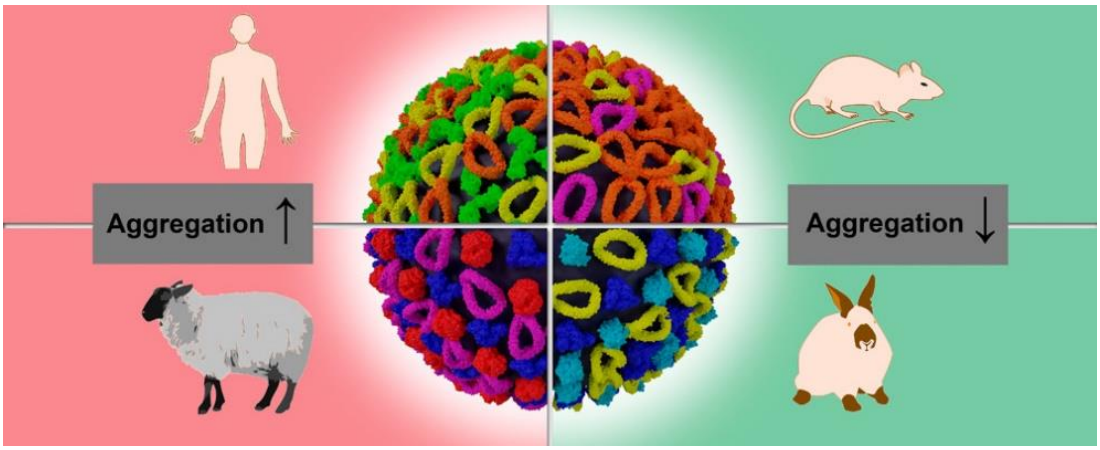


**[4] Unraveling *in vivo* corona formation**

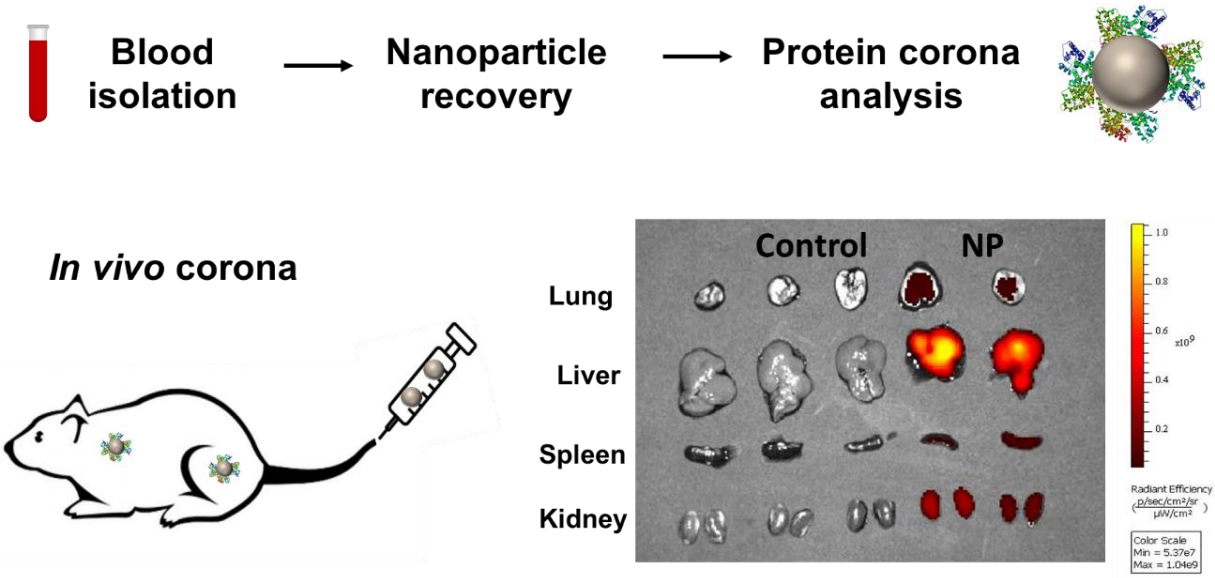

**[5] Hydrophilicity regulates the stealth properties of poly(phosphoester)-coated nanocarriers**

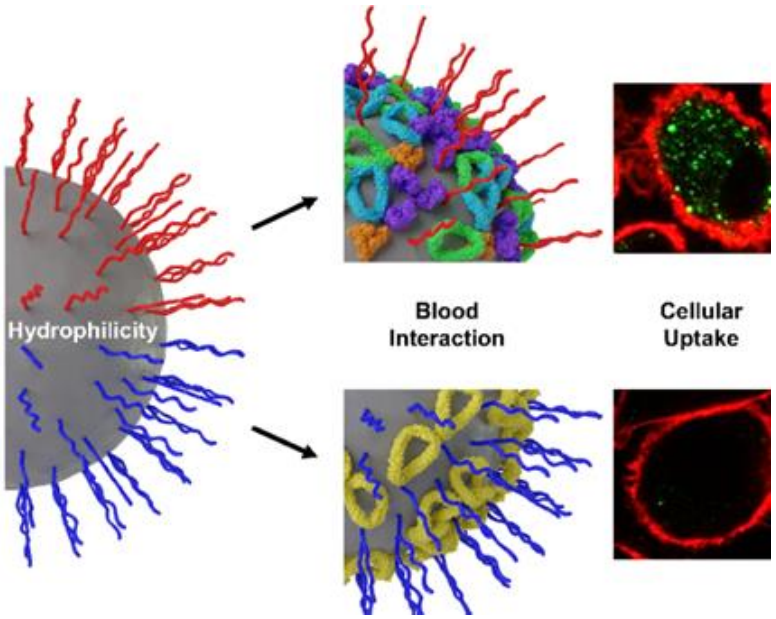


**[6] Protein corona mediated stealth properties of biocompatible carbohydrate-based nanocarriers**

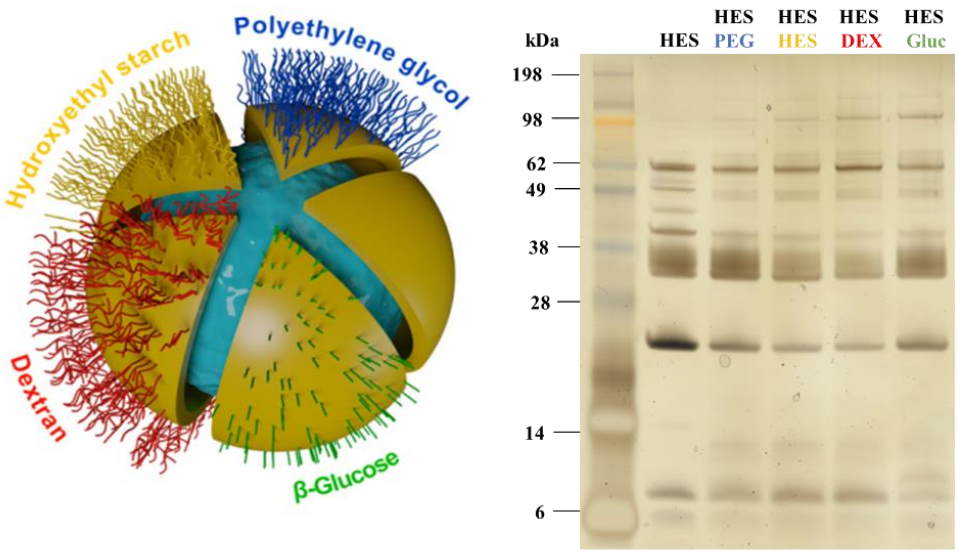

**[7] Exploiting the biomolecular corona: Pre-coating of nanoparticles enables controlled cellular interactions´**

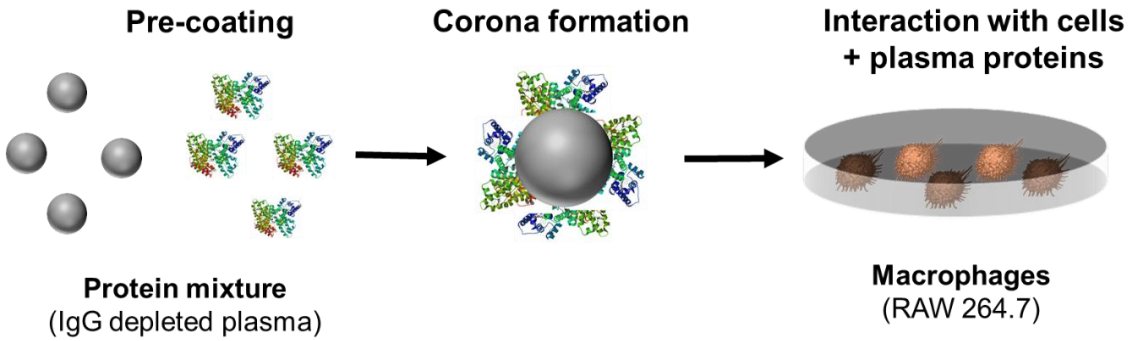


**[8] Pre-adsorption of antibodies enables targeting of nanocarriers despite a biomolecular corona**

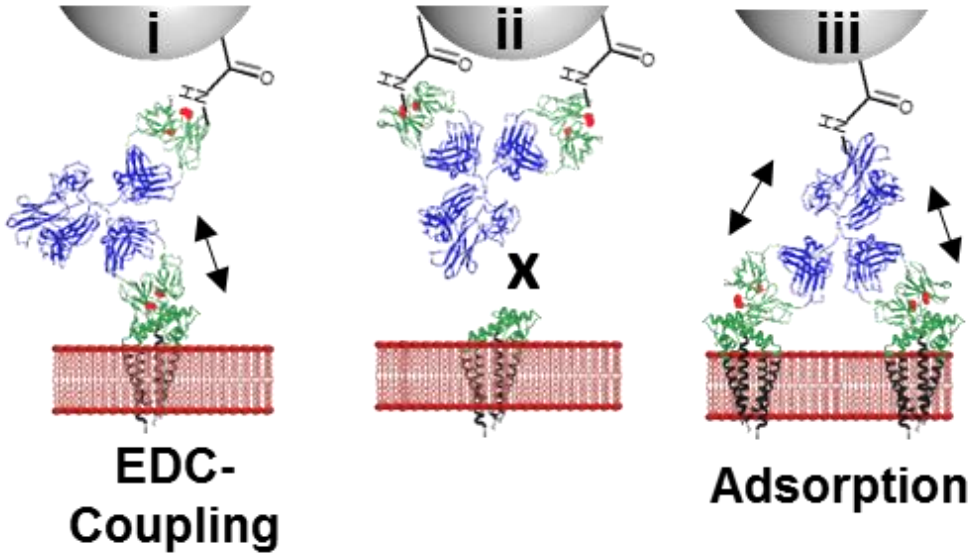

**[9] Mannose functionalized phosphoester based surfactants enable targeted cellular interactions**

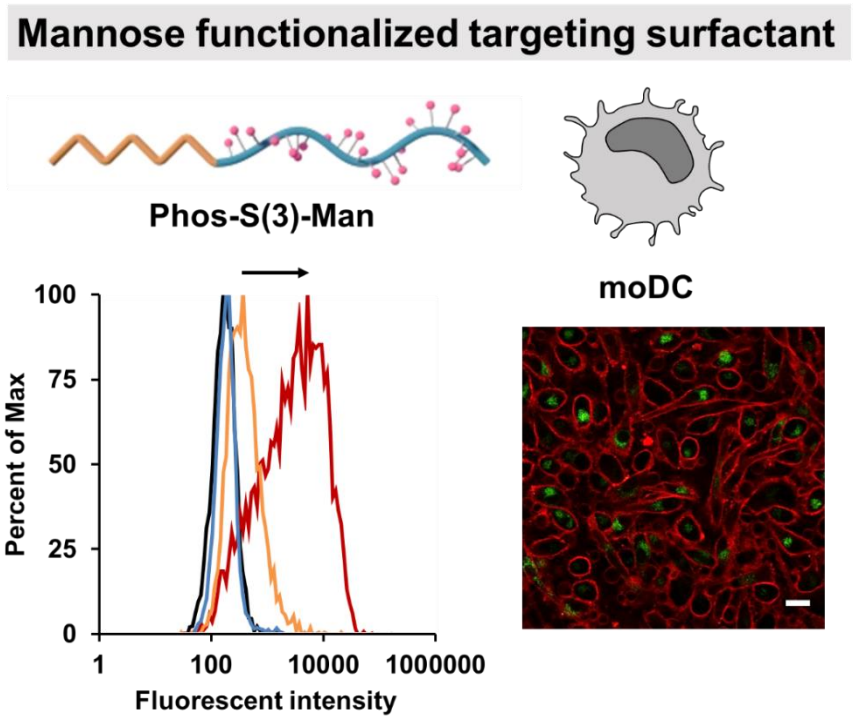


**[10] Pre-coating with protein fractions inhibits nano-carrier aggregation in human blood plasma.**

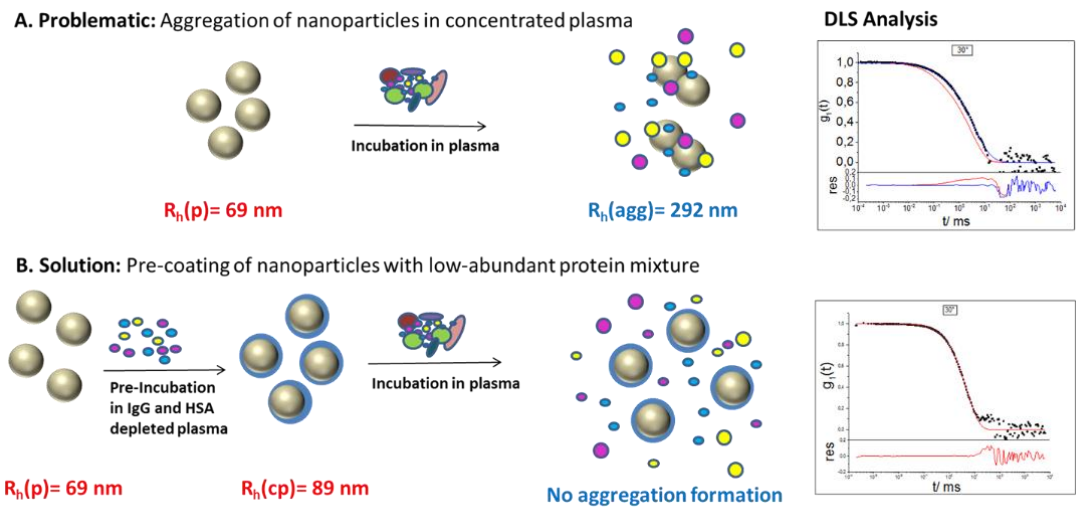

**[11] Fully degradable protein nanocarriers by orthogonal photoclick tetrazole–ene chemistry for the encapsulation and release**.

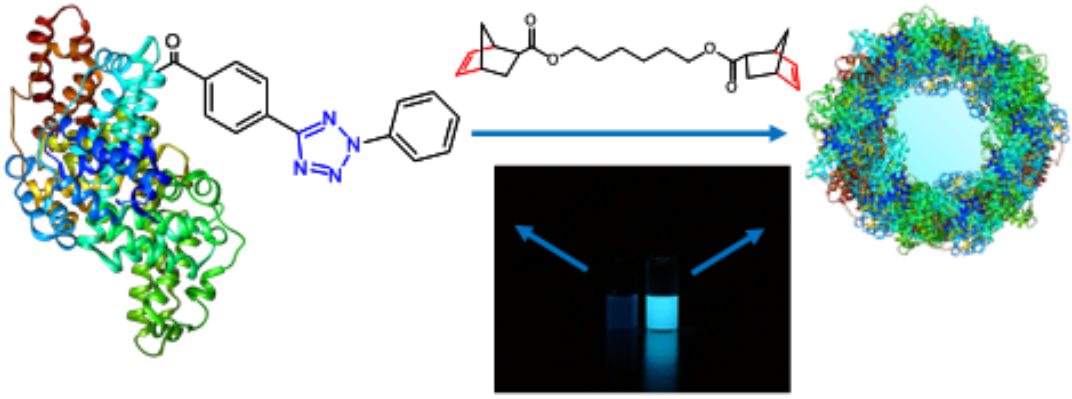

**[12] Highly Loaded Semipermeable Nanocapsules for Magnetic Resonance Imaging.**

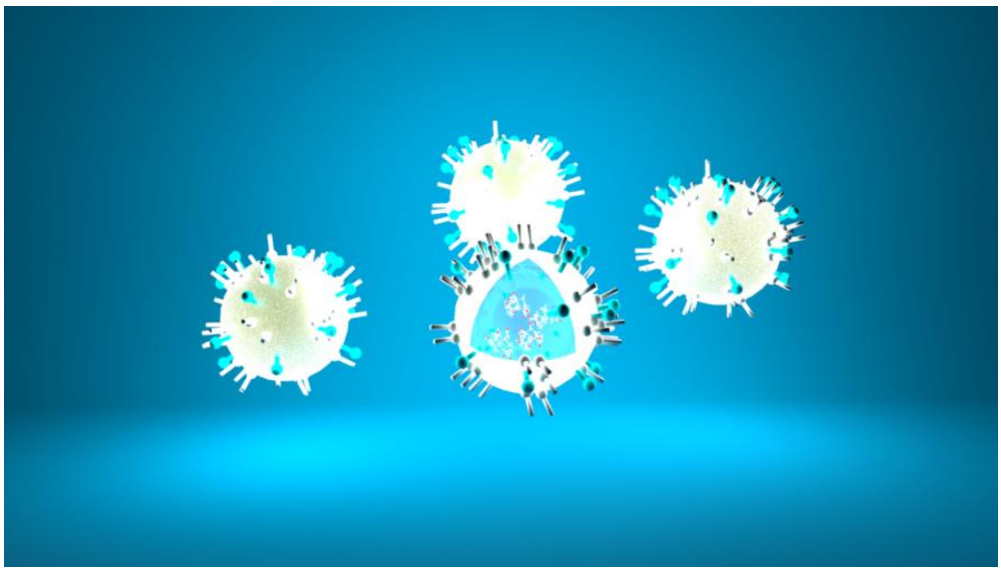

**[13] Coating nanoparticles with tunable surfactants facilitates control over the protein corona.**

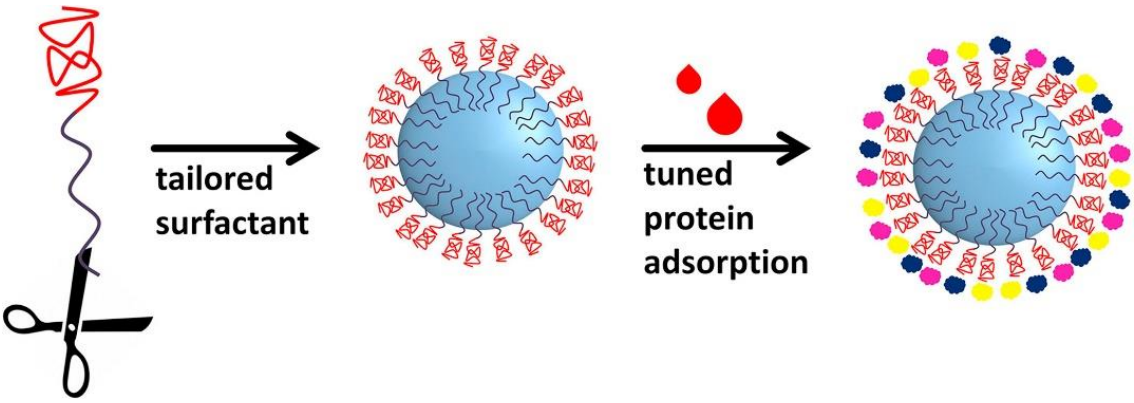


**[14] Polyglycerol Surfmers and Surfactants for Direct and Inverse Miniemulsion.**

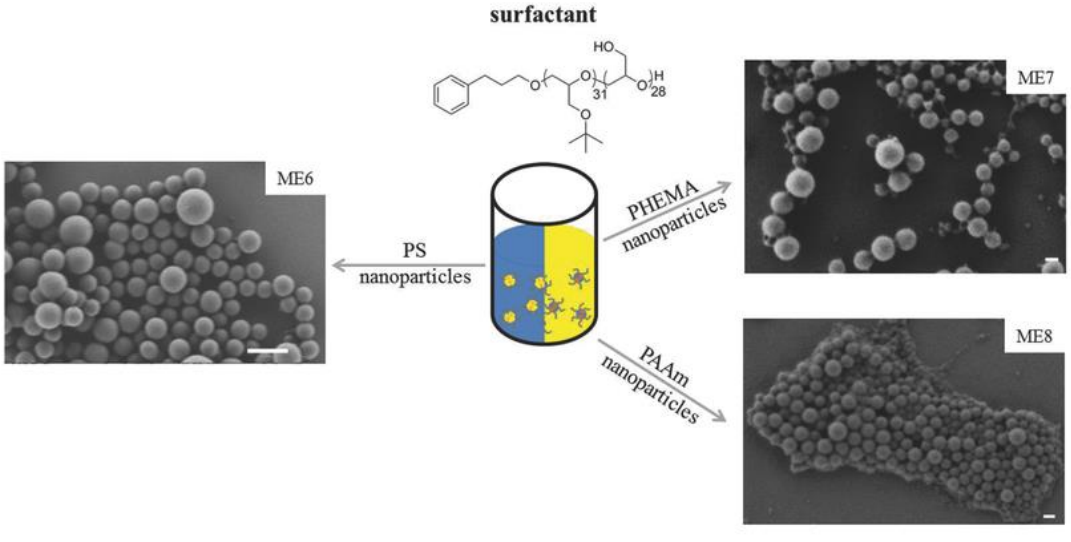

**[15] Reversible Self-Assembly of Degradable Polymersomes with Upper Critical Solution Temperature in Water.**

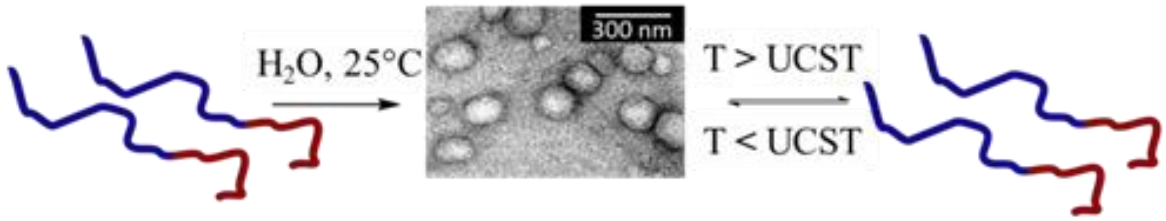


**[16] Temperature responsive poly (phosphonate) copolymers: from single chains to macroscopic coacervates.**

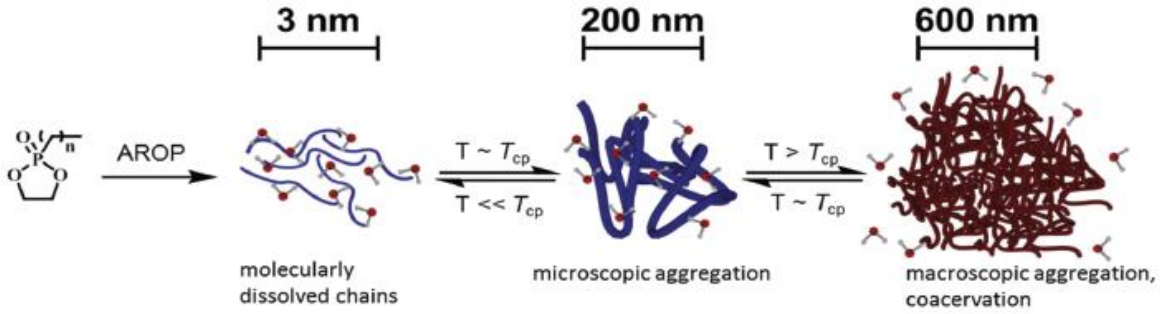


**[17] Denaturation via surfactants changes composition of protein corona**

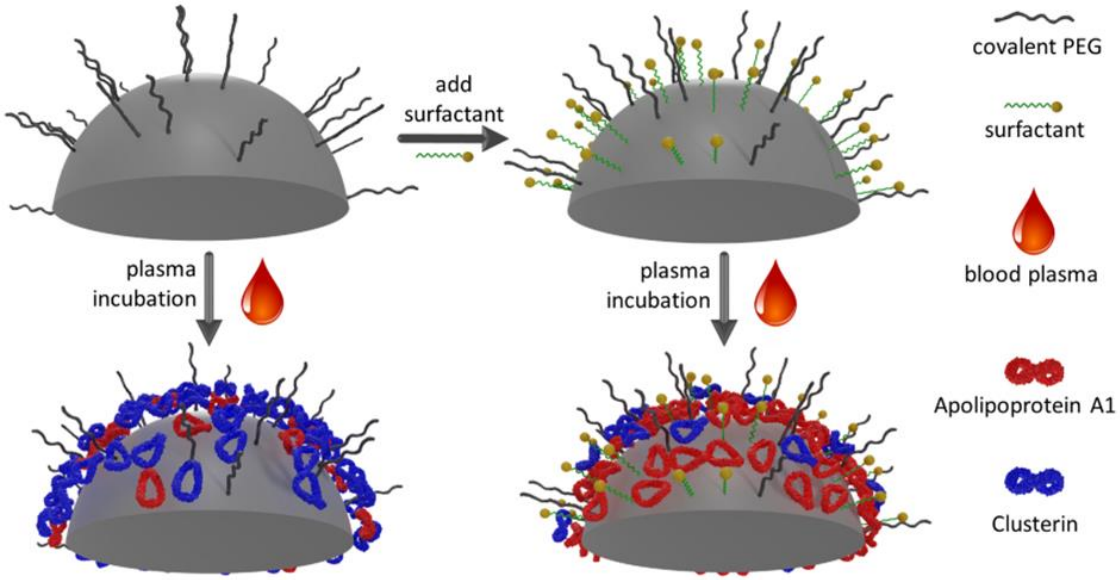


**[18] Preservation of the soft protein corona in distinct flow allows identification of weakly bound proteins**

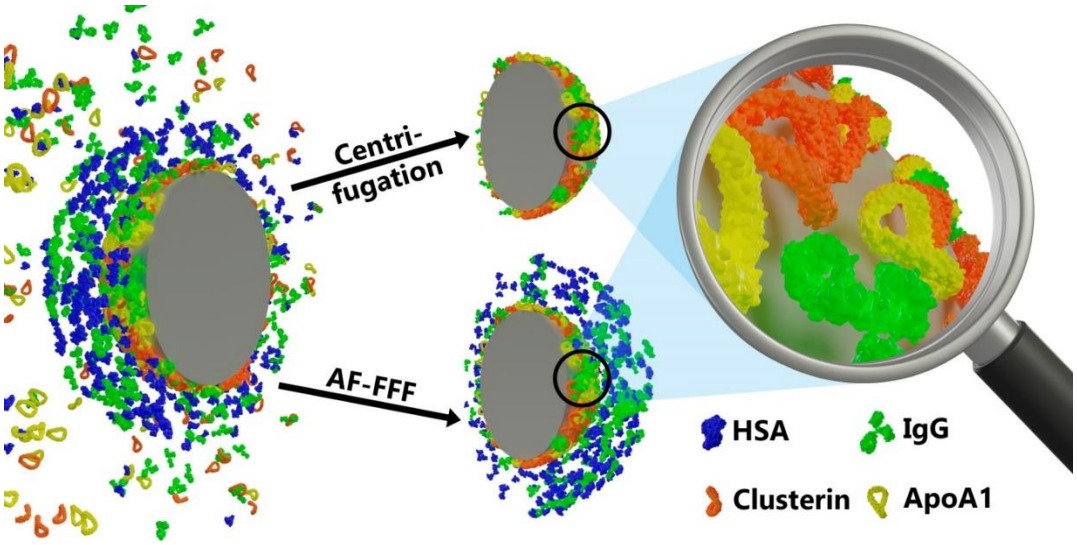


**[19] The protein corona as a confounding variable of nanoparticle-mediated targeted vaccine delivery.**

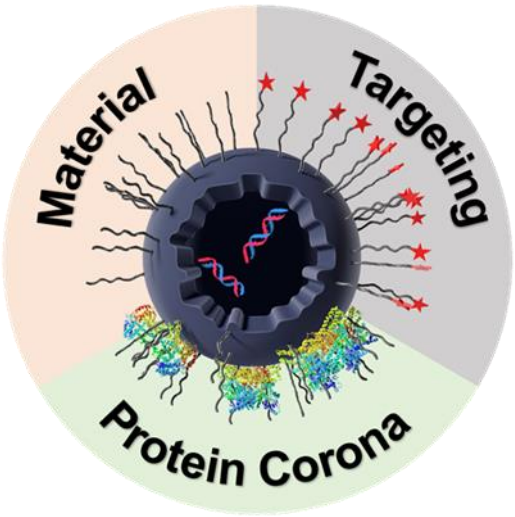
Material
Targeting
Protein Corona

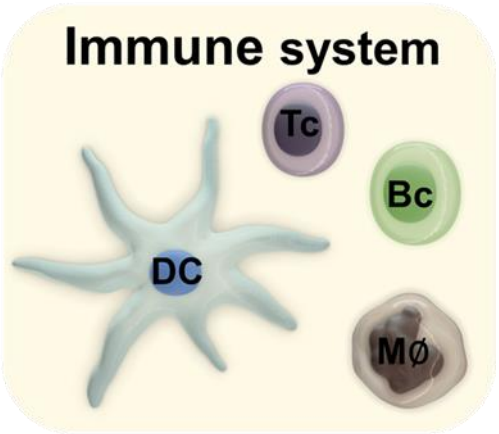
Immune system
Tc
Bc
DC
MØ

# Appendix

## Declaration

I hereby declare that I wrote the dissertation submitted without any unauthorized external assistance and used only sources acknowledged in this work. All textual passages which are appropriate verbatim or paraphrased from published and unpublished texts, as well as all information obtained from oral sources, are duly indicated and listed in accordance with bibliographical rules. In carrying out this research, I complied with the rules of standard scientific practice as formulated in the statutes of Johannes Gutenberg-University Mainz to insure standard scientific practice.

.....

[redacted]

## Curriculum vitae

[redacted]

[redacted]

## Acknowledgements

[redacted]